

Theme VIII: QUANTITATIVE EVALUATION OF DAMAGES CAUSED BY WINDS AND EARTHQUAKES
(INCLUDING TECHNICAL COOPERATIONS IN DEVELOPING COUNTRIES)

<u>Warrants for Retrofitting Highway Bridges</u>	VIII-1
<u>Anatole Longinow, Ernest Bergmann and James D. Cooper</u>	
<u>Criterion on the Evaluation of Seismic Safety of Existing Reinforced Concrete Buildings.</u>	VIII-22
<u>Kiyoshi Nakano, Masaya Hirosawa and Shin Okamoto</u>	
<u>Transferring the Technology for Wind-resistant Buildings to Developing Countries</u>	VIII-42
<u>Noel J. Raufaste, Jr.</u>	

NINTH JOINT MEETING
OF THE
U.S.-JAPAN PANEL ON WIND AND SEISMIC EFFECTS
MAY 24-27, 1977
AT THE
KEIDANREN KAIKAN

TUESDAY-May 24

OPENING SESSION

<u>9:30</u>	<u>Call to order by Dr. Tadayoshi Okubo, Head Planning and Research Administration Division, Public Works Research Institute</u>
	<u>Remarks by Mr. Takashi Inoue, Engineer General, Ministry of Construction</u>
	<u>Remarks by Mr. Justin Bloom, Acting Counselor for Scientific and Technological Affairs, U.S. Embassy</u>
	<u>Remarks by Mr. Kimio Fukushima, Chief, International Division, Promotion Bureau, Science and Technology Agency</u>
	<u>Remarks by Dr. Chester R. Benjamin, Assistant Director, International Program Division, Agricultural Research Survey, Department of Agriculture</u>
	<u>Remarks by Dr. Kaoru Ichihara, Director, Public Works Research Institute, Ministry of Construction</u>
	<u>Remarks by Dr. E.O. Pfraun, Chief, Structures, Materials and Safety Division, Center for Building Technology, NEL, National Bureau of Standards</u>
	<u>Introduction of United States Panel Members by U.S. Chairman and Japan Panel Members by Japanese Chairman</u>
	<u>Election of Permanent Chairman</u>
	<u>Adoption of Agenda</u>
<u>1:00 p.m.</u>	<u>On Distribution Models of Pressure and Wind over Stationary Typhoon Fields -- Shigemi Fujiwhara, and Kiyoshi Kurashige</u>
<u>1:25</u>	<u>Extreme Winds in the United States -- T.D. Potter</u>
<u>1:50</u>	<u>Aerodynamic Stability of a Long-span Suspension Bridge at Construction Stage -- Tetsuo Kunihiro, Nobuyuki Narita, and Koichi Yokoyama</u>
<u>2:15</u>	<u>Discussion</u>
<u>2:40</u>	<u>Present Situation of Earthquake Prediction Research in Japan -- Kazuo Hamada, Hiroshi Sato, Hiroshi Takahashi, and Akira Suwa</u>
<u>3:05</u>	<u>The Complementary Importance of Earthquake Prediction and Structural Response Estimation in Seismic Design and Planning Decisions -- R.K. McGuire</u>
<u>3:30</u>	<u>Discussion</u>
<u>3:50</u>	<u>Recess</u>
<u>4:05</u>	<u>Research and Development of Permanent Ocean-Bottom Seismograph Observation System Off the Pacific Coast of Central Honshu, Japan -- Akira Suwa, Norio Yamakawa, and Tatsuto Iinuma</u>

4:30	Vertical Distribution of the Seismic S-wave and Response Characteristics at the Site of the Iwatsuki Deep Bore Hole Observatory of Crustal Activities -- Fumio Yamamizu, Hiroshi Takahashi, Yutaka Ohta, Noritoshi Gotoh, and Keiji Shino
4:55	Researches of Active Faults in the Metropolitan Area -- Hiroshi Sato, and Toshihiro Kakimi
5:20	<u>Discussion</u>
5:45	<u>Adjourn</u>

WEDNESDAY-May 25

9:00 a.m.	<u>Characteristics of Vertical Components of Strong-Motion Accelerograms -- Tatsuo Uwabe, Setsuo Noda, Eiichi Kurata, and Satoshi Bayashi</u>
9:25	Developments in Strong-Motion Data Management -- A.G. Brady
9:50	On a Method for Synthesizing the Artificial Earthquake Wave by Using Prediction Error Filter -- Keiichi Ohtani, and Shigeo Kinoshita
10:15	<u>Discussion</u>
10:45	<u>Recess</u>
10:55	<u>Statistical Analysis of Strong-Motion Acceleration Records -- Masamitsu Chashi, Toshio Iwasaki, Susumu Wakabayashi, and Kenichi Tokida</u>
11:20	Research on Design Earthquake -- Makoto Watabe
11:45	<u>Discussion</u>
0:05 p.m.	<u>Recess (Lunch)</u>
1:00	<u>Properties of Superficial Layer for Vibration -- Yukitake Shioi, and Toshio Iwasaki</u>
1:25	<u>Studies on Soil Liquefaction Relating to the Earthquake Resistant Design of Structures -- Masamitsu Chashi, Toshio Iwasaki, and Fumio Tatsuoka</u>
1:50	<u>Earthquake Resistant Design Based on Ground Motions at Base-Rock -- Eiichi Kurabayashi, and Kazuhiko Kawashima</u>
2:15	<u>Discussion</u>
2:40	<u>Basic Earthquake for Dam Design -- J.S. Dodd</u>
3:05	<u>Study on Regional Distribution of Maximum Earthquake Motion in Japan -- Masakazu Ozaki, Makoto Watabe, Yoshikazu Kitagawa, and Sadaiku Hattori</u>
3:30	<u>Discussion</u>
3:50	<u>Recess</u>
4:05	<u>Treatments on Seismic Force in Designing Earth Structures -- Kenkichi Sawada</u>
4:30	<u>Studies on the Aseismic Properties of Underground Pipes -- Keiichi Ohtani, Nobuyuki Ogawa, and Chikahiro Minowa</u>
4:55	<u>Observation of Dynamic Behavior of Kiuura Submerged Tunnel During Earthquakes -- Shigeo Nakayama, Osamu Kiyomiya, and Hajime Tsuchida</u>

5:20	Discussion
5:45	Adjourn
THURSDAY-May 26	
9:00 a.m.	A Proposal for Earthquake Resistant Design Methods -- Kiyoshi Nakano, and Misamitsu Ohashi
9:25	On the Object Postulate for Earthquake-Resistant Code -- Kiyoshi Nakano, Yuji Ishiyama, and Yoshitsugu Aoki
9:50	Discussion
10:10	Recess
10:25	The Earthquake Response of Hysteretic Structures -- W.D. Iwan
10:50	Earthquake Resistant Design of High-Rise Buildings in Japan -- Keiichi Ohtani
11:15	Racking Strength of Wood-Frame Walls -- Roger L. Tuomi
11:40	Discussion
0:05 p.m.	Recess (Lunch)
1:00	Expanded Role of the National Science Foundation Earthquake Engineering Program -- J.B. Scalzi
1:25	Examination for an Evaluation Method of Damage of Existing Wooden Houses Caused by Earthquakes -- Kaoru Ichihara, Eiichi Kurabayashi, Tadayuki Tazaki, and Takayuki Hadate
1:50	Modified Mercalli Intensity Relationships to Wood Frame Dwelling Earthquake Insurance -- K.V. Steinbrugge, and S.T. Altermissen
2:15	Discussion
2:40	Recess
3:00	Discussion of Task Committee
5:00	Adjourn
FRIDAY-May 27	
9:00 a.m.	Warrents for Retrofitting Highway Bridges -- J.D. Cooper
9:25	Criterion on the Evaluation of Seismic Capacity of Existing Reinforced Concrete Buildings -- Kiyoshi Nakano, Masaya Hirosawa, and Shin Okamoto
9:50	Transferring Wind Technology to Developing Countries - N.J. Raufaste
10:15	Discussion
10:40	Recess
10:55	* Special Presentation * Investigation Report of the Earthquake in Rumania, March 4, 1977 - Seiji Nakano, Eiichi Kurabayashi, and Masaya Hirosawa xii

11:55 Recess (Lunch)
1:00 p.m. Report of Task Committee
2:20 Resolution
2:50 Recess
3:00 Closing Session
3:30

U.S. Panel on Wind and Seismic Effects

Membership List

May 1977

Dr. Edward O. Pfrang
Chairman
Chief, Structures, Materials and
Safety Division
Center for Building Technology, NEL
National Bureau of Standards
Room B368, Bldg. 226
Washington, D.C. 20234

Dr. S.T. Algermissen
Office of Earthquake Studies
Denver Federal Center
Branch of Earthquake Tectonics
USGS
Stop 978, Box 25046
Denver, Colorado 80225
303-234-4014

Mr. Billy Bohannan
Assistant Director
Wood Engineering Research
Forest Products Laboratory
USDA
P.O. Box 5130
Madison, Wisconsin 53705
608-257-2211

Dr. Robert D. Borcherdt
Office of Earthquake Studies
Branch of Earthquake Hazards
USGS
345 Middlefield Road
Menlo Park, California 94025
415-323-8111 (FTS 467-2755)

Dr. Charles G. Culver
Disaster Research Coordinator
National Bureau of Standards
Room B212, Bldg. 225
Washington, D.C. 20234
301-921-3126

Mr. Jerry Dodd
Bureau of Reclamation
Mail Code 230
P.O. Box 25007
Denver Federal Center
Denver, Colorado 80225

Dr. Michael P. Gaus
Head, Engineering Mechanics Section
Engineering Division
National Science Foundation
1800 G. Street, N.W.
Washington, D.C. 20550

Mr. John J. Healy
Department of the Army
DAEN-RDM
Washington, D.C. 20314
202-693-7287

Dr. William B. Joyner
Office of Earthquake Studies
Branch of Earthquake Hazards
USGS
345 Middlefield Road
Menlo Park, California 94025
413-323-8111 (FTS 467-2754)

Mr. John W. Kaufman
Aerospace Environment Division
ES42-Space Science Laboratory
National Aeronautics and Space Administration
Marshall Space Flight Center Alabama
35812, 205-453-3104

Dr. Noel E. LaSeur
Director
National Hurricane and Experimental
Meteorology Laboratory
National Oceanic and Atmospheric
Administration
P.O. Box 248265
Coral Gables, Florida 33134
305-350-4150

Dr. Richard D. Mc Connell
Office of Construction
Veterans Administration
811 Vermont Ave., N.W.
Washington, D.C. 20234
202-389-3103

Dr. Richard D. Marshall
Research Structural Engineer
National Bureau of Standards
Room B168, Bldg. 226
Washington, D.C. 20234
301-921-3475

Dr. R.B. Matthiesen
Chief, Branch of Seismic Engineering
Office of Earthquake Studies
USGS
345 Middlefield Road
Menlo Park, California 94025
415-323-8111 (FTS 467-2881)

Mr. Howard L. Metcalf
Staff Engineer
Construction Standards and Design
Directorate
Office of the Assistant Secretary
of Defense
Room 3E763
The Pentagon
Washington, D.C. 20301
202-695-2713

Mr. Keith O. O'Donnell
Assistant Chief, Structural Branch
Engineering Division, Civil Works
Directorate
Office of The Chief of Engineers
ATTN: DAEN-CWE-D
Washington, D.C. 20314

Dr. Thomas D. Potter
Director
National Climatic Center
Environmental Data Service
National Oceanic and Atmospheric
Administration
Federal Building
Asheville, North Carolina 28801
704-258-2850 x 236

Dr. Hohn B. Scalzi
Program Manager, Earthquake Engineers
Division of Advanced Environmental
Research and Technology
National Science Foundation
1800 G Street, N.W.
Washington, D.C. 20550

Mr. Charles Scheffey
Director
Office of Research
HRS-1
Federal Highway Administration
Department of Transportation
Washington, D.C. 20590
202-426-2943

Mr. Lawrence C. Shao
Chief, Structural Engineering Branch
Nuclear Regulatory Commission
Washington, D.C. 20555
202-492-8035

Dr. Warren A. Shaw
Head, Civil Engineering Department
Civil Engineering Laboratory
Naval Construction Battalion Center
Port Hueneme, California 93043

Mr. William J. Werner
Energy Building Technology and Standards
Department of Housing and Urban Development
Room 8158
451 7th Street, S.W.
Washington, D.C. 20410
202-755-0642

ALTERNATIVES

Dr. A. Gerald Brady
Physical Scientist
Office of Earthquake Studies
USGS
345 Menlo Park, California 94025
415-323-8111 (FTS-467-2881)

Dr. James D. Cooper
Structures & Applied Mechanics Division
Federal Highway Administration
Office of Research HRS-11
Washington, D.C. 20590

Mr. G. Robert Fuller
Architectural and Engineering Division
Department of Housing and Urban Development
Room 6176, 451 7th Street, S.W.
Washington, D.C. 20411

Dr. H.S. Lew
Secretary
Structures, Materials and Safety Division
Center for Building Technology, NEL
Washington, D.C. 20234
301-921-3158

Dr. Charles T. Thiel
Deputy Director
Division of Advanced Environmental Research
and Technology
National Science Foundation
1800 G Street, N.W.
Washington, D.C. 20550
202-632-5734

Mr. Drew A. Tiedemann
Bureau of Reclamation
Engineering and Research Center
Denver Federal Center
P.O. Box 25007
Denver, Colorado 80225
303-234-3029

Japanese Panel on Wind and Seismic Effects

Membership List

May 1977

Dr. Kaoru Ichihara, Chairman
Director Public Works Research Institute
Ministry of Construction

Mr. Shigemi Fujiwhara, Member
Head, Typhoon Research Division
Meteorological Research Institute

Dr. Satoshi Hayashi, Member
Vice Director
Port and Harbour Research Institute
Ministry of Construction

Mr. Toshio Iwasaki, Member
Chief Researcher,
Building Research Institute
Ministry of Construction

Mr. Toshio Iwasaki, Member
Chief, Ground Vibration Section
Earthquake Disaster Prevention Division
Chiba Branch
Public Works Research Institute
Ministry of Construction

Dr. Tetsuo Kunihiro, Member
Head, Structure and Bridge Division
Chiba Branch
Public Works Research Institute
Ministry of Construction

Mr. Eiichi Kurabayashi, Member
Chief, Earthquake Engineering Section
Earthquake Disaster Prevention Division
Chiba Branch
Public Works Research Institute
Ministry of Construction

Mr. Tatsuro Murota, Member
Chief, Structure Section
Structure Division
Building Research Institute
Ministry of Construction

Dr. Keikichi Naito, Member
Head, Meteorological Satellite Division
Meteorological Research Institute
Meteorological Agency

Dr. Kiyoshi Nakano, Member
Assistant Director
Building Research Institute
Ministry of Construction

Mr. Nobuyuki Narita, Member
Chief, Structures Section
Structure and Bridge Division
Chiba Branch
Public Works Research Institute
Ministry of Construction

Dr. Masamitsu Ohashi, Member
Head, Earthquake Disaster Prevention
Division, Chiba Branch
Public Works Research Institute
Ministry of Construction

Mr. Keiichi Ohtani, Member
Chief, Earthquake Engineering Laboratory
National Research Center for Disaster
Prevention
Science and Technology Agency

Dr. Michio Ohtsuka, Member
Acting Director,
International Institute of Seismology and
Earthquake Engineering (I.I.S.E.E.)
Building Research Institute
Ministry of Construction

Dr. Tadayoshi Okubo, Secretary-General
Head, Planning and Research Administration
Division
Public Works Research Institute
Ministry of Construction

Dr. Hiroshi Sato, Member
Chief, Research Division
Crustal Dynamics Department
Geographical Survey Institute
Ministry of Construction

Mr. Kenkichi Sawada, Member
Chief, Soil Dynamics Section
Construction Method and Equipment Division
Chiba Branch
Public Works Research Institute
Ministry of Construction

Mr. Akira Suwa, Member
Head, Seismological Laboratory
Meteorological Research Institute
Meteorological Agency

Mr. Hiroshi Takahashi, Member
Head, Second Research Division
National Research Center for Disaster
Prevention
Science and Technology Agency

Dr. Tsutomu Terashima, Member
Chief, Seismology Section
International Institute of Seismology and
Earthquake Engineering (I.I.S.E.E.)
Building Research Institute
Ministry of Construction

Mr. Hajime Tsuchida, Member
Chief, Earthquake Resistant Structures
Laboratory
Structure Division
Port and Harbour Research Institute
Ministry of Transport

Dr. Makoto Watabe, Member
Head, Structures Division
Building Research Institute
Ministry of Construction

Mr. Kaname Yahagi, Member
Chief, Foundation Engineering Section
Structure and Bridge Division, Chiba Branch
Public Works Research Institute
Ministry of Construction

Dr. Masami Hukuoka, Honorary Member
Professor of Tokyo Univ.

Dr. Shiro Ibukiyama, Honorary Member
An Executive Director
of Japan Road Company, Ltd.

Mr. Mitsuru Nagao, Honorary Member
Director of Japan International Cooperation
Agency

Mr. Kenji Kawakami, Honorary Member
An Adviser of Kubota, Tekko, Ltd.

RESOLUTIONS OF THE JOINT MEETING
U.S.-JAPAN PANEL ON WIND AND SEISMIC EFFECTS
U.J.N.R.
May 24 - 27, 1977

The following resolutions for future activities of this Joint Panel are hereby resolved:

1. The Ninth Joint Meeting was an extremely valuable opportunity to exchange technical information which was beneficial to both countries. In view of the importance of cooperative programs on the subject of wind and seismic effects, the continuation of Joint Panel Meetings is considered essential.
2. The exchange of technical information, especially revised codes and specifications relevant to wind and seismic effects shall be encouraged.
3. The cooperative research programs including exchange of personnel and equipment should be promoted.
4. Considerable advancements in various Task Committees were observed. These activities should be encourage and continued. Correspondence between Task Committee Chairmen should be encouraged, and additional meetings should be held as required.
5. Program agenda for future Joint Meetings should be developed to encourage a balanced number of presentations dealing with wind and seismic effects on structures.
6. The Tenth Joint Panel Meeting will be held in May 1978 in Washington, D.C. The specific date and itinerary of the Meeting will be determined by the U.S. Panel with concurrence by the Japan Panel.

DISTRIBUTION MODELS OF PRESSURE AND WIND OVER

STATIONARY TYPHOON FIELDS

Shigemi Fujiwhara and Kiyoshi Kurashige

Meteorological Research Institute

ABSTRACT

For pressure and wind distributions on the sea surface over typhoon and hurricane area, many trials have been proposed in order to adapt distribution models for observational data. These models have been utilized widely in many scientific and technical applications. For example, theoretical analysis, storm surge, disaster evaluation, protective measurement against typhoon damage, and so on.

The above models proposed are simple models. Unfortunately, however, the better adaptation for observed data requires more complicated models. However, the advent of the electronic computer has brought about the methods which can shorten the computational time tremendously. Therefore, the models no longer have to be simple.

In this paper, several new models are introduced and their characteristics are discussed. Then, basic differences between the formulas by various models are pointed out clearly. In order to increase the accuracy of model adaptation, a technique of revising the formulas is discussed. Taking into account the computation time of the electronic computer, a new model formula is presented and examined by comparing it with other formulas.

KEYWORDS: Distribution Models; Pressures; Sea Surface; Stationary Typhoon

INTRODUCTION

Pressure and wind distributions on the sea surface over typhoon or hurricane area seem to be complex in performing detailed analysis. However, they can be considered simply as circularly symmetric. Therefore, many trials have been proposed in order to adapt distribution models for observational data. These models have been utilized widely in many scientific and technical applications. For example, theoretical analysis, storm surge, disaster evaluation, protective measurement against typhoon damage, and so on. These models were introduced by many researchers in Japan, the United States and Philippines.

The above models were proposed for the purpose of simplification. Unfortunately, the better adaptation for observed data requires more complicated models.

However, with the recent development of the electronic computer, the shorter computation time has come to be realized. Therefore, the necessity of simplifying the models is no longer a problem.

This paper attempts to reevaluate the distribution models from the above standpoint. We have never had this sort of discussion, because these models have been considered as conventional formulas and also there have been many difficulties in computing the distances between the typhoon center and every data position at each weather map time.

The advent of the electronic computer has brought about new concepts into these distribution models. Also, the current practices require greater accuracy of adaptation for observed data.

CHARACTERISTICS OF PRESSURE DISTRIBUTION FORMULA

Among typhoon models proposed to date, several representatives are as follows:

$$\text{Schloemer (1954)} \quad P = P_c + \Delta P \exp(-Y_o/Y) \quad (1)$$

$$\text{Takahashi (1939)} \quad P = P_\infty - \Delta P/[1 + (\gamma/\gamma_o)] \quad (2)$$

$$\text{Bjerknes (1921)} \quad P = P_\infty - \Delta P/[1 + (\gamma/\gamma_o)^2] \quad (3)$$

$$\text{Fujita (1952)} \quad P = P_\infty - \Delta P/[1 + (\gamma/\gamma_o)^2]^{1/2} \quad (4)$$

where γ is a distance from the typhoon center, P shows pressure (mb) at γ , P_c is equal to P at the typhoon center, P_∞ means the average pressure value along the outer edge of the typhoon area, and $\Delta P = P_\infty - P_c$. P_c and P_∞ are calculated statistically from weather analysis maps. Parameter γ_o is defined individually in the above formulas: in (1), γ_o is equal to the radius γ_M where the maximum wind velocity is observed, in (2) and (3) γ_o means γ where $P = (P_\infty + P_c)/2$, and in (4) γ_o is equal to $\gamma_M/\sqrt{2}$.

Wind velocities within typhoon area are expressed in the following equation (the gradient wind law):

$$fv + \frac{v^2}{\gamma} = \frac{1}{\rho} \frac{\partial P}{\partial Y} \quad (5)$$

where f is Coriolis factor $2\omega \sin \psi$, ω the rotating angular velocity of the earth, ψ latitudinal degree, ρ the density of the atmosphere, v the gradient wind velocity. We can estimate v from Eq. (5) if we know the pressure distribution. Therefore, Eqs. (1) through (4) involve distribution formulas of wind implicitly.

Their characteristics are shown as follows:

Eq. (1) is very convenient with respect to theoretical arrangement as far as the adaptation for data is concerned. It has a good response over the outer regions of the typhoon area, but it is too flat to fit with observed data over the inner regions. (See Fig. 1)

Eq. (2) has also a good adaptation over the outer regions, but at the center, the pressure gradient becomes discrete. Therefore, the calculated wind velocity at the center comes to be unreasonable.

Eq. (3) is introduced basically under the rotating fluid assumption, so that it has a good adaptation over the inner regions and a bad adaptation over the outer regions.

Eq. (4) is similar to Eq. (2) over the outer regions and also similar to Eq. (3) over the inner regions, because it was designed so as to include excellent features of Eqs. (2) and (3). However, it is hard to deal with Eq. (4) practically.

In addition to the above individual deficiencies, they have some common weak points. For example, a general typhoon has several stages; the developing stage, the mature stage, the decay stage, and the warm cyclone stage. When a typhoon changes its stage from one to another, the time variance of its pressure distributions has usually come to be remarkable. But, unfortunately, the stage variation was not taken into account in the above formulas. If we introduce the following equation as a general type of Eqs. (2) and (3),

$$P = P_\infty - \Delta P / [1 + (\gamma/\gamma_0)^\alpha] \quad (6)$$

where α is determined so as to fit Eq. (6) into the observed data. It might be impossible for us to express a typhoon involving many stages by Eq. (6).

Now in order to eliminate the above weak points, it is necessary to make the problem more distinct. Namely, let us treat Eqs. (1) through (4) in the following way.

Eq. (1) is considered as an integral form of the following differential equation,

$$\frac{dP}{dx} = -\gamma_0 (P - P_0); \quad x = 1/\gamma \quad (7)$$

In the same manner, for Eq. (2),

$$\frac{dP}{dx} = \frac{1}{\Delta P} (P_\infty - P)(P - P_c); \quad x = \ln(\gamma/\gamma_0) \quad (8)$$

Also, for Eq. (3),

$$\frac{dP}{dx} = \frac{2}{\Delta P} (P_\infty - P)(P - P_c); \quad x = \ln(\gamma/\gamma_0) \quad (9)$$

Also, for Eq. (4),

$$\frac{dP}{dx} = \frac{1}{\Delta P} (P_\infty - P)(P - P_c) \cdot f(x) \quad (10)$$

$$f(x) = 1 + (1 + \rho^{2x})^{-1/2}; \quad x = \ln(\gamma/\gamma_0)$$

Eqs. (7) through (10) correspond to Eqs. (1) through (4) respectively.

In Fig. 2, characteristics of Eqs. (7) through (10) are shown schematically. Eq. (10) (Fujita type) approaches to Eq. (8) (Takahashi type) over the outer typhoon regions and it also approaches to Eq. (9) (Bjerknes type) over the inner typhoon regions. On the contrary, Eq. (7) (Schloemer type) does not show such a good approach over the inner regions. These characteristics are the same as those shown in Fig. 1.

However, Fig. 2 gives us information about an advanced formula which should be a hyperbola having two asymptotes, Eq. (8) and Eq. (9). Eq. (10) (Fujita type) is quite similar to such an advanced model, but it is not a hyperbola. Rather, it is a transcendental curve having some restrictions. It is desirable that the advanced model should be a more general type of hyperbola with less restrictions. In this Figure, the cross point T of two asymptotes shows the transitional point between the inner and outer regions of the typhoon. In these formulas mentioned above, there are two main restrictions: positions of T and gradient of asymptotes. However, if we assume a new model in which those restrictions are taken off and some freedoms are given so as to determine those values statistically by using observational data, the above problem may be solved. Namely, an introduction of new parameters (determined by data) causes an increase of freedom number and finally a better adaptation for data may be expected.

A NEW DISTRIBUTION FORMULA

A new formula is basically similar to Eq. (10). Instead of $f(x)$, $\frac{dy}{dx}$ is introduced. That is

$$\frac{dp}{dx} = \frac{1}{\Delta p} \left(\frac{dy}{dx} \right) (P_{\infty} - P) (P - P_C); x = \ln(Y/Y_0) \quad (11)$$

where y means a hyperbola, which we want to obtain. Therefore, dy/dx shows its gradient. By integrating Eq. (11),

$$P = P - \Delta p / [1 + g(x)]$$

$$g(x) \equiv Y \frac{\alpha+1}{2} / (Y_0 \cdot Y_p \frac{\alpha-1}{2}) \cdot \exp \left\{ - \left[\frac{\alpha-1}{2} \cdot \ln(Y/Y_p) - C' \right]^{1/2} \right\} \quad (12)$$

where new parameters α , Y_p and C' are referred to gradient of asymptote over the inner regions of typhoon, position of the transitional point and curvature of the hyperbola, respectively. Adding to the previous parameter Y_0 , the new constants can be determined statistically by observational data (the least square method). This new technique is proposed by Kurashige (1977). The method of determining these constants is shown in Appendix.

RELATIONSHIP BETWEEN THE NEW MODEL AND THE OTHERS

As revision of the above formulas (1) through (4), Fujita (1952) and Haraguchi (1976) have also presented their models (besides Kurashige). Therefore, we have to discuss the relationship or differences between these models and Kurashige's one. Fujita's model,

Eq. (4), as mentioned above, contained two individual distribution forms for the inner and outer regions of the typhoon. Kurashige's Eq.(12) also adopted the same concept. However, the position of T in Eq. (4) is apriori defined. Syono (1958) pointed out that the amount of negative vorticity over the outer regions in Eq. (4) was less than actual. The relationship between the vorticity ζ and wind velocity v is explained as follows:

$$\frac{\partial v}{\partial Y} + \frac{v}{Y} = \zeta \quad (13)$$

So that Syono's speculation is related to the second order derivative of γ in the pressure distribution formula. (See Eq. (5))

On the other hand, Haraguchi's model is one where two individual distribution formulas are connected empirically. Therefore, the adaptation for data shows a better result as well as Kurashige's. However, if we want to obtain characteristic values in his model, it is necessary to get a smoothed distribution curve defined previously by some other methods, and moreover the position of maximum wind velocity must be well-defined. The above conditions are unsuitable for use of the electronic computer.

Recently, Mitsuta and others (1974, 1975) examined statistically adaptations between models and observations. They reported that, on the average, each model had a rather good adaptation and there was no remarkable difference between the above models, but the deviation was rather large in an individual case. However, Haraguchi's and Kurashige's models have been proposed more recently, so that they were not included in Mitsuta's test.

Even in Kurashige's model, some uncertain problems still remain. One of them is whether the other curve besides hyperbola is convenient or not. For example, tanh x and irrational function may be taken into consideration, but unfortunately, they are so complicated that their integral forms may face difficulties. At present, the hyperbola is the most convenient one. Another of them is that the gradient of asymptote over the outer regions is apriori determined to be Takahashi type. If a sufficient data coverage is available, the above gradient should be obtained by the least square method.

As a conclusion, Kurashige's formula is apparently complicated, but its main points are the same as those in the previous models, and, moreover, it has larger freedoms than previous ones in order to get a better adaptation for data. Therefore, as far as the use of electronic computers is concerned, it does not take so much machine time as usual.

Also, a moving typhoon field is not circularly symmetric. However, as it is possible to divide the typhoon field into two parts (the general current and a stationary typhoon field), we have no problem about that.

APPENDIX

How to determine γ_0 is shown as follows. At first, data position Y and observed value P are given by data. If we take an arbitrary constant Y_1 , we can compute as

$$x = \ln(Y/Y_1), y = \ln|(P - P_c)/(P_\infty - P)|$$

Next, we consider a hyperbola with two asymptotes ($y_1 = x + \gamma$, $y_2 = ax + \beta$) as follows:

$$\alpha x^2 - (\alpha + 1) xy + y^2 + 2gx + 2fy + C = 0 \quad (14)$$

where $2g = \alpha\gamma + \beta$, $2f = -(\gamma + \beta)$, $C = \gamma\beta + \varepsilon$

and $\alpha > 1$. Using the above x and y , we can determine α , g , f and C statistically by the least square method. The cross point T is defined as

$$x_T = [2(\alpha + 1) f + 4g]/(\alpha - 1)^2$$

$$y_T = [2(\alpha + 1) g + 4af]/(\alpha - 1)^2$$

Now, the asymptote of outer regions y_1 is moved according to the parallel transformation so as to pass through the origin. Then, Eq. (14) becomes

$$\alpha' - (\alpha + 1)x'y' + y'^2 - 2f'x' + 2f'y' + C' = 0$$

where $x' = x - x_o$, $y' = y$,

$$x_o = x_T - y_T = (2f + 2g)/(1 - \alpha)$$

$$2f' = [4\alpha f + 2g(\alpha + 1)]/(\alpha - 1)$$

$$C' = \alpha x_o^2 - 2x_o g + C$$

and the cross point of two asymptotes becomes

$$x'_T = y'_T = 2f'(\alpha - 1)$$

If we convert them into (γ , P) system,

$$\gamma_o = \gamma_1 \exp(x_o) = \gamma_1 \exp\left(\frac{2f + 2g}{1 - \alpha}\right)$$

and the transitional point γ_p between the inner and the outer regions is replaced as,

$$\gamma_p = \gamma_o \exp(2f')$$

REFERENCES

Bjerknes, V. (1921): On the dynamics of the circular vortex with applications to the atmospheric vortex and wave motions. Geophysiske Publikationer, Vol. 2, pp. 1-81.

Fujita, T. (1952): Pressure distribution in typhoon. Rep. Met. Lab., Kyushu Inst. Tech. 2, No. 1-2.

Haraguchi, K. (1976): On a pressure distribution model applicable for various type cyclones. Tenki Vol. 23, pp. 615-623 (in Japanese).

Kurashige, K. (1977): On a new pressure distribution model over stationary typhoons. Pap. Met. Geophys. (to be published)

Mitsuta, Y. and others (1974): Model of severe typhoon (1). Kyoto Univ. Dev. Lab. Rep. Vol. 17, pp. 227-234 (in Japanese).

_____(1975): Studies on severe typhoon model (2). Kyoto Univ. Def. Lab. Rep. Vol. 18-B, pp. 227-243 (in Japanese).

Schloemer, R. W. (1954): Analysis and synthesis of hurricane wind patterns over Lake Okeechobee, Florida, Hydrometeorological Report, No. 31, pp. 1-49, U.S. Weather Bureau.

Syōno, S. (1958): The structure of typhoon near the ground surface. The general theory of meteorology. Chijin-Shokan, pp. 252-255 (in Japanese).

Takahashi, K. (1939): Distribution of pressure and wind in a typhoon. J. Met. Soc. Japan, 17, pp. 417-421 (in Japanese).

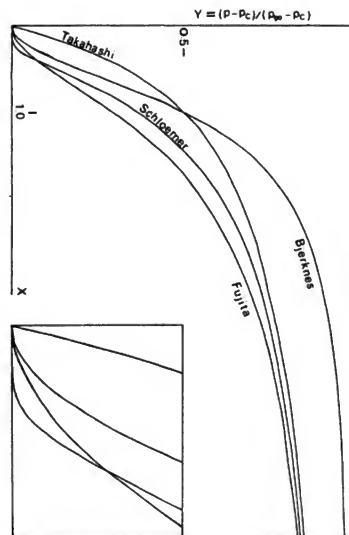


Figure 1. Comparison of pressure distribution formulas

The origin shows the center of typhoon.

The additional figure in SE corner is a magnification near the center. The cross point between Bjerknes' and Takahashi's is located at $x = 1.0$, $y = 0.5$.

Over inner regions of typhoon, Schloemer's formula shows flat and Takahashi's becomes discontinuous at the center.

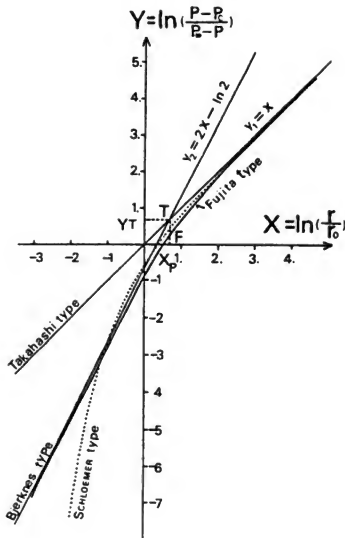


Figure 2. Comparison of formulas characteristics

Fujita type shows a transcendental curve with two asymptotes of Takahashi type and Bjerke type. T is the cross point between the above two asymptotes. Schloemer type shows to approach to Takahashi's over outer regions, but to be far from Bjerke's over inner regions.

EXTREME WINDS IN THE UNITED STATES
Thomas D. Potter and Michael Changery
Environmental Data Service
National Oceanic and Atmospheric Administration

ABSTRACT

Each year extreme winds in the U.S. cause extensive property damage and occasionally the loss of lives. This paper will first review the patterns of extreme winds in the U.S. and the associated wind damage. The types of maximum wind speed data currently available are then discussed. Finally, problems associated with using these maximum wind speed data in U.S. design standards are considered.

KEYWORDS: Design requirements; design standards; extreme winds; hurricanes; property damage.

INTRODUCTION

A large portion of the United States is subject to damage caused by wind-induced stress on structures. Many of the earliest records from explorers nearly 500 years ago refer to the occurrence of hurricanes along the Atlantic and Gulf coasts. The great heartland of the United States is well known for the large frequency of tornadoes (sometimes over 1000 per year) which often leave total destruction along their path. Other areas of the United States also suffer wind damage from various types of storms.

Until recently, however, wind has not been considered an important factor in building design. The climatologist has had little input into the problems created by winds on structural design. This is due partially to a lack of information on the characteristics of the wind and on the interaction between the wind and the structure. It is due also to the lack of a long-period homogeneous set of standard wind measurements from which design values can be obtained. This paper will examine the patterns of extreme winds and wind damage in the United States, the types and volume of maximum wind speed data currently available, and the problems in using these wind data in the current United States design standards.

WIND AND DESIGN REQUIREMENTS

Buildings and structures are now commonly being designed to heights not even considered 10 or 20 years ago. One of the most important of the loads acting upon these structures is that due to the wind. The level of safety built into these structures is directly related to the accuracy with which the wind and its effects can be determined.

In the past, the highest wind recorded in an area or location was used as the design value. Among the various problems apparent with this approach was the fact that all meteorological records are eventually broken. Thus a station with a longer period of record had a higher probability of observing an extreme wind speed - a fact which would obscure the true climatic similarity among a number of stations in an area. A second problem was the possible loss of data due to instrument failure at high wind speeds. Finally, an instrument with a better response time would record speeds higher than those recorded by a more "sluggish" system. These problems led to the adoption of a statistical estimate of design speeds.

For various engineering and meteorological reasons, wind loads are best considered in terms of a steady applied force together with a factor describing gust effects. The spectrum of horizontal velocity measured by Van der Hoven (1) showed two most prominent peaks. One peak occurs in the gust region and a second peak occurs at a period reflecting large-scale atmospheric fluctuations of no concern to the engineer. Between the two peaks is a gap ranging from 5 minutes to 5 hours which is useful for obtaining stable speed measurements. Structurally, it is not desirable to rely on only the peak gust for design purposes because this ignores the influence of a sequence of gusts which may be resonant with the structure.

In addition to being highly dependent on instrument response, gusts alone provide an uncertain estimate of the wind environment since a number of samples with similar mean speeds may all have varying peak gust values. In some instances, however, it is the gust superimposed on the load caused by a high mean speed which causes extensive damage to the surface of many structures. For example, most of the damage from Hurricane Celia at Corpus Christi, TX, in 1970 was caused by the extremely high gusts rather than the prevailing strong winds. So a knowledge of both the mean wind and gusts (determined from measurements or theory) is required to evaluate wind loads on a structure.

WIND REGIMES AND WIND DAMAGE IN THE UNITED STATES

In the United States, wind damage results from extreme winds caused by four meteorological systems: extratropical cyclones, hurricanes and other tropical cyclones, tornadoes, and severe thunderstorms. The extratropical cyclones produce their highest speeds in the winter months deriving their energy from the large thermal contrasts available in this season. Generally, the West Coast, mountain and inter-mountain areas of the Rockies, some areas of the Northern Plains and the Great Lakes receive their highest winds from these systems. Maximum wind speeds are usually less than 75 knots but may reach 100 knots in very severe extratropical cyclones. The area along and within 200 miles of the Atlantic and Gulf coasts receives its highest winds from hurricanes in which wind speeds sometimes reach 200 knots. Tornadoes produce the strongest winds observed in the United States; precise values of maximum speeds are not well established because wind instruments are usually destroyed in tornadoes but there is evidence to show that values above 300 knots are sometimes reached. The Great Plains experiences the highest frequency of tornadoes but every State in the United States (except Hawaii) has experienced at least one tornado. Occasionally, widespread outbreaks of tornadoes produce extensive structural damage and loss of life, such as in the tornadic storms of April 3-4 in 1974 (2). Portions of the United States not already mentioned usually receive their strongest winds from severe thunderstorms. A few notable exceptions to this generalization exist such as the Chinook winds in the lee of the Rockies and the Santa Ana winds of Southern California. These are usually localized in extent but may produce very strong winds which cause considerable damage.

Wind damage statistics have been collected for many years. Current statistics indicate that damage from hurricanes and other tropical storms, severe thunderstorms, and extratropical storms average approximately \$750 million per year. This figure varies, of course, from year to year and may be as high as \$2 billion in years with exceptionally severe hurricanes such as Camille in 1969. Tornado damage amounts to two-thirds the value obtained by larger scale storms - on the order of \$400 to \$500 million per year. Again, large fluctuations in annual damages may occur in years with severe tornado outbreaks.

Average damage from large-scale storms and tornadoes has been increasing year to year. This is attributed to the general population increase in the United States and the corresponding increase in area covered by dwellings and other structures, resulting in more damage even though the annual number of storms remains relatively the same on a long-

term basis. Although damage statistics may be tempered by building design considerations, the annual loss likely will continue to increase in future years. Much of this damage loss occurs along the East Coast with its high population density. Although the West Coast is heavily populated, the probability of extreme winds is rather low so the wind damage losses are relatively small. Finally, even though the population density is low in the mid-portions of the country, substantial damage occurs from the high incidence of tornadoes.

WIND MEASUREMENTS AND DATA AVAILABILITY

The United States currently has available the following four basic wind measurements in the archives:

(1) Fastest mile: This type of wind observation has been extracted since 1887 at approximately 200 locations. For these locations an additional 20 years of data could be obtained from the original records. For about 300 additional stations a limited period (10 to 25 years) could also be extracted. Daily data for nearly 150 sites are on tape for the period since 1965. Three problems are apparent in using this data set. First - at high wind speeds, the estimate of the fastest mile becomes very inexact due to the extremely small increment to be measured on the chart. Second - most locations experienced a change in instrument exposure 30 to 40 years ago when the weather office moved from a city to airport site. Suitable methods to obtain a homogeneous data set have not been developed. Current design estimates then are obtained only from the airport data. Finally, any attempt to reference the city office data to a standard height faces the problem of the change in urban profile over a period of years.

(2) Five-minute maximum: Daily values of the five-minute maximum have been taken since 1872 at the same locations mentioned previously. Beginning in 1956, it was no longer extracted from the original records. A period of 10-25 years of data can also be extracted for an additional 300 locations. None of these data have been placed on magnetic tape. The problems of mixing city and airport data mentioned for the fastest mile apply also to this measurement.

(3) Peak gust: The daily peak gust has been extracted from strip charts for approximately 450-500 stations for the past 20 to 30 years. The majority of these data are on magnetic tape. Peak gust data have not been the basis for design speeds due to the problems mentioned previously.

(4) Hourly average: This measurement, taken at approximately 3,000 locations, is presently available on tape for 800 of these locations. The hourly average is not a true value for an hourly period but a subjective assessment by the observer of the winds for a few minutes on the hour and considered representative of the entire hour. This measurement has been digitized hourly since the late 1940's and 3-hourly since 1965.

A few sets of data from special tall observation towers exist for various locations throughout the United States. Some of these data sets contain high frequency observations which permit calculations of spectral properties of the turbulent wind structure. Panofsky

(3) summarizes these special data sets which are not generally available for most locations in the United States.

In the United States the fastest mile is used for design purposes because (a) it generally falls in the gap in the energy spectrum and hence is representative of load inducing winds and (b) the parameter has been measured for a long number of years. Many investigators believe a better estimate can be obtained from a 15 or 20 minute average. Unfortunately, the cost of obtaining such averages from old records is prohibitive. At present, then, only data already extracted from the original records can be used to obtain a design speed.

THE UNITED STATES DESIGN STANDARDS

The currently accepted United States design standards are the result of the application by Thom (4) of extreme value theory to a set of annual fastest mile values. These data were all taken at airport locations for a 15-20 year period ending in the mid-1960's. Since then an additional 10 years of data have been collected. Utilizing the earlier work of Davenport (5), Thom converted these data to a standard 30 foot height by using an exponent of 1/7 in the familiar power law. This value is considered to be representative of the surface roughness for an open, uncluttered environment, and ranges to 1/3 for a heavily urbanized area.

This roughness is the drag of the wind on the earth's surface, vegetation, and man-made structures. One of the primary difficulties in developing a standardized set of city data is the unknown change in surface roughness characterizing the gradual urbanization of a site over a period of time.

There are a number of problems with the currently accepted design standard maps used in the United States.:

(1) The period of data used is generally less than 20 years. For many areas, especially the coastline, the representativeness of the design values has been questioned. Greater confidence could be achieved by including the 10 additional years of data available or developing some method of integrating the 40-60 years of city data with the airport data used.

(2) Many of the airport locations have gradually become urbanized or industrialized and the 1/7th power law may no longer be accurate. An approach based on an exponent varying with the roughness characterizing the fetch in various directions may better describe the environment at a location.

(3) It has been recognized that under high wind speed episodes in flat terrain, the 1/7th power law is suitable for the neutral atmosphere characterizing large-scale mature storm systems. However, in the strongly unstable and mixing environment of a thunderstorm, the exponent can become very small - perhaps approaching zero. For those areas of the United States receiving maximum winds from thunderstorms, the measured speed values should probably be used unchanged.

CONCLUSIONS

To summarize, wind damage in the United States is greater than one billion dollars per year. With increasing population, the damage should continue to increase in the future. Although some measurement other than the fastest mile might be used to derive the design wind, the costs to extract these data are currently prohibitive. Better design values could be obtained by including additional years of data at airport locations, developing methods to include the long period of city office data, or ensuring that the power law exponent used reflects the character of the surrounding terrain or stability of the air mass. Research is underway to overcome these limitations in current wind data to use in structural design. However, for the next few years the fastest mile wind data will continue to be used for most design purposes.

REFERENCES

- (1) Van der Hoven, I. (1957): Power Spectrum of Horizontal Wind Speed in the Frequency Range from 0.00007 to 900 Cycles Per Hour. *J. Meteorology*, Vol. 14, p. 160.
- (2) Fujita, T. T. (1975): Super Outbreak Tornadoes of April 3-4, 1974. University of Chicago.
- (3) Panofsky, H. A. (1974): The Atmospheric Boundary Layer Below 150 Meters. *Annual Review of Fluid Mechanics*, Vol. 6, pp. 147-177.
- (4) Thom, H. C. S. (1968): New Distributions of Extreme Winds in the U.S. *Jour. Struct. Div., Proc., ASCE Paper 6038*, pp. 1783-1801.
- (5) Davenport, A. G. (1960): Rationale for Determining Design Wind Velocities, *Jour. Struct. Div., ASCE Paper 2433*, pp. 39-68.

AERODYNAMIC STABILITY OF A LONG-SPAN SUSPENSION BRIDGE

AT CONSTRUCTION STAGE

T. Kunihiro

N. Narita

K. Yokoyama

Public Works Research Institute, Japan

ABSTRACT

Wind accidents on bridge structures have so far occurred at their construction stage, and this necessitates confirming the safety of a structure under construction as well as after completion. The aerodynamic safety of a suspension bridge at construction stage is especially important, because the rigidity and the relevant dynamic characteristics of the structure alter gradually as the construction work proceeds.

The aerodynamic stability of suspension bridges at construction stages for the Seven Bridge (1), the Kanmon Bridge (2), the Honshu-Shikoku Bridge (3,4) and the Narrows Bridge (5) has already been examined by others. These studies demonstrated the importance of the problem.

However, the erection method of a bridge depends largely on the conditions that, how much clearance is necessary for navigation during construction period and what kinds of erection machines are available, etc. Therefore, the results of this study can not be applied directly to other bridges.

This paper describes the design wind speed and the aerodynamic stability of suspended structure of the Hirado Ohashi Bridge.

KEYWORDS: Aerodynamic stability; suspension bridge; construction stages

INTRODUCTION

1.1 Wind Problems on a Suspension Bridge During Erection Stage

Much consideration should be given to the wind induced oscillation of a free standing tower of the main cables not being spanned, and of a suspended structure under construction.

A free standing tower is prone to be put in oscillation by the effect of synchronizing lateral force originated in the wake vortex. This type of oscillation, called Aeolian oscillation, often occurs in a high-rise structure with low rigidity and small damping. In the wind tunnel investigation for the free standing tower of the Hirado Ohashi Bridge, it was suggested that the oscillation might happen at the wind speed of 11.4 m/s and the maximum vibrational amplitude at the top of the tower was expected to reach 2.35 meters. A mechanical device using a sliding concrete block, which was connected with the tower top by wire rope, was installed to suppress the oscillation. The device was found successful in suppressing violent oscillation.

On the other hand, a large deflection and a catastrophic vibration like flutter may happen when the suspended structure is erected. The deflection can be prevented easily by reinforcing the structure or by installing a special device for cramping the deflection. However, the catastrophic oscillation must be prevented as it is fatal to the structure, and it is necessary to confirm the safety against strong wind through wind tunnel tests.

1.2 Erection Plans of Suspended Structure

The Hirado Ohashi Bridge, which is constructed over the Hirado Seto Straits and links Hirado Island to Kyushu Island, is the second largest suspension bridge in Japan. It has a center span length of 460 meters. The suspended structure carrying two-lane traffic and sidewalk is stiffened by a truss girder six meters high and 14.5 meters apart. The clearance is 30 meters above the sea level at the center span. The cross-sectional shape of the stiffening girder was selected through wind tunnel tests. The location, general view, and dimensions are shown in Fig.-1, Fig.-2, and Table-1.

The following erection method was proposed after studying the site condition, amount of work, construction machinery, economical efficiency, and so on;

- 1) The construction of stiffening girder starts from both ends near the tower, and it proceeds gradually to the midpoint of the span as shown in Fig.-3.
- 2) The unit of suspended structure in erection work is 40 meters in length and 200 tons in weight except the starting stage.
- 3) The concrete blocks in the barge are hoisted by a lifting crane set on the main cables. The state of erection work is shown in Photo-1.
- 4) The field connection of blocks are fixed immediately after lifting. But the temporary hinges are installed at the sixth point to minimize the erection stress.

By using this erection method, the construction period of suspended structure was reduced to three months, and the floor deck (I-beam grid deck without concrete slab and pavement) was erected together with stiffening truss. Three types of deck shape shown in Fig.-4 were proposed for erection stage. Crane cars can be driven on the deck in Plan-III, and this is convenient for construction work. However, Plan-III may make the aerodynamic

stability worse, so Plan-I and Plan-II were also proposed as supplementary methods. The major subject of the research was to examine aerodynamic characteristics of these three deck plans for erection through wind tunnel test. Photo-2 shows the sectional model for wind tunnel testing (6).

The natural frequency varies as the construction work proceeds. Fig.-5 shows how the vertical bending and torsional frequencies vary in accordance with the stage of construction. The natural frequency in bending mode does not shift so much, but one in torsional mode increases after the middle of steps.

DESIGN WIND SPEED FOR ERECTION STAGE

Wind load acting on a structure under construction is different from one acting on a completed structure. Namely, the expected wind speed for shorter periods may be used to evaluate the design wind speed, because the construction period is usually short. The relation between a return period (R in years), a probability of the annual extreme wind speed not exceeding a design value (q), and a life time of the structure (T in years) is given by the following formula;

$$q = (1 - 1/R)^T$$

It is reasonable that T is defined to be equal to the erection period. The erection period of suspended structure was estimated as three months, and the total duration from starting tower construction to finishing the construction of the suspended structure as fifteen months. Assuming that $T = 2$ years and $q = 0.6$, the return period R becomes 4.4 years in the case of the Hirado Ohashi Bridge.

The monthly maximum wind speed for the last thirty-five years at the Hirado Meteorological Observatory near the bridge site is given in Fig. 6. It suggests that there are few occasions of strong wind in the period from January to June. Hence this period was supposed to be the best time for erecting the suspended structure. Fig.-7 shows the relation between the return period and the expected wind speed. It follows from the figure that the expected wind speed in this period with a return period of 4.4 years ($R = 4.4$) is very low, and therefore, the following wind speed based on the return period of twenty years was used in the design;

Basic wind speed	20.2 m/s
Design wind speed	32.2 m/s
Critical wind speed for catastrophic oscillation	38.6 m/s

WIND TUNNEL TESTS

3.1 Wind Tunnel Test Method for Suspension Bridge Under Construction

Generally speaking, a sectional model, which is a rigid, geometrical copy of a typical section of a full-scale structure, is used for the aerodynamic stability test in the case of a completed bridge, because the uniformity of longitudinal mass distribution can be assumed. But a sectional model can not be used directly for a suspension bridge under construction, because the assumption can not be held valid.

Wind tunnel test methods for a suspension bridge under construction are classified as follows:

- 1) Sectional model test method making use of reduced mass parameters.

A typical length of a full structure is modeled, and it is rigged up in the tunnel by helical springs with required stiffness, and the weight of the model is simulated in accordance with a reduced mass, which represents the whole structure.

- 2) Analytical method making use of aerodynamic coefficients.

The response of whole structure can be obtained by using non-steady aerodynamic force coefficients which are measured through wind tunnel tests on a two-dimensional model.

- 3) Full-model test method.

The response can be obtained by the use of a full-model with mechanically and geometrically simulated characteristics.

In the present study, methods 1) and 2) were used.

3.2 Stability Test

3.2.1 Test Procedure

The following similarity conditions were satisfied in order to replace a full-scale structure to a two-dimensional model.

- 1) Mass parameter

$$M = \frac{\int_0^L M_c \dot{\phi}_c^2 dt + \int_0^{L_1} M_t \dot{\phi}_t^2 dt + \int_{L_1}^L M_t \dot{\phi}_t^2 dt}{\int_0^{L_2} \dot{\phi}_t^2 dt + \int_{L_2}^L \dot{\phi}_t^2 dt}$$

where M : reduced mass

M_c , M_t : mass of the prototype structure

$\dot{\phi}_c$, $\dot{\phi}_t$: mode function

and the subscripts c and t denote cable and suspended structure, respectively. The reduced moment of inertia can be calculated in a similar manner.

- 2) Vibration mode

The model is mounted by helical springs and it permits both vertical translatory and pitching motion. The natural frequencies in fundamental asymmetric modes (both bending and torsional) were observed for modelling, and no coupling between symmetric oscillation and asymmetric one was considered in the test.

The test conditions are given in Table-2. The vibration of cable is so dominant at the earlier construction steps, that the reduced mass becomes very large and the similitude law can not be maintained in the test. For this reason the stability test for the thirteenth step only can be carried out.

3.2.2 Test Results

Fig.-9 shows the relation between angle of attack α (vertical angle between wind direction and the reference axis of structure and it is taken as positive when wind blows upward) and the critical wind speed of flutter v_c .

The effect of deck shape on wind stability is clarified through the test on the thirteenth step. Model-I, having an opening at the middle of the deck, is stable up to 50 m/s at the angle of attack, $\alpha = -6^\circ - +6^\circ$. On other other hand, Model-III, having a solid deck, showed instability at $\alpha = 5^\circ$, but the critical wind speed is much higher than the design wind speed.

The variation of stability characteristics with construction steps cannot be obtained by this test. The reduced mass for 5th to 12th steps becomes so large that the stability in these steps seems to be guaranteed.

The effect of frequency ratio r (the ratio of torsional frequency to bending frequency) on the stability was examined. The test was carried out at $r = 1.65$ in the thirteenth step. The type of oscillation is a stall flutter, and the critical wind speed v_c is proportional to reduced wind speed (see Fig.-9.3 and 9.4).

3.3 Response Analysis Using Aerodynamic Forces

3.3.1 Measurement of aerodynamic forces

The aerodynamic force acting on a model was measured by a forced oscillation method in order to supplement the stability tests. In the case of driving the model, great care must be taken to balance out the inertia forces of the model so that only purely aerodynamic forces are measured (7).

The aerodynamic force coefficients measured are shown in Fig.-10. CMTI, imaginary part of the coefficient of pitching moment in pure pitching oscillation, at $\alpha = 5^\circ$ in Model-III is positive for almost the whole range of wind speed, and, on the other hand, it is negative in Model-I and Model-III except $\alpha = 5^\circ$. When CMTI is positive, the vibration system with one degree of freedom in torsional mode becomes unstable.

3.3.2 Estimation of Flutter Wind Speed

Flutter wind speed for each step of erection stage are estimated by the use of aerodynamic force coefficients. In the computer program, the motion of both cables and suspended structures is considered. The number of modes in torsional and bending oscillation is five at maximum, and the number of aerodynamic forces along the span is three at maximum. It was found that flutter may not occur at whole angle of attack in Model-I and Model-III (except $\alpha = 5^\circ$). The critical flutter speed at $\alpha = 5^\circ$ in Model-III is as follows (torsional flutter):

5th and 8th step	not present
11th step	73.6 m/s
13th step	52.4 m/s

The estimated wind speed is noted in Fig.-9.2 to compare with ones out of the sectional model test. Both results agree fairly well with each other, and it is found that the estimation method using aerodynamic force coefficients is reliable. When the coupled flutter is assumed, the estimated critical wind speed decreases slightly as shown in Table-3.

CONCLUSION

A study has been carried out to confirm the aerodynamic safety of the Hirado Ohashi Bridge under construction. In conclusion the following can be pointed out:

1) The design wind speed for construction work is estimated by the use of wind record in the last thirty-five years at the Hirado meteorological Observatory. Assuming the return period of twenty years, the expected basic wind speed, the design wind speed, and the critical wind speed for flutter are calcualted as 20.2, 32.2, and 38.6 m/s, respectively.

2) The wind tunnel test on sectional models shows that Model-I with opening in the middle of the deck is stable for whole angle of attack and Model-III with solid deck is unstable for the angle of attack more than four degrees. The critical wind speed at $\alpha = 4^\circ$ is fairly high, i.e., over 50 m/s, so that Model-III is judged to have sufficient aerodynamic stability in practical use.

3) The responses calculated with the aerodynamic force coefficients give good correlation with the test results on sectional models, and this proves that the test methods are reliable. The instability of bridge can occur in torsional flutter, and the effect of coupling of bending and torsional vibration seems to be negligible.

4) The variation of flutter wind speed with the progress of construction work is derived, and it is shown that the flutter wind speed is high at the first stage, and then it decreases gradually as the stage proceeds. This result is different from those of the Seven Bridge and the Kanmon Bridge.

5) As stated above, it is concluded that Plan-III, in which the stiffening truss and solid deck are constructed altogether, has sufficient aerodynamic stability. In the study, only aerodynamic stability tests are performed, and no attempt is done about the large deflection of suspended structure due to wind action in construction stage.

ACKNOWLEDGEMENT

The field work started in February, 1976 and ended in May of the same year. During the field work, the results of the study were fully applied. The structure, though it has a solid deck, showed no harmful vibration during erection.

The authors would like to acknowledge the staff of Structure Section of P.W.R.I. for their valuable assistance. The work described in the paper has been carried out as part of a research program on the Hirado Ohashi Bridge Design and Construction. The authors are much indebted to the staff of the Hirado Ohashi Bridge Construction Office for their earnest cooperation.

REFERENCES

- (1) Smith, I. P.: The aerodynamic stability of the Seven Suspension Bridge, NPL Aero Report 1105, May 1964
- (2) Shiraki, K. et al.: Aerodynamic Instability in Suspension Bridge under Erection, Mitsubishi Heavy Industries Tech. Review, vol. 7, No. 7 December 1970.
- (3) Ito, M. et al.: Aerodynamic stability of a suspension bridge during erection, Proc. National Meeting of JSCE, October 1974

- (4) Shiraishi, N., Urata, A., and Sakai, J.: A study of wind stability on a long span suspension bridge during erection, Proc. JSCE, No. 250 June 1976
- (5) Davenport, A. G. et al.: A study of wind action on a suspension bridge during erection and on completion, Res. Rep. BLWT-3-69, Fac. Eng. Sci., Univ. of Western Ontario, London, Canada
- (6) Narita, N. and Yokoyama, K.: Wind tunnel test on the Hirado Ohashi Bridge, Tech. Memo. P.W.R.I., No. 1102, December 1975
- (7) Okubo, T., Narita, N. and Yokoyama, K.: Some approaches for improving wind stability for cable-stayed girder bridges, Proc. Fourth Int. Conf. on Wind Effects on Buildings and Structures, London September 1975



Photo-1 Erection of suspended structure

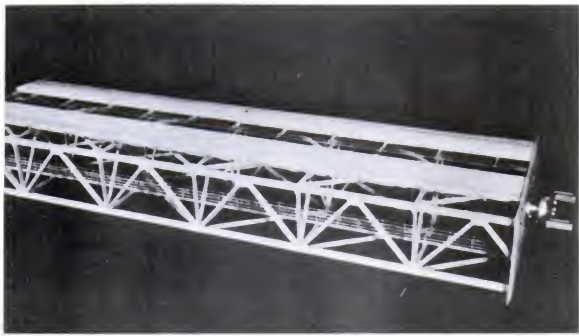


Photo-2 Model for wind tunnel (Model-I)

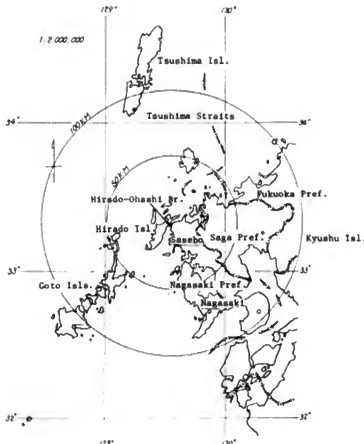


Fig.-1 Location of the Hirado-Ohashi Bridge

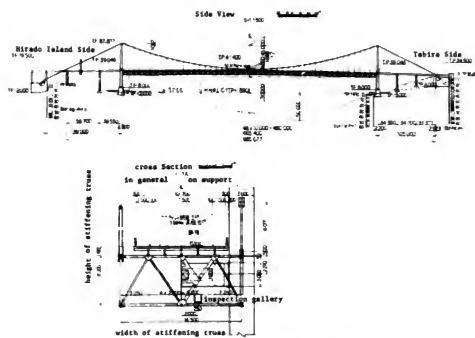
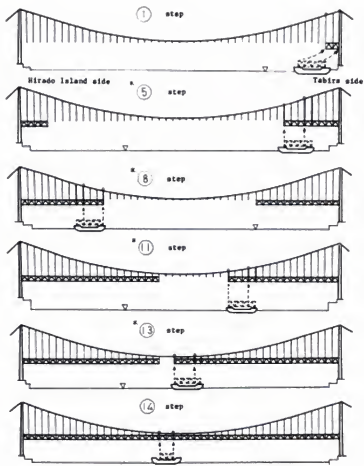


Fig.-2 General View of Hirado-Ohashi Bridge



* Frequencies were calculated

Fig.-3 Order of Suspended Structure Erection

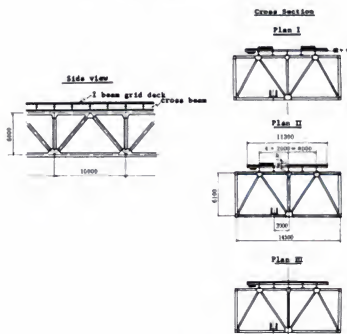


Fig.-4 Cross Section of Stiffening Truss

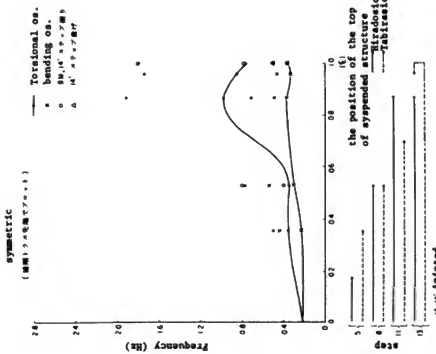


Fig.-5.1 Natural Frequency at Construction Stage
(Symmetric os.)

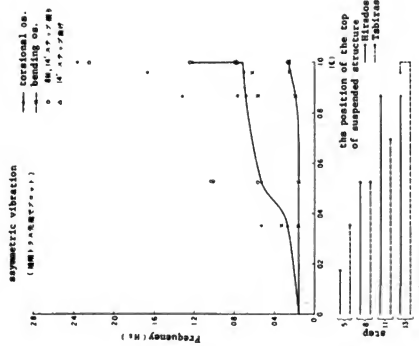


Fig.-5.2 Natural Frequency at Construction Stage
(Asymmetric os.)

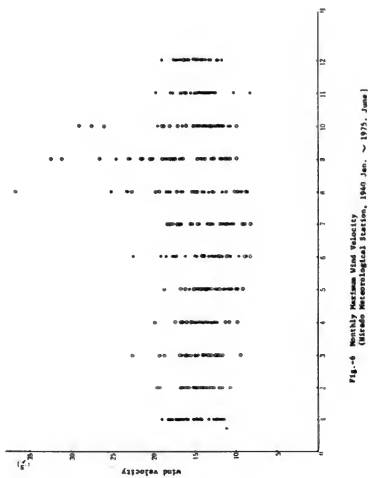


Fig.-6 Monthly Mean Wind Velocity
(Kure Atoll Meteorological Station, 1960 Jan. ~ 1975. June)

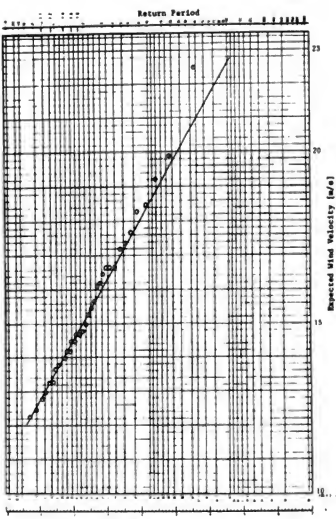


Fig.-7.1 Return Period vs. Expected Wind Velocity
at the Hirado Meteorological Station [1940 ~ 1975, Jan. ~ Mar.]

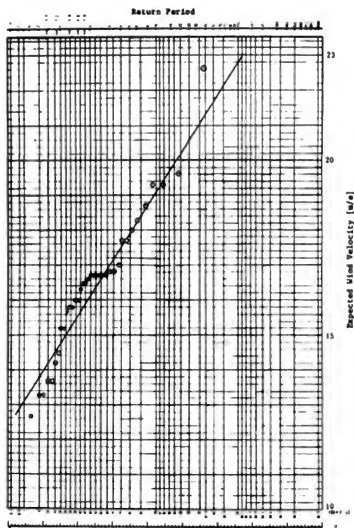


Fig.-7.2 Return Period vs. Expected Wind Velocity
at the Hirado Meteorological Station
[1940 ~ 1974, Apr. ~ Jun.]

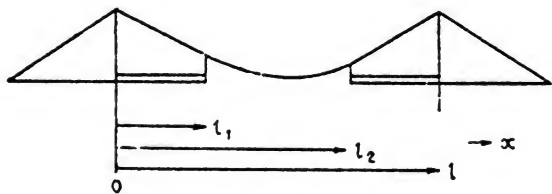


Fig. 8 Model system

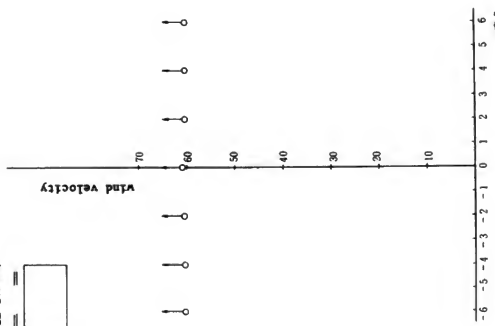
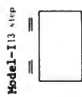


Fig.-9.1 $V_c \sim \sigma$ Curve (Model-I, 13 Step)

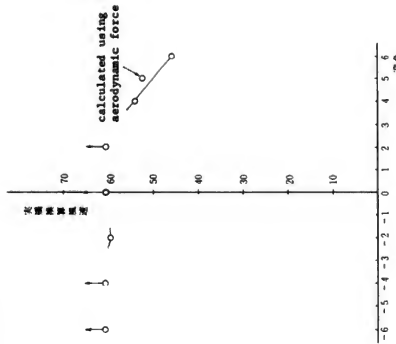


Fig.-9.2 $V_c \sim \sigma$ Curve (Model-III, 13 Step)

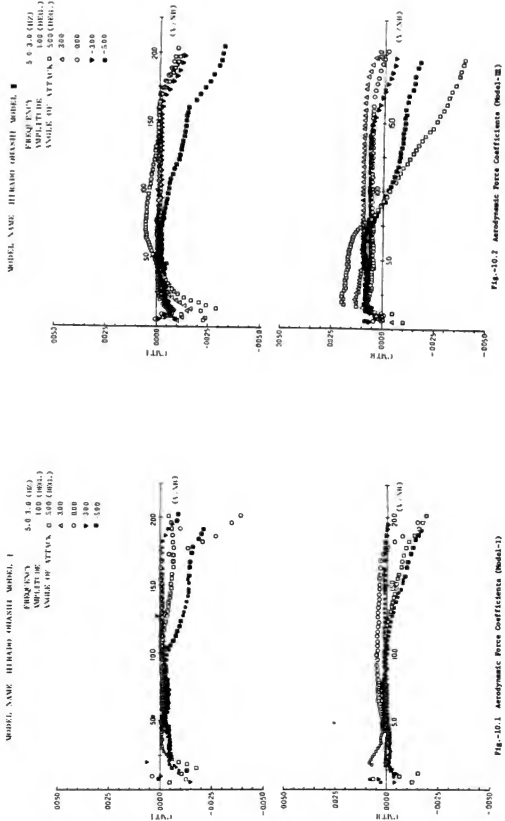


Fig.-10.1 Aerodynamic Force Coefficients (Model-1)

Fig.-10.2 Aerodynamic Force Coefficients (Model-2)

Table-1 Dimension of Hirado-Ohashi Bridge

Item	Unit	Plan-D
Span length	m	465.40
Effective span length	m	460.00
Sag	m	45.00
Backstay (lateral)		
right ... Tabira eida	m	105.00
left ... Hirado Island	m	139.00
Backstay (vertical)		
right ... Tabira eida	m	53.37
left ... Hirado Island	m	61.37
Cross sectional area (cable)	$m^2/bridge$	0.170
Dead load (whole structure)	$t/m/bridge$	11.02
" (floor deck)	$t/m/bridge$	6.99
" (stiffening truss)	$t/m/bridge$	2.50
" (cable, hanger)	$t/m/bridge$	1.53
Width of truss	m	14.50
Height of truss	m	6.00
Panel length of truss	m	5.00
" of lateral bracing	m	10.00
Width of floor deck	m	11.30
Moment of inertia of area of truss	$m^4/bridge$	1.649

Table-2.1 Reduced mass density

Mode	Step		5	8	11	13
	Torsional os. ton sec ²	Asymmetric, 1st	861,544	8,232.13	123.746	30.1326
Bending os. ton sec ^{2/m²}	Symmetric, 1st		63,012	24,701	2,200.6	32.950
	Asymmetric, 1st		1.8804	0.8459	0.7151	0.6837

Table-2.2 Test condition with sectional model

Mode	Step	5	8	11	13
Scale		1:37.59	1:37.59	1:37.59	1:37.59
Mass density (kg/model)		20.867	9.387	7.935	7.586
Polar moment of inertia	(AS1)	69.041	659.7	9.916	2.415
	(S1)	5.050	1.979	176.3	2.640

Table-2.3 Frequency ratio

Mode	Step	5	8	11	13
$N_a(AS1)/N_n$		1.71	3.28	3.55	2.85
$N_a(S1)/N_n$		1.58	1.14	1.90	2.59

Table-3 Critical Flutter Wind Speed
at $\alpha=5^\circ$ in Model-III (m/s)

Type \ Step	14	14*	13	11	8
Torsional Flutter	50.8	49.1	45.8	75.6	Not occur
Coupled Flutter	49.0	47.3	44.2	73.8	Not occur

*without pavement

PRESENT SITUATION OF EARTHQUAKE PREDICTION RESEARCH IN JAPAN

Kazuo Hamada, National Research Center for Disaster Prevention

Hiroshi Takahashi, National Research Center for Disaster Prevention

Hiroshi Sato, Geographical Survey Institute

Akira Suwa, Meteorological Research Institute

ABSTRACT

An outline of the Japanese National Program of Earthquake Prediction is introduced here. First, the progress up to date of the national program of earthquake prediction; second, the organizations related to the prediction, their main roles, and the organizational structure; third, the strategy of earthquake prediction by the Coordinating Committee for Earthquake Prediction (CCEP); fourth, the activities of the CEEP; fifth, the present state of earthquake prediction; sixth, the promotion of the prediction program, including the authors' points of view and finally, the following items of research and observations are introduced:

1. GEODETIC SURVEY
2. TIDAL OBSERVATION
3. CONTINUOUS OBSERVATION OF CRUSTAL MOVEMENT
4. SEISMIC OBSERVATION
5. VELOCITY CHANGE OF SEISMIC WAVES
6. ACTIVE FAULTS AND FOLDING
7. GEOMAGNETIC AND GEOELECTRIC OBSERVATIONS
8. LABORATORY EXPERIMENTS
9. WORKS RELATED TO GROUND WATER
10. DATA PROCESSING AND MONITORING SYSTEM

KEYWORDS: Earthquake prediction; Japan National Program; present state

PROGRESS OF EARTHQUAKE PREDICTION RESEARCH

The present research of earthquake prediction goes back to 1962, when the publication "Earthquake Prediction - Progress to Date and Plans for Future" was issued by a research group for an earthquake prediction program consisting of Japanese seismologists. This planning had drawn much attention in the world, especially in the United States. As a result, the first Japan-United States Conference on Research Related to Earthquake Prediction was held in Tokyo and Kyoto in 1964, under the auspices of the Japan-United States Cooperative Program, which still continues up to the present. In Japan, the Science Council of Japan and Geodesy Council in the Ministry of Education established some committee meetings and made recommendations and/or authorized proposals to the Prime Minister and other related Ministers with respect to promotion of earthquake prediction. Table 1 summarizes the main events related to the promotion of earthquake prediction up to the present. A national program of earthquake prediction was launched in 1965 with the financial support of the Government. The funding and planning of the program have been in 5-year increments. The program is now in the third 5-year segment and will be 13 years old by the end of the fiscal year 1977. As a result of the progress, the number of research scientists and technicians involved in the national program exceeds four hundred and several tens, and the total funding in 1977 amounted to 3.7 billion yen (approximately \$13 million, Fig. 1). During these years, approximately 130 additional positions for scientists and technicians were created, and a total of 15 billion yen will have been allocated by 1977. This budget is the largest of all projects in solid-earth science in Japan. Since the Japanese funding excludes salaries and the costs of construction of observatories, the size of the Japanese program is not small in comparison with that of the United States whose funding was \$11 million in 1976, including salaries (National Academy of Science, 1976).

ORGANIZATIONS RELATED TO THE PREDICTION PROGRAM

Organizations related to the earthquake prediction program and their main roles are shown in Fig. 2. All sorts of information of up-to-date research and observations concerning the earthquake prediction are gathered into the CCEP for judgments with respect to the earthquake occurrence in and around Japan. Main courses of information flow to the CCEP are illustrated in Fig. 3. There are about 9 organizations of universities which have their unique programs. Most requirements of budgets and new positions from these organizations are approved by the concerned ministries or agencies (Science and Technology Agency, Ministries of Education, International Trade and Industry, Transportation, and Construction) through ordinary administrative procedures. There are no review panels made up of scientists assisting a responsible agency in selecting the research projects and other requirements to be supported, unlike the United States. Nor is there a responsible lead agency which is responsible for the whole program concerning the earthquake prediction, like the State Seismological Bureau of China. In Japan, however, deep regard is given to the proposals by the Geodesy Council.

STRATEGY OF EARTHQUAKE PREDICTION BY THE CCEP

The CCEP designated some areas as the "area of specific observation, area of intensified observation, and area of concentrated observation" as the target of a strategy of earthquake prediction. The designation of an "area of specific observation" is given to areas of historically disastrous earthquakes, active faults, high seismicity in a limited area, and an important area from social and economic aspects, like a densely populated area. Whenever anomalous phenomena, such as land uplift, are observed by either nationwide observations like geodetic survey, seismic observations and tide-gauge observations or other observations in the "area of specific observation," the region of anomaly is designated as an "area of intensified observation." If the anomalous phenomena are later suspected precursory to an impending earthquake, the designation will be changed to an "area of concentrated observation," and all types of observations will be concentrated there. And, if the precursor is later more positively ascertained, all efforts will be concentrated to predict an earthquake. As illustrated in Fig. 4, the Tokai area and the southern part of the Kanto area are "areas of intensified observation." However, there is no "area of concentrated observation" up to the present.

ACTIVITIES OF THE CCEP

The CCEP has not yet issued any prediction of an earthquake, in contrast with the examples of the United States and China. However, after its establishment in 1969, the CCEP released a series of information related to an earthquake to the society in the form of general warnings; uplift in the Boso and Miura Peninsulas, no chance of a large earthquake in the Kanto region for the time being, possibility of a large earthquake in the Tokai area, the recent uplift in the lower reaches of the Tamagawa river, Kawasaki city, and most recently, the uplift in the Izu Peninsula. Thus, the CCEP also plays the role of a mediator between the scientist and the society besides the judgment of earthquake prediction.

Although any prediction of earthquake has not yet been issued in Japan, if we take "prediction" in a wide and general sense, such predictions were issued twice. A coordinating committee issued the first one to the local people through JMA (Japan Meteorological Agency) when the Matsushiro Earthquake Swarm (1965-1967) by judging from microearthquake activities preceding the occurrence of medium-size earthquakes. The second prediction in a wide and general sense was made by the CCEP before the Off-Nemuro Earthquake of 1973 by judging from the seismicity gap and the accumulated crustal deformation.

THE STATE OF EARTHQUAKE PREDICTION

Predictions of earthquakes should specify the time, magnitude, and place with the probabilities. However, neither the present state nor the present distribution of instrumentation permits useful predictions to the society on a routine basis. An earthquake prediction theory (e.g., Rikitake, 1976) or a formula to predict an earthquake is not completed, but is at the developing stage. Also, a final network of observations for the prediction on a routine basis is not made clear. What is certain is: any kind of

the present observations is not sufficient yet and we have to monitor not only one or two but several kinds of observations in order to select a phenomenon really precursory to earthquakes, rejecting all the disturbances from other sources. And a final synthetic judgment is required from observational, experimental, and theoretical aspects. Although the present state of prediction is not at an advanced, satisfactory stage, if a precursory phenomenon to a large earthquake appears very strong in a wide area, we could recognize the precursors from the present network of instrumentation. Therefore, construction of an integrated system of data gathering/release, analyses, and judgments is urged especially for the Tokai area.

PROMOTION OF EARTHQUAKE PREDICTION

The Japanese National Program of Earthquake Prediction, since it was launched in 1965, has been gradually strengthened by mutual cooperation of different organizations. The present organizational structure, however, is no longer adequate for the growing program with increasingly wide variety of observational data, larger continuous monitoring systems, broadening areas of research, and synthetic judgments from all kinds of data and research at the same time. Serious problems in the program are the chance for studying social aspects of prediction and the absence of a responsible lead agency. Under these circumstances, the Headquarters for Promotion of Earthquake Prediction was established in October, 1976, with purposes of interministrial adjustment and communication, and of promotion of comprehensive and systematic planning with respect to the national programs. This Headquarters is of the highest level of its kind in Japan and is expected to influence the state of earthquakes very much.

ITEMS OF OBSERVATIONS AND RESEARCH

Items of research and observations for the prediction program are outlined as follows:

1. GEODETIC SURVEY. A nationwide triangulation (recently, tirlateration) network consists of 6000 first-order and second-order triangulation points which are surveyed by GSI (Geographical Survey Institute) by means of geodimeters at 5-year intervals (Fig. 5). Also, nationwide levellings of first order, 20,000 km in total length, are conducted by GSI every 5 years (Fig. 6). In a special region like the Capital area, GSI has a planning of accurate geodetic measurements at the resurvey intervals of 2.5 years and other temporary geodetic measurements on occasion. Gravity surveys are conducted by GSI and universities occasionally.

2. TIDAL OBSERVATION. There are about 100 tide-gauge stations along the coast at approximately 100-km intervals. These stations belong to JMA, GSI, and HD (Hydrographic Department) primarily (Fig. 7), but their observational data are gathered into the Coastal Movement Data Center of GSI and released from this center.

3. CONTINUOUS OBSERVATION OF CRUSTAL MOVEMENT. There are various types of strain and tilt meters for continuous observation of crustal movements, but they are still at the developing stage. They are silica-bar strain meters, wire strain meters, volumetric strain

meters of buried type, tilt meters of borehole type and of tunnel type, and water-tube tilt meters. Most of them belong to universities, JMA, and CDP (National Research Center for Disaster Prevention) and are distributed at about 30 sites illustrated in Fig. 8. Recently, emphasis is placed on the continuous monitoring of crustal movements in the Tokai area as seen in the figure.

4. SEISMIC OBSERVATION. JMA has a nationwide network, consisting of about 120 stations, for large, moderate, and small earthquakes of $M \geq 3$ (Fig. 9), and regularly publishes a bulletin of the earthquake. Furthermore, JMA is now constructing additional 20 high-sensitive stations. Micro- and ultra- microearthquakes are observed at about one hundred and several tens stations which belong to approximately 20 observatories of several universities, CDP, and JMA (Fig. 10). Seven universities have their mobile parties for temporary observations of micro- and ultra-microearthquakes.

CDP installed deep-borehole seismometers and tilt meters in a 3500-m well at the Iwatsuki city about 30 km north from the center of Tokyo, so as to overcome artificial noises in the Tokyo area. And other two deep-borehole observatories will be completed in a few years also in the Tokyo area.

There are three types of ocean bottom seismometers (OBS), an anchored buoy type, a free-fall pop-up type by the University of Tokyo, and a submarine cable type by JMA. JMA intends to set several OBSs of submarine cable type off the shores of Tokai area for continuous observation on a routine basis.

5. VELOCITY CHANGE OF SEISMIC WAVES. In cooperation with universities and CDP, GS (Geological Survey) has repeatedly conducted the explosion experiment at Izu-Ōshima Island since 1968 at intervals of approximately one year, with the aim of monitoring the velocity change of seismic P waves propagating beneath Sagami Bay, which was the epicentral area of the great Kanto earthquake of 1923. No velocity change exceeding 0.1% has been observed up to the present (Fig. 11).

6. ACTIVE FAULTS AND FOLDINGS. By mutual cooperation of universities, GS, and CDP the research of active faults and foldings over the country were summarized and published (e.g., Research Group for Quaternary Tectonic Map, 1973). Matsuda's work (1972) is a classification of active faults based on an average dislocation (Table 2), and it includes his studies with respect to a recurrent interval of earthquakes along the fault. Recently, a research group of Kaizuka and his colleagues investigated the distribution of active faults, their activities, and seismic risk all over the country.

7. GEOMAGNETIC AND GEOELECTRIC OBSERVATIONS. Much emphases are placed on geomagnetic secular variation. There is a nationwide array of accurate proton-precession magnetometers as shown in Fig. 12. The natural noises contaminate the observed values of the total intensity of the geomagnetic field unexpectedly so much that it might not be easy to detect significant changes associated with an earthquake. First-order geomagnetic surveys are conducted every 5 years by GSI at about 300 sites all over the country. Continuous monitoring of the earth's resistivity changes has been carried out at Aburatsubo about 60 km south of Tokyo. Some precursors and coseismic changes have been reported (e.g., Yamazaki, 1975).

8. LABORATORY EXPERIMENTS. Apparatus for the experiments of rock failure, which simulates the circumstances prevailing within the earth's crust, were installed at five universities and GS. This kind of investigation is represented by Mogi's series of experiments.

9. WORKS RELATED TO GROUND WATER. Research on ground-water level, chemical analysis, and radon content as well as other water-related research from the viewpoint of earthquake prediction belong to the scientific fields where Japan was behind other countries. Recently, the University of Tokyo and GS, however, investigated such water-related problems (e.g., Wakita, 1976). Also, CDP is going to start on such works with a newly created research group.

10. DATA PROCESSING AND MONITORING SYSTEM. Various centers for specific activities were established: the Crustal Activity Monitoring Center in GSI; the Seismicity Monitoring Center in JMA; the Earthquake Prediction Observation Center in ERI (Earthquake Research Institute); and the Local Center of Earthquake Prediction Observation in each of five main universities. These centers are gathering and processing the widely growing variety of observation data. Most of the data are gathered and sent by a telemetering network to these centers. Furthermore, at present, a coordinated system of synthetic and rapid judgments, analyses, and data gathering/release from/to all the centers and organizations all over the country is under discussion. To promote the short-term prediction in the Tokai area, which is publicly suspected to be dangerous, a judgment committee is going to start the work under the supervision of the CCEP.

REFERENCES

Geomagnetic Research Group on Earthquake Prediction (1974): Observation of Geomagnetic Total Intensity under the Project of Earthquake Prediction Research, 1972-1973, Report of the CCEP, 12, 151-160, in Japanese.

Geological Survey (1977): Data submitted at the 36th meeting of the CCEP of Feb., 1977, in Japanese.

Matsuda, Tokihiko (1972): Earthquakes and faults from geological standpoints, Proc. 12th Conf. Earthquake Engineering, Comm. Earthquake Engineering, Japan Society of Civil Engineers, Tokyo, 7, in Japanese.

Mogi, Kiyoo (1974): Rock Fracture and Earthquake Prediction, Journal of the Society of Materials Science, Japan, 23, 2-13, in Japanese.

National Academy of Science (the United States, 1976): Predicting Earthquakes A Scientific and Technical Evaluation--With Implications for Society.

Research Group for Quaternary Tectonic Map (1973): "Quaternary Tectonic Map of Japan," National Research Center for Disaster Prevention.

Rikitake, Tsunehji (1976): Theory of Earthquake Prediction in "Earthquake Prediction," Elsevier, 245-301.

Science and Technology Agency (1976): "Handbook of Earthquake Prediction," edited by the Coordinating Committee to Promote Earthquake Prediction Research, in Japanese.

Wakita, Hiroshi (1976): The Kawasaki Uplift, Kagaku, 46, 573-579, in Japanese.

Yamazaki, Yoshio (1975): Precursory and Coseismic Resistivity Changes, Pure and Applied Geophysics (PAGEOPH), 113, 219-227.

Table 1. Progress to Date of Earthquake Prediction

Y. M.	
1961 4	The first meeting of the research group for earthquake prediction program.
1962 1	"Earthquake Prediction---Progress to Date and Plans for Future" was issued from the above research group.
1963 6	The Sectional Meeting of Earthquake Prediction was established in the Geodesy Council in the Ministry of Education.
10	The Science Council of Japan recommended the Government to promote earthquake prediction research.
1964 6	The Geodesy Council proposed to the Ministries of Education, International Trade and Industry, Transportation, and Construction on planning of earthquake prediction research.
1965 3	The Sub-Committee Meeting for Earthquake Prediction was established in the Coordinating Committee for Geophysical Research in the Science Council of Japan.
4	Beginning of financial support to the program of earthquake prediction research.
6	Yearly schedules of earthquake prediction research were made by the Sub-Committee Meeting for Earthquake Prediction.
1966 6	The yearly schedules were modified, considering the experience of the Matsushiro earthquake swarm.
1968 5	Acknowledgement at the Cabinet Council on application of earthquake prediction research, in consideration of damages caused by the 1968 Off-Tokachi Earthquake.
7	The Geodesy Council proposed to the related Ministers on application of earthquake prediction research.
1969 4	The Coordinating Committee for Earthquake Prediction was established in the Geographical Survey Institute, for exchanging information and overall judgments concerning earthquake occurrences.
1973 7	Agreement to promote earthquake prediction at the Central Conference for Disaster Prevention in the Prime Minister's Office.
1974 11	The Coordinating Committee to Promote Earthquake Prediction Research was established for administrative adjustment among the Ministries and Agencies.
1976 10	The Headquarters for Promotion of Earthquake Prediction was established in the Cabinet and the above coordinating committee to promote earthquake prediction research was displaced by this headquarters.
1977	A Judgment Committee of the Tokai Area will be established to promote short-term prediction in the Tokai area.

Table 2
 Main active faults in Japan(Matsuda, 1972)
 A; the mean rate of movement = 1-10 m/1000years
 B; " 0.1-1 "
 C; " less than 0.1 "

Location	Name of fault	Type	Length (km)	Class
Akita Pref.	Rikuu	reverse fault	60	B
Iwate Pref.	Morioka	reverse fault	40	B
Fukushima Pref.	Fukushima basin	reverse fault	50	B
Fukushima Pref.	Aizu basin	reverse fault	40	B
Niigata Pref.	Nagaoka plain	reverse fault	30	B
Nagano Pref.	Zenkoji basin	reverse fault	70	B
Nagano Pref.	Itogawa-Shizuoka	left-lateral	80	A
Shizuoka Pref.	North Izu	left-lateral	30	A
Toyama and Gifu Pref.	Atotsugawa	right-lateral	60	A
Gifu Pref.	Atera	left-lateral	70	A
Gifu Pref.	Neo valley	left-lateral	70	A
Aichi Pref.	Fukuzu	reverse fault	10	C
Kyoto Pref.	Tango	left-lateral	20	C
Hyogo Pref.	Rokko	reverse fault	50	B
Hyogo Pref.	Yamazaki	left-lateral	50	A
Tottori Pref.	Tottori	right-lateral	15	C
Southwest Japan	Median tectonic line	right-lateral	800	A

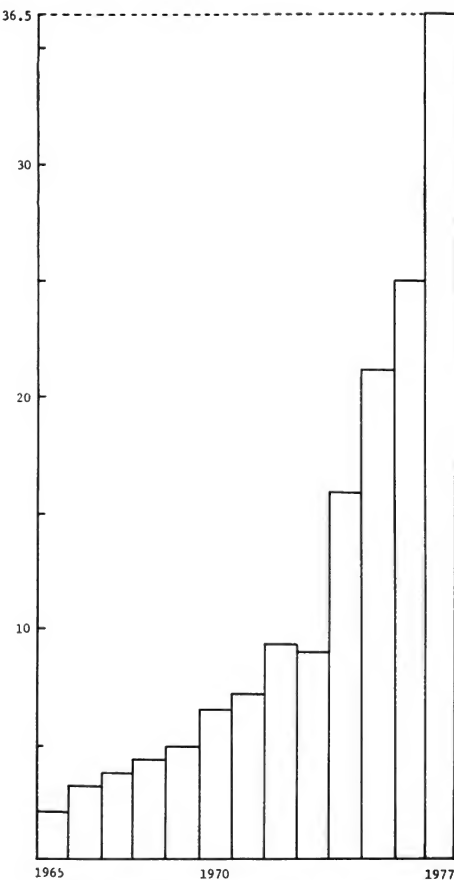


Fig. 1. Yearly budget related to the prediction program in billion yen (Science and Technology Agency, 1976)

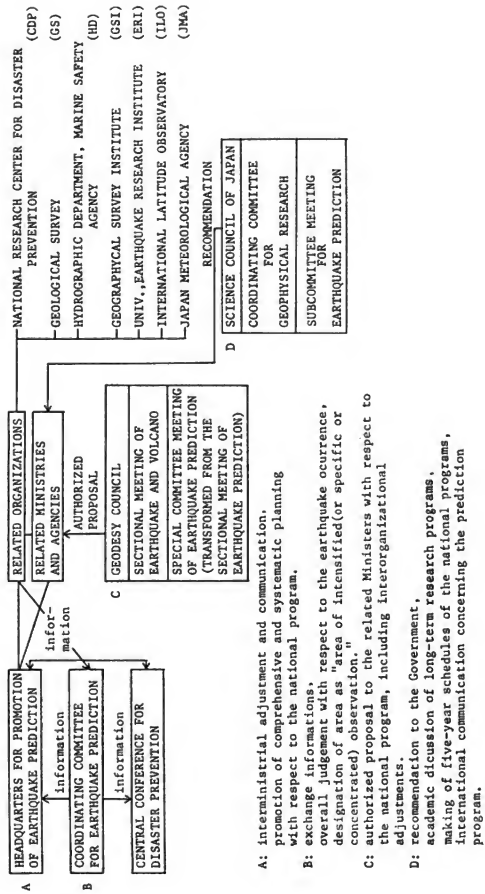


Fig. 2. Organizations related to the earthquake prediction and their main roles.

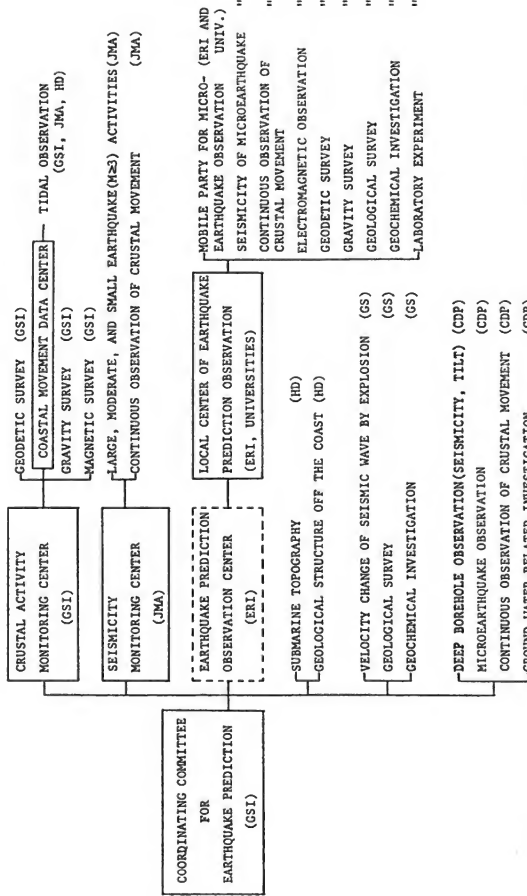


Fig. 3. Information flow to the Coordinating Committee for Earthquake Prediction and partial charges of research and observations of the prediction program.

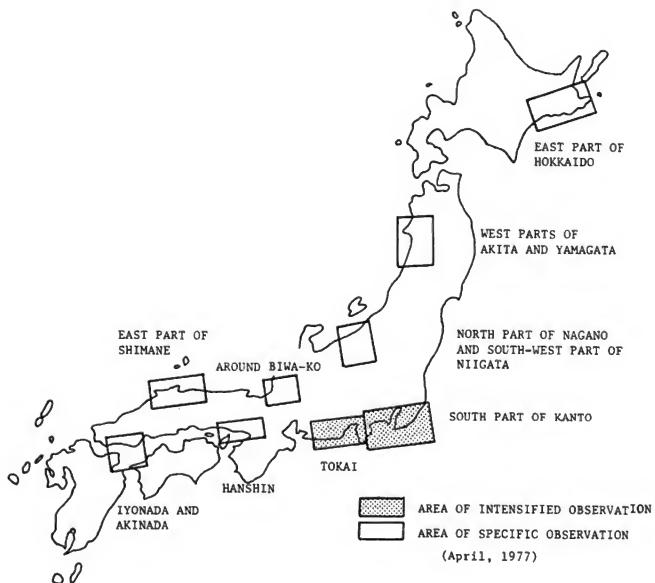


Fig. 4. Designation of area by the Coordinating Committee for Earthquake Prediction

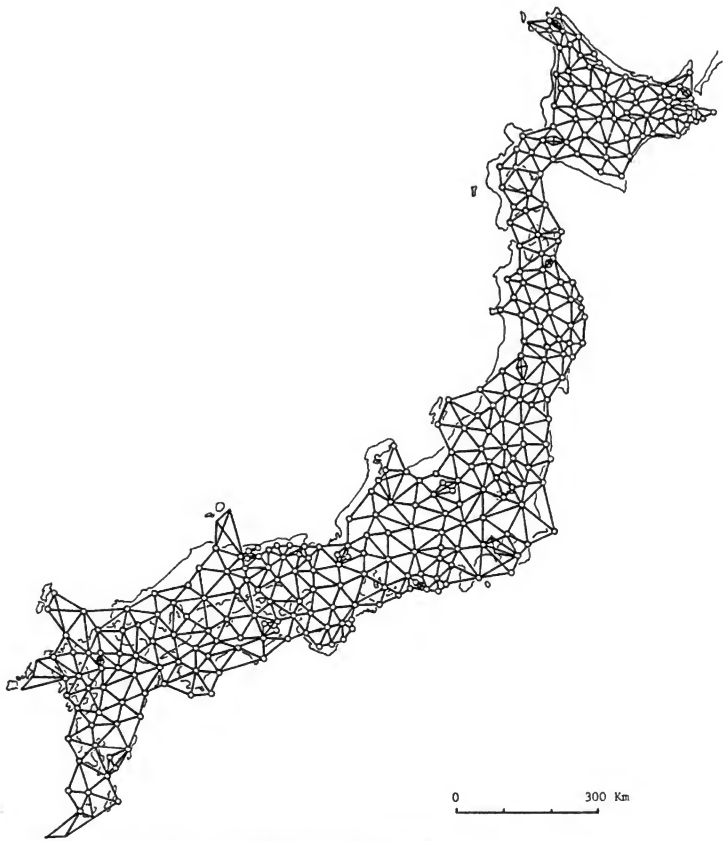


Fig. 5. Nationwide network of a first-order triangulation.

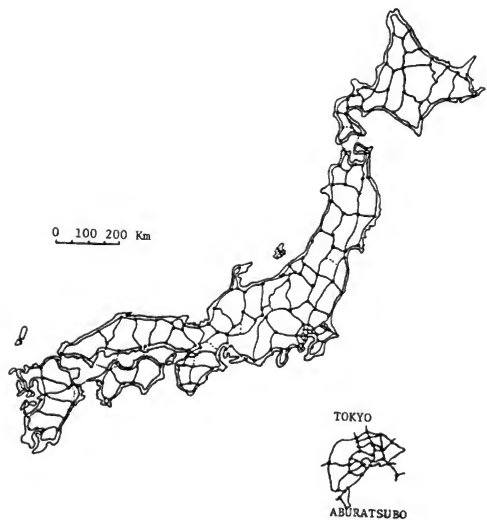


Fig. 6. Nationwide first-order levelling routes
20,000 km in total length.



Fig. 7. Tide-gauge stations registered at the
Coastal Movement Data Center.

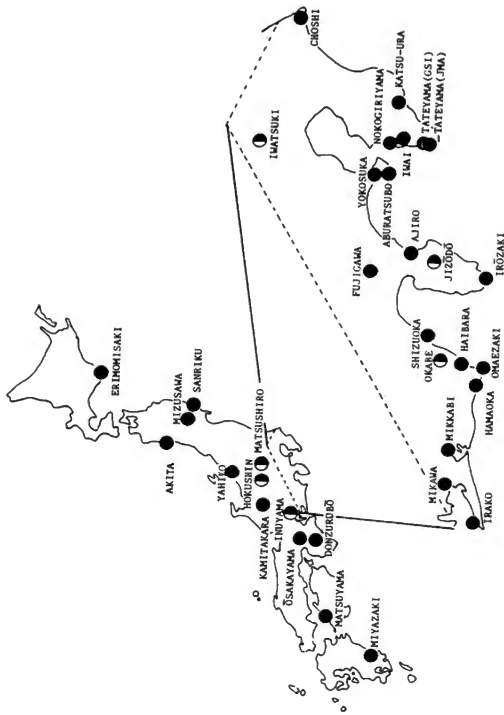


Fig. 8. Crustal movement observatories/stations of continuous observation.
 Half solid marks possess both crustal movement and microearthquake observations.



Fig. 9. Nationwide Seismometrical Network of
Japan Meteorological Agency.

Fig. 10. Microearthquake observatories/stations.

Half solid marks possess both microearthquake and crustal movement observations. One hundred and several tens in the number of observation sites, including sub-stations.

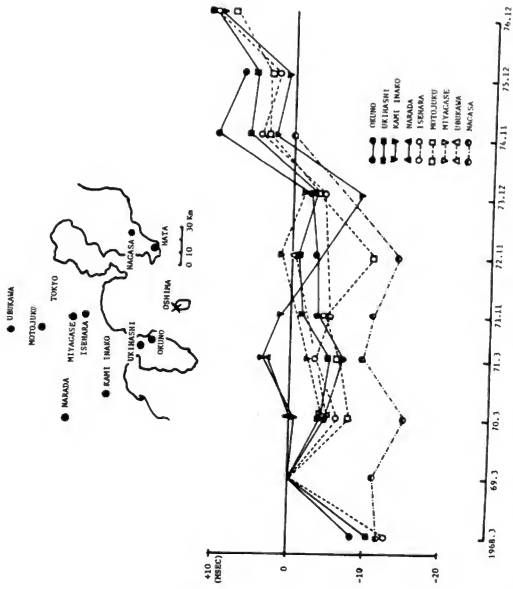


Fig. 11. Velocity change of seismic P waves propagating beneath Sagami Bay(Geological Survey, 1977)



	Stations	Geographic		Geomagnetic *)	
		Long.	Lat.	Long.	Lat.
Me	Menambetsu	144°12'	43°55'	209.1°	34.2°
Og	Oga	139 47	39 54	205.8	29.8
Ni	Nibetsu	140 16	39 48	206.3	29.7
Mz	Mizusawa	141 12	39 07	207.2	29.1
Ka	Kakicka	140 11	36 14	206.7	26.2
Kz	Katozan	139 58	35 15	206.6	25.2
No	Izushima	139 22	34 44	206.1	24.6
Sa	Izushima	139 25	34 47	206.1	24.6
Ha	Hachijo Is.	139 48	33 07	205.7	23.0
Ya	Yatsugatake	138 27	36 04	205.1	25.8
Ss	Shimosato	135 56	33 35	203.1	23.2
To	Tottori	134 14	35 31	201.4	25.0
Ky	Kanoya	130 53	31 25	196.8	20.7

*)Based on geomagnetic poles for IGRF 1965.0 (69.76°W, 78.56°N).

Fig. 12. Stations equipped with a proton precession magnetometer in Japan.
(Geomagnetic Research Group on Earthquake Prediction, 1974)

The Complementary Importance of Earthquake Prediction
and Structural Response Estimation in Seismic
Design and Planning Decisions

ROBIN K. MCGUIRE
U.S. Geological Survey, Denver, Colorado, U.S.A.

Abstract

The present uncertainty in estimating the responses of manmade and natural structures to earthquake threats is translated into cost penalties reflecting costs associated with possible failure of the structure due to underestimated response, and costs associated with overdesign of the structure (or over-conservative reaction to a hazard) due to overestimated levels of motion. The important uncertainties for seismic design and planning decisions are those associated with the size, location, and time of future earthquakes, and those associated with estimating ground motion and structural response during these events. It is shown that reducing the uncertainties in one part of the problem has only a minor effect on reducing the (social and economic) cost of earthquakes unless significant and complementary advances are also made in reducing the uncertainties of the other part.

KEYWORDS: Seismic risk; Design decisions; Minimum cost.

Introduction

Long-term earthquake design and planning decisions are made daily and will continue to be made as earthquake prediction capabilities develop and as new theories are tested to estimate ground motions and responses of structures (natural and manmade). These decisions include choosing seismic design levels, zoning land for different types of development depending on the earthquake hazard, and condemning existing low-strength buildings. The uncertainties associated with earthquake occurrence and with the ground motion and structural response generated by the event lead to cost penalties associated with these decisions. The purpose of this paper is to examine simple, typical cost penalty functions and to estimate the penalties associated with present uncertainty and with various advances in earthquake prediction capability and in ground motion and structural response estimation.

Cost penalties can be associated with the two possible outcomes of a design or planning decision regarding earthquake hazards: failure of the structure or system of interest, or survival of the structure or system because of over-design. The rare instances in which a structure experiences exactly the design response during its lifetime can be regarded as a trivial case of the second type of outcome. For the purposes of this brief study, the "earthquake demand" as well as the "structural capacity" will be measured by random-variable Y , which may (as in the example to follow) be peak ground acceleration or some other ground motion measure, or it may be a structural response measure (inter-story displacement, percent liquefaction of an earth-fill dam, etc.).

The failure cost penalty $C_F(y_d, Y)$ is a function of the design capacity y_d and the demand on the structure Y (this demand may, in the general case, be the result of one earthquake, the maximum of a series of earthquakes, or the cumulative effect of a series of earthquakes). Let y be a specific observation of Y ; then failure is defined as $y > y_d$. A possible function for C_F is shown in Figure 1. For $y \leq y_d$ there is no failure; as y increases above y_d , C_F increases from zero to a maximum value C_R which may represent the replacement cost of the structure or the maximum life loss possible.

The cost of over-design C_S is equal to the cost of earthquake design provided in the structure $C_D(y_d)$, minus the cost of earthquake design which would have just met the earthquake demand y , $C_D(y)$. A typical increase in cost of earthquake resistance as a function of capacity y_d is shown in Figure 2. The over-design penalty cost C_S is thus the "extra" capacity which is designed into the structure and which, in retrospect after having observed a seismic demand value y , is not used. C_S is obviously defined only when the observation y of Y is $\leq y_d$.

The penalty cost functions presented here may easily be interpreted as dollar costs associated with repairing and designing a specific structure. The failure penalty function may also be interpreted as the cost of life loss or loss of service of some facility; the overdesign penalty function may be considered the cost of non-development of some area of potential soil failure, or the cost of needless condemnation and razng of buildings. Capacity y_d might be chosen by optimization to minimize a total cost function (not the penalty functions). The optimum design could imply some structural repair or

casualty cost even when y exactly equals y_d (for instance, non-structural partitions might be allowed to crack in a building during the design earthquake demand); in this case the penalty functions represent increases in costs for cases in which $y > y_d$ or $y < y_d$.

The expected penalty for a given design capacity y_d can be calculated as the over-design cost (a function of y) times the distribution function of Y given $y \leq y_d$, integrated over all values, plus the failure cost (also a function of y) times the distribution function of Y given $y > y_d$, integrated over all values. Mathematically,

$$\begin{aligned} \text{EXPECTED PENALTY} = & \int_0^{y_d} C_S(y, y_d) f_Y(y) / F_Y(y_d) dy \\ & + \int_{y_d}^{\infty} C_F(y, y_d) f_Y(y) / (1 - F_Y(y_d)) dy \end{aligned} \quad (1)$$

where f_Y is the density function and F_Y the cumulative distribution function for Y . This expected penalty can be interpreted as the average penalty for a group of structures (with the same cost penalty functions) subjected to what is ostensibly the same earthquake risk, or as the expected penalty for a single structure. The advantage with working with penalty functions (over expected cost functions) is that they derive entirely from our lack of perfect knowledge of the processes governing earthquake occurrence, ground motion generation and transmission, and structural response. If there were no uncertainties in any of these processes, we would simply predict the design earthquake, calculate y , design the structure (presumably for minimum cost), and incur no penalty. Since there are uncertainties, we can calculate (through equation (1)) the associated costs, and can estimate how these costs decrease with reduced uncertainty (better theories) about physical phenomena.

Simple Example

A simple hypothetical problem has been chosen to illustrate several points. A building site is threatened by an earthquake source located 25 km away; the source produces earthquakes in the magnitude range 5-7.5, with a Richter b value of 0.88, at an average rate of one per year. Ground acceleration y is chosen as the intensity measure of interest (it is assumed for simplicity that y is a good estimator of

building damage and is a good measure to estimate design costs). The attenuation equation used is $\ln y = 6.16 + 6.5M - 1.3 \ln(R+25)$, where M is magnitude and R is source-to-site distance (25 km in this example). This attenuation equation¹ is typical of most for the range in which there is plentiful data; dispersion of observed values about the regression estimates indicates that the standard deviation of $\ln y$ is 0.51, which is a typical dispersion for California acceleration data. A lognormal distribution of y is used, corresponding to conclusions reached by many researchers.

The failure cost penalty function chosen is

$$c_F(y, y_d) = \begin{cases} 0 & y \leq y_d \\ c_R & y > y_d \end{cases} \quad (2)$$

which corresponds to the simple situation that the cost of replacement is incurred if the design intensity is exceeded. (No increase in replacement cost with seismic design level is assumed in this simple analysis.) For the over-design penalty, the following function is used:

$$c_S(y, y_d) = \begin{cases} a(y_d - y) & y \leq y_d \\ 0 & y > y_d \end{cases} \quad (3)$$

This corresponds to a linear increase in design cost with y_d . The total expected penalty is calculated using equation (1).

The penalty associated with current technology (no earthquake prediction methods available, typical dispersion in ground motion intensity estimation) will be calculated and will be compared with the (reduced) penalties associated with various advances in prediction technology and in ground motion estimation. It is assumed that, with present technology, designing the building under consideration to survive earthquake motions during its lifetime with 90-percent reliability, i.e., $F_y(y_d) = 0.9$, results in minimum total cost. The choice of design motion assuming advances in prediction technology and/or ground motion estimation is also made using a minimum cost criterion. A risk of some size is inherent in any choice of design intensity, either explicitly or implicitly, and will remain until all uncertainties in earthquake prediction, ground motion estimation, and building response estimation are eliminated or at least bounded.

¹R. K. McGuire, "Seismic Structural Response Risk Analysis, Incorporating Peak Response Regressions on Earthquake Magnitude and Distance," M.I.T. Dept. of Civil Eng., Research Report R74-51, 371 (August 1974).

Distributions of Ground Motion

Figure 3 shows the distribution of intensity y during the structure's lifetime using the assumptions and properties presented above, and using a typical state-of-the-art risk analysis². From the Poisson distribution there is a probability of 0.37 that no earthquake occurs at all, resulting in the spike of height 0.37 at $y=0$. According to the 10-percent risk design rule assumed, the value chosen for y_d is 22-percent g.

The penalty associated with this procedure can straight-forwardly be calculated via equation (1), using Figure 3 for $f_Y(y)$. Performing this calculation gives a penalty of $13.8\alpha + 0.1 C_R$, the first term due to over-design (because no earthquake occurs or because the earthquake(s) which occurs produces an intensity $y \leq y_d$) and the second term due to possible failure. The assumption that this a minimum cost design means that $\alpha = 0.0125 C_R$, and this relationship is used for subsequent cases.

Let us hypothesize first that a perfect positive earthquake prediction capability is available, i.e., that precursors have been identified which are sufficient to predict all earthquakes during a structure's lifetime, but which are not known to be necessary, so that the absence of earthquakes cannot be predicted. This is an optimistic goal for an earthquake prediction program to achieve in 5 to 10 years; we would be happy if precursors can be identified which will allow reliable predictions of the size, location, and time of the next event on a section of fault. Those faults which do not exhibit the precursory behavior would be suspected of being aseismic (during the lifetime of a structure) but, until more detailed investigations and data gathering, no specific aseismic prediction would be made. The distribution of ground motion from the predicted event depends upon its size; distributions of y for three events (magnitude 5, 6, and 7) are shown in Figure 4. The minimum cost criterion is used, and it is assumed also that only one event is predicted during the structure's lifetime. The expected penalty for each design depends on the magnitude of the predicted event (it increases with magnitude) and this penalty can be calculated with equation (1). To determine an expected penalty for a single structure before the earthquake is predicted (or equivalently to calculate the average penalty for a large number of structures to be affected

²R. K. McGuire, "Fortran Computer Program for Seismic Risk Analysis," U.S. Geological Survey Open-File Report 76-67, 90 (1976).

by a range of predicted magnitudes) we use the exponential magnitude distribution and integrate over all values between M=5 and M=7.5. Performing this calculation gives an expected over-design penalty, for cases in which earthquakes can be predicted, of 11.1 a. The expected failure penalty, calculated by weighting according to the exponential magnitude distribution, is 0.077 C_R . Using the relationship between a and C_R described above, the total expected penalty is 80 percent of that for the risk analysis case. It must be concluded that the expected cost penalties associated with long-term earthquake design and planning decisions will not be reduced greatly by a positive earthquake prediction capability.

If a perfect positive and negative prediction capability is available (i.e., we can predict earthquakes and no earthquakes), the expected penalties are reduced because there are no penalties (and no costs) for structures which will not be shaken. Assuming (from the Poisson distribution described above) that this happens 37 percent of the time, the penalties associated with a positive prediction capability are reduced 37 percent, to 50 percent of the penalty calculated for risk analysis. We are thus faced with the interesting conclusion that, given present uncertainties in ground motion estimation, more benefits in long-term planning decisions will be realized in an earthquake prediction program by identifying faults and areas where earthquakes will not occur, rather than where they will occur.

To determine the effect on cost penalties of advances in ground motion estimation, the three cases above (no earthquake prediction capability, positive capability, positive and negative capability) were repeated assuming first that uncertainty in ground motion is reduced by one-half (σ of $\ln y = 0.25$), and second that it is reduced to zero. The cost penalties were calculated in a manner identical to that described above. Table 1 summarizes the expected penalties under various hypothesized advances in prediction technology and/or ground motion estimates, as percentages of the expected penalty under present technology (first row, first column). Table 2 indicates a similar comparison for the total expected cost for each case, calculated as the design cost plus the failure cost times the probability of failure, i.e., $ay_d + C_R(1 - F_Y(y_d))$, integrated over the various possibilities where applicable.

It can be seen from the first column of Table 1 (or 2) that (as discussed above) the reduction in expected penalty is small when going from present technology to a

positive prediction capability, primarily because of the large uncertainty in ground motion given the prediction. Similarly, reading across the first row of Table 1 (or 2) the reduction in expected penalty due to reducing uncertainty in ground motion is small, primarily because of the large uncertainty in earthquake size, location, and time of occurrence. It is only when advances in both earthquake prediction and ground motion estimation are made, that substantial reductions in expected penalties and total costs are achieved.

Conclusions

It is shown by this simple study that advances must be made in both earthquake prediction capability, and in ground motion and structural response estimation technology, for the costs associated with long-term design and planning decisions to be significantly reduced. Large reductions in these costs will not be achieved by an earthquake prediction capability alone, nor will they be achieved solely by more advanced theories to estimate ground motion and structural response. This is the case whether one examines the expected cost penalties due to uncertainties in estimating structural responses during future earthquakes, or whether total expected design and failure costs are used as the criterion for comparison. Design and planning costs will be reduced somewhat by a perfect positive prediction capability (meaning that earthquake precursors have been identified which are sufficient but not necessary for prediction purposes); more cost reduction will occur when a perfect positive and negative prediction capability is available (meaning that faults can be identified which can be assumed to be aseismic in the future, for planning and design purposes).

Table I

**Expected Cost Penalties as Percent of Present
Penalty due to Uncertainties in Earthquake
Occurrence and in Ground Motion**

		Present	Ground Motion Uncertainty	
		Present	1/2 of Present	No Uncertainty
Earthquake prediction capability	None	100%	60%	56%
	Positive* capability	80%	33%	0%
	Positive and negative capability	50%	21%	0%

*Analysis only for sites where events are predicted.

Table II

**Total Expected Costs as Percent of Present
Cost of Earthquake Design and Failure**

		Present	Ground Motion Uncertainty	
		Present	1/2 of Present	No Uncertainty
Earthquake prediction capability	None	100%	82%	76%
	Positive* capability	94%	66%	38%
	Positive and negative capability	60%	42%	24%

*Analysis only for sites where events are predicted.

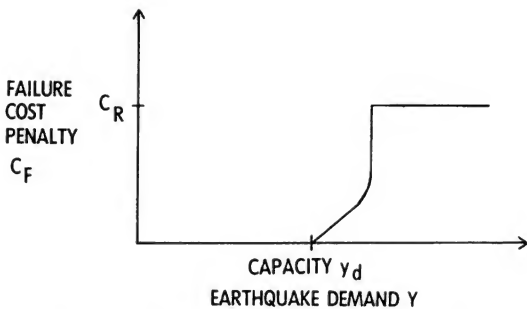


FIG. 1- FAILURE COST PENALTY AS FUNCTION OF EARTHQUAKE DEMAND.

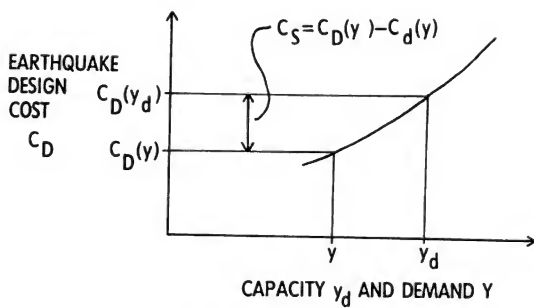


FIG. 2- DESIGN COST AS FUNCTION OF CAPACITY.

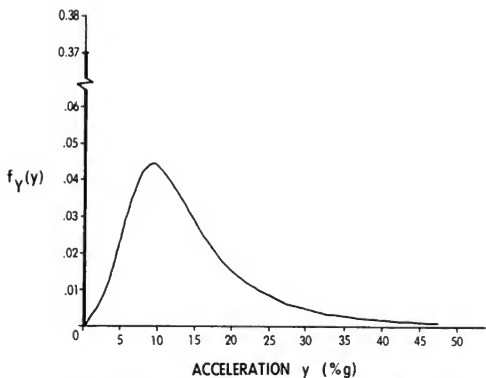


FIG. 3- DISTRIBUTION OF ACCELERATION, RISK ANALYSIS.

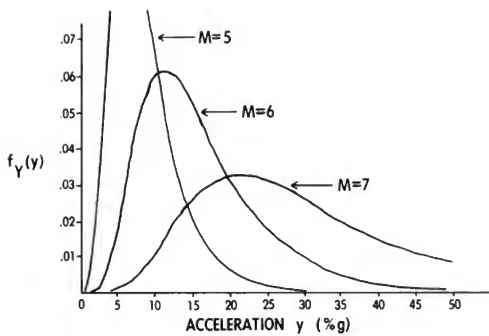


FIG. 4- DISTRIBUTION OF ACCELERATION, 3 PREDICTED EARTHQUAKES.

RESEARCH AND DEVELOPMENT OF PERMANENT
OCEAN-BOTTOM SEISMOGRAPH OBSERVATION SYSTEM
OFF THE PACIFIC COAST TO CENTRAL HONSHU, JAPAN
Akira Suwa, Head, Seismology & Volcanology Division
Norio Yamakawa, Chief, 1st Laboratory of the Division
Tatsuto Iinuma, Chief, 3rd Laboratory of the Division
Meteorological Research Institute
Japan Meteorological Agency

ABSTRACT

Eighty to ninety percent of all the earthquakes in the world occur in the sea area. However, there is not a single permanent ocean-bottom seismograph yet; this is the weakest point in seismic activity monitoring and earthquake prediction. The Seismology and Volcanology Division of the Meteorological Research Institute has been engaged in the development of a permanent ocean-bottom seismograph observation system off the Pacific coast of Tokai District, central Honshu, which is one of the major items included in the 3rd Five-Year Plan of the National Program of Earthquake Prediction Research in Japan (1974-1978).

The observation system being developed consists of the combination of submarine and land equipment. The submarine equipment consists of one terminal apparatus and several intermediate apparatus, i.e., pressure vessels containing seismograph and tsunami-meter sensors, and signal transmitters, which are connected in series by a submarine co-axial cable. This equipment is laid one hundred and twenty kilometers off Omaezaki, Shizuoka Prefecture, at the ocean-bottom down to 3,000m below sea level. On the other hand, the land equipment consists of receiving and repeating apparatus in the shore station (Omaezaki Weather Station), and receiving and data processing apparatus at the Earthquake and Tsunami Center (Japan Meteorological Agency in Tokyo).

This development project has been progressively implemented. Trial layings of the submarine equipment have been carried out already and actual layings are planned in 1978.

KEYWORDS: Cables; development of submarine equipment; earthquake prediction; ocean-bottom seismograph.

MAJOR AIMS OF THIS OBSERVATION SYSTEM DEVELOPMENT

Two-thirds of the globe's surface is covered with sea water, and accordingly, 80 to 90% of all the earthquakes take place in the sea area.

Ten to fifteen percent of the world's earthquakes occur in and near the Japan Archipelago. And the Japan Meteorological Agency is responsible for permanent monitoring of large, moderate, and small earthquakes ($M \geq 3$) which occur in this area. It is estimated that the number of these earthquakes is approximately 10,000 per year. Moreover, it is also estimated that the number of micro- and ultra micro-earthquakes ($M < 3$) in this area is more than 10,000,000 per year. The observation of these earthquakes is significant for realizing earthquake prediction, though they have no direct influence on our daily life.

Most of these numerous earthquakes have their hypocenters under the sea bottom near the Japan Archipelago. Remarkably, all the recorded great earthquakes with a magnitude of $M \geq 8$, which caused huge damages, occurred in the sea bottom off the Pacific coast between the coastline and the Japan Trench, Nankai Trough and so on, with the single exception of the Nobi Earthquake in 1891.

While the Japan Meteorological Agency is always carrying out permanent observations at 130 locations or more together with a number of university laboratories conducting their local observations, the concerned seismographs are all land based ones and not a single piece of permanent observation equipment is located at the sea bottom.

Consequently it has not been determined exactly how many and in which areas minor earthquakes occur in the sea bottom. Moreover, even for major earthquake occurrences, concrete and precise data on the location of the epicenter, the depth of the hypocenter and the magnitude have not been available.

This means a lack of monitoring devices for seismic activities in the sea bottom, producing serious obstacles in processing tsunami warnings and earthquake informations, as well as realizing earthquake prediction and forecast. The monitoring devices are indispensable for disaster prevention.

Under such circumstances, the Japan Meteorological Agency is going to implement a program for the immediate application of land observation data combined with permanent sea bottom observation data which are obtained by seismographs connected in series at the sea bottom down to thousands of meters, the deepest part, under the sea level, off Sanriku District, Sagami Bay to the Boso Peninsula, Tokai District, and Shikoku, all of which are the locations with frequent earthquake occurrences.

The development of the on-line and real-time system of permanent ocean-bottom seismograph observation off the Pacific coast of central Honshu, Japan, is presently being implemented by the Meteorological Research Institute as one of the major items included in the 3rd Five-Year Plan of the National Program of Earthquake Prediction Research in Japan (1974-1978). The system is transferred to routine observation by the Japan Meteorological Agency after completion of the Plan.

The sea area, off the Pacific coast of central Honshu, was selected because it was around this area where great earthquakes of the M8.5 class occurred at least four times

in history with intervals of 145 to 402 years. 123 years have already passed since the last occurrence of such a great earthquake and there is a seismicity gap, as shown in Figure 1, even when small earthquakes are taken into consideration. Such being the case, the Coordinating Committee for Earthquake Prediction of Japan also specifically designated Tokai District of central Honshu, as an "Area of Intensified Observations."

Studying the data from a large earthquake that occurred in 1854, the last case observed in the past in this area, it is well anticipated that, if such a large-scale earthquake takes place again, not only Tokai District will suffer very serious damages but also Tokyo, Kanasawa, Kobe, etc. will be subjected to damages as well.

Although the existence of a seismicity gap does not in itself reflect the imminent sign of a large scale earthquake, we cannot deny the existence of the ominous silence usually observed before a storm. In this respect, further change in seismic activity within this sea area requires a special attention.

Furthermore, a large budget is required for the development of this system, and even with such a budget and the most up-to-date sophisticated technology, there still remains various risks. Fortunately, the depth of the water in this area is not so deep as the other three areas.

The authors together with Hideteru Matsumoto, senior researcher, and other staff members, Yasuo Nagayama, Akio Takayanagi, Michio Takahashi and Toshimitsu Tsukakoshi, have been making every effort to carry out the research and development of this system at the Research Division. However, research and development activities are not being carried out solely by the Meteorological Agency. Nippon Telegraph and Telephone Public Corporation, the Faculty of Science and the Earthquake Research Institute of Tokyo University, and the Hydrography Department of the Maritime Safety Agency have extended special cooperation. As to the production of equipment the Nippon Electric Company, Ltd., and related companies have been engaged in this project.

CONSTITUTION OF A SUBMARINE SYSTEM

The observation of ocean-bottom earthquakes using the submarine cable system has only been attempted once in the past by the U.S.A., and this system was less complicated than that which is now being developed by the authors, et al. In 1965, the Lamont-Doherty Geological Observatory of Columbia University installed a cable in the Pacific Ocean approximately 180km (100 nautical miles) off Point Arena, California, to a depth of nearly 4,000m and equipment such as seismographs were attached only at the tip of the cable.

Staff members including the authors were successively dispatched to the above observatory in order to acquire knowledge of their valuable techniques and experiences.

However, the Lamont-Doherty Geological Observatory was forced to give up their research after only several years of study mainly due to frequent trouble, which resulted from wire breaks in the cable and slight water leakage in the pressure vessel, caused by geographical and geological features.

The series type system now being developed by the Meteorological Research Institute of the JMA is more intricate, therefore, precise studies on the geographical and geological

features of the sea bottom are required in order to select the best route for the cable laying. The laying work must be carried out with extra caution because modifications after the completion and replacement of broken components are almost impossible with this kind of system.

The system is composed of a submarine system which is installed at a depth of nearly 3,000m in the sea approximately one hundred and twenty kilometers off the coast of Omaezaki, Tokai District, and a land system. The submarine system consists of one terminal apparatus and several intermediate apparatus of high reliability, i.e., pressure vessels containing seismograph and tsunami-meter sensors, and signal transmitters, which are connected in series by the co-axial submarine cable. The land system consists of the receiving and repeating apparatus in the shore station (Omaezaki Weather Station), and of the receiving and data processing apparatus at the Earthquake and Tsunami Center (Japan Meteorological Agency in Tokyo).

Figure 2 indicates the above mentioned system. The submarine transmitting system is an application of the transmitting techniques of the ocean-bottom co-axial cable used for the most recently developed long-range submarine telephone and telegram lines. In other words, of the two types of real-time and on-line transmitting systems, one is multi-cable systems in which components are divided into several channels and electric power is transmitted through a different channel, and the other is the co-axial cable system in which all components are combined in one channel through which electric power is also transmitted. The co-axial cable system has been employed for our observation system. All components of the observation equipment installed at the tip of the cable and at intermediate points transmit signals using the ocean-bottom co-axial cable by way of an FM-FDM system. An electric current is fed by way of a constant current feeding system in which electric currents run through the center conductor of the co-axial cable, and are released into the sea water from the terminal equipment attached to the ocean-bottom earth and then sent back to the coastal station through shore earth.

We have developed large size pressure-resistance containers for the terminal equipment (inner diameter 300m; inner length 820m), as a large variety of sensors needs to be incorporated. However, the largest of the pressure-resistant containers (inner diameter 204m; inner length 700mm) currently being used for ocean-bottom relaying equipment will be employed for intermediate apparatus. This will enable cable ships available in Japan to carry out the laying work. The pressure vessels are incorporated with 3 directional short-period (seismograph) sensors on gimbals (natural frequency 4.5Hz), an equalizing amplifier, signal transmitter, etc. The terminal equipment will also be equipped with a medium-period seismograph and pinger which is used for measuring the actual laying position of the equipment at the ocean-bottom.

A tsunami-meter is installed in order to contribute directly to the improvement of tsunami warning activities which are essential for the prevention of natural disasters. Sensors will be installed at the sea bottom to measure the change in hydraulic pressure and thereby detect tsunami. A quartz pressure transducer of the sensor which is used for this system (manufactured by the Hewlett-Packard Co., the U.S.A.) records changes in

frequency when there is a pressure change. This tsunami-meter sensor is covered with oil filled rubber to insulate it from brine.

The advantage of using this tsunami-meter has been confirmed through evaluation of its characteristics in a pressure chamber, thermostatic chamber, etc., and also by continuous test observations in the sea for five months at the marine observatory tower of the Meteorological Research Institute off the coast of Ito City, Shizuoka Prefecture. Although this tsunami-meter is a total pressure type which detects the overall pressure from the sea surface to the bottom, its resolvability is approximately 1 cm even at a depth of 3,000m, and has the comprehensive characteristic of being able to release sufficiently strong signals, compared to other surrounding noise, when a 10cm change in terms of water depth occurs. Furthermore, observation errors of a 10m high tsunami are 10cm or less.

The prerequisites for the apparatus to be used for this submarine system, both sensors and transmitters, are that they be highly efficient, reliable, and safe, and in addition, extremely compact.

RESEARCH AND DEVELOPMENT PROGRESS

The research and development of this permanent observation system for submarine seismic observation have been making steady progress in accordance with the annual program as shown in Table 1. In 1974, the initial year of the program, the system design of the total system including the land part was conducted, and as an integral part of this, various tests using a breadboard model were also carried out. Then, hardware was developed on the basis of the system design, and various tests have been conducted on the characteristics of these developed products and evaluated.

No damage should be incurred on any of the submarine system equipment while loading it on the cable ship or during the construction work. A route which meets the geographical and geological requirements must be carefully determined prior to the construction work. Geographical and geological conditions must have little possibility of sea-bottom landslides and wire breaks, and a small gradient, and also they must be as flat as possible to avoid a cable bridge. It is especially important that the intermediate apparatus are not left hanging in the water as a result of the geographical and geological features of the sea-bottom. Also, one end of the cable of this submarine system is placed a few thousand meters at the deep sea-bottom, whereas in the case of a submarine cable for telephone and telegram, both ends are at the two coastal stations.

The above-mentioned points make it necessary to first conduct elaborate studies on the geographical and geological features of the sea area to be used. Since the work also involves construction of heavy terminal equipment (the weight in water is approximately 1 ton including the cage), special methods will have to be employed in order to accomplish the work successfully, and trial layings of the terminal equipment are indispensable.

In view of the above-mentioned conditions, a bathymetric chart and a submarine structural chart of the sea bottom to be used, which are the results of a detailed survey conducted in 1974 by the Hydrography Department of the Maritime Safety Agency, were made available by the same Department to the Meteorological Research Institute; and four proposed

routes for submarine cable installation were determined on the basis of such charts and the bathymetric record of the same survey, and also by taking into consideration the opinions of the experts in the Hydrography Department and the Nippon Telegraph and Telephone Public Corporation.

Furthermore, in 1975 and 1976, the Meteorological Research Institute commissioned the Corporation to carry out research on geographical and geological features concerning sea-bottom of the proposed routes, and had a private land survey company perform surveys of the sea bottom along the coastal area south of the Omaezaki Weather Station. The Corporation was also commissioned to implement trial operations aiming at establishing a laying system of the sea bottom terminal equipment.

The Corporation carried out bottom sampling and sounding along all the proposed routes on board the Kuroshio-Maru (3,344.9 tons), the newest cable ship, employing a multi-beam bathymeter (which is capable of simultaneous sounding and inclination measurement in a transverse direction to the course), the NNSS (U.S. Navy Navigation Satellite System), and a computerized automatic control system. As a result, among the four proposed routes which run from NNE to SSW along the zone between the Suruga Trough to the Nankai Trough and the submarine canyon off the Tenryu River, the central route was determined to meet the necessary geographical and geological conditions, while others did not.

The Corporation, in 1976, carried out a trial laying and refloating of the terminal and intermediate equipment by use of a dummy system on board the Kuroshio-Maru. The laying of the sea-bottom system is planned to start from the terminal. The terminal will be lowered to the sea-bottom from the bow of the cable ship, and then the laying of the intermediate equipment will take place from the stern by operations in the ship. The lowering of the terminal will be performed by adopting the so-called single wirehanging process which ties the heavy terminal equipment and the ocean-bottom earth with 1,000m long cable (approx. 500m in the trial) to the signal transmitting co-axial cable. However, since the conventional type non-armored co-axial cable has a 7-ton tensile strength and therefore presented large risks, a high tension non-armored co-axial cable (15-ton tensile strength) was newly developed and used. This new cable endured well at the maximum tensile strength, i.e., 9 tons, at the time of refloating.

In this co-axial cable of the sea bottom system, a section of approximately 40km which was to be laid in the shallow sea-bottom (down to approximately 500m) adopts a single or double armored co-axial cable in order to avoid any trouble in relation to the operation of dragnet fishing. In the very shallow sea-bottom (down to 50m) along the sea shore, various kinds of trouble tend to occur due to wave action and tidal currents. Therefore, the double armored co-axial cable guarded by a steel protector is adopted and furthermore, the cable is buried in the sea-bottom mud. The sole manufacturer of the submarine co-axial cable in Japan is the Ocean Cable Company.

The research and development project of this permanent sea-bottom earthquake observation system has been steadily progressing with the support of the earnest people concerned. While numerous difficulties have been encountered and overcome, there still remains a lot of problems to be analyzed and solved in the coming days. The practical laying of the submarine system is planned to be implemented in summer or fall of 1978, and preparations are now being made.

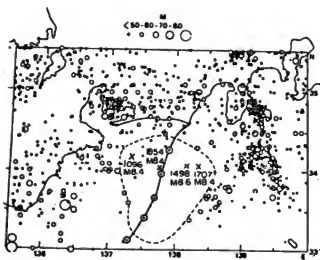


Figure 1. Distribution of Epicenters of Shallow Earthquakes off the Tokai District (1926-72) and the Permanent Ocean-Bottom Seismograph Observation System

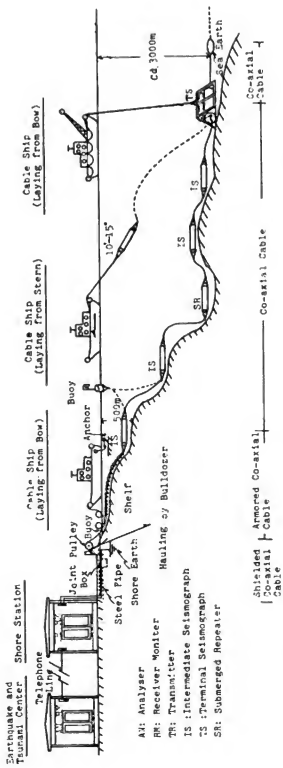


Figure 2. Outline and Laying Method of the Ocean-Bottom Seismograph Observation System

Table I. Research and Development of Permanent Ocean-Bottom Seismograph Observation System
YEARLY PLAN

	F.Y. 1974	F.Y. 1975	F.Y. 1976	F.Y. 1977	F.Y. 1978
Terminal system	Development of medium-period seismograph	Development of short-period seismograph and pressure vessel	Development of transmitter		
Intermediate system	Development of one apparatus	Production of tsunami-meter	Production of one apparatus (excl. tsunami-meters)	Production of two apparatus	Production of cables
Submarine cable			Partial designing and production (cable for trial)	Production of cables	Production of cables
Relay facilities				Production of one ocean-bottom repeater; Construction and settlement of coastal repeating station	Construction and settlement
Central facilities					Implementation
Performance test			Implementation	Implementation	Implementation
Effective disposition	Implementation	Implementation	Implementation	Implementation	Implementation
Studies on utilization	Implementation	Implementation	Implementation	Implementation	Implementation
Laying			Trial		Actual
Total system	System designing	Studies on system designing		Comprehensive experimentation	

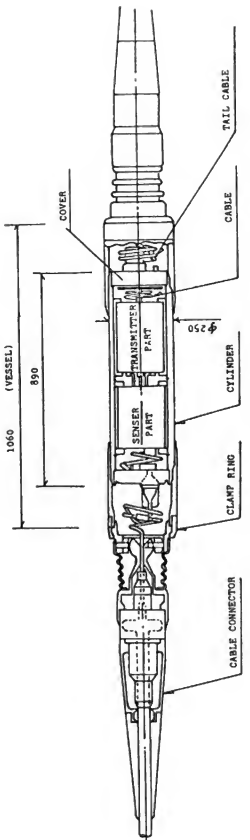


Figure 3-1. Composition of the Intermediate Apparatus

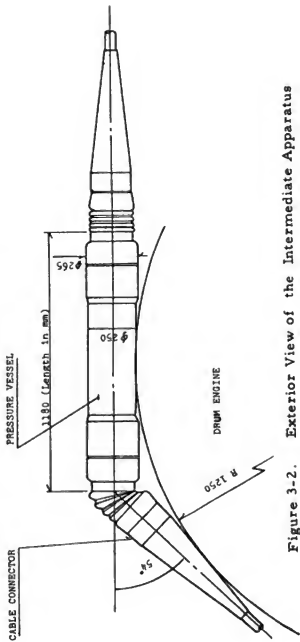


Figure 3-2. Exterior View of the Intermediate Apparatus

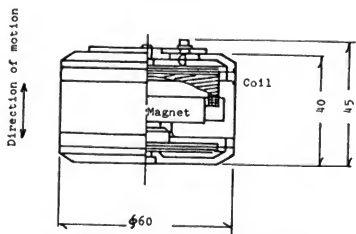


Figure 4. Seismometer Sensor

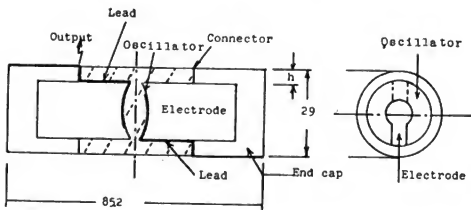


Figure 5-1. Tsunami-meter Sensor

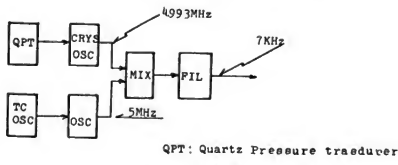


Figure 5-2. Tsunami-meter Block Diagram

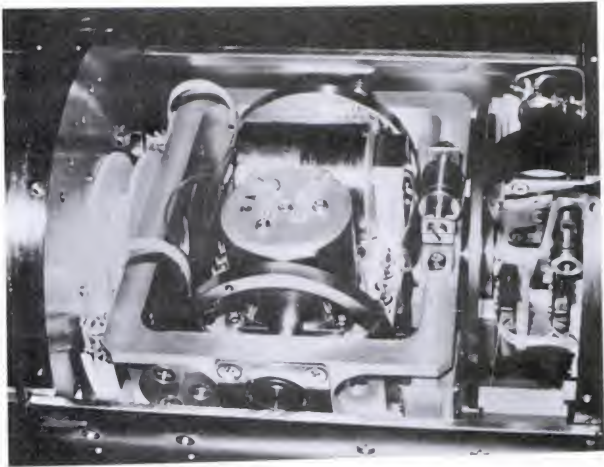


Figure 6. Short-Period Seismometer Sensor

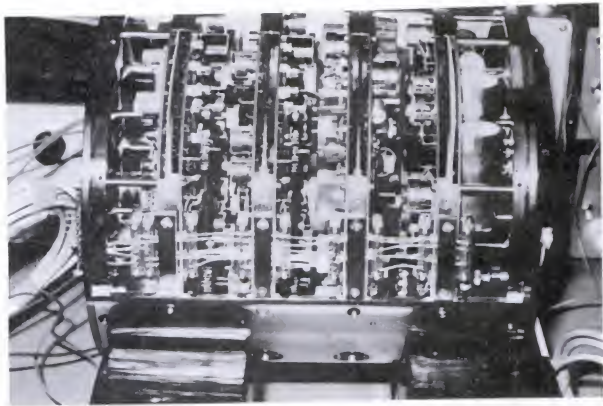


Figure 7. Transmitter of the Terminal Apparatus

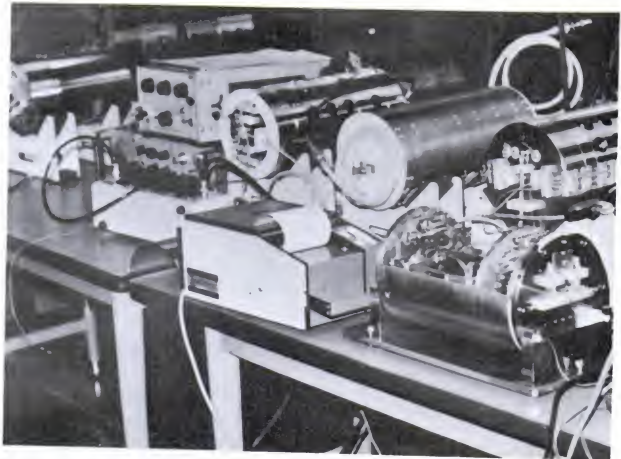


Figure 8 Overall Test of a Breadboard Model of the Submarine System



Figure 9 Test of Tsunami-meter in the Sea (20m deep)



Figure 10 Trial Layings of the Terminal Apparatus

VERTICAL DISTRIBUTION OF THE SEISMIC
S-WAVE VELOCITIES AT THE SITE OF THE IWATSUKI DEEP
BOREHOLE OBSERVATORY OF CRUSTAL ACTIVITIES
Fumio Yamamizu and Hiroshi Takahashi
National Research Center for Disaster Prevention
Noritoshi Gotoh, Yutaka Ohta and Keiji Shiono
Hokkaido University

ABSTRACT

From the earthquake engineering point of view, in-situ velocity measurement of the seismic S-wave was carried out down to a depth of 3500 meters at the site of the Iwatsuki Deep Borehole Observatory constructed by the National Research Center for Disaster Prevention.

S-waves were produced mainly by ordinary small chemical explosions in a shallow bore-hole and supplementarily by an SH-wave generator (an S gun) firmly pressed on the ground surface. A set of three-component seismometers of moving-coil type with natural frequency of 4.5 Hz was installed in a capsule which could be fixed at any depth in the borehole. Repeated measurements were made at 16 different depths from the surface to the bottom. The S-wave by the S gun was clearly recorded down to the depth of 1500 m. Identification of the S-wave onset on the record of the explosion was unexpectedly easy, even for depths deeper than 1500 m, because very good phase correspondence between the S phase from the S gun and the S phase from the explosion was obtained. Therefore, the reading of the S-wave onset was most reliable.

The estimated S-wave velocity structure was 0.44, 0.76, 1.3, 1.6 and 2.6 km/sec with the boundary depths of 300, 1000, 2000 and 2800 m, respectively, from the surface to the bottom of the borehole. The boundary at 2000-m depth was uncertain unlike the other three boundaries. This boundary may not exist, or the velocity may change gradually with depth.

The P-wave velocity structure was estimated at the same time, and the velocity values were 1.8, 2.1, 2.9 and 4.7 km/sec with the boundaries very close to those of S-wave velocity. But the 2000-m depth boundary was not found.

KEYWORDS: Deep borehole; earthquake, in-situ velocity measurement; S-wave; vertical distribution of seismic wave.

INTRODUCTION

With the recent increase of large size structures, it has become essential that the response characteristics related to the sub-surface structure at depth, probably several kilometers deep, should be evaluated; in other words, the existence of a thick sedimentary layer is indispensable for the earthquake resistance of high and/or long structures (Seis. Expl. Group of Japan, 1976).

As a first step to understand the response characteristics of a thick, deep sedimentary layer, the velocity of S-waves was directly measured in-situ down to the depth of 3500 meters, at the Iwatsuki Deep Borehole Observatory of Crustal Activities constructed by the National Research Center for Disaster Prevention. Since there has been no direct S-wave measurement made for the depths over several hundred meters, the present measurement over 3500 m depth was the first trial in Japan, probably even in the world. Firstly, the detection and identification of S-waves are emphasized and then the general trend of their velocities is properly evaluated.

To produce S-waves, we used small chemical explosions in a shallow borehole and we also used a specially designed SH-wave generator, called an S gun. The SH-wave predominantly generated by the S gun (Jolly 1956, Komaki 1959, Shima and Ohta 1967) was recorded clearly down to the depth of 1500 m. Through the comparison of records from the explosion and the S gun, it was possible to extract S-wave characteristics contained in the record from the explosion. Therefore, the S-wave identification at depth by simple detonations has become unexpectedly easy and the reading of the S-wave onset is reliable.

OBSERVATION

The Iwatsuki Deep Borehole Observatory of Crustal Activities fronts on the Moto-Arakawa River, Iwatsuki-city, Saitama-ken, Japan. Four shot holes were drilled on this riverbed about 100 meters southeast from the observation well, and the S gun was firmly pressed on the surface of the same bed about 50 m east from the well.

A set of instruments was well designed with the purpose of efficient task of the observation and easy operation not to miss recordings. The block diagram of the observation system is shown in Fig. 2. The apparent dynamic range of this recording system is over 70 db, including the effect of the analog voltage divider. All seismometers used were of the moving-coil type, with natural frequency of 4.5 Hz for the underground use, and 1.0 Hz for the surface use. A set of seismometers on the surface was also operated in order to determine the attenuation of S-wave energy by comparing the records at varying depths and at the surface.

The measurement was sequentially carried out at the following 16 depths, 100, 200, 300, 500, 750, 1000, 1500, 2000, 2500, 3000, 3482, 3249, 2745.3, 2245, 1750 and 1250 meters.

ANALYSIS

The analysis proceeded along a line in which the priority was given to detection and identification of S-waves, and then the general trend of S-wave velocities were evaluated. This was also inevitably required because the interval between depths of measurement was rather rough, namely 100 or 250 m.

In the determination of the S-wave velocity structure on the basis of the obtained travel-time diagram, any other data concerning the observation well (for example, the sonic, the density logging) were not taken into account. All efforts were concentrated on determining the objective S-wave structure from the travel-time only. After that, all the data were compared with each other, and the harmony between them was examined.

PROCESSING OF RECORDS

Along the line stated above, at first, the record from the S gun which predominantly produced the SH-wave was processed (Fig. 3). Traces shown in Fig. 3 were resynthesized by the analog signal converter shown in Fig. 4. Since the horizontal direction of the seismometers in the borehole was not known, this converter was used, so that the expected SH-wave could be emphasized. The result was very clear especially for the trace of 1500m depth. This converter was also applied to records of the explosion, but the result was not improved. Probably, the reason was that the explosion produced both SH- and SV-waves. Accordingly, the S/N ratio was improved primarily by various digital filtering. Filtered traces are shown in Fig. 5.

Comparing Fig. 3 with Fig. 5, relatively long-period wave groups are clearly recognized on the record of the explosion at the time of appearance of the SH-wave on the record of S gun. The records in Fig. 5 were made by various filterings, so that this relatively long-period wave group could be emphasized, because these wave groups are taken as S-waves. The solid circle in the figure shows the S-wave onset. Only the onset at 3250 m is less objective.

Next, the trace of the vertical seismometer is drawn up (Fig. 6) so as to determine the P-wave velocity structure. There are almost three wave groups: the first wave group is the precursor with small amplitudes, appearing at the depths as deep as 2500 m, the second is the true P-wave group, and the third group following the P waves has large amplitudes. Judging from a rough estimation of their velocities, they correspond to the dilatational wave propagating through the cemented zone around the observation well protected by the wall and through the water filled in the well. Especially, from the fact that in the large-amplitude wave group those reflected by the well bottom are recognized, it is obvious that the third wave group has propagated in the well water.

TRAVEL-TIME DIAGRAM AND VELOCITY STRUCTURE

The onsets of S and P waves were read with the precision of 1/100 sec. After that, the travel-time was corrected, as if the source were just above the well at the surface. In the correction, detailed velocities of S and P waves near the surface were used and

these were the results of the P, S velocity loggings as deep as the depth of 120 meters, which were carried out at an area close to the observatory.

In Fig. 7, the corrected travel-times were plotted and straight lines were drawn through the plots. All the points except one or two are on the lines, and furthermore, even those exceptional points are away from the lines by only 3/100 sec. Therefore, straight lines seemed to be very reasonable.

From this travel-time diagram, we can directly determine the velocity structures of S and P waves. It is summarized in Fig. 8 together with the structure near the surface. The S-wave velocity structure consists of four layers, and the velocity structure consists of three layers to the deep basement, excepting the vicinity of the surface. The boundaries at the depth of 300, 1000 and 2800 m coincide with each other in both the S- and P-wave structures. The only discrepancy occurs in the boundary at 2000 m. Since the ratio of S velocity at this boundary is $1.3/1.6=0.8$, it is not significant. On the other hand, the travel-time of that interval seems to be increasing gradually with increase in the depth, and so it is also possible that the two layers are taken as one mirage layer. Accordingly, both the structures of S and P waves are in good agreement with each other.

COMPARISON WITH OTHER DATA

Other data concerning the Iwatsuki Deep Borehole, that is, the sonic wave (P wave), the density and the electrical loggings and the geologic columnar section, etc. had been examined (Takahashi and Hamada, 1975). The sonic logging was basically a continuous measurement. Although the variation of velocity was very complex and scattering, the general tendency of the sonic logging and the absolute values are in good agreement with the present estimated structure. Two discontinuities at depths of 1000 and 2800 m are clearly seen in the sonic logging, and also obvious in the columnar section, corresponding to the boundary of Pleistocene-Miocene and Miocene-Pretertiary, respectively. In the sonic logging, velocities are almost constant or slightly increasing between 1000 and 2800 m depths except small scatterings near a depth of 1200 m. They also agree with the results shown in Fig. 8. Such general tendency is also shown in the density and electrical loggings.

Accordingly, the resultant S- and P-wave velocity structure are reasonable and in harmony with all the other data of the observation well.

CONCLUSION

Measurements of velocities of S and P waves were carried out down to a depth of 3500m at the Iwatsuki Deep Borehole Observatory. The results are summarized in Fig. 8. And they are in good harmony with all other data of observation well. Except at the ground surface, the S-wave velocity structure consists of four layers, and the velocity structure of P wave three layers. If we regard the intermediate depth layers as a mirage layer, the boundaries for S and P waves are consistent with each other.

The S gun plays an important role for detection of an S wave contained in the simple detonation, and so the reading of S-wave onset has become more reliable and accurate.

This is one of the good harvests of the present measurement, and also suggests a technical method of the deep S wave in-situ velocity measurement for the future research.

In conclusion, the experiment was carried out under the cooperation of five groups, NRCDP, Hokkaido Univ., Teikoku Oil Co., Akashi Seisakusho Co. and Allaround Consultant of Geological Survey Co. We want to express our gratitude to the scientist and technicians who participated in this experiment, especially to Mr. Suzuki at NRCDP who partly conducted the experiment. Also we would like to express our sincere thanks to Dr. Hamada who was a member of the planning team at the early stage of this experiment and kindly read the manuscript making valuable suggestions and encouragements.

REFERENCES

Jolly, R. N. (1956): Investigation of Shear Waves. *Geophysics*, 21, 905-938.

Komaki S. (1959): Fundamental Experiments on Generation of Shear Waves. *Journ. Seis. Exploration Group*, 18, 19-100. [in Japanese]

Shima, E. and Y. Ohta (1967): Experimental Study on Generation and Propagation of S-waves I, Designing SH-wave Generator and its Field Tests. *Bull. Earthq. Res. Inst.*, 45, 19-32.

Takahashi, H. and K. Hamada (1975): Deep Borehole Observation of the Earth's Crust Activities Around Tokyo - Introduction of the Iwatsuki Observatory. *Pure. & Appl. Geophys.* 113, 311-320.

The Seismic Exploration Group of Japan (1976): Experimental Studies on Generation and Propagation of Seismic Waves, Chapt. 5, Sec. 6. [in Japanese].

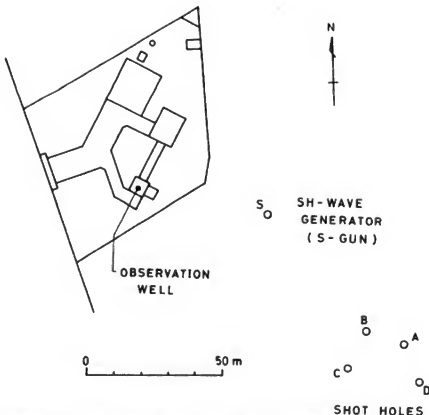


Fig. 1 Arrangement of the observation well, shot-holes and the SH-wave generator.

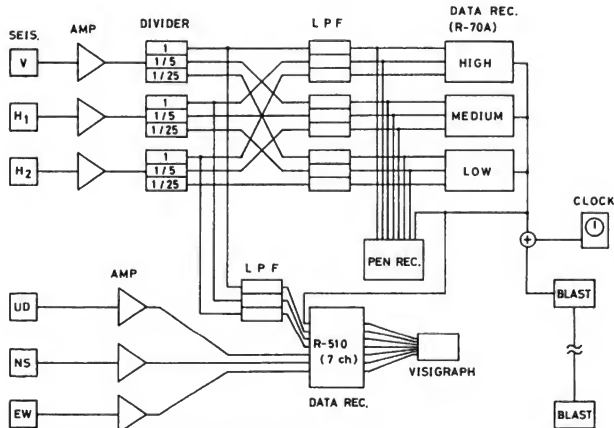


Fig. 2 Block diagram of the observation system.

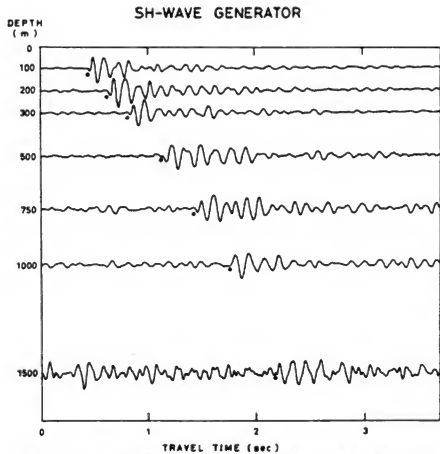


Fig. 3 Resynthesized records of the SH-wave generator.
Solid circles show the onset of S waves.

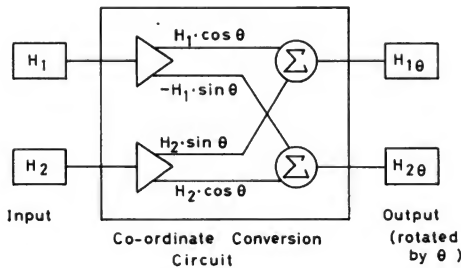


Fig. 4 Block diagram of an analog signal converter.

EXPLOSION
Horizontal component, filtered.

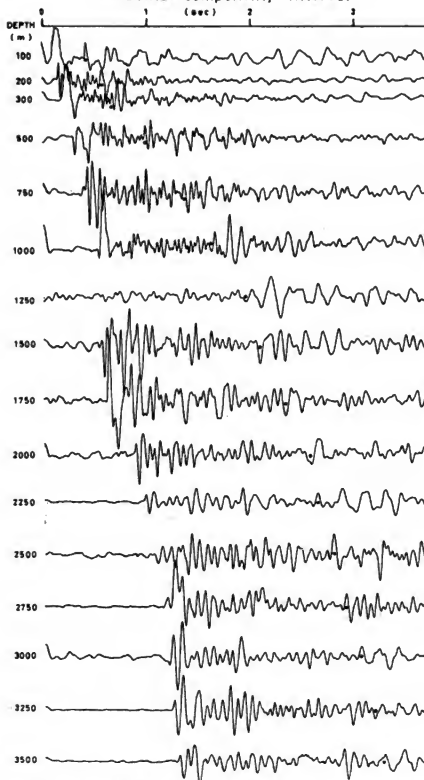


Fig. 5 Records of the horizontal component seismometer with the suitable filtering. Solid circles show the detected onset of S wave.

EXPLOSION

Vertical component, no filtering.

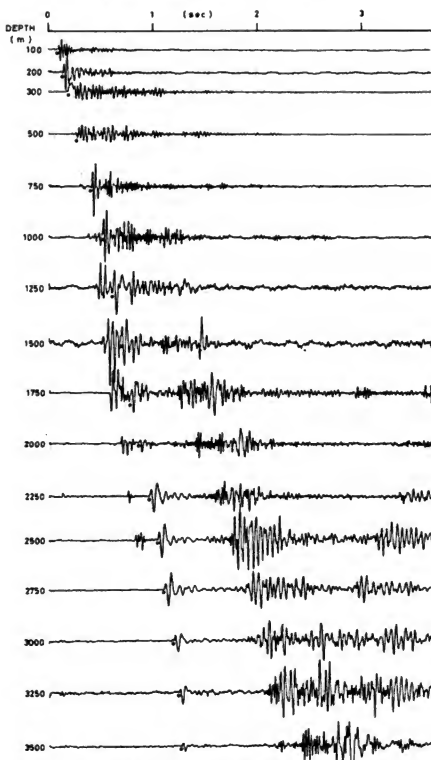


Fig. 6 Records of the vertical seismometer without filtering.
Solid circles show the true P wave.

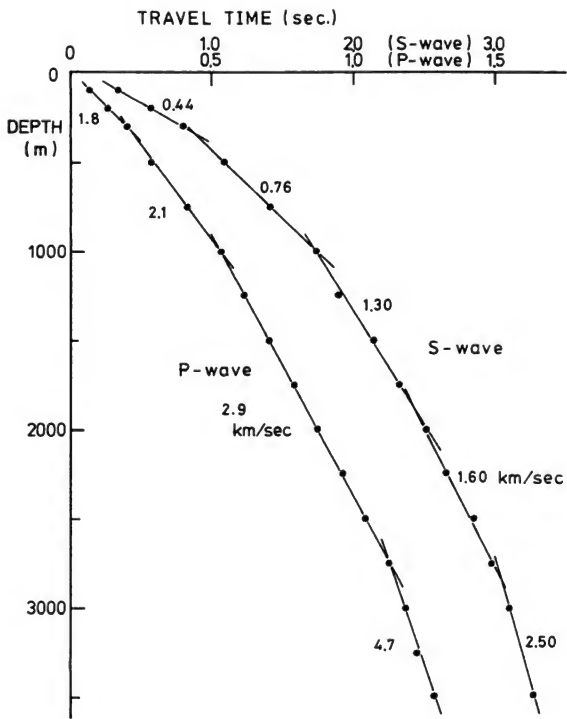


Fig. 7 Travel-time diagram of S and P waves

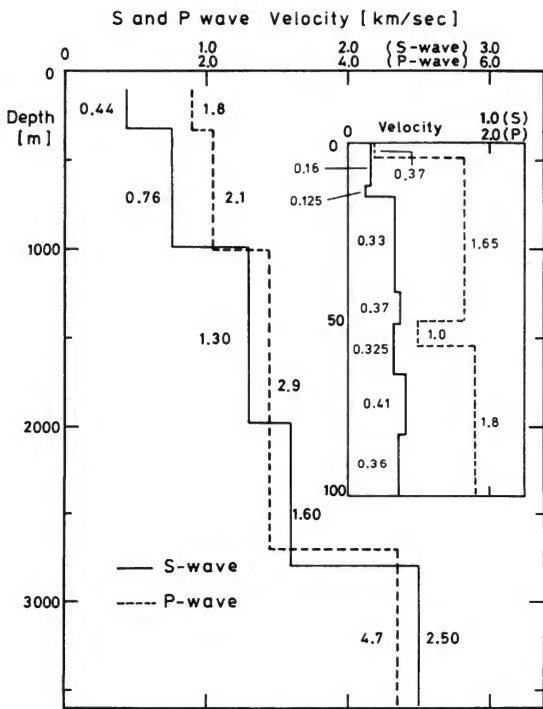


Fig. 8 Velocity structure of S and P waves.

RESEARCH ON ACTIVE FAULTS IN THE METROPOLITAN AREA

Hiroshi Sato, Geographical Survey Institute

Toshihiro Kakimi, Geological Survey of Japan

ABSTRACT

The present state of research on active faults in the metropolitan area is discussed. The paper describes the discovery of two active faults, the Tachikawa Fault and the Arakawa Fault, in the Kanto plain. The paper also points out that at present there is no definitive method(s) to detect active faults covered by thick sediment. The geophysical methods commonly employed in underground research work present problems when the methods are used for research on active faults in urban areas. Geochemical methods should be considered.

KEYWORDS: Detection of active faults; earthquake prediction; research on active fault

INTRODUCTION

It is well known that a sudden movement of a fault results in an earthquake. Fault which had moved in geologically recent time, namely Quartenary, is considered to move in the future. Such a fault is called an active fault and it is possible to estimate the magnitude and the mean recurrence time by knowing its length and displacement. Research on active fault are important for earthquake prediction and earthquake hazard mitigation. However, active faults in urban areas have not been well understood yet because of the many difficulties in performing research on active faults. Recently, importance of counter-measure for earthquake hazards in urban areas is emphasized, and research on active faults under metropolitan areas have been urged. This paper describes the present state of the research on active faults in the metropolitan area.

EARTHQUAKE DISASTER IN THE METROPOLITAN AREA

Since 1603 when the Shogunate was established in Edo, the metropolis of Japan has been attacked by destructive earthquakes more than thirty times, and those of intensity 6 or more in JMA scale have been recorded eight times.

The earthquakes that caused severe damages to the metropolis can be classified into two categories, that is, major earthquakes in the Sagami Bay and destructive earthquakes under the urban area. More than half of the earthquakes that attacked Edo are considered to be the latter type. Nowadays, the possibility of the occurrence of a major earthquake in the Sagami Bay in the near future is considered small and that of a destructive earthquake in the inland is considered not so small, as we have not had large earthquakes in the metropolitan area since the Nishisaitama earthquake occurred in 1931. The mean time interval of destructive earthquakes in this area is nearly 30 years, so the occurrence of a destructive earthquake under Tokyo is very apprehensive today.

Earthquakes that caused damages to Edo or Tokyo are divided into two groups from their focal depth. The Ansei Edo earthquake of 1854 is estimated (from the distribution of damages) to be a shallow earthquake whose focal depth was 30 Km or less, and the Tokyo earthquake of 1894 is considered to be a relatively deep one. In the southern Kanto district, there is an active seismic zone in the depth of 40 - 60 Km and the Tokyo earthquake of 1894 is estimated to be in this zone. Though the likelihood of occurrence of a relatively deep earthquake is larger than that of a shallow earthquake, the latter may give more severe damages to the Tokyo area.

The distribution of destructive earthquakes in Kanto appears to be closely related with the tectonic line extending from the northwestern part of the Kanto plain to the southeastern part. So, the studies of the tectonic structure are important for the evaluation of seismic hazards in the metropolis of Japan. (Fig. 1).

GEOLOGICAL STRUCTURE AND ACTIVE FAULTS IN THE KANTO PLAIN

The geological structure of south Kanto is characterized by thick sediment of Neogen and Quartenary and also by active seismicity zone of 50 - 60 Km in depth. In such thick

sediment areas, it might be possible to estimate a linear structure of base rocks, namely fault, from the discontinuity in the thickness of sediment, but it is difficult to know whether the fault had moved or not in geologically recent time. (Fig. 2)

The known or estimated active faults at present in the southern Kanto district are shown in Fig. 3. As seen in the figure, the faults are located mainly in the western part of the plain, and their strikes are prominent in the direction from northwest to southeast.

Some active foldings are estimated to be in the central and eastern part of the plain. These foldings might be considered a faulting in deep layer, resulting foldings in the upper layer. Among the active faults in the metropolitan area the most important ones on the hazard mitigation are the Tachikawa fault and the Arakawa fault.

Tachikawa Fault

This is the active fault running from Oome city to Tachikawa city (west of Tokyo) and its length is estimated to be 20 Km or more. It was very recently that the existence of this fault became definitive from the interpretation of air photographs and field investigations, and this poses a problem for land use in this area. The fault pass under the Tachikawa airdrome of the U.S. air force and the airdrome will be turned over to the Japanese government in the near future. Its mean vertical displacement rate is estimated to be 0.2 mm/year, resulting in the present total displacement of about 4 m to the Tachikawa plain which was formed nearly 20,000 years ago.

Any historical earthquake originated from the Tachikawa fault is not known, but at least one earthquake resulted from the fault within the last 10,000 years, when it displaced a sedimental layer formed nearly 10,000 years ago. If we assume that the displacement of the fault is about 1 m during one earthquake, the mean recurrence time of the earthquakes originated from the fault is estimated to be about 5,000 years.

Arakawa Fault

This fault is estimated from investigations of tectonic movements of late Quartenary in the Kanto plain. A clear boundary of tectonic blocks has been found along the Arakawa River, and an active fault should be considered to be there to explain the discontinuity in the movements. Although its existence is not confirmed yet by field investigations, the fault is estimated to be west down reverse fault of B class, that is, mean displacement rate in the order of 0.1 - 0.2 mm/year.

Recently a clear gap of about 400 m in the depth of base rock was found at the north of Tokyo by the artificial explosion at Yumenoshima in Tokyo Bay. Some researchers suppose that this gap is a part of the Arakawa fault. Considering the estimated strike of the fault and the distribution of the historical earthquake, the Arakawa fault might be considered as a part of the medium line in the Kanto district.

Exact location and length of the Arakawa fault are not known, but it is the nearest fault to the central part of the metropolis of Japan, therefore, research of the Arakawa fault is greatly needed.

RESEARCH OF ACTIVE FAULTS IN THE METROPOLITAN AREA

The first synthesis research of active faults in the metropolitan area have been conducted by the Committee for Disaster Prevention of Tokyo. The committee emphasized the importance of active faults on the hazard mitigation, and compiled a map of active faults and foldings. However, present information about active faults in the southern Kanto plain is not sufficient because of many difficulties encountered in the research.

Recently, a research project on active faults under sedimental layer has been initiate under the promotion by the Science and Technology Agency of Japan. The project is aimed to explore a new way of investigating active faults covered by thick sediment by using many kinds of geophysical methods. Although these geophysical methods are commonly used for geophysical prospectings of underground structure some problems remain when they are used for the research on active faults under young sediment. It is important to know the amount of displacement in the young sediment due to faulting, but physical property of the young sediment is much affected by the amount of included water, then it is difficult to detect the displacement from the difference of the physical property of the sediment. The present project is to search effective ways to apply these geophysical methods for the studies of active faults under thick sediments with the cooperation by governmental institutes related to the research for earthquake prediction.

The following is a short summary of the present research.

Gravity Survey

Areal distribution of gravity anomalies reflects the geological structure of the underground, so it is possible to know the depth of base rock and its fall-off by surveying the gravity values minutely. Therefore, the Geographical Survey Institute is now doing gravity surveys with the allotting of one point at every 1 Km in the metropolitan area. Fig. 4, is the preliminary result of the survey. The figure is made by filtering out long wave component in the bouguer anomaly. As seen in the figure, a linear structure of the bouguer anomaly extending in the west-east direction is remarkable in the northern part of the Kanto plain.

As mentioned previously, the strikes of the active fault known in the southern Kanto district are NW-SE direction, so the line like anomaly found by the gravity survey is noteworthy.

Micro Earthquakes

In western Japan where the depth of base rock is very shallow, the activity of micro earthquakes has a close relation with active faults, that is, many micro earthquakes along active faults are observed. Such phenomena, however, have not yet been known in eastern Japan. Recently, a linear distribution of micro earthquakes of shallow depth was found by the observations of very high sensitivity at Iwatuiki in the area where an active folding is estimated, and the distribution of the micro earthquakes is well accordant with this active folding.

At present, any micro earthquake activity is not known along the Techikawa fault and the Arakawa fault, but there is a possibility that micro earthquakes might be observed there when the observation net is well established.

Elastic Wave Prospecting

Elastic waves are effective means to prospect underground structures, but there are problems when it is applied for the research on active faults in the urban area, that is, it is difficult to use gunpowder as a source of elastic wave, so it is necessary to search for another source usable in the urban area. Another problem is that physical property of shallow sedimental layer is much affected by the ground water and also contrasts between the sediments are very small. It is, therefore, necessary to develop a new receiving system of high resolving power and the way of data analysis. The Geological Survey of Japan is now developing a new system of elastic wave sounding for active fault under sedimental layer.

Electrical Method

This is an effective way to research active faults from the difference of electric property such as resistivity in the sedimental layers, but there are many artificial disturbances in the measurements of the resistivity in urban areas, so it is necessary to eliminate artificial noises in the measurement. The Geomagnetic Observatory of Kakioka is now studying a method to search an active fault by the measurement of ground resistivity and other electric properties of the ground.

Conclusive Remarks

At present, there is no definitive method to detect active faults covered by thick sediment. The geophysical methods are useful ways to search ground structure through the sediment, but they have difficult problems to solve when they are applied for the research on active faults, and geochemical methods should be considered. Aside from these geo-physical and chemical methods, geological drilling and topographical research have to be conducted by a new approach for the research. We expect much progress in the research on active faults, as well as in earthquake hazard mitigation in the metropolitan area, by synthesizing the studies from the present project.

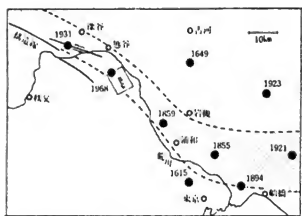
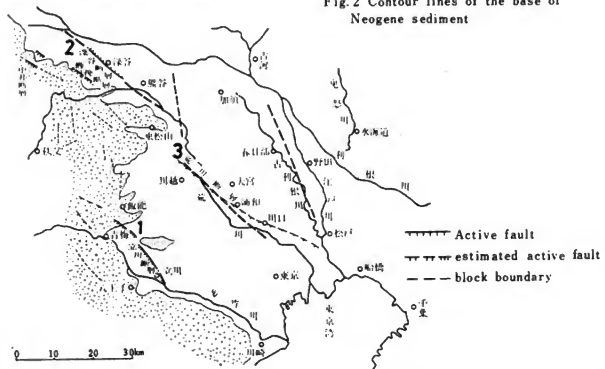


Fig. 1 Destructive earthquakes and estimated tectonic line in the metropolitan area



Fig. 2 Contour lines of the base of Neogene sediment



Name	Strike	Length	Mean Displacement Velocity
1. Tachkawa	N 45 W	20 Km	0.2/1000
2. Fukaya	N 50 W	10 Km	0.2/1000
3. Arakawa	N 50 W	?	0.1 0.2/1000

Fig. 3 Active faults and block boundaries in the Kanto District



Fig. 4 Tachikawa fault

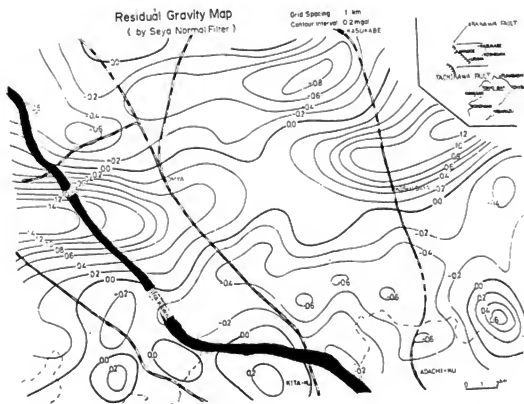
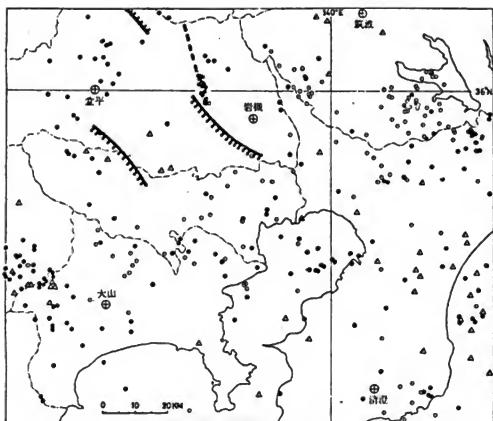


Fig. 5 Distribution of gravity anomaly in the metropolitan area



期間1974年12月～1976年1月

△ 0～5 km
 focal depth ● 0～30km
 ○ 30～40km

Fig. 6 Distribution of micro-earthquakes in Kanto District.

CHARACTERISTICS OF VERTICAL COMPONENTS

OF STRONG-MOTION ACCELEROGRAMS

Tatsuo Uwabe

Setsuo Noda

Eiichi Kurata

and

Satoshi Hayashi

Port and Harbour Research Institute

ABSTRACT

Characteristics of vertical components of the 574 strong-motion accelerograms were studied in order to determine the effects of vertical ground motions on dynamic stability of structures. The following were made clear.

1) According to accelerograms with the maximum acceleration of over 50 gals the ratio of the maximum acceleration on the vertical component to that on the horizontal component was less than 1/2.

2) The occurrence time of the maximum acceleration on the horizontal component was different from that on the vertical component. At the time when the safety factors against sliding and overturning were the smallest, the ratio of the vertical acceleration to the horizontal acceleration was less than 1/3.

3) The stability analysis of the gravity type quaywalls based on a current design method of port facilities was performed considering the vertical seismic coefficient. Consequently, the vertical seismic coefficient was found to have little influence on the safety factor for gravity type quaywalls.

KEYWORDS: Design; horizontal acceleration; seismic coefficients; stability; strong-motion accelerogram; structures; vertical acceleration.

INTRODUCTION

A ground motion during an earthquake consists of a vertical component besides horizontal components. It is generally recognized that vertical accelerations usually have smaller amplitude and higher frequency components as compared with horizontal accelerations, hence the vertical accelerations have little influence on stability of civil engineering structures and buildings. However, it is pointed out from the case studies of damage records that the vertical motion might have severe influence on the stability of structures in some cases.

According to the present methods of earthquake resistant design, the vertical motion is considered as a vertical seismic coefficient in some cases, and in other cases it is not clearly provided but indirectly included in design conditions. Because of insufficient data on the vertical motions during earthquakes, the effects of the vertical motion in the design procedures are not based on enough information on amplitude and frequency characteristics of the motion but are decided from a sort of empirical knowledge on dynamic characteristics and stability of structures as a whole.

In order to collect more reliable data for a seismic design, such engineering features of vertical motions as amplitude, predominant frequency, ratio of vertical acceleration to horizontal ones are investigated by using strong-motion accelerograms. Furthermore, for the purpose of clarifying the effects of vertical motion on stability of structures, gravity type quaywalls which are typical type among harbour structures are analyzed by present design procedures based on a seismic coefficient method (1).

STRONG-MOTION ACCELEROGRAMS

Strong-motion accelerograms used in this paper are drawn from "Annual Report on Strong-Motion Earthquake Records in Japanese Ports" (2) published annually by the Port and Harbour Research Institute, Ministry of Transport and also from "Strong-Motion Earthquake Records from Public Works in Japan" (3) by the Public Work Research Institute, Ministry of Construction. Maximum amplitude of accelerograms used herein is over 10 gals in either of the two horizontal components. The 294 records during May 1963 to December 1974 are selected from the publications by PHRI and the 280 records during January 1968 to December 1973, from the publications by PWRI. Table 1 shows the number of records in each maximum acceleration range. Additionally, most of these were recorded by SMAC-B₂ accelerograph, of which specifications are listed in Table 2. Because of limited time for analysis, only 25 records published already by PHRI are used in the study based on the digitized vertical components. The digitized accelerograms are listed in Table 3.

INVESTIGATION ON CHARACTERISTICS OF VERTICAL ACCELERATION

Ratio of Maximum Vertical Acceleration to Maximum Horizontal Acceleration

As shown in Fig. 1 maximum vertical acceleration (A_{vmax}) is compared to the maximum horizontal accelerations (A_{hmax}) for all 574 records. In this figure ratios of the former to the latter (A_{vmax}/A_{hmax}) are also indicated by straight lines. Fig. 2 shows a frequency

distribution of the ratios A_{vmax}/A_{hmax} for all records and also shows the frequency in each acceleration range. In these records the 3 records show particularly large ratios, that is, 1.30, 1.60 and 1.67. According to Fig. 1 the ratios A_{vmax}/A_{hmax} are less than 1/2 for most records of which maximum horizontal accelerations are over 50 gals. In this case the maximum horizontal acceleration means the larger one in the two horizontal components. But the real horizontal acceleration in each instant must be the resultant of these components, and the maximum resultant acceleration in the horizontal direction is always larger than the maximum horizontal acceleration and becomes 2 times in the largest case. Therefore, the ratio A_{vmax}/A_{hmax} becomes smaller, if the maximum resultant acceleration is used instead of the maximum horizontal acceleration.

Factors Having Influence Upon Ratio of Maximum Vertical Acceleration to Maximum Horizontal Acceleration

As shown in Fig. 1 the ratios A_{vmax}/A_{hmax} are widely scattered. If it is made clear what factors have influence upon the ratio, it may give useful information for the earthquake resistant design. Since phenomena of ground motion during earthquakes are very complicated, mathematical and statistical studies are desirable for estimating the factors correctly. Prior to such approach, the influence of various factors including maximum horizontal acceleration, epicentral distance, magnitude of earthquake, subsoil condition and others on the ratio A_{vmax}/A_{hmax} are preliminarily investigated hereinafter.

(1) Maximum Horizontal Acceleration

In Fig. 1 the ratios A_{vmax}/A_{hmax} are fairly scattered in case of small maximum horizontal accelerations and decrease to almost less than 1/2 in case of large maximum horizontal acceleration.

(2) Epicentral Distance

Fig. 3 shows the distributions of the ratios A_{vmax}/A_{hmax} in relation to the epicentral distance for all records, and Fig. 4 also shows the ratios for the records with the maximum horizontal acceleration of over 50 gals. Both in Fig. 3 and Fig. 4 the ratios tend to scatter and show no definite correlation with the epicentral distance. But, for extremely short distance the ratios become over 1, and this fact may be worthy of attention for considering the near epicentral area.

(3) Magnitude of Earthquake

In Fig. 5 the ratios A_{vmax}/A_{hmax} which are obtained from records with the maximum horizontal acceleration of over 50 gals are against the magnitude of earthquakes. It is shown in Fig. 5 that there is no particular feature in the relationship between the ratio and the magnitude of earthquakes.

(4) Subsoil Condition

Accelerograms which were collected by the Port and Harbour Research Institute are used for investigation on subsoil conditions. As shown in Table 4 the sites of the observation stations are classified into three groups which were already reported in the study on the average response spectra of the horizontal components of the accelerograms at the sites (4). The relationship between A_{vmax} and A_{hmax} in each group is shown in Figs. 6 to

8, and the ratios $A_{v\max}/A_{h\max}$ are similarly plotted to the epicentral distance. But there is no significant difference in characteristics among these groups.

(5) The Others

Wakayama zi-S station in the observation network of the PHRI and Kinokawa-ohashi station (Station No. 112) of the PWRI observation network are only 1.4 km away from each other and succeeded to record the ground motions during the same earthquakes. Fig. 9 shows the observation results from these stations. In the figure the results are respectively numbered in sequence of date of earthquake events for each station but the same numbers are used for records by the same events. In the case of the epicentral distance of 5.2 km the ratios $A_{v\max}/A_{h\max}$ which are obtained from earthquake magnitude of 3.6 to 5.0 are fairly well scattered. Comparing the results at both stations from the same earthquakes, the ratios are similarly over 1.0 for the event No. 5 and less than 0.5 for the event No. 9. Fig. 10 shows the observation results at several stations during a great earthquake (1968 Tokachi-oki earthquake, Magnitude: 7.9). In the figure the ratios $A_{v\max}/A_{h\max}$ tend to scatter, even though they were recorded at stations of similar epicentral distance.

Phase Difference Between Maximum Vertical Acceleration and Maximum Horizontal Acceleration

According to the strong-motion accelerograms, it appears that the occurrence time of the maximum horizontal acceleration does not usually coincide with that of the maximum vertical acceleration. Therefore, discussion based on the maximum accelerations of both components is to be presented toward the most extreme case in which both of the maximum accelerations occur at the same time. This assumption is on the safe side from the viewpoint of design. But, for rational earthquake resistant designs it is desirable to make clear by the observed data whether both the maximum accelerations occur at the same time or not. The following investigation is performed on the ratio of the vertical acceleration to the horizontal acceleration (A_v/A_h) when the structure becomes the most unstable.

In order to make the problem simpler, a stability of a rigid block on a solid plane is analyzed by the seismic coefficient method. A resultant force due to gravity and seismic force, and its direction are expressed by the following equations,

$$R = mg\sqrt{(1+k_v)^2 + k_h^2} \quad (1)$$

$$K = \tan \theta = \frac{k_h}{1+k_v} \quad (2)$$

where R = resultant force acting on the block

m = mass of the block

g = acceleration of gravity

k_v = seismic coefficient in the vertical direction

k_h = seismic coefficient in the horizontal direction

K = resultant seismic coefficient

θ = angle between directions of resultant force and gravity

The block becomes more unstable with increase of the resultant seismic coefficient. From the digitized records listed in Table 3 the resultant accelerations of the two components in the horizontal direction are calculated and the resultant seismic coefficients at each instant are obtained from the equation (2), in which the resultant acceleration in the horizontal direction and the vertical acceleration are introduced. When the resultant seismic coefficient becomes maximum, the block is in the most unstable condition against sliding and overturning. Fig. 11 shows the vertical acceleration (A_v) and the horizontal acceleration (A_h) for this maximum condition. Usually maximum resultant seismic coefficient occurs when the horizontal acceleration is almost maximum but the corresponding vertical acceleration is not so large. If the difference of the occurrence time between $A_{v\max}$ and $A_{h\max}$ is taken into consideration, the ratios $A_{v\max}/A_{h\max}$ become almost less than 1/3.

Frequency Characteristics of Vertical Acceleration

Fourier spectra and response spectra of the digitized records are calculated. In this case the minimum epicentral distance is 14 km, and then the records from the near epicentral area are not included. Judging from Fourier spectra of 20 records out of total 25 records, it was not found that the vertical motion may contain higher frequency components in comparison with the horizontal motion. As an example of the results the spectra of the three components having similar shape are shown in Fig. 12. Response spectra for relative displacement, relative velocity and absolute acceleration are also calculated. According to the calculation the spectra of the vertical component and the horizontal components are almost similar in shape except 6 records out of 25. Fig. 13 shows a typical example of the absolute acceleration spectra similar in shape and Fig. 14, an example of the spectra different in shape. Owing to the limited number of records available, it is not recognized that there were any particular influences by subsoil conditions and earthquakes on spectra.

Accelerograms at Wakayama Port on March 30, 1968

Strong-motion accelerograms shown in Fig. 15 were recorded at Wakayama port (epicentral distance: 5.2 km, Subsoil condition: group B) in Wakayama city during a local earthquake (magnitude: 5, focal depth: 0 km) on March 30, 1968. The maximum acceleration of N-S component was 176 gals, 253 gals in E-W component and 405 gals in vertical component. Notable feature of the record was very large vertical acceleration in comparison with the horizontal acceleration. Although the principal part of the vertical component did not come out clearly in Fig. 15, it consisted of fairly high frequency components of about 20 Hz. The maximum accelerations both in the vertical and the horizontal directions occurred at different instants, that is, the horizontal acceleration was about 25 gals when the maximum vertical acceleration occurred and the vertical acceleration was about 40 gals when the maximum horizontal acceleration occurred.

What is specially noteworthy is the fact that none of the facilities at Wakayama port were damaged by the earthquake in spite of the fairly large acceleration on the vertical component and the relatively large acceleration on the horizontal components. It is consequently recognized that the earthquake motion with fairly high frequency components and

the different occurrence time on the maximum accelerations both in the horizontal and in the vertical direction do not have so much influence on the stability of the structures.

INFLUENCE OF VERTICAL ACCELERATION ON STABILITY OF GRAVITY TYPE STRUCTURES

Influence on Safety Factor Against Sliding for Rigid Block

When both the horizontal and the vertical accelerations exist, a safety factor against sliding for such a rigid block as concrete caisson on a firm ground is expressed by the following equation,

$$SF = \frac{(1-k_v)}{k_h} \quad (3)$$

where SF = safety factor against sliding

= coefficient of friction between block and ground

k_h and k_v = seismic coefficients in horizontal and in vertical direction, respectively. Three kinds of situations are considered for the calculation of safety factors against sliding for block. In the first situation, only the horizontal seismic coefficient corresponding to A_{hmax} is taken into consideration. The second situation is when the safety factor is the minimum value by the equation (3) in which the seismic coefficients are equivalent to the resultant horizontal acceleration and the vertical acceleration in each instant. In the third situation, the safety factor is calculated by the equation (3) in terms of the seismic coefficients corresponding to A_{hmax} and A_{vmax} . For the comparisons of safety factors in three situations, A_{hmax} is normalized as 250 gals and the coefficient of friction is assumed to be 0.6 for all cases.

If the safety factor in the second case is assumed to be rational for the stability analysis of structures during earthquake, the safety factor in the first case is overestimated about 4% and is underestimated about 5% in the third case. These results, though obtained in the particular conditions will provide some information on the influence of the vertical acceleration on the stability of structures.

Influence on Stability of Gravity Type Quaywall

Referring to the investigation mentioned above, the influence of the vertical acceleration on the stability of gravity type structures will be discussed with the aid of the present design procedures. The gravity type quaywalls are selected for discussion. In the present design procedures of port facilities (5) the seismic coefficient in the vertical direction is not considered. This conception is not based on the investigation of the earthquake records but on the empirical judgment that the effects of the vertical acceleration on the stability of structures will be compensated by applying a proper value of seismic coefficients in the horizontal direction. Therefore, safety factors considering the vertical seismic coefficient will be examined using the present design procedures.

Model quaywalls are shown in Figs. 16 and 17. One is a common size of wall with a water depth of -5.5 m, the other is a relatively large wall with a water depth of -12 m. In the stability analysis the horizontal seismic coefficient are changed as 0.15, 0.10 and

0.05, and the vertical seismic coefficients are fixed as one half of the horizontal one in both the upward and downward directions. Such design conditions as crown height, sea water level, angle of friction of backfill soil, surcharge, ratio of width to height of caisson and residual water level are also changed in several ways. Safety factors against sliding and overturning, and bottom reaction are calculated, and their changes due to the vertical seismic coefficient are also examined.

According to the analysis, the vertical seismic coefficient acting in the upward direction reduces the safety factors and the rate of reduction of the safety factors increases proportionally with increase in the horizontal seismic coefficient. For example, safety factors in which the vertical seismic coefficient are considered decrease 1.5% in the case of the horizontal seismic coefficient of 0.05 and 10% in the case of 0.20 in comparison with the cases in which the vertical seismic coefficient is not considered. These rates of the reduction of safety factors remain unchanged, even if the design parameters except the horizontal seismic coefficient are changed. It is indicated that bottom reactions vary complicatedly with the direction of the vertical seismic coefficient and other design parameters. The rate of change of the safety factors is commonly within several percents, but in special cases it changes up to 20% for the structure with a safety factor of 1.0 against sliding.

This discussion is limited to the particular condition in which the vertical seismic coefficient is one-half of the horizontal one. But the influence of the vertical motion on safety factors and bottom reaction will certainly decrease in the case when the difference of occurrence time between $A_{h\max}$ and $A_{v\max}$ is taken into consideration. From the analysis above, it will be concluded that the vertical component of earthquake motion may give only a small variation, less than several percents, in safety factors for gravity type structures, and in the practical design it is possible to compensate this degree of small variation by applying a proper value of horizontal seismic coefficients.

CONCLUSIONS

- 1) According to the accelerograms of the maximum horizontal acceleration of more than 50 gals, the ratio of the maximum acceleration on the vertical component to that on the horizontal component (greater acceleration on the resultant of two horizontal components) is less than 1/2.
- 2) Any significant relationship can not be found between the ratio of the maximum vertical acceleration to the maximum horizontal acceleration and the factors such as maximum horizontal acceleration, epicentral distance, magnitude of earthquake and subsoil conditions at the sites.
- 3) The ratios of the maximum vertical acceleration to the maximum horizontal acceleration are fairly scattered in the accelerograms which are recorded at stations during earthquakes with almost the same epicentral distance and the same magnitude.
- 4) The occurrence time of the maximum acceleration on the horizontal component is different from that on the vertical component. At the time when the safety factors against

sliding and overturning for gravity type structures are the smallest, the ratio of the vertical acceleration to the horizontal acceleration is less than 1/3.

5) Fourier spectra and response spectra of the vertical component and the horizontal components of the earthquake motions in which epicentral distances are more than 14 km show almost similar frequency characteristics.

6) During a local earthquake near Wakayama city on March 30, 1968, the accelerogram with the vertical component of 405 gals was recorded at Wakayama port with the epicentral distance of 5.2 km. Inspite of the fairly large vertical acceleration, none of the facilities at the port were damaged.

7) Using the present design method for harbour structures, the stability analysis for gravity type quaywalls was performed in order to examine the effect of the seismic coefficient in the vertical direction. So far as the quaywalls investigated herein are concerned, the vertical seismic coefficient has not so considerable influence on the stability.

ACKNOWLEDGEMENT

This report is indebted to the fruits of projects on observation of strong-motion earthquakes. The authors wish to express their thanks to persons concerned in the networks on the Port and Harbour Research Institute and the Public Work Research Institute.

REFERENCES

- (1) Tatsuo Uwabe, Setsuo Noda and Eiichi Kurata: Characteristics of Vertical Components of Strong-Motion Accelerograms and Effects of Vertical Ground Motion on Stability of Gravity Type Quay Walls, Report of the Port and Harbour Research Institute, Vol. 15, No. 2, June 1976, pp. 289-317.
- (2) Annual Report on Strong-Motion Earthquake Records in Japanese ports, Technical Note of the Port and Harbour Research Institute, Ministry of Transport, No. 10, No. 15, No. 55, No. 62, No. 64, No. 80, No. 98, No. 100, No. 116, No. 136, No. 160, No. 181, No. 202.
- (3) Strong-Motion Earthquake Records from Public Works in Japan, Technical Memorandum of Public Work Research Institute, Ministry of Construction, No. 430, No. 641, No. 718, No. 815, No. 913, No. 967.
- (4) Satoshi Hayashi, Hajime Tsuchida, Eiichi Kurata: Average Response Spectra for Various Subsoil Conditions, Third Joint Meeting, U.S.-Japan Panel on Wind and Seismic Effects, UJNR, May 1971.
- (5) Design Manual of Harbour Structures in Japan, The Japan Port and Harbour Association, April 1967.

Table I Number of Accelerograms

Max. acceleration range in gals	Number of accelerograms		
	PHRI (Mar. 1963 - Dec. 1974)	PWRI (Jan. 1968 - Dec. 1973)	Total
10 - 20	135	103	238
20 - 50	106	114	220
over 50	53	63	116
Total	294	280	574

Table 2 Specifications of SMAC-B₂ accelerograph

Number of elements	Natural period of pendulum (sec)	Damping constant	Sensitivity (gal/mm)	Max. recording acceleration (gals)
2 in horizontal 1 in vertical	0.14	critical damping	12.5	500
Recording system	Recording speed (mm/sec)	Recording time (min)	Timing (sec)	Dimension of instrument (cm)
Scratching stylus paper	10	3	1	54 x 54 x 37

Table 4 Stations classified by subsoil condition

Group	Subsoil condition	Station
A	Rock, very dense granular layer with N value of over 50	Miyako-S, Kashima-S, Kushiro-S, Koken-S, Ofunado-bochi-S, Akita-S
B	Sandy, silty and clayey layer with medium density except group A and C	Muroran-S, Hachinohe-S, Shiogama-S, Tomakomai-S, Shiogamakojo-S, Onahama-S, Chiba-S, Keihinji-S, Shinagawa-S, Yamashitahen-S, Tagonoura-S, Shimizukojo-S, Kinuura-S, Nagoyazokan-S, Yokkaichijii-S, Yokaiichichitose-S, Kobeji-S, Hiroshima-S, Kochi-S, Hososhima-S, Kanazawa-S, Sakata-S, Wakayamaji-S, Tsuruga-S, Ofunado-S, Kashinaji-S, Okitsu-S
C	Loose sandy layer with N value of less than 5.	Aomori-S, Kagoshima-S

Table 3 Strong-motion accelerograms including digitized vertical component

Observation station	Record number	Strong-motion accelerogram			Earthquake data					
		Max. acceleration (gal)		epicentral distance (km)	date and time		north latitude (degree)	east longitude (degree)	focal depth (km)	magnitude
		N-S	E-W	U-D						
Kushiro-S	S-634	68.0	64.7	21.3	183	1971. 8. 2. 16.25	41.5	143.4	60	7.0
	S-674	94.1	66.3	25.0	74	1972. 5. 11. 9.45	42.5	145.0	40	5.8
	S-733	166.0	120.0	56.3	132	1973. 6. 17. 12.55	42.9	146.0	40	7.1
	S-741	56.9	49.8	15.0	173	1973. 6. 24. 11.43	42.9	146.5	30	7.1
	S-804	13.8	13.8	6.3	146	1974. 1. 25. 4.13	41.7	144.0	40	6.0
Tomakomai-S	S-877	62.3	53.2	12.5	15	1974.11. 9.16.23	42.6	141.8	120	6.5
	S-235	207.7	179.9	131.0	243	1968. 5. 16. 9.49	40.7	143.7	20	7.9
Hachinohe-S	S-670	49.6	56.5	21.3	85	1972. 3. 20. 0.58	41.0	141.8	40	6.4
	S-252	232.7	180.6	88.0	188	1968. 5. 16. 9.49	40.7	143.7	20	7.9
	S-669	54.3	44.8	23.8	57	1972. 3. 20. 0.58	41.0	141.8	40	6.4
	S-857	61.2	49.1	17.5	53	1974. 9. 4. 18.20	40.1	141.7	20	5.6
	S-786	36.8	60.7	25.0	46	1973.11.19.22. 2	38.8	142.2	20	6.4
Kashima-kojo-S	S-782	46.1	55.6	27.5	111	1973.11.19.22. 2	38.8	142.0	20	6.4
	S-612	41.2	54.1	20	42	1971. 6. 13. 13. 6	36.2	141.0	40	5.3
	S-647	34.3	127.4	12.5	17	1971.10.11.19.16	35.9	140.5	40	5.2
	S-770	28.8	70.0	10.0	26	1973. 9. 30.13.18	35.7	140.7	40	5.9
	S-813	35.8	98.1	11.3	38	1976. 3. 3. 13.50	35.6	140.8	40	6.1
Kehin-Yamashita	S-845	48.8	31.6	13.8	82	1974. 7. 8. 14.45	36.4	141.4	20	6.3
	S-882	67.6	75.2	20.0	47	1974.11.16. 8.32	35.8	141.2	40	6.1
	S-658	53.1	46.9	12.5	282	1972. 2. 29.18.23	33.3	141.3	40	7.0
Nagoya-Zokan-S	S-585	81.3	76.0	22.5	59	1971. 1. 5. 6. 9	34.4	137.2	40	6.1
	S-578	45.5	53.3	15.6	82	1971. 1. 5. 6. 9	34.4	137.2	40	6.1
	S-577	86.0	79.5	32.5	80	1971. 1. 5. 6. 9	34.4	137.2	40	6.1
	S-788	55.3	55.3	23.8	42	1973.11.25.18.19	33.9	135.4	40	5.8
	S-655	21.4	72.9	5.0	14	1972. 2. 17. 7. 5	39.8	140.0	20	4.0

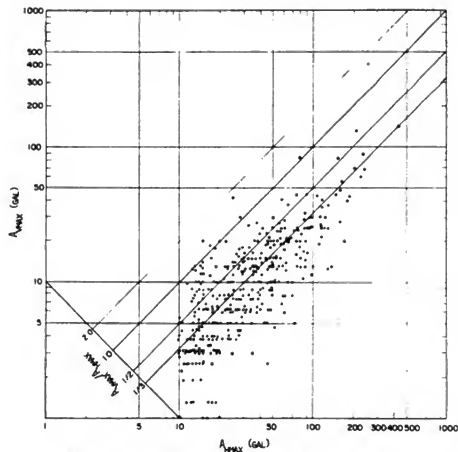


Fig. 1 Relationship between max. vertical acceleration ($A_{v\text{max}}$) and max. horizontal acceleration ($A_{h\text{max}}$)

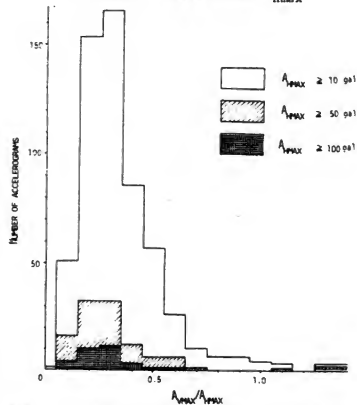


Fig. 2 Frequency distribution of ratios of max. vertical acceleration to max. horizontal acceleration ($A_{v\text{max}}/A_{h\text{max}}$)

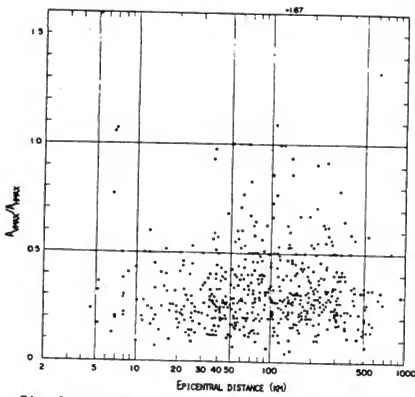


Fig. 3 Distribution of ratios of max. vertical acceleration to max. horizontal acceleration ($A_{v\text{max}}/A_{h\text{max}}$) to epicentral distance

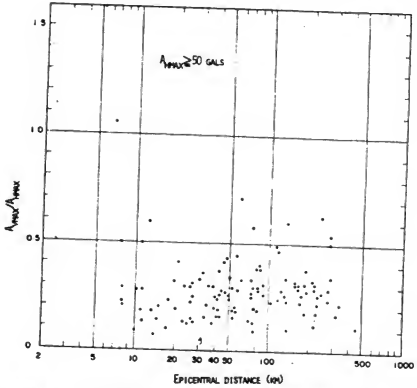


Fig. 4 Distribution of ratios of max. vertical acceleration to max. horizontal acceleration ($A_{v\text{max}}/A_{h\text{max}}$) to epicentral distance, $A_{h\text{max}} \geq 50$ gals

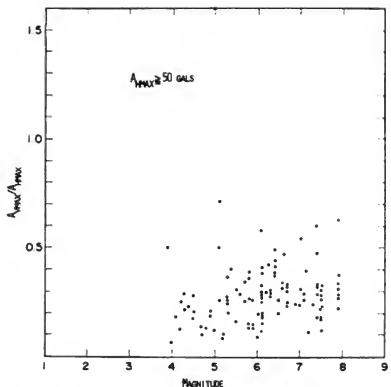


Fig. 5 Distribution of ratios of max. vertical acceleration to max. horizontal acceleration ($A_{v\text{max}}/A_{h\text{max}}$) to magnitude of earthquake

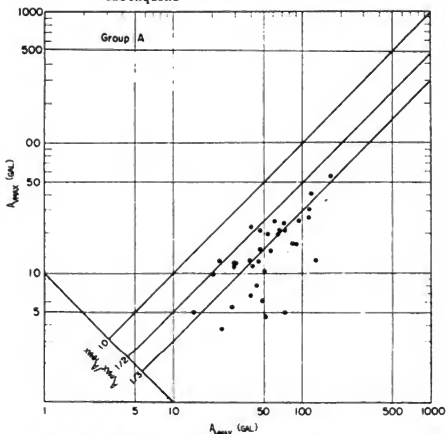


Fig. 6 Relationship between max. vertical acceleration ($A_{v\text{max}}$) and max. horizontal acceleration ($A_{h\text{max}}$), for Group A

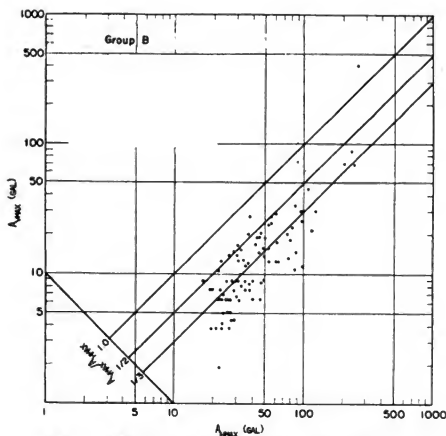


Fig. 7 Relationship between max. vertical acceleration ($A_{v\text{max}}$) and max. horizontal acceleration ($A_{h\text{max}}$), for Group B

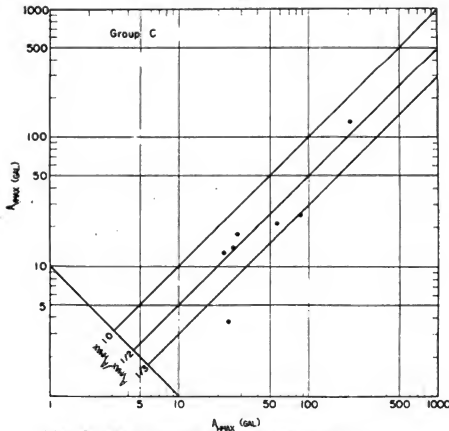


Fig. 8 Relationship between max. vertical acceleration ($A_{v\text{max}}$) and max. horizontal acceleration ($A_{h\text{max}}$), for Group C

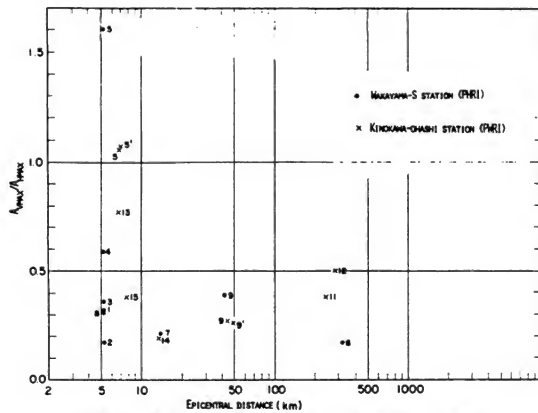


Fig. 9 Ratios of max. vertical acceleration to max. horizontal acceleration (A_{vmax}/A_{hmax}) at Wakayama-zi-S station

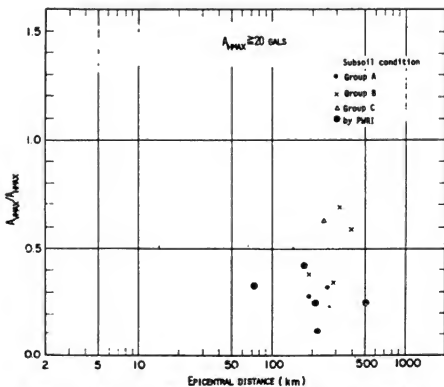


Fig. 10 Ratios of max. vertical acceleration to max. horizontal acceleration (A_{vmax}/A_{hmax}) during Tokachi-oki earthquake in 1968

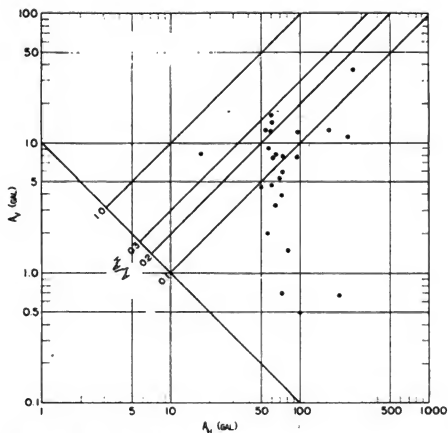


Fig. 11 Relationship between vertical acceleration (A_v) and resultant horizontal acceleration (A_h) corresponding to max. resultant seismic coefficient

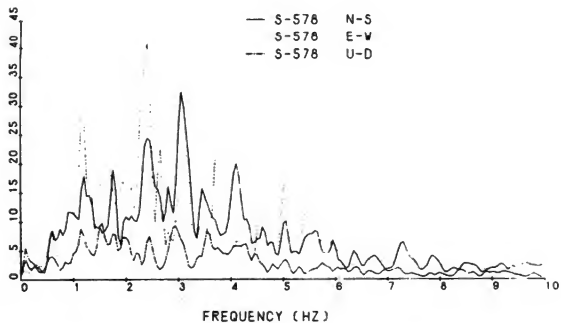


Fig. 12 An example of Fourier spectra similar in shape

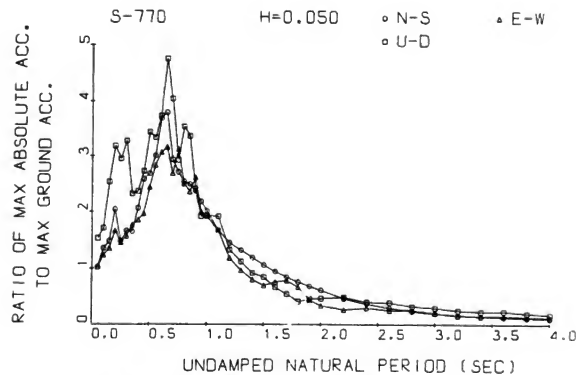


Fig. 13 An example of response spectra similar in shape

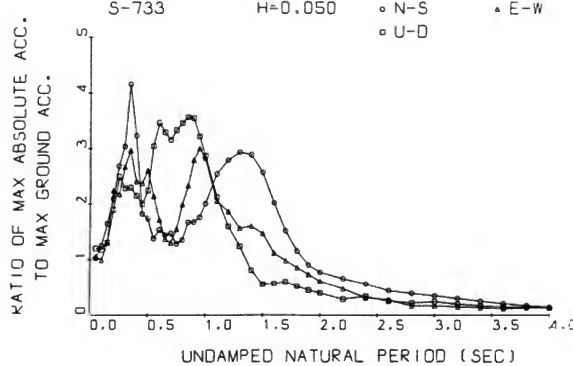


Fig. 14 An example of response spectra different in shape

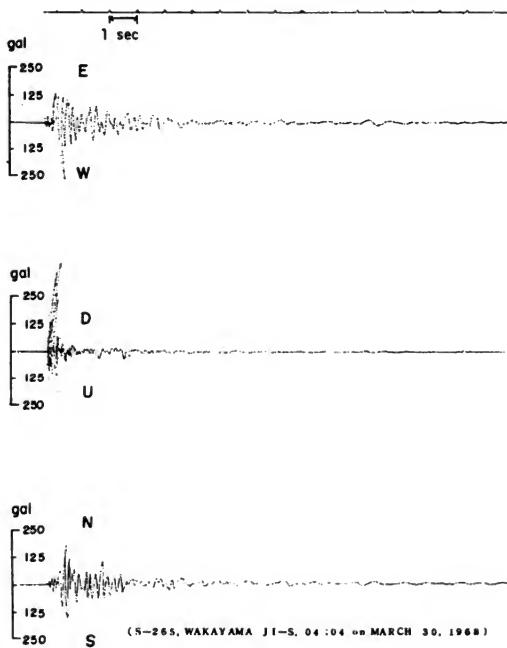


Fig. 15 Accelerograms recorded at Wakayama port

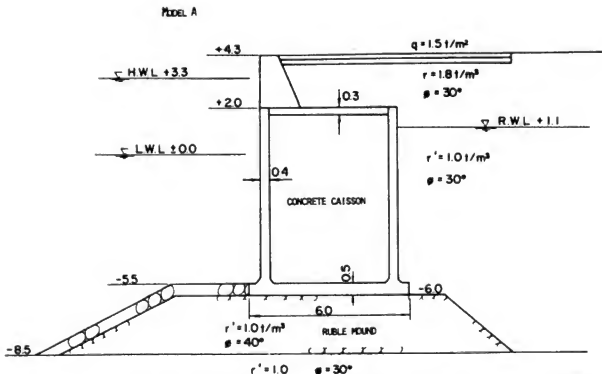


Fig. 16 Cross section of gravity type quaywall,
sea water depth of -5.5 m

Model B

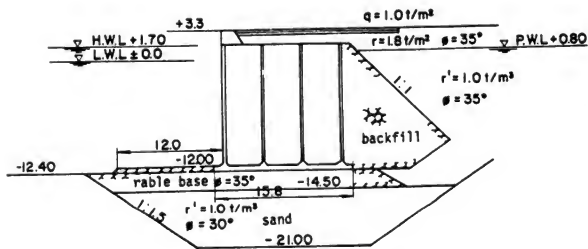


Fig. 17 Cross section of gravity type quaywall,
sea water depth of -12 m

Developments in Strong-Motion Data Management

A. GERALD BRADY
U.S. Geological Survey, Menlo Park, California

ABSTRACT

Some recent developments in the procedures for digitization and subsequent analysis of strong-motion earthquake accelerograph records are described. The standard digitizing and analysis procedures of the California Institute of Technology's Earthquake Engineering Research Laboratory have been well documented for several years now and apply well to the long-duration, high-amplitude recordings that were the main content of the project. This paper provides further descriptive material dealing with the care needed in using standard analysis procedures on records which cannot be described as standard. In particular, short duration records, where except for a few peaks the amplitudes are low, have noise problems that can only be reduced by considerable reduction of the frequency range containing valid data. The Seismic Engineering Branch of the U.S. Geological Survey, in continuing the digitization and analysis of significant records, has modified the standard procedures where experience has shown such adjustments are necessary, and plans to make further modification where appropriate.

INTRODUCTION

Strong-motion earthquake accelerograph records have been digitized with various techniques since significant ones were first recorded. A detailed description of the methods used over the years up to the present day would show the gradual improvement in digitizing during this time, indicative of the concern amongst users of this data for the extraction of the maximum amount of information. This quest continues, and indeed it is obvious that any report describing "current" techniques under such circumstances must be expected to appear immediately out of date to some readers. The digitizing of records has been carried out, in the main, in order to analyse them more thoroughly than can be

KEYWORDS: Accelerograms, Digitization, High Frequencies, Low Frequencies

done by visual study. Of interest has been the time history of ground velocity and displacement, the frequency content of the different bursts of energy in the record, and the effects on simple idealized structures assumed to be excited by the ground motion, and portrayed in response spectra.

By the early 1960's it was realized that the results of most analyses of digitized records depended to an appreciable extent on the individual technique of the people doing the digitizing and planning the subsequent computer analysis. A comparative digitizing effort, carried out by research staff at Caltech, U.C. Berkeley, the University of Michigan and the University of Illinois, clarified a number of points pertaining to the digitizations and analyses.¹ At that time parabolic corrections were made to the accelerations, and calculations of displacement showed up the dependence of these displacements on the details of the computing techniques. Response spectra calculations were also shown to depend on such parameters as the integration step length and the record duration, as well as the obvious basic dependence on the digitizer of the original record.

In 1968 Caltech's Earthquake Engineering Research Laboratory embarked on a digitization and analysis project whose main goal was to provide data in digital form by standard procedures developed over the early stages. Reports² and magnetic tapes containing the data from 381 digitized records were distributed throughout the country and to some overseas destinations, and their use attest to their acceptance. Procedures are fully described in the reports for digitization of the various types of records making up the total, and for routine analyses. These standard analysis procedures include the following:

1. Preparation of uncorrected scaled data by making use of time marks and fixed traces where available.

¹A. G. Brady, "Studies of Response to Earthquake Ground Motion," EERL Report, Calif. Inst. of Tech., Pasadena, Calif. (1966)

²"Strong Motion Earthquake Accelerograms," Vol. I, Part A (Report No. EERL 70-20), Vol. II, Part A (Report No. EERL 71-50), Vol. III, Part A (Report No. EERL 72-80), Vol. IV, Part A (Report No. EERL 72-100), Calif. Inst. of Tech., Pasadena, Calif. (1970-1972)

2. Preparation of corrected data by making use of the instrumental constants in an instrument correction, and by removal of high frequency and low frequency noise in a band pass filtering operation.
3. Calculation of response spectra for five different values of damping and over a frequency range equal to that of the pass band used in the correction stage.
4. Calculation of the Fourier amplitude spectrum of the record by use of Fast Fourier Transform techniques.

Many countries in seismic areas of the world have similarly embarked on the planning and installation of instrumentation networks and have subsequently developed analysis techniques for use on those significant records that they have recovered and digitized. The Caltech project has frequently been used as a standard guide for these endeavors and has served well in this capacity when care has been exercised in transferring the procedures to the users particular circumstances.

DIGITIZATION

An appreciable amount of information can be obtained from the record before any digitization attempt. Peak values of acceleration can be scaled off, using the sensitivity of an individual transducer's mechanical and optical properties. The total duration of the instrumental record can be determined from the time marks. The duration of various levels of strong-motion can be determined, such as the length of time between the first and last amplitudes of 100 cm/sec^2 (or $0.1g$). In some cases where the instrument has been triggered by the first vertical accelerations reaching it, (P waves), and the horizontal components show S wave arrivals clearly, then S-T times can be read off for use in epicenter determinations and other travel time calculations.

Engineering uses of accelerogram records prior to digitizing is limited to the investigation of upper story records where modal vibrations of a structure become apparent, particularly after the first transient motions have dissipated. Some preliminary estimates of mode shapes, depending on the number of records throughout the height of the structure, and of their natural frequencies, can be made. This allows calculation of base shears and overturning moments during normal mode vibrations as they occur during earthquake excitation.

For computer analysis of the dynamic behavior of buildings during base input motion, ground motion records must first be digitized. The records from upper levels of structures must be digitized if a detailed computer investigation is required of building motions, stiffnesses and mode shapes. Also, for investigations that require the integration of carefully prepared accelerations, for velocity and displacement time histories, the original accelerations need digitization.

High Frequency Considerations of Hand Digitizing

Hand digitizing refers for the time being to moving a cross-hair by hand, following a trace, and selecting individual points whose coordinates are recorded automatically when signalled by the operator. Subsequent computer programs, which assume that the traces are straight lines between elected points, demand that among the points chosen are all the local peaks and all changes of slope. In order that the same control on high frequency noise can be maintained throughout the duration of the digitized record the average density of selected points must be kept up in the weak-motion portions to the level maintained in the strong-motion portions.³

The following line of reasoning can now be applied to the further analysis of this raw data. Suppose for the sake of an example that the average digitizing rate of a particular trace corresponded to 50 points per second of record time, chosen because 25 Hz content was seen to be present and capable of digitizing. Portions of the record that contained 20-25 Hz signals would be digitized just at the peaks, i.e., two points per cycle, while signals at the 10 Hz frequency level would be identified with approximately 5 points per cycle. Lower frequency content, appearing smoother in the record, would be well-defined with many points per cycle. For analyses that required the highest accuracy, i.e., maintaining the accuracy already present, equal-step interpolation must be performed at a Δx equal to the least count of the digitizing machine. Otherwise, peaks will be missed during interpolation. However, a compromise must be reached because data of this density is too large in volume to handle. The compromise must consider the fact that the final data, in order to portray accurately the 25 Hz content originally

³J. B. Berrill and T. C. Hanks, "High Frequency Amplitude Errors in Digitized Strong Motion Accelerograms," in "Analyses of Strong Motion Earthquake Accelerograms", Vol. IV, Parts Q, R, and S, Report No. EERL 74-104, Calif. Inst. of Tech., Pasadena, Calif. (1974)

seen, must be at a density that offers approximately 6 points per cycle, and therefore 150 points per second. The 25 Hz content could be satisfactorily represented with 50 points per second only if each time the 25 Hz waves appeared they were always in phase with each other and their peaks occurred at multiples of 0.02 sec. This of course is never the case.

If 25 Hz is the highest frequency that can be seen and digitized, the digitization at an average density of 50 points per second will contain unacceptable digitization noise at frequencies above 25 Hz and low-pass filtering at 25 Hz is called for. Maintenance of a final data density of 150 points per second is still required.

The compromise between data density and the accuracy of peak values leads to some confusion when comparisons are made⁴ between the maximum acceleration of a record when scaled off the original (or off the raw digitized data) and the maximum acceleration after correction. If the correction procedures have required interpolation at a density with Δx greater than the least count of the machine, then it is probable that this scaled peak will be lost, and a lower peak value will result. As an example, with records containing 12-16 Hz components, whose peak accelerations occur in this frequency range, corrected data with $\Delta t = 0.02$ sec have had peak values in the range of 0.75 to 0.3 of the uncorrected peak values.

High Frequency Considerations for Machine Digitizing

Various other possibilities of selecting points are available and in use on some digitizing systems. Although the cross-hair is moved by hand along the trace in question, the automatic relaying of points into some storage device can take the form of a set number of points transferred each cm in the X-direction (i.e., Δx , or Δt kept constant) or a set number of points transferred each second of real time (in which case Δx or Δt depends on the speed of the operator following the trace).

Totally automatic digitizing can be of two principle types. The first consists of automatically scanning the entire recorded film and measuring the greyness at each matrix element location, followed by computer analysis to recover the traces. The second consists

⁴"Strong Motion Earthquake Accelerograms," Index Volume, Report No. EERL 76-02, Calif. Inst. of Tech., Pasadena, Calif. (1976)

of automatically following a particular trace having been given a starting position, and recording X and Y coordinates according to some fixed procedure.

In all of these cases, the procedure can be compared with the description in the previous section on hand digitizing and appropriate measures taken to insure that the quality of the high frequency content remaining in a record is accurately known.

LONG PERIOD ANALYSIS

The baseline correction procedure of the Caltech standard data processing project removes from the accelerogram all Fourier components with periods longer than an upper period limit chosen on the basis of careful tests. For the particular equipment used at Caltech, and for the typical records used in the project, namely with sensitivities of 7 to 14 cm/g and with record speeds of the order of 1 cm/sec, this upper limit was about 14 seconds. A filter was developed with a cut-off period of 14 sec and roll-off termination at 20 sec - the corresponding frequencies are 0.07 and 0.05 Hz. Subsequent investigations confirmed that for this typical Caltech data the errors in the 14 or 16 second components could be up to 4 cm of displacement, while errors in the 8 second components were of the order of 1 cm of displacement.⁵ Shorter periods had correspondingly smaller errors. These displacement errors were apparent irrespective of the acceleration amplitudes, which for most of the records in the project were relatively high - the selection of the records had been originally made on the basis of peak accelerations being greater than 0.1g. It has recently become clear that for records of low acceleration amplitudes, or of accelerations of large amplitudes but corresponding to small displacement pulses as in records close in to small shocks, or in short records, some further adjustment of the long period limit is required.

Short Records

Recent experience with records shorter than approximately 60 sec has shown that the upper limit for long periods must be selected with due consideration to record length. It is not advisable to assume that a satisfactory quantitative measure of the Fourier

⁵T. C. Hanks, "Strong Ground Motion of the San Fernando, California, Earthquake: Ground Displacements," Bull. Seis. Soc. America, 65, 1, p. 193 (1975)

components with periods longer than 1/4 or 1/3 of the total record length can be obtained from any record. Consequently, for records shorter than 60 sec, revised cut-off and roll-off termination periods must be used. A suitable choice has been found to be the restriction of periods retained in the corrected data to 15 seconds or 1/4 of the record length, whichever is smaller.

Records With Small Displacements

Treatment of the long period limits in this case is rather obvious, after a few trials are run on any particular record. The long period limit must be chosen so that the errors in the displacement at this long period are negligible when compared to the actual displacements expected when the accelerogram is integrated twice. For an 8 cm/g sensitivity, use can be made of a table such as the following in order to estimate the longest period to retain:

Longest period retained (sec)	16	8	4	2	1
Expected errors in displacement (cm)	4	1	.25	.06	.015

The required ground displacements from a filtered accelerogram should be, say, 10 times these expected errors in order that the displacements retain an acceptable signal to noise ratio. Adjustments to these figures can be made for instruments with different sensitivities, and recorder speeds different from 1 cm/sec, and further adjustments of the long period limit can subsequently be made if desired in order that resulting displacements compare favorably, in amplitude and frequency content with actual displacements predicted on the basis of seismological studies.

CONCLUSIONS

This paper has discussed the areas in which it is appropriate to make some changes in the standard data processing of strong-motion earthquake records. Included have been the following conclusions:

Hand digitization of records, (trace following by hand, and points selected individually), in which the highest frequency capable of being examined and digitized is 25 Hz, should be accompanied by computer analyses which treat the data at a density of 150

points per second. Careful considerations along similar lines must be given to any digitization that is more automated.

The long period limit for corrected data must, in general, be reduced for accelerograms that are shorter than 60 sec, for accelerograms that have short duration, high amplitude pulses, corresponding to small displacement pulses, and for accelerograms with generally low amplitudes.

ON A METHOD FOR SYNTHESIZING THE ARTIFICIAL EARTHQUAKE WAVES

BY USING THE PREDICTION ERROR FILTER

Keiichi Ohtani and Shigeo Kinoshita

National Research Center for Disaster Prevention, Science & Technology Agency

ABSTRACT

Several methods for synthesizing the artificial earthquake waves have been reported for the purpose of dynamic analysis and earthquake-resistant design of structures. In the present report, the authors discuss a method by using "the prediction error filter," in which there are less numbers of the required parameters than those in other methods and also these parameters are more easily estimated. This method is based on the linear prediction model for the earthquake wave in the time domain. Therefore, parameters by which the prediction error filter is constructed are computed from the sequence of covariance matrices that represent the characteristics of earthquake waves in the time domain.

As compared with the methods using the finite Fourier expansion by harmonic functions, this method uses the finite Fourier expansion by uncorrelated random variables, and the filter is designed in the time domain. Also, the number of terms of this expansion is automatically determined by using "An Information Criterion" (AIC) proposed by Akaike. The relationship introduced by the authors for synthesizing correlated multi-dimensional waves show an example of synthesis by using an observed strong-motion accelerogram.

KEYWORDS: Accelerogram; artificial earthquake; covariance; filter; finite Fourier expansion; prediction error; random variables; synthesis; wave

INTRODUCTION

Mathematical processes of the simulation of various random phenomena have growing applications. In the field of earthquake engineering, the simulation for strong-motion earthquake waves provides a valid starting point for the dynamic analysis and the earthquake-resistant design of structures in seismic regions, and also in playing an important role in the shaking table tests. Accordingly, several methods for synthesizing artificial waves have been already reported (1). The present report discusses a simple method for synthesizing artificial waves by using the prediction error filter, in which required parameters are fewer than those in other methods and also they are easily estimated. The suggestion that the application of prediction error filter to earthquake wave would be efficient was made in two references (2,3).

In the authors' method by using the prediction error filter, a filtered white noise model is used for generating the artificial earthquake waves as shown in Fig. 1. The procedure is to use the digital computer for generating a random number, to multiply this by a gain function (i.e., a function of the covariance matrix of final prediction error), and then to pass the resultant sequence through a linear filter (i.e., the prediction error filter with the sequence of covariance matrices of a given earthquake wave). Matrices $F(n,n)$, $B(n,1)$, in which $n=1,\dots,p$, are referred to as the filter parameters, and are required in order to design this filter and to describe the characteristics of the filter. Also, the covariance matrix $S(p)$ of final prediction error is required in order to describe the characteristics of input for the filter. The induction of those matrices and the construction of the prediction error filter are discussed in sections 2 and 3, respectively.

Generally, there are two difficulties associated with the simulation of earthquake waves. One is that the two horizontal components and the vertical component of observed earthquake waves are not statistically independent. However, this difficulty is probably out of the question in this method, because correlations between these components are taken into account by designing the filter from the sequence of covariance matrices. The other difficulty is the nonstationarity of observed earthquake waves, especially because this method is based on a theory of stationary stochastic process. Assuming the frequency stationarity, the amplitude nonstationarity is induced by passing the input random number through the time-dependent function of covariance matrix of prediction error, i.e., a shape function in matrix form. On the other hand, the simulation of the frequency nonstationarity is difficult. Putting the filter parameters as time-dependent matrices, the nonstationarity representation of frequency characteristics is theoretically possible. But, generally, the time constant of prediction error filter composed from observed earthquake waves is so large that the simulated waves can not run after the variation of the original waves. However, a simulation of one dimensional nonstationary process by using the prediction error filter and the Kalman filtering technique was reported in reference 2. In the present report, the object of the author's study, i.e., the simulation of multi-dimensional artificial earthquake wave, is bound within the stationary case.

INDUCTION OF FILTER PARAMETERS AND COVARIANCE MATRIX OF PREDICTION ERROR

When a linear subspace $M(q)$ is given, the forward prediction of $X(k)$ can be defined as the projection of $X(k)$ on this subspace. Then, the forward prediction of $X(k)$,

$$\bar{X}(k; q) = \sum_{n=1}^q F(q, n) X(k-n) \quad (2.1)$$

is estimated by solving the so-called forward Yule-Walker equations.

$$\begin{aligned} E\{\{X(k) - \sum_{m=1}^q F(q, m) X(k-m)\} X'(k-n)\} \\ = R(n) - \sum_{m=1}^q F(q, m) R(n-m) \\ = 0, \quad n=1, \dots, q \end{aligned} \quad (2.2)$$

Prediction matrices $F(q, n)$, where $n=1, \dots, q$, in Eq. (2.1) are the solution of the above simultaneous equations. Also, the forward prediction error is,

$$\underline{X}(k; q) = X(k) - \bar{X}(k; q) \quad (2.3)$$

Similarly, the backward prediction of $X(k-(q+1))$,

$$\bar{X}(k-(q+1); q) = \sum_{n=1}^q B(q, n) X(k-n) \quad (2.4)$$

the backward Yule-Walker equations,

$$\begin{aligned} E\{\{X(k-(q+1)) - \sum_{m=1}^q B(q, m) X(k-m)\} X'(k-n)\} \\ = R(n-(q+1)) - \sum_{m=1}^q B(q, m) R(n-m) \\ = 0, \quad n=1, \dots, q \end{aligned} \quad (2.5)$$

and the backward prediction error

$$\underline{X}(k-(q+1); q) = X(k-(q+1)) - \bar{X}(k-(q+1); q) \quad (2.6)$$

are obtained as corresponding to (2.1), (2.2) and (2.3) in the forward prediction scheme, respectively.

Furthermore, the forward Yule-Walker equations with regard to the subspace $M(q+1)$ are partitioned into the following relations,

$$\begin{aligned}
R(n) &= \sum_{m=1}^{q+1} F(q+1, m) R(n-m) \\
&= R(n) - \sum_{m=1}^q F(q+1, m) R(n-m) - F(q+1, q+1) R(n-(q+1)) \\
&= 0, \quad n=1, \dots, q+1
\end{aligned} \tag{2.7}$$

From (2.2), (2.5) and (2.7), we have

$$\begin{aligned}
\left\{ \sum_{m=1}^q F(q, m) R(n-m) \right\} - \left\{ \sum_{m=1}^q F(q+1, m) R(n-m) \right\} - F(q+1, q+1) \left\{ \sum_{m=1}^q B(q, m) R(n-m) \right\} \\
= 0, \quad n=1, \dots, q+1
\end{aligned} \tag{2.8}$$

i.e.,

$$F(q+1, m) = F(q, m) - F(q+1, q+1) B(q, m), \quad m=1, \dots, q \tag{2.9}$$

Analogously, following relations are obtained in the backward scheme:

$$B(q+1, m+1) = B(q, m) - B(q+1, 1) F(q, m), \quad m=1, \dots, q \tag{2.10}$$

As shown in the next section, the prediction error filter is constructed by using matrices $\{F(q+1, q+1), B(q+1, 1), q=0, \dots, p-1\}$ which appeared in relations (2.9) and (2.10). That is, these matrices are required to construct the filter and are referred to as the filter parameters. The filter parameters are computed by using the recursive formulae which are due to Whittle (4).

The stochastic characteristics of input for this filter is governed by the covariance matrix $\underline{S}(p)$ of the final prediction error $\underline{X}(k;p)$. Although the final prediction error does not necessarily become a white noise, in general the spectral structure of this error is so flat that the white noise approximation for this error is possible from engineering viewpoints. Therefore, the stochastic characteristics of input for the filter is governed by $\underline{S}(p)$,

$$\begin{aligned}
\underline{S}(p) &= E[\underline{X}(k;p) \underline{X}'(k;p)] \\
&= E\{[X(k) - \bar{X}(k;p)] X'(k)\} \\
&= R(0) - \sum_{n=1}^p F(q, n) R(-n)
\end{aligned} \tag{2.11}$$

Actually, the square root of diagonal component of matrix $\underline{S}(p)$ is used as a gain function in the direction corresponding to the diagonal component. Analogously, the covariance matrix of background prediction error is computed. Especially, the covariance of forward prediction error and that of backward one are equivalent in one dimensional case.

CONSTRUCTION OF PREDICTION ERROR FILTER

In this section, we will consider the construction of the prediction error filter. As the prediction error filter is based on the wave matching in the time domain, the filter is constructed by using the filter parameters induced in the foregoing section and the delay operator D .

First, the following notations are defined as follows:

$$F(n, 0) = -I, \quad B(n, n+1) = -I, \quad n=1, \dots, p$$

By using these notations and the delay operator D , (2.1) and (2.4) become (3.1) and (3.2) respectively.

$$\bar{X}(k; q) = - \sum_{n=0}^q F(q, n) D^n X(k) \quad (3.1)$$

$$\bar{X}(k-(q+1); q) = - \sum_{n=1}^{q+1} B(q, n) D^n X(k) \quad (3.2)$$

From (2.9), (2.10), (3.1) and (3.2), we have the following two relations,

$$\begin{aligned} \underline{X}(k; q+1) &= - \sum_{n=0}^{q+1} F(q+1, n) D^n X(k) \\ &= -F(q+1, 0) + \sum_{n=1}^q [F(q, n) - F(q+1, q+1) B(q, n)] D^n + F(q+1, q+1) D^{q+1}] X(k) \\ &= \underline{X}(k; q) - F(q+1, q+1) \underline{X}(k-(q+1); q) \end{aligned} \quad (3.3)$$

and

$$\begin{aligned}\underline{X}(k-(q+2); q+1) &= - \sum_{n=1}^{q+2} B(q+1, n) D^n X(k) \\ &= -D(B(q+1, 1) - \sum_{n=1}^q (B(q, n) - B(q+1, 1) F(q, n)) D^n + D^{q+1}) X(k) \\ &= D(\underline{X}(k-(q+1); q) - B(q+1, 1) \underline{X}(k; q))\end{aligned}\quad (3.4)$$

where $\underline{X}(k; 0) = X(k)$ and $\underline{X}(k-1; 0) = DX(k) = X(k-1)$.

Employing Eqs. (3.3) and (3.4) recursively from $q=0$ to $q=p-1$, three-dimensional prediction error filter is constructed as shown in Fig. 2. In this figure, the diagonal component of filter parameters represents the characteristics of the corresponding direction and the off-diagonal one represents the degree of correlation between the two corresponding directions.

FREQUENCY CHARACTERISTICS OF PREDICTION ERROR FILTER

The more the filter's order increases, the more the spectral structure of the original wave is absorbed into the filter. In the final order p , the filter has the spectral envelope of the original wave as the characteristics of the filter. The remaining spectral fine structure is the frequency characteristics of the final prediction error $\underline{X}(k; p)$. Namely, if the final order p is determined as such, the final prediction error becomes a white noise, and then a white noise with the covariance matrix $\underline{S}(p)$ could be used as the input of the filter in this stochastic model.

The autoregressive spectrum estimation procedure is used in order to represent the frequency characteristics of the filter. Forward prediction matrices, i.e., regression matrices $F(p, n)$, where $n=1, \dots, p$, are obtained from the filter parameters by using (2.9) and (2.10). From these matrices and the covariance matrix of the final prediction error, the spectral envelope of the original wave, i.e., the spectral density matrix $P(g)$, is estimated in the following form (5)

$$P(g) = \frac{1}{2\pi} A^{-1}(z) \underline{S}(p) [A^*(z)]^{-1}, \quad |g| \leq \pi \quad (4.1)$$

where

$$A(z) = I - \sum_{n=1}^p F(p, n) z^{-n}, \quad z = \exp(ig) \quad (4.2)$$

The resonance frequency and the damping coefficient of each vibration mode appeared in every direction components are computed by solving the algebraic equation $A(z)=0$ in one-dimensional case. In the complex s plain, the frequency response function of the second order system has

$$\frac{1}{(s - \frac{2\zeta_n \omega_n s + \omega_n^2}{n})} \quad (4.3)$$

By the transformation $z = \exp(sT) = \exp(i\zeta)$, (4.3) becomes (6)

$$H_n(z) = K_n \exp(-\zeta_n \omega_n T) \cdot \frac{z}{(z - z_n)(z - z_n^*)} \quad (4.4)$$

where

$$z_n = \exp\left(-\zeta_n \omega_n + i\omega_n \sqrt{1 - \zeta_n^2} T\right) \quad (4.5)$$

and

$$K_n = \frac{\sin(\omega_n \sqrt{1 - \zeta_n^2} T)}{\omega_n \sqrt{1 - \zeta_n^2}} \quad (4.6)$$

Accordingly, the transfer function of this system has

$$\begin{aligned} |H_n(z)|^2 &= H_n(z) H_n(z^{-1}) \\ &= K_n^2 \frac{z}{(z - z_n)(z - z_n^{*-1})} \frac{z}{(z - z_n^*)(z - (z_n^*)^{-1})} \end{aligned} \quad (4.7)$$

In the actual ground motion, each of the direction components of recorded wave has the spectral density function having the product of this type of transfer function. Therefore, taking out the factor of fourth order such as (4.7) from the power spectrum density function, the resonance frequency and the damping coefficient of each vibration mode are computed. In one dimensional case, the roots of the characteristic equation $A(z)=0$ are denoted with z_n , $n=1, \dots, p$. Then, (4.1) becomes

$$\begin{aligned} P(g) &= \frac{\underline{S}(p)}{2\pi \prod_{n=1}^p |1 - z_n^{-1} z|_n^2} \\ &= \frac{(-1)^p \underline{S}(p)}{2\pi \prod_{n=1}^p z_n^*(z - z_n)(z - z_n^{*-1})} \end{aligned} \quad (4.8)$$

Therefore, if the roots of $A(z)=0$ are z_n and z_n^* , the factor of fourth order such as (4.7) is extracted. Namely, when $A(z)$ is decomposed with the factor of second order and that of first order, the resonance frequency and the damping coefficient of each vibration mode are computed by using the relation (4.5) and the root of the factor of second order. Solving the characteristic equation $A(z)=0$, the Bairstow's method is convenient in the numeric computation. In this method, the resonance frequency is exactly estimated, but the stability and the estimation of the damping coefficient are not expected to be as accurate as the estimation of the resonance frequency.

MATHEMATICAL MEANINGS OF PREDICTION ERROR FILTER

By repeated application of (3.3), we have

$$X(k) = \underline{X}(k; 0)$$

$$= \sum_{q=1}^p F(q, q) \underline{X}(k-q; q-1) + \underline{X}(k; p) \quad (5.1)$$

This is a basic equation of the prediction error filter. In this section, a mathematical meaning of this equation is discussed.

By applying the Gram-Schmidt orthonormalization process to a sequence of $X(k-n)$, $n=1, \dots, p$ and finally $\underline{X}(k)$, an orthonormal sequence is obtained. The first p orthonormal random variables are

$$V(n) = \frac{\underline{X}(k-n; n-1)}{\| \underline{X}(k-n; n-1) \|^2}, \quad n=1, \dots, p, \quad (5.2)$$

where

$$\underline{X}(k-n; n-1) = X(k-n) - \bar{X}(k-n; n-1) \quad (5.3)$$

and

$$\bar{X}(k-n; n-1) = \sum_{m=1}^{n-1} (X(k-n), V(m)) V(m) \quad (5.4)$$

Before the final step of the Gram-Schmidt orthonormalization process is applied, it is necessary to find the following relations. Namely, as $\bar{X}(k;n-1)$ is the projection of $X(k)$ on the $n-1$ dimensional subspace $M(n-1)$ spanned by the sequence of $X(k-m)$, $m=1, \dots, n-1$ and $\underline{X}(k;n-1)$ is the orthogonal component of $X(k)$ to this subspace, we have the following relations.

$$\bar{X}(k; n-1) = \sum_{m=1}^{n-1} (X(k), V(m)) V(m),$$

i.e.,

$$(\bar{X}(k; n-1), V(m)) = 0, m=n, \dots, p \quad (5.5)$$

and

$$\underline{X}(k; n-1) = X(k) - \bar{X}(k; n-1),$$

i.e.,

$$(\underline{X}(k; n-1), V(m)) = 0, m=1, \dots, n-1 \quad (5.6)$$

Applying the final step of the Gram-Schmidt orthonormalization process to $X(k)$, a relation is obtained,

$$X(k) = \bar{X}(k; p) + \underline{X}(k; p)$$

$$= \sum_{n=1}^p (X(k), V(n)) V(n) + \underline{X}(k; p) \quad (5.7)$$

By using (5.6), this relation is expanded as follows:

$$\begin{aligned} X(k) &= \sum_{n=1}^p ((X(k) - \underline{X}(k; n-1)), V(n)) V(n) + \underline{X}(k; p) \\ &= \sum_{n=1}^p \frac{(\underline{X}(k; n-1), \underline{X}(k-n; n-1))}{||\underline{X}(k-n; n-1)||^2} \underline{X}(k-n; n-1) + \underline{X}(k; p) \end{aligned} \quad (5.8)$$

This expression is the finite Fourier expansion of $X(k)$ by an uncorrelated sequence of vector valued random variables $\underline{X}(k-n; n-1)$, $n=1, \dots, p$ and $\underline{X}(k; p)$.

In one-dimensional case, the norm of $\underline{X}(k-n; n-1)$ and that of $\underline{X}(k; n-1)$ are equal, i.e., the covariance of $\underline{X}(k-n; n-1)$ and that of $\underline{X}(k; n-1)$ are equal. Then, Fourier coefficients are equivalent to partial correlation coefficients, i.e.,

$$r(n) = \frac{(\underline{X}(k; n-1), \underline{X}(k-n; n-1))}{||\underline{X}(k; n-1)|| ||\underline{X}(k-n; n-1)||}. \quad (5.9)$$

That is, $r(n)=F(n,n)$ is the partial correlation of $X(k)$ and $X(k-n)$ after the effect of $X(k-m)$, $m=1,\dots,n-1$ has been removed by regression. Also, from (5.9) and Schwartz inequality, the absolute value of $r(n)$ is less than one and this is the stability condition of the prediction error filter in one-dimensional case.

NUMERICAL EXAMPLE

We first consider how to determine the final order p of the prediction error filter. In order to determine the order p , the "An Information Criterion" (AIC) proposed by Akaike is used (7). The AIC is a criterion for obtaining the maximum information about the distribution of future value obtained from the model. The degrees of freedom for the model's parameter is determined by using the AIC. In this case, a second order process with zero mean is treated. Therefore, an identical Gaussian process is considered. Then, the AIC is

$$AIC(n)=N \cdot \ln\{\det[\underline{S}(n)]\} + 2M^2 n \quad (6.1)$$

where M is the number of dimension (8). The order p is the value of n for which the $AIC(n)$ is minimized.

As an original record for simulation, we used the strong-motion accelerogram at the Golden Gate Park site of San Francisco earthquake (1957.3.22). A numerical computation was done in two-dimensional case, i.e., $X_1(k)$ and $X_3(k)$ which represent the N-S component and the U-D one, respectively. We employed 300($=N$) samples with 20 msec($=T$) from the main part of accelerogram.

Grasping the characteristics of this part, the sample spectral density matrix $I(g)$ was estimated by the following relation (5)

$$I(g) = \frac{1}{2\pi N} Z(g)Z^*(g), \quad |g| \leq \pi \quad (6.2)$$

where $Z(g)$ is the sample Fourier transform:

$$Z(g) = \sum_{n=1}^{N} x(nT) \exp(-ign) \quad (6.3)$$

As the spectral density matrix is a Hermitian matrix, the contents are represented by two diagonal components, and the real part and the imaginary one of the off-diagonal component. They are shown in Figs. 3-6. In these Figs., the transverse axis is expressed in $g/(2\pi T)$ Hz. Among these four Figs., Fig. 3 (N-S component), Fig. 5 (co-spectrum) and Fig. 6 (quadrature spectrum) show the distinguished spectral peaks. But, Fig. 4 (U-D component) shows almost flat spectral structure so that the difficulty of simulation for this component is expected.

A two-dimensional prediction error filter is shown in Fig. 7. The final order p which was computed from (6.1) was 12 within $n=14$. Table 1 is the list of the filter

parameters obtained by using the recursive formulae which are due to Whittle. The relations $f_{1,1}(n) \approx b_{1,1}(n)$, $f_{3,3}(n) \approx b_{3,3}(n)$, $n=1, \dots, p$ are found from this table. In one-dimensional case, this relationship is $r(n) = f_{1,1}(n) = b_{1,1}(n)$, $n=1, \dots, p$. Introducing a mathematical model of multi-reflection type, these parameters $r(n)$, $n=1, \dots, p$ play the role of reflection coefficients. The off-diagonal components of matrices $F(n,n)$, $B(n,1)$, $n=1, \dots, p$ are so small compared with unity that the degree of correlation between two direction components is not conspicuous.

Corresponding to the components of the matrix $I(g)$, those of the estimated spectral density matrix $P(g)$ which represents the characteristics of the prediction error filter, are shown in Figs. 3 to 6. As a whole, the matrix $P(g)$ envelopes the matrix $I(g)$. But, the final order $p=12$ is so small that the separation of spectral peaks is not sufficient in the high frequency region.

The input for this filter is synthesized by using a sequence of random numbers between zero and one, i.e., $e(n)$, $n=1, \dots$. By using this sequence, two-dimensional independent Gaussian white noise with zero mean and one variance is obtained by the following relations (9),

$$u(n) = \sqrt{2 \ln[e(n)]} \sin(2\pi e(n+1)), \quad (6.4)$$

$$v(n) = \sqrt{2 \ln[e(n)]} \cos(2\pi e(n+1)) \quad (6.5)$$

Taking the covariance matrix $\underline{S}(12)$ into consideration, the input for this filter is

$$\underline{x}_3(n;p) = \sqrt{\{\underline{S}(12)\}_{2,2}} v(n), \quad (6.6)$$

$$\begin{aligned} \underline{x}_1(n;p) &= \sqrt{\{\underline{S}(12)\}_{1,1} - \{\underline{S}(12)\}_{1,2}^2} \{\underline{S}(12)\}_{2,2}^{-1} u(n) \\ &\quad + \{\underline{S}(12)\}_{1,2} \{\underline{S}(12)\}_{2,2}^{-1} \underline{x}_3(n;p) \end{aligned} \quad (6.7)$$

Fig. 8 shows a sample of synthesized two-dimensional wave during the first four seconds. In the following four figures, the components of the sample spectral density matrix of the synthesized wave between the five second and the ten second, are shown. As a whole, these components envelope the characteristics of the corresponding components of the estimated spectral density matrix $P(g)$.

CONCLUSION

In the present report we developed a method for synthesizing the artificial earthquake waves. The method uses a finite Fourier expansion by uncorrelated random variables, while the other methods use the finite Fourier expansion by harmonic functions. As an advantage of this method, the characteristics of the strong-motion earthquake waves are represented by a smaller number of parameters. Therefore, this method would be convenient to file a large number of strong-motion records.

REFERENCES

- (1) Hoshiya, M. (1974): Probabilistic analysis of structural vibration, Kajima-Shuppan. [in Japanese].
- (2) Matsui, E., T. Nakajima, T. Suzuki and H. Omura (1972): An adaptive method for speech analysis based on the Kalman filtering theory, Report of the Electrotechnical Laboratory, 36, 3, 42-51. [in Japanese].
- (3) Riley, D. C. and J. P. Burg (1972): Time and space adaptive deconvolution filters, Presented at the 42nd annual meeting of the SEG.
- (4) Whittle, P. (1963): On the fitting of multivariate autoregressions, and the approximate canonical factorization of a spectral density matrix, Biometrika, 50, 129-134.
- (5) Parzen, E. (1968): Multiple time series modeling, Technical Report No. 12, Department of Statistics, Stanford University.
- (6) Jury, E. I. (1964): Theory and application of the Z-transform method, John Wiley & Sons, 298.
- (7) Akaike, H. (1974): A new look at the statistical model identification, IEEE Trans. A.C., 19, 6, 716-723.
- (8) Jones, R. H. (1974): Identification and autoregressive spectrum estimation, IEEE Trans. A.C., 19, 6, 894-898.
- (9) Gold, B. and C. M. Rader (1969): Digital processing of signals, McGraw-Hill, 144-146.

GLOSSARY OF SYMBOLS

T: Sampling time

N: Number of sample points

 $x(n \cdot T)$, $n=1, \dots, N$: Sequence of observed acceleration vectors which are sampled with the sampling time T $X(n)$, $n=1, \dots, N$: Sequence of vector valued Gaussian random variables with zero mean $M(q)$: q-dimensional linear subspace spanned by the sequence of $X(k-n)$, $n=1, \dots, q$ $\bar{X}(k;q)$: Projection of $X(k)$ on $M(q)$ $\underline{X}(k;q)=X(k)-\bar{X}(k;q)$: Prediction error of $X(k)$ which is orthogonal to $M(q)$ $E[]$: Expectation operator X' : Transpose of X

p: Final order of the prediction error filter

D: Delay operator; $D^n X(k)=X(k-n)$

I: Unit matrix

 $R(n)=E[X(k)X'(k-n)]$, $n=0, 1, \dots$: Sequence of covariance matrices $S(q)$: Covariance matrix of the prediction error $\underline{X}(k;q)$ $F(p,n)$, $n=1, \dots, p$: Forward prediction matrices $B(p,n)$, $n=1, \dots, p$: Backward prediction matrices $F(n,n)$, $B(n,1)$ $n=1, \dots, p$: Prediction error filter parameters $f_{j,k}(n)$, $b_{j,k}(n)$: (j,k) components of $F(n,n)$ and $B(n,1)$, respectively

w: Circular frequency

$g=\omega T$: Normalized circular frequency, $|g| \leq \pi$
 $P(g)$: Spectral density matrix
 z^* : Complex conjugate of z
 A^* : Adjoint matrix of A
 $\langle X, Y \rangle = E[X'Y]$: Inner product of X and Y
 $\|X\| = \sqrt{\langle X, X \rangle}$: Norm of X
 $V(n), n=1, \dots, p$: Sequence of orthonormal vector valued random variables
 $r(n), n=1, \dots, p$: Sequence of partial correlation coefficients
 $AIC(\cdot)$: An information criterion
 $I(g)$: Sample spectral density matrix
 $Z(g)$: Sample Fourier transform
 $\{u(n), v(n)\}, n=1, \dots$: Sequence of two dimension Gaussian vectors with zero mean

n	$f_{11}(n)$	$f_{13}(n)$	$f_{31}(n)$	$f_{33}(n)$	$b_{11}(n)$	$b_{13}(n)$	$b_{31}(n)$	$b_{33}(n)$
1	0.740	0.124	-0.008	0.538	0.749	-0.093	0.032	0.529
2	-0.709	-0.100	-0.010	-0.633	-0.715	0.021	-0.020	-0.626
3	0.357	0.043	0.008	0.405	0.359	-0.003	0.006	0.401
4	-0.380	0.183	0.035	-0.264	-0.387	0.120	0.072	-0.265
5	-0.112	-0.002	0.015	0.069	-0.116	0.044	-0.007	0.068
6	-0.066	-0.326	-0.049	-0.019	-0.069	-0.118	-0.127	-0.006
7	-0.098	-0.179	0.009	0.031	-0.108	0.036	-0.072	0.038
8	-0.149	-0.102	0.062	0.068	-0.167	0.181	-0.044	0.070
9	-0.085	0.148	-0.015	-0.182	-0.089	-0.023	0.071	-0.181
10	0.016	-0.114	-0.009	-0.026	0.019	-0.026	-0.043	-0.017
11	-0.023	0.117	0.011	-0.077	-0.027	0.033	0.051	-0.080
12	0.163	0.303	-0.017	-0.171	0.183	-0.079	0.131	-0.181

$$S(12) = \begin{bmatrix} 3610 & 392 \\ 392 & 1571 \end{bmatrix}$$

Table 1 Parameters of two dimensional prediction error filter

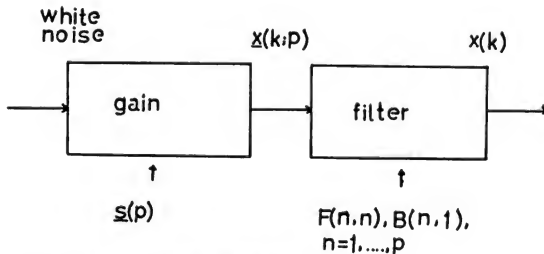


Fig. 1 Filtered White Noise Model

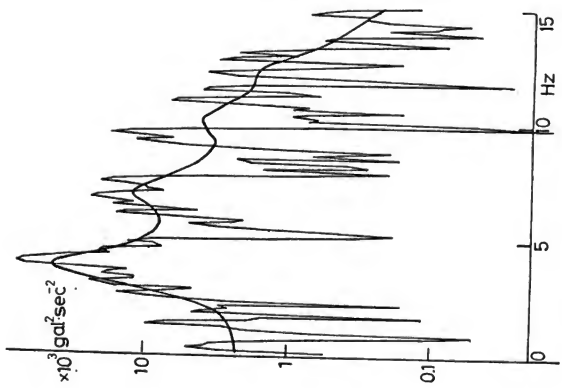


Fig. 3 Power Spectrum (recorded N-S)

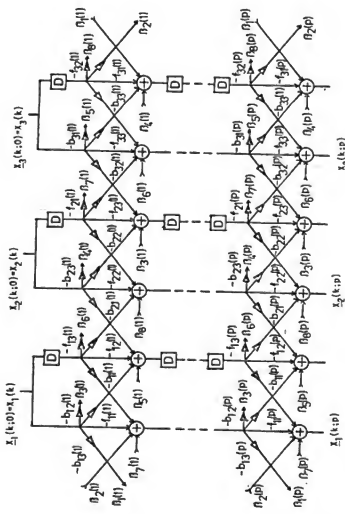


Fig. 2 Three Dimensional Prediction Error Filter

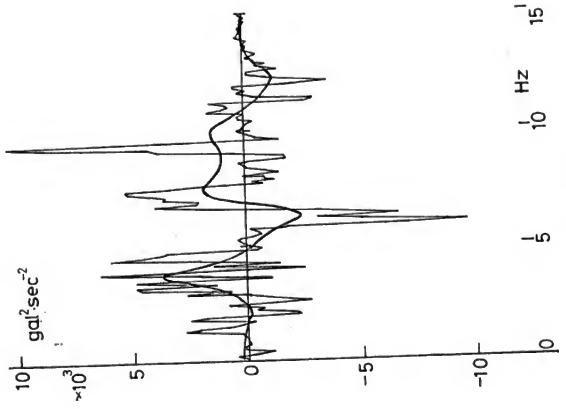


Fig. 5 Co-spectrum (recorded U-D)

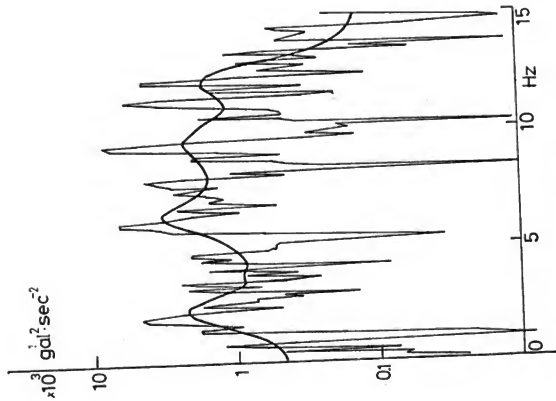


Fig. 4 Power Spectrum (recorded U-D)

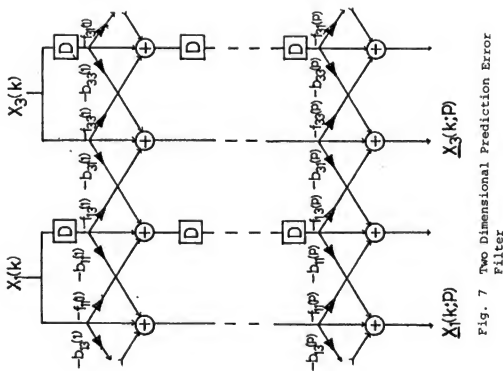


Fig. 7 Two Dimensional Prediction Error Filter

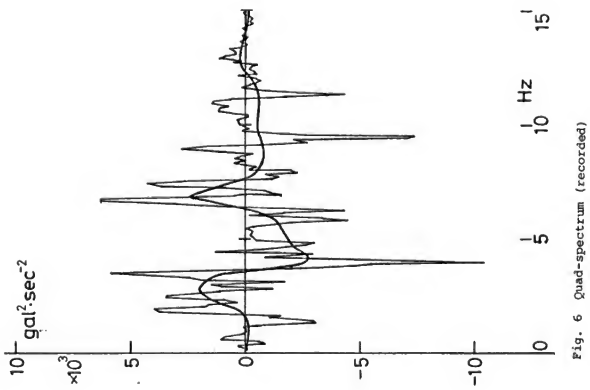
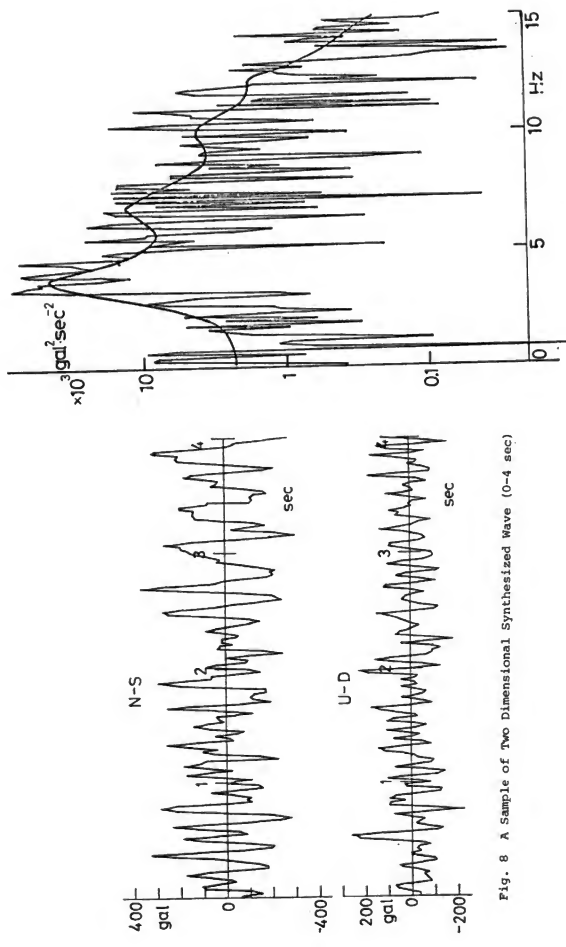


Fig. 6 Quad-spectrum (recorded)



IV-45

Fig. 8 A Sample of Two Dimensional Synthesized Wave (0-4 sec)

Fig. 9 Power Spectrum (synthesized N-S)



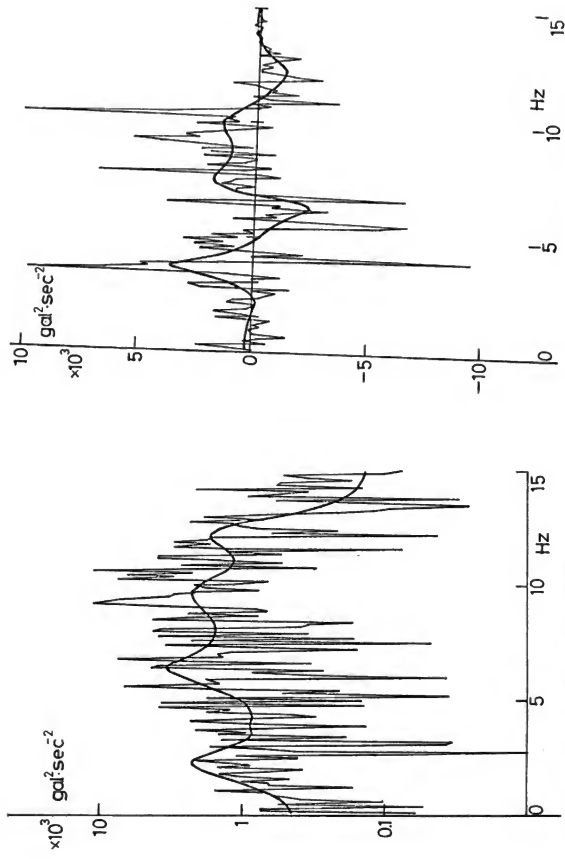


Fig. 10 Power Spectrum (synthesized U-D)

Fig. 11 Co-spectrum (synthesized)

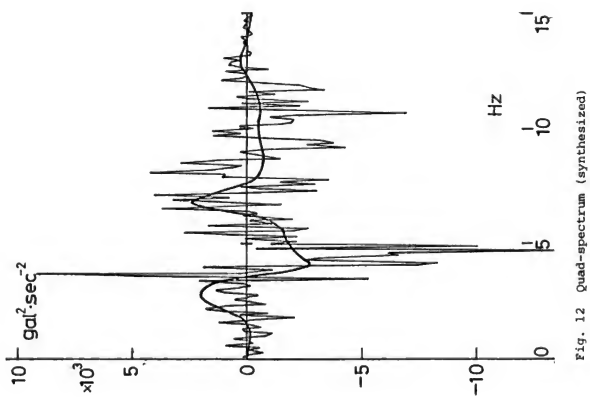


Fig. 12 Quad-spectrum (synthesized)

STATISTICAL ANALYSIS OF STRONG-MOTION ACCELERATION RECORDS

Masamitsu Ohashi, Head, Earthquake Disaster Prevention Division

Toshio Iwasaki, Chief, Ground Vibration Section, Earthquake Disaster Prevention Division

Susumu Wakabayashi, Research Engineer

Ken-ichi Takida, Research Engineer

All of the Public Works Research Institute, Ministry of Construction

ABSTRACT

This paper briefly discusses the present status of strong-motion observation for engineering structures in Japan. Next, it presents the results of the multiple regression analysis of 301 strong-motion acceleration records to evaluate the effects of earthquake magnitude, epicentral distance and subsoil condition on characteristic variables of ground accelerations such as maximum horizontal acceleration, time duration of major motion, ratio of vertical to horizontal accelerations, etc. The paper also shows the results of a quantification analysis of average response accelerations obtained from 277-component horizontal acceleration records to clarify the effects of seismic and subsoil conditions on average response spectra.

From the analysis performed, empirical formulas which can statistically estimate maximum horizontal acceleration, duration of major motion, and number of zero-crossing in terms of earthquake magnitude, epicentral distance, and subsoil condition, are proposed. Frequency characteristics of horizontal motions and ratios of vertical to horizontal accelerations are evaluated and averaged depending on subsoil conditions. Furthermore, various average response spectrum curves for a linear single-degree-of-freedom system are proposed in terms of earthquake magnitude, epicentral distance, and subsoil condition.

KEYWORDS: Design; earthquake magnitude; epicentral distance; statistical analysis; strong-motion acceleration records.

INTRODUCTION

In establishing reasonable procedures for earthquake resistant design of structures, it seems essential to properly evaluate characteristics of ground motions and structural behavior during strong earthquakes. A number of strong motion accelerographs are installed at various engineering structures and on their neighboring grounds in Japan to understand dynamic properties of ground motions and structural responses. The strong-motion observation network for engineering structures in this country has progressed significantly after experiencing the Niigata Earthquake of 1964 and the Tokachi-oki Earthquake of 1968. At the present time more than 1,000 sets of strong-motion accelerographs are equipped at structures and on grounds near the structures, and many meaningful acceleration records are already available. Although the records triggered include those of structural responses, only the records on ground surfaces are employed in the present analysis.

Characteristic variables of acceleration records and response spectral accelerations of a linear single-degree-of-freedom system computed from ground accelerations are statistically investigated. Records used are classified into four groups, depending on the subsoil conditions at the observation stations, from rocky ground to soft alluvial ground.

Although there will be a number of factors which affect characteristics of ground motions, three principal factors might be: earthquake magnitude, geographical situation of the focal area of a concerned earthquake related to the structural site, and subsoil condition at the site. Accordingly, in this study, characteristic variables of ground accelerations are statistically analyzed in terms of these three factors. It is expected that the results of the analysis will give the designer invaluable information when performing seismic design of structures.

The study shown in this paper was performed as one of comprehensive work done in the Aseismic Technology Development Committee established at the Technology Center for National Land Development with a commission from the Public Works Research Institute. The results from the study are utilized as basic materials in standard design seismic forces and seismic loads of "New Criteria of Earthquake Resistant Design (Draft)," (1,2) proposed by the Ministry of Construction in March, 1977.

OBSERVATION OF STRONG-MOTION EARTHQUAKES AT ENGINEERING STRUCTURES IN JAPAN

In Japan the observation of strong-motion earthquakes for engineering structures was initiated when SMAC-type accelerographs were developed in 1953. The observation network has gradually advanced since the experiences of severe structural damages due to the Niigata Earthquake of 1964 and the Tokachi-oki Earthquake of 1968. As of March, 1976, the total number of SMAC accelerographs installed on various structures and neighboring grounds is 1048, as shown in Fig. 1 and Table 1. It is believed, however, that additional accelerographs are needed in order to obtain reliable records for major earthquakes which might take place in any areas of this country.

At the present time about one third of the installed accelerographs are on the ground surfaces, and the rest on structures. Fig. 1 illustrates the present network of strong-

motion observation for various structures. These instruments are generally installed by individual organizations such as governmental agencies and private companies which are in charge of construction and maintenance of the structures.

In addition to the stations with strong-motion accelerographs, there are a number of stations where electromagnetic-type seismographs are equipped. Moreover, dynamic behavior of subsoils during earthquakes is also being studied using downhole seismometers at several points (some at depths greater than 100 m) as well as using standard seismometer and SMAC accelerograph measurements on the surface. These studies will provide pertinent information for establishing seismic design methodology of engineering structures.

Records obtained from these field study programs have been published periodically by institutions concerned (3). Records obtained at port and harbor structures are digitized, analyzed and published at the Port and Harbour Research Institute. Records triggered at highway bridges, tunnels, dams, and embankments are processed mainly at the Public Works Research Institute. Furthermore, records at building structures are treated mostly at the Building Research Institute.

Incidentally, in order to promote the strong-motion observation program in Japan, the Strong-Motion Observation Council is established at the National Research Center for Disaster Prevention, Science and Technology Agency, with the cooperation of universities, governmental organizations, public corporations, and private companies. The council has been preparing a nationwide strong-motion observation program, and also has been publishing important acceleration records collected from all field studies covering the above-mentioned structures and others.

ANALYSIS OF ACCELERATION RECORDS

A statistical analysis of measured acceleration records was attempted to quantitatively express characteristic variables of ground motions as functions of seismic conditions and subsoil properties at the observation point. Records analyzed were extracted from the publications issued by the Earthquake Research Institute of the University of Tokyo, the National Research Center for Disaster Prevention of Science and Technology Agency, Port and Harbour Research Institute of the Ministry of Transport, the Public Works Research Institute of the Ministry of Construction, and the Railway Technical Research Institute of the Japanese National Railways.

The present analysis employed those records which were obtained during earthquakes with the Richter magnitude of 5.0 or higher and the hypocentral depth of 60 km or shallower, and also those records which include at least one record with the maximum acceleration of 50 gals or higher for an earthquake. Records with the maximum acceleration less than 10 gals were excluded. The total number of the records used is 301 (the number of components treated is $3 \times 301 = 903$) for 51 earthquakes.

Factors considered in the analysis are as follows:

- (1) Seismic properties: Richter magnitude M , epicentral distance Δ (km)
- (2) Subsoil conditions: Observation stations are classified into the following four groups depending on subsoil conditions, with reference to the stipulation in "Specifications for Earthquake Resistant Design of Highway Bridges," Japan Road Association (5,6).

- 1st Group: Rock
- 2nd Group: Diluvium
- 3rd Group: Alluvium (Except the 4th Group)
- 4th Group: Soft Alluvium

The definition of this classification is described in Table 2.

(3) Characteristic variables of acceleration records:

- (a) Absolute maximum horizontal acceleration (larger value of two perpendicular horizontal motions): H_{\max} (gals)
- (b) Period of vibration about the time when acceleration becomes H_{\max} : T_1 (sec)
- (c) Duration of major motion: T_d (sec)
- (d) Ratio of vertical to horizontal accelerations: $v = V_{\max}/H_{\max}$
- (e) Number of zero-crossing during the time interval of T_d : N_z
- (f) Mean period of vibration during the time interval of T_d : $T_m = 2T_d/N_z$

The determination of the above characteristic variables are illustrated in Fig. 2.

Each of the characteristics values (expressed as X below) was assumed to be represented by the following two types of expressions:

$$\text{Type-1: } X = a_1 \cdot 10^{b_1 M + c_1 \Delta} \quad (1)$$

$$\text{Type-2: } X = a_2 + b_2 M + c_2 \Delta \quad (2)$$

where X = characteristic value (namely, H_{\max} , T_1 , T_d , N_z , and T_m)

M = earthquake magnitude on the Richter scale

Δ = epicentral distance (km)

a_1 , b_1 , c_1 ; a_2 , b_2 , c_2 = constants for each characteristic value

The analysis was conducted for five different cases, namely four groups of subsoil conditions plus the average subsoil conditions including the entire data. In determining the expressions for H_{\max} , only eq. (1) was investigated and the term Δ in eq. (1) was substituted by $(\Delta + \Delta_0)$, where Δ_0 was taken as 0, 10, 20, 30 and 40 km.

Table 3 indicates the distribution of 301 records used in the analysis. Table 4 shows formulated regression equations and correlation coefficients. These are obtained from the analysis based on the multiple regression analysis. The table shows the results for three characteristic values H_{\max} , T_d and N_z , and it is seen that multiple correlation coefficients are greater than 0.5. Since correlation coefficients for expressions of Type-1 were generally greater than those for Type-2, the results for only Type-1 were generally greater than those for Type-2, the results for only Type-1 are shown in the table. Although the correlation coefficient was the largest in the cases of $\Delta_0 = 10$ km among the five cases analyzed (Table 3), H_{\max} equations in Table 4 were for the cases of $\Delta_0 = 0$ for simplicity. Figs. 3(A) to (E) illustrate the expressions for H_{\max} in the cases of $\Delta_0 = 0$ as functions of M and Δ for the four groups of subsoil conditions and the average subsoils.

As for the other three characteristic values T_1 , v and T_m , the multiple correlation coefficients are found to be less than 0.5. This means that there is no distinct relation among these values and M and Δ . For these variables the mean values and the standard deviations are evaluated, and are listed in Table 5.

The results of the analysis described above may be summarized as follows:

- (1) The maximum horizontal acceleration (H_{\max}), the duration of major motion (T_d), and the number of zero-crossing (N_z) can be approximately expressed as functions of earthquake magnitude and epicentral distance, as shown in Table 4.
- (2) The maximum horizontal acceleration (H_{\max}) becomes larger as the earthquake magnitude (M) increases and the epicentral distance (Δ) decreases. The average values of H_{\max} for $M=8$ and $\Delta=50$ km are estimated to be 130, 270, 200 and 400 gals for rock, diluvium, alluvium, and soft alluvium, respectively. The corresponding values of H_{\max} for $M=8$ and $\Delta=100$ km are estimated to be 85, 150, 110 and 200 gals. The decrease in H_{\max} values with increase in the epicentral distance is not considerable for rock compared with the other three subsoils.
- (3) The duration of major motions (T_d) defined in Fig. 2 becomes greater as the earthquake magnitude (M) increases and as the epicentral distance (Δ) increases. Fig. 4 (A) and (B) show the relation between Δ and T_d for $M=8$, and the relation between M and T_d for $\Delta=100$ km, respectively. It is seen from those results that the duration of major motions is between 10 and 30 seconds for ground motions of earthquakes with the Richter magnitude between 7 and 8 at the epicentral distance of 100 km.
- (4) The relation between the number of zero-crossing (N_z) and the epicentral distance (Δ) is considerably affected by subsoil conditions. The value of N_z increases with increase in Δ for harder grounds such as rocky and diluvial soils. For softer soils, it seems that N_z is affected by M , but not by Δ . The number of repetitions of major motions (N), which can be approximately $N_z/2$, is 30 to 100 for various subsoil conditions.
- (5) The period of vibration about the time of H_{\max} occurrence, T_1 , the ratio of vertical to horizontal acceleration, v , and the mean period of vibration during the major motion, T_m , are not clearly related with M and Δ . The following two points, however, can be seen from Tables 4 and 5.
 - (a) The mean values of T_1 and T_d become larger as the subsoil condition becomes softer. This tendency is obvious for soft alluvial soils. The ratio of T_1 to T_m varies from 1.20 to 1.26, and these ratios are nearly constant irrespective of the subsoil conditions.
 - (b) The mean values of v being 0.32 to 0.34 are not strongly affected by the subsoil conditions. Since the standard deviation is in the range of 0.15 to 0.21, it may be reasonable to assume that the vertical acceleration is equal to one-half of the horizontal acceleration for design purposes. Fig. 5 illustrates an example of the relationship between Δ and v . In the figure the mean value of v is equal to 0.32.

ANALYSIS OF EARTHQUAKE RESPONSE SPECTRA

The Port and Harbour Research Institute, the Ministry of Transport and the Public Works Research Institute, the Ministry of Construction have been conducting response spectrum analysis for major ground motions obtained at various ground conditions during moderate to strong earthquakes (7,8). The present analysis discusses the results of the response spectra analysis performed at the two Institutes for 277 horizontal components of ground motions, which were triggered during 68 earthquakes with the Richter magnitude between 4.5 and 7.9 and the hypocentral depth of 60 km or shallower.

Factors considered in the analysis are as follows:

- (1) Seismic properties: Earthquake magnitude on the Richter scale M , and epicentral distance Δ km.
- (2) Subsoil conditions: Observations are classified into four, in the same manner as they were in the previous section. (See Table 2 for the definition of the classification of subsoils.)
- (3) Characteristic variables of acceleration records and their response spectral values:
 - (a) Maximum horizontal acceleration (two perpendicular components for one record):
 A_{\max} (gals)
 - (b) Absolute response acceleration: S_A (gals), which is computed from digitized values of triggered records by assuming a linear viscously damped single-degree-of-freedom system with the natural periods T of 0.1, 0.15, 0.2, 0.25, 0.3, 0.35, 0.4, 0.5, 0.6, 0.7, 0.8, 0.9, 1, 1.5, 2, 2.5, 3, and 4 seconds and the damping ratio h of 5% of critical.

In estimating S_A and A_{\max} the analysis assumes the following:

- (i) A quantification analysis can be applied to the estimation of S_A in terms of earthquake magnitude M , epicentral distance Δ , and subsoil conditions S , by assuming an expression as

$$\log_{10} \bar{S}_A = C(M) + C(\Delta) + C(S) \quad (3)$$

where

\bar{S}_A = estimated value of S_A (gals)

$C(M)$, $C(\Delta)$, and $C(S)$ = weighting functions depending on M , Δ , and S , respectively.

- (ii) A quantification analysis can be also applied to the estimation of A_{\max} in terms of the three factors used above by assuming an expression,

$$\log_{10} \bar{A}_{\max} = C'(M) + C'(\Delta) + C'(S)$$

where

\bar{A}_{\max} = estimated value of A_{\max} (gals)
 $C'(M)$, $C'(\Delta)$, $C'(S)$ = weighting functions depending on M , Δ , and S ,
respectively.

Classification of 277-component records employed in the analysis is shown in Tables 6 and 7. Magnitudes M in the tables are irregularly divided into five groups with consideration of the scatter in the data used and also convenience of practical application of the results.

Table 8 shows the results of the quantification analysis for S_A , and lists the ranges of the weighting functions $C(M)$, $C(\Delta)$, and $C(S)$ in Eq. (3). The table also gives the multiple correlation coefficients of these three functions. Furthermore, Figs. 6 to 9 illustrate the response spectral curves (T and S_A relation) which are obtained from Table 8. In these figures, the maximum values of ground acceleration A_{\max} which are also estimated from the quantification analysis are tabulated. From these two types of information, the acceleration magnification factor β ($= \bar{S}_A / \bar{A}_{\max}$) can be evaluated. The values of A_{\max} shown here, however, may not be used for the estimation of the absolute maximum horizontal accelerations (H_{\max}), but for the estimation of β , these values may be used. For estimating H_{\max} , the results described in the previous section may be employed.

Degrees of the effects of the three factors (M , Δ , and S) on \bar{S}_A are shown in Fig. 10, by indicating the variation of the ranges of $C(M)$, $C(\Delta)$, and $C(S)$ with T . On the other hand, Fig. 11 shows an example of frequency distribution for 277 values of S_A / \bar{S}_A (the ratio of response spectral accelerations computed directly from the measured records to those estimated by the results of the quantification analysis) for the natural period of $T=0.6$ seconds. Shapes of frequency distribution of S_A / \bar{S}_A for the other natural periods are found to be similar to that of Fig. 11.

From the analysis shown above, the following significant points can be made:

- (1) Values of \bar{S}_A at the same epicentral distance increase with increase in the earthquake magnitude.
- (2) Values of \bar{S}_A for the same earthquake magnitude decrease as the epicentral distance becomes smaller.
- (3) As for the effects of subsoil conditions on \bar{S}_A , the effect on rock ground is considerably different from those on the other three subsoil conditions. Values of \bar{S}_A for rock are smaller than those for the other subsoils, except for the subsoils with the natural periods shorter than 0.3 seconds. For the range of comparatively longer periods, the values of \bar{S}_A tend to become larger for softer subsoils.
- (4) The shapes of T vs. S_A curves do not change much with the variations of M and Δ . It is supposed from Figs. 6 to 9 that for the range of longer natural periods the values of β will increase as M becomes greater, and as Δ becomes longer.
- (5) Among the effects of the three factors, earthquake magnitude ($M=4.5$ to 7.9), epicentral distance ($\Delta=6$ to 405 km), and subsoil condition (rock to soft alluvium), the effects of M are found to be the greatest for the entire range of natural periods. The

effects of Δ are close to those of M for the shorter period range, and become small for the longer period range. The effects of subsoil condition are small in comparison with those of M and Δ for the entire period range. This may be reasonable from the fact that the ranges of M and Δ are both considerably large. It is noted, however, that for the range of the periods between 0.5 and 2 seconds the effects of subsoils become rather great.

(6) Multiple correlation coefficients in the quantification analysis of \bar{S}_A vary between 0.53 and 0.72. The coefficients generally become larger as the natural periods become longer. Multiple correlation coefficient in the analysis \bar{A}_{\max} is approximately 0.6.

(7) Frequency distribution of S_A/\bar{S}_A does not vary much with the change in natural periods. In view of this, it may be possible to stochastically assess design seismic forces in consideration of the importance of structures.

The results described so far are for the case of the damping ratio of $h=0.05$ only. Values of \bar{S}_A for damping ratio other than 0.05 can be approximately estimated by multiplying the values of \bar{S}_A for $h=0.05$ by C_h shown in Fig. 12, which are derived from the previous investigation (9,10).

As an example of use of the results shown above, let us estimate the average response of a structure with the natural period of $T = 0.35$ seconds and the damping ratio of $h = 0.1$, when subjected to an earthquake with the Richter magnitude of $M=7.5$ to 7.9 and the epicentral distance of $\Delta=60$ to 120 km. From Fig. 9(C) and Fig. 12,

$$\begin{aligned} S_A &= \bar{S}_A (T=0.35 \text{ sec.}, h=0.5) \times C_h (h=0.1) \\ &= (200 \sim 300) \times 0.78 = (156 \sim 240) \text{ gals} \end{aligned}$$

The value of S_A varies depending on the subsoil conditions at the site of the structure, being 156 gals for rock, 211 gals for dilluvium, 240 gals for alluvium, and 234 gals for soft alluvium. Response accelerations of structures with different dynamic properties can be estimated in the similar way, depending on the earthquake magnitude, the epicentral distance, and the subsoil condition.

It should be noted that in the above analysis the structures are assumed as linear systems with viscous dampings. A similar analysis for nonlinear structures may be necessitated in the succeeding steps.

CONCLUSIONS

The following remarks may be made as the conclusions of the statistical analyses of strong motion records measured in Japan.

- (1) The absolute maximum horizontal acceleration, the duration of major motions, and the number of zero-crossings can be approximately evaluated as functions of the earthquake magnitude and the epicentral distance, and the subsoil conditions.
- (2) The mean value of the ratio of vertical to horizontal accelerations is found to be around 1/3. The ratio may be conservatively taken as 1/2, for design purposes.

- (3) Response spectral curves, by which structural response accelerations can be estimated in terms of earthquake magnitude, epicentral distance, and subsoil conditions, are proposed.
- (4) Among the three factors, the earthquake magnitude M , the epicentral distance Δ , and the subsoil condition S , which affect the response acceleration of a structure during an earthquake, the effects of M are found to be the greatest. The effects of Δ are close to those of M for the range of shorter natural periods, and become smaller for the range of longer natural periods. The effects of subsoil conditions are comparatively small, but become comparatively large for the range of natural periods between 0.5 and 2 seconds. It is remarkable that response accelerations for the range of the natural periods between 0.5 and 2 seconds become larger as the subsoils become softer.
- (5) The results presented in this paper would be useful in evaluating the characteristics of seismic forces and seismic loads for the earthquake resistant design of structures.

ACKNOWLEDGMENTS

This study has been performed as one of comprehensive research projects done in the Aseismic Technology Development Committee which was established at the Technology Center for National Land Development with a commission from the Public Works Research Institute, Ministry of Construction. The authors express their thankful appreciation to Professor Shunzo Okamoto (President of Saita University and the Chairman of the Committee), Professor Keizaburo Kubo (Chairman of the Subcommittee on Seismic Forces and Subsoils), Professor Motohiko Hakuno and Kenji Ishihara (Vice-Chairman of the Subcommittee), and Professor Tsuneo Katayama (Member of the Subcommittee) for their helpful guidance. The authors also thank Mr. Mitsuaki Saeki (Japan Engineering Consultants, Co.) for his strenuous work in processing a great deal of strong-motion records.

REFERENCES

- (1) Ministry of Construction, "New Criteria of Earthquake Resistant Design (Draft)," March, 1977 (in Japanese); and Masamitsu Ohashi, Kiyoshi Nakano, "A Proposal for Earthquake Resistant Design Methods," Ninth Joint Meeting, U.S.-Japan Panel on Wind and Seismic Effects, U.J.N.R., Tokyo, Japan, May 24-27, 1977.
- (2) Public Works Research Institute, "Report on Research and Development of Aseismic Technology," March, 1977 (in Japanese)
- (3) E. Kuribayashi, H. Tsuchida and M. Watabe, "On the Maintenance of the Strong-Motion Accelerograph and the Data Processing of the Records," Seventh Joint Meeting of Wind and Seismic Effects, U.J.N.R., May, 1975
- (4) Strong-Motion Earthquake Observation Council, "The Project for Observation of Strong-Motion Earthquakes and its Results in Japan," National Research Center for Disaster Prevention, Science and Technology Agency, Tokyo, Aug., 1972.
- (5) Japan Road Association, "Specifications for Earthquake-Resistant Design of Highway Bridges," Jan., 1971 (in Japanese)

- (6) T. Iwasaki, "Earthquake-Resistant Design of Highway Bridges in Japan," Bulletin No. 29, Public Works Research Institute, May, 1972
- (7) M. Saeki, T. Katayama and T. Iwasaki, "On Characteristics of Earthquake Acceleration Records and Response Acceleration Spectra Obtained on Grounds in Japan," Proceedings of 31st Annual Meeting of JSCE, Oct., 1976 (in Japanese)
- (8) T. Iwasaki, T. Katayama, "Statistical Analysis of Strong-Motion Earthquake Response Spectra," Japan-U.S. Seminar on Earthquake Engineering Research with Emphasis on Lifeline Systems, Tokyo, Japan, Nov. 8-12, 1976
- (9) E. Kuribayashi, T. Iwasaki, Y. Iida and K. Tuji, "Effects of Seismic and Subsoil Conditions on Earthquake Response Spectra," Proceedings of International Conference on Microzonation for Safer Construction, Research and Application, Seattle, Washington, Vol. II, October-November, 1972
- (10) E. Kuribayashi, T. Iwasaki, K. Tuji, "Several Factors Affecting Earthquake Response Spectra," JSCE Meeting on Earthquake Engineering, July, 1971 (in Japanese).

Table 1 Number of Strong-Motion Accelerographs (SMAC-Type)

Number of Accelerographs Installed at	(as of March, 1976)		
	At Structures	On Grounds	Total
Buildings	424	48	472
Highway Bridges	89	79	168
Railways	38	57	95
Ports	5	51	56
Telephone Offices	94	0	94
Power Plants	27	11	38
Nuclear Power Plants	21	20	41
Dams	9	10	19
River & Coastal Dykes	15	28	43
Storage Tanks	3	4	7
Others (Tunnels, Subways, Pipelines, etc.)	5	10	15
Total	730	318	1,048

Table 2 Definitions of Classification of Subsoil Conditions

Category	Definitions	Abbreviation
I	(1) Ground of the Tertiary era or older defined as bedrock hereafter in this table (2) Diluvial layer with depth less than 10 meters above bedrock	Rock
II	(1) Diluvial layer with depth greater than 10 meters above bedrock (2) Alluvial layer with depth less than 10 meters above bedrock	Diluvium (Dil.)
III	Alluvial layer with depth less than 25 meters, which has soft layer with depth less than 5 meters	Alluvium (All.)
IV	Softer than the above	Soft Alluvium (Soft All.)

Table 3. Classification of 301 Records Analyzed

Magnitude M	Subsoil Condition	Epicentral Distance Δ (km)					Total
		20< Δ	20 \leq Δ <60	60 \leq Δ <120	120 \leq Δ <200	200 \leq Δ	
5.0 \leq M<6.0	Rock	2	3				5
	Dil.	3	12	3			18
	All.	4	16	5	2	2	29
	Soft All.	2	5	7	1		15
6.0 \leq M<6.5	Rock		3	6	3	1	13
	Dil.		7	8	2	1	18
	All.		12	13	8	1	34
	Soft All.		3	6	6	1	16
6.5 \leq M<7.0	Rock		1	2	1		4
	Dil.		1	6	6		13
	All.	1	5	10	10	1	27
	Soft All.		1	4	9	4	18
7.0 \leq M<7.5	Rock			1		3	4
	Dil.				2	12	14
	All.				2	14	16
	Soft All.			1	1	5	7
7.5 \leq M<7.9	Rock				1	2	3
	Dil.				3	8	11
	All.			2	6	16	24
	Soft All.				1	11	12
Total		12	69	74	64	82	301

Note. 1) Numbers of records for four subsoil conditions are 29 for rock, 74 for diluvium, 130 for alluvium, and 68 for soft alluvium.

Table 4 Regression Equations for H_{max} , T_d and N_z

Characteristic Value	Subsoil Condition	Empirical Equations	Partial Correlation Coefficient		Multiple Correlation Coefficient r
			Magnitude M	Epicentral Distance Δ	
H_{max}	Rock	$H_{max} = 28.5 \times 10^{0.207M_x - 0.598}$	0.33	-0.47	0.48
	Dil.	$H_{max} = 13.2 \times 10^{0.330M_x - 0.806}$	0.50	-0.59	0.59
	All.	$H_{max} = 32.1 \times 10^{0.254M_x - 0.757}$	0.47	-0.61	0.61
	Soft All.	$H_{max} = 6.5 \times 10^{0.423M_x - 0.977}$	0.65	-0.72	0.71
	Total	$H_{max} = 18.4 \times 10^{0.302M_x - 0.800}$	0.51	-0.62	0.62
T_d	Rock	$T_d = 3.89 \times 10^{-4} \times 10^{0.466M_x + 0.589}$	0.59	0.40	0.89
	Dil.	$T_d = 1.37 \times 10^{-2} \times 10^{0.262M_x + 0.485}$	0.29	0.26	0.71
	All.	$T_d = 2.75 \times 10^{-2} \times 10^{0.291M_x + 0.265}$	0.37	0.17	0.41
	Soft All.	$T_d = 2.28 \times 10^{-1} \times 10^{0.199M_x + 0.233}$	0.25	0.16	0.52
	Total	$T_d = 2.08 \times 10^{-2} \times 10^{0.274M_x + 0.394}$	0.32	0.23	0.65
N_z	Rock	$N_z = 1.43 \times 10^{-2} \times 10^{0.410M_x + 0.444}$	0.41	0.22	0.75
	Dil.	$N_z = 4.23 \times 10^{-1} \times 10^{0.0974M_x + 0.661}$	0.11	0.35	0.66
	All.	$N_z = 6.28 \times 10^{-1} \times 10^{0.272M_x + 0.0313}$	0.39	0.02	0.54
	Soft All.	$N_z = 4.05 \times 10^{0.190M_x - 0.0646}$	0.22	-0.04	0.29
	Total	$N_z = 4.68 \times 10^{-1} \times 10^{0.243M_x + 0.195}$	0.30	0.12	0.54

Table 5. Averages and Standard Deviations

of T_1 , v , and Subsoil T_m

		Subsoil Condition			
		Rock	Diluvium	Alluvium	Soft Alluvium
T_1 (sec)	Average	0.36	0.43	0.49	0.75
	S.D.	0.52	0.39	0.30	0.42
v	Average	0.34	0.33	0.34	0.32
	S.D.	0.15	0.18	0.18	0.21
T_m (sec)	Average	0.30	0.34	0.39	0.41
	S.D.	0.36	0.22	0.22	0.35
T_1/T_m		1.20	1.26	1.26	1.23

Note: 1) S.D. = Standard Deviation

Table 6. Classification of 277-Component Records for the Response Spectrum Analysis

Magnitude M	Subsoil Condition	Epicentral Distance Δ (km)					Total
		$\Delta < 20$	$20 \leq \Delta < 60$	$60 \leq \Delta < 120$	$120 \leq \Delta < 200$	$200 \leq \Delta$	
$4.5 \leq M < 5.4$	Rock	6	4				10
	Dil.	4	10				14
	All.	12	8	8	2		30
	Soft All.	6					6
$5.4 \leq M < 6.1$	Rock		4	2			6
	Dil.	4	4	4			12
	All.	2	12	6			20
	Soft All.	4	2	4			10
$6.1 \leq M < 6.8$	Rock		4	6			10
	Dil.		4	4	2		10
	All.	4	32	22	8	2	68
	Soft All.		6	4	2	2	14
$6.8 \leq M < 7.5$	Rock			4	3	2	9
	Dil.			2	4	2	8
	All.				4	4	8
	Soft All.					4	4
$7.5 \leq M < 7.9$	Rock				2	2	4
	Dil.				6	2	8
	All.		2	6	4	2	14
	Soft All.				2	10	12
Total		42	92	72	39	32	277

Note: 1) Numbers of components for four subsoil conditions are 39 for rock, 52 for diluvium, 140 for aluvium, and 46 for soft alluvium.

Table 7 Classification of 277-Component Records and Mean Values in Each Category

Factor	Category	Number of Components	Mean Value		
			Peak Ground Acc. AG (gals)	Magnitude M	Epicentral Distance Δ (km)
Magnitude (M)	I $4.5 \leq M \leq 5.4$	60	66.0	5.0	31
	II $5.4 \leq M \leq 6.1$	48	67.5	5.8	43
	III $6.1 \leq M \leq 6.8$	102	63.6	6.3	76
	IV $6.8 \leq M \leq 7.5$	29	58.1	7.1	194
	V $7.5 \leq M \leq 7.9$	38	112.4	7.7	197
Epicentral Distance (Δ)	I $6 \leq \Delta < 20$ km	42	110.6	5.3	12
	II $20 \leq \Delta < 60$ km	92	68.2	5.8	38
	III $60 \leq \Delta < 120$ km	72	59.1	6.2	83
	IV $120 \leq \Delta < 200$ km	39	56.2	7.0	159
	V $200 \leq \Delta \leq 405$ km	32	71.3	7.3	271
Subsoil Conditions (S)	I Rock	39	59.9	6.2	87
	II Diluvium	52	69.4	6.2	86
	III Alluvium	140	73.2	6.1	74
	IV Soft Alluvium	46	75.1	6.4	143
Total	-	277	70.9	6.2	90

Table 8 Estimation of Average Response Acceleration S_A (Ratio $S_A = C/(M(C) - c(S))$) for Systems with Natural Period of T and Damping Ratio of 0.05, by Quantification Analysis of 27 Components of Strong-motion Records

(in gals)

Natural Period	Category of Earthquake Magnitude	C (ft)	Category of Epicentral Distance (mi)												C (ft)	
			0 to 10			10 to 20			20 to 30			30 to 40				
			0	10	20	0	10	20	0	10	20	0	10	20		
T ₁	5.28E-5.6 5.42E6.1 6.13E+6.8 7.52E7.9	111	IV	V	VI	605<120	1205<200	2005<405	Block	Diffusion	Absorption	Salt	IV	IV	0.56	
0.1	-0.66	-0.56	-0.53	-0.40	0	0.71	0.43	0.31	0.00	0	2.10	2.03	2.06	2.03	0.56	
0.15	-0.65	-0.56	-0.53	-0.35	0	0.69	0.48	0.37	0.00	0	2.19	2.11	2.15	2.10	0.53	
0.2	-0.73	-0.55	-0.54	-0.30	0	0.78	0.51	0.32	0.02	0	2.23	2.17	2.21	2.11	0.54	
0.25	-0.77	-0.60	-0.55	-0.27	0	0.84	0.56	0.37	0.08	0	2.13	2.11	2.16	2.11	0.55	
0.3	-0.79	-0.57	-0.55	-0.26	0	0.82	0.55	0.35	0.11	0	2.04	2.11	2.17	2.12	0.56	
0.35	-0.79	-0.54	-0.52	-0.23	0	0.76	0.48	0.33	0.10	0	1.97	2.10	2.17	2.15	0.55	
0.4	-0.82	-0.51	-0.51	-0.25	0	0.74	0.48	0.30	0.17	0	1.92	2.09	2.16	2.16	0.57	
0.5	-0.97	-0.81	-0.51	-0.23	0	0.80	0.46	0.30	0.13	0	1.88	2.05	2.15	2.19	0.53	
0.6	-1.05	-0.81	-0.69	-0.21	0	0.77	0.45	0.32	0.12	0	1.79	2.00	2.13	2.20	0.67	
0.7	-1.14	-0.85	-0.50	-0.19	0	0.83	0.47	0.39	0.14	0	1.70	1.95	2.07	2.17	0.70	
0.8	-1.17	-0.87	-0.53	-0.23	0	0.77	0.44	0.36	0.11	0	1.68	1.96	2.06	2.16	0.68	
0.9	-1.17	-0.87	-0.55	-0.24	0	0.71	0.38	0.30	0.17	0.08	1.67	1.94	2.05	2.11	0.67	
1	-1.19	-0.84	-0.55	-0.20	0	0.66	0.33	0.15	0.06	0	1.64	1.95	2.03	2.10	0.67	
1.5	-1.20	-0.86	-0.59	-0.27	0	0.64	0.34	0.16	0.09	0	1.53	1.75	1.86	1.93	0.77	
2	-1.22	-0.81	-0.67	-0.23	0	0.58	0.30	0.11	-0.03	0	1.39	1.57	1.66	1.71	1.12	
2.5	-1.23	-0.87	-0.74	-0.39	0	0.54	0.29	0.13	-0.02	0	1.36	1.51	1.55	1.52	0.70	
3	-1.18	-0.86	-0.71	-0.41	0	0.51	0.25	0.13	-0.06	0	1.27	1.42	1.45	1.42	0.69	
4	-1.15	-0.84	-0.73	-0.40	0	0.45	0.21	0.10	-0.10	0	1.19	1.31	1.36	1.26	0.68	

Note: • Indicates a station installed SMAC accelerographs
(1,048 accelerographs totally)

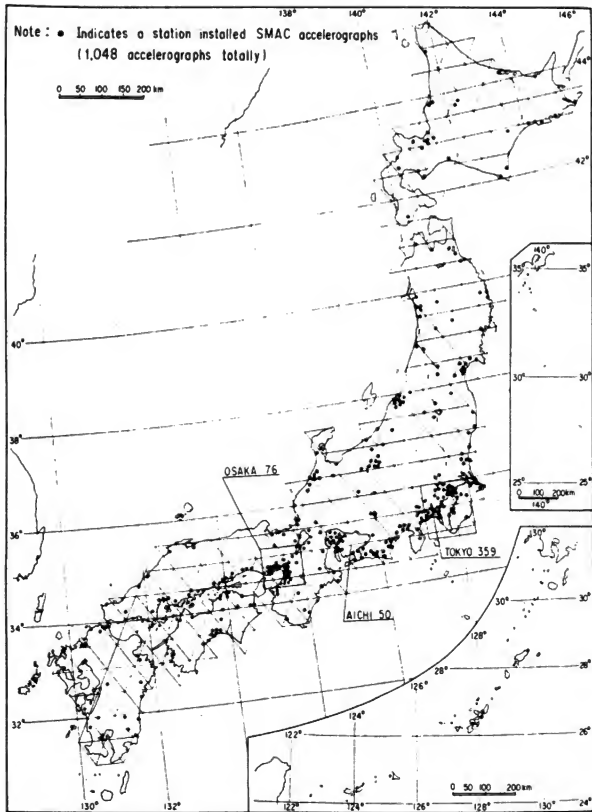
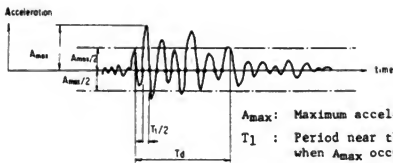


Fig. 1 Strong-Motion Observation Network in Japan as of March, 1976



A_{max} : Maximum acceleration
 T_1 : Period near the time
 when A_{max} occurs
 T_d : Duration of major motion
 (= Time interval between
 the initial time and the
 last time when A is
 equal to the half of
 A_{max})
 N_z : Number of zero-crossing
 within the time of T_d
 ($n=12$ for the case shown)

Fig. 2 Definitions of T_1 , T_d and N_z

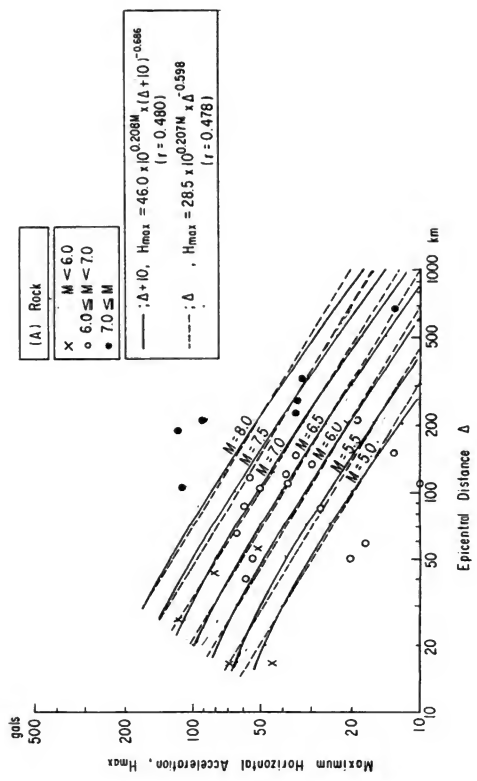


Fig. 3(A) Epicentral Distance versus Maximum Horizontal Acceleration
for Four Subsoil Conditions

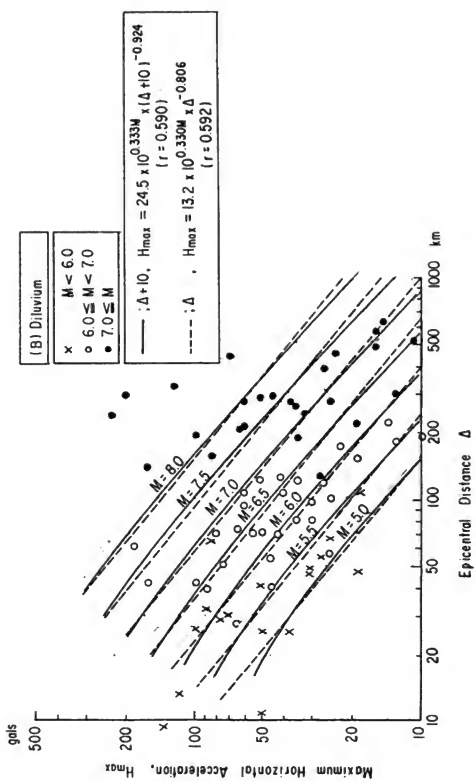


Fig. 3(B) Epicentral Distance versus Maximum Horizontal Acceleration for Four Subsoil Conditions

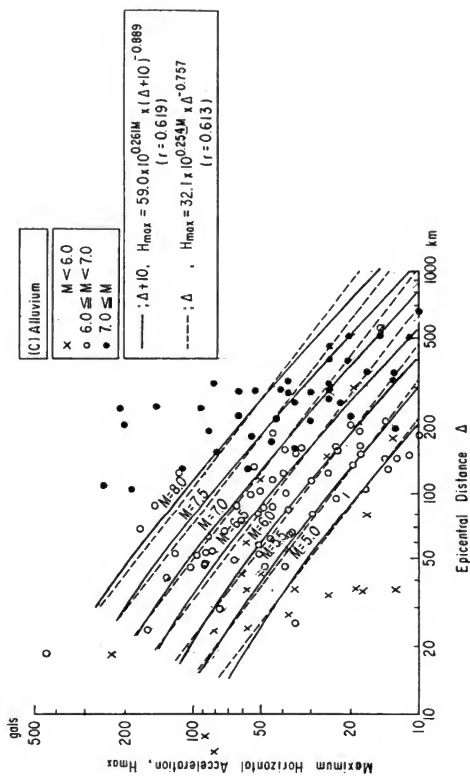


Fig. 3(C) Epicentral Distance versus Maximum Horizontal Acceleration
for Four Subsoil Conditions

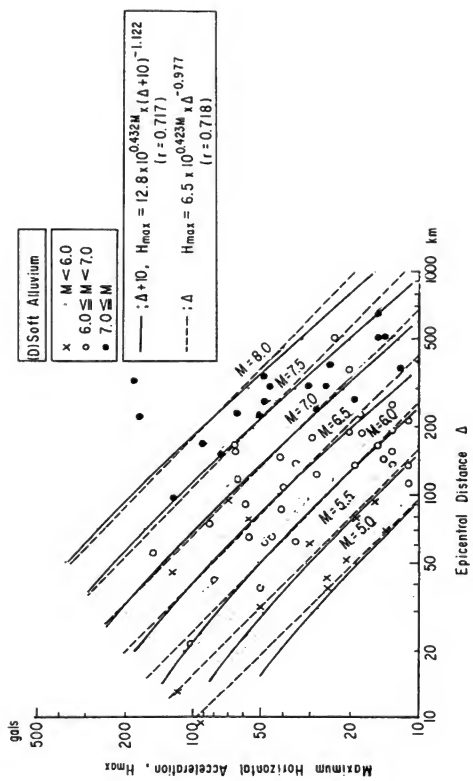


Fig. 3 (D) Epicentral Distance versus Maximum Horizontal Acceleration
for Four Subsoil Conditions

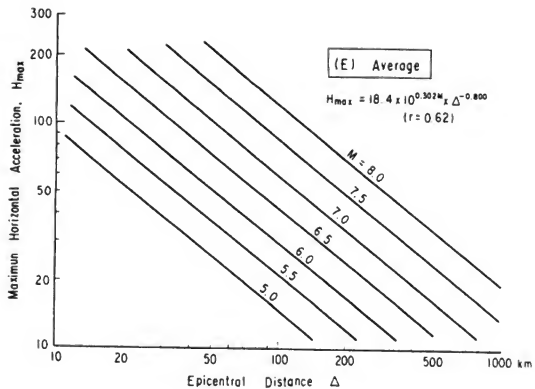
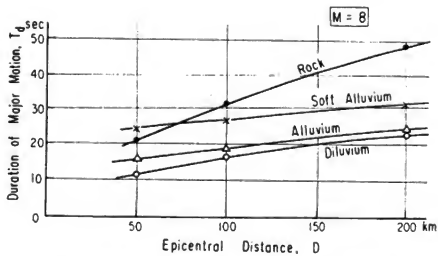
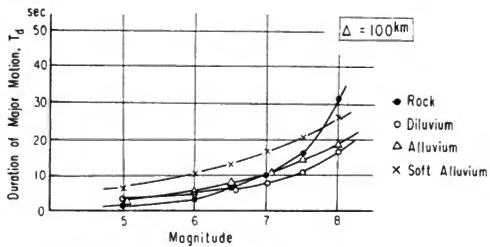


Fig. 3(E) Epicentral Distance versus Maximum Horizontal Acceleration for Average Subsoils



(A) Epicentral Distance versus Duration of Major Motion for Magnitude of 8

Fig. 4 Duration of Major Motion Defined by Fig. 2



(B) Earthquake Magnitude versus Duration of Major Motion at Epicentral Distance of 100 Km

Fig. 4 Duration of Major Motion Defined by Fig. 2

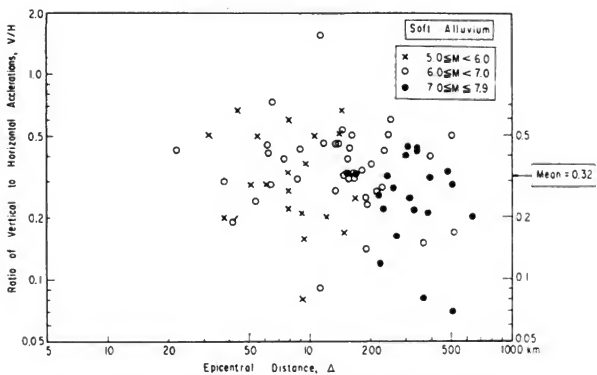
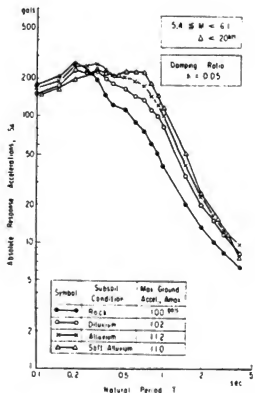
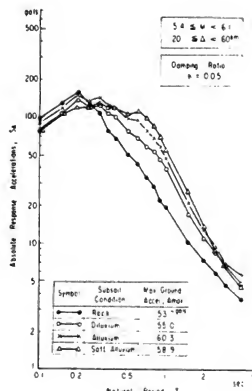


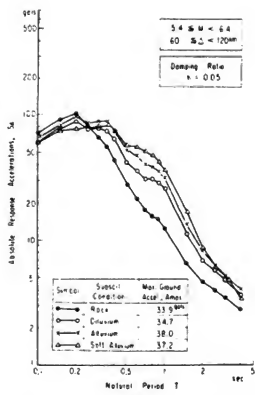
Fig. 5 Example of Ratios of Vertical to Horizontal Accelerations



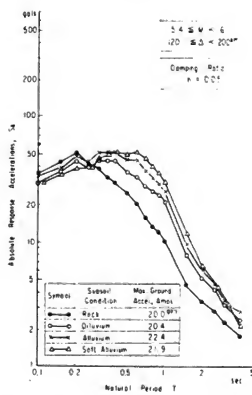
(A)



(B)

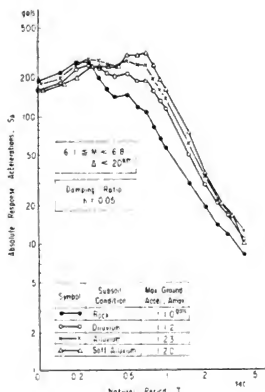


(C)

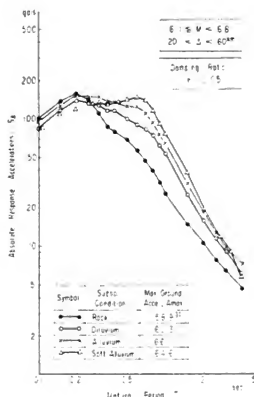


(D)

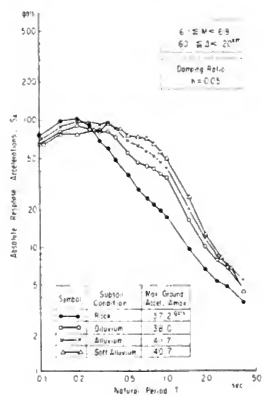
Fig.6 (A)~(D) Response Spectrum Curves for Maximum Response Accelerations in Case of $5.4 \leq M < 6.1$



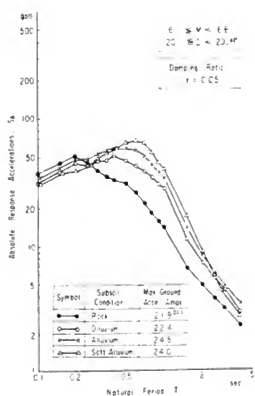
(A)



(B)

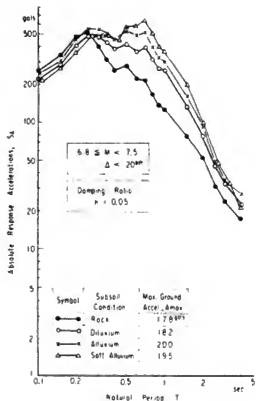


(C)

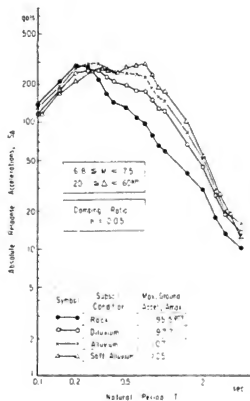


(D)

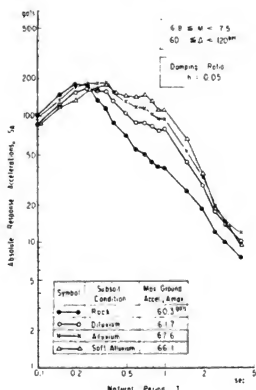
Fig.7(A)~(D) Response Spectrum Curves for Maximum Response Accelerations in Case of $6.1 \leq M < 6.8$



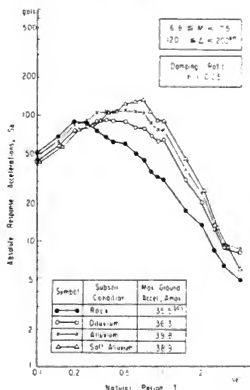
(A)



(B)

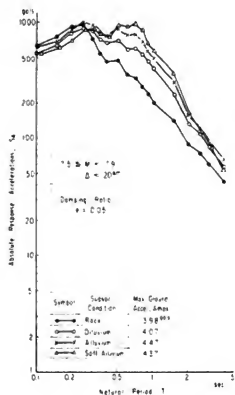


(C)

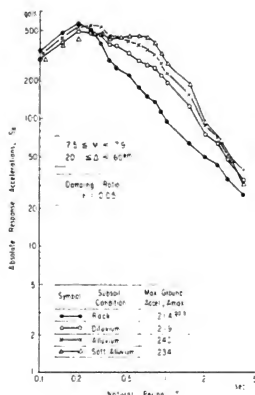


(D)

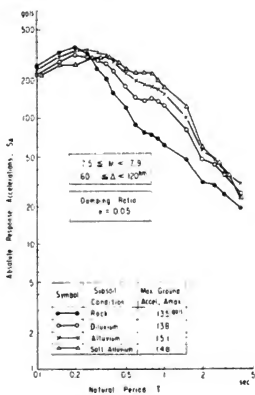
Fig. 8(A) ~ (D) Response Spectrum Curves for Maximum Response Accelerations in Case of $6.8 \leq M < 7.5$



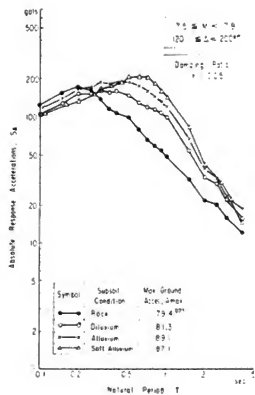
(A)



(B)



(C)



(D)

Fig.9(A)~(D) Response Spectrum Curves for Maximum Response Accelerations in Case of $7.5 \leq M \leq 7.9$

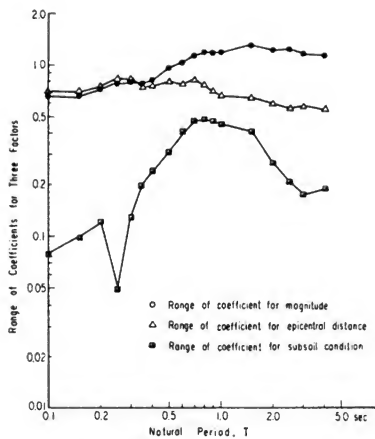


Fig. 10 Natural Period versus Ranges of Coefficients for the Three Factors (Magnitude, Epicentral Distance, and Subsoil Condition)

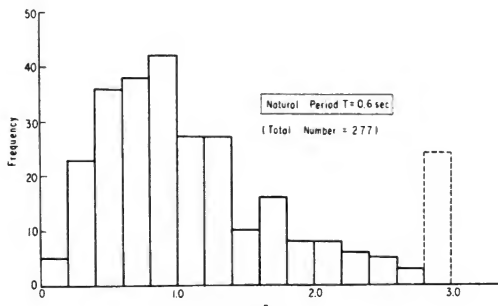


Fig.11 Distribution of S_A / \bar{S}_A

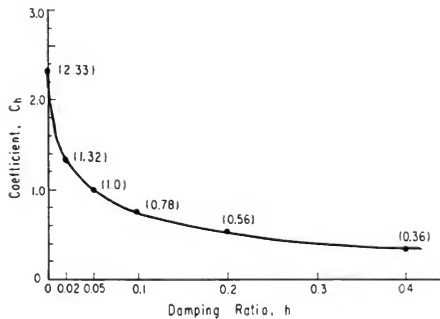


Fig. 12 Effect of Damping Ratio (C_h) on Response Spectrum Values ($C_h = 1.0$ when $h = 0.05$)

RESEARCH ON DESIGN EARTHQUAKE

Makoto Watabe

Building Research Institute

Ministry of Construction

ABSTRACT

The maximum values of accelerations, velocities and displacements of the ground motions due to earthquakes are first discussed utilizing the historical data as well as some theoretical approaches. Then, duration time and the deterministic intensity function of the accelerograms are introduced. The predominant periods and spectral shapes of the strong motion accelerograms are also reported. Historical earthquake data were utilized to assess the earthquake risks in Japan. Finally the explanation of proposed "design earthquake" concludes this report.

KEYWORDS: Design earthquake; deterministic intensity function; historical data; maximum values; random characteristics; seismic zoning; spectral shapes; theoretical analysis.

INTRODUCTION

One of the essential factors for aseismic designs of structures is to estimate the intensity and characteristics of ground motions. Numerous research on this matter has been carried out and the results are summarized here. Recognizing that seismic waves are initiated by irregular slippage along faults followed by numerous random reflections, refractions, and attenuations within the complex ground formations through which they pass, the stochastic modelling of strong ground motions is a realistic form which can be applied in practice. Noting the above fact, stochastic quantities are induced as much as possible in this report.

MAXIMA OF EARTHQUAKE GROUND MOTIONS

(1) Evaluation by overturning of the tombstones:

Fig. 1 illustrates the relation between the epicentral distance (km) and the maximum acceleration estimated by overturned tombstones, based on the earthquake data with the magnitudes greater than 7 since 1927 in Japan. According to this figure, the maximum acceleration may exceed the value of 0.4g and the upper bound of the maximum acceleration at ground surface appears to be around 0.6g.

(2) Evaluation by the records of the strong motion seismographs:

The maximum accelerations measured by the strong motion accelerographs on the hard subsoil layers are tabulated in Table 1. In Fig. 2, the relation between the epicentral distances and the maximum velocity values measured by the strong motion seismographs are indicated with the parameter of the magnitude (1). It may be noticed that the maximum velocity ever recorded by the seismographs is approximately 35 kines as seen in Fig. 2.

(3) Estimation of upper bound from the critical strain level of the rocks (2):

Assuming the critical maximum strain of the fracture of the rocks (ϵ_{cr}) as $\epsilon_{cr} = 10^{-4}$ and shear wave velocity value in the rock (Vs) as Vs=3km/sec., the maximum velocity value is estimated as 30 kines by the following equation,

$$\mu(z,t) = f(t - \frac{z}{Vs}) \quad \epsilon = \left| \frac{\sigma_z}{\sigma_0} \right|_{max} = \left| \frac{\partial f}{\partial t} \frac{1}{Vs} \right|_{max} = \frac{V}{Vs} \leq \epsilon_{cr}$$

where μ = amplitude of seismic wave in terms of time,

z = coordinate along the wave propagation,

t = time,

V_s = shear wave velocity,

ϵ = strain

From the above estimation, it is suggested that there is little change for the maximum velocity to exceed the value of 30 kines.

(4) Proposal by Professor K. Kanai:

With his vast experience on earthquake engineering, Professor Kanai proposed the following equation for the relationship between the hypocentral distance (x) and the

maximum velocity (V_{max}) with the parameter of the magnitude of the earthquake (3),

$$V_{max} = 10^{0.61M - (1.66 + \frac{3.6}{x}) \log x - (0.631 + \frac{1.83}{x})}$$

where V_{max} = the maximum velocity on the surface of the bed-rock (kines)

 M = the magnitude of the earthquake

 x = the hypocentral distance (km)

Also, the radius (D km) of the spherical volume within which hypocenters of after-shocks of the earthquake exist can be expressed in terms of the magnitude (M) followingly (4);

$$D(\text{km}) = 10^{0.353M - 1.134}$$

Assuming that the above value D is the depth of the hypocenter and using Kanai's equations of maximum velocity, the relationship between the maximum velocity and the epicentral distance can be expressed as illustrated in Fig. 3 with the parameter of the magnitude. The intersection of the relevant magnitude line and the dotted line indicate the radium (D km) in the above equation or, let us say, the depth of the hypocenter. Fig. 3 suggests that the maximum probable velocity value will never exceed the value of 60 kines.

(5) The ratio of the maximum acceleration to the maximum velocity:

From the 75 sets of the strong motion accelerograms and the corresponding velocity records obtained in both Japan and the United States, the mean value of these ratios is 9.95 in horizontal components and the standard deviation of those ratios is 1.7, while in the vertical component, the above accelerograms and the corresponding velocity records do not coincide in the time domain. However, these maxima will be regarded as closely correlated if the above time difference of the peaks is limited within one second. Selecting such records, the mean value of the ratios of the maximum acceleration to the maximum velocity is 11.0 in horizontal components and the standard deviation of those ratios is 1.8. In vertical component, the mean value and the standard deviation of those ratios are 13.8 and 1.7, respectively. Incidentally, for the horizontal components, the mean value of the ratios of the maximum acceleration to the corresponding maximum displacement is 20.6 and the standard deviation of those ratios is 3.3. In the case of vertical component, the mean value and the standard deviation of those ratios are 18.0 and 1.9, respectively. Using the same materials including vertical components as well, a stochastic analysis is also made on the cross-correlations between the maximum values of acceleration, velocity, displacement and Housner's spectral intensity with zero and 0.2 dampings. The results are indicated in Table 2 from which it may be suggested that "measures" to represent intensity of ground motions such as values mentioned above are extremely cross-correlated. Therefore, the choice of these "measures" can be rather arbitrary. This analysis also provides linear relations between these maxima. The results are indicated in Table 3, and suggest reasonable ratios between two values of maxima such as horizontal and vertical acceleration,

velocity, displacement and spectral intensity. The ratios indicated in Table 3 give closer values which are proposed by M.D. Trifunac and A. G. Brady (5) as follows,

$$A_H = 5.89 V_H^{1.2}$$

$$A_v = 9.97 V_v^{1.07}$$

$$A_v = 0.64 A_H$$

$$V_v = 0.4 V_H^{1.2}$$

where A and V represent maximum acceleration and velocity, respectively, and the suffixes H and v represent horizontal and vertical components, respectively.

RELATIONS BETWEEN HORIZONTAL AND VERTICAL COMPONENTS OF EARTHQUAKE GROUND MOTIONS

(1) The ratio of the maximum acceleration in vertical component to those in the corresponding two horizontal components:

From the same sets of the strong motion accelerograms mentioned previously (5), ratios between horizontal and vertical components are obtained. It might be reasonable to associate the epicentral distance with these ratios of the vertical maximum accelerations to the horizontal accelerations. The results suggest that the shorter the epicentral distance is, the larger this ratio becomes. This ratio of the maximum acceleration in vertical component to those in the corresponding two horizontal components, R(d), can be approximated as follows,

$$R(d) = e^{-0.0022(\frac{x}{x_0} + 300)}$$

where x is the epicentral distance in kilometers and x_0 is the unit distance of the kilometers.

(2) Random characteristics of the accelerations ratios (horizontal and vertical components).

In spite of the above results, this ratio of the maximum acceleration in vertical components to those in the corresponding two horizontal components follows the complete characteristics of Gaussian random process as may be observed in Fig. 4, in which the probability distribution of variables as logarithms of the above ratio are plotted with solid lines and the reference plots (in dotted line) of true Gaussian distribution. As previously introduced, Table 3 suggests stochastically reasonable ratios between horizontal and vertical components (diagonal elements in Table 3). It should be noted that the ratio of intensity between horizontal and vertical components is rather stable, whatever intensity scale may be chosen such as acceleration, velocity, displacement or spectral intensity.

DURATION TIME AND DETERMINISTIC INTENSITY FUNCTION

From 76 accelerograms obtained by 56 strong motion earthquakes during the years between 1968 and 1971 in Japan, the duration time (t) of accelerograms determined by the engineering judgment can be expressed in terms of the magnitude of the earthquake (M),

$$t = \frac{M-2.5}{3.23} \text{ (sec.)}$$

According to research work on length (L , km) and displacement (D , m) of the active faults, the following relationships are known (6),

$$\log D=0.60 M-3.91 \quad \log L=0.6 M-2.91 \quad R=D/S$$

where S = average displacement velocity (m/year)

M = magnitude of caused earthquake

R = period of earthquake occurrence (year).

With the rupture velocity of 3 km/sec. along the fault, total rupture duration of the earthquake can be calculated using the above relation. The results are also indicated in Fig. 5.

Figs. 6(a) and 6(b) are the deterministic intensity functions determined from the actual accelerograms by smoothing the oscillatory irregular waves. If $a(t)$ is the accelerogram, $\xi(t)$ is the deterministic intensity function and $a'(t)$ is the stationary random process of the accelerogram, $a(t)$ is expressed as,

$$a(t) = \xi(t) a'(t) \quad a'(t) = a(t)/\xi(t)$$

If real $\xi(t)$ is to be obtained, $a'(t)$ must satisfy the condition of the stationary random process such as the Gaussian distribution of probability and run's test. Thus true $\xi(t)$ can be obtained by step-by-step smoothing techniques through checking the stationary random process of $a'(t)$. Figs. 6(a) and 6(b) suggest the deterministic intensity function of ideal model (7), and the generalization of this pattern is somewhat controversial, but desirable from an engineering point of view. It also should be noted that the deterministic intensity functions for the vertical components are not identical to those for the horizontal components as seen in Fig. 6. Another approach to obtain the pattern of deterministic intensity function was shown by J. Penzien and T. Kubo (8).

SPECTRAL CHARACTERISTICS

Spectral shape of the accelerograms on the surface of the bed-rock:

The transfer function to transmit the seismic wave around the bed-rock layers might be regarded uniform in frequency domain, i.e., the spectral shape of the transfer function is "White." The spectral shape of the accelerograms on the surface of the bed-rock may be subjected to the influence of the spectral shape of source mechanisms and the surroundings of the hypocenters. The velocity response spectrum $Sv(T,h)$ at free field bed-rock is assumed to be the function of magnitude M and hypocentral distance x in addition to period T and damping ratio h ,

$$Sv(T,h) = 10^{a+M-b \log x - c}$$

Using 27 accelerograms obtained at free field bed-rock, coefficients a, b and c for every period of spectrum are determined by least square sum techniques. The results are shown in Fig. 7(a) and Fig. 7(b) as examples. It can be clearly seen in Fig. 7(a) that higher frequency components are predominant in response spectrum for smaller magnitude while lower frequency components are predominant in response spectrum for larger magnitude. By these figures, Fig. 7(a) and Fig. 7(b), any response spectra at free field bed-rock can be obtained.

CONCEPT OF PRINCIPAL AXES OF THE ACCELEROGRAAMS

In this paper, only the outline of the concept of principal axes of ground motions is introduced. Details are explained in reference 9. First, 3 components of accelerograms along three orthogonal coordinate axes are defined through the relations,

$$a_x(t) = \xi(t) b_x(t), a_y(t) = \xi(t) b_y(t), a_z(t) = \xi(t) b_z(t)$$

where $b_x(t)$, $b_y(t)$ and $b_z(t)$ are stationary random processes and $\xi(t)$ is the deterministic intensity function giving appropriate non-stationarity to the ground motion process. If $a_x(t)$, $a_y(t)$ and $a_z(t)$ are considered to be zero-mean non-stationary random processes, the covariance functions

$$E[a_i(t)a_j(t+\tau)] = \xi(t) \xi(t+\tau) E[b_i(t)b_j(t+\tau)] \quad i,j = x,y,z$$

where E denotes ensemble average, it can be used to characterize the ground motion process. Since random processes $b_x(t)$, $b_y(t)$ and $b_z(t)$ are stationary, all ensemble averages on the right side of the above equation are independent of time t; therefore, showing dependence only upon the time difference τ . Since real earthquake accelerograms demonstrate a very rapid loss in correlation with increasing values of $|\tau|$, the influence of coordinate directions on the covariance functions can be investigated by considering the relations,

$$E[a_i(t)a_j(t)] = \xi(t)^2 E[b_i(t)b_j(t)] \quad i,j = x,y,z$$

Defining covariance matrix $\underline{\beta}$ as

$$\underline{\beta} = \begin{bmatrix} \beta_{xx} & \beta_{xy} & \beta_{xz} \\ \beta_{yx} & \beta_{yy} & \beta_{yz} \\ \beta_{zx} & \beta_{zy} & \beta_{zz} \end{bmatrix}$$

where $\beta_{ij} = E[b_i(t)b_j(t)]$, the total covariance matrix can be written in the form $\underline{u}(t) = \xi(t)^2 \underline{\beta}$.

By coordinate transformation of $a_x(t)$, $a_y(t)$ and $a_z(t)$ along new three orthogonal coordinate axes, the covariance matrix can be transformed into diagonal elements only, that is,

$\theta_{ij}=0$; $i \neq j$. Such new axes which satisfy the above conditions are defined as principal axes where no cross-term of covariance exists and 3 variances of diagonal elements become the maximum, minimum and intermediate. Using the defined orthogonal transformation, principal axes of ground motion have been located for six different earthquakes. Variances and covariances of the recorded accelerations $a_x(t)$, $a_y(t)$ and $a_z(t)$ along the three accelerograph axes x, y and z respectively, were obtained. By selecting successive intervals over the entire duration of motion, the changes in direction of principal axes with time can be checked. Fig. 8 shows the horizontal directions of one principal axis for the above mentioned six earthquakes using sufficiently long time intervals to reasonably stabilize the principal coordinate directions. The corresponding variances are indicated by arrow lengths applied to the radial scale. In most cases the principal axis shown in Fig. 8 is the major principal axis; however, in some cases, usually for intervals near the ends of the motions when intensities have decreased considerably, the major principal axis is at right angles to the directions shown. The minor principal axis is in each case nearly vertical. When averaging over the entire duration of motion and averaging for the six earthquakes, the resulting ratios of intermediate and minor principal variances to the major principal variance are approximately 3/4 and 1/2, respectively, i.e., $(\mu_{11}/\mu_{22})_{\text{avg}} \approx 3/4$ and $(\mu_{33}/\mu_{11}) \approx 1/2$. Using these numerical values to obtain principal covariances, the principal cross-correlation coefficients become

$$\rho_{12} = (\mu_{11}-\mu_{22})/(\mu_{11}+\mu_{22})=0.14, \quad \rho_{23} = (\mu_{22}-\mu_{33})/(\mu_{22}+\mu_{33}) = 0.20 \text{ and}$$

$$\rho_{13} = (\mu_{11}-\mu_{33})/(\mu_{11}+\mu_{33})=0.33.$$

Finally it is suggested that the potential use of the concept of principal axes to explore physical phenomena, such as tracing the center of energy release, should be investigated.

SEISMIC ZONING IN JAPAN

In Japan, history of earthquakes from the 7th century up to the present time extending over 1300 years can be available. The total number of destructive earthquakes with magnitudes more than 6 amount to 600. Fig. 9 shows epicenters and magnitudes of earthquakes in and around Japan during these 1300 years. For instance, applying Professor Kanai's equation, introduced in the previous section, to all historical earthquakes, frequency distribution at a specific site, $f(V_{\max})$, can be evaluated, which represents the number of earthquakes in the past with the maximum velocity, V_{\max} , at this specific site. The probability density function for the maximum velocity, $p(V_{\max})$, can be obtained as follows,

$$p(V_{\max})=f(V_{\max})/T$$

where T is the length of historical years of earthquake.

By integration,

$$P(V_{\max,0}) = \int_{V_{\max,0}}^{\infty} p(V_{\max}) d(V_{\max})$$

probability distribution function $P(V_{\max,0})$ can be obtained, which represents the probability of such an earthquake whose maximum velocity, at this specific site, is larger than $(V_{\max,0})$ in a year. Inverse of such probability, $1/P(V_{\max,0})$ is termed as "return period (Tr)" of $(V_{\max,0})$. If some specific return Tr is chosen, say 200 years $(P(V_{\max,0})=0.005)$, then the corresponding $(V_{\max,0})$ can be evaluated. According to Poisson's distribution, the probability $P(t)$ of experiencing the ground motions, the maximum velocity of which exceeds $(V_{\max,0})$ the corresponding return period Tr during the lifetime of a building t, can be evaluated,

$$P(t) = 1 - e^{-t/Tr}$$

Taking $t/Tr=0.1$, $P(t)$ equals 0.095. Assuming the chance of experiencing more than $(V_{\max,0})$ earthquake during the lifetime of building t is 0.3, then t/Tr becomes 0.36. Various researchers proposed seismicity maps in Japan applying similar analyses introduced here. The entire map of Japan is divided into rectangles, the dimensions of which are 20' in both longitude and latitude. Then seven different seismicity maps of Japan (10,11,12,13) of return period 100 years are normalized to assign unity (1.0) for the rectangular division of the maximum value in each map. Using these normalized maps, the mean value of these seven different maps, the mean value plus two standard deviations of these maps and the maximum value of these maps in each rectangular division are obtained. The results are shown in Fig. 10(a), Fig. 10(b) and Fig. 10(c), which are considered to be the appropriate seismic zoning coefficients for aseismic design of structures.

DESIGN EARTHQUAKE

Now let the deviation of estimating intensity of ground motions in terms of magnitude and hypocentral distance be considered. Applying the best fit method to estimate intensities (for instance, maximum velocities) in terms of magnitudes and hypocentral distances of 75 earthquakes, coefficients of deviation for intensity of ground motions are obtained. 0.8 is the smallest possible value for the coefficients of deviation to assess the intensity of ground motions in terms of given magnitude and hypocentral distance. Some other research paper on the coefficient of deviation also suggests the similar value (14).

SUMMARY

(i) As for the maximum velocity value, Fig. 3 might be regarded reasonable, considering the results of critical maximum strain. Also, the maximum velocity ever recorded is 35 kines as seen in Fig. 2 and the upper bound area in Fig. 3 is obtained by extrapolating the values actually recorded. It is quite controversial to define the maximum acceleration

value. However, in a stochastic sense, this value can represent a reasonable measure for the intensity parameter. This may mean to exclude a single peak value of the acceleration with frequency higher than 20 Hz for the stochastically significant value. The values indicated in Table 4 can be regarded as the "mean value of the maximum," therefore, in actual cases, many of the maximum values may exceed the values in the table, which indicate the values for vertical components, as well, by applying linear coefficients shown in Table 3.

(ii) Total duration of design earthquake may be calculated by the equation introduced in Chapter 4, in terms of magnitude of earthquake. As for the duration of the stationary part of ground motions the following equation was derived from fault length of rupture, with assumption of rupture velocity of 3 km/sec.,

$$t = 10^{0.04 - 3.38} \text{ (sec.)}$$

where M is the magnitude of assumed earthquake and t is the duration in second of stationary part which can be applied to the deterministic intensity function.

(iii) The deterministic intensity function for design earthquake may be determined by applying an ideal model proposed in reference 7. This ideal model assumes deterministic intensity functions which increase linearly or parabolically for the stationary part and then decay exponentially.

(iv) Fig. 7(a) and Fig. 7(b) may be recommended as response spectra of design earthquake on bed-rock.

(v) The concept of principal axes may be quite useful for multi-dimensional ground motions.

(vi) It must be fully considered that earthquake ground motions are so random natured that they are not to be permitted to give any explicit values but to give values with mean and deviation.

Proposed procedures to obtain design earthquake are discussed below.

(1) Time history of design earthquake:

- a) Assume magnitude and hypocentral distance and then calculate the maximum velocity using Kanai's equation and the equation for radius (D) of spherical volume.
- b) Use Table 3 to obtain maximum acceleration and spectral intensity (SI), both in horizontal and vertical directions.
- c) Calculate total and stationary duration of the assumed earthquake by equations introduced in summary (ii). Then, assume an ideal model of deterministic intensity if necessary.
- d) Determine spectral characteristics using Fig. 7(a) or Fig. 7(b) if necessary.
- e) Produce accelerograms either through simulated earthquake or modification of real accelerograms and then establish multi-dimensional time history ground motions if necessary.
- f) Principal axes accelerograms are strongly recommended for design earthquake.

- g) Multiply 1.8 (mean plus 1 standard deviation) to accelerograms derived above for important structure and 2.6 (mean plus 2 standard deviation) for very important structures or very dangerous structures.
- h) If the time histories of design earthquake on the ground surface is necessary, apply conventional or non-linear wave propagation techniques.

(2) Response spectrum for design earthquake:

- a) Assume a maximum possible earthquake ground motion, for instance magnitude 8 and hypocentral distance 50 km and then by Fig. 7(a) or Fig. 7(b) establish response spectrum for the maximum possible ground motions.
- b) According to the importance factor of structure, choose Fig. 10(a) for less important structures , Fig. 10(b) for general structures or, Fig. 10(c) for important structures . For the response spectrum in any districts, multiply seismic zoning coefficients of relevant districts to the response spectrum derived in (i) as the maximum possible one.
- c) Apply linear coefficients indicated in Table 3 to obtain response spectrum for vertical component if necessary.
- d) Multiply 1.8 (mean plus 1 standard deviation) to the spectral values in (ii) and (iii) for important structures.
- e) Amplification spectrum of subsoil layers may be multiplied for the design response spectrum on the ground surface.

BIBLIOGRAPHY

- (1) Watabe, M. and Kitagawa, Y., 1973, Characteristics of Strong Motion Earthquake Obtained in Japan, 5th U.J.N.R.
- (2) Muramatsu, I. et al., 1963, Observation of Micro-Earthquake in Mino District in Gifu Prefecture, General Japan Journal of Phys. of the Earth.
- (3) Kanai, K., 1966, Improved Empirical Formula for Characteristics of Strong Earthquake Motions, Proc. Japan Earthquake Symposium, (in Japan), pp. 1-4.
- (4) Iida, K., 1963, A Relation of Earthquake Energy to Tsunami Energy and the Estimation of the Vertical Displacement in a Tsunami Source, Journal of Earth Science Nagoya Univ. Vol. 11, pp. 49-67.
- (5) Trifunac, M. D., and Brady A. G., 1975, On the Correlation of Seismic Intensity Scales with the Peaks of Recorded Strong Ground Motion, B.S.S.A. Vol. 65, 139-162.
- (6) Matsuda, T., 1975, Magnitude and Recurrence Interval of Earthquakes from a Fault, Zishin Vol. 28, pp. 269-283.
- (7) Jennings, P. C., Housner, G. W., and Tsai, N. C., April 1969, Simulated Earthquake Motions, Earthquake Engineering Research Laboratory, California Institute of Technology, Pasadena.
- (8) Penzien, J., and Kubo, T., 1977 Characteristics of Three-Dimensional Ground Motions Along Principal Axes, San Fernando Earthquake, WCCE.
- (9) Penzien, J., and Watabe, M., 1975, Simulation 3-Dimensional Earthquake Ground Motions, International Journal of Earthquake Engineering, McGraw-Hill.

- (10) Goto, H., and Kameda, H., November 1968, A Statistical Study of the Maximum Ground Motion in Strong Earthquakes, Dobokugakkai, No. 159
- (11) Takanashi, K., July 1974, Risk Analysis for Earthquake, Saigaikagaku-Kenkyu-kai
- (12) Omote, S., and Muramatsu, S., Acceleration Expectancy in Japan Derived from Up-to-Date Data.
- (13) Hattori, S., and Kitagawa, Y., 1974, On the Regional Distribution of Earthquake Danger in Japan, Bull. I.I.S.E.E. Vol. 112, pp. 83-102.
- (14) O'Brien, L. J., et al., March 1976, The Correlation of Peak Ground Acceleration Amplitude with Seismic Intensity and Other Physical Parameters, Computer Science Corporation.

Table 1 : Max. Acceleration by Strong Motion
Accelerographs on Hard Subsoil

Earthquake	Date	M	Location	Epicentral Distance	Subsoil	Max. Acceleration (gal)
Matsushiro	1966. 4.5	6.1	Hoshina A	8.0		550
	1966. 5.28	4.9	Matsushiro B	3.5		370
	1966. 8.8	-	Hoshina B			390
Tokachioki	1968. 5.16	7.9	Miyako	115	Hard	118
			Moromanbashi		-	69
			Kibiyadenden	50	Gravel	27
Higashi-Matsuyama	1968. 7.1	6.4	Shintomebashi	32	Hard	75
			Sakagewabashi	48	-	55
	1970. 1.21	6.7	Moromanbashi	20	Rock	182

Table 2 : Coherence Among Measures to Represent the Intensity of Ground Motions

	A	V	D	SI _{0.0}	SI _{0.2}
A	0.905	0.841	0.587	0.830	0.902
V	0.892	0.798	0.876	0.957	0.986
D	0.739	0.888	0.702	0.826	0.770
SI _{0.0}	0.815	0.923	0.786	0.924	0.970
SI _{0.2}	0.911	0.960	0.791	0.960	0.897

A half above the diagonal : Horizontal and horizontal
A half below the diagonal : Vertical and vertical
Diagonal matrix : Horizontal and vertical
A : Maximum acceleration V : Maximum velocity
D : Maximum displacement SI : Housner's intensity
(ξ : Damping ratio)

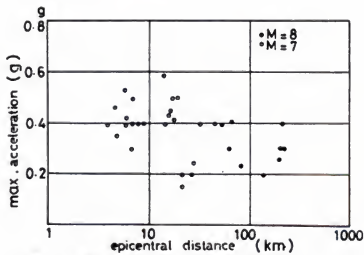
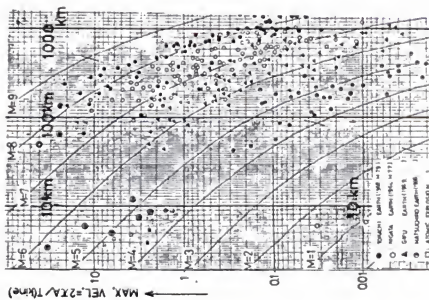
Table 3 : Linear Relations Between Maxima

X Y	A	V	D	SI _{0.0}	SI _{0.2}
A	1.669 (0.532)	0.0961 (8.701)	0.0389 (15.98)	0.579 (1.429)	0.227 (3.945)
V	9.921 (0.0880)	1.753 (0.448)	0.440 (2.000)	5.921 (0.162)	2.242 (0.431)
D	17.67 (0.0406)	1.839 (0.476)	1.555 (0.468)	11.81 (0.0710)	4.290 (0.181)
SI _{0.0}	1.551 (0.511)	0.157 (5.821)	0.0741 (10.63)	1.887 (0.489)	0.371 (2.610)
SI _{0.2}	4.819 (0.186)	0.469 (2.035)	0.216 (3.614)	2.855 (0.334)	2.038 (0.435)

H : Horizontal Components
V : Vertical Component
A half above the diagonal : Horizontal and horizontal
A half below the diagonal : Vertical and vertical
Diagonal matrix : Horizontal and vertical
X(row) = coef. Y(column)
Inside parenthesis ; Y(column) = coef. X(row)
example : AH = 1.669 · Av = 8.701 VH
Av = 0.532 · AH = 9.921 Vv

Table 4 : The Mean Maximum Values

	Horizontal	Vertical (epicentral distance within 20km)
Max. acceleration (gals)	573	356.8
Max. velocity (kines)	55	31.4
Max. displacement (cm)	24.2	17.1
Spectral intensity (cm) h=0.2	123.3	67.0

Fig.-1 Max. Acceleration Estimated by
Overturning of TombstonesFig.-2 Max. Velocity by Strong Motion
Seismograph

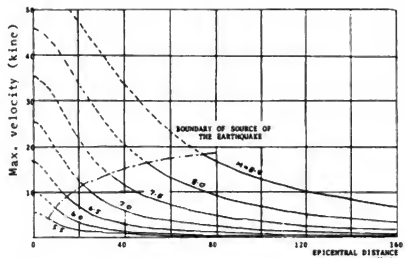


Fig.-3 Epicentral Distance and Max. Velocity

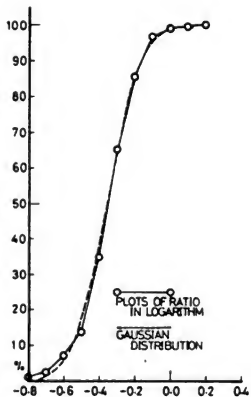


Fig.-4 Probability Distribution
Plots of Variables as
Logarithm of Ratio (Vertical
VS. Horizontal Housner's
Intensity with 20% Damping)

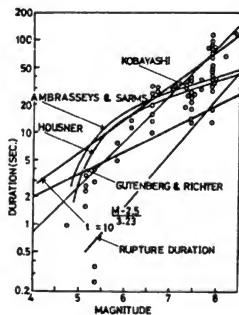


Fig.-5 Duration and Magnitude Proposed by Various Researchers

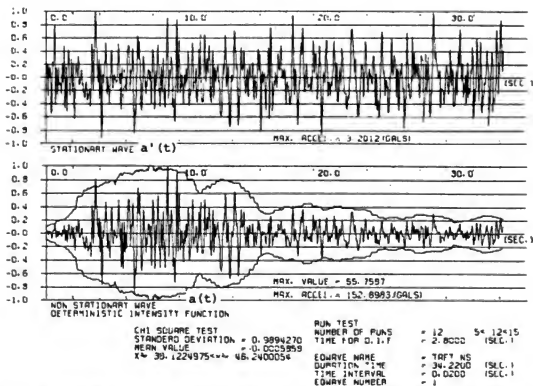


Fig.-6a Deterministic Intensity Function (Horizontal Components)

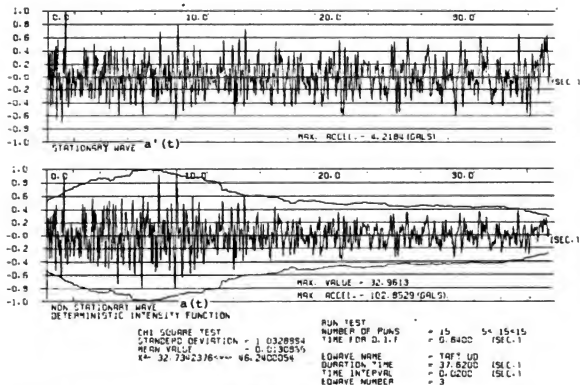


Fig.-6b Deterministic Intensity Function (Vertical Component)

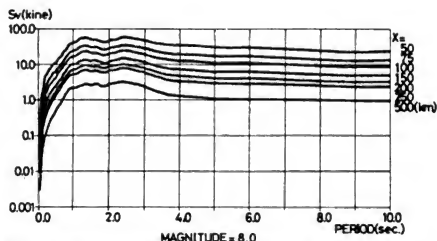


Fig.-7a Velocity Response Spectrum of Ground Motions at Hard-rock due to Earthquake with Magnitude 8.0
(Fraction of Critical Damping : 0.05)

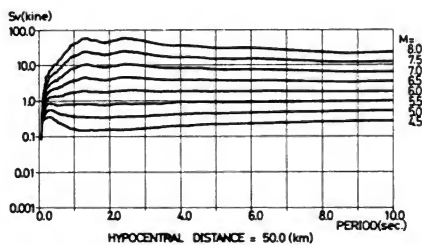
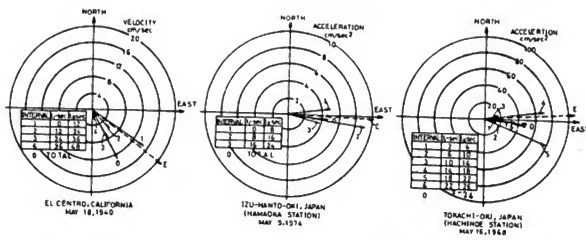


Fig.-7b Velocity Response Spectrum of Ground Motions at Hard-rock due to Earthquake of 50km Hypocentral Distance
(Fraction of Critical Damping : 0.05)



E-EPICENTER DIRECTION

Fig.-8 Principal Axis Directions for 3 Different Recorded Earthquake Ground Motions.

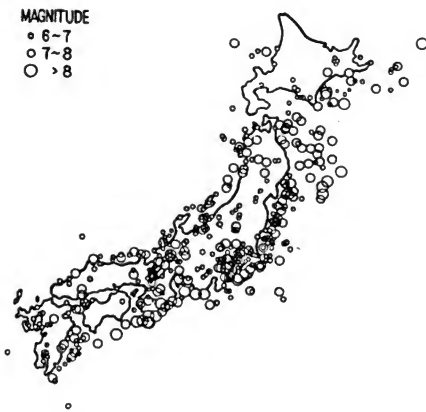


Fig.-9 Magnitude and Location of large Earthquakes in and Around Japan



Fig.-10a Seismic Zoning Coefficient Map
(Mean Value of Each Division)

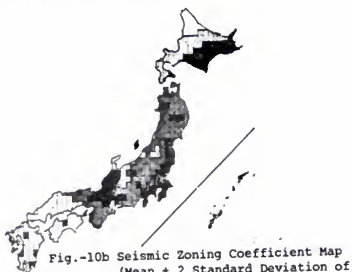


Fig.-10b Seismic Zoning Coefficient Map
(Mean + 2 Standard Deviation of
Each Division)

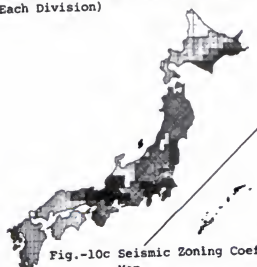


Fig.-10c Seismic Zoning Coefficient
Map
(Maximum of Each Division)

DETERMINATION OF WAVE PROPAGATION VELOCITIES IN

SUBSURFACE SOIL LAYERS

Yukitake Shioi, Chief, Civil Engineering Section

International Institute of Seismology and Earthquake Engineering

Building Research Institute, Ministry of Construction

Toshio Iwasaki, Chief, Ground Vibration Section

Earthquake Disaster Prevention Division

Public Works Research Institute, Ministry of Construction

ABSTRACT

Activities of the Committee on Earthquake Observation on Soil-Structure Interaction have been described. One of the committee's research activities is the research involving the construction of a model structure, soil investigations, dynamic tests and analysis of dynamic soil-structure interaction.

This paper discusses the results of forced vibration tests conducted on a model structure with a vibrator which generated harmonic waves. These waves were then compared with the Rayleigh and Love waves.

KEYWORDS: Harmonic wave; Love waves; model structure; Rayleigh waves; soil-structure interaction; vibrator.

INTRODUCTION

It is empirically and theoretically well known that the vibration of structures on the ground by such energy as an earthquake principally depends on the properties of the superficial layer. In other words it is possible to presume the main ground motions to the structures if we can relate the physical properties of layers to the variables of the vibratory characteristics. Substituting the superficial waves with the Rayleigh and Love waves, we have attempted to obtain the values of coefficients relevant to the ground vibration with the observed records of the harmonic wave propagation generated artificially on a small surface base. Also, the characteristics of these data were examined. As a matter of fact, we took measures to study these characteristics on the propagation waves by means of a high frequency vibrator based on the surface.

This test was a part of the forced vibration tests conducted under the direction of the Committee on Earthquake Observation on Soil-Structure Interaction presided by Professor Yutaka Osawa at the Tokyo University in a comprehensive research project for the Establishment of New Aseismic Design Method. This testing method is somewhat similar to the methods employed by Jeukelon, Foster and Fry at the Waterways Experiment Station (1).

We expect that the accumulated results from these vibratory tests may serve as an exploratory calculation method on the ground movement under various conditions of aseismic design of underground structures and, of countermeasures against the vibration by circulations, etc.

ACTIVITIES OF THE COMMITTEE ON EARTHQUAKE OBSERVATION ON SOIL-STRUCTURE INTERACTION (4)

The research theme commenced since the fiscal year of 1974. During the past second year the Technology Center for National Land Development established a committee on earthquake observation on soil-structure interaction (Chairman: Professor Yutaka Osawa), under the authority of the Building Research Institute, Ministry of Construction. The committee attempted to make a research plan covering all the necessary stages for the future.

In the fiscal year of 1975, construction of an upper structure, dynamic tests on a soil-structure model, and observation of earthquake motions on and around the foundation structure have been accomplished. In addition, theoretical and experimental procedures to analyze dynamic behavior of soils and structures have been investigated.

The research includes construction of a model structure, soil investigations, instrumentation, measurement of seismic motions, dynamic tests and analysis of dynamic soil-structure interaction. The research is expected to be completed in three years. The work accomplished or to be accomplished in the middle of the year is as follows: (See Fig. 1)

- a) Forced vibration test: The forced vibration test using a vibrator was made to study the dynamic characteristics of the model structure, of the neighboring building, and of the wave propagation.
- b) Construction of upper model structure: An upper structure having four steel columns (4-Ø 267.4 x 6.) and one reinforced concrete slab, 4m long, 4m wide and 1m high, was constructed in Fuchinobe, Sagamihara City, Kanagawa Pref.

- c) Earthquake observation: Four transducers were installed in the model foundation structure and six transducers were placed around the model. Six observational data were obtained to determine the dynamic behavior of the subsoil foundation system.
- d) Analysis of dynamic soil-structure interaction: Analytical evaluation of dynamic behavior of the simply shaped structure may be done. For a detailed and complicated system, however, it seems that quantitative investigations and experimental procedures are more significant.

This report discusses the work listed in a) above.

PROPERTIES OF SURFACE WAVE

The vibration of the superficial layers becomes maximum at the surface wave during earthquake from the viewpoint of energy. Among the surface waves, the Rayleigh and Love waves are typical. Their formulas are shown as follows (3), (Fig. 2):

Rayleigh Wave (See Fig. 3)

$$u = A \cdot n [\exp(-\gamma \cdot z) \sin (\omega t - nx) - (2 \gamma / n \cdot s/n) / (1 + s^2/n^2) \exp (-sz)] \sin (\omega t - nx)$$

$$w = A [2\gamma / (1 + s^2/n^2) \cdot \exp(-sz) - \gamma \exp (-\gamma z)] \cos (\omega t - nx)$$

Love Wave

$$v = [B \cos (qz) + C \sin (qz)] \cos (pt - fy)$$

$$v' = D \exp (-q'z) \cos (pt - fy)$$

where,

u = displacement in x direction

v = displacement in y direction (at upper layer)

v' = displacement in y direction (at lower layer)

w = displacement in z direction

A, B, C, D = arbitrary constant

ω = circular frequency on $x - z$ plane

p = circular frequency on $x - y$ plane

n = wave number

f = frequency

$$\gamma^2 = n^2 - \omega^2/v_v^2$$

$$s^2 = n^2 - \omega^2/v_H^2$$

v_v = velocity of P wave

v_H = velocity of S wave

$$q^2 = (p/v_v)^2 - f^2,$$

$$q'^2 = f^2 - (p^2/v_H^2)$$

(prime means of lower layer)

The phase velocities of each surface waves are shown as follows:

$$v_R = k v_v = \omega L_R / 2\pi$$

$$K^6 - 8 K^4 + (24 - 16\alpha^2) K^2 + 16 (\alpha^2 - 1) = 0$$

$$\alpha^2 = (1 - 2\mu) / (2 - 2\mu) = G / (2G + \lambda)$$

$$v_L = p / f = v_H (1 + q^2 L_L^2 / 4\pi^2)^{1/2} = p L_L / 2\pi$$

where,

v_R = velocity of Rayleigh wave

v_L = velocity of Love wave

L_R = wave length of Rayleigh wave

L_L = wave length of Love wave

μ = Poisson's ratio of subsoil

G = shear modulus of subsoil

λ = Lame's constant

OUTLINE OF THE TEST

The vibration tests were performed to research the above mentioned subjects in December, 1975 at which time we installed a high frequency vibrator on a model of reinforced concrete footing ($4^m \times 4^m \times 1^m$). The layout of the model, the fixed observatory instruments and so on, are shown in Fig. 1, but the superstructure of the model was not yet constructed at that time.

The site is on the complex of Sagamihara Engineering Center of Nippon Steel Co./LTD at Fuchinobe, Sagamihara City, Kanagawa prefecture (See Fig. 4). The geological structure consists of Nakatsu layer in the tertiary period, Sagami layers in the diluvial epoch, Sagamino gravel layer, Musashino and Tachikawa loams and subsoil from the bottom, and the upper layers are shown in Fig. 5. The results from the standard penetration tests, seismic prospectings, and so on at the site are given in Fig. 6. The most important layer in this test is the loam extending 14m down. Its physical constants from Fig. 6 and from other existing reports are assumed to be 0.5 to 1.11 km/sec. for the velocity of the P wave, 0.15 to 0.30 km/sec. for the velocity of the S wave, and 0.33 to 0.45 for Poisson's ratio. The predominant frequencies of micro-tremor at this site are recognized at 0.7, 2.1 and 5 Hz. The specifications of the vibrator are shown on Table 1 and it is possible to change continuously the vertical and horizontal frequencies. The frequency range in the test is distributed at 8 to 30 Hz for the vertical, axial, and transverse directions.

To measure the ground vibrations, "pickups" were placed to observe the types of velocity and displacements at constant intervals on the axial direction and we used a master control system for operation and recording at the station (See Fig. 1). The measurement in velocity type was adopted for ground vibration and measurement in displacement type was adopted for soil-structure interaction and vibration of neighboring buildings. The latter results may be introduced again for further studies in the future.

RESULTS

The wave lengths and shear moduli given by substituting the measured frequencies and phase velocities into the equations in article 3 are shown in Table 2 and 3. The vibration test was mainly carried out at the range of frequency around 20 Hz, being relatively stable, because higher frequency was limited in order to protect the vibrator itself and lower frequency could not give clear waves owing to insufficient existing force.

The phase velocities on the horizontal and vertical directions were measured with various pickups. As a result, these differences do not affect the observed values of phase velocity. On the other hand, the dynamic behavior of the ground as seen in Figs. 7 and 8, shows such aspect as the Rayleigh wave at the propagation of the vertical wave but it does not look as clearly as the Love wave at the propagation of the horizontal waves (5).

Assuming that the velocities and shear moduli in Table 2 and 3 represent dynamic properties of the layer in depth of a half wave length, it is possible to express this relation in Figs. 9 and 10. Although it is difficult to indicate the corresponding layer, it seems reasonable from Figs. 3 and 7 that the layer in depth of 0.4 to 0.5 wave length shares the most severe deformation.

The above mentioned results have good correspondence with soil test results and seismic prospecting results. This fact makes us believe that this method of determining dynamic properties of the ground from phase velocity with a vibrator is practical and useful. Now we can point out the merits of this method,

- (1) availability of any type of pickups and of any component of waves.
- (2) continuous measurement of properties of layers downward, depending on different frequencies.
- (3) detailed measurement for shallow layers.
- (4) simple and economic measurement with a vibrator, pickups and recorders.

The disadvantages of this method are:

- (1) requirement to improve the accuracy of the measured phase velocity.
- (2) necessity of electric power.
- (3) difficulty to apply it to the ground under some obstacles, up and down surface, deep layers and so on.

On account of the deformation level in this test, approximately 2×10^{-4} , the resulting values are not directly applicable to such a big vibration as an earthquake but useful to the vibrations caused by circulations, construction works, factories, and so on.

CONCLUSIONS AND ACKNOWLEDGMENT

It is found that if we want to know the dynamic properties of the ground, we can easily obtain comparatively accurate values from shake tests on the ground with a vibrator.

Now there still remain some problems to pursue such as expansion of frequency range, minimization of the base, more comparisons with other methods, device for simpler operation, and so on.

We would like to express our grateful thanks to Professor Osawa and the members of the committee and to the persons who cooperated with this field test.

REFERENCES

1. Vibrations of Soils and Foundations, by Richart, Hall and Woods, Prentice-Hall.
2. Ditto, translated in the Japanese by T. Iwasaki and A. Shimazu, Kashima Shuppankai.
3. Vibration Manual for Civil Engineer (in Japanese), The Japan Society of Civil Engineers.
4. Earthquake Observation on Soil and Structure I, II, III, March in 1975, 1976, 1977 (in Japanese), Building Research Institute.
5. Bulletin of the International Institute of Seismology and Earthquake Engineering, Vol. 14, 1977. Surface Waves Generated by a Vibrator, by S. Hattori.

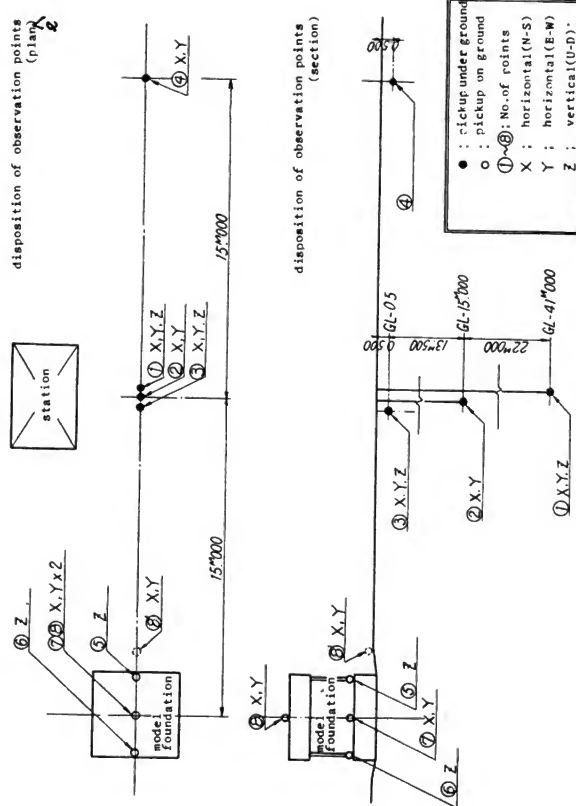


Fig.1 Disposition of observation points

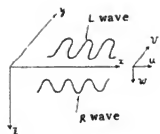


Fig. 2 Modes of Rayleigh and Love waves

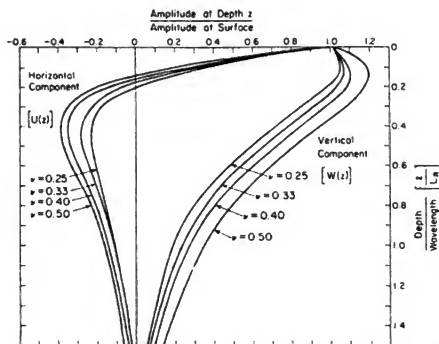


Fig. 3 Amplitude ratio vs. dimensionless depth for Rayleigh wave

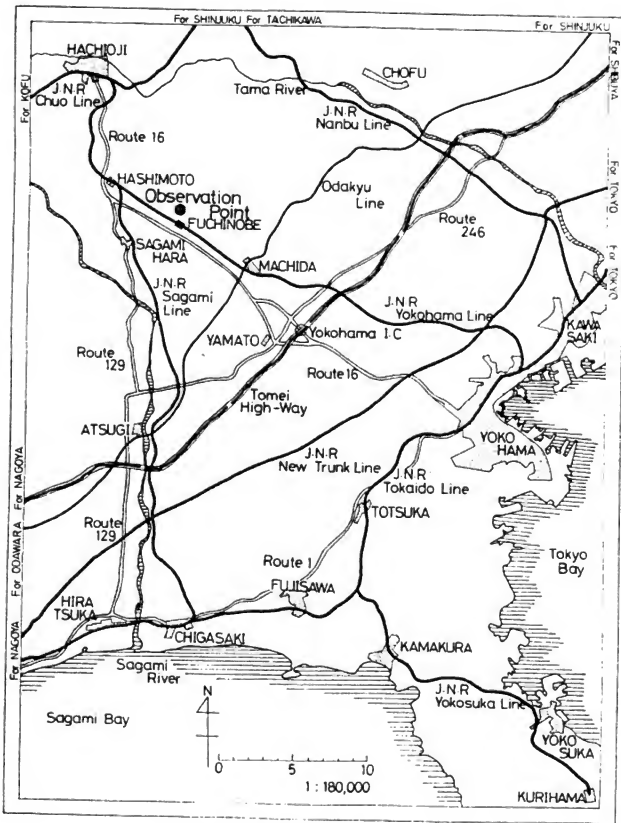


Fig. 4 Experimental site 4)

point	No 2	reference									
title	Survey for dynamic properties of soil	U									
place	2-2-24 Fuchinobe, Sagamihara, Kanagawa	D									
date	20 - 25 March, 1975	P : Pressuremeter									
altitude	111.5290	standard TP									
method	Rotary boring										
name	N. Yamada	chief									
name	S. Miyaji										
scale	water level depth (m)	thickness (m)	sampling point (m)	symbol	soil	color	remark	consistency	pene- tration value (N)	standard penetration test	scale
0	111.5290	0	0.55		loam	dark brown	reclaimed soil	—	0.00	0.00	0
1	114.76	0.55	3.40	P-1 (12.00)	loam	light brown		medium	1.30	6.00	1
2			P-2					soft	2.32	6.50	2
3			0.90	P-3 (14.00)	loam	brown containing sand	slightly	medium	3.00	7.00	3
4	111.38	3.95	2.75	P-4 (16.00)	loam	light brown	mixed with dark brown	medium	4.00	7.50	4
5	110.64	4.85	0.95	P-5 (18.00)	loam	brown	mixed with white	hard	5.00	8.00	5
6			3.30	P-6 (10.00)	loam	brown		hard	6.00	8.50	6
7	-107.69	7.60	0.90	P-7 (12.00)	loam	light brown	light stone	hard	7.00	9.00	7
8	-106.70	8.55	1.10		clay	brown	12.m0	medium	7.50	9.50	8
9			0.4		loam			—	8.00	10.00	9
10			0.4					—	9.00	11.00	10
11			0.4					—	10.00	12.00	11
12	-103.04	11.85	0.4					—	11.00	13.00	12
13	-102.56	12.75	0.4					—	12.00	14.00	13
14	-101.64	13.85	0.4					—	13.00	15.00	14
15			0.4					—	14.00	16.00	15
16			0.4					—	15.00	17.00	16
17			0.4					—	16.00	18.00	17
18			0.4					—	17.00	19.00	18
19			0.4					—	18.00	20.00	19
20			0.4					—	19.00	21.00	20
			6.29					—	20.00	22.00	
								—	20.10	22.10	

Fig. 5 Result from geological survey

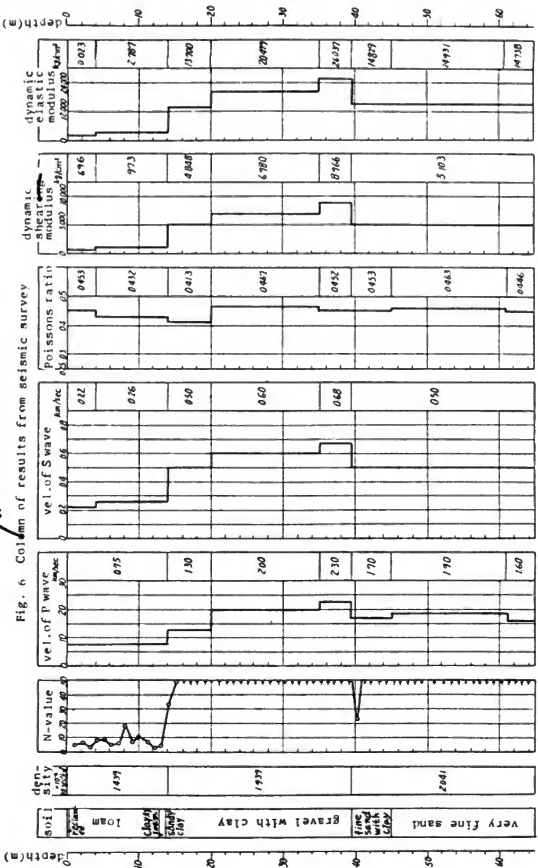
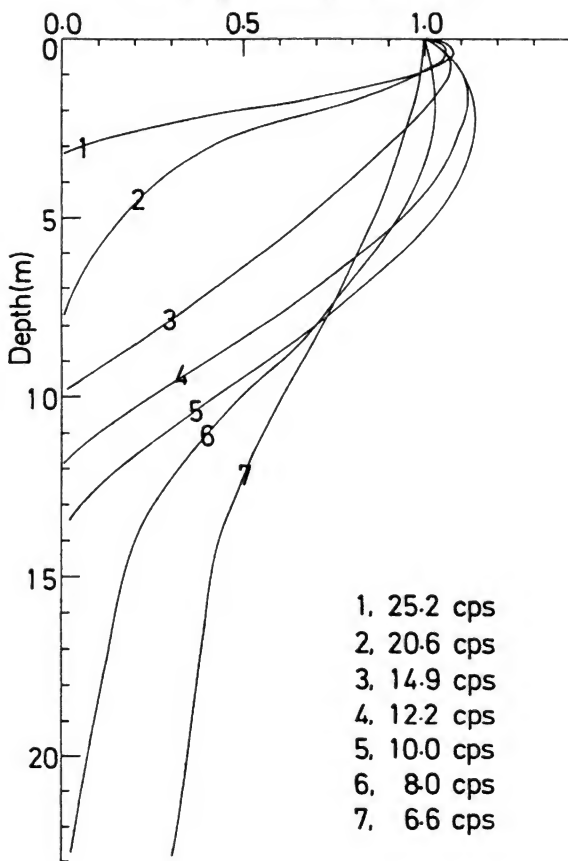


Fig. 7 (a) Amp. distribution
(Rayleigh wave; Ver. comp.)



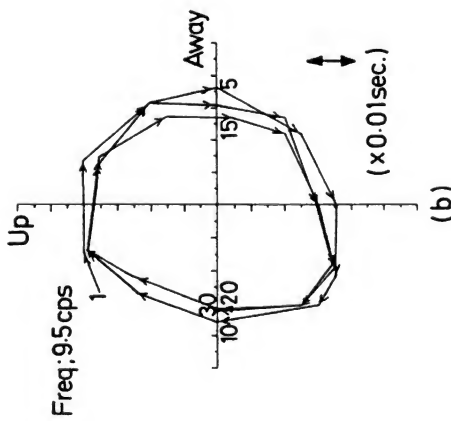
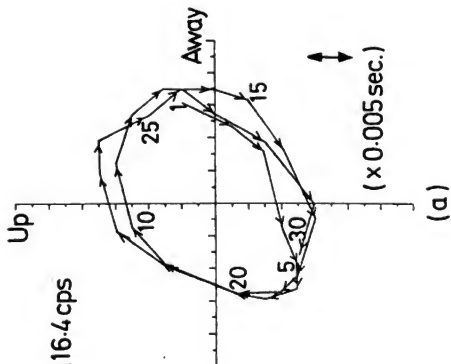
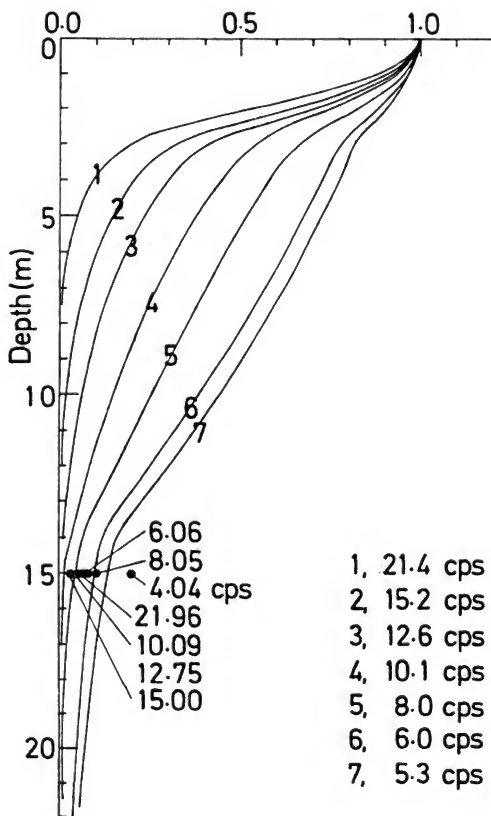


Fig. 7 (b) Observed particle orbit's

Fig. 8 Amp. distribution
(Love wave)



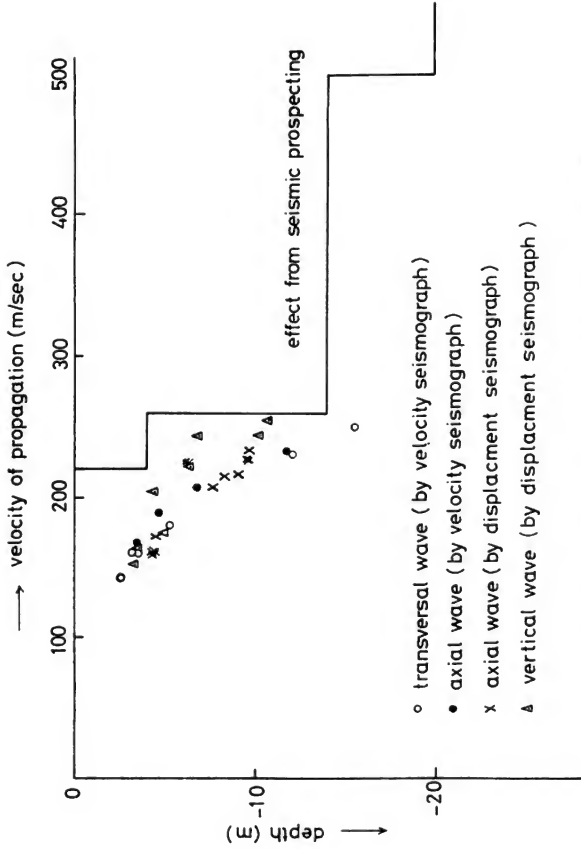


Fig. 9 Distribution of propagating velocity of wave

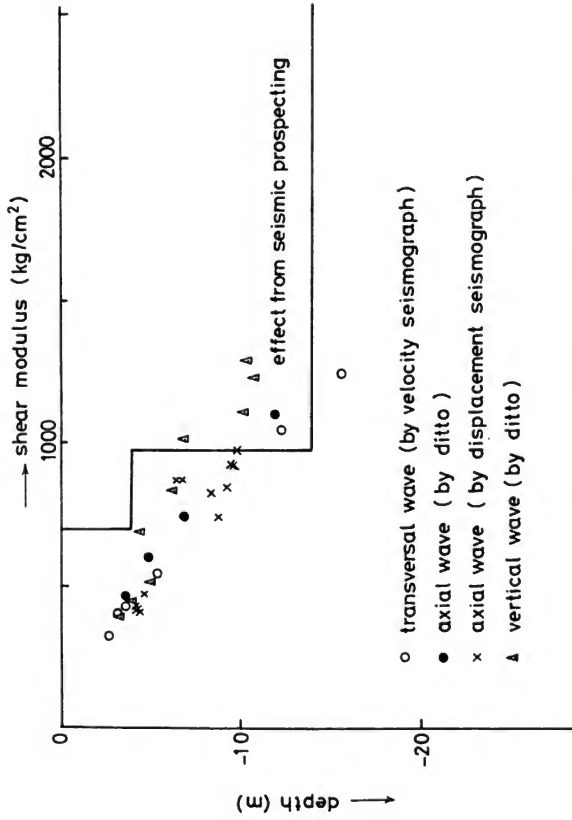


Fig. 10 Distribution of shear modul

Table - 1 Main Specification of Hi-Frequency Vibrator

Item (Vibrator)	Content	Item (Motor)	Content
Exciting system	Simultaneous reversal rotation system with 3 - unbalanced weight and 3 horizontal axes	Type	Convertible velocity induction motor in air ventilation type
Exciting moment	1 - 250 kg·cm (continuously changeable)	Out-put	5.5 kW
Max. force	3000 kg (> 17 Hz)	Power	3 phase A.C., 200/220 V 50/60 Hz
Frequency	1 - 20, 2 - 40 Hz	Rotational frequency	0 - 1100/0 - 1300 rpm
Accuracy	$\pm 1\%$ against Max. value.	Control system	Control by thyristor system
Dimension	1020 (mm) in width 880 (mm) in length 880 (mm) in height	Weight	900 kg (incl. motor)

Table 2

Values by velocity vibrograph

Values on horizontal shaking by displacement vibrograph

Table - 3

Values on Vertical shaking by displacement vibrograph									
Direction	Section	ω	ψ^*	ω^*	L	$L/2$	ρ	G	Reference
Axial	5 - 15	75	255	12.0	21.4	10.7	2.0	1801	Exciting force 1t
		114	245	18.1	13.5	6.8	1.7	1020	ditto
		145	204	23.0	8.8	4.4	1.7	707	ditto
	20 - 30	75	255	12.0	21.4	10.7	1.9	1235	ditto
		113	175	18.0	9.7	4.9	1.7	521	ditto
		145	153	23.0	6.6	3.3	1.7	398	ditto
Vertical	5 - 15	75	245	12.0	20.4	10.2	1.9	1140	ditto
		113	175	18.1	9.7	4.9	1.7	521	ditto
		136	163	21.1	7.7	3.9	1.7	452	ditto
	20 - 30	75	245	12.0	20.5	10.3	1.9	1140	ditto
		114	223	18.1	13.5	6.2	1.7	845	ditto
		151	204	24.0	8.5	4.3	1.7	707	ditto
					* measured				

STUDIES ON SOIL LIQUEFACTION RELATED TO
EARTHQUAKE RESISTANT DESIGN OF STRUCTURES

Masamitsu Ohashi, Chief, Earthquake Disaster Prevention Division

Toshio Iwasaki, Chief, Ground Vibration Section

Fumio Tatsuoka, Research Engineer, Ground Vibration Section

All from the Public Works Research Institute, Ministry of Construction, Japan

ABSTRACT

In order to evaluate dynamic behavior of structural foundations and embedded structures during earthquakes, it is essential to estimate the effects of the surrounding soils on these structures. The authors have conducted a literature survey on the effects of liquefied soils on bridge foundations and also conducted laboratory experiments using models of pile foundations including surrounding soils.

Furthermore, a simplified method to evaluate liquefaction potential of sand deposits was investigated on the basis of numbers of blows (so called N-values) by the standard penetration test. Proposed herein are the critical N-values which can be used in determining liquefaction potential. This method can estimate whether the sand deposit may likely liquefy or not during future severe earthquakes by means of comparing N-values measured at the site of interest with the critical values proposed. These critical values were determined on the basis of dynamic triaxial tests on undisturbed sand samples and N-values measured at the points where the undisturbed samples were obtained.

These studies are to clarify the effects of liquefied soils on pile foundations and to establish design methodology of pile foundations considering the effects of soil liquefaction.

KEYWORDS: Bridge foundations; dynamic triaxial tests; liquefaction; model tests; pile foundations; sand; standard penetration test; shake table.

INTRODUCTION

In order to appropriately evaluate dynamic behavior of pile foundations or embedded structures during earthquakes, it is essential to estimate the effects of the behavior of the surrounding soils on these structures. It can be supposed that the surrounding soils do not move severely in normal cases and normally resist movements of the structures, but sometimes the surrounding soils cause large movements of the structures when the soils vibrate severely as a result of resonant state of the soils and furthermore in special cases the surrounding soils do not support these structures at all when soil liquefaction takes place.

To provide a proper solution to this problem, it seems necessary to precisely analyze the behavior of the structures considering the effects of soil-structure interactions. When the surrounding soils liquefy during earthquakes, the problem becomes more complicated. In this case, the effects of liquefied soils on the structures will be much more severe.

The authors have conducted a literature survey on the effects of liquefied soils on bridge foundations and also conducted laboratory experiments using models of structures including surrounding soils. This attempt was to clarify the effects of liquefied soils on pile foundations, and to establish design methodology of pile foundations considering the effects of soil liquefaction.

Another problem to be considered in the aseismic design of bridges with pile foundations in sand deposits with high liquefaction potential is the evaluation of liquefaction potential of sand deposits. In the simplified procedures for evaluating liquefaction potential generally used in Japan, the N-value obtained from the standard penetration tests are used in evaluating the liquefaction potential of the sand deposit.

If the N-value of the sand deposit of interest is lower than a critical value, say $N=10$, it is judged that this sand deposit will liquefy during severe earthquake motions. In this study dynamic triaxial tests on undisturbed sand samples were conducted and at the same time N-values were measured at the points from where undisturbed samples were secured. Then the appropriate critical N-values were determined on the basis of the relationship among dynamic shear strength, N-value and insitu effective overburden pressure. It was found that even in the case where the dynamic shear strengths are identical, the N-values may vary according to the variation of soil properties which can be represented by the content of fine soils and the mean diameter of soil particles.

The results of this study are summarized as follows:

1) The supporting capacities of surrounding soils may become considerably smaller when liquefaction takes place.

In some cases, dynamic forces of soils acting on piles may become considerably larger in the course of liquefaction. When the complete liquefaction takes place, both the supporting capacities and the dynamic forces can be approximately estimated by assuming that a liquefied sand layer is heavy water.

2) In the course of liquefaction, soil-pile foundation systems may resonate to the input motions, and may vibrate severely.

3) Critical N-values for evaluating the liquefaction potential should be determined by taking into account the facts that the N-values decrease with increase in the content of fine soils in sand deposits. Also, the dynamic shear strength does not decrease much as compared with the decrease in the N-values.

DAMAGE TO BRIDGE FOUNDATIONS DUE TO LIQUEFACTION

It has been recognized that one of the main causes of damage to bridges which were constructed in alluvial deposits and reclaimed lands is an unstable performance of ground soils. It is also well known that liquefaction of sandy soils induce catastrophic movements of ground and loss of bearing capacities of ground. A number of damages to bridge structures with pile foundations were observed during the Niigata Earthquakes of 1964 in Japan (Iwasaki (1973)) and during the Alaska Earthquake of 1964 in the United States (Kachadoorian (1968)). Similar damages were also reported for other earthquakes in Japan (Iwasaki (1973)) and for the San Francisco Earthquake of 1906 (Youd and Hoose (1976)). Liquefactions have been observed in alluvial deposits and reclaimed lands during major earthquakes including the above earthquakes. In Japan, 44 earthquakes induced liquefaction phenomena during the period from 1872 to 1968 (Kuribayashi and Tatsuoka (1974)).

In viewing damages to engineering structures caused by soil liquefaction, numerous studies on evaluation of liquefaction potential of sandy deposits have been conducted by using dynamic soil testing equipment such as dynamic triaxial apparatus and a dynamic simple shear apparatus. Furthermore, studies have also been conducted with shaking table tests to determine the effects of the loss of bearing capacities caused by liquefaction on the behavior of heavy structures (Yoshimi et al. (1975), Ishihara, et al. (1975)). However, little effort has been made on the study of the effects of soil liquefaction on the dynamic behavior of pile foundations (Shikamori, Sato and Hakuno (1973), Yoshida and Uematsu (1975), Iwasaki, Tatsuoka and Sakaba (1976)). Accordingly methodology of aseismic design of pile foundations considering the effects of liquefaction is still in the process of formation.

Intending to establish a rational aseismic design criterion of pile foundations which are constructed in soil deposits with high liquefaction potential, a series of shaking table tests of pile foundations placed in liquefying sand deposits was performed.

EXPERIMENT ON DYNAMIC BEHAVIOR OF PILE FOUNDATION MODELS

Test Arrangements - In this experiment small models of pile foundations were prefabricated on a shaking table. Five different tests listed in Table 1 were conducted. Typical test arrangements for Test 1 and Test 2 are illustrated in Figs. 1 and 2, respectively. A saturated loose sand layer including a small model of a pile foundation was placed in a container on a shaking table. To actuate the shaking table an electro-magnetic actuator was used for Test 1. A displacement controlled hydraulic actuator was used for Tests 2 to 5. Sand layers were prepared by pouring air-dried sand into water. Initial relative densities of the sand layers ranged from 24 to 40 percent. The water level coincided

with the sand surface at the beginning of shaking. As shown in Figs. 1 and 2, accelerometers and strain gauges were installed to measure movements of the shaking table, sand layers and pile foundation models. Earth pressure cells and pore pressure cells were also equipped to measure earth pressures acting on piles and excessive pore water pressures. Sinusoidal table motions were applied in all tests (Tests 1 to 5). Wave form of acceleration measured at the table was of triangular form in the case of Test 1, as shown in Fig. 3 where the table acceleration is denoted as A_1 . However, in the other tests (Test 2 to Test 5) where a hydraulic actuator was used, the measured table acceleration was close to sinusoidal motion, as shown in Figs. 4 and 5. Several motions with different frequencies were employed as input motions. Frequencies were selected on the basis of the natural frequencies of pile foundation models submerged in water. The base acceleration was determined in view of outbreak of gradual increase in excessive pore water pressure in sand layers. Actuators used in the experiments were not sufficient enough to keep an accurately constant base acceleration during a test run. This is due to a great change in rigidity of sand layers, which are caused by soil liquefaction. Actually, the base acceleration changed somewhat in the course of liquefaction of sand layers, as shown in Figs. 3 through 5.

Four different pile foundation models were examined (see Table 1). Their natural frequencies when submerged in water are 3.8, 4.0, 10 and 14 Hz, respectively. Their natural frequencies in air are slightly higher than those in water. Each of these models consists of several solid aluminum bars with 2 cm in diameter and a top mass. The values of the natural frequencies of models were adjusted by choosing the number of bars and the weight of the top mass. These models were fixed at the bottom, as shown in Figs. 1 and 2 to facilitate the boundary condition. The degree of fixity would be considered to be larger than that in actual cases.

Principles of Similarity - Frequencies of input motion and natural frequencies of pile foundation models submerged in water were determined in the following manner. Model tests in the field of soil mechanics can be classified into two groups by their objectives. The first group is to find fundamental parameters required to be taken into account when analyzing the behavior of the prototype by an analytical method. This analytical method can be, of course, applied to the model test. In this case, the rigorous satisfaction of principles of similarity is not of first importance. The second group is to quantitatively estimate the behavior of the prototype from the results of model tests. In this case the principles of similarity should be determined and satisfied. At present, it is of first importance to find the controlling factors in the behavior of structures in liquefying soils. Therefore, reported herein is the result of tests of the first category. Accordingly, the similitude between the prototype and the model was satisfied in terms of the following (but others such as the permeability of sand layers could not satisfy the principles of similarity):

(i) Length (L): Scale ratio considered for length was on the order of 1:10 to 1:30. Therefore, model sand layers with the height of 70 cm correspond to actual sand deposits of 7 to 21 m in depth.

(ii) Density of sand layer (MLT^{-2}): Since actual sands were used, the ratio of density of soils was on the order of 1:1.

(iii) Acceleration (LT^{-2}): Since body force induced by gravity is the same between models and prototypes, the ratio for body force induced by horizontal motions should be on the order of 1:1. And the ratio for horizontal acceleration was also on the order of 1:1.

(iv) Time (T): From (i) and (iii) the ratio for time is determined as

$$1 : \sqrt{L} = 1 : \sqrt{10} \text{ to } 1 : \sqrt{30} = 1:3.2 \text{ to } 1:5.5.$$

(v) Natural frequencies of model pile foundations submerged in water (f_p), frequencies of input motion (f_i), and fundamental natural frequencies of sand layers with the excessive porewater pressure of zero and the shear strain level of $\tau = 10^{-4}$ or less (f_g), (T^{-1}): These scale ratios are determined from (iv) as $1:\frac{1}{T} = 1:\frac{1}{3.2}$ to $1:\frac{1}{5.5} = 1:0.32$ to $1:0.18$.

Estimated frequencies f_g for model sand layers were around 18 and 24 Hz as shown in Table 1. These values correspond to the natural frequencies of the prototype sand layers, 3.2 to 7.7 Hz. On the other hand, the fundamental natural frequency of a soil deposit f_1 (Hz) can be approximately estimated by:

$$f_1 = \frac{V_s}{4H} \text{ (Hz)} \quad (1)$$

in which V_s denotes the average shear wave velocity (m/sec) and H means the depth (m) of soil deposit of interest. Since the usual values of V_s for shallow alluvial sand deposits range from 150 to 250 m/sec, the fundamental frequency of sand deposit with the depth of 7 to 21 m ranges from $150/(4 \times 21) = 1.8$ Hz to $250/(4 \times 7) = 8.9$ Hz. These values correspond well to the values derived from scale ratios and the fundamental frequencies of model sand layers (=3.2 to 7.7 Hz).

Since predominant frequencies of strong earthquake motion observed on the actual sand deposits are estimated to be less than the above values, the frequency of input motion in model tests f_i should be less than the natural frequencies of model sand layers f_g (18 and 24 Hz). Therefore, as the values of f_i in the model tests, 12 Hz for Iruma sand and 10 Hz and 20 Hz for Toyoura sands were selected.

Furthermore, it can be estimated that the fundamental natural frequencies of ordinary bridges with pile foundations, f_p , are less than the predominant frequency of strong earthquake motion observed on shallow sand deposits when the value of f_p are determined on the assumption that liquefied sand layer with the depth of 7 to 21 m are removed. Therefore, three of the five model tests conducted were cases where the natural frequencies of model pile foundations submerged in water, f_p , are less than the frequency of input motion, f_i , which correspond to actual ordinary cases. In addition to these cases where $f_p < f_i$, other two cases where $f_p = f_i$ and $f_p > f_i$ were examined in order to evaluate the importance of the relationship between these two values, f_p and f_i in assessing the dynamic behavior of pile foundations in liquefying sand layers.

Test Records - For Test 1, acceleration records at the table at three positions in the sand layer and at three positions of the model pile foundation are shown in Fig. 3. Excessive porewater pressure in the sand layer and earth pressure acting on the pile foundation are also illustrated in the figure during the elapsed time of 8 to 14 seconds

counting from the beginning of shaking. Similar records in the cases of Test 2 and Test 4 are shown in Figs. 4 and 5, respectively. One of the most peculiar performances observed in these tests is non-stationary behavior of the sand layer and the pile foundation, and non-stationary dynamic interaction between them, while the table movement is almost stationary. Furthermore, it can be noted that the responses of different pile foundation models are not similar to each other. Especially, the variation of the response of the pile foundation in Test 4 is quite different from those in Test 1 and Test 2.

In order to clarify the dynamic behavior of the sand layer and the pile foundation, envelopes of dynamic amplitudes recorded were illustrated in Fig. 6 for Test 1. Since in the case of Test 1 excessive porewater pressures reached their maximum stationary values at the elapsed time between 11 and 12 seconds and the acceleration in the entire sand layer decreased to almost zero at the same time, it could be estimated that liquefaction in the entire sand layer initiated at the elapsed time between 11 and 12 seconds in the case of Test 1. It should be noted in the case of Test 1 that the maximum response of the pile foundation occurred at the elapsed time of about 10 seconds when excessive porepressure did not reach the maximum value yet and the sand layer was vibrated in ordinary fashion. And at $t=10$ seconds, dynamic earth pressure acting on the pile foundation and strains in the pile also had their maximum values. In addition to this, it is also noted in the case of Test 1 that the response (acceleration) of the pile foundation decreased to the small value after the entire sand layer had liquefied. Corresponding to this decrease in acceleration of the pile foundation, earth pressure acting on the piles and strains in the pile also decreased to the small values. Following this, recovery from liquefaction started at the elapsed time of about 30 seconds, and after this moment the response of pile foundation increased again. Although this recovery phenomenon is also very interesting, this will not be discussed herein because such a phenomenon is unlikely to take place in the prototype during severe ground shaking in an actual earthquake. In this test, the ratio of time in the model and that in the prototype is considered on the order of 1:3.2 to 1:5.5. Therefore, the elapsed time of 30 seconds in the model corresponds to 96 to 165 seconds in the prototype. This duration time seems longer than the duration of major ground motion during a strong earthquake. Furthermore, it is recognized that recovery from liquefaction began after the cease of earthquake motion in the actual earthquakes experienced. From these reasons, only phenomena observed before the recovery from liquefaction will be discussed in this report.

Variations of Responses of Pile Foundation Models in the Course of Liquefaction - In
Fig. 7 shown is the variation of response ratio β_p of the pile foundation with respect to frequencies of input motion in the case of Test 1. The response ratio β_p is defined as

$$\beta_p = \frac{|\alpha_{A6}|}{|\alpha_{A1}|} \quad (2)$$

where $|\alpha_{A1}|$ represents the amplitude of the acceleration at the base and $|\alpha_{A6}|$ represents the amplitude of the acceleration at the bottom of the top mass of the pile foundation. The solid curve in Fig. 7 represents the response curve of the pile foundation model

measured when submerged in water and the black solid circles denote the response ratio of the pile foundation model measured in liquefying sand layer at several increments of elapsed time. Numbers near the black solid circles represent the elapsed time in seconds from the beginning of shaking. It is seen from this figure that the response ratio of the pile foundation model, β_p , once increased before $t=10$ seconds and then decreased abruptly to a smaller value of 0.2 at $t=12$ seconds. Also illustrated in Fig. 7 are the response ratio of sand layer $\beta_g = |\alpha|/|\alpha_{A1}|$, excessive pore water pressure ratio u/u_{\max} and the amplitude of dynamic earth pressure acting on the pile foundation $|p_d|$. These values are illustrated in relation with β_p . It is clearly seen from this figure that at the moment of the maximum response of the pile foundation model, sand layer had not liquefied yet and the dynamic earth pressure had the maximum value and also that after the occurrence of liquefaction in the entire sand layer the response of pile foundation and the dynamic earth pressure also decreased to smaller values.

Similarly Figs. 7, 8, 9 and 10 represent the variation of responses of pile foundation models in the cases of Test 2, Test 4 and Test 5, respectively. In these figures, squares denote responses of pile foundation models at the moment when liquefaction is not initiated in any part of the sand layer, triangles show responses at the moment when liquefaction is taking place in the upper part of the sand layer, and circles represent responses when liquefaction is taking place in the entire sand layer. It can be noted from these figures that while the variation of the response of the pile foundation model in the case of Test 2 is quite similar to that in the case of Test 1, those in the case of Test 4 and in the case of Test 5 are considerably different from that in the case of Test 1 or that in the case of Test 2. The cause for these differences among these tests will be discussed later.

Fig. 11 illustrates instantaneous positions of the sand layer and the pile foundation model at several instants of time ($t=8.0$ to 12 seconds) in the case of Test 1. In this figure, each stage (a) through (d) in each column represents the variation of positions of the sand layer and the pile foundation model with a short interval during the half of the vibration period (=1/24 second). In each figure, circles represent the value of $-\alpha/|\alpha_{A1}|$ in which α denotes the instantaneous value of acceleration recorded by the accelerometers A2 through A4 equipped in the sand layer, and $|\alpha_{A1}|$ represents the amplitude of the base acceleration. In an ideal sinusoidal movement, $-\alpha/|\alpha_{A1}|$ can be an index representing the displacement modes. And solid circles represent those for the pile foundation model. Arrows represent the instantaneous directions of the movements at each point and the short vertical straight lines represent the maximum values of $-\alpha/|\alpha_{A1}|$ at each point during the half of the vibration period. Triangles denote the instantaneous values of earth pressures acting on the pile. The positive sign corresponds to the increase of earth pressures sensed by the earth pressure cell which faced to the right in these figures. At the bottom of Fig. 11 shown are the excessive pore pressure ratio u/u_{\max} . It is seen from this figure that at the elapsed time of 8 seconds when excessive pore water pressures were very small, movements of the sand layer and those of the pile foundation model are close to each other during the half of the vibration period. Then, as time goes on and excessive pore pressures increase, the difference between the movement of the sand layer and that of

the pile foundation model increases gradually. This would mean that the capability of the sand layer to support the pile foundation model is decreasing with decrease in the effective stress in sand layer (which corresponds to increases in excessive pore water pressure). As seen in Figs. 3 through 11, liquefied parts in the sand layer expand from the surface toward the bottom. Therefore, the free length of the pile foundation model which are not supported by the surrounding sand layer increased with increase in excessive pore pressure in the sand layer. This means that the natural frequency of the pile foundation in the sand layer, which is defined as f_p , decreased with increase in the free length of pile foundation.

Then, it would be beneficial to examine the response of the pile foundation model from the viewpoint of structural dynamics. First, let's suppose a single-degree-of-freedom vibrating system which corresponds to the pile foundation model in the sand layer. The maximum value of the response ratio $\beta_p = 3.6$ of the pile foundation model, which took place at the elapsed time of 10 seconds, could be regarded as that of the vibrating system which resonates to the sinusoidal input motion with the frequency of $f_i = 12$ Hz. Then, the apparent damping ratio (h) of the vibrating system could be derived as,

$$h \approx \frac{1}{2 \times 3.6} \approx 0.14 \quad (3)$$

In Fig. 12 shown are the response curve of the equivalent single degree-of-freedom vibrating system with the damping of 0.14 and are the phase relation between the input force and the motion of the system. Using this response curve, the apparent natural frequency of the pile foundation model embedded in the sand layer f_p^* in the case of Test 1 was obtained as follows. It could be supposed that the natural frequency of the pile foundation embedded in non-liquefied sand layer at the strain of around 10^{-4} is similar to the natural frequency of the sand layer, that is, $f_g = 18$ Hz in the case of Test 1. Therefore, just after the beginning of shaking the natural frequency of the pile foundation embedded in the sand layer, f_p^* would be around 18 Hz. This means then $f_i/f_p^* = (12/18) < 1.0$. Therefore, the approximate value of f_i/f_p^* at the elapsed time of $t=8.0$ seconds can be obtained from the intersection point between $\beta_p = 2.1$ (β_p at $t = 8.0$ seconds) and the response curve for $f_i/f_p^* < 1.0$. By the same procedure, the values of f_i/f_p^* were obtained for the following elapsed time $t = 10.0, 10.8, 11.3, 12.2$ seconds as shown in Fig. 12. It is seen from this figure that the ratio of the frequency of input motion to the natural frequency of the pile foundation model embedded in the sand layer, f_i/f_p^* , increased with time and eventually approached the value in the case of the pile foundation model submerged in water, $f_i/f_p = 12/3.8 = 3.2$. Since the value of f_i was kept constant as 12 Hz, the increase of f_i/f_p^* means the decrease of f_p^* . Also shown in Fig. 12 is the phase relation ϕ between the motion at the bottom of the top mass and the motion at the base. In this figure, the values of ϕ were obtained from Fig. 11 and the values of f_i/f_p^* were obtained from the procedure described above. The general coincidence of the measured phase relation with that of the single-degree-of-freedom vibrating system with damping ratio $h = 0.14$ means that the variation of the response of the pile foundation, β_p , in

liquefying sand layer was caused by the variation of the apparent natural frequency of the pile foundation model in the sand layer, β_p .

As a next step, the effects of the response of the sand layer on the response of the pile foundation model should be taken into account, because the response of sand layer varied in the course of liquefaction as shown in Figs. 3 through 11. In the case of the pile foundation with a very small rigidity, the response of this pile foundation would be completely affected by the response of the sand layer before effective stress in the sand reduces to zero. On the other hand, this effect would be rather small in the case of the pile foundation with a relatively large rigidity. This would be the cases of these tests (Tests 1 to 5). For example, in the case of Test 1, the maximum response ratio of the pile foundation β_p , is about 3.6 at $t = 10$ seconds and at this moment the response ratio of the sand layer near the surface was about 1.9 which is less than 3.6 ($=\beta_p$). This means that the large response of the pile foundation model at $t = 10$ seconds was caused mainly by the resonance of the pile foundation model embedded in the sand, as illustrated in Fig. 12.

A Summary of Model Tests of Pile Foundation Tests

A summary of the whole test results in Fig. 13 shows the relationship between the response ratios (β_p) of the pile foundation models and the ratios (f_i/f_p) of frequencies of input motions to the natural frequencies of the pile foundation models submerged in water. This figure indicates clearly that a comparative relation among the frequencies of input motions f_i , the natural frequencies of the pile foundation models submerged in water (f_p) and the initial natural frequencies of the sand layer (f_g) is fundamental in determining the dynamic behavior of the pile foundation models in liquefying sand layer. Since all of the tests shown in Fig. 13 are the cases where f_g is larger than f_i or f_p , these tests can be divided into the following three groups:

(a) $f_g > f_i > f_p$ (Tests 1 to 3): In these tests, the response ratios of the pile foundation models, β_p , are small at the beginning of shaking as indicated by hollow squares in Fig. 13, and as the sand layer begins to liquefy, β_p starts to increase, reaching its maximum value as indicated by black triangles. At this moment, the sand layer has not liquefied completely. And following this moment, β_p begins to decrease and eventually β_p becomes a small value as indicated by hollow circles in Fig. 13. These small values of β_p correspond well to those of the response ratios of the pile foundation models submerged in water. The phenomenon described above could take place in the prototype as one of the worst cases. Therefore, the maximum value of β_p in the course of liquefaction in sand deposits should be estimated accurately in the case of the prototype so that this phenomenon can be taken into account in aseismic design of pile foundations.

(b) $f_g > f_i = f_p$ (Test 4): In this test, β_p simply increases from the beginning of shaking to the state of the liquefaction in the entire sand layer. The eventual response ratio in the completely liquefied sand layer is as large as the value at the resonance of the pile foundation model submerged in water. If there could be such a case where $f_i = f_p$ in the prototype, severe damages could take place, because the response might become quite large.

(c) $f_g > f_p > f_i$ (Test 5): In this test, the tendency of the variation of β_p is similar to that of Test 4. However, unlike in Test 4, the eventual value of β_p in the completely liquefied sand layer is rather small, because the response ratio of the pile foundation model submerged in water is small due to the fact that the value of f_i/f_p is much less than 1.0. In this case, the damage to the pile foundation would be minor. However, this case would be unlikely to exist in the prototype, because the value of f_p would be smaller than f_i in most cases in the prototype.

SIMPLIFIED PROCEDURES IN EVALUATING LIQUEFACTION POTENTIAL

Present Status

In the specifications for Earthquake Resistant Design of Highway Bridges (Japan Road Association - 1971), a special attention is given to the design of highway bridges constructed in sandy layers vulnerable to liquefaction during earthquakes and in very soft cohesive layers. The bearing capacities of these layers are neglected in the design, in order to assure high earthquake resistance of structures built in these layers. An article "Sandy Soil Layers Vulnerable to Liquefaction" states: saturated sandy soil layers which are within 10 meters below the actual ground surface, have a standard penetration test N-value less than 10, have a coefficient of uniformity less than 6, and also have a D_{20} -value of the grain size accumulation curve between 0.04 mm and 0.5 mm, shall have a high potential for liquefaction during earthquakes. Bearing capacities of these layers shall be neglected in design.

Saturated sandy soil layers which have a D_{20} -value between 0.004 and 0.04 mm or between 0.5 and 1.2 mm may liquefy during earthquakes, and shall be given an attention. Estimation in the case shall be made in accordance with the available information on liquefaction problems.

When a special investigation is performed, the above article may not be required to apply.

On the other hand, it is well known that standard penetration N-values may vary considerably due to the variation of the grain size of sand deposits. For example, it is a general tendency that in so-called alluvial sandy deposits, N-values are considerably large for gravelly sand deposits and are quite small for silty sand deposits. Therefore, it can be easily supposed that N-values do not hold a constant value even for the cases where the dynamic shear strengths are constant. The difference of N-values in the two cases would be caused by the other soil properties such as the grain size rather than the dynamic shear strengths. Accordingly, if an identical critical N-value, say 10, is applied to all types of sand deposits in evaluating liquefaction potential, this critical N-value may be too small for gravelly sand deposits and may be too large for silty sand deposits. For these reasons, it is specified in the above-mentioned specifications that the uniformity coefficient U_c and D_{20} -value should be taken into account in the evaluation of liquefaction potential in addition to the N-value. However, it has become clear recently that there is no evidence that the U_c -values of sands have a definite relation to liquefaction potential. Furthermore, it seems that the D_{20} -value specified in the above-mentioned specifications

are not always proper as an index representing grain size for the evaluation of liquefaction potential.

For these reasons, the present study discusses the relationship among standard penetration N-values, grain size distribution characteristics and dynamic shear strengths which were obtained from dynamic triaxial tests on undisturbed sandy samples. It was found from the relationship that the critical N-value in the evaluation of liquefaction potential could be smaller for sand deposits with small grain sizes.

Dynamic Triaxial Tests on Undisturbed Sandy Samples

Sampling of undisturbed sand samples and standard penetration tests were performed at two sites, i) Akebono - Tatsumi Site and ii) Haneda Site. Both sites are along the Bay of Tokyo. A typical boring log at Akebono-Tatsumi Site is shown in Fig. 32. Undisturbed samples were secured by a reformed Bishop sampler in which the inner diameter of the sampler is 5.4 cm and the length of the sampler is 65.0 cm. Sand samples with low contents of fine soils were frozen at site by dry ice to avoid disturbances which may be caused during the transportation from the site to the laboratory for testing. Silt samples were not frozen to avoid the disturbance due to volume expansion caused by freezing. Figs. 15 through 18 show typical grain size analysis curves. Almost all sand samples secured are fine sands with D_{50} less than 0.3 mm and with high contents of fine soils less than 0.074 mm.

Dynamic triaxial tests were conducted on samples with the diameter of 5.0 cm and the height of 10.0 cm. Applied isotropical effective confining pressures were equal to insitu effective overburden pressures and enough back pressures were applied to make the Skempton's B-value larger than 0.96 (Fig. 19). Figs. 20 and 21 show typical test results which describe the relationship between the applied stress ratio and the number of repetitions in both cases of undisturbed samples and disturbed samples. Disturbed samples were made by pouring completely disturbed de-aired saturated soils which were made from undisturbed samples into a mold. It is seen from this figure that the strength of disturbed samples is smaller than those of undisturbed samples for the same density. In this study, the dynamic shear strength in dynamic triaxial tests was defined as

$$R_l = \left(\frac{\sigma_{dp}}{20'c} \right)_l = \left[\begin{array}{l} \text{the stress ratio } \left(\frac{\sigma_{dp}}{20'c} \right) \text{ when the simple amplitude} \\ \text{of axial strain } \Delta e_a (\%) \text{ becomes 3\%, at the number} \\ \text{of repetitions.} \end{array} \right] \quad (4)$$

The value of R_l were read off from the relationship between $\sigma_{dp}/(20'c)$ and the number of repetitions. Fig. 22 indicates a relationship between dynamic shear strength of undisturbed samples and that of disturbed samples (obtained from Figs. 20 and 21).

Dynamic Shear Strength $(\tau/\sigma_v') Comparable With Dynamic Shear Stress Ratio $(\tau/\sigma_v')_e$$

Dynamic shear stress ratio $(\tau/\sigma_v')_e$ which are induced in grounds by earthquake motions were defined as the maximum shear stress ratio in the computed time history of shear stress ratio τ/σ_v' , at the depth of interest. Earthquake response analysis of grounds were performed by the wave propagation theory with the equivalent linearization method with

respect to deformation properties of soils. In this study, underground acceleration records were used as input base motions. The maximum acceleration in the computations was taken as 150 gals at the base (assumed at the depth of 127 m).

In evaluating liquefaction potential, the dynamic shear strength should be compared with the dynamic shear stress ratio due to earthquake motions (See Fig. 14). In this procedure, to obtain the dynamic shear strength $(\tau/\sigma_v')_d$, which is compared with the computed dynamic stress $(\tau/\sigma_v')_e$, some corrections should be made on the dynamic shear strength R_d , which are obtained from dynamic triaxial tests. These corrections are expressed as,

$$(\tau/\sigma_v')_d = C_1 \cdot C_2 \cdot C_3 \cdot C_4 \cdot C_5 \cdot R_d \quad (5)$$

(i) C_1 : This is the correction factor for confining pressure. In this study, the insitu earth pressure at rest, K_o , was estimated to be around 0.5. In this case, the effective mean principal stress in the insitu stress condition becomes $(1 + 2 K_o) \cdot \sigma_v / 3$ where σ_v is the effective overburden pressure. On the other hand, the effective mean principal stress in dynamic triaxial tests is σ_v , as shown in Fig. 19. As it was shown by Ishihara and Li (1972) that dynamic shear strength of samples under stress conditions with different K_o values should be evaluated for the same effective mean principal stress, the correction factor C_1 becomes,

$$C_1 = \frac{1 + 2K_o}{3} = \frac{2}{3} \quad (6)$$

(ii) C_2 : This is the correction factor for wave form of loading. While actual earthquake motions are random with respect to time, the loading wave forms used in dynamic triaxial tests were sinusoidal with constant amplitudes. According to Ishihara and Yasuda (1972), the value of C_2 ranges from 1/0.55 to 1/0.7, in which C_2 has a larger value for a shock-type earthquake motion and has a smaller value for a vibration type one. In this study, a moderate value equal to 1.5 was adopted.

(iii) C_3 : This is the correction factor for the effect of disturbance which are inevitable in the processes of sampling, freezing, transportation and testing procedures in dynamic triaxial tests. It can be supposed that the dynamic shear strength of soils may decrease due to these disturbances. Fig. 22 shows the relationship between the values of R_d of undisturbed samples defined by Eq. (4) and those of completely disturbed samples. It is clearly seen from this figure that the difference between two values is too large to be neglected. Therefore, it seems that the value of C_3 should be larger than 1.0. However, at present, the precise value of C_3 can not be evaluated.

(iv) C_4 : This is the correction factor for the effect of the densification, which are also inevitable during the above-mentioned operations. In fact, some densifications were observed in samples. As denser sand samples have larger dynamic shear strengths, C_4 can be, in general, less than 1.0. Considering that densifications of samples are caused by disturbances during operations, it was estimated in this study that $C_3 \cdot C_4 = 1.0$.

(v) C_5 : This is the correction factor for compensating the effects of directions of excitation. Although the precise value of C_5 can not be evaluated, here it is assumed that $C_5 = 1.0$.

Eventually, the product of all the correction factors became about 1.0. Therefore, in this study the dynamic shear strength were obtained as

$$(\tau/\sigma_v')_L = R_L \quad (7)$$

To estimate the value of $(\tau/\sigma_v')_L$ at the point where only the N-values or both the N-values and other soil properties such as mean grain size and contents of fine soils were obtained but no undisturbed samples were available, the relationship among $(\tau/\sigma_v')_L$ -values, N-values and soil property parameters should be established. In this study, it was supposed that $(\tau/\sigma_v')_L$ -values can be represented as

$$(\tau/\sigma_v')_L = R_L = F(N, S, D_{50}) \quad (8)$$

in which N means the standard penetration test N-value, S denotes the content of fine soils ($< 74\mu$) in percentage and D_{50} denotes the mean grain size in mm. As a great deal of dynamic triaxial tests on clean sands have been conducted at various laboratories, it is necessary to establish the method of evaluation of clean sand deposits as the first step. For this purpose, insitu relative density should be evaluated. As an indirect method, Meyerhof (1957) proposed the following equation:

$$D_r = 21 \sqrt{\frac{N}{\sigma_v' + 0.7}} \quad (9)$$

where D_r is relative density in percentage, N is the standard penetration N-value and σ_v' is the effective overburden stress in kg/cm². This equation was proposed on the basis of the test results on clean sands by Gibbs and Holtz (1957). Figs. 23 and 24 represent the comparison between the relative density obtained from eq. (9) and that obtained directly by $D_r = (e_{max} - e)/e_{max} - e_{min}$ where the values of void ratio e were obtained from undisturbed sand samples by a reformed Bishop sampler. These samplings were performed at Kawagishi-cho, Niigata City by the Japanese Society of Soil Mechanics and Foundation Engineering (1976). The values of e_{max} and e_{min} were obtained on completely disturbed air-dry samples. These figures indicate that the value of the relative density D_r obtained by eq. (9) is almost identical with that obtained directly by $D_r = (e_{max} - e)/(e_{max} - e_{min})$. Fig. 25 shows the relationship between the dynamic shear strength from dynamic triaxial tests on clean sands with no fine soils less than 0.074 mm and the relative densities $D_r = (e_{max} - e)/(e_{max} - e_{min})$. These tests were conducted at various laboratories as listed in Table 2. The average relationship among data plots in Fig. 25 can be represented by

$$R_L = 0.0042 D_r \quad (10)$$

where D_r denotes $(e_{max} - e)/(e_{max} - e_{min})$ in percentage. If there is not a large difference between the strength of an undisturbed clean sand and that of a completely disturbed clean sand, the dynamic shear strength $(\tau/\sigma_v')_L$ can be estimated by the following procedure:

$$(N, \sigma_{v'},) + D_r = 21 \sqrt{\frac{N}{\sigma_{v'} + 0.7}} \text{ (eq. (9))} + R_\lambda = 0.0042 D_r \text{ (eq. 10)}$$

$$+ (\tau/\sigma_{v'})_L = R_\lambda \text{ (eq. (7))} \quad (11)$$

Fig. 26 shows the relationship between $(\tau/\sigma_{v'})_L$ obtained by dynamic triaxial tests on undisturbed samples which were conducted in this study and the value of $D_r = 21\sqrt{N}/(\sigma_{v'} + 0.7)$. It can be clearly seen that the $(\tau/\sigma_{v'})_L - D_r$ relationship of silty fine sands which were tested in this study is quite different from the average $(\tau/\sigma_{v'})_L - D_r$ relationship of clean sands. Therefore, it seems that the direct application of eq. (11) to this case gives considerably under-estimated values of $(\tau/\sigma_{v'})_L$.

Estimation of $(\tau/\sigma_{v'})_L$ - Values at Akebono-Tatsumi Site

The values of $(\tau/\sigma_{v'})_L$ at the site of Akebono-Tatsumi were estimated by the following procedure, because it was found that eq. (11) could not be applied directly to this case.

(a) $(\tau/\sigma_{v'})_L$ -values were obtained as $(\tau/\sigma_{v'})_L = R_\lambda$ at the points where undisturbed samples were obtained and the values of R_λ were obtained by dynamic triaxial tests.

(b) $(\tau/\sigma_{v'})_L$ -values at the points where only N-values were measured and no other information is available were estimated as follows:

$$(N, \sigma_{v'},) + D_r = 21 \sqrt{\frac{N}{\sigma_{v'} + 0.7}} \text{ (eq. (9))}$$

$$+ R_\lambda = 0.21 + 0.0021 D_r \text{ (eq. (13))} + (\tau/\sigma_{v'})_L = R_\lambda \text{ (eq. (7))}$$

$$R_\lambda = 0.21 + 0.0021 \cdot D_r \quad (13)$$

Eq. (13) represents the average relationship of the test data from this study and the average relationship is shown in Fig. 26.

(c) $(\tau/\sigma_{v'})_L$ -values at the points where N-values and grain size analysis curves of the samples were obtained were estimated as follows. First, it was supposed that the reason why the $(\tau/\sigma_{v'})_L$ -values of sands tested in this study are larger than those of clean sands for the same value of $D_r = 21\sqrt{N}/(\sigma_{v'} + 0.7)$ is that sands tested in this study are fine sands and include fine soils less than 0.074 mm to some extent. Therefore, DR_λ was defined as the difference in the dynamic shear strength $(\tau/\sigma_{v'})_L = R_\lambda$ for the same value of D_r between the value of the data obtained in this study and the average value of clean sands. This definition is illustrated in Fig. 27. As almost all of the samples tested in this study were fine sands where the mean grain size D_{50} were less than 0.3 mm, only the correlation between the DR_λ -value and the content of fine soils were examined as shown in Fig. 28. While there is a wide scattering in the plots, it may be seen from this figure that DR_λ -values increase with increase in the content of fine soils (S). This relationship may be expressed as,

$$D(\tau/\sigma_{v'})_L = DR_\lambda = 0.0022S - 0.0075S \leq 0.175 \quad (14)$$

Therefore, the (τ/σ_v') _g-values in this case were estimated as follows:

$$(\tau/\sigma_v')_g = \{(\tau/\sigma_v')_g \text{ by eq. (11)}\} + \{D(\tau/\sigma_v')_g \text{ by eq. (14)}\} \quad (15)$$

Comparison Between $(\tau/\sigma_v')_e$ and $(\tau/\sigma_v')_g$ at Akebono-Tatsumi Site

Firstly, the critical N-value = 10 specified in the specifications for the Earthquake-Resistant Design of Highway Bridges were evaluated as follows. In Fig. 30 shown is the value of $(\tau/\sigma_v')_e$ which was calculated for a point at Akebono-Tatsumi site. In this calculation, the maximum acceleration at the base was taken as 150 gals and four different earthquake motions recorded at the depth of 127 m near this site were utilized. Also shown in this figure are the values of $(\tau/\sigma_v')_g$ which were obtained from eq. (11) on the assumption that the N-values at this site were 10 irrespective of depth and the sands in this point were clean. Therefore, the dynamic shear strength R_g of these sands can be obtained from eq. (10). It can be seen from Fig. 30 that the value of $(\tau/\sigma_v')_g$ obtained as above are almost identical to the value of $(\tau/\sigma_v')_e$ for the entire depth of interest. Therefore, it was evaluated that the critical N-value of 10 is a proper value for clean sand deposits with the value of $(\tau/\sigma_v')_e$ which were estimated in this study.

Secondly, the values of $(\tau/\sigma_v')_g$ obtained by eq. (11) using the measured N-values and σ_v' , were compared with the calculated values of $(\tau/\sigma_v')_e$ as shown in Fig. 31. It can be seen from this figure that the overall values of $(\tau/\sigma_v')_g$ are less than those of $(\tau/\sigma_v')_e$. This means that this deposit may liquefy during severe earthquake motions. However, as eq. (11) is based on the test results on clean sands, this conclusion may not be proper.

Therefore, $(\tau/\sigma_v')_g$ -values were estimated by the three methods (a), (b) and (c) presented earlier. In Fig. 32, black squares represent the $(\tau/\sigma_v')_g$ -values obtained by the method (a), hollow circles and triangle circles represent the $(\tau/\sigma_v')_g$ -values obtained by the method (b) and horizontal lines represent the ranges of $(\tau/\sigma_v')_g$ -value obtained by the method (c). And the hatched zone shows the estimated range of $(\tau/\sigma_v')_g$. It can be seen from this figure that the estimated values of $(\tau/\sigma_v')_g$ are, in general, larger than the estimated values of $(\tau/\sigma_v')_e$. This conclusion is rather different from that which can be derived from Fig. 31. This means that when the liquefaction potential of sand deposits are evaluated on the basis of dynamic triaxial tests, these tests should be conducted on undisturbed samples if these samples include much fine soils.

An additional survey was performed at the Haneda site. The data obtained from this survey were added to those of the Akebono-Tatsumi site as shown in Figs. 33 and 34. In these figures, data with letters A means those of the Akebono-Tatsumi site. It is seen from these figures that the general trend is almost similar for both sites.

The Critical N-values Based on Dynamic Triaxial Tests on Undisturbed Sand Samples

Fig. 33 shows the relationship between the dynamic shear strength of undisturbed samples R_g and the relative density $D_r = 21 \sqrt{N/\sigma_v'} + 0.7$ obtained by using N-values and insitu effective overburden pressures σ_v' . On the basis of this relationship, the critical N-values were determined for fine sands with different content of fine soils as follows. It should be noted that the almost mean grain diameter D_{50} of sands tested are less than 0.3 mm.

Therefore, the following discussions can be applied only for sands with D_{50} less than 0.3mm. While there is a large scatter in the data shown in Fig. 34, the average relationship of these plots can be represented conservatively as:

$$DR_L = 0.0035S \quad (16)$$

where S denotes the content of fine soils in percentage. The value of R_L is represented as:

$$\begin{aligned} R_L &= 0.0042 \times 21 \sqrt{\frac{N}{\sigma_v' + 0.7}} + 0.0035 S \\ &= 0.0882 \sqrt{\frac{N}{\sigma_v' + 0.7}} + 0.0035 S \end{aligned} \quad (17)$$

To obtain the relationship in fine sands with D_{50} less than 0.3 mm between the critical N-value for the evaluation of liquefaction potential and the content of fine soils, the critical N-value of 10 was selected as the value for clean sand deposits with $\sigma_v' = 0.5 \text{ kg/cm}^2$. This value was evaluated from the above-mentioned specifications. In the specifications, it is specified that saturated sandy soil layers within 10 m of the actual ground surface and with a standard penetration test N-value less than 10 may be vulnerable to liquefaction. Therefore, as the mean value of σ_v' , for this sandy soil layer, 0.5 kg/cm^2 was selected. If this critical N-value of 10 can be applied to clean sand deposits like those at Niigata City, the standard value of R_L , R_{L0} , can be obtained by substituting $N=10$, $\sigma_v' = 0.5$ and $S=0$ into eq. (17) as

$$R_{L0} = 0.255 \quad (18)$$

Next, by substituting $R_L = 0.255$ and $\sigma_v' = 0.5$ into eq. (17), the relationship between the critical N-value for sands including fine soils and the content of fine soils S can be expressed as:

$$N = 0.00189 (72.9 - S)^2 \quad (19)$$

From eq. (19), the critical N-values for various values of S can be obtained as,

$$\begin{aligned} N &= 10 \quad \text{for} \quad S = 0\%, \\ N &= 7.5 \quad \text{for} \quad S = 10\%, \\ N &= 5.3 \quad \text{for} \quad S = 20\%, \\ N &= 3.5 \quad \text{for} \quad S = 30\% \text{ and} \\ N &= 2.0 \quad \text{for} \quad S = 40\%. \end{aligned}$$

From these values, the design critical N-values for sand deposits whose D_{50} -values are less than 0.3 mm can be tentatively proposed as,

N = 10	for	S = 0 - 10%,
N = 7	for	S = 10 - 20%,
N = 5	for	S = 20 - 40% and
N = 3	for	S = 40 - 60%.

Since these values were obtained from the small number of field data, more research is necessary. Therefore, the critical N-values recommended for design purposes should be determined after more field data are accumulated.

CONCLUSIONS

Dynamic behavior of pile foundations in liquefying soil deposits is considered to be one of soil-structure interaction problems during earthquakes. As this problem is very complicated, only qualitative results can be derived from the experimental tests conducted in this study. The following remarks can be made.

(1) Since liquefaction phenomena progress with respect to time and with respect to space, the effects of liquefied sands on the piles vary as functions of time and space. It can be normally recognized that the response of a pile foundation with a normal rigidity is small during earthquakes before liquefaction initiates. The response increases abruptly after liquefaction begins, and decreases when complete liquefaction takes place. During the complete liquefaction, soils behave as heavy liquid, and piles are subjected to hydrodynamic pressures due to the liquefied soils.

(2) The relationship among the natural frequency of the pile foundation supported by the surrounding soil deposits before liquefaction initiates, the natural frequency of the pile foundation submerged in completely liquefied soils and the predominant frequency of input motion is the most important factor. Dynamic behavior of pile foundations in the course of liquefaction of sand layers will be considerably affected by this relationship.

(3) While the complete liquefaction continues, the soil-pile foundation system behave as a submerged structure. Since its natural frequency becomes smaller, it may resonate when subjected to seismic motion with longer periods. Accordingly it will be important to assess the components of longer periods involved in induced seismic motions.

For simplified procedure in evaluating liquefaction potential, critical N-values are proposed on the basis of dynamic triaxial tests on undisturbed samples and the standard penetration tests.

While additional research works are necessary, the tentatively proposed critical N-values for sands whose D_{50} -values are less than 0.3 mm are:

N = 10	for the content of fine soils S = 0 to 10%,
N = 7	for S = 10 - 20%,
N = 5	for S = 20 - 40%,
N = 3	for S = 40 - 60%.

ACKNOWLEDGEMENTS

The studies described in this paper were greatly assisted by Messrs. Susumu Yasuda, Makoto Hirose, Seiichi Yoshida, Masahide Ikemoto, Yoshio Sakaba and Hironobu Noma. Their experimental works are especially appreciated.

The field soil surveys at the Akebono-Tatsumi site and Haneda site were conducted by Kawasaki National Road Construction Office, Kanto Regional Bureau, Ministry of Construction, with a cooperation of the Public Works Research Institute. Mr. Koji Miyata, Director of Kawasaki National Road Construction Office gave the authors an invaluable opportunity to investigate insitu dynamic soil properties with emphasis on liquefaction potential. The authors express their cordial appreciation to him and the staff members at the above office.

REFERENCES

Gibbs, H. J., and Holtz, W. G., (1957), "Research on Determining the Density of Sands by Spoon Penetration Tests," Proc. of 4th ICSMFE. London, Vol. 1.

Ishihara, K., and Li, S., (1972), "Liquefaction of Saturated Sand in Triaxial Torsion Test," Soils and Foundations, Vol. 12, No. 2, June.

Ishihara, K., and Yasuda, S., (1972), "Sand Liquefaction Due to Irregular Excitation," Soils and Foundations, Vol. 12, No. 4., Dec.

Ishihara, K., and Matsumoto, K. (1975), "Bearing Capacity of Saturated Sand Deposits During Vibration," Proc. of the 4th Japan Earthquake Engineering Symposium, 1975.

Iwasaki, T. (1973), "Earthquake-Resistant Design of Bridges in Japan," Bulletin of Public Works Research Institute, No. 29.

Iwasaki, T., Tatsuoka, F., and Y. Sakaba (1976), "A Shaking Table Test on Dynamic Behaviors of Model Pile Foundations Embedded in Sand Layers," Proc. of 14th Annual Meeting of Earthquake Engineering, JSCE (in Japanese).

Japan Road Association (1971), "The Specifications for Earthquake Resistant Design of Highway Bridges."

Kachadoorian, R. (1968), "Effects of the Earthquake of March 27, 1964, on the Alaska Highway System," Geological Survey Professional Paper 545-C, U.S. Department of the Interior.

Kuribayashi, E., and Tatsuoka, F. (1975), "Brief Review of Liquefaction During Earthquakes in Japan," Soils and Foundations, Vol. 15, No. 4., Dec.

Meyerhof, G. G., (1957), "Discussion of Gibbs and Holtz Paper," Proc. of 4th ICSMFE, London, Vol. III.

Shikamori, M., Sato, Y., and Hakuno, M. (1973), "Effects of Noncomplete Liquefaction of Soils on Embedded Structures," Proc. of Annual Meeting of JSCE (in Japanese).

Yoshida, T., and Uematsu, M. (1973), "A Model Test of Piles in Liquefying Sand," Proc. of Annual Meeting of JSCE (in Japanese).

Yoshimi, Y. and Tokimatsu, T. (1975), "Liquefaction of Sand Deposits during Earthquakes Near Structures," Proc. of 4th Japan Earthquake Engineering Symposium, 1975 (in Japanese).

Youd, T. L., and Hoose, S. N. (1975), "Liquefaction During 1906 San Francisco Earthquake," Journal of the Geotechnical Division, ASCE, Vol. 102, No. GT5.

TEST CASE	SAND	DR ³⁾ (%)	Number ⁴⁾ of Piles	Head Weight (kg)	5) f _p (Hz)	6) f _i (Hz)	7) ^a A ₁₁ (gal)	Shaking Period (sec.)	8) f _g (Hz)
T1	Iruma ¹⁾ Toyoura ²⁾	40	9	44	3.8	12	40 ~ 100	60	18
T2		27	4	53	4	10	60 ~ 80	30	24
T3		34	6	18	10	20	80 ~ 130	15	
T4		24	6	18	10	10	60 ~ 80	30	
T5		40	9	13	14	10	60 ~ 120	30	

1) Iruma Sand ($G_s=2.88$, $D_{50}=0.52\text{mm}$, $U_c=1.52$, $\epsilon_{max}=0.93$, $\epsilon_{min}=0.66$)
 2) Toyoura Sand ($G_s=2.64$, $D_{50}=0.16\text{mm}$, $U_c=1.46$, $\epsilon_{max}=0.96$, $\epsilon_{min}=0.64$)
 3) Relative Density
 4) Each Pile is made of aluminum bars with 70cm in length and 2cm in diameter.
 5) Natural Frequency of Pile Foundation in Water
 6) Frequency of Input Motion
 7) Amplitude of Base Acceleration before Perfect Liquefaction
 8) Estimated Natural Frequency of Non-liquefied Sand Layer ($\gamma=10^{-4}$)

Table 1. List of Test Cases

LEGEND

- A : Accelerometers
- E, OE : Earth pressure cells
- △ P : Poropressure cells
- S : Strain gauges

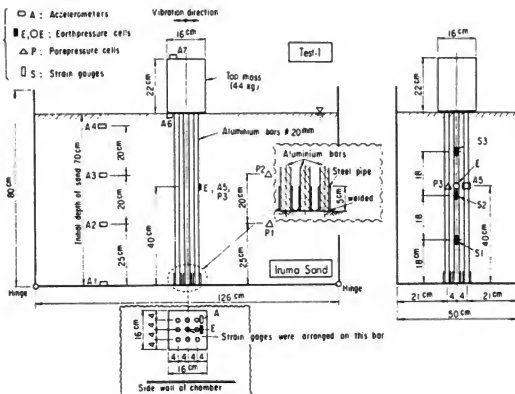


Fig. 1 Test Arrangements for Test 1

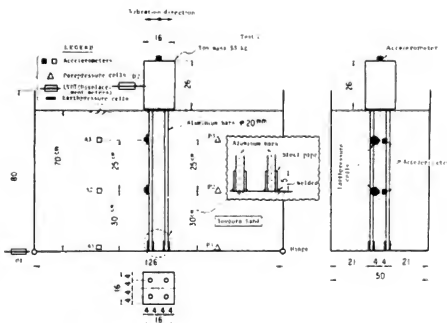


Fig. 2 Test Arrangements for Test 2

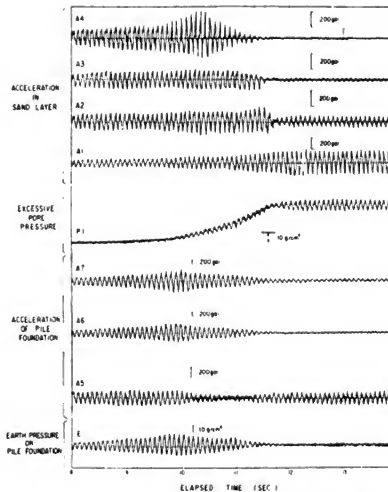


Fig. 3 Typical Test Records (Test 1) (See Fig. 1)

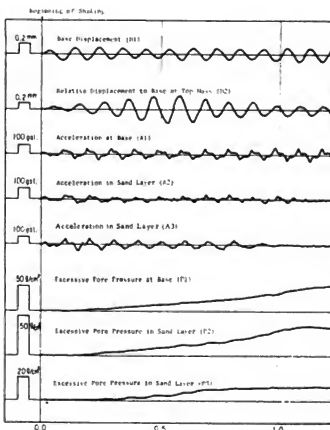


Fig. 4 Typical Test Records (Test 2) (See Fig. 2)

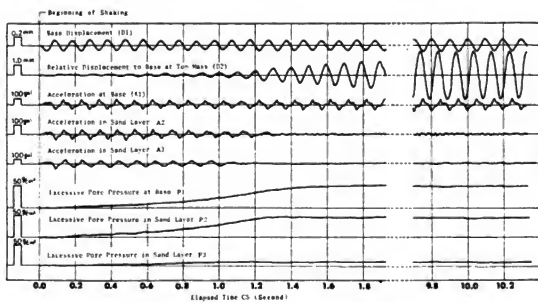


Fig. 5 Typical Test Records (Test 4) (See Fig. 2)

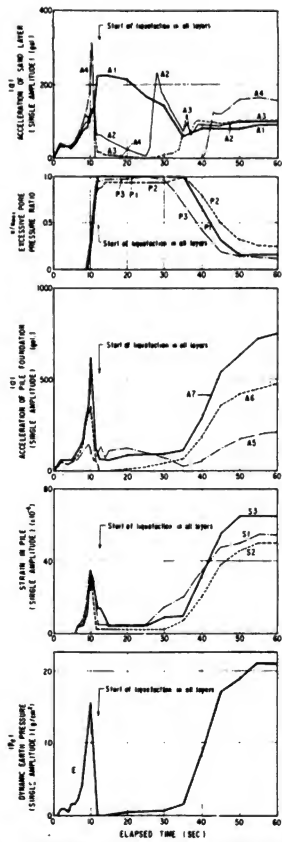


Fig. 6 Amplitudes of Recorded Quantities (Test 1)

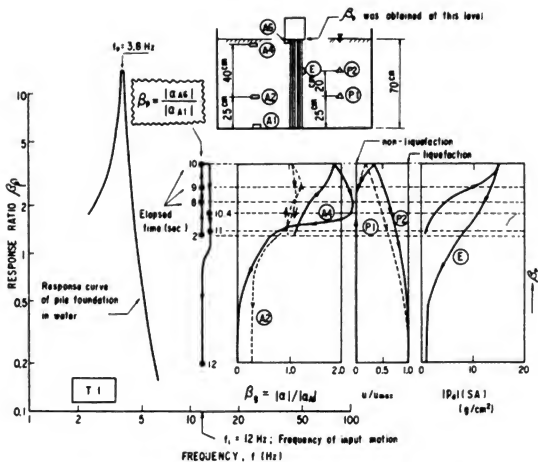


Fig. 7 Variation of Response of Pile Foundation in the course of Liquefaction of Sand Layer (Test 1)

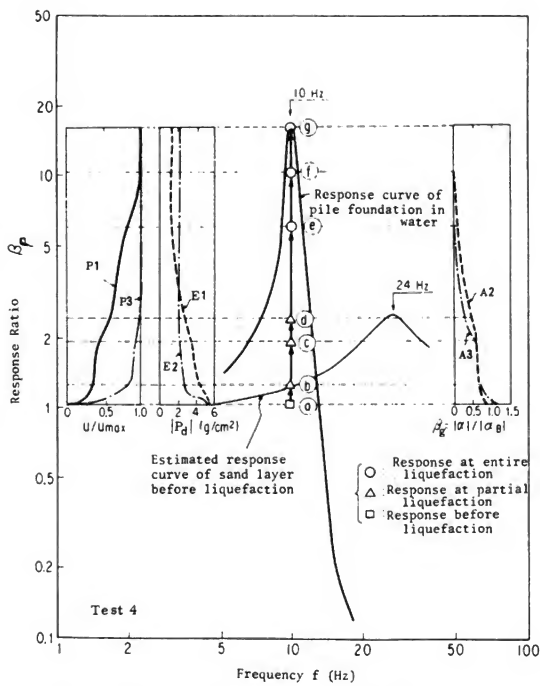


Fig. 9 Variation of Response of Pile Foundation in the course of Liquefaction of Sand Layer (Test 4)

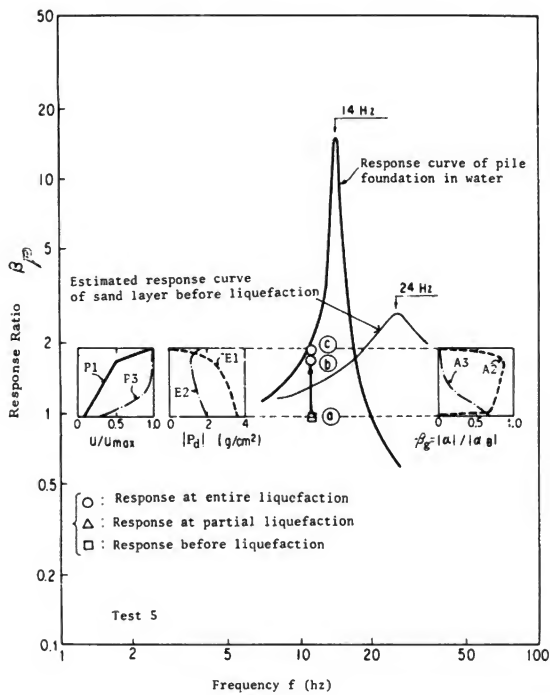
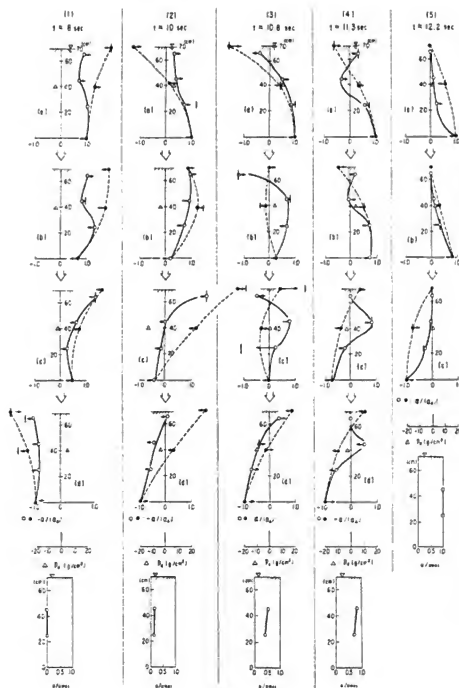


Fig. 10 Variation of Response of Pile Foundation in the course of Liquefaction of Sand Layer (Test 5)



1405

(a) Through (c) or (d) represent the movements of pine sawyer and red borer during 10 years. (a) 1/128 sec.

$\phi_{\perp} = 0 / (g_s) \pi$ and larger

卷之三

ACKNOWLEDGMENT

8. Ca^{+} with pressure. Existing force of Ca^{+}
pressure set faces to the right direction

Journal of Health Politics, Policy and Law

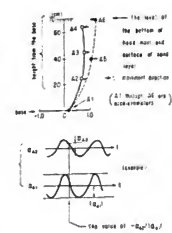


Fig. 11 Instantaneous Positions of Sand Layer and the Pile Foundation Model (Test 1)

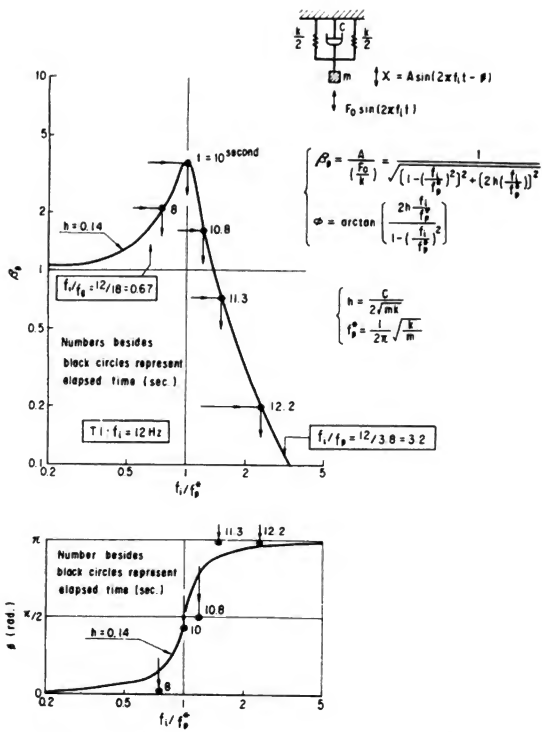


Fig. 12 Estimation of Apparent Natural Frequency of Pile Foundation Model Embedded in Liquefying Sand Layer (Test 1)

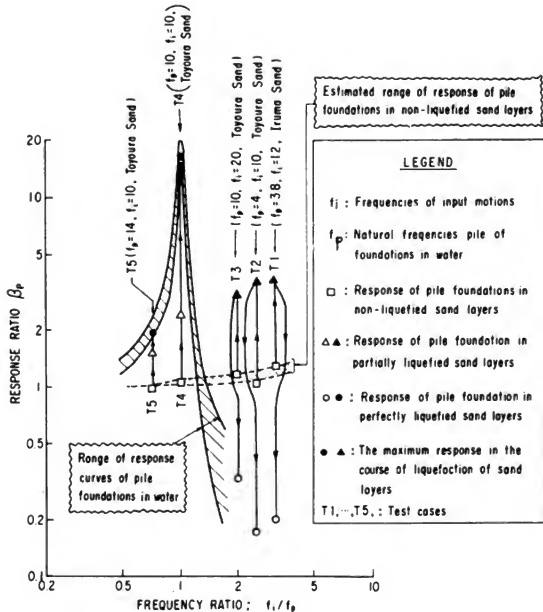


Fig. 13 Summary of Whole Tests

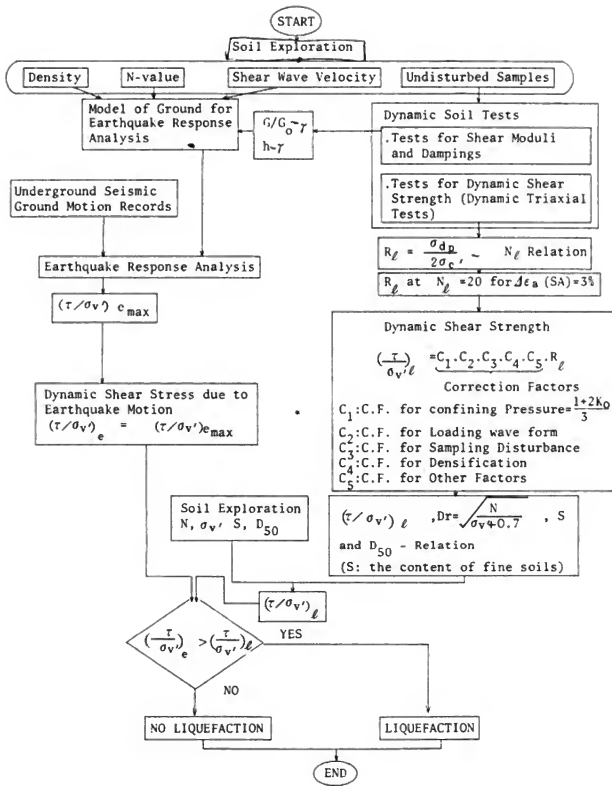


Fig. 14 Flow Chart of Precise Evaluation of Liquefaction Potential

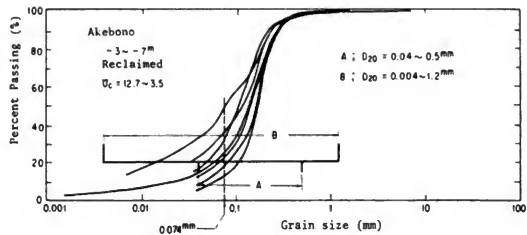


Fig. 15 Typical Grain Size Accumulation Curves
 (Akebono, Reclaimed Sand Layer)

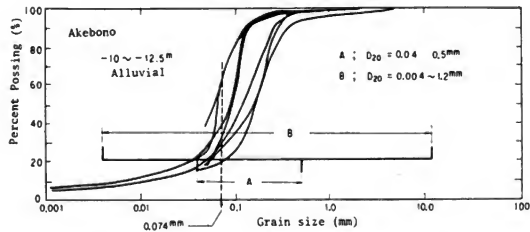


Fig. 16 Typical Grain Size Accumulation Curves
 (Akebono, Alluvial Sand Layer)

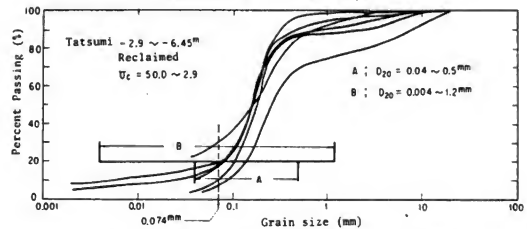


Fig. 17 Typical Grain Size Accumulation Curve S
 (Tatsumi, Reclaimed Sand Layer)

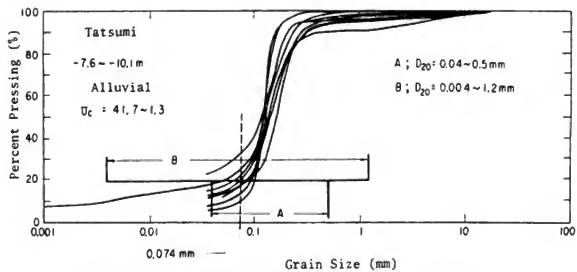
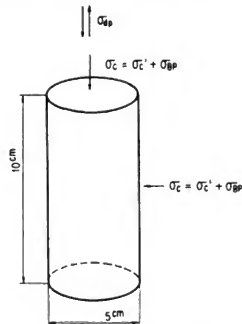


Fig. 18 Typical Grain Size Accumulation Curve
(Tatsumi, Alluvial Sand Layer)



σ_c' (Effective confining pressure) = σ_v' (In situ effective overburden pressure)
 σ_{BP} (Back pressure) $\sigma_{\text{BP}} \geq I_{sh}$ (In situ static porepressure)

All of the tests were performed on samples with Skempton's B-value larger than 0.96.

Fig. 19 Stress Condition in Dynamic Triaxial Tests

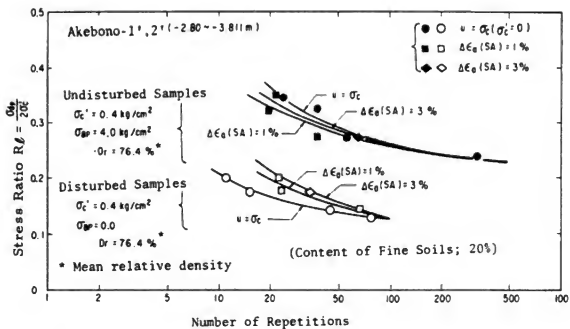


Fig. 20 Typical Dynamic Triaxial Test Results (Akebono)

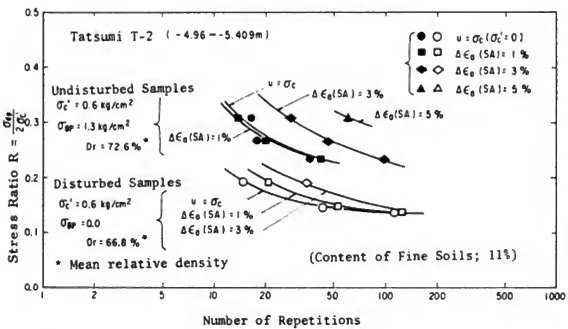


Fig. 21 Typical Dynamic Triaxial Test Results (Tatsumi)

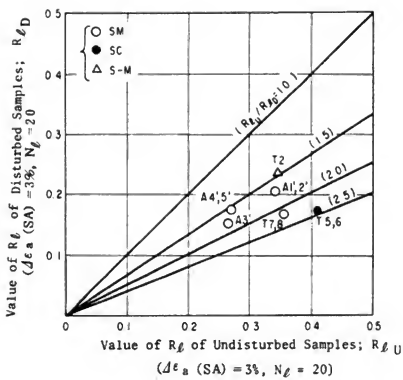


Fig. 22 Relationship of Dynamic Shear Strength of
Undisturbed Samples and Disturbed Samples

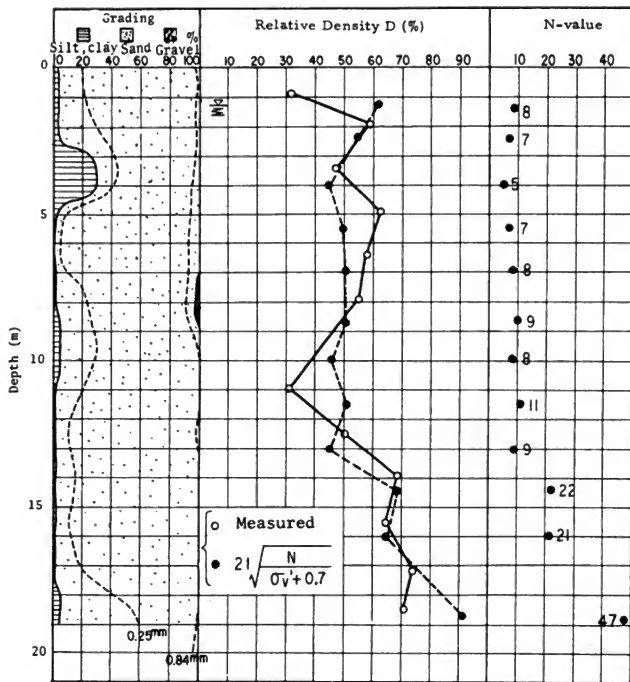


Fig. 23 Comparison between Measured Relative Density

$$Dr = \frac{e_{max} - e}{e_{max} - e_{min}} \times 100 \text{ and } Dr = 21 \sqrt{\frac{N}{\sigma_v' + 0.7}}$$

at Kawagishi-cho, Niigata

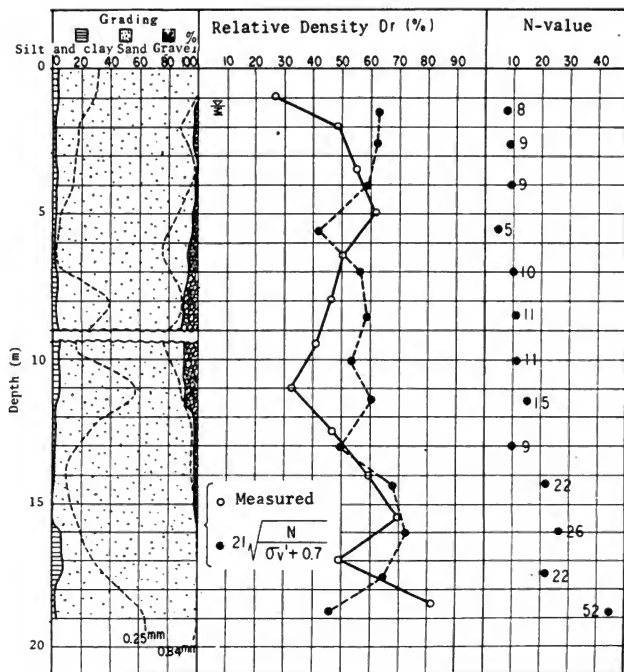


Fig. 24 Comparison between Measured Relative Density

$$Dr = \frac{e_{max} - e}{e_{max}} \times 100 \quad \text{and} \quad Dr = 21 \sqrt{\frac{N}{\sigma_v' + 0.7}}$$

at Kawagishi-cho, Niigata

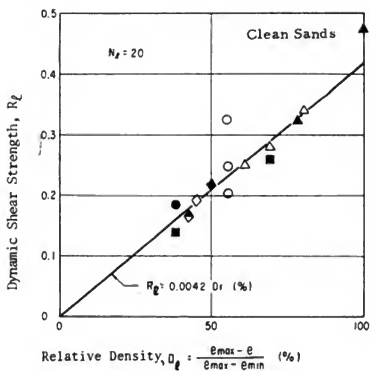


Fig. 25 $R_L - D_L$ Relationship of Clean Sands

Table 2 Summary of Dynamic Triaxial Test Results on Clean Sands

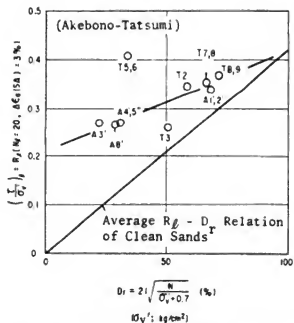


Fig. 26 $D_h - R_f$ Relationship of Sands of Akebono-Tatsumi Site

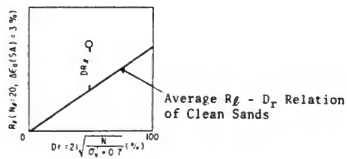


Fig. 27 Definition of DR_f

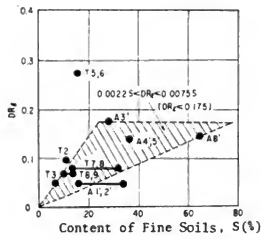


Fig. 28 S-D R_f Relationship

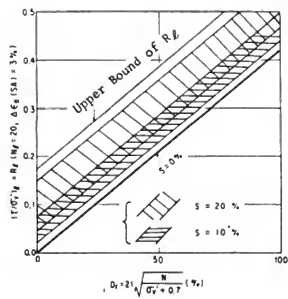


Fig. 29 $D_T - R_f$ Relationship Based on Fig. 28

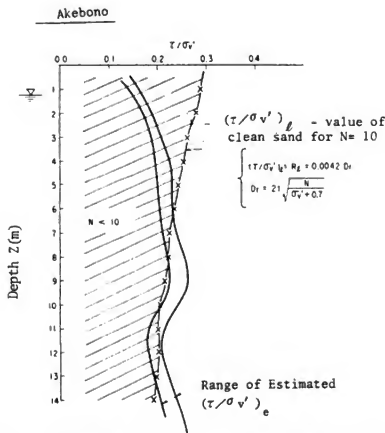


Fig. 30 Comparison of $(\tau/\sigma_{v'})_f$ of Clean Sand for $N = 10$ with $(\tau/\sigma_{v'})_e$

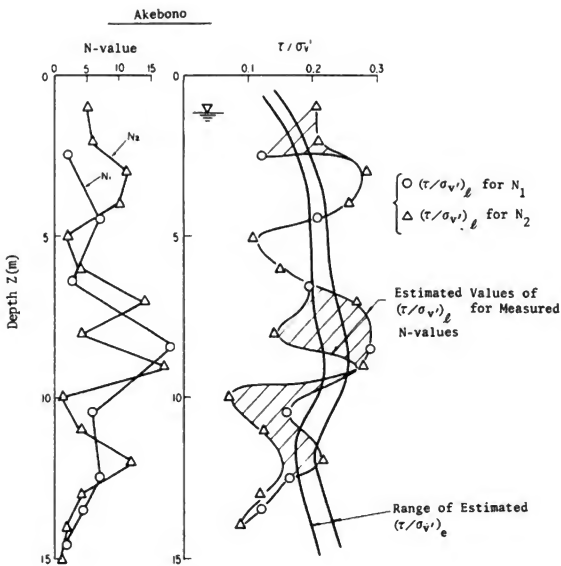


Fig. 31 Comparison of (τ / σ_v') of Clean Sand for Measured N-values with (τ / σ_v') _e

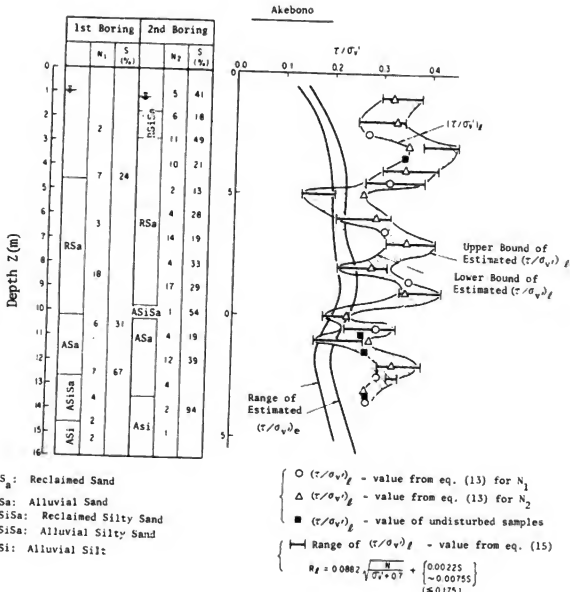


Fig. 32 Comparison of (τ/σ_v') Based on Dynamic Triaxial Tests on Undisturbed Samples with $(\tau/\sigma_v')_e$

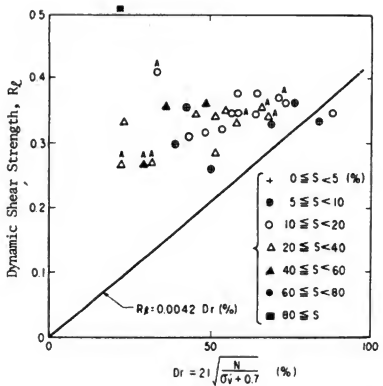


Fig. 33 $D_T - R_s$ Relationship of Sands of Two Sites

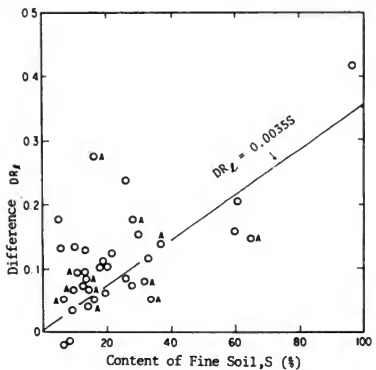


Fig. 34 $S - DR_s$. Relationship of Sands of Two Sites

EARTHQUAKE RESISTANT DESIGN BASED ON GROUND MOTIONS AT BASE-ROCK

Eiichi Kuribayashi, Chief, Earthquake Engineering Section

Kazuhiko Kawashima, Research Engineer, Earthquake Section

Public Works Research Institute

ABSTRACT

It is generally known that dynamic behaviors of structures are influenced by their ground conditions and that earthquake ground motions recorded are dependent on their ground conditions. In order to specify common input earthquake motions for design of every structure on and under ground, it is useful to select base-rocks in ground, where effects of grounds near surface are small enough to be ignored, as an input terminal where earthquake motions are to be specified. In order to improve such seismic designs, discussions on necessary conditions of base-rock and on accuracies of base-rock motions estimated by theoretical calculations are presented. Earthquake responses of bridges are also presented as a numerical example.

KEYWORDS: Analytical method; base-rock; bridge foundations; deconvolution procedure; earthquake records; ground conditions; ground transfer functions; shear wave.

INTRODUCTION

Advances in technology would make it possible to construct huge structures with deeply embedded foundations. In the current seismic designs of structures the usual practice is to specify earthquake motions at a gravity center as an input even in huge structures. However, based on observations of underground earthquake motions, the earthquake motions are not uniform in grounds. Therefore, it is necessary to take into account such trends in the seismic design of structures. On the other hand, it is generally recognized that earthquake motions recorded are appreciably influenced by local ground conditions. It is, therefore, inadequate to employ the recorded earthquake motions directly, disregarding the differences of ground conditions in the seismic design. One of the approaches to consider such problems is to select a suitable widespread formation of the ground (base-rock), where effects of ground near the surface (subsurface ground) are small enough to be ignored, as a common input terminal of earthquake motions. When the earthquake motions at the selected formation are found to be independent of the properties of the subsurface ground, their characteristics can be directly compared with each other among various sites. By specifying input earthquake motions at the base-rocks, the subsurface ground motions can be determined based on the assumptions of upward shear wave propagations in the grounds. The earthquake responses of structures can then be determined by appropriate analytical models.

Although the base-rocks are generally selected based on their geological and soil conditions, it should be noted that they are essentially selected in accordance with the characteristics of earthquake motions specified there (base-rock motions). The base-rock motions are expected to be compared on the same basis among various sites as an index expressing seismic intensities considered in design and we can appropriately incorporate the subsurface ground conditions so as to specify input motions for every structure constructed on and underground (Fig. 1-1).

When the base-rock motions have such conditions, the remaining significant factors which influence the base-rock motions would be magnitudes (Richter scale) and epicentral distances. Fig. 1-2 shows earthquake motions classified in terms of such factors. From an engineering point of view, it is considered desirable to apply earthquake motions in design which lie on the dotted line in Fig. 1-2. The level of intensity will depend on the factors determined based on the dynamic behaviors, magnitudes, shapes of the structures, etc. For instance, earthquake ground motions used for seismic analyses of suspension bridges in Japan are shown in Fig. 1-3.

This paper presents the conditions of base-rocks to improve seismic designs based on base-rock motions and discusses the accurate base-rock motions estimated by theoretical calculations. Also, earthquake responses of bridges are presented as a numerical example to estimate base-rock motions.

BASE-ROCKS AND BASE-ROCK MOTIONS

Assuming propagations of shear waves in horizontally stratified two elastic layers as shown in Fig. 2-1, equations of motion can be expressed disregarding damping terms as

$$G_j \frac{\partial^2 v_j}{\partial x^2} = \rho_j \frac{\partial^2 v_j}{\partial t^2} \quad (j = 1, 2) \quad (2-1)$$

where,

j : suffix expressing j th formation $(j = 1, 2)$

G_j : shear modulus of j th formation

ρ_j : mass density of j th formation

Fourier transformation of Eq. (2-1) gives

$$V_j \frac{\partial^2 \bar{v}_j}{\partial x^2} = -\omega^2 \bar{v}_j \quad (2-2)$$

where,

$$V_j = \sqrt{G_j / \rho_j} \quad (2-3)$$

in which \bar{v}_j express transformed solutions of v_j . The general solution of Eq. (2-1) can be written as,

$$\bar{v}_j = A_j e^{-i\omega \frac{x_j}{V_j}} + B_j e^{i\omega \frac{x_j}{V_j}} \quad (2-4)$$

in which A_j and B_j are arbitrary constants and express amplitude of downward and upward shear waves at $x_j = 0$, respectively. Determinations of the constants A_j and B_j based on boundary conditions give the solution in the form as,

$$\bar{v}_1 = 2 B_1 \frac{\cos \frac{\omega x_1}{V_1}}{\sqrt{\cos^2 \frac{\omega H}{V_1} + \alpha^2 \sin^2 \frac{\omega H}{V_1}}} e^{-i\delta} \quad (2-5)$$

$$\bar{v}_2 = 2 B_2 \cos \left(\frac{\omega x_2}{V_2} + \delta \right) e^{-i\delta} \quad (2-6)$$

where,

$$\alpha = \rho_1 V_1 / \rho_2 V_2 \quad (2-7)$$

$$\delta = \tan^{-1} \left(\alpha \tan \frac{\omega H}{V_1} \right) \quad (2-8)$$

From Eqs. (2-4) to (2-6) two types of ground transfer functions can be defined, i.e., suppose the ground transfer function $H^{Q/B}_2(\omega)$ be defined as ratio between ground motions

in the first or second layers (\bar{v}_1 or \bar{v}_2) and the amplitude of upward (incidental) motions (B_2), then it can be written as

$$H_{(w)}^{\bar{v}_1/B_2} = \frac{2 \cos \frac{\omega x_1}{V_1}}{\sqrt{\cos^2 \frac{\omega H}{V_1} + \alpha^2 \sin^2 \frac{\omega H}{V_1}}} \cdot e^{-i\delta} \quad (1st \text{ layer})$$

$$H_{(w)}^{\bar{v}_2/B_2} = 2 \cos \left(\frac{\omega x_1}{V_1} + \delta \right) e^{-i\delta} \quad (2nd \text{ layer}) \quad (2-9)$$

and suppose the transfer function $H^{Q/V}(w)$ be defined as ratio between ground motions in the first or second layers (\bar{v}_1 or \bar{v}_2) and ground motions at the interface $x_2 = 0$ ($v_{x_2} = 0$), then it can be written as

$$H_{(w)}^{\bar{v}_1/v_{x_2}} = \frac{\cos \frac{\omega x_1}{V_1}}{\cos \frac{\omega H}{V_1}} \quad (1st \text{ layer})$$

$$H_{(w)}^{\bar{v}_2/v_{x_2}} = \frac{\cos \left(\frac{\omega x_1}{V_1} + \delta \right)}{\cos \delta} \quad (2nd \text{ layer}) \quad (2-10)$$

The ground transfer functions defined by Eqs. (2-9) and (2-10) change in accordance with the parameter α as shown in Table 2-1. It is obvious from Table 2-1 that both types of transfer functions in the second layer are unconditionally independent with properties of the first layer when $\alpha = 0$, i.e., the shear modulus of the second layer is infinitely large compared with that of the first layer. It implies that both the incidental and ground motions in the second layer are independent of the properties of first layer in such conditions. Even in the case when $\alpha \neq 0$, no reflections and refractions of propagating shear waves develop in the second layer, provided that the second layer is uniform continua in grounds. In such conditions the incidental motions in the second layer are independent of the first layer.

It is recognized therefore that the second layer can be selected as base-rock in either case when the second layer is infinitely stiff as compared with the first layer or when the second layer is uniform continua in the ground. In the former condition, both the incidental and ground motions in the second layer can be selected as base-rock motions while in the latter condition, only the incidental motions can be selected as base-rock motions.

The ground with the above conditions do not exist in practice. It is required therefore to relieve the above conditions from practical point of view in accordance with objectives and accuracies needed in the analyses. For example, in the former condition, influences of the first layer (subsurface ground) on the ground motions in the second layer (base-rock motions) would be controlled to be small, provided that the second layer is considerably stiff comparatively to the first layer, and, in the latter condition, incidental motions in the second layer would be considered as base-rock motions as long as the second layer continues almost uniformly with the depth where shear waves propagate for a period of predominant motions.

ACCURACY OF BASE-ROCK MOTIONS ESTIMATED

In order to obtain base-rock motions from recorded motions it is required to incorporate effects of local subsurface conditions. A one-dimensional analytical model based on vertically propagating shear waves with equivalent linear materials is currently established for such purposes. An accuracy of base-rock motions calculated theoretically by the deconvolution procedures was correlated with the recorded underground motions. Three underground motion accelerations observed at Ukishima Park near Tokyo (Table 3-1) were employed for this purpose. Three motions were the most significant ones recorded up to the present.

Underground Transfer Functions Estimated from Observations

Soil profile at Ukishima Park (Fig. 3-1) consists of upper alluvium soft formations and lower diluvial hard formations which lie 50 m beneath the ground surface. Earthquake motions were recorded at four points, i.e., at the ground surface, 27 m, 67 m and 127 m beneath the ground surface. Power spectra were calculated to estimate predominant frequencies as shown in Figs. 3-2 to 3-4 and it was found from these results that they are approximately 4-7 c/s for A-earthquake motion and 0-1 c/s for B- and C-earthquake motions. The former motion was obtained from small earthquake in magnitude with relatively short epicentral distance while the latter motions were obtained from large earthquakes in magnitude with long epicentral distances.

Ground transfer functions (amplitude) between each recording point were calculated as shown in Fig. 3-5. It is noted from the result that although the ground motions have significant differences in their predominant frequencies, the ground transfer functions obtained from the motions are almost independent of such characteristics.

Theoretical and Estimated Ground Transfer Functions

The ground transfer functions were theoretically determined by calculations based on the deconvolution procedures. An analytical model was formulated based on the soil profile of Fig. 3-1. The shear moduli of soils were evaluated by estimated shear wave velocities v_s (m/sec) based on a relationship with the N-values obtained by field tests as

$$v_s = 60 \sqrt{N} \quad (3-1)$$

The shear moduli of soils G_0 determined based on Eq. (3-1) correspond to the value at low amplitude strain level. Since the ground motions studied were very small, it was found appropriate to analyze them by using G_0 .

Fig. 3-6 shows the comparisons of theoretical and observed underground transfer functions. A damping ratio of 2% of the critical was assumed in the theoretical calculations.

Theoretical and Measured Underground Motions

The underground motions were computed for C-earthquake theoretically by specifying the recorded surface motion. The deconvolution procedure was applied using the analytical model formulated in the preceding paragraph. Fig. 3-7 shows comparisons between computed

and recorded underground motions. Both motions are considered to be in fairly good agreement. It would be possible to improve the computed motions by formulating more accurate analytical models based on precise investigations of ground.

Based on the results presented it was recognized that the deconvolution procedures based on shear wave propagations are effective in taking account of local ground conditions into recorded earthquake motions.

NUMERICAL EXAMPLES FOR CALCULATION OF BASE-ROCK MOTIONS AND EARTHQUAKE RESPONSES OF BRIDGE

Analytical Model

A discrete analytical model as shown in Fig. 4-1 was formulated to calculate earthquake responses of the embedded foundation. The equation of motions of the system can be written as

$$\begin{aligned} (\underline{\underline{M}}_P + \underline{\underline{M}}_e) \ddot{\underline{u}}_P + \underline{\underline{C}}_P \dot{\underline{u}}_P + \underline{\underline{K}}_P \underline{u}_P \\ + \underline{\underline{C}}_e (\dot{\underline{u}}_P - \dot{\underline{u}}_g) + \underline{\underline{K}}_e (\underline{u}_P - \underline{u}_g) = \underline{0} \end{aligned} \quad (4-1)$$

where,

$\underline{\underline{M}}_P$: mass matrix of structure

$\underline{\underline{M}}_e$: mass matrix of surrounding soils

$\underline{\underline{C}}_P$: damping matrix of structure

$\underline{\underline{K}}_P$: stiffness matrix of structure

$\underline{\underline{C}}_e$: damping matrix expressing radiational dampings

$\underline{\underline{K}}_e$: stiffness matrix expressing springs between structure and surrounding soils

$\underline{u}_P, \dot{\underline{u}}_P, \ddot{\underline{u}}_P$: absolute displacement, velocity and acceleration vectors of structure

$\underline{u}_g, \dot{\underline{u}}_g$: absolute displacement and velocity vectors of subsurface ground

in which the subsurface ground motions of \underline{u}_g and $\dot{\underline{u}}_g$ are assumed to be specified. Denoting as

$$\begin{aligned} \underline{\underline{M}} = \underline{\underline{M}}_P + \underline{\underline{M}}_e \\ \underline{\underline{C}} = \underline{\underline{C}}_P + \underline{\underline{C}}_e \\ \underline{\underline{K}} = \underline{\underline{K}}_P + \underline{\underline{K}}_e \end{aligned} \quad (4-2)$$

Eq. (4-1) can be written as

$$\underline{\underline{M}} \ddot{\underline{u}}_P + \underline{\underline{C}} \dot{\underline{u}}_P + \underline{\underline{K}} \underline{u}_P = \underline{\underline{C}}_e \dot{\underline{u}}_g + \underline{\underline{K}}_e \underline{u}_g \quad (4-3)$$

The vector \underline{u}_p can be conveniently decomposed into a quasi-static displacement vector \underline{u}_{ps} and a dynamic displacement vector \underline{u}_{pd} , i.e.,

$$\underline{u}_p = \underline{u}_{pd} + \underline{u}_{ps} \quad (4-4)$$

By definition of quasi-static displacement in the form as

$$K \underline{u}_{ps} + K_e \underline{u}_g = 0 \quad (4-5)$$

\underline{u}_{ps} can be written as

$$\underline{u}_{ps} = - K^{-1} K_e \underline{u}_g \equiv - K_s \underline{u}_g$$

Substitutions of Eqs. (4-4) and (4-6) into Eq. (4-3) gives

$$M \ddot{\underline{u}}_{pd} + C \dot{\underline{u}}_{pd} + K \underline{u}_{pd} = M K_s \ddot{\underline{u}}_g + (C_e + C K_s) \dot{\underline{u}}_g \quad (4-7)$$

Usually the damping term on the right hand side of Eq. (4-7) is less significant comparing with the inertia terms so that it can be dropped from the equation without introducing significant errors. Then Eq. (4-7) can be written as

$$M \ddot{\underline{u}}_{pd} + C \dot{\underline{u}}_{pd} + K \underline{u}_{pd} = M K_s \ddot{\underline{u}}_g \quad (4-8)$$

Eq. (4-8) can be solved by mode-superposition procedures provided that the damping matrix on the left hand side of the equation is assumed to be triangularized in the same manner as the mass and stiffness matrices in the form of damping ratio of critical.

Numerical Example

The Itajima Bridge is a composite steel girder bridge with five simple spans as shown in Fig. 4-2. In this numerical example, earthquake response of second pier-foundation of the bridge from right hand side was investigated based on earthquake motions recorded on ground surface near the bridge (approximately 400 m apart from the bridge, refer to Fig. 4-3). An earthquake motion acceleration selected was induced by Hyuganada Earthquake (April 1, 1968, $M = 7.5$, $\Delta = 100$ Km) and had the maximum amplitude of 185 gals as shown in Fig. 4-4.

Based on soil investigations conducted near the pier-foundation (Fig. 4-5) it was found that the soil profile consists of upper soft loam formations with an averaged N-value of 7 and lower stiff gravel formations with averaged N-values of 30 or more. Assuming the relation of Eq. (3-1), the relative stiffness a defined by Eq. (2-7) between the loam and gravel formations was estimated approximately as 0.48 for low amplitude ground vibrations and 0.34 for high amplitude ground vibrations. It was expected therefore that ground motions in the gravel formations would be less significantly influenced by the loam

formations during high amplitude ground vibrations. Then, based on the relieved criteria of base-rocks in the preceding chapter it was judged that the gravel formations underlying 10 m below the surface could be selected as base-rock at this site. On the other hand, ground conditions had not yet been investigated enough at the recording site. Based on topography of the sites it was assumed that the gravel formations existed at the bridge site continues to the recording site and underlies 20 m below the surface. This assumption coincided with the evidence that predominant frequency of the ground was approximately 3-4 c/s in field microtremor observations at the site.

The ground motion and incidental motion at the top face of gravel formations were theoretically calculated as shown in Figs. 4-6 and 4-8, respectively, by the deconvolution procedures taking into account the shear moduli of loam formations with their strain dependences. Fig. 4-7 shows comparisons of response acceleration spectrum between the recorded surface motion and theoretically calculated base-rock motion (Fig. 4-6). The pier-foundation and surrounding subsurface ground were modeled as shown in Fig. 4-9 by the analytical model described in the preceding paragraph. The loam formations were idealized by one dimensional shear column model with equivalent linear soil properties. The weight of girder supported by the pier was treated as an additional lumped mass at the pier top. The mass of surrounding soils defined by Eq. (4-1) was disregarded in the analyses. Vibration modes and natural periods (1st - 3rd) calculated for the subsurface ground and pier-foundation are shown in Fig. 4-10.

Earthquake responses of the pier-foundation were calculated based on Eq. (4-8) by applying the base-rock motion displayed in Fig. 4-6 at the base of shear column model. The damping ratio of 5% of the critical was assumed in the calculation. The maximum responses of displacements and accelerations are shown in Fig. 4-11 and representative response time histories at the top of pier are displayed in Fig. 4-12.

CONCLUSIONS

Based on the results presented, the following conclusions can be deduced:

(1) In order to specify common input earthquake motions for design of every structure on and underground at various sites, the useful approach is to select base-rocks in ground, where effects of ground near surface (subsurface ground) are small enough to be ignored, as common input terminals where earthquake motions, independent of subsurface ground properties, are to be specified.

(2) Formations considered can be selected as base-rocks at the site either when they are infinitely stiff as compared with the overburden subsurface grounds ($a = 0$) or when they are uniform continua in ground. In the former condition, both the incidental motions and the ground motions in those formations are selected as base-rock motions, while in the latter condition, the incidental motions in those formations are selected as base-rock motions. It is required to relieve the above conditions, however, from practical points of view in accordance with objectives and accuracies needed in design.

(3) Based on the correlative studies conducted for the underground earthquake motions, deconvolution procedures based on vertically propagating shear waves with equivalent linear material properties were effective in incorporating local subsurface ground conditions into earthquake motions recorded on grounds.

(4) The seismic analyses based on base-rock motions were successively applied to the Itajima Bridge.

ACKNOWLEDGEMENT

The authors wish to express their sincere appreciation to Mr. Toshio Iwasaki and Mr. Susumu Wakabayashi, Chief and Research Engineering of PWRI, in making digitized ground motion records available to us. Special thanks are also due to Mr. Matuo Shibata and Mr. Tadaaki Miyata, Engineers of PWRI, for their cooperation in the present investigation.

REFERENCES

- 1) Kanai, K., Relation Between the Nature of Surface Layer and Amplitude of Earthquake Motions, (I) BERI, 30 (1952), pp 31-37 (II) BERI, 31 (1953), pp. 219-226, (III) BERI, 31 (1953), pp. 275-279, (IV) BERI, 34 (1956), pp. 167-184.
- 2) Kanai, K., et al., Comparative Studies of Earthquake Motions on the Ground and Underground, (I) BERI, 37 (1959), pp. 53-87, (II) BERI, 44 (1966), pp. 609-643.
- 3) Kagami, H. and Kobayashi, H., A Numerical Analysis of the Propagation of Shear Waves in Multi-Layered Ground, Proceedings of Japan Earthquake Engineering Symposium, Oct., 1966, pp. 15-20.
- 4) Public Works Research Institute, Locations of Strong Motion Accelerometers (No. 3), Ministry of Construction, 1973.
- 5) Kuribayashi, E., Iwasaki, T. and Takagi, Y., Digitized Strong Motion Acceleration Records (No. 1 to No. 3), Technical Report No. 876, Public Works Research Institute, Ministry of Construction, 1974.
- 6) Iwasaki, T., Wakabayashi, S. and Horiuchi, S., Digitized Underground Strong Motion Acceleration Records, Technical Report No. 1103, Public Works Research Institute, Ministry of Construction, 1976.
- 7) Penzien, J., Scheffey, C. F. and Parmelee, R. A., Seismic Analyses of Bridges on Long Piles, Proc. ASCE, Vol. 90, No. EM3, 1964, pp. 223-254.
- 8) Kuribayashi, E., Kawashima, K. and Miyata, T., Earthquake Resistant Design Based on Ground Motions at Base-Rock, Technical Report No. 1192, Public Works Research Institute, Ministry of Construction, 1977.
- 9) Kuribayashi, E., Kawashima, K. and Miyata, T., Stress Analyses of Piles Due to Shear Deformation of Subsurface Ground in Earthquakes, Technical Report No. 972, Public Works Research Institute, Ministry of Construction, 1974.

Table 3-1. Underground Earthquake Motion Acceleration Studied(Ukishima Park, NS Component)

Earthquake Motion	Date	Epicenter	Epizentral Distance (Km)	Magnitude	Maximum Ground Motion Acceleration [gals]			
					Ground Surface	-27m	-67m	-127m
A	1970. 9. 30	East Kanagawa Pref.	15	4.8	11.8	10.7	5.5	4.3
B	1972. 12. 4	Off Hachijo Island	285	7.2	11.2	14.6	7.4	6.4
C	1974. 5. 9	South Izu Peninsula	135	6.9	12.2	9.2	5.0	5.9

Table 2-1. Transfer Function of Two Layered Ground.

Layers	Depth	Ground Motion (Displacement) $\sigma = 0$	Transfer Function Based On Incident Wave		Transfer Function Based On Ground Motion at Interface	
			$\sigma = -1$	$\sigma = 0$	$\sigma = 0$	$\sigma = 1$
Upper Layer	Ground Surface $s = \infty$	$\frac{2e^{i\sigma\theta}}{\sqrt{C + \sigma^2 S^2}}$ B_1	$\frac{2e^{i\sigma\theta}}{\sqrt{C + \sigma^2 S^2}}$	$\frac{2}{\cos \frac{\omega H}{V_1}}$	$\frac{1}{\cos \frac{\omega H}{V_1}}$	$\frac{1}{\cos \frac{\omega H}{V_1}}$
Interface Between Upper and Lower Layers	$s = \infty$	$\frac{2e^{i\sigma\theta} \cos \frac{\omega H}{V_1}}{\sqrt{C + \sigma^2 S^2}}$ B_1	$2e^{i\sigma\theta} \cos \frac{\omega H}{V_1}$	$2e^{i\sigma\theta} \cos \frac{\omega H}{V_1}$	$\frac{\cos \frac{\omega H}{V_1}}{\cos \frac{\omega H}{V_1}}$	$\frac{\cos \frac{\omega H}{V_1}}{\cos \frac{\omega H}{V_1}}$
Lower Layer	$s = \infty$	$2e^{i\sigma\theta} \cos \theta \cdot B_1$	$2e^{i\sigma\theta} \cos \frac{\omega H}{V_1}$	$2e^{i\sigma\theta} \cos \frac{\omega H}{V_1}$	2	1
			$2e^{i\sigma\theta} \cos \left(\frac{\omega H}{V_1} + \delta \right) B_1$	$2e^{i\sigma\theta} \cos \left(\frac{\omega H}{V_1} + \theta \right)$	$\frac{2 \cos \frac{\omega H}{V_1}}{\cos \frac{\omega H}{V_1} + \sin \frac{\omega H}{V_1} \sin \theta}$	$\frac{\cos \frac{\omega H}{V_1}}{\cos \frac{\omega H}{V_1}}$

$$C = \cos \frac{\omega H}{V_1}, \quad S = \sin \frac{\omega H}{V_1}, \quad \sigma = \frac{P_1 V_1}{P_2 V_2}$$

$$\sin \delta = \frac{eS}{\sqrt{C + \sigma^2 S^2}}, \quad \cos \delta = \frac{C_s}{\sqrt{C + \sigma^2 S^2}}$$

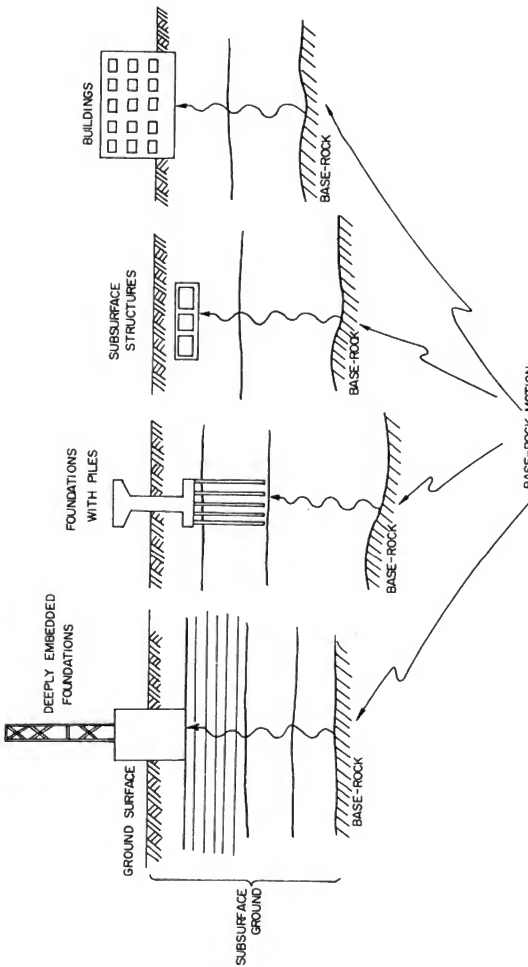


Fig. I-I SEISMIC ANALYSIS BASED ON BASE-ROCK MOTIONS

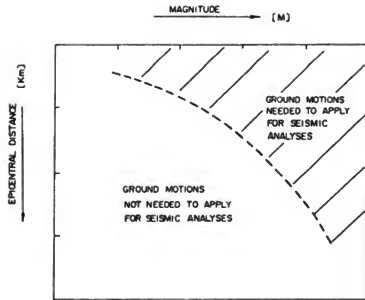


Fig. I-2 GROUND MOTIONS USED FOR SEISMIC ANALYSES

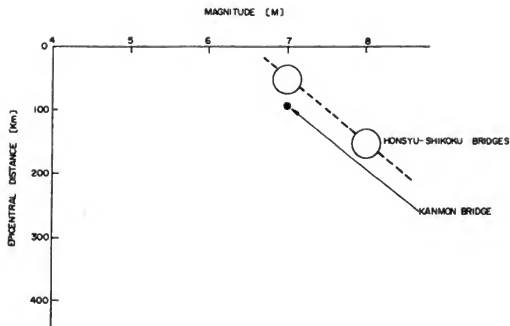


Fig. I-3 GROUND MOTIONS USED FOR SEISMIC ANALYSES OF SUSPENSION BRIDGES CONSTRUCTED OR PLANNED TO CONSTRUCT

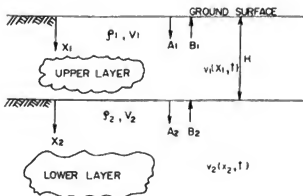


Fig. 2-1 SUBSURFACE GROUND MODEL

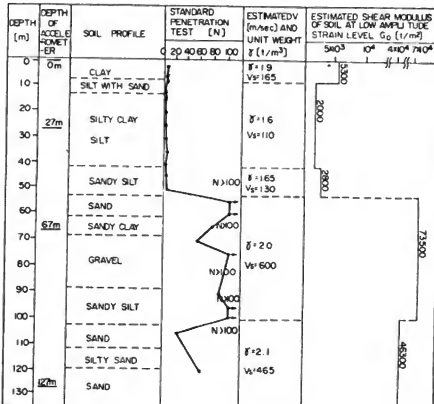


Fig. 3-1 SOIL PROFILE AT UKISHIMA PARK [6]

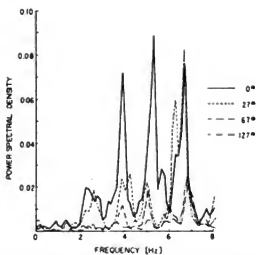


Fig.3-2 POWER SPECTRUM OF A-EARTHQUAKE GROUND MOTION

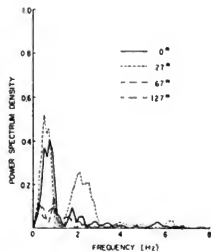


Fig.3-3 POWER SPECTRUM OF B-EARTHQUAKE GROUND MOTION

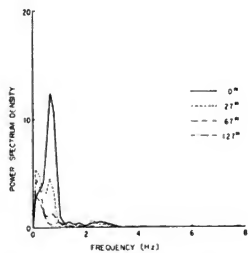


Fig 3-4 POWER SPECTRUM OF C-EARTHQUAKE GROUND MOTION

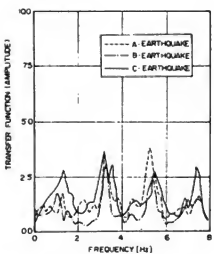


Fig 3-5 (a) TRANSFER FUNCTION OF GROUND
BETWEEN GROUND SURFACE AND
27m BENEATH GROUND SURFACE
(0°/ 27°)

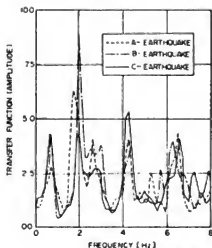


Fig 3-5 (b) TRANSFER FUNCTION OF GROUND BETWEEN
27m AND 67m BENEATH GROUND SURFACE
(27m/ 67m)

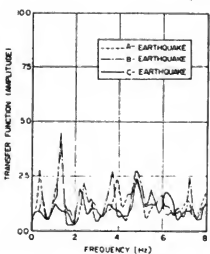


Fig 3-5 (c) TRANSFER FUNCTION OF GROUND BETWEEN
67m AND 127m BENEATH GROUND SURFACE
(67m/ 127m)

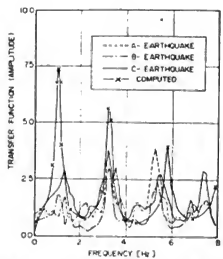


Fig 3-6 (a) COMPARISON OF COMPUTED AND MEASURED TRANSFER FUNCTIONS [0m/27m]

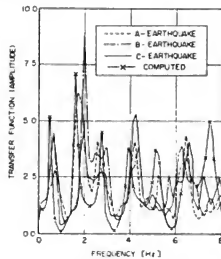


Fig 3-6 (b) COMPARISON OF COMPUTED AND MEASURED TRANSFER FUNCTIONS [27m / 67m]

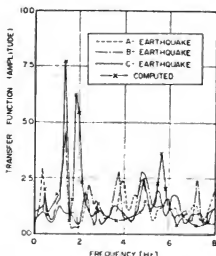


Fig 3-6 (c) COMPARISON OF COMPUTED AND MEASURED TRANSFER FUNCTIONS [67m/127m]

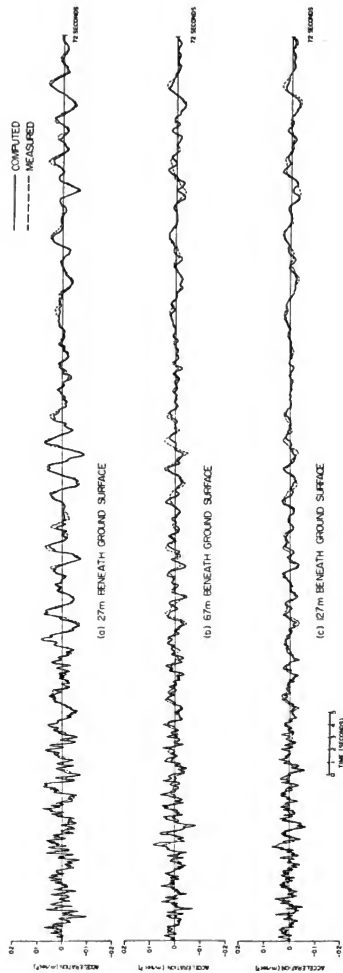


FIG. 3-7 COMPARISONS OF COMPUTED AND MEASURED UNDERGROUND EARTHQUAKE ACCELERATION MOTIONS

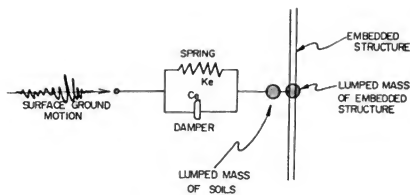


Fig. 4-1 DISCRETE ANALYTICAL MODEL OF DEEPLY EMBEDDED STRUCTURE

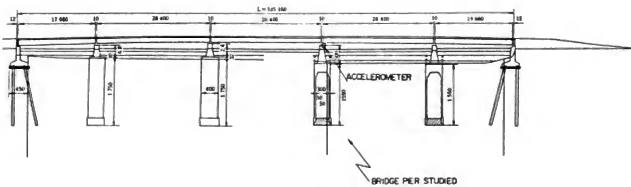


Fig. 4-2 GENERAL VIEW OF ITAJIMA BRIDGE (4)

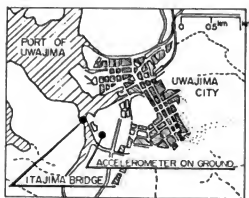


Fig. 4-3 LOCATIONS OF ITAJIMA BRIDGE
AND ACCELEROMETER ON
GROUND SURFACE (4)

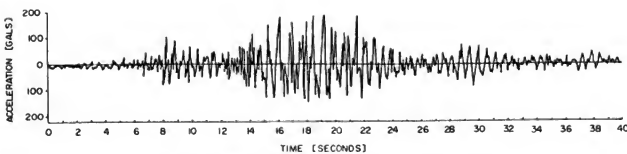


Fig 4-4 EARTHQUAKE GROUND MOTION ACCELERATION [GALS]
RECORDED ON GROUND SURFACE

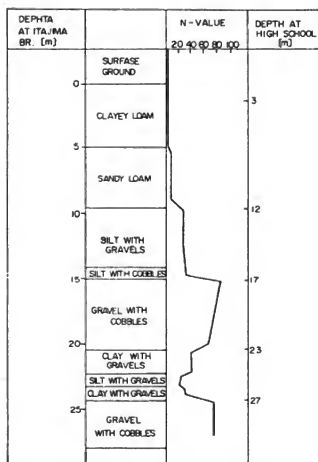


Fig 4-5 SOIL PROFILE AT ITAJIMA BRIDGE (4)



Fig 4-6 CALCULATED BASE-ROCK ACCELERATION

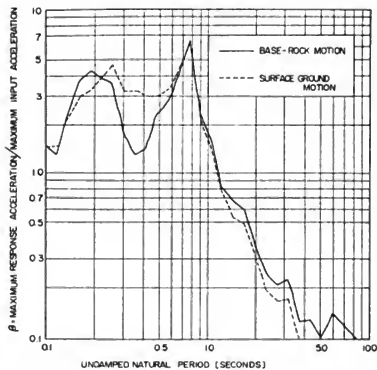


Fig. 4-7 COMPARISON OF RESPONSE ACCELERATIONS BETWEEN
BASE-ROCK AND SURFACE GROUND MOTIONS

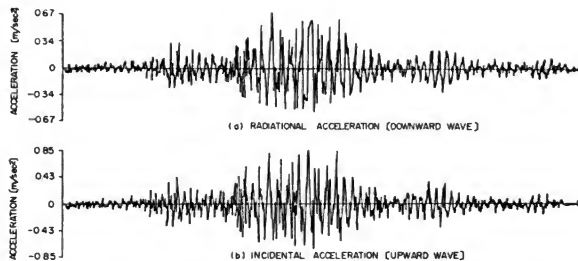


Fig. 4-8 CALCULATED INCIDENTAL AND RADIATIONAL MOTIONS [ACCELERATION]
AT BASE-ROCK

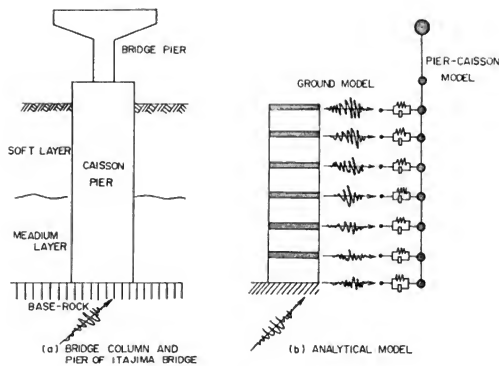


Fig. 4-9 ANALYTICAL MODEL OF BRIDGE FOUNDATION WITH SURROUNDING SUBSURFACE GROUND

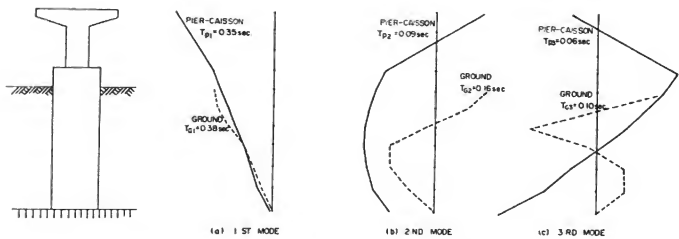


Fig. 4-10 VIBRATION MODES OF PIER-CAISSON AND GROUND

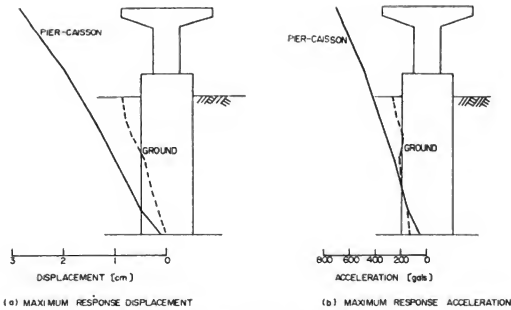


Fig. 4-11 CALCULATED MAXIMUM RESPONSES

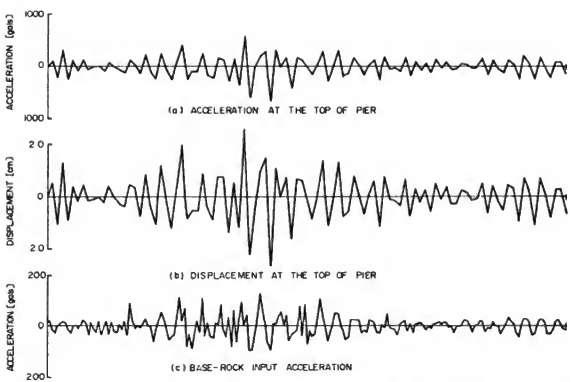


Fig. 4-12 CALCULATED RESPONSE ACCELERATION AND DISPLACEMENT AT TOP OF PIER

BASIC EARTHQUAKE FOR DAM DESIGN

Jerry S. Dodd

U.S. Bureau of Reclamation, Denver, Colorado

ABSTRACT

Modern computational techniques permit mathematical dynamic analysis of concrete and embankment dams. Steps in the analysis are: (1) specify location, depth, and magnitude of critical specifically located earthquakes, (2) attenuate seismic waves to site, (3) determine site response to seismic waves, (4) analyze response of structure, (5) evaluate results. This discussion addresses the first step and proposes the establishment of a minimum earthquake -- the basic earthquake -- for damsites in the western United States.

KEYWORDS: Earthquakes, Dams; Dynamic Analysis

INTRODUCTION

Modern computational techniques permit mathematical dynamic analysis of concrete and embankment dams. Steps in the analysis are: (1) specify location, depth, and magnitude of critical specifically located earthquakes, (2) attenuate seismic waves to site, (3) determine site response to seismic waves, (4) analyze response of structure, (5) evaluate results. However, with respect to the first step, there should be a small earthquake which is independent of location and which does not control or dominate the design of a dam, and therefore, should be a basis of comparison for specifically located earthquakes to determine if their effects will exceed those of a small earthquake. Also this approach permits during the design of a dam a rational means for the consideration of small earthquakes, which are difficult to define as specifically located earthquakes. The following evaluation is based on information about western United States.

RELATIONSHIP OF EARTHQUAKE MAGNITUDE AND INTENSITY

No direct relationship exists between magnitude and epicentral intensity. However, a general correlation does exist and has been studied by many investigators. Derived relationships of three investigations (Gutenberg and Richter, 1956; Toppozada, 1975; Krinitzsky and Chang, 1975) are shown in Fig. 1. Without violating the precision of these equations the relationship between magnitude and epicentral intensity can be more simply stated as:

$$M = 2 + I/2$$

or

$$I = 2(M-2)$$

where M = Richter magnitude

I = Modified Mercalli intensity

A comparison of three common Intensity scales is shown in Fig. 2.

EARTHQUAKE CLASSIFICATION

A classification of earthquakes for engineering seismology incorporating the above relationship is shown in Table I.

TABLE I
Engineering Classification of Earthquakes

<u>Classification</u>	<u>Magnitude Range</u>	<u>Epicentral Intensity</u>
Micro	Up to 2.0	
Very Minor	2.1 to 2.9	I
Minor	3.0 to 4.4	II, III, IV
Moderately Strong	4.5 to 5.9	V, VI, VII
Strong	6.0 to 6.9	VIII, IX
Major	7.0 to 7.9	X, XI
Great	8.0 and Up	XII

"Strong," "Major," and "Great" have been used for some time by the United States Geological Survey to describe the magnitude of earthquakes. The remaining classification nomenclature is also employed by the Geological Survey (W. Person, personal communication). The intensity relationship is from the above equation. "Micro" earthquakes are not felt and are detected only with instruments. "Very minor" earthquakes are on the threshold of human perceivability. The classification of "Minor" is used for those earthquakes with a magnitude range of 3.0 to 4.4. These are felt earthquakes but inflict at most only slight damage in the United States and correspond to epicentral intensities of II, III, and IV. The "Moderately strong" earthquake is that classification between minor and strong.

Minor earthquakes can be considered as not having associated surface rupture of the ground surface, see Fig. 3. An exception may be smaller earthquakes which occur on faults capable of producing creep and moderately strong or larger earthquakes. The magnitude 3.5 earthquake shown on Fig. 3 is an earthquake on the Imperial fault in California, which earlier ruptured at the ground surface in 1940 as the result of a magnitude 7.1 earthquake. Whether this 3.5 magnitude earthquake actually caused surface rupture is still open to discussion. Shallow moderately strong earthquakes may produce ground rupture on the fault generating the earthquake. Shallow strong and larger earthquakes are very likely to produce ground rupture on the source fault.

From the study by Krinitzsky and Chang (1975), it is reasonable to assume that minor earthquakes do not possess near field effects, see Fig. 4. That is, higher frequency content and complicated wave forms generated near the earthquake source are filtered out of the seismic signal by the time it reaches the ground surface. A reasonable conclusion is that a minor earthquake results only in far field vibrations at the ground surface.

BASIC EARTHQUAKE

The basic earthquake is defined as the minimum earthquake considered in the design of a dam. It yields the maximum ground motion which can be expected for a minor earthquake. Because of uncertainties with respect to the location and occurrence of minor earthquakes -- primarily because of the lack of good historical and instrumental data -- it is prudent in dam design to assume a ubiquitous nature for minor earthquakes. In many areas of the western United States it is likely that imposing the basic earthquake will be more severe than the resulting site ground motions determined from specifically located earthquakes.

The bedrock characteristics of the basic earthquake are:

1. Peak acceleration of .10 g.
2. Maximum duration ($g \geq .05 g$) of 8 sec.
3. No surface fault rupture.
4. No near field effects.

Krinitzsky and Chang (1976) show that for far field the limit of observed data for peak acceleration for an intensity between IV and V is .10 g (Fig. 5). Correspondently, Gutenberg and Richter (1956) correlated an acceleration of .10 g with an intensity VII (Fig. 6). Employing the limit of observed data from Krinitzsky and Chang is conservative.

For rock the upper bound of duration for accelerations exceeding .05 g for intensities between IV and V is 8 sec. as shown by Krinitzsky and Chang (1976) (Fig. 7). This also appears conservative. Bedrock can be assumed to be rock. Studies by Duke, et al. (1972) found that peak accelerations during the 1971 San Fernando earthquake in southern California were higher in rocks than surficial deposits (alluvium) for 40 to 60 km from the epicenter.

An engineering geologic description of the three primary earth materials is:

Bedrock - A generic term that embraces any of the continuous and generally indurated or compact earth material that makes up the earth's crust and is exposed at the earth's surface as outcrops or is covered by surficial deposits or topsoil.

Surficial Deposits - The young, generally loose and normally unstratified earth material occurring at or near the earth's surface as a bedrock cover and of two major classes: (1) dislocated and generally eroded or weathered bedrock materials transported by water, wind, ice, gravity, and man to another place, and (2) sedentary deposits formed in situ as a result of weathering and chemical processes or by the accumulation of organic matter.

Topsoil - The darker colored upper portion of a soil profile, the organic layer and organic rich A layer.

GOVERNING EARTHQUAKE

Using the data from Krinitzsky and Chang (1975), as shown in Fig. 8, a general guideline can be developed indicating when the basic earthquake will govern or when a specifically located earthquake will dominate. This is shown on Fig. 9. Also shown is a curve for a peak acceleration of .10 g developed from seismic wave attenuation studies of others and depicts the most moderate attenuation characteristics expressed in these studies (Gutenberg and Richter, 1942; Housner, 1965; Blume, 1965; Kanai, 1966; Esteva, 1970; Schnabel and Seed, 1973; Duke, et al. 1972; Donovan, 1973; Trifunac and Brady, 1976). The actual attenuation employed in the dynamic design of a dam is more likely to generate a curve to the left of this curve rather than between this curve and the Krinitzsky and Chang curve. This means generally that specifically located earthquakes need to be evaluated only within 125 km of the dams site. Also the controlling epicentral distances for governing specifically located earthquakes for earthquake classifications greater than magnitudes 4.4 can be estimated.

REFERENCES

Barosh, P. J., "Use of Seismic Intensity Data to Predict the Effects of Earthquakes and Underground Nuclear Explosives in Various Geologic Settings," Bulletin 1279, U.S. Geological Survey, Washington, D.C., 1969.

Blume, J. A., "Earthquake Ground Motion and Engineering Procedures for Important Installations Near Active Faults," Proceedings of the Third World Conference on Earthquake Engineering, New Zealand, Vol. IV, pp. 53-67, 1965.

Bonilla, M. G., "Surface Faulting and Related Effects," Earthquake Engineering, R. H. Wiegel, ed., Prentice Hall, Englewood Cliffs, Chapter 3, pp. 47-74, 1970.

Donovan, N. C., "A Statistical Evaluation of Strong Motion Data Including the Feb. 9, 1971 San Fernando Earthquake," Proceedings of the Fifth World Conference on Earthquake Engineering, Rome, Italy, 1973.

Duke, C. M., Johnsen, K. E., Larson, L. E., and Engman, D. C., "Effects of Site Classification and Distance on Instrumental Indices in the San Fernando Earthquake," UCLA Eng-7247, University of California, Los Angeles, June 1972.

Esteva, L., "Seismic Risk and Seismic Design Decisions," Seismic Design for Nuclear Power Plants, R. J. Hansen, ed., M.I.T. Press, Cambridge, Massachusetts, 1970.

Gutenberg, B., and Richter, C. F., "Earthquake Magnitude, Intensity, Energy, and Acceleration," Bulletin, Seismological Society of America, Vol. 32, pp. 163-191, 1942.

Gutenberg, B., and Richter, C. F., "Earthquake Magnitude, Intensity, Energy, and Acceleration (Second paper)," Bulletin, Seismological Society of America, Vol. 46, pp. 105-145, 1956.

Housner, G. W., "Intensity of Earthquake Ground Shaking Near the Causative Fault," Proceedings of the Third World Conference on Earthquake Engineering, New Zealand, pp. 94-111, 1965.

Kanai, K., "Improved Empirical Formula for Characteristics of Strong Earthquake Motions," Proceedings of Japan Earthquake Symposium, 1-4 (in Japanese), 1966.

Krinitzsky, E. L., and Chang, F. K., "Earthquake Intensity and the Selection of Ground Motions for Seismic Design" State-of-the-Art for Assessing Earthquake Hazards in the United States - Report 4, Miscellaneous Paper S-73-1, U.S. Army Engineer Waterways Experiment Station, 1975.

Krinitzsky, E. L., and Chang, F. K., "Design Earthquakes," Unpublished, U.S. Army Engineer, Waterways Experiment Station, 1976.

Linehan, D., "Geological and Seismological Factors Influencing the Assessment of a Seismic Threat to Nuclear Reactors," Seismic Design for Nuclear Power Plants, R. J. Hansen, ed., M.I.T. Press, Cambridge, Massachusetts, 1970.

Schnabel, P., and Seed, H. B., "Accelerations in Rock for Earthquakes in the Western United States," Bulletin, Seismological Society of America, Vol. 63, pp. 501-516, 1973.

Toppozada, T. R., "Earthquake Magnitude as a Function of Intensity Data in California and Western Nevada," Bulletin, Seismological Society of America, Vol. 65, pp. 1223-1238, 1975.

Trifunac, M. D., and Brady, A. G., "Correlations of Peak Accelerations Velocity and Displacement with Earthquake Magnitude, Distance and Site Conditions," Earthquake Engineering and Structural Dynamics, Vol. 4, pp. 455-471, 1976.

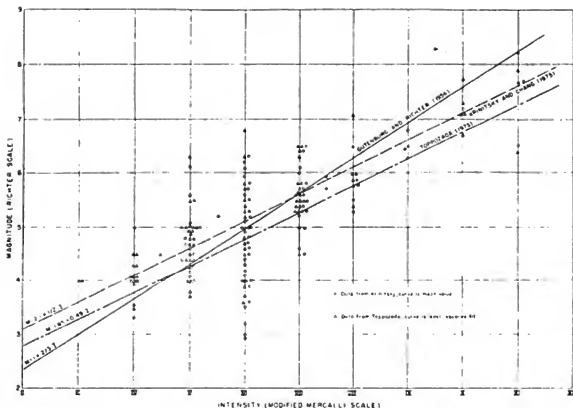


FIGURE 1. Comparisons of several curves relating magnitude and intensity values in the western United States (Gutenberg and Richter curve from Krinitzky and Chang, 1975).

MODIFIED MERCALLI INTENSITY SCALE	GEOFIAN INTENSITY SCALE (RUSSIA)	JAPANESE INTENSITY SCALE
I Non felt; Marginal and long-period effects of large earthquakes	I Oscillations of site ground are detected only with instruments	0 Non felt by humans, registered only by seismographs.
II Felt by persons at rest, or super-thin, or have felt it abroad	II In individual cases felt only by semi-savvy persons at rest	I Slight, felt only by persons at rest or by those who are especially observant of earthquakes
III Felt outdoors; Hanging objects swing. Very common loss of sense of light trucks. Durian movement. May not be noticed even on an earthquake.	III Oscillations felt by few persons	
IV Hanging objects swing. Vibration like passing of heavy truck. Shaking similar to very slight wind. Small objects move. Glasses shake. In upper range of IV windows wane and frame crack.	IV Noticed by many persons. Windows or doors may rattle.	II Weak felt by most persons. Slight shaking of windows and Japanese - knock of sliding doors.
V Earthquakes direction unknown. Trees are swayed. Leaves rattled. Doors swing. Shutters pictures move. Pendulum's start, stop, change rate.	V Objects swing. Radio mouth, glasses, remote outer plaster crumble.	III Moderate strong. Buildings shake, windows and doors rattle, hanging objects swing, some pendulums start to stop, some people run outside.
VI Felt by many. Many frightened and run out doors. Persons with unsteady. Windows, shades, pictures break. Books off shelves. Furniture rattles. Pictures move. Small objects move. Walls and adobe cracked. Small bells ring.	VI Light damage to buildings. Thin cracks in plaster, cracks in tile surfaces etc.	IV Strong, strong shaking of buildings, objects overturn, houses split and/or vessels
VII Difficult to predict. Reduced by doors of houses, windows, doors, windows, walls, roofs, etc. Broken cracks in masonry. Walls cracked, water seeped. Small cracks, separation of stones or granite blocks. Large blocks ring. Concrete or garden articles bending and/or snap.	VII Considerable damage to buildings, masonry, plaster and lining of individual pieces, thin cracks in walls.	V Very strong. Bricks and plaster walls crack, stone blocks, granitess and similar objects overturn, thick trees are bent and pulled, walls are broken, vehicles are stamp dismounted
VIII Strengthening of major cars affected. Damage to machinery, some partial collapse. Twisting, falling, breaking of pipes, cables, telephone and tank. Frame houses moved in front behind doors. Branches broken. Changes in ground surface. Cracks in earth ground and/or snap.	VIII Damage in buildings, large cracks in walls, falling of cornices or cornices.	
IX General panic. Woods fissures, damaged, good memory seriously damaged. Frame structures, not better, shifted off base, collapsed. Large cracks in ground, damage to reservoirs. Underground pipes broken. Ground cracked, sand and mud mixed, permeable fountains, land curves.	IX Collapse of some buildings, debris, corn of earth, roofs, floors, terraces.	VI Disastrous destruction of 1-30 cm. corn of Journal houses, house large landslides, fissures at the base of great mountains, landslides caused by mud and water-attacks.
X Major damage to houses, roads, railways, serious damage to embankments. Large landslides. Water through banks of small rivers, lakes, etc. Roads bent slightly.	X Collapse of many buildings, debris in ground about 1 meter high.	
XI Roads torn, gravity. Underground pipelines completely out of service	XI Numerous fissures, large landslides in mountains	VII Rupture destruction of more than 30 percent of the houses, high landslides, fissures and fault movements
XII Damage nearly total. Large rock masses dislodged. Lines of high and low are altered. Objects thrown into the air.	XII Large-scale changes in relief	

FIGURE 2. Comparison of the Modified Mercalli, the Geofian and the Japanese Intensity Scales (after Barosh, 1969 and Krinitzky and Chang, 1975).

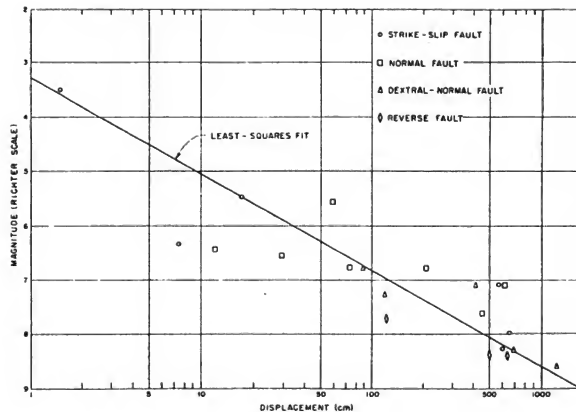


FIGURE 3. Magnitude versus maximum displacement on main fault at surface (after Bonilla, 1970).

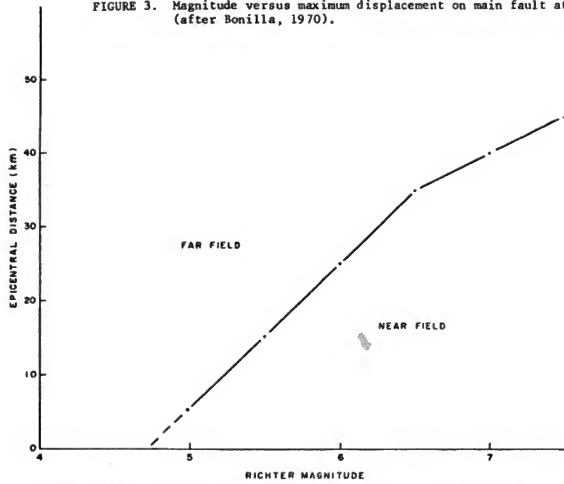


FIGURE 4. Near field and far field limits (after Krinitzsky and Chang, 1975)

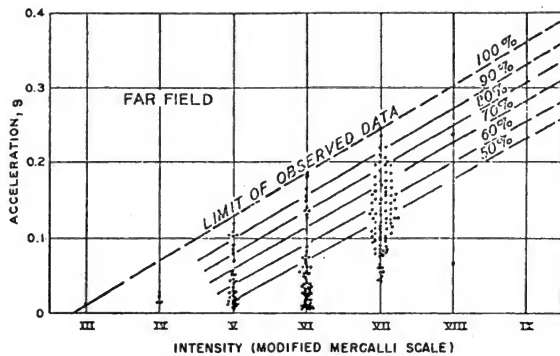


FIGURE 5. Acceleration values for MM intensity in the far field (after Krinitzsky and Chang, 1976).

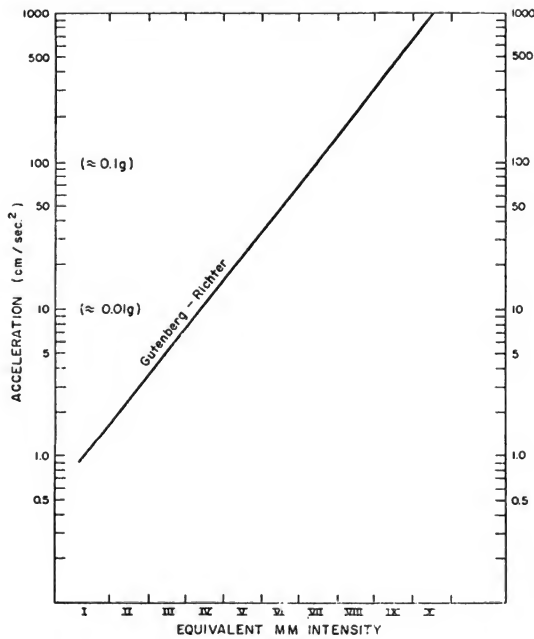


FIGURE 6. Intensity versus acceleration (after Linehan, 1970).

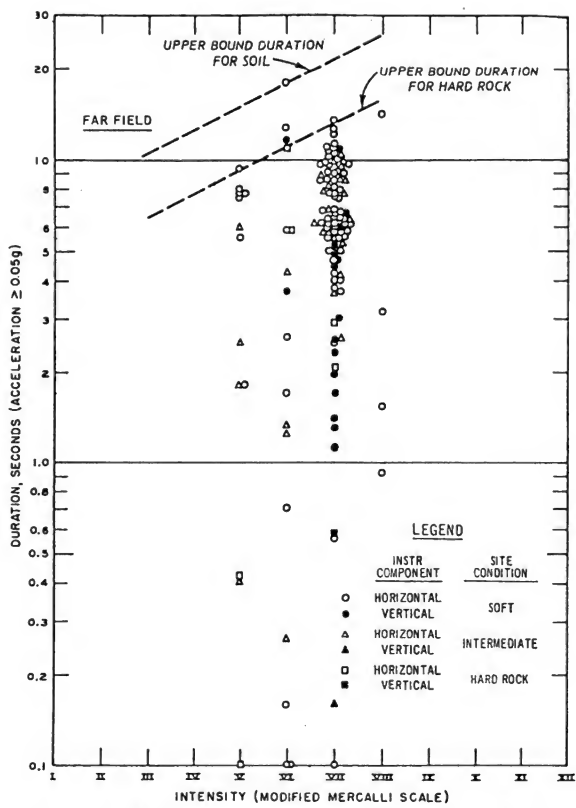


FIGURE 7. Durations for MM intensity in the far field (after Krinitzsky and Chang, 1976)

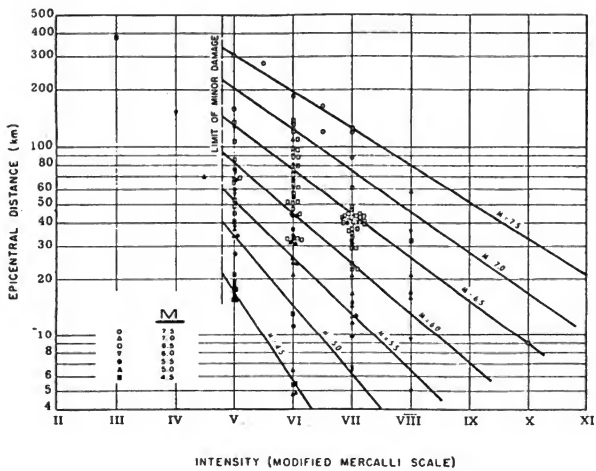


FIGURE 8. Intensity versus magnitude, M (Richter scale), and epicentral distance, western United States (from Krinitsky and Chang, 1975).

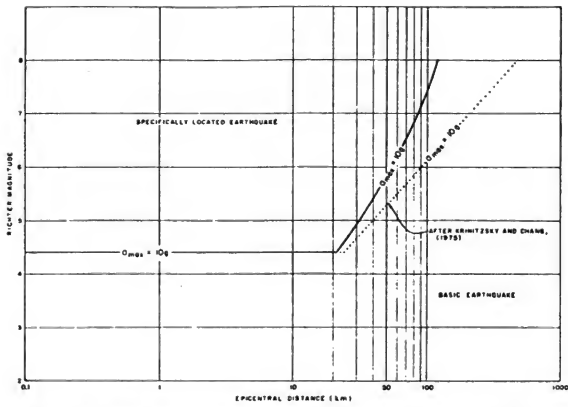


FIGURE 9. Governing earthquake - magnitude versus epicentral distance.

STUDY ON REGIONAL DISTRIBUTION OF MAXIMUM EARTHQUAKE MOTIONS IN JAPAN

Masakazu Ozaki, Head, Str. Div., B.R.I., Ministry of Const, Japan

Yoshikazu Kitagawa, Res. Memb., Str. Div., B.R.I., Min. of Const., Japan

Sadaiku Hattori, Res. Memb., I.I.S.E.E., B.R.I., Min. of Const., Japan

ABSTRACT

Research activities in the earthquake danger have been critically reviewed. Many researchers concentrated on the study of the past earthquake data and statistical analyses of these data.

This paper presents an application of Gumbel's theory of extremes for the prediction of the intensity of future earthquakes. The paper concludes with a new regional seismic coefficient map of Japan.

KEYWORDS: Earthquake danger; Gumbel's theory of extremes, literature review; regional seismic coefficient map; statistical analysis.

1. INTRODUCTION

One of the most important problems in earthquake engineering is to predict statistically the intensity of future earthquakes from the past earthquake data, since at the present time the precise earthquake forecast is difficult. In the process of the prediction, the selection of the past earthquake data and statistical method of analysis are most important, because the available earthquake data are not sufficiently large.

Many investigations have been carried out in these two subjects in Japan. However, there has been no research on the prediction of the intensity of future earthquakes based on the theory of extremes developed by Gumbel. This paper deals with the expected values of the intensity of future earthquakes on base rock as well as on the surface of ground by introducing Gumbel's Theory of Extremes.

2. GENERAL REVIEW ON THE EARTHQUAKE DANGER IN JAPAN

The earthquake danger in a certain place may be defined by the seismic activity in the vicinity and the characteristics of the soil-layers. In order to clarify the earthquake danger more reliably, it is necessary to investigate the regional distribution or variation of the seismic activity and the characteristics of soil-layers.

General reviews indicate that some research has been conducted considering seismic activity only, i.e., magnitude frequency distribution and focal distribution, disregarding the regional difference of soil characteristics. A few investigations seem to be performed considering the influence of the soil characteristics, but not sufficiently.

Since Dr. H. Kawasumi published his regional map on the earthquake danger in 1951, the research activities have increased in number as many as 10 in Japan. The outline of the research conducted on the earthquake danger in the vicinity of Japan is as follows:

Dr. H. Kawasumi^{1*} observed the following relation between the seismic intensity I in J.M.A. and the maximum acceleration amplitude α on the ground,

$$\alpha \text{ (gal)} = 0.45 \times 10^{0.5I} \quad (1)$$

Taking into account the fact that the regional distribution of the intensity is closely related to the epicentral distance and the magnitude of an earthquake, he also determined the relation between the epicenters and his magnitudes M_k for the earthquakes in the olden times (A.D. 679-1925) when no observed data had been given, utilizing the descriptions in ancient documents. Kawasumi also defined the relation among M_k , I, and the epicentral distance Δ . Taking Eq. 1 into consideration, the relation is represented in terms of M , α and Δ as follows:

*The superscript numerals refer to the corresponding numerals in Table 1.

$$\log \alpha = M - 0.540 - 2.3 \log (\Delta/\Delta_0) - 0.000915 (\Delta - \Delta_0)$$

$$= M - 0.540 - \log (r/r_0) - 0.00834 (r - r_0) \text{ for } r \leq r_0 = 100 \text{ km} \quad (2)$$

where r means the hypocentral distance, $\Delta_0 = 100 \text{ km}$, $r_0 = \sqrt{100^2 + 18^2}$.

Using the data for the period 679-1948 and Eq. 2, the expected maximum acceleration was calculated at arbitrary points for the return period τ years and was determined by the following equation,

$$\frac{\sum_{\alpha=0}^{\infty} n(\alpha)}{T} = \frac{1}{\tau} \quad (3)$$

where $n(\alpha)$ and T are the frequency of maximum acceleration amplitude and the data period in year. He obtained finally the regional distribution of the expected maximum acceleration amplitude for the return periods ($\tau = 50, 75, 100$ and 200 years) at every half degree point in latitude and longitude.

Dr. I. Muramatsu² analyzed the destructive earthquakes in latitude and longitude since 1926 and obtained the following equations as the relation among M , r and maximum velocity amplitude V ,

$$V \text{ (cm/sec)} = C(M)r^{-1} e^{-r/r_c(M)}$$

$$\log C(M) = 0.655M - 1.719 \quad (4)$$

$$\log r_c(M) = 0.145$$

Dividing the earthquake data into two periods A.D. 679-1867 and A.D. 1868-1956 and using these data in each period, he made the same analysis as Dr. Kawasumi and pointed out that the distribution of the expected maximum acceleration amplitude resembled each other, but the absolute values were fairly different between both cases. So that the regional distribution of the expected maximum velocity amplitude V_0 for the return period ($\tau = 50$ years) using Eq. 4 and the data between 1868-1964 years was obtained by the following equation,

$$\frac{\sum_{V=V_0}^{\infty} n(V)}{T} = \frac{1}{\tau} \quad (5)$$

where $n(V)$ is the frequency of the maximum velocity amplitude.

After analyzing the seismic records observed underneath the ground at the depth of 300 m, Dr. K. Kanai and T. Suzuki³ concluded that the amplitude of the velocity spectrum V of earthquake motions at base rock was nearly constant with regards to period t as follows:

$$t \leq 10^{0.39M-1.70} \quad (6)$$

and that amplitude is determined by the following equation:

$$\log V = 0.61M - (1.66 + \frac{3.60}{r}) \log r - (0.631 + \frac{1.83}{r}) \quad (7)$$

So that using Eqs. 5 and 7 and the earthquake data with damages for the period 599-1964, they obtained the regional distribution of the expected maximum velocity spectral amplitude at the base rock for the return periods ($t = 75, 100, 200$ years).

H. Goto and H. Kameda⁴ applied a certain probabilistic model to make up for insufficient earthquake data in ancient time. They assumed the occurrence of earthquakes to be independent events and defined that the records in the period B_k were the sample values of n times Bernoulli trials, in which $n_{11}, n_{12}, \dots, n_{1m}$ times trials were related to the seismic intensities I_1, I_2, \dots, I_m . The probability P_k of each trial was a degree of importance for the period B_k in the whole records, and the earthquake danger in each period was estimated with P_k . At that time, the seismic acceleration amplitude $X(t)$ was indicated as $\beta f(t; \tau) g(t)$ and the mean maximum acceleration amplitude a_f relating to the parameter β was given as $a(V) = 50 T_0^{-1.316}$, $a(VI) = 320(T_0/0.4)^{-1.316}$ and $a(VII) = 470(T_0/0.4)^{-1.316}$, where $f(t; \tau)$, $g(t)$ and β are a deterministic time function, a non-dimensional stationary stochastic process and a constant with dimension of acceleration, and T_0 means a predominant period. Taking these into consideration, the probability distributions of the maximum acceleration amplitude $\psi_f(a_f)$ and the maximum velocity amplitude $\psi_f(v_{mf})$ at arbitrary points for a certain period were given as follows:

$$\left. \begin{aligned} \psi_f(a_f) &= \sum_{K_1=0}^{n_{11}} \cdots \sum_{K_m=0}^{n_{1m}} \left\{ \prod_{j=1}^m [\psi_s(a_f; I_j)]^{K_{ij}} \cdot b \cdot (K_{ij}; n_{ij}; P_f) \right\} \\ \psi_f(v_{mf}) &= \sum_{K_1=0}^{n_{11}} \cdots \sum_{K_m=0}^{n_{1m}} \left\{ \prod_{j=1}^m [\psi_s(v_{mf}; I_j)]^{K_{ij}} \cdot b \cdot (K_{ij}; n_{ij}; P_f) \right\} \end{aligned} \right\} \quad (8)$$

and the regional distributions of the expectation $E[a_f]$, $E[v_{mf}]$ were calculated in the following equations:

$$\left. \begin{aligned} E[a_f] &\approx \int_0^\infty \{1 - \psi_f(a_f)\} da_f \\ E[v_{mf}] &\approx \int_0^\infty \{1 - \psi_f(v_{mf})\} dv_{mf} \end{aligned} \right\} \quad (9)$$

where the return period τ is 75 years and the predominant period is 0.5 sec.

T. Okubo and T. Terashima⁵ modified the expected maximum acceleration amplitude proposed by Dr. Kawasumi on the distribution of earthquake intensity in the major earthquakes after the Kanto Earthquake in 1923. In their map, Japan was divided into four divisions by recombining Kawasumi's map and the distribution of intensity V or more.

K. Takahashi⁶ defined that a mean annual accumulative intensity frequency $f(\alpha)$ at the observatories of J.M.A. could be shown in the following equation as the first approximation,

$$f(\alpha) = \frac{f_0}{\alpha(1 + \alpha/25)} = \frac{f_0}{\alpha(1 + 0.002\alpha F)} \quad (10)$$

where $\alpha = 0.8 \times 10^{0.5(I-1)}$, f_0 and F are a regional coefficient and times of felt earthquakes, respectively.

He estimated the expected maximum values at any point with the following data: (a) the times of felt earthquakes for the period 1884-1970 year, (b) the mean annual frequency of earthquakes with Intensity III or more for the period 1884-1970 year, (c) the mean annual frequency of Intensity V or more for the period 1506-1970 year. So that final regional distribution of the expected maximum acceleration amplitude was obtained by means of weighted mean values as the result of the above-mentioned method.

S. Hattori and Y. Kitagawa⁷ applied Ishimoto-Iida's formula

$$n(A)dA = k A^{-m} dA \quad (11)$$

to the maximum displacement amplitude at each observational station of J.M.A., using the observed data for the period 1967-1972.

In Eq. 11 $n(A)$ is the frequency of the maximum displacement amplitude A , k and m are constants at each observational station. At that time, m and k were determined as follows:

$$m = \frac{\sum_{i=1}^S \log e}{\sum_{i=1}^S \log A_j - S \log A_j} + 1.0, \log k = \log N (A > A_j) + \log (m - 1) + (m - 1) \log A_j,$$

where S , A_j , A_i and $N (A > A_j)$ are the total number of the data, the smallest maximum amplitude, the i -th maximum amplitude counted from the largest one and accumulative frequency of $A > A_j$, respectively. Taking these values and the data period into consideration, the regional distribution of the expected maximum displacement amplitude was obtained for the return periods ($t = 25, 50, 100$ years).

S. Omote and K. Matsumura⁸ obtained the regional distribution of the expected maximum acceleration amplitude using the data for the period 1885-1973. At that time, magnitude M in J.M.A. for the period after 1926 was transformed into M_k by $M_k = 2M - 8.7$. The method of analysis was almost the same as that of Dr. Kawasumi except the following equation was used instead of Eq. 1).

$$\alpha = 0.253 \times 10^{0.5I} \quad (12)$$

Moreover, S. Omote, H. Hanai and S. Nagamatsu⁹ made the regional distribution of the expected earthquake motions at the base rock using Eq. 7 and a probability model of earthquake occurrences represented by a Poisson process. At that time, they used the earthquake data from the periods 679-1972 and 1741-1972 for the same return periods ($T = 50, 200$ years).

S. Nagahashi¹⁰ defined the expected maximum velocity response amplitude SV_o as follows:

$$\log SV_o = a M - b \log r - c \quad (13)$$

where a , b and c are the functions of natural period modified by the characteristics of the observational site from the strong-motion records.

And he obtained the regional distribution of the expected SV_o values having 0.3, 1.0 and 3.0 sec. in natural period and 0.05 in the damping of response system for the return period 50 years, using the data for the period 1885-1975. At that time, M_k for the period 1885-1925 was transformed into M by Muramatsu's equation $M_k = 0.88M + 1.2$.

The research described above is summarized in Table 1.

3. THEORY OF EXTREME VALUES

3-1. Gumbel's First Asymptotic Distribution

The simplest method by which the extreme values of a variate can be predicted is known as that of the First Asymptotic Distribution of Gumbel (1958)¹¹. Whether the distribution is a reasonable one to employ in a specific application is a matter of judgment. Such a judgment can be exercised by considering how well the inputs fit the distribution and by taking into account any factor which may tend to influence the trend toward the extreme values. While the goodness of fit is a statistical problem, the criterion by which it is judged depends on the intended application and no priori rule can be formulated in its regard. The deviation in trend to extreme is usually a physical problem and its prediction cannot always be made on a purely statistical basis but may require insight into the nature of the phenomenon to be predicted.

1) INPUTS

The prediction of extreme values is made by carrying out certain statistical operations on a set of maximum values of the variate to be predicted. Such a set is obtained either by sampling subsets of a totality or by the sequential measurement of a process over specific intervals of time suitably spaced. The method is the same in either case, but since the environmental phenomena of interest are essentially time-dependent, the exposition that follows is expressed in the parlance pertinent to time functions.

Thus, the inputs required are:

- a) A compilation of set maxima, x
- b) The total number of set maxima, N

2) ORDERING OF INPUTS

When N is large, the set maxima (adjusted) are ordered by magnitude, either ascending or descending. In what follows, the ascending order is used. The generic value of the ranking index of the set maxima is denoted by x_m , thus:

$$x_1 < x_2 < \dots < x_m < \dots < x_N$$

3) ORDINAL FREQUENCY θ_m

To each set maximum x_m corresponds the ordinal frequency

$$\theta_m = \frac{m}{N+1}$$

4) INPUT STATISTICS

The mean value of x_m

$$\bar{x} = \frac{1}{N} \sum_{m=1}^N x_m$$

The variance

$$\sigma^2 = \frac{1}{N} \sum_{m=1}^N [x_m - \bar{x}]^2$$

The corresponding dispersion

$$\sigma = \sqrt{\sigma^2}$$

5) REDUCED VARIATE y_m

The set maximum x_m is plotted at the position given by the reduced variate

$$y_m = -\ln [-\ln (\theta_m)]$$

6) SLOPE $\frac{1}{a}$

The slope is calculated by the least square technique as

$$\frac{1}{a} = \frac{\frac{1}{N} \sum_{m=1}^N (x_m - \bar{x}_m) (y_m - \bar{y}_m)}{\frac{1}{N} \sum_{m=1}^N (y_m - \bar{y}_m)^2}$$

7) MODE U

The mode is calculated by the least square technique as

$$U = \bar{x}_m - \frac{\bar{y}_m}{a}$$

8) EXPECTED MAXIMUM VALUE $x(y)$

The regression line of expected maxima is

$$x(y) = U + \frac{Y}{a}$$

3-2. Gumbel's Second and Third Asymptotic Distributions

The First Asymptotic Distribution of Gumbel predicts extreme values of a variate approaching infinity as the return period approaches infinity. In most applications to forecasting, this tendency of growth does lead to predictions of reasonable accuracy. This is obtained when the observed values ranked by magnitude and related to a probability of occurrence crowd the regression line of the expected values. There exist, however, cases for which there is, indeed, a marked tendency of the observed values to deviate increasingly from the regression line as the return period increases. Such cases occur when physical causes operate to impose constraints of ever greater severity as the variate tends to grow in magnitude.

The reliable treatment of such problems requires extremal probability distributions to be somewhat more flexible than the First Asymptotic Distribution. A convenient one is Gumbel's Second or Third Asymptotic Distribution. As against the First, which is a two-parameter distribution (mode and slope), the Second or Third is a three-parameter distribution (asymptote, characteristic value, and exponent). However, the enhanced flexibility introduced by the third parameter is paid for in increased complexity, and a relatively simple and direct determination of parameters, as in the case of the First Distribution, is not quite in hand. The way out is to have recourse to a computer and derive the parameters by iteration. A method for accomplishing this is outlined herein.

The cumulative probability corresponding to Gumbel's Second Asymptotic Distribution is given by

$$2\theta(x) = \exp \left(-\left[\frac{V - \epsilon}{x_m - \epsilon} \right]^K \right)$$

where x is the variable, ϵ its limiting value, V its characteristic value and K an exponent. The problem is to derive them from the input data. The inputs are a set of maximum values measured over a specific interval.

The cumulative probability corresponding to Gumbel's Third Asymptotic Distribution is given by

$$3\theta(x) = \exp \left(-\left[\frac{W - x_m}{W - V} \right]^K \right)$$

where x is the variable, W its limiting value, i.e., the expected maximum value that the variable is likely to attain in the infinitely long run, V its characteristic value and K an exponent.

The set of maximum values x_m is arranged in ascending order and plotted against the corresponding ordinal frequency

$$\beta_m = \frac{m}{N+1}$$

where N is the total number of data points. The mean value, variance and dispersion x_N , σ_N^2 , σ are obtained as for the First Asymptotic Distribution.

The reduced variate $_2Z_m$ for the Second Asymptotic Distribution when introduced onto the expression

$$_2Z_m = -k_n \left(\frac{V - \epsilon}{x_m - \epsilon} \right)^K$$

and the reduced variate $_3Z_m$

$$_3Z_m = -k_n \left(\frac{W - x_m}{W - V} \right)^K$$

will plot as a straight line against

$$y_m = -k_n [-k_n (\beta_m)]$$

Note that in the outline that follows the subscript m is employed to define either an input x_m or a value directly related to inputs y_m , β_m , etc.

Note also that the characteristic value is that value of x which corresponds to the cumulative probability $\beta = \frac{1}{e} = 0.368$, i.e., to $y = 0$. In the First Asymptotic Distribution, such a value is termed the mode.

1) VARIANCE σ_N^2

Variance $\sigma_N^2(V, \epsilon, K)$ for the Second Asymptotic Distribution can be obtained as

$$\sigma_N^2(V, \epsilon, K) = \frac{1}{N} \sum_{l=1}^N (_2Z_m - y_m)^2$$

$$= \frac{1}{N} \sum_{l=1}^N (-K \cdot k_n \left[\frac{V - \epsilon}{x_m - \epsilon} \right] - y_m)^2$$

Variance $\sigma_N^2(V, W, K)$ for the Third Asymptotic Distribution is as follows:

$$\sigma_N^2(V, W, K) = \frac{1}{N} \sum_{l=1}^N (_3Z_m - y_m)^2$$

$$= \frac{1}{N} \sum_{l=1}^N (-K \cdot k_n \left[\frac{W - x_m}{W - V} \right] - y_m)^2$$

2) EXPONENT K

Using the least square method, the exponent K for the Second Asymptotic Distribution can be expressed in terms of ϵ and V .

$$\frac{\partial \sigma_N^2}{\partial K} = -\frac{2}{N} \sum_1^N [-K \cdot i_n (\frac{V - \epsilon}{x_m - \epsilon}) - y_m] [-i_n (\frac{V - \epsilon}{x_m - \epsilon})]$$

$$K = -\frac{\sum_1^N y_m i_n (\frac{V - \epsilon}{x_m - \epsilon})}{\sum_1^N \{i_n (\frac{V - \epsilon}{x_m - \epsilon})\}^2}$$

The exponent K for the Third can also be expressed in terms of W and V

$$K = -\frac{\sum_1^N y_m \cdot i_n (\frac{W - x_m}{W - V})}{\sum_1^N \{i_n (\frac{W - x_m}{W - V})\}^2}$$

Then the variance $\sigma_N^2(V, \epsilon)$ and $\sigma_N^2(V, W)$ are

$$\sigma_N^2(V, \epsilon) = \frac{1}{N} \sum_1^N [-K(V, \epsilon) \cdot i_n (\frac{V - \epsilon}{x_m - \epsilon}) - y_m]^2$$

and

$$\sigma_N^2(V, W) = \frac{1}{N} \sum_1^N [-K(V, W) \cdot i_n (\frac{W - x_m}{W - V}) - y_m]^2$$

3) PARAMETRIC SEQUENCE OF THE CHARACTERISTIC VALUE V

The characteristic value V is obtained by iteration. A new characteristic value V_{p+1} is related to its previous value V_p through recurrence relation

$$V_{p+1} = V_p + [-\frac{1}{2}]^{C_p} \cdot \Delta V$$

where p is an interation index and ΔV is an arbitrary incremental value.

Note that the characteristic value V corresponds to the mode U of the First Distribution. Therefore, an approximate characteristic value V_0 is obtained by letting $V_0 = \text{Mode of First Distribution}$.

The exponent C_p appearing in the recurrence relation denotes the number of times the inequality sign changes in step 2.6. The initial value of C_p is zero.

4) PARAMETRIC SEQUENCE OF THE ASYMPTOTES ϵ AND W

The asymptote ϵ or W is also obtained by iteration. A new value of the asymptote ϵ_{q+1} or W_{q+1} is related to the previous value ϵ_q or W_q through the recurrence relation

$$\epsilon_{q+1}(V) = \epsilon_q(V) + [-\frac{1}{2}]^{C_q} \cdot \Delta \epsilon$$

or

$$w_{q+1}(V) = w_q(V) + [-\frac{1}{2}]^{C_q} \cdot \Delta w$$

where q is a sequential index and $\Delta \epsilon$ or Δw is an arbitrary incremental value whose selection should be based, if possible, on physical reasoning.

The exponent C_q denotes the number of times the inequality sign changes in Step 5).
The initial value of C_q is zero.

5) CRITERION FOR THE ASYMPTOTE VALUES $\epsilon(V_p)$ and $w(V_p)$

If

$$\sigma_N^2(V_p, \epsilon_{q+1}) < \sigma_N^2(V_p, \epsilon_q)$$

or

$$\sigma_N^2(V_p, w_{q+1}) < \sigma_N^2(V_p, w_q)$$

the sign change count is

$$c_{q+1} = c_q$$

If

$$\sigma_N^2(V_p, \epsilon_{q+1}) > \sigma_N^2(V_p, \epsilon_q)$$

or

$$\sigma_N^2(V_p, w_{q+1}) > \sigma_N^2(V_p, w_q)$$

the sign change count is

$$c_{q+1} = c_q + 1$$

Repeat calculation from $c_{q=0}$ until $c_q = 3, 4$, or 5 and find the minimum value of σ_N^2 .
The selection of $c_q = 3, 4$, or 5 depends upon the nature of the problem.

6) CRITERION FOR THE CHARACTERISTIC VALUE V (FOR ALL POSSIBLE VALUES OF ϵ OR w)

If the minimum value of $\sigma_N^2(V_{p+1}, \epsilon)$ or $\sigma_N^2(V_{p+1}, w)$ is smaller than that of
 $\sigma_N^2(V_p, \epsilon)$ or $\sigma_N^2(V_p, w)$ the sign change count is

$$c_{p+1} = c_p$$

If the minimum value of $\sigma_N^2(V_{p+1}, \epsilon)$ or $\sigma_N^2(V_{p+1}, W)$ is larger than that of $\sigma_N^2(V_p, \epsilon)$ or $\sigma_N^2(V_p, W)$ the sign change count is

$$C_{p+1} = C_p + 1$$

Repeat calculation from $C_p = 0$ until $C_p = 3, 4$, or 5 and find the smallest value of $\sigma_N^2(V_p, \epsilon)$ for all possible combinations of V and ϵ or $\sigma_N^2(V_p, W)$ for all possible combinations of V and W by iteration. The selection of $C_p = 3, 4$, or 5 also depends on the nature of the problem.

The exact solution of V, ϵ and K for the Second Asymptotic Distribution or V, W and K for the Third corresponds to the smallest value of $\sigma_N^2(V, \epsilon)$ or $\sigma_N^2(V, W)$.

Note that the value of exponent K is a function of V and ϵ or V and W for which the variance $\sigma_N^2(V, \epsilon)$ or $\sigma_N^2(V, W)$ is the smallest and is calculated for each step of V_p and ϵ_q or V_p and W_q .

4. EARTHQUAKE DATA

The earthquake data considered to be available at present in Japan can be divided into five periods as follows:

- (I) Period 416-1872 - Magnitude M_k and epicenters were determined by Dr. Kawasumi using the descriptions in ancient documents. These values are shown in the Science Calendar¹². No data except damages are included.
- (II) Period 1885-1925 - Both M_k and M are shown in such a relation as $M_k = M + 0.5$ in the Science Calendar. No data except damages are included.
- (III) Period 1885-1925 - Both M_k and M are shown with the same relation as the data (II) in the Science Calendar. Moreover the data in the major earthquakes above are included in the Catalogue of Major Earthquakes by J.M.A.¹³
- (IV) Period 1926-1960 - The results of instrumental observations are reported in the Catalogue of Major Earthquakes by J.M.A., in which all the earthquakes with the magnitude $M \geq 5.0$ are considered to be included.
- (V) Period in and after 1961 - The data in this period are reported in the Catalogue of Major Earthquakes or the Seismological Bulletin of J.M.A., in which almost all the earthquakes with the magnitude $M \geq 4.0$ are considered to be included because of advanced instruments comparing with those in the period 1926-1960.

It is generally assumed that the seismic activity has been or will be nearly as constant in an area as in the whole vicinity of Japan. If the assumption above is made and the data of the earthquakes occurred in the period are completely included, such phenomena should be recognized for any data as follows; (1) the gradient of the accumulative energy curve, that is, the mean annual energy released by earthquakes is nearly constant and (2) the mean annual accumulative magnitude frequency distribution is similar for any period of data.

Mean annual magnitude frequency distribution and mean annual energy released by the earthquakes for the data period of (I) - (V) are shown in Figs. 1 and 2. As seen in these figures, the data (I) - (V) can be classified into two parts, data A (I, II) and

data B (III, IV, V), and there are remarkable differences between the data in A and the data in B.

It is necessary to pay attention for the data A as follows: (1) the data A were made according to the descriptions in the ancient documents and (2) the distribution of population in the time when the documents were made had to be very uneven. The reason is easily inferred why the data A are not only small in quantity and low in accuracy but also uneven regionally. On the other hand it is doubtful whether the period of the data B is long enough for the seismic activity to be regarded as being constant.

After considering the facts above, two kinds of data are used in the present paper as follows:

1. The data B with modified magnitude - The data B are examined and modified in the following. The accumulative energy curves using the original magnitude and modified magnitude are shown in Fig. 3. As seen in Fig. 3 the gradient of energy curve before 1925 is larger than that after 1926.

It seems necessary to modify the magnitude for the period 1885-1925, because the magnitude for the period 1885-1925 was Kawasumi's magnitude and the magnitude for the period thereafter has been determined based on the instrumental observation. Assuming that the gradient of the accumulative energy curve is nearly constant and that the gradient value for the period 1926-1973 is representative in the vicinity of Japan, three types of modification for the magnitude are made as follows: (1) M-0.5 for the period 1885-1925, (2) M-0.6 for the period 1896-1915 and M-0.5 for the periods 1885-1895 and 1916-1925, and (3) M-0.7 for the period 1896-1915 and M-0.5 for the periods 1885-1895 and 1916-1925. In Fig. 3, it is seen that the resultant accumulative energy curve makes almost a straight line in the modification (2). The mean annual magnitude frequency distribution for the period 1885-1925 after the above modification is compared with that for the period 1926-1973 in Fig. 4. As seen in Figs. 3 and 4, the modification (2) seems to be most suitable for data B.

2. The data after the period 1946 when the distribution of population was relatively even - As for the data before 1926, the following treatments with characteristics of acceleration were applied.

- (1) The major earthquakes having 100 gals or more were estimated from the destructive earthquakes in the Science Calendar.
- (2) Considering the annual magnitude frequency distribution curves in Fig. 4, it is assumed for the small or medium earthquakes less than 100 gals that the frequency of earthquakes occurrence was the same as that after 1926 year. The magnitude before the period 1885 was estimated from M_k .

5. EXPECTED VALUES OF EARTHQUAKE INTENSITY BY THE THEORY OF EXTREMES

5-1. PRESUMPTION OF EARTHQUAKE INTENSITY

Many empirical formulae concerning the relationship of intensity, magnitude and epicentral distance have been proposed by many investigators in addition to those mentioned in Chapter 2; Gutenberg and Davenport (1942), Blume (1965), Housner (1965), Milke and

Davenport (1969), Esteva (1970), Watanabe (1971), Donovan (1972), Soknabel and Seed (1973), Katayama (1974), Trifunac and Brady (1975). Fig. 5 shows the relationship between the maximum acceleration and epicentral distance in the case of magnitude M=6.5⁴. Good agreement can be seen among these empirical formulae in the range of epicentral distance 20-250 km except those by Gutenberg and Richter, and by Blume.

In this paper, Kanai's formula (7) which indicates velocity spectrum on the base rock was utilized for the presumption of earthquake intensity.

Using Kanai's formula (7), maximum acceleration a_{\max} , maximum velocity v_{\max} and maximum displacement d_{\max} on the surface of ground can be obtained as follows:

$$a_{\max} = 10^{0.61M - (1.66 + \frac{3.60}{r})} \log_{10} r + (0.167 - \frac{1.83}{r}) \cdot \frac{1}{T} \cdot G(T)$$

$$v_{\max} = 10^{0.61M - (1.66 + \frac{3.60}{r})} \log_{10} r - (0.631 + \frac{1.83}{r}) \cdot G(T)$$

$$d_{\max} = 10^{0.61M - (1.66 + \frac{3.60}{r})} \log_{10} r \left(1.430 + \frac{1.83}{r} \right) \cdot T \cdot G(T)$$

where $G(T)$ is dynamic characteristics of the ground and is approximated by

$$G(T) = \frac{1}{\sqrt{\{1 - \left(\frac{T}{T_G}\right)^2\}^2 + \left\{\frac{0.2}{\sqrt{T_G}} \cdot \left(\frac{T}{T_G}\right)\right\}^2}}$$

$$\text{when } T = T_G$$

T: Predominant period of earthquake motion

T_G : Predominant period of the ground

Therefore, considering $T = T_G$ maximum acceleration, velocity and displacement on the surface of the ground are approximated as follows:

$$a_{\max} = \frac{5}{\sqrt{T_G}} \cdot 10^{0.61M - (1.66 + \frac{3.60}{r})} \log_{10} r + (0.167 - \frac{1.83}{r})$$

$$v_{\max} = 5\sqrt{T_G} \cdot 10^{0.61M - (1.66 + \frac{3.60}{r})} \log_{10} r - (0.631 + \frac{1.83}{r})$$

$$d_{\max} = 5\sqrt{T_G} \cdot 10^{0.61M - (1.66 + \frac{3.60}{r})} \log_{10} r - (1.430 + \frac{1.83}{r})$$

5-2. EXPECTED VALUES OF EARTHQUAKE INTENSITY

1) Expected Values of Maximum Acceleration and Velocity in Tokyo

The expected values of maximum acceleration and velocity on the surface of ground at the center of Tokyo (35.7°N . 139.8°E) are predicted using the past 326 year earthquake data (magnitude and epicentral distance) mentioned in Chapter 4.2. Fig. 6 shows the expected values of maximum acceleration on the surface of the ground, of which the predominant period T_G is 0.3, 0.5, 0.8 and 1.2 sec., obtained by Gumbel Asymptotic Distribution.

The expected values of maximum velocity are shown in Fig. 7 obtained by Kanai's formula (7). Tables 2 and 3 show the calculated values of maximum acceleration for each year and the expected maximum acceleration and velocity vs. return period on the surface of the standard ground ($T_G = 0.3$ sec.) at the center of Tokyo, respectively.

2) Regional Distribution of Expected Maximum Acceleration on the Surface of Standard Ground

The expected maximum acceleration on the surface of the standard ground ($T_G = 0.3$ sec.) is calculated at the location of every 0.5° in latitude and longitude by Kanai's formula and Gumbel's Asymptotic Distribution. The past earthquake data used are described in Chapter 4.2. Regional distribution maps of the expected maximum acceleration corresponding to the return periods of 50, 100 and 200 years are shown in Figs. 8, 9 and 10, respectively.

3) Regional Distribution of Expected Maximum Velocity in Bedrock

The expected maximum velocity at the base rock is obtained at the location of every 0.5° latitude and longitude by Kanai's formula and Gumbel Asymptotic Distribution.

The past earthquake data since 1885 are used as described in Chapter 4.1. Regional distribution maps of the expected maximum velocity corresponding to the return periods of 50, 100 and 200 years are shown in Figs. 11, 12 and 13, respectively.

Figs. 14 and 15 show the expected maximum acceleration and displacement at the base rock corresponding to the return period of 100 years, respectively.

6. PRACTICAL APPLICATION ON THE EARTHQUAKE DANGER

As is clear from Table 1, the periods of the data used and of the analyses in the respective research vary from a scientific point of view. For practical purposes, that is, especially the regional seismic coefficients for aseismic design of structures, these results may not be available directly, because it is disagreeable to say that the results express the regionality of seismic activity in the vicinity of Japan completely and objectively. Moreover it seems not to be always desirable in aseismic design that there are many kinds of the regional distribution of the expected values. So a new regional seismic coefficient map was made after examining all results from the following standpoints: (i) the accuracy of each value in earthquake data, (ii) the regional evenness of data information, (iii) the quantity or the period length of data, (iv) the method to calculate the maximum earthquake motions from M and r , (v) the method to determine the expectation of the maximum earthquake motions and (vi) the representative method to obtain the results.

The regional distribution maps of the expectation values based on the regionality of seismic activity only were selected from various maps and normalized to assign unity for the

maximum value in each map at the point of every half degree in both longitude and latitude. The regional distribution of seismic coefficients was determined by means of the weighted mean values by multiplying each normalized one by each weight determined from the six items above.

The final results are shown in Fig. 16, which are considered to be the appropriate regional seismic zoning coefficients for aseismic design of structures. As seen in Fig. 16, Japan is divided into three divisions by the criterion of seismic activity, that is, A) area with high earthquake danger, B) medium danger area and C) low danger area.

ACKNOWLEDGEMENT

This study was partially supported by the project of Establishment of New Aseismic Design Method monitored by Ministry of Construction, Japan. The authors wish to express their thanks to Professor St. Denis, University of Hawaii, for introduction of Gumbel's Second and Third Asymptotic Distribution by iteration method; to Dr. Otsuka, Head of I.I.S.E.E. and Dr. M. Watabe, Head of Str. Div. at present, for valuable discussion on regional seismic/zoning coefficient; to Mr. Y. Serizawa, member of B.R.I., for drawing of figures.

Table-1 General Reviews of Researches for Earthquake Danger in Japan

No.	Researcher	Period of Data	Method of Analyses	Unit	Result Return Period(τ)
1)	Kawasumi,H.	679 - 1948	$(N=0.45 \cdot 10^{25} \cdot 1 \cdot \log(M))^{\tau}$, in a random-ground motion, $\log(M) = 10.192$, $\log(V/V_0) = 1.007$, $V = 1000m \cdot \sqrt{1000m} \cdot \sqrt{1000m}$	$\frac{1}{2} \cdot n(\Delta) = T/\tau$ $I = I_0$	Expected maximum acceleration on the ground
2)	Muramatsu,I.	1958 - 1964	$\log(CM) = 0.655M - 1.719$ $\log(E(M)) = 10.45M + 1.253$	$\frac{1}{2} \cdot n(V) = T/\tau$ $I = I_0$	Expected maximum velocity on the ground
3)	Kanai,K. and T.Suzuki	599 - 1964	$V = 10^3$ $N = 0.6M^{-1}(100-350) \cdot \log(-0.63+83M) \cdot I = I_0$	$\frac{1}{2} \cdot n(V) = T/\tau$ $I = I_0$	Expected maximum velocity at the base rock
4)	Goto,H. and H.Kameda	679 - 1964	$4(VV_0) \cdot \#(D) = F(\tau_{\text{max}}, K_{\text{max}}, I_{\text{max}}, P_1, V_1)$ $\#(D) = F(\tau_{\text{max}}, K_{\text{max}}, I_{\text{max}}, P_1, \alpha)$	$E(V) = \int_0^\infty \left\{ 1 - e^{-\#(V)} \right\} dV$ $E(I) = \int_0^\infty \left\{ 1 - e^{-\#(I)} \right\} dI$	Expected maximum velocity and acceleration on the ground
5)	Okubo,T. and T.Tomoshina	679 - 1948 1923 - 1967	Kawasumi's Shop + Experience more than J.M.A. Int. ∇	$\tau = 50$ years based on Kawasumi's Shop on the ground	Seismic coefficient $\tau = 50$ years based on the acceleration on the ground
6)	Takahashi,K.	1986 - 1970	$\frac{h(\Omega)}{h} = \frac{h(\Omega(1-4\pi/15))}{h(\Omega)} = \frac{h(\Omega(1-0.024\pi))}{h(\Omega)}$	$\frac{h(\Omega)}{h} = 0.25 \cdot \frac{1}{10}$	Expected maximum acceleration on the ground
7)	Hatori,S. and Y.Kitagawa	1967 - 1972	$n(A) \cdot da = K''^m \cdot da$ $\log N = \log(121/61)$	$\int_{A_0}^{\infty} K''^m \cdot da = 1$	Expected maximum displacement on the ground
8)	Omote,S. and K.Matsuura	1985 - 1973	$I = M_k^{-1}$ Same to No.1)	$S(I) = C I^{-41} \cdot S(I_0) / \sqrt{I} \cdot \tau = 1$ $\alpha = 0.255 \cdot 10^{-m}$	Expected maximum acceleration on the ground
9)	Omote,S., H. Honai and S.Nogamotsu	1961 - 1972	$V = 10^3$ $N = 0.6M^{-1}(100-350) \cdot \log(-0.63+83M) \cdot I = I_0$	$\lambda(V) = \frac{1}{V} \cdot e^{-\#(V)} = ne^{-\#(V)}$	Expected maximum acceleration at the base rock
10)	Nogashita,S.	1985 - 1975	$\log(SV(\omega)) = d(\omega M - b) \cdot \log(-C\omega)$ $M_b = 0.88M + 1.2$, $b = 0.05$	$\log(SV) \propto -\log \omega^n$	Expected maximum velocity at the base rock

Table - 2 Calculated Values of Maximum Acceleration (gal)
for Each Year in Tokyo ($T_G = 0.3$ sec.)

A. D.	Epicentral distance	Magnitude	$a_{max}(T_G=0.3)$	A. D.	Epicentral distance	Magnitude	$a_{max}(T_G=0.3)$
1926	4810	6.2	89.75	1950	84.96	6.5	61.18
1927	14166	6.0	14.08	1951	58.60	6.2	68.36
1928	7610	5.8	26.87	1952	104.41	5.5	11.07
1929	7030	6.1	45.91	1953	226.82	6.6	15.76
1930	9828	7.0	99.61	1954	126.80	6.4	29.25
1931	71.71	7.0	157.93	1955	74.33	5.3	13.77
1932	12089	6.1	20.63	1956	50.82	6.0	62.88
1933	114.21	5.6	11.14	1957	155.63	5.0	2.99
1934	5886	5.2	16.68	1958	43.95	4.4	8.09
1935	14920	6.3	19.83	1959	123.03	5.6	9.95
1936	14285	6.3	21.19	1960	177.37	5.9	8.66
1937	11998	6.6	42.12	1961	147.25	5.9	11.53
1938	11399	6.6	35.62	1962	79.25	4.9	7.16
1939	67.22	5.3	15.91	1963	136.45	6.1	17.16
1940	117.23	6.1	21.47	1964	132.40	6.2	20.68
1941	75.36	6.0	36.09	1965	152.50	6.7	33.62
1942	141.15	6.6	32.90	1966	57.10	4.9	11.42
1943	151.62	6.6	29.48	1967	87.38	5.6	16.04
1944	23.50	5.5	82.90	1968	70.10	6.1	46.09
1945	68.01	5.7	27.44	1969	65.84	4.5	5.33
1946	71.17	6.3	59.73	1970	84.05	5.1	8.70
1947	118.30	6.0	18.52	1971	70.85	4.9	8.41
1948	74.03	5.4	15.94	1972	58.60	5.1	14.58
1949	114.38	6.7	52.90				

Table - 3 Expected Maximum Acceleration and Velocity Values vs Return Period in Tokyo

	Return Period (years)			Unit
	50	100	200	
A_{max}	162.7	217.0	287.7	gal.
V_{max}	7.77	10.4	13.7	cm/sec

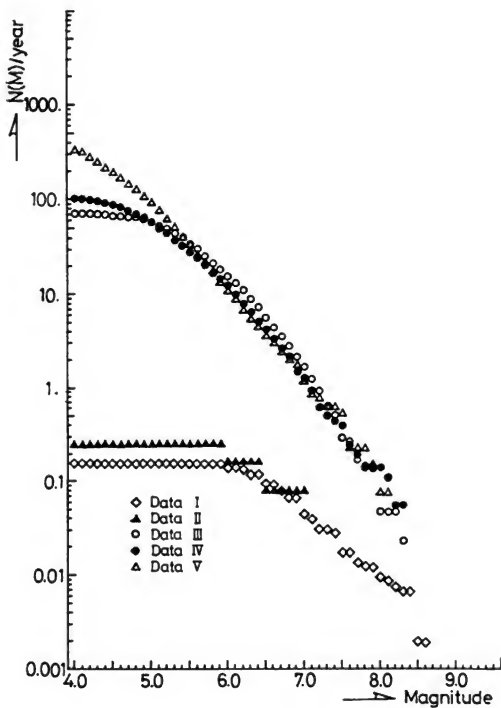


Fig. 1. Frequency Distribution of Mean Annual Magnitude
for Data I to V.

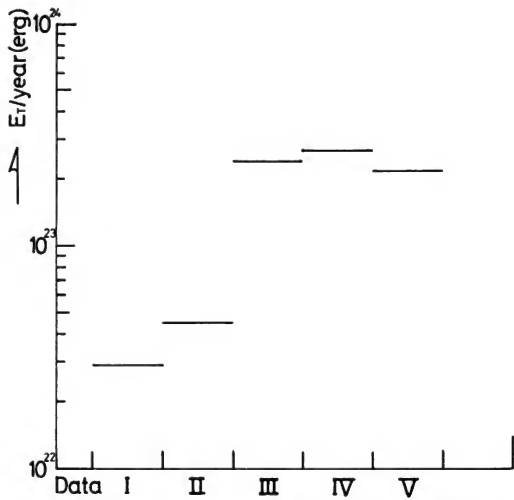


Fig. 2. Mean Annual Energy Released by Earthquake Data (I to V)

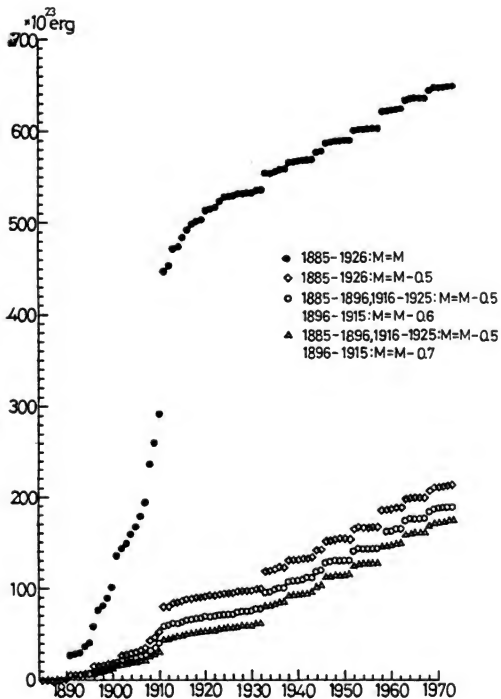


Fig. 3. Accumulative Energy Curves of Original and Modified Data

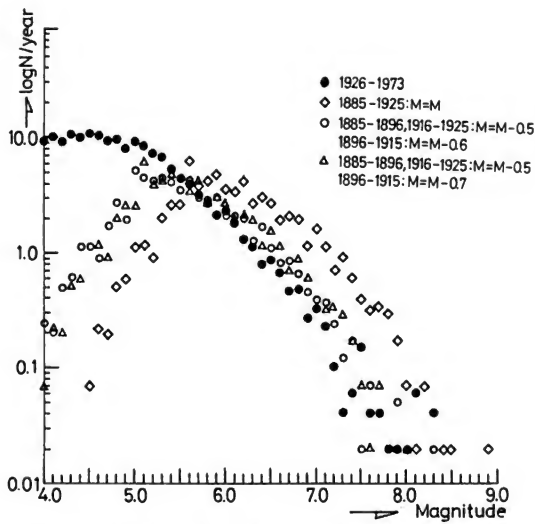


Fig. 4. Frequency Distribution of Mean Annual Accumulative Magnitude

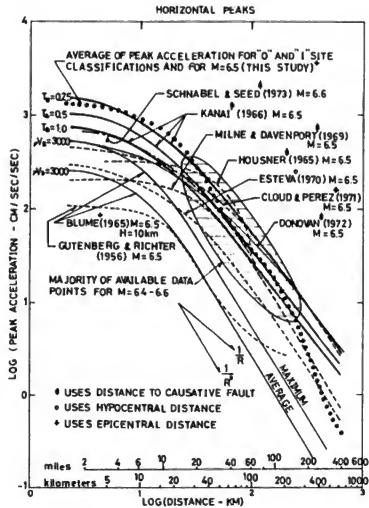


Fig. 5. Comparison of the Correlations of Maximum Acceleration and - Distance in Case of M=6.5 (After Trifnac, M. D. and Brady, A. G.)

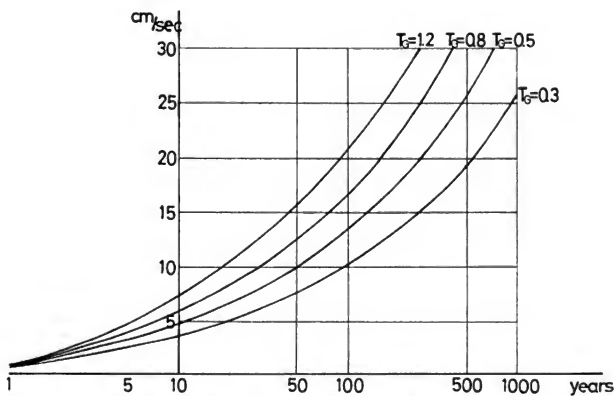
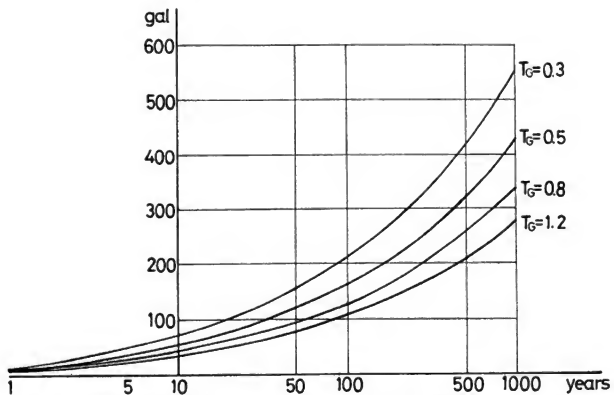


Fig. 7. Expected Maximum Velocity Values (cm/sec.) vs. Return Period in Tokyo



Fig. 8. Regional Distribution of the Expected Maximum Acceleration Values (gal) at the Free Surface of Ground ($T_G=0.3$ sec., $T=50$ years)

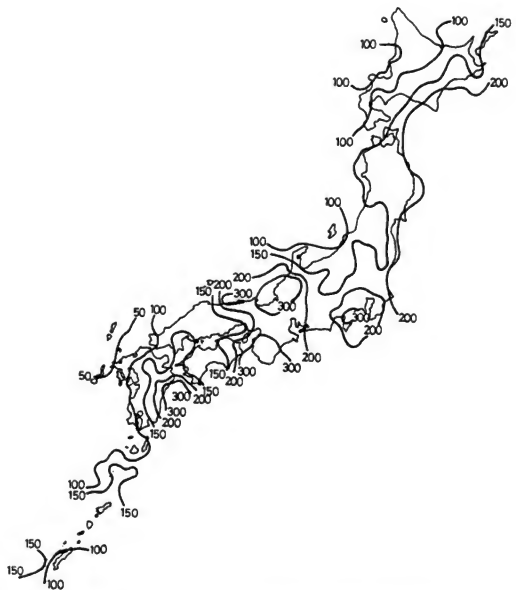


Fig. 9. Regional Distribution of the Expected Maximum Acceleration Values (gal) at G. L. ($T_G = 0.3$ sec., $\tau = 100$ years)

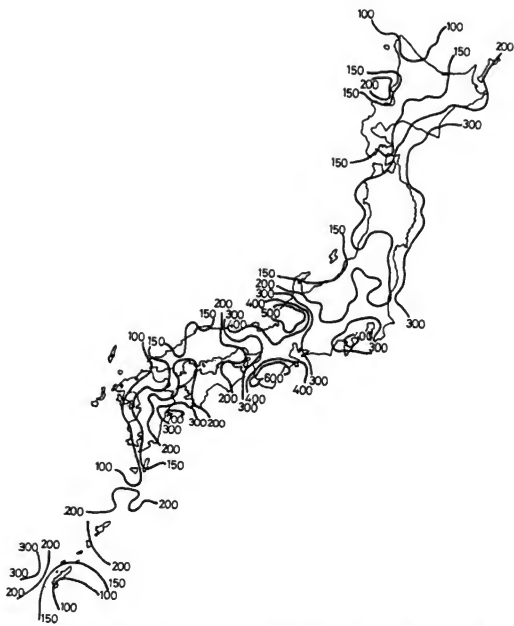


Fig. 10. Regional Distribution of the Expected Maximum Acceleration Values (gal) at the G. L. ($T_G=0.3$, sec, $T=200$ years)



Fig. 11. Regional Distribution of the Expected Velocity Values (cm/sec) at the Base Rock ($t=50$ years)



Fig. 12. Regional Distribution of the Expected Velocity Values (cm/sec) at the Base Rock ($t=100$ years)



Fig. 13. Regional Distribution of the Expected Velocity Values (cm/sec) at the Base Rock ($T=200$ years)



Fig. 14. Regional Distribution of the Expected Acceleration Values (gal) at the Base Rock ($T_G=0.5$ sec., $T=100$ years)



Fig. 15. Regional Distribution of the Expected Displacement
Values (cm) at the Base Rock ($T_G=5.0$ sec., $T=100$ years)

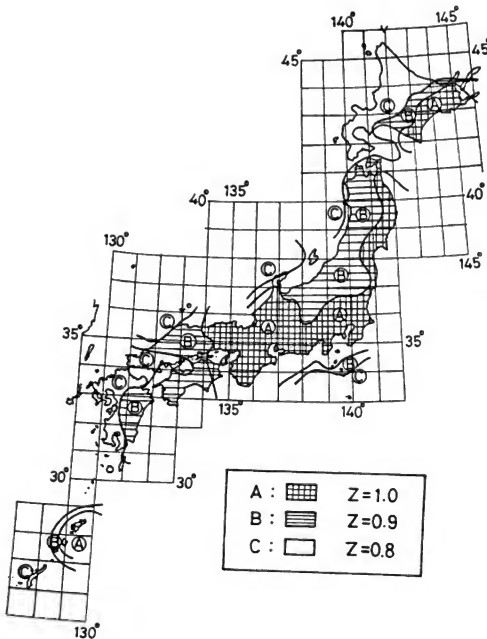


Fig. 16. Regional Seismic Zoning Coefficient for the Aseismic Design

TREATMENTS ON SEISMIC FORCE IN DESIGNING EARTH STRUCTURES

Kenkichi Sawada, Chief, Soil Dynamics Section

Public Works Research Institute

ABSTRACT

Treatment of earthquake forces in the design of retaining walls and of embankment slopes is discussed. The discussion centers around the philosophy and considerations given when Japan Road Association revised its Earth Work Manual in Road Construction.

KEYWORDS: Culverts; design principle; fill slope; earth structure; earthwork manual; priority; retaining wall; seismic forces

1. PREFACE

Statistical analysis of damages to earth structures, preservation of records and other treatments on the damages were discussed in my previous report. This paper will analyze the actual circumstances by considering the very basic problems in designing particular earth structures.

The earth structures have been built for many years by trial and error method with accumulated knowhow rather than by so-called design process, thus the process of design was not particularly required in these years.

It is considered that the design procedure for earth structures becomes particularly important only when constructing a large structure or construction of a structure in a minimum time was a prerequisite. It may be said that the design of stable slope and retaining wall became important because the height of the slope was large and also because consolidation of soft ground became important when a high construction speed was needed.

Recently, the Japan Road Association revised its Earth Work Manual in Road Construction in which an important problem was the treatment of the seismic force in the design after the social movement toward incorporation of the seismic force in designing the earth structures. This also may be considered a new prerequisite as stated in the above example. In this manual, influence of seismic force has become more important when designing especially retaining walls, embankment on soft ground, and culvert. This subject will be outlined below.

2. CONSIDERATION FOR RETAINING WALLS

Seismic force on retaining wall is now treated in a manner stated below in design. The retaining walls exceeding eight meters in height will be now designed for earthquake. For retaining walls lower than eight meters, those resisting forces or abilities that are not taken into account in normal computations, such as the passive earth pressure at front face or design under the worst condition of the rear earth fill (that is, loss of cohesion that may occur only during a long period of use), are considered resistive against increased loads due to earthquake. That is, the lower walls require no particular consideration for earthquake and they are considered to be safe for seismic forces.

The next problem is in the area of calculations for retaining wall exceeding eight meters in height with seismic forces. The previously mentioned Earth Work Manual employs equations for earth pressure principle proposed by Mononobe-Okabe during earthquakes.

The Mononobe-Okabe equations propose to tilt a retaining wall imaginarily forward by an angle corresponding to seismic coefficient in order to statically calculate a seismic force applied to the wall during an earthquake. This type of equation is also used in many other manuals. However, one of the characteristics of the road embankment is its sloped surface at the rear of the retaining wall instead of horizontal surface. Therefore, especially when a retaining wall is required at the bottom of a long sloped ground, these equations may often result in an overdesigned wall. In order to provide horizontal friction forces sufficient to resist the forces such as earth pressure, inertia force assumed to be

applied to main portion of retaining wall, and seismic earth pressure, the length of bottom slab required is enormously large.

To solve this type of problem in design, various design manuals for retaining walls are responding in many different approaches. For example, the design manual prepared by the Japan Highway Public Corporation simply clarifies this problem by employing Terzaghi's equations for earth pressure with proportional increase of $(1 + k)$ corresponding to coefficient k . With this modification for the equations, the use of excessive earth pressure in design can be prevented. For retaining walls for structures other than road construction, this kind of problem is not likely to occur since the rear top of most retaining walls is considered to be associated with horizontal ground surface.

Depending upon the angle of friction assumed on slip surface of soil back to the wall, the direction of earth pressure force will vary greatly, resulting in a serious influence on the stability. Value of this angle is normally assumed to be zero at the time of an earthquake, but it is inconsistent to make its static value simply zero since it may still have statically a fractional value of internal friction angle of the earth. Also the equations proposed by Mononobe-Okabe do not consider the cohesion force, but it may be agreeable to consider the effect of cohesion force in some way since an earthquake and loss of cohesion force of earth next to wall are not likely to occur at the same time. The Earth Work Manual qualitatively discusses the effect of cohesion force in the hope of limiting the size of slip surface.

With these various approaches employed in the Manual, the Manual establishes a rational design method that offers dimensional ranges acceptable in the actual practices. However, it is widely said that the studies on soil mechanics start and end in coping with the problems of the earth pressure, so that step by step improvement of the design method for the retaining walls stated in the Manual is likely to be expected but problems will never be completely solved.

3. CONSIDERATION FOR EMBANKMENT SLOPE

Various types of problems are also pointed out for the stability of the earth fill slope, as in the case of the retaining wall. Not only for retaining walls but also for the earth fill slopes the need for encountering the effect of earthquake by some method was strongly discussed in the process of hearing for the Earth Work Manual.

Conventionally the stability of the slope has been analyzed by the use of the slip surface method which is equivalent to seismic coefficient method. However, justification for accurately computing the safety factor in dynamic design was questioned in the hearing even if the method itself was valid for static design problems, since the test method for soil dynamics did not completely reproduce job site conditions, failure models were oversimplified and soil properties of job site varied too much from one location to another. For this reason, the committee for the Manual once concluded that the statical calculations with simply increased safety factor would be adequate for earthquake. This approach was identical to that of retaining wall. Since the earth fill slope had no extra resisting abilities uncounted in the calculations, the value of safety factor had to be increased in

the actual practices. Then, the safety factor as extra room for strength was in question but it was once set to be about 0.5 by a majority of the committee members. However, in the final stage, this method was abandoned since it was not well grounded to take up as a method to be specified in the Manual.

In the end, the soil was classified into the clayey soil and sandy soil, and they were specified separately in the Earth Work Manual. The former has a recovery of strength after construction, and the increase of strength after construction is expected to provide an extra stability to the slope, as in the case of retaining walls. Thus, no special consideration was given to the earthquake. However, for the sandy soil, only a basis for determining possibility of liquefaction of poor soil was described without including detailed requirements. It seems to be very important to examine the dynamic properties of clay, but no requirements are provided for examining strength properties since it was simply agreed in the committee that the earth structures would gain strength required for safety after their construction. It was found that a dynamic test method capable of producing results clear as these by dynamic triaxial test used for checking poor sandy soil was not available at this time.

Thus, methods for analyzing the sliding of slope were not positively stated in the Earth Work Manual. It should be noted that some manuals are using the circular arc slip surface methods. However, many variations can be expected in details in the method of the Manual where the sliding plane of various forms is combined with the seismic coefficient method. A few examples will be described hereinafter, but some of them are somewhat identical to those already reported as "earthquake-resistive properties of earth fill" at the 5th joint meeting.

There are three methods in the linear sliding plane approaches: (1) sliding plane is treated as infinitely long slope as employed by National Railway Laboratories and others; (2) resistance at the bottom edge of the slip surface is compensated in the method used by Seed and Goodman; and 3) sliding plane passing through the toe of the slope is used by the Design Standards for Harbour Structures.

The circular arc slip surface methods are: (1) standard method applying seismic force to center of gravity of each slice; (2) design criteria for earth fill dam applying seismic force on slip surface; (3) design standards for Harbour Structures where influence of seismic force is not applied to resistance term; (4) report of research by National Railway and proposed design criteria for an artificial island of Tokyo Bay by Japan Road Association where the seismic coefficient is applied only to earth fill in providing resistance to earthquake; and (5) so-called folded line method where a special form is assumed for the sliding mass of earth fill.

The latter methods (circular arc type) are employed when the results of the computations by standard methods are unable to assure stability due to exceptionally large sizes of structure or unusual form or to provide basis for calculations by accurately studying mechanism of phenomenon with various devices and by various types of simplifications. By this approach, each of these phenomena is examined in detail for evaluating its contribution to resistance, and thus extra forces hidden in the calculations will be reduced accordingly.

4. DESIGN BY DISPLACEMENT CRITERIA

In the design of a retaining wall, one problem is the value of the destructive displacement to be used, and this is not the problem concerned with the earthquake alone. It was tried to make provisions for displacement in the Manual. As reported previously, there will be a number of different types of failure in earth structures caused by actual earthquakes. However, a type of failure similar to that modeled in an analysis is hardly found. In fact a slight projection of retaining wall after an earthquake may be found, but complete overturning or sliding is rarely found. Most of the failures stop after a certain degree of progress. Even if an overall failure occurs it is usually made as a part of overall slope failure instead of its own independent failure. Also in the case of earth fill, overall failure rarely occurs unless a liquefaction is present.

All of these phenomena are called "failure" so that various types of recognitions for the failure become unclear. A number of phenomena existing in reality are all cast in the limited number of forms, resulting in a shortage of useful information. It may be natural to find this kind of problem in old references investigated but a complete record may not be obtained in earthquake damage investigation conducted in recent years unless the problem stated above is reformed in investigation. When an actual damage is seen, each person may classify it differently from others. Also, a damage may look as if it can be classified into certain types at a glance, but an engineering method for quantitatively determining the damage by a survey has not been studied consciously.

Slip failure of road embankment caused by earthquake in the middle district of Oita Prefecture may be a good example of this problem. At a glance or from photographs of damage, the contents of damage look very clear but it is extremely difficult to record it quantitatively as a prototype. It seems very difficult to imagine a real state of a damage from drawings of data gathered only from Survey of Soil Property for Disaster Restoration Work. Regardless of the consequences, it may be an only way to produce drawings according to a pattern.

Because of this uncertainty, many people are used to thinking that consideration for failure of earth structures by earthquake is unnecessary. However, this is mainly because conventional analytical models cope with a boundary condition where a failure may start, but it should be understood that a structure can be utilized even after this boundary state is exceeded. The discussion may be advanced with such a view in which the use of structures is precluded taken as a limit. For this purpose, also an effort to adopt a design method determining a failure by displacement criteria may be required. However, this method has not been adopted in the recent revision of the Manual.

5. PROGRESS OF DESIGN PRINCIPLE

Empirical techniques of design for earth structures have been useful for the design of structures with limited sizes. But, uncontrollable factors will appear when the sizes of structures increase. At first, the difficulty in design is overcome by modifying values expressing the characteristics of soils used in design. When this approach becomes no more appropriate to design, other mechanical or qualitative development must be expected.

The problem in evaluating the influence of earthquake may be the same as that stated above. This problem can't be solved simply by increasing the accuracy of the same analytical method. This problem requires a certain new method. As presently done so often, resorting to the strength characteristics such as "c" and " ϕ " (which are not related to strain) as a result of analysis of soil properties is an accustomed method in normal approaches of mechanics. However, possibility of solving problems within this conventional area of approach is becoming very small.

6. CONSIDERATION FOR CULVERTS

Lastly, the influences of earthquakes are not taken into consideration in the design principle for culverts in the Manual. However, in the design of gate type culverts, one paragraph of the Manual requires an analysis with earth pressures acting only on one side during earthquake even if the earth pressures may be acting on both sides in reality. In this case, the method for computing the earth pressures during the earthquake is not designated.

7. IMPRESSIONS

(1) Revision

Subjects related to earthquake in the revised Earth Work Manual have been described above, and now my impressions will be stated below.

An important point is that major changes covering a wide area of subjects may be required instead of conventional type revisions in the sense of narrow area if a design manual for earth structures is to be revised in the future. Methods used in many revisions up to now are to revise parametric values of earth mechanics while maintaining the same qualitative mechanism. This traditional approach may be limited in its effects even if the accuracy of the values of parameters is improved by means of many experiments since the approach is not considering non-uniformity of the quality of earth structures.

As a result, this may raise a question whether properties of earth structures can be expressed by accumulation of minor items as expressed in normal mechanics. Normally, in research activities, more details are investigated as the research progresses. But the entire picture can be more exactly understood if macroscopical view is taken as long as the magnitudes of disturbance of the properties are identical. A solution might be to employ a probabilistic approach. But, simply using the probability concept is not desirable to us since solutions by considering soil mechanics are more important at this stage of the development.

Now let us examine these subjects in more detail. As long as we try to understand a phenomenon by the use of data and analysis, contradictions between requirements for analytical accuracy and actual state will go non-reversibly towards more contradictory direction. In such a case, a proper compromise may be necessary. Usually the compromise is considered to be passive, but, in this case, it should be more positive in nature and this can be achieved if it solves the problem. The use of slip surface method may be a kind of compromise to the present state of mechanics, but it is very practical especially for producing proper

compromise now is response to the present needs. However, it should not be limited only in an area where values of coefficients are prepared unless it contains wider mechanical area.

(2) Renovation

It must also be considered that the problem of renovation in earth structures is very particular compared to other structural materials. With other materials, renovation of a failed structure means that broken portions are completely replaced by new materials, though it may be sometimes very difficult to determine a limit of broken portion. This is quite different from the earth structures since broken portions of soils are rarely replaced by other new soils. This phenomenon is rather quantitative in nature since a form is rearranged by adding soils to the broken, deformed portions. On the other hand, there is an example of rather qualitative renovation. A final renovation work is executed directly on an emergency work made immediately after a failure of earth structure. Thus, in earth structures, wear rather than failure is often more adequate expression to use.

As long as the failure of earth structure is treated as stated above, it may be very difficult to expect a complete answer to the design. That is why a consistent description in a limit of a system will give a justification as stated previously.

But, it is understood that this type of system must experience a qualitative improvement of the method at a certain stage. Research and design are mutually combined in such types of relationships. In earth structures, however, this kind of stage is long overdue, and the result is slow progress. Though only these kinds of findings are useful for design, they are not all of the present fruits. A great number of data resulted from various types of enormous in-house analytical experiments must be totally integrated to utilize them for the improvement of the method.

(3) Terms

We are accustomed to the use of existing concepts when observing something. Especially in soils engineering, concepts developed in other fields of science are often used without modification since analytical soil dynamics is very slow in its progress. The present approach may be handy for an approximate understanding but chance for true understanding can't be achieved simply by this borrowing of concepts. Also a significant progress can't be achieved as long as a chaos exists in the technical terms. The chaos also exists in the magnitude of sizes and forces but more importantly in the areas of social demand for quality and changes in environmental conditions.

(4) Priority

In the discussions held for revisions of the Earth Work Manual, a concept of priority in design of earth structures was once taken into consideration in an attempt to prevent the failure of structures having top priorities. It will be very hard for me to understand if this concept is brought to an attention only for compensating the design method employing "c" and " θ ". It is not sufficient to use the priority concept only for immediately solving discrepancy that has not been resolved by "c" and " θ ".

This gives an impression that all unclear subjects are to be approached with the priority concept. It may be possible to establish the priority concept to restrict the

designs for high priority structures for preventing the failure, but it is very difficult to determine the priority for actual structures agreeable to people. Also the priority or value is not a constant factor in nature. Changes in the priority or value are normal and it is not a simple phenomenon. The changing state doesn't mean dimensions or shapes of structure itself but means social demands.

If the priority is understood in this way, it may be a type of an expression for indicating social importance. As stated above the priority concept was brought to an attention as an important concept in the design of earth structures but its meaning failed to obtain the common understanding.

(5) Postscript

Lastly I consider conditions where structures made of earth can be produced. If only the probability of failure during earthquake is taken into account, production of structures by soil may become impossible. Exposure to any other type of disaster must also be taken into consideration. Also, it may be possible to discuss a difference in human senses between products made of earth and those made of steel as a factor in considering earth structures.

STUDIES ON THE ASEISMIC PROPERTIES OF UNDERGROUND PIPES

Keiichi Ohtani, Chief, Earthquake Engineering Laboratory

Nobuyuki Ogawa, Research Member, Earthquake Engineering Laboratory

Chikahiro Minowa, Research Member, Earthquake Engineering Laboratory

National Research Center for Disaster Prevention, Science and Technology Agency

ABSTRACT

This paper describes the experiments of underground pipes by using the large-scale shaking table of the National Research Center for Disaster Prevention, the analysis results of dynamic water pressure on pipelines caused by earthquake motions, and the problem of the slip between the surface of pipe and the soil.

Two kinds of experiments were executed. In the first experiment a linear pipeline (steel) was buried in the ground at the vicinity of this shaking table. The test pipeline was excited by the waves which were generated from the shaking table and transmitted through the ground. The behaviors of this pipeline and the ground would not always be similar because of the differences in the rigidities between pipe and soil and in the boundary conditions of pipeline ending. In this experiment, slight differences were measured between the behaviors of the test pipeline and the ground.

In the second experiment, a steel pipeline with a branch pipe was set on this shaking table and one end of the main pipe was clumped in the shaking table foundation. And this pipeline was buried in the sand pit. The bending strains and restoring forces of this pipeline were measured. The dynamic strains had the values similar to those of static strains for the same displacements. The hysteresis loops, drawn by the restoring force and displacement at the clumped end, had the energy absorption. The necessity for the second experiment was based on the slip which had grown around the pipe surface in disastrous earthquakes. The slip values of the infinite length pipeline with a branch pipe were calculated for sinusoidal ground waves.

In addition to these problems concerning water supply pipelines, etc., the water pressure in the pipelines has to be considered. In this paper, the procedure for estimating the distributions of dynamic water pressures caused by earthquakes without the so-called water hammer has been developed. For example, the dynamic water pressures for model pipelines are calculated.

KEYWORDS: Dynamic water pressure; shaking table; underground pipes; vibration experiments.

1. INTRODUCTION

In the cases of damaging earthquakes, such as the 1923 Kanto Earthquake and the 1974 Izuhanto-oki Earthquake and so on, the underground pipelines were severely damaged. Some of the damage happened to be brought about by landslides and falling stones accompanied with earthquakes. But in most cases damages would be brought about by the ground motions during earthquakes. There would be many pipe breaks in the vicinities of structures, and the boundaries of different ground properties would be more vulnerable than in general sites. Almost all of the pipes would be broken by the axial and bending deformations, and the increase of water pressure would occur during earthquakes. The damage patterns of pipes would vary in accordance with the types of pipe materials, the ages of being buried, the methods of pipe joints and pipe sizes.

The aseismic properties of underground pipe lines were already studied by many researchers - A. Sakurai, and the Ministry of Construction, and so on, and many valuable results were brought by them. In the present paper, the experiments using the large-scale shaking table, the vibration experiment of an underground pipeline of finite length and the forced displacement experiment of T-shaped underground pipelines are discussed. In addition, the dynamic water pressure caused by earthquake are calculated.

2. THE VIBRATION EXPERIMENT OF AN UNDERGROUND PIPELINE OF FINITE LENGTH

The ground vibrations around the shaking table amount to 3-10 gal during the shaking table excitations with the heavy loading weight. This level of vibration corresponds to the earthquake of Intensity III of Japan Meteorological Agency scale. These ground vibrations were used for the underground pipeline experiments. The steel pipeline 6.5m long and 139.8 mm in diameter was buried in the depth of about 40 cm, parallel with the direction of this shaking table excitation. Accelerations and strains measured were only in the axial direction component of this test pipeline. Also, the ground acceleration of this component was measured. The ground acceleration measured was about 3 gal, and the apparent transmitting velocities were supposed to be 150-800 m/s with the dispersion by another experiment. The axial strain values of the test pipeline during the excitations were 4×10^{-6} in maximum. According to Figs. 2 and 3, differences in behaviors of this test pipeline and the ground were found to be small.

The displacement equation in the axial direction component of the underground pipeline, using the coefficient of subgrade reaction, is expressed as follows:

$$EA \frac{\partial^2 u}{\partial x^2} = \rho \frac{\partial^2 u}{\partial t^2} + k_{ga} (u_g - u) \quad (1)$$

where E = Young's modulus of the pipeline, A is cross section area of pipeline, ρ is the unit length mass of the pipeline, k_{ga} is the interaction spring between ground and pipeline, x is the co-ordinate in parallel with axial direction, u_g is the absolute ground displacement, u is the absolute pipe displacement. k_{ga} would be obtained approximately as follows:

The pipeline was assumed to be buried in the infinite depth for convenience. The wavelength in the axial direction was also assumed to be infinite. Thus, this problem was reduced to two-dimensional procedure. The equation for obtaining k_{ga} by the use of polar co-ordinate $r-\theta$ was given as follows:

$$\frac{\partial^2 u_x}{\partial r^2} + \frac{1}{r} \frac{\partial u_x}{\partial r} + \frac{1}{r^2} \frac{\partial^2 u_x}{\partial \theta^2} + \frac{\rho_0}{G} \frac{\partial^2 u_x}{\partial t^2} = 0 \quad (2)$$

where G is the shear modulus of the ground, u_x is the ground displacement for the axial direction (perpendicular to the $r-\theta$ plane), ρ_0 is the unit volume mass of ground.

The solution of this equation would be assumed as $u_x = e^{i\omega t} \cdot R(r) \cdot \Theta(\theta)$. It would be sufficient to assume the uniform radiation wave only, because of infinite medium. The boundary forces and displacements along the pipe surface would be assumed to be continuous. Therefore, the displacements along the pipe surface are written as follows:

$$u_x(a, t) = - \frac{H_0^{(2)}(\frac{\omega a}{V})}{2\pi G \frac{\omega a}{V} H_1^{(2)}(\frac{\omega a}{V})} Q_0 e^{i\omega t} \quad (3)$$

where a is the radius of the pipe, V is the shear velocity of the ground, $Q_0 e^{i\omega t}$ is the axial force acting on the pipeline, ω is the circular frequency, $H_0^{(2)}(\frac{\omega a}{V})$ and $H_1^{(2)}(\frac{\omega a}{V})$ is the Hankel function of the 2nd kind.

$u_x(a, t)$ corresponds to $u_g - u$ in the first expression. Thus, k_{ga} would be given as follows:

$$k_{ga} = \frac{2 G \frac{\omega a}{V} H_1^{(2)}(\frac{\omega a}{V})}{H_0^{(2)}(\frac{\omega a}{V})} \quad (4)$$

where k_{ga} is expressed in complex numbers, and the values of $k_{ga}/(2\pi G)$ are shown in Table 1. Because this problem was analyzed in two dimensions, the static value of k_{ga} would be equal to zero.

The solution of the first expression for the stationary sinusoidal waves with the boundary conditions of the free ends is written as follows:

$$u(x, t) = \frac{k_{ga} e^{i\omega t}}{(EA + iC_a) \frac{\omega^2}{Va^2} + (k_{ga} - \rho\omega^2)} U_0 \left(e^{-\frac{\omega x}{Va}} + \frac{\sin(\frac{\omega x}{Va}) \cosh(\lambda_a x)}{Va \lambda_a \sinh(\lambda_a x)} \right. \\ \left. + \frac{\cos(\frac{\omega x}{Va}) \sinh(\lambda_a x)}{Va \lambda_a \cosh(\lambda_a x)} \right) \quad (5)$$

where

$$\lambda_a^2 = \frac{k_{ga} - \rho\omega^2}{EA + iC_a w} \quad u_g = e^{i\omega(t - \frac{x}{V_a})} \quad (5 \text{ cont'd.})$$

V_a is apparent transmitting velocity of the ground excitation, C_a is the damping of the pipeline, and $2l$ is the length of the pipeline.

Besides, another solution for the first expression with the use of modal analyses would be expressed as follows:

$$u(x,t) = \sum_{n=0}^{\infty} (\beta_n \phi_n(x) q_n(t)) \quad (6)$$

where β_n is the nth modal participation factor, $\phi_n(x)$ is the nth natural function, and $q_n(t)$ is the nth normal co-ordinate.

$$f_n^2 = \left(\frac{V_p^2}{4\pi^2} \right) \left(\frac{n^2 \pi^2}{4 l^2 \rho} + \frac{k_s}{EA} \right) \quad (7)$$

$$h_n^2 = \left(\frac{1}{4\pi^2 f_n^2} \right) \left(\frac{n^2 \pi C_a}{4 l^2 \rho} + \frac{C_d}{\rho} \right) \quad (8)$$

where V_p is the transmitting velocity of longitudinal waves along the pipeline, k_s is the spring between the pipe and the ground, and C_d is the damping of the ground.

Supposing the sinusoidal ground excitation $u_g = e^{i\omega(t-x/V_a)}$ as the input wave for the underground pipeline, β_n would be expressed as follows:

$$\beta_n = \frac{1}{2} \left(\frac{\sin \pi \left(\frac{n}{2} + \frac{l_0}{L} \right)}{\pi \left(\frac{n}{2} + \frac{l_0}{L} \right)} + (-1)^n \frac{\sin \pi \left(\frac{n}{2} - \frac{l_0}{L} \right)}{\pi \left(\frac{n}{2} - \frac{l_0}{L} \right)} \right) \quad (9)$$

where l_0 is the length of the pipeline and L is the wavelength.

According to these considerations, if the input ground wave have sufficiently long wavelengths in comparison with the pipe length, the pipeline would give almost the same behaviors to the ground. However, in the short wavelength input waves, the pipeline would give complicated behaviors.

The slight differences between the test pipeline and the ground in this measurement will be explained by these reasons.

3. THE FORCED DISPLACEMENT EXPERIMENT OF T-SHAPED UNDERGROUND PIPELINE

In the disastrous earthquakes, the pipelines are supposed to slip along the boundary of the pipe and ground. In this case, the axial spring between the pipe and the ground is assumed to be represented by the bilinear loop. Supposing the sinusoidal ground waves, k_{ga} may be expressed with the first term of Fourier series for the bilinear loop as follows:

$$k_{ga} = k_1(C + iS) \quad (10)$$

where,

$$C = \frac{1}{\pi}(\phi - \frac{1}{2}\sin(2\phi))(1-a)+a, \quad S = \frac{1}{\pi}(1-a)\sin^2(\phi)$$

$$k = 2\pi\xi G k_r, \quad \phi = \cos^{-1}(1 - \frac{U_e}{U}), \quad U_e = \frac{2\pi a k_g W h}{k_1}$$

a is the bilinear coefficient, U is the relative displacement between the pipeline and the ground, k_r is the elastic spring between the pipeline and the ground, ξ is the decrease coefficient of G , h is the thickness of the backfill soil over the pipeline, W is the unit volume weight of the backfill soil, k_g is the coefficient of dynamic friction between the pipe surface and the soil.

If the sinusoidal ground wave $U_g e^{i\omega(t - \frac{x}{V_a})}$ is applied to the T-shaped pipeline, parallel with the axial direction of the main pipe, the displacement of the pipeline at the junction would be given in the condition of infinite length for each pipe as follows:

$$\frac{U_j}{U} = \frac{\lambda_b^3 I_b (1 + \delta) k_{bb}}{(\lambda_m A_m + \lambda_b^3 I_b (1 + \delta)) (k_{bb} - \rho_b \omega^2)} \quad (11)$$

$$+ \frac{k_{ga} A_m \lambda_m}{(\lambda_m A_m + \lambda_b^3 I_b (1 + \delta)) ((E A_m + i C_m \omega) \frac{\omega^2}{V_a^2} + k_{ga} - \rho_m \omega^2)}$$

$$4 \lambda_b^4 = \frac{k_{bb} - \rho_b \omega^2}{E I_m + i C_{bb} \omega} \quad 4 \lambda_{bo}^4 = \frac{k_{bm} - \rho_m \omega^2}{E I_m + i C_{bm} \omega}$$

$$\lambda_m^2 = \frac{k_{ga} - \lambda_m \omega^2}{E A_m + i C_m \omega} \quad \delta = \frac{2 \lambda_{bo}^2 I_m}{2 \lambda_{bo}^2 I_m + \lambda_b^2 I_b}$$

where I_m and I_b stand for section moments of inertia of the main pipe and branch pipes, ρ_m and ρ_b stand for unit length masses of the main and branch pipes, C_{bm} and C_{bb} stand for the damping factor of the main and branch pipes attributed to bending vibrations, C_m stands for the damping factor of the main pipe attributed to the axial vibrations, k_{bm} and k_{bb} mean the ground springs for the bending displacements of the main and branch pipes, V_a means the apparent transmitting velocity of the input ground wave in the direction of the main pipe axis.

Figs. 8, 9 and 10 are the calculation results of the expression (11) for the parameter values of $U_e = 0.2\text{cm}$, $U = 10\text{cm}$, $k_{bm} = k_{bb} = 28\text{kg/cm}^2$, $W = 1.9\text{g/cm}^3$, $h = 120\text{cm}$. In the calculations, the damping factors of the pipes were neglected. Judging from Figs. 8, 9 and 10, the relative displacements (slips) between the ground and pipe at the junction would increase if input waves have short wavelengths. The pipeline with branch pipes would have small relative displacements. As a result of this relative displacement, the concentrated bending moments would occur at the junction points.

To examine these concentrated bending-moment strains, the experiment illustrated in Fig. 5 was executed. The steel pipeline with the same pipe section as in the first experiment was set on the shaking table. One end of this main pipe was clumped in the shaking table foundation. And this test pipelines of T-shape was buried in the sand pit. The bending strains and restoring forces caused by the shaking table displacements were measured. The dynamic strains excited by the 1Hz sinusoidal waves were found to have the value similar to the static strains for the same displacements. The hysteresis loops at the clumped end showed the absorption of energy, as illustrated in Fig. 7.

4. DYNAMIC WATER PRESSURE OF PIPELINE CAUSED BY EARTHQUAKE MOTION

Dynamic water pressure of pipeline caused by earthquake motion is one of the design factors of water supply system. On this subject Nakagawa (Ref. 7) performed theoretical studies and offered some practical conclusion on maximum water pressure at the stop end, bend, junction, etc. of pipeline due to sinusoidal earthquake motion. We made an attempt to approach more actual conditions, that is, to estimate the dynamic pressure distribution in the pipeline system.

Basic assumptions are as follows:

- (1) Any part of the pipeline is forced to have the same motion as the ground around it during the earthquake.
- (2) Earthquake motion is stationary sinusoidal wave at any place.
- (3) Only the dynamic water pressure due to axial motion of pipeline is considered.
- (4) Propagation of pressure wave in the pipeline is considered to be one dimensional.
- (5) Pipeline system is in the horizontal plane.

Then, considering the earthquake motion, the equations of motion and continuity of water in a pipe element are

$$\frac{\partial}{\partial t} \left(v + \frac{\partial \xi}{\partial t} \right) = - \frac{1}{\rho} \frac{\partial P}{\partial x} - Qv \quad (12)$$

$$\frac{\partial P}{\partial t} = -\rho a^2 \frac{\partial}{\partial x} \left(v + \frac{\partial \xi}{\partial t} \right)$$

where x is the co-ordinate along the axis of pipe, t the time, P the pressure change from stationary value, v the particle velocity of water caused by earthquake motion (relative velocity of vibration to pipe), ξ the ground displacement along the axis of the pipe (component in axial direction of the pipe), a the velocity of pressure wave propagation, ρ the density of water, and Q the linearized resistance.

Put $\xi(x,t) = \xi e^{(wt-kx)}$, and considering stationary solution $v=v(x)e^{j\omega t}$, and $p=P(x)e^{j\omega t}$, we get:

$$v(x) = v_A e^{-sx} + v_B e^{sx} - \frac{j\omega(a^2 k^2 - \omega^2)}{j\omega Q + a^2 k^2 - \omega^2} \xi e^{-jkx} \quad (13)$$

$$p(x) = p_A e^{-sx} + p_B e^{sx} - \frac{\rho a^2 \omega Q k}{j\omega Q + a^2 k^2 - \omega^2} \xi e^{-jkx}$$

where P_A , P_B , etc. are constants to be determined by boundary conditions, $s=j\omega k/a$, $k=1-j(Q/\omega)$ and $j=\sqrt{-1}$.

Considering that a is constant in pipeline system for simplicity, and using the boundary condition (equality of pressure and continuity of flow) for bend, T-junction, etc., we can express a general formula for dynamic pressure amplitude as follows:

$$\text{Pressure amplitude} = \text{Velocity amplitude of ground motion } (j\omega \xi) x \quad (14)$$

$$\text{Wave impedance in pipeline } (\rho a k) x B$$

where B is determined by ω , Q and network system of pipeline considering the direction of the ground motion.

In order to obtain pressure distribution in general pipeline systems, we can use numerical computations based on solution (13) as follows. Considering a network system of pipeline including N -nodal points (stop end, bend, etc.), which have linear boundary condition on pressure and flow, the boundary condition at a nodal point $i=1, 2, \dots, N$ is written in matrix form:

$$\begin{bmatrix} P_i \\ [W_{i1}, W_{i2}] \end{bmatrix} \begin{bmatrix} 1 \\ V_i \end{bmatrix} = (R_i) \quad (15)$$

Supposing a two-dimensional horizontal ground motion, and substituting the solution (13) of each pipeline, we will have a simultaneous linear equation including the boundary conditions of all nodal points and ground motions.

$$[W] (P) = (S) \quad (16)$$

Solving this equation, we may obtain P_A , P_B , and the pressure distribution of pipeline system.

Fig. 11 shows an example. In this example it is assumed that the frequency of ground motion $f=1.4\text{Hz}$, propagation velocity of ground motion (apparent velocity at ground surface) $v_g=100\text{m/sec.}$, and damping $Q=0$. Ten nodal points are shown by No. 1-10, where No. 1, 8, and 10 may be infinite points which absorb pressure energy and have no reflection waves. In this figure, the pressure distribution is normalized by $\rho a \omega \xi = 0.9\text{kg/cm}$ so as to show the effect of infinite points.

From some computations as shown above (Ref. 8) we can say that,

- 1) Dynamic water pressure in the pipeline to be caused by earthquake motion has frequency characteristics which will depend on pipeline system and ground.
- 2) Water pressure is considerably damped at infinite points in pipeline system, but considerably high pressures may arise in some parts of the pipelines which have many stop ends.

3) Pressure distribution in pipeline system shows some difference depending on the ground motion, but it seems to have a specific mode depending on the structure of pipeline system, and the maximum pressure amplitude does not always appear at a stop end or junction point.

5. CONCLUSION

The behavior of underground pipelines during earthquakes is expected to give smaller vibrations in comparison with that of the ground, because of the difference in the stiffness. In the cases of the pipelines with branch pipes, the earthquake loads would be considered to be concentrated in the junction points. In the design of water supply system, great care must be paid to the distribution of pipelines where large dynamic water pressures might be caused by earthquakes.

The properties of earthquake ground motions should be clarified for the aseismic design of underground pipeline as well as for the other structures. Considering the input earthquake waves to the pipeline, the apparent transmitting velocities should be an important factor because of their wavelengths. For the purpose of investigations for the apparent transmitting properties of earthquake ground motions, it is necessary to intensify the earthquake observations on the surface.

6. REFERENCES

- 1) Sakurai, A., et al. (1970): Dynamic stresses of underground pipelines during earthquakes 2, Technical Report: C69087, Central Res. Inst. Electric Power Industry, etc.
- 2) Public Works Research Institute (1975): Technical Memorandum of Public Works Research Institute No. 1037.
- 3) Hohjo, S., et al. (1974): Earthquake and pipe lines (2), Ductile Cast Iron Pipe No. 16.
- 4) Miyajima, N., et al. (1975): Stress on the underground pipeline during earthquakes, Proceedings of the Fourth Japan Earthquake Engineering Symposium.
- 5) Ishimaru, S., et al. (1973): Ductility factor control method, Transactions of the Architectural Institute of Japan, No. 174.
- 6) Minowa, C. (1976): Dynamic experiment of an underground pipeline, The Report of the National Research Center for Disaster Prevention, No. 16.
- 7) Nakagawa, Y. (1969): Theoretical research on the dynamic water pressure of water supply system during earthquakes, Journal of Japan Water Works Association, No. 416.
- 8) Ogawa, N. (1976): Study on the dynamic water pressure of water supply system during earthquakes, Journal of Japan Water Works Association, No. 501.

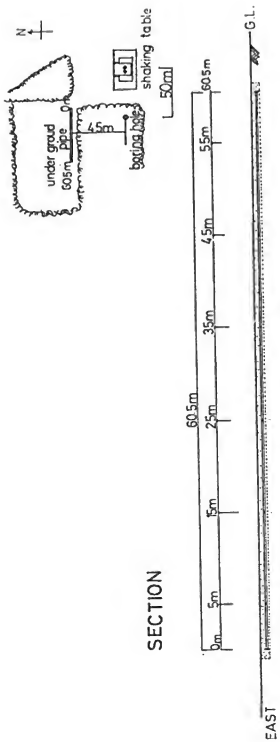


Fig. 1 The Outline of First Experiment

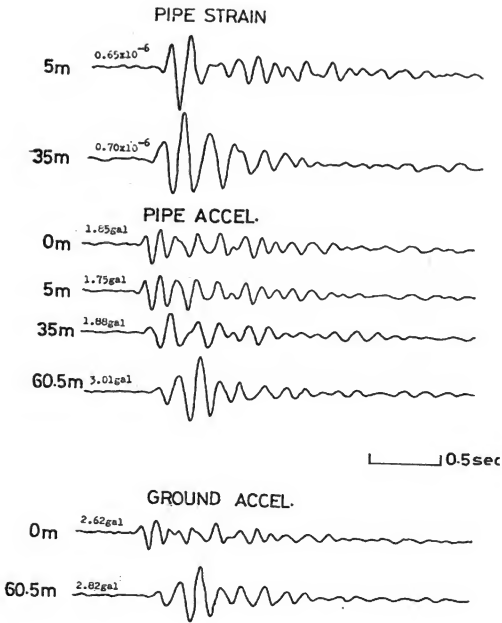


Fig. 2 Measured Waves by an Impulse

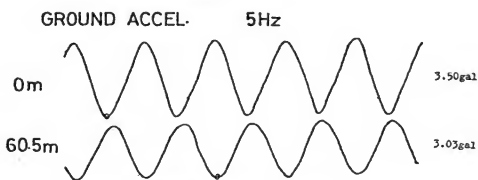
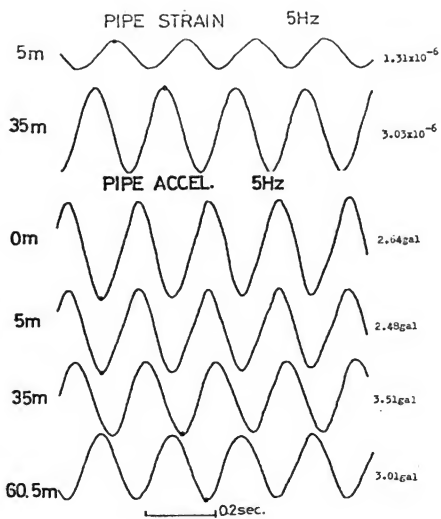


Fig. 3 Measured Sinusoidal Waves

MODAL PARTICIPATION FACTOR
FOR SINUSOIDAL WAVE

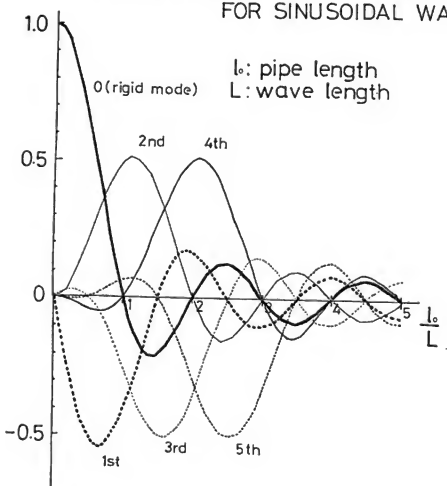


Fig. 4 Participation Factor of a Finite Length Pipe
PLAN

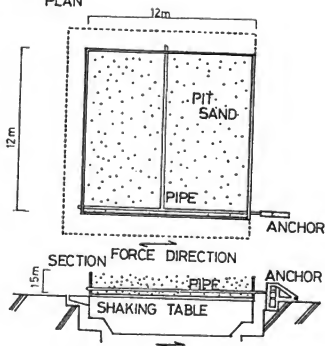
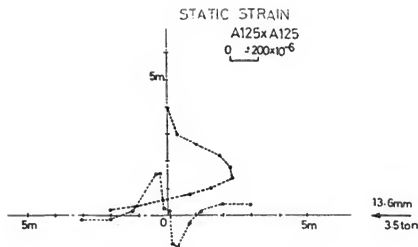


Fig. 5 The Outline of Second Experiment



DYNAMIC STRAIN OF BRANCH PIPE

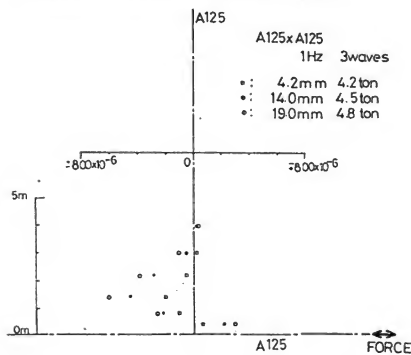


Fig. 6 Strain Distribution

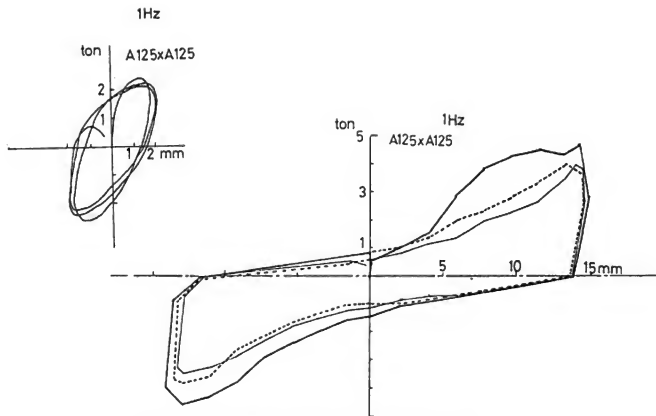


Fig. 7 Hysteresis Curves at the Anchor Point

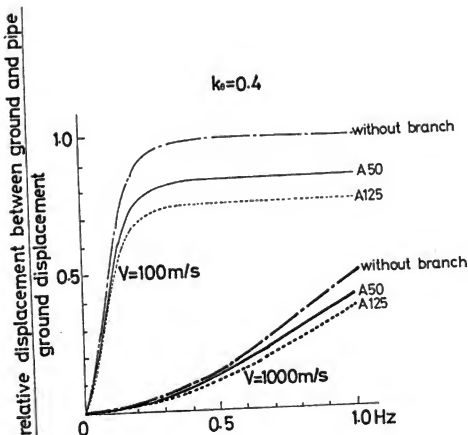


Fig. 8 Slip of a Junction Point

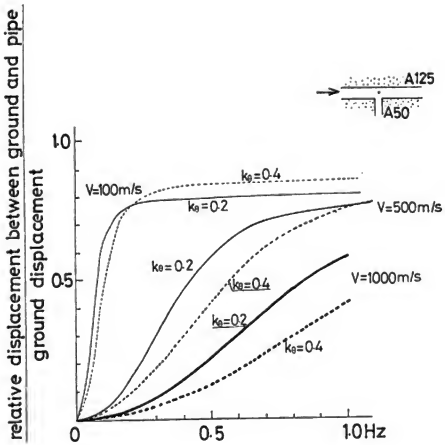


Fig. 9 Slip of a Junction Point

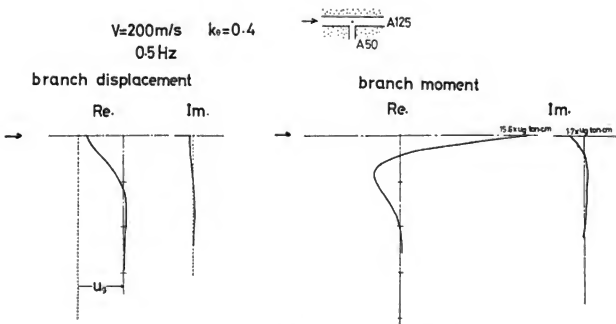


Fig. 10 Displacement and Strain of a Branch Pipe

Numerical Example

Distribution of

Normalized Value

$$\left| \frac{P}{w^2 a^5} \right|$$

in the Pipe Line

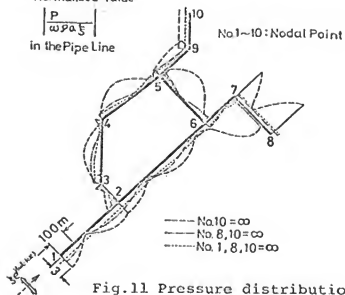


Fig.11 Pressure distribution
in model pipe line

Table 1. $k_{ga}/2\pi g$

$\frac{wa}{V}$	Real	Imaginary
0.00001	0.0845	0.011
0.00005	0.0974	0.015
0.0001	0.1043	0.017
0.0005	0.1244	0.025
0.001	0.1356	0.030
0.005	0.1705	0.049
0.01	0.1907	0.063
0.05	0.2576	0.129
0.1	0.2970	0.189

OBSERVATION OF DYNAMIC BEHAVIOR OF KINUURA SUBMERGED TUNNEL
DURING EARTHQUAKES

Shigeo Nakayama, Chief of Subaqueous Tunnels and Pipe Lines Laboratory
Osamu Kiyomiya, Member of Subaqueous Tunnels and Pipe Lines Laboratory
Hajime Tsuchida, Chief of Earthquake Resistant Structures Laboratory
All of Structures Division, Port and Harbour Research Institute
Ministry of Transport

ABSTRACT

Kinuura Submerged Tunnel, which is located at Kinuura Port and Aichi Prefecture, is equipped with a number of instruments comprising of accelerometers, strain meters, bar stress transducers, and a displacement meter, which are intended to serve the purpose of the tunnel maintenance and to provide data for studying the behavior of the submerged tunnel during earthquakes.

The measurement of earthquake response of the tunnel has been carried out since August, 1973 when the tunnel was opened to traffic. Fifteen earthquakes have been recorded up to January, 1977. A part of the data thus obtained and its analysis have already been reported by the authors (1). This paper describes the analysis of the data and the result of earthquake response calculations carried out by using these earthquake records.

KEYWORDS: Accelerometer; axial force; bar stress transducer; bending moment; displacement meter; dynamic behavior of tunnel; power spectrum; strain meter; submerged tunnel.

1. SUMMARY OF THE TUNNEL AND INSTRUMENTATION

Kinuura Submerged Tunnel which connects the cities of Handa and Hekinan is a two-lane highway tunnel having a total length of 1,560 m. The submerged portion of the tunnel is 480 m in length and consists of six reinforced concrete elements, 80 m long. The soil conditions at the tunnel site consist of a well compacted sandy gravel layer below a depth of -17 to -18 m and a filled-up layer to the depth of -5 to -10 m from the surface. Intervening layer in Handa side between the foregoing two layers is a very soft, unconsolidated, clay layer, however, the intervening layer in Hekinan side is hard clay with N-value of 9-13.

The arrangement of instruments installed in the tunnel is shown in Fig. 1. A total of 19 accelerometers is installed, one each in the axial and normal directions to the tunnel axis at the ground surface on both sides of the tunnel, thus totalling four; two each at the top and bottom of each of the two ventilation towers and two more for vertical acceleration measurement at the top of the ventilation tower on Handa side to catch rocking motion, totalling ten; and five in the submerged elements. A pair of strain meters are installed at three sections of the tunnel under the navigation channel, totalling six. A total of eight bar stress transducers, at each junction of the ventilation towers and the submerged tunnel elements is installed.

Bar stress transducers were initially used for the execution control. Also, one displacement meter is installed in the middle of the submerged tunnel. The trigger level for the starter of these instruments is set at three gals and the system is so designed as to take the records for three minutes. The recording systems are located in the ventilation towers.

2. EARTHQUAKE DATA AND ANALYSIS

Earthquake data obtained and analyzed are given in Table 1. Earthquake Nos. KUWT-4 through KUWT-6 were omitted in the tabulation because they were recorded only in some instruments.

All of the earthquakes recorded were medium scale (not exceeding magnitude 6), and the intensities at Kinuura were Scale II-III in the Japan Meteorological Agency Scale. Shown in Fig. 2 are some of the records during the earthquakes. A study of the data obtained by accelerometers indicates that the values of the maximum acceleration on the ground surface of Hekinan side were in most cases greater than those on the ground surface of Handa side, and this appears to be attributable to the difference in the soil properties between the ground at both sides of the tunnel. Unlike the foregoing difference, however, almost identical values were shown on both sides in the case of the maximum accelerations recorded at the ventilation towers. From this point of view, it is presumed that the ventilation towers have responses to earthquake different from those of the tunnel elements. At the tunnel section under the navigation channel, the record of KUWT-1 and that of KUWT-2 showed little difference in the values of the maximum acceleration. As for KUWT-3 and KUWT-7, however, the values of maximum acceleration increased as the location became closer to Handa

side. At the approach portion of the tunnel, the values of the maximum acceleration were somewhat greater than those for the tunnel elements. In the ventilation towers, the maximum acceleration at the top was greater than that at the bottom.

The Fourier analysis of waveforms indicates that the predominant periods of KUWT-1 and KUWT-2 are significantly different from those of KUWT-3 and KUWT-7. This difference is considered to be attributable to the difference in the characteristics of these earthquakes. The earthquake waveform at the bed layer was calculated by the theory of multiple reflections using the ground surface records obtained in KUWT-7. Shown in Fig. 3 are the maximum accelerations for each stratum as calculated from the records obtained at Handa side and also the maximum acceleration as measured at the ventilation tower (P-5, -6, -14 and -15) and at the on-ground portion (P-3) of the tunnel. It can be seen from the figure that the maximum acceleration of the structure in the ground was almost equal to or slightly smaller than that of the ground itself.

3. EARTHQUAKE RESPONSE CALCULATIONS

Using the earthquake records, earthquake response calculations were carried out and compared with the measured values. The method of these earthquake response calculations was proposed by TAMURA and HAMADA (2,3), i.e., the method in which the responses of the ground and structure are obtained by replacing the ground and the structure by an idealized system composed of mass, spring and dashpot. As input records, P-2 and P-9 in KUWT-2, and P-1, P-2, P-8 and P-9 in KUWT-3, were used. The input records were gained by the theory of multiple reflection.

Table 2 shows the bending moments and axial forces as calculated from the measured values by the bar stress transducers and strain meters. Fig. 4 to 9 shows the results of earthquake response calculations. For these calculations, the damping constant was taken as 0.0 except for some cases. Black dots in these figures represent the bending moments and axial forces calculated from the measured values given in Table 2 and the measured values of acceleration. As for the bending moments, the values calculated from the strain meters agreed fairly well with those obtained by earthquake response calculations as shown in Fig. 4.

The values obtained by the bar stress transducers were somewhat lower than the calculated moments. This disagreement may have been caused by the fact that the bar stress transducers, having been primarily intended for the execution control, were not designed for high precision measurement. According to the results of earthquake response calculations in other cases, the maximum bending moments generally occurred at the tunnel proximate to the shore protection structures. However, the calculated maximum moments from the measured values occurred at the same point and also at the middle of the tunnel section under the navigation channel. In view of this, further studies will be made as to the cause of this result.

In the case of axial forces, the measured values agreed well with the corresponding calculated values where the damping constant was taken as 0.0 as shown in Fig. 5. When the damping constant was taken as 0.1, the sectional forces were 1/2 or 1/3 of the value as shown by dash lines in Fig. 5.

As shown in Figs. 5 and 6, the maximum axial forces occurred on the opposite side to the place where the input record had been obtained. When the power spectrum of the earthquake waveforms were compared with the predominant period of the ground obtained from the measurement by microtremor, it was found that the period of earthquake record of P-2 in KUWT-2 are close to the predominant period of the ground on Hekinan side, but are not close to that of the ground on Handa side.

What can be considered in this respect is that the assumption of the soil conditions made in the ground modelling might have been somewhat inadequate. From this point of view, the tunnel was divided into halves at the midpoint under the navigation channel, the earthquake response calculation of each half of the tunnel was made with the earthquake record obtained on that side, and then the two results were superposed.

In consequence, the peak of the sectional force, which was conspicuous in the opposite side to the one in which the input was made, disappeared, and a comparatively flatter curve of axial force distribution as shown in Fig. 7 was obtained.

Fig. 8 was plotted by using the earthquake record of P-3 in KUWT-3. The maximum response accelerations turned out to be greater in the submerged portion of the tunnel. As to P-3, P-11, and P-16 in the submerged portion and P-1 and P-8 at the ground surface, the calculated values agreed fairly well with the measured values.

Fig. 9 is plotted by using the earthquake record of P-2 in KUWT-3 which was in axial direction. Slightly differing from the case of P-1, the acceleration in the navigation channel was smaller, but the calculated values were approximately in accord with the measured values. There were cases where the maximum response acceleration of the navigation channel portion was greater than those on both sides or where the measured values were substantially lower than the calculated values.

This will have to be clarified by future studies. It is to be noted in Table 2 that, except for the measured values in KUWT-3 by the strain meters of S-1 and S-2, the axial strains were greater than the bending strains. The maximum axial strains measured by the bar stress transducers of K-1 and K-3 in KUWT-3 was 3.75×10^{-6} . Since the corresponding maximum axial strain obtained from the earthquake response calculations was 3.78×10^{-6} , there was a fair agreement between them. The measured bending strain was 0.92×10^{-6} which was about a quarter of the axial strain, but the maximum bending strain as obtained by the earthquake response calculations was 5.78×10^{-6} , which is about six times as great as the measured bending strain. Although the calculated bending strain curve was of such a shape that its amplitude became large gradually, the measured and the calculated values agreed well with each other in respect with the predominant period in the power spectrum. Figs. 10 and 11 show the axial and bending strains, and the power spectrum, respectively, of KUWT-3.

Predominant periods in the measured bending strain were 0.79 and 0.60 second and those in the calculations were 0.79 and 0.68 seconds, respectively. As for the axial strains, 1.02, 0.85 and 0.60 seconds, and 0.93, 0.85 and 0.57 seconds were predominant for the measured and the calculated values, respectively.

4. CONCLUSIONS

While the epicenters of KUWT-1 and KUWT-2 were at a long distance from the submerged tunnel site, those of KUWT-3 and KUWT-7 were proximate to the tunnel site. All of these earthquakes were of comparatively small scale but each had its own characteristics. The fact that they had different characteristics clarifies that the ground as well as the submerged tunnel had behaviors depending on the earthquake characteristics. It was also found that, in the earthquakes originated far from the tunnel site, the long period components were predominant in ground motion, and the tunnel had almost the same behaviors as the ground. On the contrary, where the epicenters are located near the tunnel site, the ground motion was governed by the short period components, and the behaviors of the tunnel differed slightly from those of the ground.

The vibration of the submerged tunnel as a whole was governed by the surrounding soil conditions at respective sections of the tunnel, and the ground vibration characteristics along the axis of the tunnel were different from those in direction normal to the tunnel axis. It is, therefore considered necessary to investigate topography and soil properties both in the direction of the tunnel axis and in the direction normal to the tunnel axis in order to determine the natural period of the ground.

The greatest value of the maximum acceleration was found at the ground surface. The values of the maximum accelerations in the ventilation towers and the submerged section of the tunnel were almost equal to or slightly smaller than those at the ground surface. At the upper part of the ventilation tower, the maximum acceleration was found to be smaller than that at the ground surface.

As for the strains which occurred in the submerged tunnel, the axial strains were found to be predominant over the bending strains in all cases except one record in KUWT-3, and the maximum axial force calculated by the measured strain was about 1,100 tons. In view of the results of earthquake response calculations, it is very important to determine soil condition, spring constant, damping constant, etc.. Since the moduli of elasticity of soils vary with the levels of the ground strain during earthquakes, the value of spring constant should be determined on the basis of elastic-plastic analysis or triaxial vibration tests, particularly if the strong earthquakes are to be considered. In these calculations, there were cases wherein the measured strains showed fairly good agreement with the value by the earthquake response calculations. In such cases, it was found that the power spectrum for both had also similar predominant periods. Values of the calculated accelerations were somewhat larger than the measured values. This was particularly so under the navigation channel where the calculated accelerations were large. Unfortunately, there was no case in the present observations where perfect record of strains was obtained at all of the three sections of the submerged tunnel.

Thus, the distribution of the sectional forces with respect to the submerged tunnel axis should be taken up as the subject of the future research studies.

REFERENCES

- 1) Shigeo Nakayama, Osamu Kiyomiya and Hajime Tsuchida, "Observation of Dynamic Behavior of the Kinuura Submerged Tunnel during Earthquakes," Summary of Lecture at 13th Earthquake Engineering Conference.
- 2) Masanori Hamada, "Computations of Earthquake Response of Submerged Tunnel," Proc. of 26th Annual Research Conference of Japan Society of Civil Engineers.
- 3) Choshiro Tamura, Shunzo Okamoto and Masanori Hamada, "Dynamic Behavior of a Submerged Tunnel during Earthquakes," Report of the Institute of Industrial Science, the Tokyo University, Vol. 24, No. 5.
- 4) Osamu Kiyomiya, Shigeo Nakayama and Hajime Tsuchida, "Observations of Dynamic Response of Kinuura Submerged Tunnel During Earthquakes and Dynamic Response Analysis," Technical Note of Port and Harbour Research Institute, No. 221.

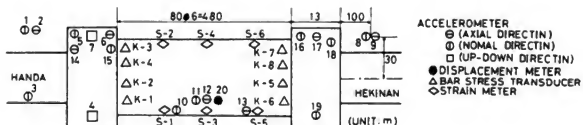


Fig. 1 Arrangement of meters

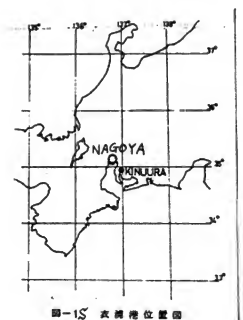


Fig. 1S Location of Tunnel

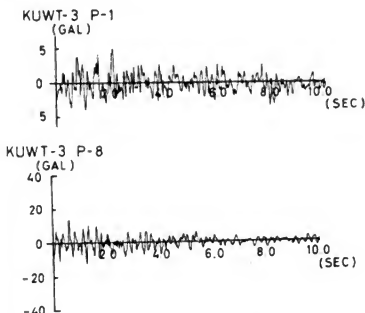


Fig. 2 EARTHQUAKE RECORDS

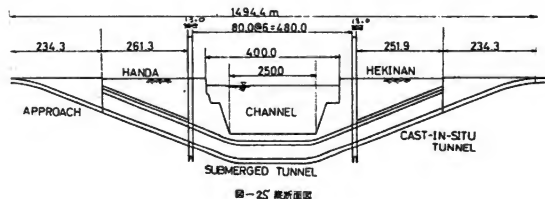


Fig. 2S Longitudinal Section of Tunnel

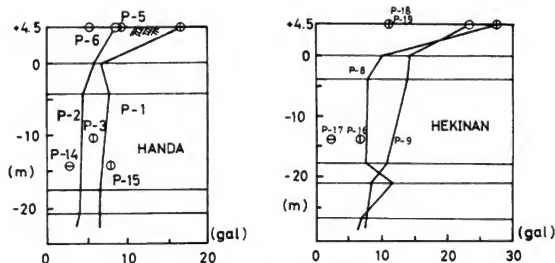


Fig. 3 Acceleration in the ground

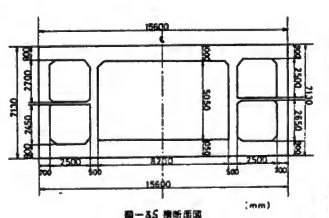


Fig. 3S Typical Cross Section

Table - 1 EARTHQUAKE RECORDS

Earthquake No.	Date	Location of Origin	Magnitude	Depth (km)	Epicentral distance (km)
KUWT - 1	1973.11.25	N 33° 51' E 135° 25'	5.9	60	185
KUWT - 2	1973.11.25	N 33° 53' E 135° 23'	5.8	60	185
KUWT - 3	1974. 2.10	N 35° 2' E 136° 56'	5.3	40	30
KUWT - 7	1974. 8.16	N 35° 15' E 136° 11'	4.9	50	50

Table - 2 MEASURED BENDING MOMENTS
AND AXIAL FORCES

Earthquake No.	Axial Strain (10^{-6})	Axial Force (ton)	Bending Strain (10^{-6})	Bending Moment (t-m)
KUWT-2 K-1 & K-3	1.84	239	0.33	110
KUWT-2 K-2 & K-4	6.34	823	2.09	696
KUWT-2 K-5 & K-7	2.55	331	1.15	383
KUWT-2 K-6 & K-8	8.65	1,123	5.80	1,931
KUWT-2 S-1 & S-2	6.5	844	1.5	703
KUWT-3 S-1 & S-2	0.37	324	5.66	2,655
KUWT-3 K-1 & K-3	3.75	487	0.92	306

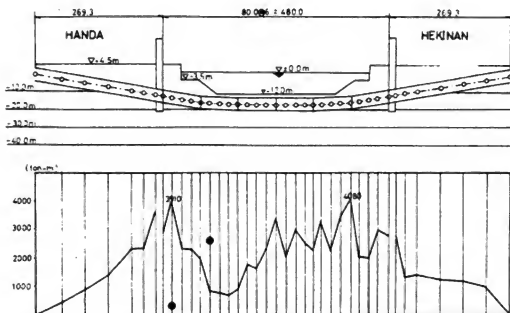


Fig-4 Maximum bending moment (KUWT-3 P-1)

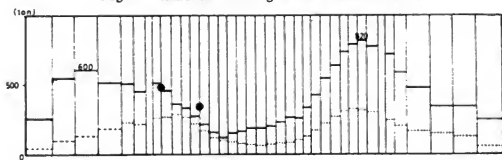
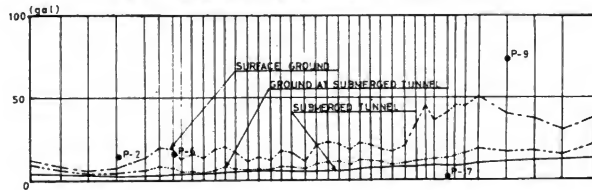
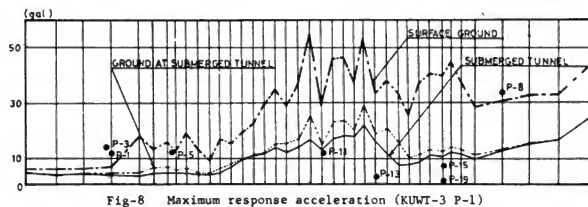
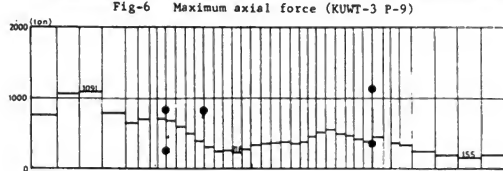
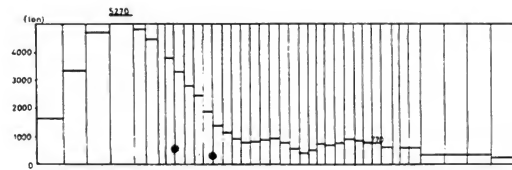


Fig-5 Maximum axial force (KUWT-3 P-2) h=0.1



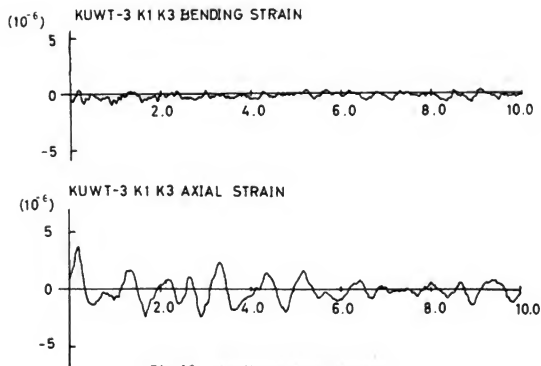


Fig-10 Bending & axial strain

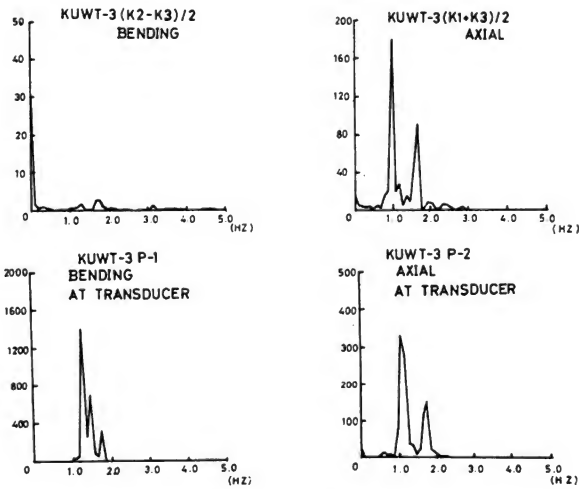


Fig-11 Power spectrum

A PROPOSAL FOR EARTHQUAKE RESISTANT DESIGN METHODS

Kiyoshi Nakano, Assistant Director, Building Research Institute,
Ministry of Construction

and

Masamitsu Ohashi, Head, Earthquake Disaster Prevention Division,
Public Works Research Institute, Ministry of Construction

ABSTRACT

This paper describes the outline of a Proposal for Earthquake Resistant Design Methods, which was completed by the Ministry of Construction in March, 1977.

KEYWORDS: Coefficients in aseismic design; design method; proposed earthquake resistant design method; seismic hazard zoning map.

1. INTRODUCTION

A Proposal for Earthquake Resistant Design Methods owes a great deal to the results of the investigations of a major ministerial project on new technology for synthesized earthquake resistant design in the Ministry of Construction, which were carried out from 1972 through 1976. The proposal also had absorbed the results of investigations by universities, public and private laboratories. The purpose of the proposal is to establish a practical and rational earthquake resistant design method.

2. OUTLINE OF A PROPOSAL FOR EARTHQUAKE RESISTANT DESIGN METHODS

Damages of the structures caused by the Niigata Earthquake (1964), Tokachioki Earthquake (1968), and San Fernando Earthquake (1971) stimulated to improve and rationalize the earthquake resistant design methods. For this purpose, a new major ministerial project was conducted from 1972 through 1976 and a Proposal for Earthquake Resistant Design Methods was presented by the Ministry of Construction in March, 1977.

This project consisted of 6 themes and 20 sub-themes as shown in Appendix I.

The proposal has been divided into 3 parts. In part I, a fundamental conception commonly applied to bridges, soil structures, underground structures and buildings is proposed. In part II, practical calculations excluding buildings are advanced based on Part I. Part III deals with the calculation methods for buildings.

The contents of the proposal are shown in Appendix II. The proposal is compiled according to the following principles:

(1) Standardization of Fundamental Conception

Each earthquake resistant design method has its own background. It has improved by itself by studying the damages of structures caused by past earthquakes, analyzing the earthquake ground motions which were obtained by the strong motion observation network, and investigating the characteristics of structures and their members. Consequently, the design methods have been diversified in accordance with the uses and types of each structure.

In the project, existing earthquake resistant design methods were reviewed and a fundamental conception for designing bridges, soil structures, underground structures and buildings was proposed.

(2) Clarification of Design Procedure

Until recently, the earthquake resistant design has been apt to concentrate on the calculation methods. The fundamental design procedure has not satisfactorily been clarified. The proposal clarifies the fundamental design procedure considering characteristics of earthquake ground motion, seismic performance, and safety.

(3) Systematization of Design Procedure

Earthquake resistant design is required to follow a proper procedure in accordance with the characteristics of subgrounds and structures.

The proposal presents a fundamental conception for the earthquake resistant design in order to indicate correct procedures to follow.

3. PART I, FUNDAMENTAL CONCEPTION

3.1 Fundamental Conception of Aseismic Design

In the earthquake resistant design, following items should be considered:

- (1) Characteristics of structures
- (2) Uses of structures
- (3) Types of structures
- (4) Scales of structures
- (5) Circumstances of structures

(6) Damages of structures and surrounding grounds caused by past earthquakes.

Fig. 3.1 shows a fundamental procedure of aseismic design. In the procedure, the process to calculate seismic force or earthquake response is classified into 4 methods as below:

- (1) Seismic coefficient method
- (2) Modified seismic coefficient method
- (3) Seismic deformation method
- (4) Dynamic analysis method

The method to be selected among these is determined by considering the characteristics of structures.

3.2 Standard Seismic Loadings for Aseismic Design

Seismic zoning is presented herein in order to indicate the characteristics of earthquake ground motion at each site. The occurrence of past earthquakes, the records of strong-motion earthquakes and the earthquake activities in relatively wide areas were taken into account in the zoning.

To determine the intensity of earthquake ground motion at a certain site, the seismic zoning as stated above and the characteristics of ground should be taken into consideration.

Seismic loadings for aseismic design is evaluated by the coefficients concerning the seismic zoning and the characteristics of grounds according to the particular method of earthquake resistant design.

3.3 Ground Examinations and Seismic Performance of Grounds

Investigating the documents about the damages of grounds caused by past earthquakes is important in the earthquake resistant design of structures. If it is necessary, the characteristics of grounds and soils at the construction site should be examined. Seismic loadings are determined considering the results of investigations and examinations stated above.

The proposal presents herein soil and ground examinations and stability of grounds. It also systematizes the methodology for examination and confirmation regarding the stability of grounds.

3.4 Seismic Performance of Structural Members

The proposal has aimed at systematizing the methodology to evaluate and promote the seismic performance of structural members in reinforced concrete, steel and reinforced concrete composite, prestressed concrete, steel and other structures.

4. PART II EARTHQUAKE RESISTANT DESIGN OF CIVIL ENGINEERING STRUCTURES

4.1 General

Current seismic design specifications for construction excluding buildings have been formulated on the basis of experiences gained through earthquake damage in the past and investigations on seismic design criteria. The seismic design criteria introduced in this chapter were established based on the fundamental conceptions presented in the previous chapter (Part I) in difference to the current seismic design specifications. In the case of designing special types of structure, it is recommended to make use of this aseismic design specification selectively according to the structural properties considered.

4.2 Coefficients in Aseismic Design

In the case of estimating the seismic loadings specified in Part I, the coefficients in aseismic design shall not be lower than the values allowed in the following provisions.

4.2.1 Design Coefficients in the Seismic Coefficient Method

The horizontal design seismic coefficient can be determined by the following formula:

$$K_H = \Delta_1 \cdot \Delta_2 \cdot \Delta_3 \cdot K_o \quad (4.1)$$

- (1) The standard horizontal design seismic coefficient K_o can be taken as 0.2.
- (2) Seismic zone factor Δ_1 is shown in Table 4.1 by referring to the seismic zoning map displayed in Fig. 4.1.
- (3) Ground condition factor Δ_2 is shown in Table 4.2.
- (4) A factor Δ_3 dependent on other conditions can be determined through considerations on uses and types of structures. The structural type factor is shown in Table 4.3.

4.2.2 Design Coefficients in the Modified Seismic Coefficient Method

The horizontal design seismic coefficient can be determined by the following formula:

$$K_H = \Delta_1 \cdot \Delta_2 \cdot \Delta_4 \cdot \Delta_5 \cdot \Delta_6 \cdot K_o \quad (4.2)$$

- (1) The standard horizontal design seismic coefficient K_o , seismic zoning factor Δ_1 , and ground condition factor Δ_2 can be the same values employed in the seismic coefficient method.
- (2) A factor Δ_4 dependent on the response characteristics of structures is presented for four groups of ground conditions in Fig. 4.2. In the case when natural period is smaller than 0.5 seconds, a factor Δ_4 can be taken as 1.0.
- (3) A factor Δ_5 dependent on structural characteristics can be taken as 1.0 in the case when the allowable stress design procedure is to be applied. However, in the case when the ultimate strengths of structure are to be checked in design, a factor Δ_5 can be properly determined in accordance with the ductilities expected in plastic zone of structural members.
- (4) A factor Δ_6 dependent on other conditions can be properly determined through considerations on uses and types of structures and so on. When it is considered not necessary to pay special attentions to these matters, a factor Δ_6 can be taken as 1.0.

4.3 Principal Features of Aseismic Design Criteria

4.3.1 Development of New Seismic Zoning Map and Intensity of Design Earthquake Motions

The seismic zoning maps and intensities of design earthquake motions applied in the current seismic design specifications are not necessarily uniform. There are slight differences among these according to the types of structure considered. It has been, therefore, requested to establish a unified seismic zoning map.

In the proposal, a unified seismic zoning map applicable for all types of structure is presented.

4.3.2 Development of New Aseismic Design Criteria for Foundations

It has been pointed out that the design criteria employed in the current seismic design of foundations are not necessarily uniform since they have been formulated separately.

In the proposal, a unified criteria for aseismic design of spread foundations, caisson foundations, pile group foundations, steel-walled-pipe pile foundations, and multi-column foundations are presented.

4.3.3 Development of New Seismic Design Criteria for Reinforced Concrete and Steel Structures

Evaluation systems of ductilities are presented for reinforced concrete structures. The results of investigation concerning the buckling effects on seismic stability are introduced into the design of thin walled steel structures.

4.3.4 Development of New Seismic Design Criteria for Soil Structures

The basic principles for aseismic design criteria of soil structures are presented. An empirical seismic design criterion, in which a seismic design calculation can be omitted as long as the structure has standard shape, material, size and construction procedure, is also presented.

Technical means to improve soft subsurface soil layers are presented.

4.3.5 Development of New Seismic Design Criteria for Underground Structures

The seismic design criteria for important underground structures such as water, gas, electricity and communication facilities, which are often called as life lines systems, are presented as well as the seismic design criteria for petroleum pipe lines and submerged tunnels.

4.3.6 Development of New Criteria for Restoration Systems of Existing Structures

Evaluation systems of seismic performance and restoration systems of existing structures are presented.

4.3.7 Improvements of Design Details

Design details are presented so that detailed devices, which help improve seismic performance of structures, are adequately provided.

5. PART III BUILDING CONSTRUCTION

5.1 Introduction

In this part, an aseismic design method for the building structures, non-structural elements, foundations, and retaining walls is introduced.

Compared with the conventional design method, the proposed method is based on the most recent research in seismology, earthquake engineering and structural engineering. One of the important characteristics of this method is that the appropriate design procedure can be applied according to the structural properties and the occupancy of the building.

5.2 Characteristics of the Proposed Design Method

5.2.1 Design Procedures and Steps

This aseismic design method involves six design procedures and each procedure has two steps.

One or more of the six procedures would be selected, according to the structural properties and the occupancy of the building, materials, seismic resisting system, height, use or occupancy, etc.

The step 1 of these design procedures should satisfy the condition that the response of the structural members as well as the non-structural elements due to frequent earthquakes should not exceed the elastic range of the materials and the damages caused should be small enough that the repair would be scarcely required due to such earthquakes.

The step 2 which follows step 1 should satisfy the condition that the building structure would not collapse due to the maximum possible earthquakes such as Great Kanto Earthquake in 1923.

The schematic chart of these design procedures and steps are set forth in Table 5.1.

5.2.2 Seismic Force

The total lateral seismic force is basically determined by the following formula:

$$F = C \cdot W \quad (5.1)$$

where C is the seismic design coefficient given by formulas (5.2a), (5.2b), (5.3a) or (5.3b), and W is the total dead load of the building and applicable portions of other loads.

The seismic design coefficient for step 1 shall be determined in accordance with the following formula:

$$C_1 = Z \cdot G_0(T) \cdot eCo \quad (5.2a)$$

where Z is the seismic hazard zoning factor prescribed in section 5.2.3, $G_0(T)$ is the soil profile spectrum for approximation as given in section 5.2.4, T is the fundamental natural period of the building in seconds, and $eCo = 0.2$ is the standard base shear coefficient for step 1.

In the procedure I-A or I-B in Table 5.1 the height of the building concerned is low and the value of T is small. Accordingly, $G_0(T)$ is considered to be constant and 1.0. Therefore, formula (5.2a) is reduced to (5.2b)

$$C_1 = Z \cdot eCo \quad (5.2b)$$

The seismic design coefficient for step 2 shall be determined in accordance with either of the following formulae:

$$C_2 = Z \cdot G(T) \cdot K_1 \cdot pCo \quad (5.3a)$$

$$C_2 = Z \cdot G(T) \cdot K_2 \cdot pCo \quad (5.3b)$$

where $G(T)$ is the soil profile spectrum as specified in section 5.2.4, $pCo = 1.0$ is the standard base shear coefficient for step 2, and K_1 and K_2 are the structural coefficients as given in section 5.2.5.

5.2.3 Seismic hazard zoning factor

Sesimic hazard zoning factor Z was determined by the seismicity and by applying the theory of extremes, statistics and engineering judgment. The values of Z are given in Fig. 5.1 Seismic Hazard Zoning Map.

5.2.4 Soil Profile Spectrum

The effects of the soil profile properties and the natural period of the building are expressed as the soil profile spectra given in Fig. 5.2.

One of these spectra, $G(T)$, is for approximation and the other four $G_i(T)$ correspond to four soil profile types.

The soil profile types are defined as follows:

Soil profile type 1 is a profile with rocks, stiff and well consolidated sands, etc.

Soil profile type 2 is a profile with sands, stiff clays, stiff loams, etc.

Soil profile type 3 is a profile which would not belong to other types.

Soil profile type 4 is a profile with soft clays, loose sands, etc.

5.2.5 Structural Coefficient

It is a well known fact that the ductile structure could absorb more energy than the brittle structure and it is not practical to design the building to be completely elastic when subjected to the maximum possible earthquake motion. Accordingly the structural coefficients K_1 and K_2 are calculated and they would be denoted as the response modification factors which depend on the energy absorption capacity of the building during the earthquakes. The values of these factors are given in Table 5.2, according to the structural materials and system, and ductility level. K_1 would be used in procedure II-A and K_2 in procedure II-B, III-A and III-B, as shown in Table 5.1.

5.2.6 Seismic Hazard Exposure Factor

According to the use or the character of the occupancy of the building, the appropriate design procedure could be elected or the seismic hazard exposure factor could be adopted for use in step 1 or 2. The value of the factor is not specified in this method, because the reliable theory to determine the value is not developed yet. But it can be suggested that the probability of failure, the dispersion of the seismic resistant capacity as well as the dispersion of the seismic force, social utilities and the acceptable level of human risk should be studied to determine the value of the seismic hazard exposure factor.

5.3 Concluding Remarks

The proposed aseismic design method has been founded on the principle that make possible the application of new theory and research as well as the use of new materials and new structural systems. If one of the six design procedures would be selected properly, the building designed might be safe enough for the earthquakes with a minimum design effort and a minimum volume of structural materials.

But, the details of the design method might not be complete yet, therefore, the following studies would be necessary in the near future:

- i) re-examination of various parameters
- ii) case study for different types of buildings
- iii) simplification of the method for practical use

(SUPPLEMENT)

In Part II, the seismic design coefficient is denoted as the following formula:

$$K_H = \Delta_1 \cdot \Delta_2 \cdot \Delta_3 \cdot K_o$$

This formula corresponds to the following formula in Part III.

$$C_1 = Z \cdot G_o(T) \cdot eCo$$

or

$$C_1 = Z \cdot eCo$$

And the following correspondences would be given:

$$K_H = C_1$$

$$\Delta_1 = Z$$

$$\Delta_2 = G_o(T)$$

$$\Delta_3 = \text{seismic hazard exposure factor}$$

$$K_o = eCo$$

The modified seismic design coefficient in Part II is denoted as the following formula:

$$K = \Delta_1 \cdot \Delta_2 \cdot \Delta_4 \cdot \Delta_5 \cdot \Delta_6 \cdot K_o$$

In Part III:

$$C_2 = Z \cdot G_o(T) \cdot K_1 \cdot pCo$$

or

$$C_2 = Z \cdot G_1(T) \cdot K_2 \cdot pCo$$

here, we have:

$$\begin{aligned}K &= C_2 \\ \Delta_1 &= Z \\ \Delta_2 \cdot \Delta_4 &= G_0(T) \text{ or } G_1(T) \\ \Delta_5 &= K_1 \text{ or } K_2 \\ \Delta_6 &= \text{seismic hazard exposure factor} \\ K_o &= pC_0\end{aligned}$$

APPENDIX I - Themes of Research Project on New Criteria for Earthquake Resistant Design of Structures

I Research on Earthquake Ground Motions

1. Characteristics of Earthquake Ground Motions on Baserock
 - 1) Seismic Records obtained
 - 2) Source Mechanism and Propagation of Seismic Waves
 - 3) Earthquake Ground Motions on Various Subsoils
 - 4) Earthquake Ground Motions of Long Period Components
2. Evaluation of Standard Seismic Inputs Depending on Subsoils
 - 1) Standard Design Seismic Inputs

II Research on Dynamic Properties of Soils

1. Failure Mechanism and Strength of Soils
 - 1) Behavior of Loose Sands and Soft Clayey Soils
 - 2) Dynamic Strength of Soils
 - 3) Seismic Damage to Embankments and Slopes

III Dynamic Properties and Dynamic Strength of Structural Members

1. Dynamic Strength of Structural Members
 - 1) Plastic Properties of Bridge Piers
 - 2) Dynamic Behavior of Bridge Piers
 - 3) Dynamic Strength of Building Members
 - 1) Reinforced Concrete Columns
 - 2) Reinforced Concrete Walls
 - 3) Steel Reinforced Concrete Columns
2. Dynamic Strength of Structural Joints
 - 1) Dynamic Strength of Structural Joints for Prefabricated Buildings
 - 2) Dynamic Strength of Steel Structural Joints
 - 3) Dynamic Strength of Structural Joints for Prestressed Concrete Buildings and Steel Reinforced Concrete Structures
 - 4) Dynamic Strength of Structural Joints of Reinforced Structures

IV Research on Vibrational Characteristics and Earthquake Response Analyses of Structures

1. Dynamic Interactions of Soils and Structures
 - 1) Sesimic Measurements at Structures and Surrounding Soils
 - 1) Bridges
 - 2) Buildings

- 2) Dynamic Analyses of Soil-Building Systems
- 3) Dynamic Interactions of Soil-Bridge Foundation Systems

- 2. Failure Mechanism of Structures
 - 1) Failure Mechanism of Wooden Building Structures

- V Establishment of Criteria on Earthquake Resistant Design of Structures
 - 1. Establishment of New Criteria on Earthquake Resistant Design
 - 1) Civil Engineering Structures
 - 2) Building Structures
 - 2. Establishment of New Earthquake Resistant Design of Various Structures
 - 1) Establishment of Prefabricated Building Structure
 - 2) Establishment of Buried Pipes
 - 3) Establishment of Non-Structural Members

- VI Research on Countermeasures Against Earthquake Disaster
 - 1. Procedures for Assessing Earthquake Resistance for Existing Structures
 - 1) Criteria on Evaluating Earthquake Resistance of Reinforced Concrete Buildings
 - 2. Rehabilitations of Existing Structures
 - 1) Strength and Deformation of Structural Members for Reinforced Concrete Buildings and Steel Reinforced Concrete Buildings
 - 3. Establishments of Procedures for Preventing Earthquake Disaster
 - 1) Development of Procedures for Predicting Seismic Risk

APPENDIX II - Contents of a Proposal for Earthquake Resistant Design Methods

Introductory Remarks

Part I. Fundamental Conception

- 1. Scope
- 2. Definition of Terms
- 3. Fundamental Conception of Aseismic Design
 - 3-1. Fundamental Procedure of Aseismic Design
 - 3-2. Methods of Calculation for Aseismic Design
 - 3-2-1. Classification
 - 3-2-2. Selection
 - 3-2-3. Precaution
 - 3-3. Safety
- 4. Standard Seismic Loadings for Aseismic Design
 - 4-1. Past Earthquakes
 - 4-2. Engineering Characteristics of Earthquake Ground Motions
 - 4-2-1. Characteristics of Earthquake Ground Motions
 - 4-2-2. Seismic Zoning
 - 4-2-3. Intensity of Earthquake Ground Motions at Construction Site
 - 4-3. Design Seismic Loadings
 - 4-3-1. General Remarks
 - 4-3-2. Design Coefficients in the Seismic Coefficient Method
 - 4-3-3. Design Coefficients in the Modified Seismic Coefficient Method

- 4-3-4. Design Coefficients in the Seismic Deformation Method
- 4-3-5. Seismic Loads in the Dynamic Analysis Method
- 5. Ground Examinations and Seismic Performance of Grounds
 - 5-1. General
 - 5-2. Soil Examinations
 - 5-2-1. General Remarks
 - 5-2-2. Examinations for Dynamic Properties of Soils
 - 5-3. Ground Examinations
 - 5-3-1. General Remarks
 - 5-3-2. Examinations for Dynamic Characteristics of Grounds
 - 5-3-3. Dynamic Analysis of Grounds
 - 5-3-4. Examinations for Classification of Grounds
 - 5-4. Stability of Grounds During Earthquakes
 - 5-4-1. General Remarks
 - 5-4-2. Examinations for Stability of Sandy Grounds
 - 5-4-3. Examinations for Stability of Clayey Grounds
- 6. Seismic Performance of Concrete Members
 - 6-1. Properties of Concrete and Steel Materials
 - 6-1-1. Concrete
 - 6-1-2. Reinforcements
 - 6-2. Seismic Performance of Reinforced Concrete Structural Members (Excluding Buildings)
 - 6-2-1. General Remarks
 - 6-2-2. Fundamentals for Design
 - 6-2-3. Ultimate Strength and Ductility
 - 6-3. Seismic Performance of Reinforced Concrete Structural Members for Buildings
 - 6-3-1. General Remarks
 - 6-3-2. Fundamentals for Design
 - 6-3-3. Ultimate Strength and Ductility
 - 6-4. Seismic Performance of Steel and Reinforced Concrete Structural Members for Buildings
 - 6-4-1. General Remarks
 - 6-4-2. Fundamentals for Design
 - 6-4-3. Ultimate Strength and Ductility
 - 6-5. Seismic Performance of Prestressed Concrete Structural Members for Buildings
 - 6-5-1. General Remarks
 - 6-5-2. Fundamentals for Design
 - 6-5-3. Ultimate Strength and Ductility
- 7. Seismic Performance of Steel Members
 - 7-1. Properties of Steel Materials
 - 7-2. Seismic Performance of Steel Structural Members (Excluding Buildings)
 - 7-2-1. General Remarks

- 7-2-2. Fundamentals for Design
- 7-2-3. Ultimate Strength and Ductility
- 7-3. Seismic Performance of Steel Structural Members for Buildings
 - 7-3-1. General Remarks
 - 7-3-2. Fundamentals for Design
 - 7-3-3. Ultimate Strength and Ductility
- 8. Seismic Performance of Other Members
 - 8-1. General
 - 8-2. Seismic Performance of Wooden Structural Members for Ordinary Wooden Houses
 - 8-2-1. General Remarks
 - 8-2-2. Ultimate Strength and Ductility
 - 8-3. Seismic Performance of Non-Structural Members for Buildings
 - 8-3-1. General Remarks
 - 8-3-2. Fundamentals for Design
 - 8-3-3. Ultimate Strength and Ductility
 - 8-4. Seismic Performance of Underground Pipes

Part II. Earthquake Resistant Design of Civil Engineering Structures

- 1. General
 - 1-1. General Remarks
 - 1-2. Usage and Classifications of Structures in Aseismic Design
 - 1-3. Coefficients in Aseismic Design
 - 1-3-1. Outline
 - 1-3-2. Design Coefficients in the Seismic Coefficient Method
 - 1-3-3. Design Coefficients in the Modified Seismic Coefficient Method
 - 1-3-4. Design Coefficients in the Seismic Deformation Method
 - 1-3-5. Seismic Loads in the Dynamic Analysis Method
 - 1-4. Effects of Earthquakes During Construction
- 2. Aseismic Design of Foundations
 - 2-1. General Remarks
 - 2-2. Effects of Earthquakes
 - 2-3. Foundation Grounds and Allowable Bearing Forces
 - 2-4. Methods of Calculation of Stress, Displacements and Stability
 - 2-4-1. Outline
 - 2-4-2. Spread Foundations
 - 2-4-3. Caisson Foundations
 - 2-4-4. Pile Group Foundations
 - 2-4-5. Steel Walled Pipe Pile Foundations
 - 2-4-6. Multi-Column Foundations
- 3. Aseismic Design of Concrete and Steel Structures
 - 3-1. General Remarks
 - 3-2. Effects of Earthquakes
 - 3-3. Methods of Calculation of Stress and Displacement

- 3-3-1. Bridges (Reinforced Concrete Pier and Abutments)
- 3-3-2. Bridges (Steel Piers)
- 3-3-3. Concrete Dams (Gravity, Hollow Gravity and Arch Dams)
- 3-3-4. Tanks
- 3-3-5. Others

- 4. Aseismic Design of Soil Structures
 - 4-1. Effects of Earthquakes
 - 4-2. Methods of Calculation for Stability
 - 4-2-1. Outline
 - 4-2-2. Fill-Type Structures
 - 4-2-3. Artificial Island
 - 4-2-4. Artificial Ground
 - 4-2-5. Cutting Slope
 - 4-3. Improvement of Ground
 - 4-4. Safety
- 5. Aseismic Design of Underground Structures
 - 5-1. Effects of Earthquakes
 - 5-2. Stability of Surrounding Ground
 - 5-3. Methods of Calculation of Stress and Displacement
 - 5-3-1. Outline
 - 5-3-2. Underground Pipes
 - 5-3-3. Submerged Tunnels and Common Ducts
 - 5-4. Safety
- 6. Seismic Performance of Existing Structures
 - 6-1. System for Evaluating Seismic Performance
 - 6-2. System for Retrofitting Existing Structures
- 7. Design Details
 - 7-1. Foundations
 - 7-2. Substructures and Devices for Preventing the Fall of Superstructures
 - 7-2-1. Reinforced Concrete Piers and Abutments
 - 7-2-2. Devices for Preventing the Fall of Superstructures
 - 7-3. Soil Structures
 - 7-4. Underground Structures
 - 7-4-1. Outline
 - 7-4-2. Joints

Part III. Building Construction

- 1. General
 - 1-1. Scope
 - 1-2. Object of Aseismic Design
 - 1-3. Fundamental Method of Aseismic Design
 - 1-4. Design Procedures of Aseismic Design

- 1-4-1. Kinds of Design Procedures
- 1-4-2. Selection of Design Procedures
- 1-5. Methods of Aseismic Design
 - 1-5-1. Design Procedure I-A
 - 1-5-2. Design Procedure I-B
 - 1-5-3. Design Procedure II-A
 - 1-5-4. Design Procedure II-B
 - 1-5-5. Design Procedure III-A
 - 1-5-6. Design Procedure III-B
- 1-6. Parameters for Aseismic Design
 - 1-6-1. Seismic Hazard Zoning Factor
 - 1-6-2. Standard Base Shear Coefficient
 - 1-6-3. Soil Profile Types
 - 1-6-4. Fundamental Natural Period
 - 1-6-5. Vertical Distribution of Lateral Force
 - 1-6-6. Seismic Hazard Exposure Factor
 - 1-6-7. Limitation of Structural Discontinuities
 - 1-6-8. Story Drifts Limitation
 - 1-6-9. Structural Coefficient
 - 1-6-10. Ultimate Load Carrying Capacity
 - 1-6-11. Allowable Stresses and Allowable Load Carrying Capacity
- 2. Aseismic Design Method for Reinforced Concrete Buildings
 - 2-1. General
 - 2-2. Design Procedure
 - 2-3. Structural Coefficient
 - 2-4. Ultimate Story Shear Capacity
 - 2-5. Design of Building Elements and Structural Design Requirements
- 3. Aseismic Design Method for Steel Reinforced Concrete Buildings
 - 3-1. General
 - 3-2. Design Procedure
 - 3-3. Structural Coefficient
 - 3-4. Ultimate Story Shear Capacity
 - 3-5. Design of Building Elements and Structural Design Requirements
- 4. Aseismic Design Method for Steel Buildings
 - 4-1. General
 - 4-2. Design Procedure
 - 4-3. Structural Coefficient
 - 4-4. Ultimate Story Shear Capacity
 - 4-5. Design of Building Elements and Structural Design Requirements
 - 4-6. Story Drifts Limitation
- 5. Aseismic Design Method for Prestressed Concrete Buildings
 - 5-1. General
 - 5-2. Design Procedure

- 5-3. Structural Ceofficient
- 5-4. Ultimate Story Shear Capacity
- 5-5. Design of Building Elements and Structural Design Requirements
- 6. Aseismic Design Method for Conventional Wooden Buildings
 - 6-1. General
 - 6-2. Design Procedure
 - 6-3. Structural Coefficient
 - 6-4. Ultimate Story Shear Capacity
 - 6-5. Design of Building Elements and Structural Design Requirements
- 7. Aseismic Design Method for Non-Structural Elements
 - 7-1. General
 - 7-2. Required Aseismic Consideration for Non-Structural Elements
 - 7-3. Load and Story Drifts
 - 7-4. Selection of Construction Methods and Design of Elements
- 8. Assismic Design Method for Foundations and Retaining Walls
 - 8-1. General
 - 8-2. Design of Foundations
 - 8-3. Design of Retaining Walls
- 9. Safety Against Earthquakes of Existing Buildings
 - 9-1. System for Evaluating Earthquake Resistant Capacity
 - 9-2. System for Reinforcing Existing Buildings

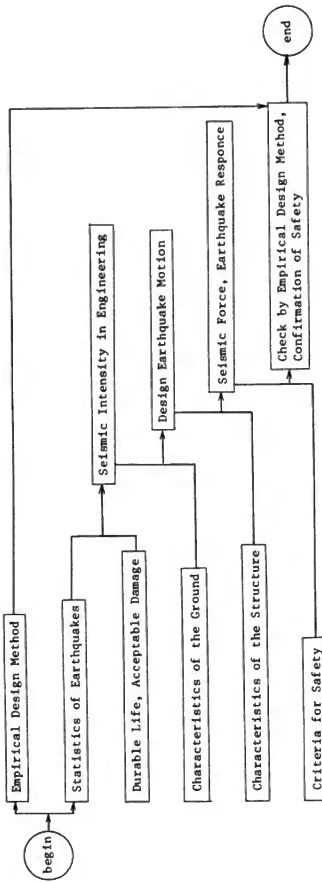


Fig. 3.1 Basic Procedure for Earthquake Resistant Design

Table 4.1 Seismic Zone Factor Δ_1

Zone	Value of Δ_1
A	1.0
B	0.85
C	0.7

Table 4.2 Ground Condition Factor Δ_2

Group	Definitions ¹⁾	Value of Δ_2
1	(1) Ground of the Tertiary era or older (defined as bedrock hereafter)	0.9
	(2) Diluvial layer ²⁾ with depth less than 10 meters above bedrock	
2	(1) Diluvial layer ²⁾ with depth greater than 10 meters above bedrock	1.0
	(2) Alluvial Layer ³⁾ with depth less than 10 meters above bedrock	
3	Alluvial layer ³⁾ with depth less than 25 meters, which has soft layer ⁴⁾ with depth less than 5 meters	1.1
4	Other than the above	1.2

(Notes)

- 1) Since these definitions are not very comprehensive, the classification of ground conditions shall be made with adequate consideration of the bridge site.
Depth of layer indicated here shall be measured from the actual ground surface.
- 2) Diluvial layer implies a dense alluvial layer such as a dense sandy layer, gravel layer, or cobble layer.
- 3) Alluvial layer implies a new sedimentary layer made by a landslide.

Table 4. 3 Structural Type Factor Δ_3

Definitions	Value of Δ_3
Steel Structures Concrete Structures Steel Reinforced Concrete Structures	1.0
Huge Massive Structures Soil Structures	0.5

Table 5.1 SEISMIC DESIGN COEFFICIENT AND DESIGN METHOD ACCORDING TO
DESIGN PROCEDURES AND STEPS

DESIGN PROCEDURE	SCOPE	STEP 1	STEP 2
I-A	CONVENTIONAL WOODEN BUILDINGS	$C_1 = Z \cdot eCo$ ELASTIC DESIGN WITH SEISMIC DESIGN COEFFICIENT AND ALLOWABLE STRESSES	STRUCTURAL DESIGN REQUIREMENTS
I-B	REINFORCED CONCRETE BUILDINGS WITH SHEAR WALL SYSTEM, etc.		
II-A	ORDINARY BUILDINGS	$C_1 = Z \cdot g_0(T) \cdot eCo$ ELASTIC DESIGN WITH APPROXIMATE MODIFIED SEISMIC DESIGN COEFFICIENT AND ALLOWABLE STRESSES	$C_2 = Z \cdot g_0(T) \cdot K_1 \cdot pCo$ PLASTIC DESIGN WITH APPROXIMATE MODIFIED SEISMIC COEFFICIENT AND APPROXIMATE ULTIMATE STORY SHEAR CAPACITY
II-B			$C_2 = Z \cdot g_1(T) \cdot K_2 \cdot pCo$ PLASTIC DESIGN WITH MODIFIED SEISMIC COEFFICIENT AND ULTIMATE STORY SHEAR CAPACITY
III-A	HIGH RISK BUILDINGS		$C_2 = Z \cdot g_1(T) \cdot K_2 \cdot pCo$ DYNAMIC DESIGN WITH MODAL ANALYSIS
III-B	SUPER HIGH RISE BUILDINGS		$C_2 = Z \cdot g_1(T) \cdot K_2 \cdot pCo$ DYNAMIC DESIGN WITH MODAL ANALYSIS AND TIME HISTORY ANALYSIS

 C_1 : SEISMIC DESIGN COEFFICIENT FOR STEP 1 eCo : STANDARD BASE SHEAR COEFFICIENT FOR STEP 1 C_2 : SEISMIC DESIGN COEFFICIENT FOR STEP 2 pCo : STANDARD BASE SHEAR COEFFICIENT FOR STEP 2 Z : SEISMIC HAZARD ZONING FACTOR K_1 : STRUCTURAL COEFFICIENT FOR APPROXIMATION $g_0(T)$: SOIL PROFILE SPECTRUM FOR APPROXIMATION K_2 : STRUCTURAL COEFFICIENT $g_1(T)$: SOIL PROFILE SPECTRUM T : FUNDAMENTAL NATURAL PERIOD OF BUILDING

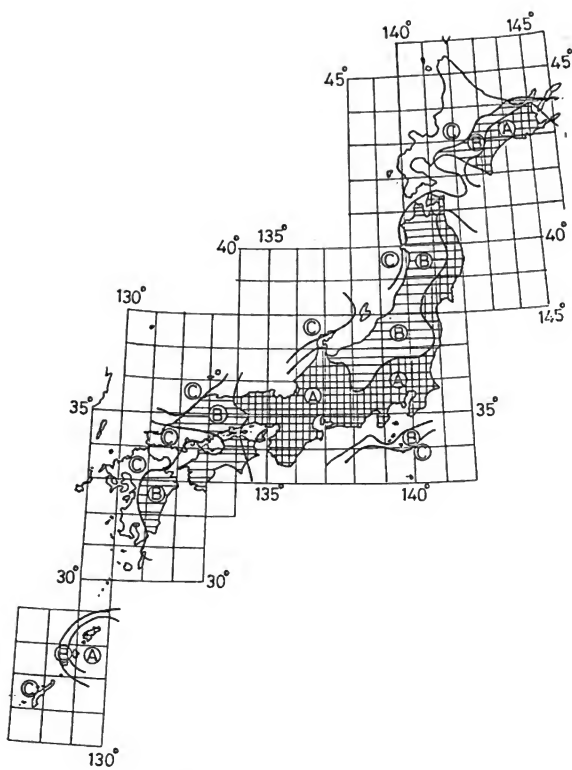


Fig. 5.1 Seismic Zoning

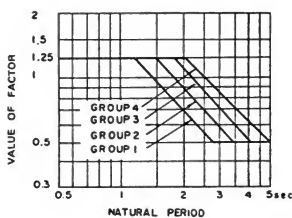
Table 5.2 STANDARD STRUCTURAL COEFFICIENT

	STRUCTURAL COEFFICIENT	DUCTILITY LEVEL		
		A	B	C
REINFORCED CONCRETE BUILDINGS	K_1	0.4	0.5	0.6
	K_2	0.3	0.4	0.5
STEEL REINFORCED CONCRETE BUILDINGS	K_1	0.3	0.4	0.5
	K_2	0.3	0.3	0.4
STEEL BUILDINGS	K_1	0.3	0.5	0.6
	K_2	0.3	0.4	0.5
WOODEN BUILDINGS	K_1	0.4		
	K_2	0.3		

DUCTILITY LEVEL A : DUCTILE BUILDINGS

DUCTILITY LEVEL B : INTERMEDIATE BUILDINGS

DUCTILITY LEVEL C : BRITTLE BUILDINGS

Fig. 4.2 Factor A₄

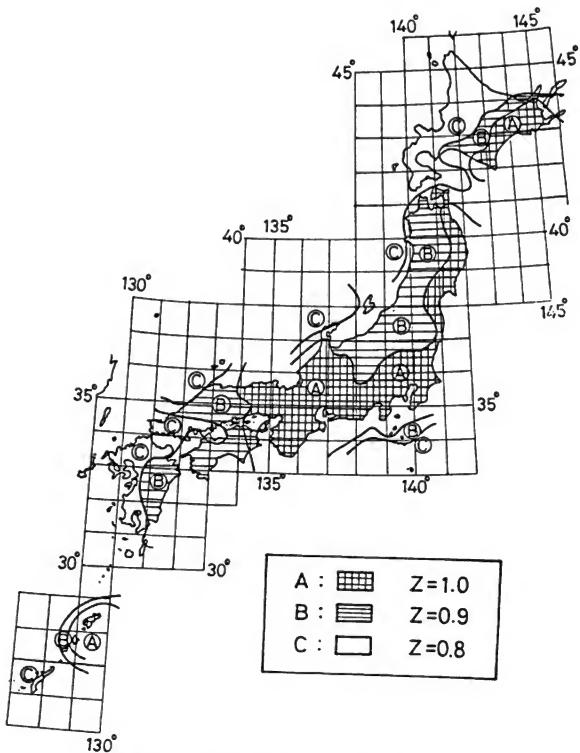


Fig. 5.1 Seismic Hazard Zoning Map of Japan

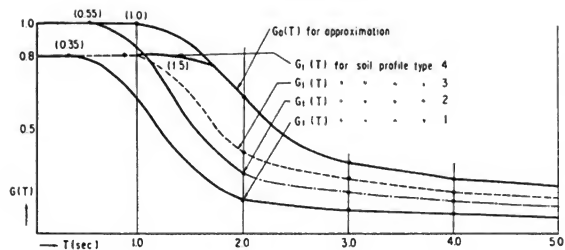


Fig. 5.2 Soil Profile Spectra

ON THE OBJECT POSTULATE FOR EARTHQUAKE-RESISTANT CODE

Kiyoshi Nakano, Assistant Director

Yuji Ishiyama, Chief Research Engineer

Yoshitsugu Aoki, Research Engineer

Kazumasa Watanabe, Research Engineer

Building Research Institute, Ministry of Construction

ABSTRACT

What the object of the earthquake-resistant code should be and how to define the object are the concerns of the object postulate. Since the seismic forces and the earthquake-resistant capacity of the buildings have certain dispersions, it is necessary to introduce the concept of the reliability to define the object postulate. This report deals with research on 1) dispersions, 2) relation between the earthquake-resistant capacity and the construction cost, 3) acceptable level of human risk, and 4) principle of social utility to optimize the importance factor, in order to define the object postulate for the earthquake-resistant code.

KEYWORDS: Acceptable level of human risk; construction costs; earthquake resistant code; expected seismic force; object postulate; reliability theory; social utility.

1. INTRODUCTION

Any design process is implicitly or explicitly constructed on a design system which is sometimes called a design code. It was shown by Niels C. Lind (1) that present structural design codes could well be understood by searching for basic eight principles or postulates. In his earlier paper, Kiyoshi Nakano (2) proposed an important postulate concerned with the probability of the death of occupants caused by the failure of structures.

The authors propose some postulates in addition to the above postulates, and classify the postulates, and examine their relations to structural codes. Furthermore, the object postulate, one of the most important postulates, is considered extensively.

2. CLASSIFICATION OF STRUCTURAL DESIGN POSTULATES

The following eight postulates which are included in several design codes were shown by Niels C. Lind.

- 1) Load postulate
- 2) Strength postulate
- 3) Design method (postulate)
- 4) Principle of constant reliability
- 5) Postulate of data sufficiency
- 6) ISO format
- 7) Cornell's format
- 8) Linearized factor format

The authors proposed the following postulates in addition to the above postulates (2,3),
9) Earthquake load postulate proposed in AIJ draft (4)

$$(a) \mu_r \leq \frac{\mu_a}{I_r},$$

$$(b) \frac{\delta_r}{H_r} \leq \frac{1}{125},$$

$$(c) \frac{\sum_{r=1}^i \delta_r}{\sum_{r=1}^i H_r} \leq \frac{1}{150}, \quad i = \text{number of stories},$$

where,

μ_r = ductility factor of the r -th story,

μ_a = permissible ductility factor which is fixed in accordance with the kind of structures (such as steel structures, reinforced concrete structures, etc.),

I_r = importance factor which is fixed in accordance with the occupancy of structures and with the structural importance of structural members,

δ_r = inter-story deformation (inter story drift) of the r -th story, which is caused by elasto-plastic response,

H_r = story height of the r-th story.

10) The postulate for optimizing monetary expenses

$$\frac{\partial L}{\partial \eta} = 0, \quad (2-1)$$

where,

$$L = I + pF, \quad (2-2)$$

L = expected value of losses

I = initial expenses,

p = probability of failure,

F = losses caused by the failure = αI ,

$$n = (I - A_0)/A_1 \quad (2-3)$$

= central safety factor = (R^*/S^*) ,

R^* = expected value of resistance,

S^* = expected value of load effect,

A_0, A_1 = constants corresponding to the kind of structures.

11) Starr's postulate (2,5),

$$P_f = p (R^* \leq S^*) \leq r_{cr} \cdot \theta \cdot A, \quad (2-5)$$

where,

P_f = probability of failure,

r_{cr} = standard death rate (death rate per one hour, unit is 10^{-9}),

θ = probability of the death of occupants caused by the failure of structures,

A = factor which is fixed in accordance with occupancies (1.0 for housings and office buildings which are indispensable for life, 1000 for leisure facilities).

12) Nakano's postulate (2),

$$P_f \leq r_{cr} \cdot \theta (1 + b + g) \cdot A, \quad (2-6)$$

where,

b = coefficient of density (number of occupants per unit floor area),

g = coefficient of evacuation (constant fixed in accordance with easiness of evacuation in case of emergency).

The combination of the postulates in various design codes are shown in Table 2-1. Furthermore, we have attempted a classification of the postulates as shown in Table 2-2. That is, the traditional design processes are governed by three kinds of postulates: load strength postulate, comparison postulate, and object postulate. The object postulate is concerned with design philosophy on social needs for structural safety, therefore we shall consider the object postulate more extensively.

3. SURVEY ON EARTHQUAKE-RESISTANT CAPACITY AND ITS DISPERSION

It is almost impossible to measure the earthquake-resistant capacity of each building as a total system. Accordingly, we tried to evaluate it by an expert survey which would make use of the intuition of the experts most effectively. About two hundred experts from four different fields of structural engineering; 1) constructors, 2) administrators, 3) designers and 4) researchers or educators, participated in this survey. From the result of this survey, the earthquake-resistant capacity and its dispersion of buildings are given in Fig. 3-1. In Fig. 3-2, the weighted factors are set forth depending on seven major factors; 1) designer, 2) design cost, 3) design term, 4) constructor, 5) construction cost, 6) construction term, and 7) material.

From Fig. 3-1, it can be seen that the cast in situ reinforced concrete wall buildings, super high rise steel buildings and high rise steel buildings are considered to have good earthquake-resistant capacities. On the contrary, the reinforced concrete block buildings, conventional wooden buildings and prefabricated wooden buildings seem to have rather small resistant capacity against earthquakes.

As to the dispersions of earthquake-resistant capacity, the super high rise buildings, prestressed concrete buildings and prefabricated H-steel reinforced concrete buildings have small variance and the value of c.o.v. (coefficient of variance) is about 0.25. The cast in situ reinforced concrete buildings, conventional wooden buildings and low rise steel buildings have large variance and the value of c.o.v. is about 0.45.

From Fig. 3-2 we can assume that among seven major factors concerning earthquake-resistant capacity, the level of the designer and the level of the constructor are the most influential factors.

From the result of this survey, it was also found that the administrators and the constructors take an optimistic view of earthquake resistant capacity of buildings, and that the designers and the researchers or educators have a pessimistic one.

4. RELATION BETWEEN EARTHQUAKE-RESISTANT CAPACITY AND CONSTRUCTION COST

It is evident that the construction cost of the building would be influenced by the seismic design coefficient which is one of the main factors controlling the earthquake-resistant capacity. In this chapter, the relation between the seismic design coefficient and the construction cost is discussed. To analyze the problem, the following assumptions are adopted.

- 1) Elastic design with seismic design coefficients and allowable stresses is used.
- 2) The range of seismic design coefficient is from 0.2 to 1.0.
- 3) Two cases of construction cost ratio; i) columns and girders, and ii) column, girders, beams and slabs, are considered. The construction cost of foundations, other non-structural members and finishings are not included in both cases.
- 4) The costs of columns and girders are dependent on the seismic design coefficient, but the beams and slabs are independent of it.
- 5) The costs of columns and girders are approximated by the formula proposed by Nakagawa (6).

6) Two structural systems; i) steel frame buildings and ii) reinforced concrete buildings, are considered. The numbers of stories are five and ten.

Under these assumptions the cost ratio is given in accordance with following formula;

$$\gamma = 1 + R (C - 0.2) \quad (4-1)$$

where,

$$\gamma = \text{cost ratio} (= \frac{\text{cost by seismic design coefficient equals } C}{\text{cost by seismic design coefficient equals } 0.2})$$

R = cost coefficients as given in Table 4-1

C = seismic design coefficient ($0.2 \leq C \leq 1.0$)

Two examples of Eq. (4-1) are shown in Fig. 4-1-(1) for steel frame buildings and Fig. 4-1-(2) for reinforced concrete buildings.

5. ACCEPTABLE LEVEL OF HUMAN RISK

The point of view of the security of human lives may be considered as one of the most important criteria for structural design.

In the domain of the security of human lives, we find some discussions that propose several criteria; such as those of David E. Allen, of H. G. Otway, of Starr, of K. Nakano and of K. Watanabe. But we cannot find any proposition that achieves the practical level.

We dared to attempt to overcome such a difficult state, and this report proposes an acceptable level of human risk, observing the fluctuations in the evolution of the ordinary death rate and assuming the existence of insensible range of the fluctuations in the death rate.

- 1) The sense of average risk level is supposed to be based on the average death rate \bar{d} for a period of several years which precede the point of time for this sense. This average death rate may be considered as the basic death rate for the sense of risk.
- 2) Taking the standard deviation σ_d in the evolution of death rate for the same period as that of the average death rate, the rate of fluctuation of death rate Δd is obtained as $\Delta d = \sigma_d / \bar{d}$.
- 3) The observation through a sufficiently long term of the rates of fluctuation, each of which is calculated on the same period of time, permits to suppose that the rate of fluctuation is nearly constant. So that if the mean level of the rates of fluctuations $\bar{\Delta d}$ is obtained,

$$\Delta d = \bar{\Delta d} = \text{Constant.}$$

- 4) Thus the insensible range of fluctuation of death rate σ_{dins} is supposed as $\sigma_{dins} = \bar{\Delta d} \cdot d$.

As for the acceptable level of human risk, this report proposes the acceptable death rate from earthquake, d_{sac} .

It may be considered that the average death rate \bar{d} includes a part of the death rate from earthquakes in certain proportion e . The death rate from earthquakes, \bar{d}_s , included in the average death rate is obtained as $\bar{d}_s = e \cdot \bar{d}$.

The acceptable death rate from earthquake, d_{sac} , is proposed as the sum of the part of the death rate from earthquakes included in the average death rate \bar{d}_s and the insensible range of fluctuation of death rate σ_{dins} : $d_{sac} = \bar{d}_s + \sigma_{dins} = e \cdot \bar{d} + \sigma_{dins}$.

On the supposition that the number of deaths from earthquake is proportional to the number of destroyed buildings, a proposition is established that the acceptable rate of destruction from earthquake, P_{fac} , is to be obtained as a proportional value to the acceptable death rate from earthquakes, d_{sac} :

$$P_{fac} = d_{sac} \cdot \frac{P}{Y \cdot N_b \cdot f_s},$$

where,

P = population of the area concerned

Y = probability of deaths in case of destruction of a building (the number of deaths/the number of destroyed buildings)

N_b = number of buildings in the area concerned.

f_s = frequency of earthquakes on the area concerned.

6. PRINCIPLE OF SOCIAL UTILITY TO OPTIMIZE IMPORTANCE FACTOR

The object postulate is concerned with social utilities, that is, we assume that the value of structure is comprised of the construction cost (negative utility) and the social-human utilities. We are going to establish an object postulate which formulates the value of importance factor corresponding to the maximum total utilities.

The following concepts are used in this discussion,

- (1) Load means a scalar having an expected value \bar{s} and a coefficient of variance Ω_s .
- (2) Strength means a potential of structures corresponding to a certain limit state designated in design. The strength is also a scalar having an expected value \bar{R} and a coefficient of variance Ω_R .
- (3) Magnifying factor of strength means the ratio defined by the following equation

$$\theta = R/R_0, \quad (6-1)$$

where,

R = actual strength of structure,

R_0 = strength corresponding to a certain limit state under a defined standard load effect S_0 .

Particularly, we shall distinguish the value of magnifying factor for ordinary buildings from that for public buildings. The ratio of magnifying factors is called an importance factor, and it may be defined as follows:

$$\theta^* = \theta/\theta_0, \quad (6-2)$$

where,

θ_0 = magnifying factor for ordinary buildings.

(4) Probability of reaching limit state is defined as follows:

$$P = P (\theta_0 R_0 < S) \quad (6-3)$$

$$P_2 = P (\theta R_0 < S) \quad (6-4)$$

Equation (6-3) is applied to ordinary buildings and equation (6-4) is applied to public buildings such as hospitals, public facilities, public halls, and so on.

(5) Social utilities are presented by four utilities, U_1 , U_2 , U_3 and U_4 as shown in Table 6-1.

Table 6-1 Social utilities

STATE OF ORDINARY BUILDINGS	STATE OF PUBLIC BUILDINGS	
	(1) Undamaged $\theta R_0 \geq S$	(2) Damaged $\theta R_0 < S$
(1) Undamaged State ($\theta_0 R_0 \geq S$)	U_1	U_3
(2) Damaged State ($\theta_0 R_0 < S$)	U_2	U_4

(6) Construction cost means the present value of initial construction cost. We define C_0 , construction cost in the payment time, and T_0 , time lag between the payment time and the time of putting the building in use. The construction cost can then be shown by the following equation with the interest rate r ,

$$C = C_0 (1 + r)^{T_0} \quad (6-5)$$

With the above conception, we can examine the social utilities for the building. In the first year, the expected value of social utility is as follows:

$$U^{(1)} = (1-p) (1-p_2) U_1 + p (1-p_2) U_2 + (1-p) p_2 U_3 + pp_2 U_4 \quad (6-6)$$

where,

$$P = \text{prob } (\theta_0 R_0 < S)$$

$$P_2 = \text{Prob } (\theta R_0 < S).$$

The present value of social utility in the second year is

$$U^{(2)} = \frac{1 - P_2}{1 + r} U^{(1)} \quad (6-7)$$

Similarly, the present value in the nth year is

$$U^{(n)} = \left(\frac{1 - P_2}{1 + r}\right) U^{(n-1)} \quad (6-8)$$

Consequently, the sum of the social utility in life span of the building T is obtained as follows:

$$U_s = \sum_{i=1}^T U^{(i)} = U^{(1)} \sum_{i=0}^{T-1} \left(\frac{1 - P_2}{1 + r}\right)^i \quad (6-9)$$

The total utility is represented by the following equation,

$$U = U_s - C \quad (6-10)$$

We must maximize the value of U from a viewpoint of social safety or urban safety. Therefore, we obtain the following postulate by differentiating Eq. (6-10) with respect θ ,

$$-\frac{\partial P_2}{\partial \theta} = \left[\frac{\partial C}{\partial \theta}\right] / \left[\frac{\partial U_s}{\partial P_2}\right] \quad (6-11)$$

The optimum value of importance factor can be obtained from the above equation when the distribution functions of random values S and R are given. Actually, if the distribution functions of load effect and strength are normal distributions $N[\bar{S}, \sigma_s]$, $N[\bar{R}, \sigma_R]$ respectively, the optimal values of magnifying factor and importance factor are expressed approximately by the following equations respectively:

$$\theta = \frac{1}{\theta_0} + \delta \sqrt{2 \ln \left(\frac{1}{\sqrt{2\pi} k \delta} \right)}, \quad (6-12)$$

$$\theta_* = \frac{1}{\theta_0^2} + \frac{\delta}{\theta_0} \sqrt{2 \ln \left(\frac{1}{\sqrt{2\pi} k \delta} \right)}, \quad (6-13)$$

where,

$$\delta = \frac{\sqrt{\sigma_R^2 + \sigma_S^2}}{\bar{R}} \quad (6-14)$$

$$k = \left(\frac{\partial C_0}{\partial \theta} / C_0 \right) / \mu \quad (6-15)$$

and

$$\mu = \frac{(1+r)^T - 1}{(1+r)^{T^*} - 1} \cdot \frac{1 - U_1/U_1}{(1+r)^{T-T^*}} + \frac{(1+r)^T - 1 - rT}{(1+r)^{T^*} - 1} \cdot \frac{1 + pU_2/U_1}{r(1+r)^{T-T^*}} \quad (6-16)$$

The auxiliary parameter δ and k are called synthetic coefficient of variance and cost performance sensibility, respectively, and the parameter T^* means the turnover year of the buildings. The relation among the optimal values of magnifying factor θ , synthetic c.o.v. δ and the cost performance sensibility k is shown in Fig. 6-1.

7. CONCLUDING REMARKS

From Chapters 3 to 6, we have suggested several approaches to settle the object postulate for the earthquake-resistant code. The details of each chapter should be investigated more extensively and intensively. Though more suitable ways to determine the object postulate might be discovered in the future, the following items are the most influential factors to settle the object postulate from the surveys we have conducted.

- 1) earthquake-resistant capacity of buildings
- 2) expected seismic force
- 3) earthquake-resistant capacity and construction cost
- 4) acceptable human risk
- 5) social utility

8. REFERENCES

- (1) Niels C. Lind, Consistent Partial Safety Factors, Journal of the Structural Division, Proceedings of ASCE, June, 1971, pp. 1651-1669.
- (2) Kiyoshi Nakano, State-of-the-Art Report on Safety of Building Structures. Report of the Building Research Institute, No. 73, March, 1976.
- (3) Kiyoshi Nakano, Yoshitsugu Aoki and Kazumasa Watanabe, A Proposal for a Rational Aseismic Structural Design Process. BRI Research Paper No. 68, Building Research Institute, September, 1976.
- (4) Committee Report, Architectural Institute of Japan, 1975.
- (5) Chauncey Starr, Social Benefit versus Technological Risk. Science, Vol. 165, September 19, 1969, pp. 1232-1238.
- (6) Atsushi Nakagawa, Structural Cost Planning of High Rise Buildings. Kenchiku Gitjutsu No. 238, June, 1971.

Table 2-1 Postulates included in structural design codes

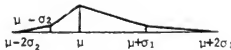
Name of Code	Postulate										
	1	2	3	4	5	6	7a	7b	8	9	11
ISO draft	*	*	*	*	*	*					
AIJ RC code	*	*	*								
AIJ earth-quake load draft	*	*								*	
NORDIC CODE (A-Type)	*	*		*	*		*	*			*
NORDIC CODE (B-Type)	*	*	*			*				(*)	
Proposal of Lind	*	*	*		*						
Proposal of Cornell	*	*		*	*		*	*			
Proposal of Ravindra	*	*	*	*	*						*
FIP-CEB Code	*	*	*			*					

Table 2-2 Classification of postulates

The first Group: LOAD-STRENGTH POSTULATE	Main Postulates: 1, 2 Sub Postulates: 6, 8, 7b	The main postulates are basic postulates for design system. The sub postulates are the modification of the main postulate for the purpose of facilitating probabilistic treatment of design variables.
The Second Group: COMPARISON POSTULATE	Main Postulates: 3, 4 Background Postulates: 5, 7a Sub Postulates: 9, 10, 11, 12	The main postulate 3 is representing the classical design procedure. The main postulate 4 is representing probabilistic concepts. The background postulates supplies logical support for the postulate 4. The sub postulates are used together with the postulate 3 to introduce considerations of deformation.
The Third Group: OBJECT POSTULATE	Main Postulates: 3, 9, 10, 11, 12	The postulate 3 is an object postulate as well as the comparison postulate. The postulates 10, 11, and 12 are used together with the postulate 4.

μ : mean value

σ_1, σ_2 : standard deviation



CONVENTIONAL WOODEN
BUILDINGS

PREFABRICATED WOODEN
BUILDINGS

CAST IN SITU REINFORCED
CONCRETE BUILDINGS

CAST IN SITU REINFORCED
CONCRETE WALL BUILDINGS

PREFABRICATED REINFORCED
CONCRETE WALL BUILDINGS

STEEL REINFORCED
CONCRETE BUILDINGS

PREFABRICATED H-STEEL
REINFORCED CONCRETE
BUILDINGS

SUPER HIGH RISE
STEEL BUILDINGS

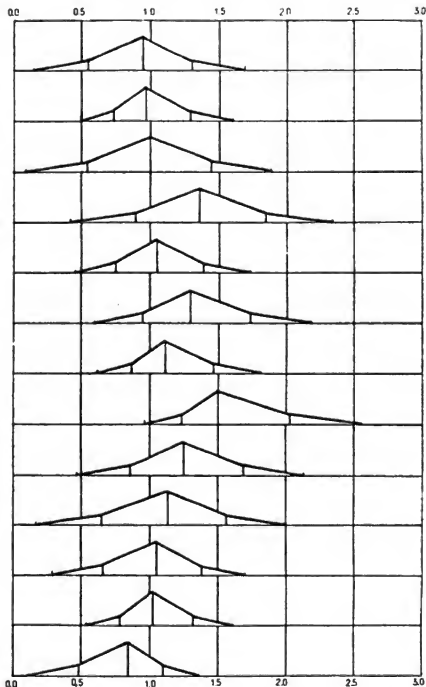
HIGH RISE STEEL
BUILDINGS

LOW RISE
STEEL BUILDINGS

LARGE SPAN STEEL
BUILDINGS

PRESTRESSED CONCRETE
BUILDINGS

REINFORCED CONCRETE
BLOCK BUILDINGS



(Normalized by the mean value of cast in situ reinforced concrete buildings)

Fig. 3-1 RELATIVE EARTHQUAKE-RESISTANT CAPACITY AND ITS
DISPERSION OF BUILDINGS

Factor (1) : Level of Designer
 (2) : Design Cost
 (3) : Design Term
 (4) : Level of Constructor
 (5) : Construction Cost
 (6) : Construction Term
 (7) : Material

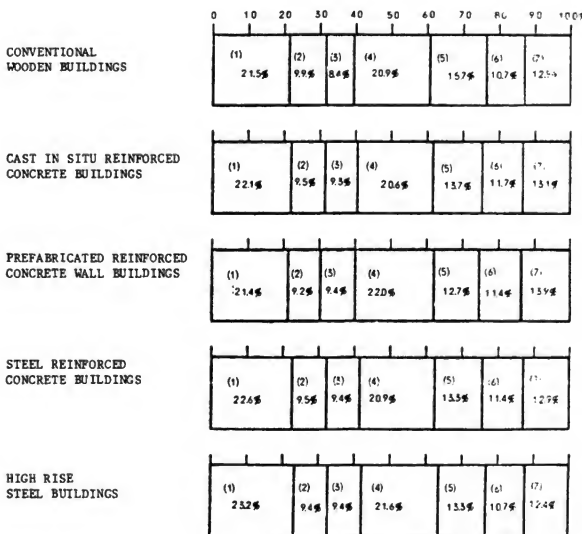


Fig. 3-2 WEIGHTED FACTORS OF EARTHQUAKE-RESISTANT CAPACITY

Table 4-1-(1) Cost Coefficients of Steel Frame Buildings

N	n		R		
	x	y	$\mu = 1.0$	$\mu = 0.6$	$\mu = 0.5$
5	5	3	2.0	1.2	1.0
	5	5	2.0	1.2	1.0
	∞	5	2.0	1.2	1.0
	∞	∞	2.0	1.2	1.0
10	5	3	2.0	1.2	1.0
	5	5	2.0	1.2	1.0
	∞	5	2.0	1.2	1.0
	∞	∞	2.0	1.2	1.0

Table 4-1-(2) Cost Coefficients of Reinforced Concrete Buildings

N	n		R		
	x	y	$\mu = 1.0$	$\mu = 0.4$	$\mu = 0.3$
5	5	3	3.2	1.25	0.95
	5	5	3.0	1.22	0.92
	∞	5	3.1	1.23	0.93
	∞	∞	3.1	1.24	0.93
10	* ∞	∞	3.7	1.43	1.10
	5	3	4.0	1.60	1.17
	5	5	3.8	1.53	1.13
	∞	5	3.8	1.55	1.15
	∞	∞	4.0	1.60	1.17

N : number of stories

n : number of spans

 μ : cost ratio of columns and girders to total structural cost
($\mu = 1.0$ means that cost of columns and girders is total structural cost)

* : aseismic shear wall, columns and girders system

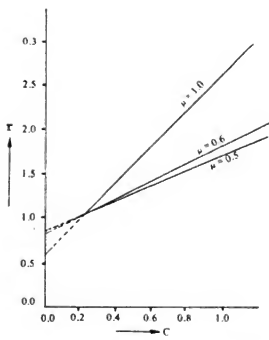


Fig. 4-1-(1) Cost Ratio of Steel Frame Buildings

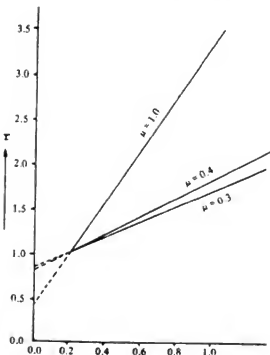


Fig. 4-1-(2) Cost Ratio of Reinforced Concrete Buildings
 ($N=5$, $n=0$ in both directions, no aseismic shear walls)

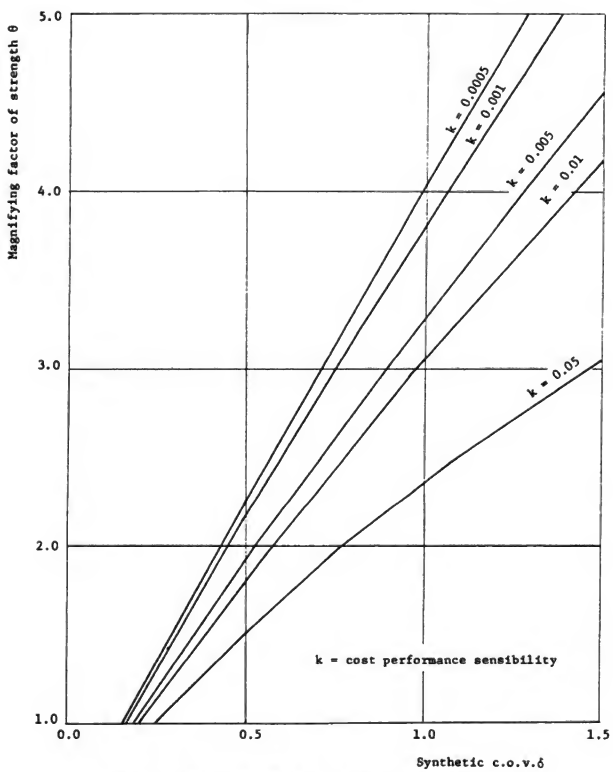


Fig. 6-1 Relation among k , θ and δ

The Earthquake Response of Hysteretic Structures

W. D. IWAN and N. C. GATES
California Institute of Technology, Pasadena, California

ABSTRACT

The earthquake response of a broad class of hysteretic structures is investigated. Inelastic response spectra are determined. Based on these spectra, an effective linear period and damping are defined for each type of hysteretic structure as a function of ductility. A simple empirical formula is presented which may be used to estimate the response of a general hysteretic structure given the linear response spectrum of the excitation. The predictions obtained from this formula are compared with those of another frequently used scheme for estimating the response of hysteretic structures.

INTRODUCTION

Most modern building structures are designed to respond in a ductile manner during a major earthquake. In a steel structure, ductility is associated with the local yielding of steel structural elements. For cyclic loading, the resulting load-deformation behavior is hysteretic and the hysteresis loops are quite stable with successive loading. In reinforced concrete structures, ductility arises both from the yielding of the steel reinforcing and the cracking and crushing of the concrete. The resulting load-deformation behavior is again hysteretic. However, in this case, the hysteresis loops tend to degrade in both energy dissipation and stiffness with successive loading. It is important for the safe design of structures that the response of both degrading and nondegrading hysteretic structures be well understood.

There have been numerous studies of the earthquake response of simple non-degrading hysteretic structures. Based on studies of the most elementary systems, it has been suggested that for moderate to long structural periods, the peak amplitude of response of the hysteretic system is very nearly the same as that of a linear system with the same nominal period and viscous damping independent of the ductility ratio of the response [1]. There have been relatively few studies of the earthquake response of degrading structures and no general design guidelines have yet been

proposed. However, the equal displacement rule is often employed for this type of structure as well [2].

The purpose of the present investigation is to examine the earthquake response of a general class of single-degree-of-freedom hysteretic structures and to evaluate the merit of certain simplified methods for estimating the response of such structures.

INELASTIC RESPONSE SPECTRA

It is assumed that the equation of motion of the structure or a particular mode of the structure can be written in the form

$$\ddot{x} + 2\zeta_0 \omega_0 \dot{x} + \omega_0^2 f[x(t)]/k_0 = a(t) \quad (1)$$

where x is the generalized relative displacement, ζ_0 is the fraction of viscous damping, ω_0 is the natural frequency, $f[x(t)]$ is the generalized restoring force, k_0 is the nominal stiffness, and $a(t)$ is the excitation acceleration. In what follows, it is assumed that $\zeta_0 = 2\%$. The nominal period of the system is $T_0 = 2\pi/\omega_0$.

The generalized restoring force $f(x)$ is assumed to be hysteretic. In this investigation, the particular form of $f(x)$ is derived from a combination of linear elastic and coulomb slip elements as indicated in reference [3]. The restoring force model incorporates the major features associated with linear, simple hysteretic and degrading hysteretic behavior. Six specific systems are considered and the restoring force diagrams for these systems are shown schematically for cyclic loading with monotonically increasing amplitude in Figure 1.

The symbol BLH denotes the bilinear hysteretic restoring force model. The other systems are designated by a three number code. The first set of two digits specifies the ratio of the strength of the simple hysteretic component of the model to that of the degrading component with 1.0 denoted by 10. The second set of two digits specifies the ratio of the generalized yield displacement of the simple hysteretic component to that of the degrading component with 1.0 denoted by 10. The third set of two digits specifies the ratio of the failure loads associated with tensile and compressive failure for the basic degrading component of the model with 0.1 denoted by 10. In reinforced concrete, the simple yielding component of the model would be representative of the behavior of the reinforcing steel and the degrading component

would be representative of the behavior of the concrete. In this case, the third set of digits would be roughly proportional to the ratio of the cracking to crushing strength of the concrete. The limiting fully yielded stiffness for each case is taken to be 5% of the nominal stiffness k_0 .

The ductility ratio of the response is defined as

$$\mu = x_{\max} / x_y \quad (2)$$

where x_{\max} is the maximum amplitude of response and x_y is the generalized yield displacement of the simple yielding component of the system.

In the present investigation, the structural model described by equation (1) is excited by an ensemble of twelve earthquake acceleration time histories $a(t)$ which are chosen to be representative of a variety of different types of earthquake excitation. An effective peak acceleration level A^* is determined for each earthquake by finding the scale factor necessary to minimize the mean square difference between the 2% damped response spectrum of the earthquake in question and the NRC 1.60 design response spectrum [4] in the period range of 0.2 to 4.0 seconds. The latter spectrum is adjusted to a mean value spectrum by subtracting one σ from the published spectrum. The twelve earthquakes and their effective peak accelerations are given in Table I.

The response of each structural model to each earthquake of the ensemble is calculated numerically. The yield level of the structural model x_y is varied until a desired ductility ratio μ is obtained and the resulting maximum generalized displacement x_{\max} is recorded. In the present investigation, this is done for nine different nominal structural periods ranging from 0.4 to 4.0 seconds and ductility ratios of 2, 4 and 8. The resulting values of x_{\max} are used to construct inelastic response spectra for each hysteretic system. In order to minimize the effects of the local variations in the spectral content of each earthquake, the inelastic response spectra are normalized by A^* and averaged over the twelve earthquakes. This defines a family of normalized averaged inelastic response spectra for each structural model. A typical family of inelastic pseudo-velocity response spectra is shown in Figure 2 for the highly degrading system 02-10-00. Also shown for comparison are the averaged linear response spectra for 2, 5 and 10% viscous damping.

OPTIMAL EFFECTIVE LINEAR PARAMETERS

An examination of Figure 2 reveals that the overall shape of the averaged inelastic spectrum for a given value of μ closely resembles that of some linear spectrum except for a translation along a line of constant spectral displacement (a line with slope of minus one on the log-log PSV diagram). For example, a linear spectrum for $\zeta = 5\%$ may be translated to fit very closely the inelastic spectrum for $\mu = 2$. This fact may be used to define a linear system which gives very nearly the same spectral response as a given hysteretic system.

Let $SD_{nl}(EQ(j), SYS(k), \mu, T_i, \zeta_o)$ be the spectral displacement of the k^{th} hysteretic system $SYS(k)$ with nominal period and damping T_i and ζ_o at ductility μ to the j^{th} earthquake, $EQ(j)$. Let $SD_l(EQ(j), T, \zeta)$ be the spectral displacement of a linear system with period T and viscous damping ζ to the j^{th} earthquake $EQ(j)$. Then, consider a shifted linear spectrum defined by $SD_l(EQ(j), T_i(T_e/T_o), \zeta_o + \zeta_e)$. In this way, T_e/T_o represents a period shift ratio and ζ_e an added damping with respect to the linear spectrum. Let δ_{ijk} be the difference between the nonlinear inelastic spectral displacement and the shifted linear spectral displacement defined by

$$\delta_{ijk} = \frac{SD_l(EQ(j), T_i(T_e/T_o), \zeta_o + \zeta_e)}{SD_{nl}(EQ(j), SYS(k), \mu, T_i, \zeta_o)} - 1 . \quad (3)$$

Then, a measure of the overall difference or error between the averaged nonlinear and averaged shifted linear spectrum will be

$$\bar{\epsilon}(k) = \left[\frac{1}{9} \sum_{i=1}^9 \left(\sum_{j=1}^{12} \delta_{ijk} \frac{SD_{nl}}{SD_{nl}} \right)^2 \right]^{\frac{1}{2}} . \quad (4)$$

$\bar{\epsilon}(k)$ will be referred to as the root mean square (rms) averaged spectral error.

An optimal period shift and added damping can be defined for each hysteretic system by minimizing $\bar{\epsilon}(k)$ with respect to T_e/T_o and ζ_e . Let the optimal parameters be noted by T_{e_m}/T_o and ζ_{e_m} and let $\bar{\epsilon}_m(k)$ be the minimum value of $\bar{\epsilon}(k)$. Then

$$\bar{\epsilon}(k) = \bar{\epsilon}_m(k), \text{ a minimum, when } T_{e_m}/T_o = T_{e_m}/T_o \text{ and } \zeta_e = \zeta_{e_m} . \quad (5)$$

This defines an optimal effective linear system for any particular nonlinear system.

The optimal period shift and added damping for the six hysteretic systems considered herein is presented in Table II along with the minimum rms averaged spectral error $\bar{\epsilon}_m$ as a function of ductility ratio. It is observed that the averaged spectral error is in no case greater than 6%. Hence, it is concluded that the optimal effective linear parameters are capable of providing an excellent description of the averaged inelastic response spectrum for hysteretic structures of the type considered. As a general trend, it will be noted that both the optimal period shift and damping tend to increase with increasing ductility μ for all systems. It will also be noted that the more degrading systems tend to have greater period shift particularly at the largest ductilities. The effective added damping is in the range of 6 to 12% for all cases.

A SIMPLE EMPIRICAL MODEL

If graphed as a function of μ without regard to system, the results presented in Table II suggest a simple empirical formula for approximating T_e/T_o and ζ_{e_m} . This may be expressed in the form

$$\begin{aligned} T_e/T_o &= 1 + \frac{1}{10}(\mu-1) \\ \zeta_e (\%) &= 6(\mu-1)^{\frac{1}{3}}. \end{aligned} \tag{6}$$

This formula may be used to predict the response of a nonlinear hysteretic structure given the linear response spectrum of the excitation. This is accomplished by shifting the period from its nominal value by an amount T_e/T_o and introducing an additional viscous damping ζ_e . The accuracy of this formula will now be examined and compared with another simple prediction method.

EVALUATION OF RESPONSE PREDICTIONS

The merit of any scheme for predicting the earthquake response of a hysteretic structure may be measured by the magnitude of the error between the actual and predicted response over the period range of interest. The ability of a given scheme to predict gross response features can best be seen with reference to a smooth or averaged response spectrum as shown in Figure 2. In this case, the root mean square averaged spectral error $\bar{\epsilon}(k)$ defined by equation (4) is an appropriate error measure. The ability of a scheme to predict the finer details of the response can

best be seen with reference to a particular earthquake with all of its spectral variations. For this purpose, an unaveraged root mean square spectral error $\epsilon(k)$ will be an appropriate error measure where

$$\epsilon(k) = \left[\frac{1}{108} \sum_{i=1}^9 \sum_{j=1}^{12} \delta_{ijk}^2 \right]^{\frac{1}{2}} \quad (7)$$

In this investigation, the response predictions of the empirical formula will be compared with those of the optimal parameters and those of the Newmark-Hall method [1]. The Newmark-Hall method was originally formulated as a technique for generating an inelastic response spectrum from a smooth linear design spectrum. In this method, the linear spectrum is modified according to different rules depending on period range. For periods greater than or equal to some value T' , the method follows the equal displacement rule and the inelastic displacement or pseudo-velocity spectrum is identical to the linear spectrum. For periods in an interval slightly less than some value T'' , the inelastic spectral displacement is obtained from the linear spectral displacement by multiplying by a factor of $\bar{\mu}/\sqrt{2\bar{\mu}-1}$ where $\bar{\mu}$ is an effective ductility ratio. Between T' and T'' the spectral behavior changes continuously.

In order to obtain a direct comparison with the empirical formula, the Newmark-Hall method is herein applied directly to the averaged linear 2% damped spectrum or to the corresponding spectrum of an individual earthquake as required rather than to a smoothed or bounding spectrum. Use of a bounding spectrum has been found to give response results which are considerably over conservative. The values of T' and T'' are taken to be 0.5 and 0.4 seconds respectively and the effective ductility ratio $\bar{\mu}$ is taken to be equal to μ . This latter assumption has very little effect since the method gives results which are independent of μ over most of the period range considered.

Table III gives the rms spectral error $\epsilon(k)$ and the rms averaged spectral error $\bar{\epsilon}(k)$ resulting from response predictions based on the optimal parameters presented in Table II, the effective parameters from empirical formula (6) and the Newmark-Hall method. It is seen that all of the methods considered give better response predictions for an averaged or smoothed response spectrum than for the

spectrum of a particular earthquake. This is evident from the much lower values for the averaged spectral error $\bar{\epsilon}$ as compared to the unaveraged spectral error ϵ . For the optimal parameters, the ratio of ϵ to $\bar{\epsilon}$ is approximately four and for the two predicting schemes, the ratio is approximately two. This particular feature of the data is not at all surprising in light of the variations in frequency content associated with any particular earthquake of an ensemble.

An important observation from Table III is that for given ductility, the spectral errors resulting from either the empirical formula or the Newmark-Hall method are comparable for all of the systems considered. Hence, it may be concluded that very marked differences in hysteretic behavior of the type considered herein have only a secondary effect on the accuracy of a given response prediction technique. This does not imply that there are no systematic differences in the response of one system versus another, but it does imply that these differences are of the order of the error inherent in the two simple prediction schemes.

For all ductilities considered, Table III indicates that the spectral error ϵ resulting from the empirical formula is comparable to that resulting from use of the optimal parameters. This error is typically of the order of 20% which would be satisfactory for most design purposes. The error resulting from the Newmark-Hall method is generally more than twice that of the empirical formula. Even for the simple bilinear hysteretic system, the spectral errors resulting from the Newmark-Hall method are of the order of 50%. Overall, for all systems and ductilities, the unaveraged spectral error ϵ is 18.3% for the optimal parameters, 20.9% for the empirical formula and 54.5% for the Newmark-Hall method.

Additional insight into the merit of the two simple prediction schemes considered in Table III may be gained from an examination of the distribution of the individual spectral errors δ_{ijk} . For this purpose, all of the different systems, earthquakes, periods and ductilities are taken together. The results are shown in Figure 3. Figures 3(a), (b) and (c) give the results of the empirical formula and Figures 3(d), (e) and (f) the results of the Newmark-Hall method. It will be seen that the mean spectral error associated with the empirical formula is substantially smaller than that associated with the Newmark-Hall method for all values of ductility. The mean error for the empirical formula is always less than 2% while that for the

Newmark-Hall method ranges from 17% to 32%. In addition, the standard deviation of the error for the empirical formula is roughly one-half that for the Newmark-Hall method. It is true that the Newmark-Hall method is more conservative than the empirical formula. However, this conservatism is often excessive and is offset by the fact that the results of the Newmark-Hall method show considerably greater scatter than those of the empirical formula.

As an illustration of the ability of the simple empirical formula to predict the response of a given hysteretic structure to a particular earthquake, the predicted inelastic response spectra for two different systems are shown in Figures 4(a) and (b) along with actual response data. Also shown are the predicted spectra given by application of the Newmark-Hall method. In each case, the excitation is the scaled accelerogram for 8244 Orion Blvd., 1st floor, San Fernando, 1971, N00W (HOL). This accelerogram was chosen because of the presence of several pronounced peaks and valleys in its response spectrum. This helps to demonstrate the effects of local variations in spectral content.

It will be seen from Figure 4 that the predictions of the empirical formula are generally in good agreement with the data over the range of periods considered while the Newmark-Hall method tends to be somewhat overly conservative. This is consistent with the results of Figure 3. Even more significant, however, is the fact that the empirical formula appears to be capable of accounting to some extent for local variations in spectral content. For example, at a nominal period of 1 second, there is a marked valley in the linear and Newmark-Hall inelastic spectrum but this is not reflected in the behavior of the numerical integration results which, for the system BLH, actually exhibit a maximum. The inelastic spectrum predicted by the empirical formula possesses a local maximum at this period. On the other hand, from a nominal period of 3 to 4 seconds there is a sharp increase in the value of spectral displacement as predicted by the linear or Newmark-Hall inelastic spectrum while the numerical results show a local decrease. The empirical formula also predicts a decrease in spectral displacement. The superiority of the empirical formula in predicting detailed spectral behavior may be attributed in part to the fact that this method takes into account a shift in the effective period of oscillation of the structure while the Newmark-Hall method does not.

CONCLUSIONS

Based on the results of the present investigation of a class of single-degree-of-freedom hysteretic systems, the following conclusions are made.

- (1) Over the midperiod range of 0.4 to 4.0 seconds and for ductility ratios in the range of 2 to 8, it is possible to approximate the response of both simple and degrading hysteretic structures from a linear response spectrum by using an effective period shift and added damping. The use of optimal parameters leads to root mean square averaged spectral errors of less than 5% and unaveraged root mean square spectral errors of less than 20%.
- (2) A simple empirical formula for the effective period shift and added damping is capable of providing response predictions which are quite acceptable from a design point of view. The overall root mean square averaged spectral error for all systems and ductilities considered is of the order of 11% and the unaveraged root mean square spectral error is of the order of 21%.
- (3) The differences in hysteretic behavior considered herein have only a secondary effect on the accuracy of the results of the empirical formula.
- (4) The response predictions resulting from the empirical formula represent a significant improvement over the results obtained using currently accepted criteria for estimating the response of ductile structures.

ACKNOWLEDGMENT

The authors wish to thank Mr. C. Krousgill for his assistance in the computational aspects of this investigation. This research was sponsored by Grant No. ATA 74-19135 from the National Science Foundation, Research Applied to National Needs. Any opinions, findings, and conclusions or recommendations expressed in this paper are those of the authors and do not necessarily reflect the views of the National Science Foundation.

REFERENCES

- ¹N. M. Newmark and W. J. Hall, "Procedures and Criteria for Earthquake Resistant Design," Building Practices for Disaster Mitigation, Building Science Series 46, NDS, February 1973, pp. 209-237.

²Applied Technology Council, "An Evaluation of a Response Spectrum Approach to Seismic Design of Buildings," A Study Report for the N.D.S., Washington, D.C., September 1974.

³W. D. Iwan, "Response of a Simple Stiffness Degrading Structure," Proceedings of the Sixth World Conference on Earthquake Engineering, New Delhi, India, 1977, Volume III, pp. 121-126 (preprint).

⁴U.S. Atomic Energy Commission, Regulatory Guide 1.60, "Design Response Spectra for Seismic Design of Nuclear Power Plants," 1973.

Table I
**Ensemble of Earthquakes Employed in Investigation
 with Effective Acceleration Level**

Earthquake	Actual Peak Accel. (g's)	Effective Peak Accel., A* (g's)
Vernon, Long Beach, 1933, S8E	0.154	0.169
Helena, Montana, 1935, N9E	0.145	0.123
El Centro, Imperial Valley, 1940, S04E	0.348	0.410
Olympia, Washington, 1949, S04E	0.165	0.236
Taft, Kern Co., 1952, S69E	0.179	0.218
Eureka, 1954, N11W	0.168	0.266
Array No. 8, Parkfield, 1966, N50E	0.237	0.140
Borego Mountain, 1968, S90W	0.057	0.125
Pacolima Dam, San Fernando, 1971, S14W	1.170	0.952
8244 Orion Blvd., 1st Fl., San Fernando, 1971, N00W	0.255	0.415
445 Figueroa St., San Fernando, 1971, S38W	0.119	0.174
Smoothed Golden Gate Park (artificial), S80E	0.150	0.264

Table II
**Optimal Effective Linear System Parameters
 T_{e_m}/T_o , ζ_{e_m} and Associated Root Mean Square Averaged Spectral Error $\bar{\epsilon}_m$**

System	Ductility, $\mu = 2$			Ductility, $\mu = 4$			Ductility, $\mu = 8$		
	T_{e_m}/T_o	ζ_{e_m} (%)	$\bar{\epsilon}_m$ (%)	T_{e_m}/T_o	ζ_{e_m} (%)	$\bar{\epsilon}_m$ (%)	T_{e_m}/T_o	ζ_{e_m} (%)	$\bar{\epsilon}_m$ (%)
BLH	1.130	6.06	5.3	1.317	8.75	3.9	1.573	10.25	5.7
02-06-10	0.979	5.93	1.7	1.281	11.44	3.5	1.594	11.66	3.2
50-06-10	1.128	7.68	5.3	1.328	10.88	2.8	1.574	11.06	4.7
02-10-10	1.068	6.53	3.1	1.449	10.76	4.1	1.850	12.00	6.0
02-10-00	1.082	2.37	5.0	1.559	7.88	3.6	2.050	11.00	5.4
10-10-00	1.202	6.15	4.5	1.434	9.75	4.0	1.692	9.80	5.9

Table III
**Root Mean Square Spectral Error ϵ and Root Mean Square
 Averaged Spectral Error ($\bar{\epsilon}$) for Different Response Models in Percent**

System	Optimal Parameters			Empirical Formula (6)			Newmark-Hall Method [1]		
	$\mu = 2$	$\mu = 4$	$\mu = 8$	$\mu = 2$	$\mu = 4$	$\mu = 8$	$\mu = 2$	$\mu = 4$	$\mu = 8$
BLH	19.6 (5.3)	22.0 (3.9)	23.3 (5.7)	19.2 (6.3)	22.0 (4.2)	23.0 (6.1)	47.7 (30.0)	59.0 (37.4)	56.7 (36.7)
02-06-10	6.4 (1.7)	13.7 (3.5)	18.3 (3.2)	22.8 (15.6)	18.3 (9.9)	19.5 (7.9)	59.8 (52.7)	69.4 (43.4)	65.1 (43.4)
50-06-10	15.9 (5.3)	19.4 (2.8)	21.2 (4.7)	18.3 (7.8)	22.3 (4.9)	22.2 (8.6)	55.0 (41.1)	65.3 (44.0)	60.2 (39.8)
02-10-10	13.6 (3.1)	16.3 (4.1)	17.4 (6.0)	15.4 (6.5)	19.5 (7.6)	19.4 (8.4)	52.4 (39.8)	56.0 (34.1)	50.4 (29.3)
02-10-00	19.4 (5.0)	18.8 (3.6)	20.6 (5.4)	22.4 (18.1)	26.1 (19.9)	25.2 (18.0)	31.3 (12.5)	46.2 (21.6)	46.8 (26.8)
10-10-00	16.9 (4.5)	17.4 (4.0)	22.2 (5.9)	17.1 (9.9)	20.3 (8.6)	20.5 (7.6)	39.8 (23.8)	56.1 (32.9)	49.5 (29.8)
All systems	15.9 (4.4)	18.1 (3.7)	20.6 (5.2)	19.4 (11.6)	21.6 (10.6)	21.7 (10.4)	48.6 (35.8)	60.7 (38.2)	55.2 (34.8)

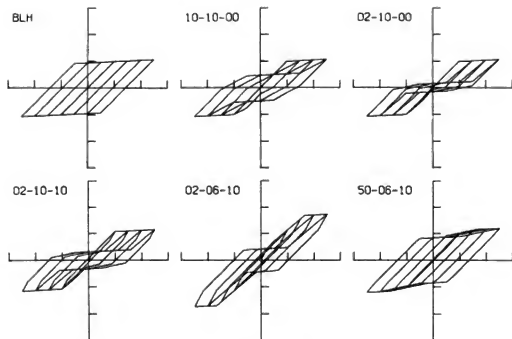


Figure 1

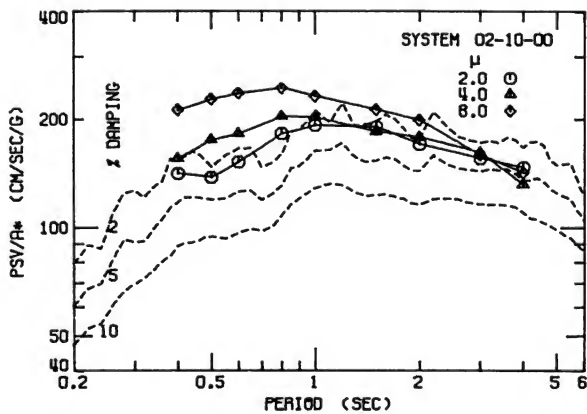


Figure 2

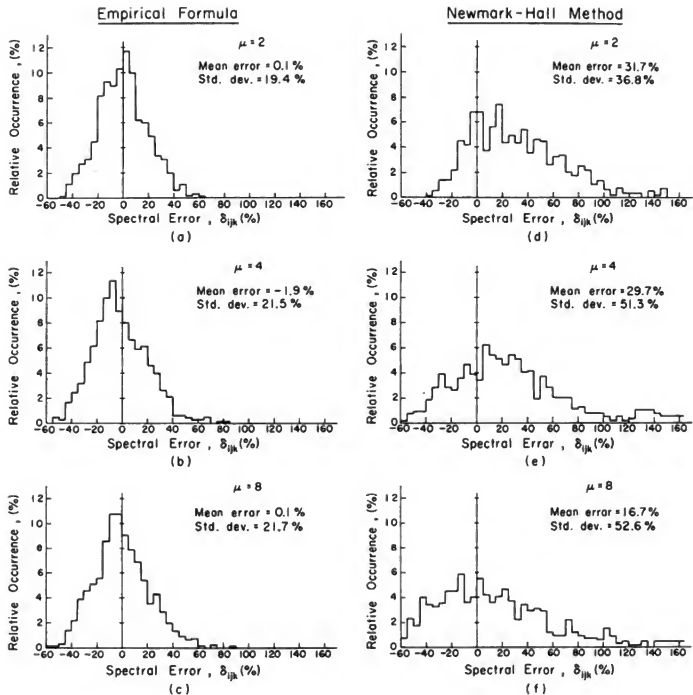


Figure 3

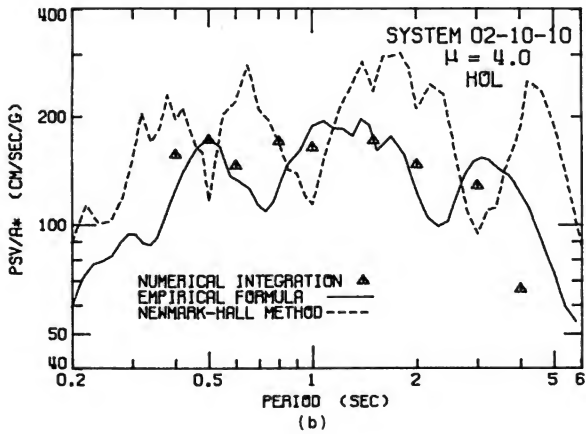
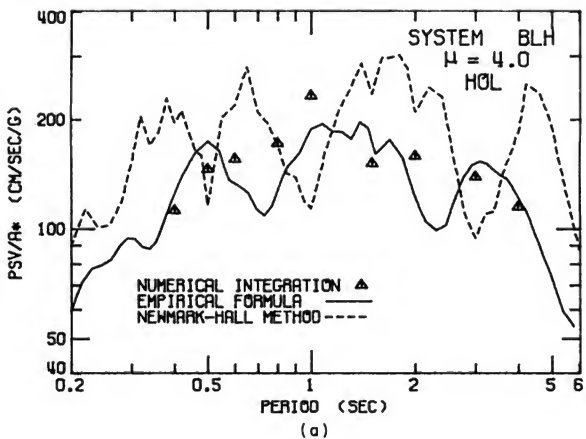


Figure 4

EARTHQUAKE RESISTANT DESIGN OF HIGH-RISE BUILDINGS IN JAPAN

Keiichi Ohtani, Chief, Earthquake Engineering Laboratory

National Research Center for Disaster Prevention

Science and Technology Agency

ABSTRACT

In January, 1964, the building height limitation which had been stipulated in the Structural Standard Law of Japan since 1921 was replaced with the building volume limitation. Number of high-rise buildings exceeding 45 meters in height came out to be about 300 cases. These buildings are examined thoroughly for the aseismic safety by dynamic analysis instead of static analysis, and received judge-and-rating as to the propriety of structural design from the committee consisting of specialists.

In this report, I discuss the present state of design, especially of dynamic analysis, using the design specification presented to the above committee. The number of data used in this report is 78 for SRC (composite steel and reinforced concrete structure) and 160 for S (steel structure) omitting special type structures such as high chimneys, towers, etc. As this study is the research of materials based on the actual design specification, I refer to the problems of aseismic design or the future subjects of research and development by considering the trend of design.

KEYWORDS: Building height limitation; building volume limitation; flexural-shear model; earthquake resistant design; high-rise buildings; histogram for building uses; shear model.

1. INTRODUCTION

The building height in Japan was limited to 31 meters since the Kanto Earthquake. The study of possibility of realization of the hihg-rise buildings was started by the Building Constructor Society with trust from the Ministry of Construction. In September, 1963, the Architectural Institute of Japan published the original draft of the "Guide Line for Aseismic Design of Tall Buildings" ("Guide Line"), and in January, 1964, the Structural Standard Law of Japan was altered from the building height limitation to the building volume limitation. It is certain that the rapid developments in the techniques of the response analysis of structure for earthquakes (the dynamic analysis of structure) along with a recent remarkable progress of electronic computers were the background of this alteration of the law.

Although we had been annoyed by the absolute deficiency of land and overcrowded state of buildings in the city region of Japan, we took the interest to raise the open space ratio of the city, and to rearrange the city for more green spaces by consideration of the building volume limitation.

In order to assure the structural safety of tall buildings exceeding 45 meters in height, an Examination Board was set up in the Ministry of Construction in September, 1964. The Board was transferred to the Evaluation Committee of High-Rise Building Structures, the Building Center of Japan, in August, 1965.

The structural designs of high-rise buildings are carried out generally in accordance with the "Guide Lines," usually employing dynamic response analysis. Documents and drawings of the structural design are presented to the Building Center of Japan by a structural engineer and he explains the outline of design to all members of the committee. After this hearing, a sub-committee consisting of appropriate number of the committee members and several other specialists, if necessary, is organized to investigate the design in detail. The sub-committee reports its conclusion to the main committee, and the decision on approval is made by the vote of all committee members. Detailed explanation on the function of the Evaluation Committee appears in the literature. Finally it is subjected to approval of the Ministry of Construction.

Number of high-rise buildings which have been approved by either the Examination Board in the Ministry of Construction or by the Evaluation Committee of High-Rise Building Structures in the Building Center of Japan is about 300 cases from March, 1963 to February, 1977. Omitting special type structures such as high chimneys, towers, etc., from these cases, and classifying them into S (steel structure for the main parts) and SRC (composite steel and reinforced concrete structure for the main parts) types, their general trend of current earthquake resistant design are briefly discussed in this report.

2. USE AND SIZE OF BUILDINGS

Numbers of data which have been used in this report are 78 cases for SR and 160 cases for S. These numbers are all the data available to the author, and form 95% of the pertinent data.

The histograms for the use of buildings are as follows:

for SRC (see Fig. 1-a)	
office (include those of stores and halls)	36 cases (46%)
hotel (include those of offices)	12 cases (15%)
apartment house (include those of offices)	16 cases (21%)
bank	7 cases (9%)
hospital	7 cases (9%)

for S (see Fig. 1-b)

office (include those of stores and halls)	101 cases (63%)
telephone station and broadcasting station	13 cases (8%)
hotel (include those of offices)	23 cases (14%)
store and department store	10 cases (6%)
apartment house (include those of offices)	9 cases (6%)
other use	4 cases (2%).

From the trend of use, it is noted that the buildings, which are adopted into SRC, are used in many cases for the apartment house, hospital and bank. It seems to be all right to consider that the reason for this adoption into SRC are to raise the rigidity of structure and to restrain the deformation. On the other hand, about 2/3 of the high-rise buildings, which are constructed with S, are used for the office.

The histograms for number of stories are illustrated in Figs. 2-a,b,b'. When the number of stories is distributed 10 to 60 stories, its peak is 14 to 18 for SRC, 14 to 30 for S. The basements ranged 0 to 5 storeis for SRC, 0 to 6 for S. It has a trend that the S structure is 4 or 5 stories taller and 1 story deeper than the SRC.

The total floor area of the buildings is distributed from 5,000 to 220,000 m² and is concentrated on 30,000 to 40,000 m². The typical floor area occupied 1,000 to 1,500 m² for the most part. Though the height of the highest building in Japan is 226.2 m, the heights are 50 to 75 m for most buildings. Although the deepest foundation bed sets on GL-43 m, the depths of the foundation bed are located GL-12 ~ 20 m for most cases.

3. VIBRATION CHARACTERISTICS

3-1 Modeling of Structure

The structure is so complex for space or plane and the mechanical property of materials is not so simple that it is impossible to analyze the structural characteristics which remain intact. In the case of dynamic analysis, the model constructed in mathematically simple forms is necessary.

A general method of modeling is the method that concentrates the mass at each floor level and connects some springs from floor to floor, so called the idealized lumped mass vibration system. The shear model and the flexual-shear model are used for elastic response analysis, but the employment of the flexual-shear model is more widely used than the shear model in recent years.

A general method of the use of springs for inelastic response analysis is as follows: the force-deformation curves of the open frame (Rahmen) and of the quake resisting wall are determined respectively as shown in Fig. 3, and then the curve of the story is obtained

by cumulating these curves. And simplifying the curve of the story, the story spring is approximated to the polygonal line as bi-linear or tri-linear.

The shear model is used for inelastic response analysis. If the flexural-shear model is used for elastic analysis, the equivalent shear model which is constructed with the same fundamental period and vibrational mode of the above model is used for inelastic analysis.

The histograms of the viscous damping ratio for the fundamental period (h_1) are shown in Figs. 4-a, b where its peak is 5% for SRC and 2% for S. The results of vibration tests, indicated that the actual structure did not have the damping mechanism which was in proportion to the frequency. In the structural designs, a method which increases the damping for the higher modes as the type of frequency proportion, assuming constant values for the fundamental and the 2nd modes (for the 3rd mode and so on, if necessary), has been more and more employed.

3-2 Natural Periods and Design Base Shear Coefficients

The relationships between the fundamental period (T_1) and the number of stories (N) are plotted in Figs. 5-a,b, 6-a,b where N in Fig. 5 denotes the number of all stories including the basements and penthouse and, N in Fig. 6 the number of stories above ground only (except the basement and the penthouse). In these figures, one-dot-dash-line is for $T_1=0.1N$ from the formula proposed in the SEACOC code, and the region sandwiched between one-dot-dash-line and the two-dots-dash-line is for $T_1=(0.06\sim 0.1N)$ from the formula recommended in the "Guide Line." The relation between " T_1 " and "N" is approximated by a formula $T_1=0.06N$ for SRC, $T_1=0.08N$ for S in Fig. 5, and $T_1=0.08N$ for SRC, $T_1=0.1N$ for S in Fig. 6.

Since the relation between the 2nd order period (T_2) and the fundamental period (T_1) has small dispersions, a linear equation $T_2=0.364T_1$ for SRC and $T_2=0.354T_1$ for S by the method of least squares passing through the zero point can be found as shown in Figs. 7-a,b. The difference in both approximate expressions is so little that it would be almost adequate to consider a relation $T_2=0.36T_1$ as the approximate expression.

The relation between " T_1 " and " C_B " are plotted in Figs. 8-a,b where C_B is the design base shear coefficient. The "Guide Line" has recommended $C_B=(0.18\sim 0.36)/T_1$ and $0.05 \leq C_B \leq 0.2$, and has advanced an opinion that the C_B decreases from above formula to $(0.15\sim 0.30)/T_1$. From the actual state of designs, most of them are in the range of $C_B=(0.24\sim 0.42)/T_1$ and the designers have attempted to design structures using the more severe criterion than the "Guide Line." This is because they expect that the satisfactory structural safety is to be achieved only specifying the sufficient capacity of section, even if it means a little wasteful design, since the high-rise buildings have had no experience of greater earthquakes and their safety has not been sufficiently proved in practice.

4. INPUT EXCITATIONS AND THE MAXIMUM INPUT ACCELERATIONS

The histograms of the employed earthquake accelerograms are shown in Figs. 9-a,b where its trend are alike for both cases of SRC and S. El-Centro NS is used in almost all designs as the standard excitations and Taft EW is used in the cases of 80 ~ 90 percents. It is hoped truly that the high-rise buildings are going to be designed by El-Centro

NS and Taft EW in Japan. The accelerograms observed in Japan, Tokyo 101 NS, Sendai 501 NS, Osaka 205 EW, etc. are employed. It is pointed out in a few cases that Hachinohe EW, which gives large responses of the structure with longer fundamental period, and El-Centro EW, which has large effects on the structures with fundamental period of about 2 sec, are also employed.

Figs. 10-a,b give the maximum input accelerations for elastic or inelastic response analysis, generally 200 ~ 250 gal for the former, and 350 ~ 400 gal for the latter.

In the design methods based on the maximum input acceleration, even if several waves are employed, only one wave of them gives the maximum response because that they all have individual frequency characteristics. Namely, in practice it is equivalent to the design employing one wave, and therefore in several cases, the design method based on the maximum input velocity is employed. For the value of the maximum velocity corresponding with the maximum acceleration, 25 kine for elastic analysis and 40 kine for inelastic analysis are used.

For the scale for estimation of the response of structure, its standard value has been used as follows:

The maximum angle of story deformation:

1/250 ~ 1/200 for elastic analysis,

1/150 ~ 1/100 for inelastic analysis.

The ductility factor: $\mu \leq 2$ for inelastic analysis.

5. PROBLEMS OF THE DESIGN FOR HIGH-RISE BUILDINGS

Using the value of the design for high-rise buildings, studying the present state of the design and dynamic analysis, I raise several points with regard to the design and future subjects of research as follows:

1) Institution of Input Excitation

As the "Guide Line" has recommended that a suitable input excitation must be chosen in consideration of site or foundation condition, the actual states of the design has hardly taken into consideration the aforementioned condition. The development of the "Standard Excitation" and the method that takes into account the seismicity and dynamic characteristics of ground at the site of the structure are necessary.

2) Level of Input Excitation

In the present design method, 250 gal for elastic analysis and 400 gal for inelastic analysis are widely employed, though there has been no investigation on the safety of structure when the greater earthquake than the designed one occurs. It is necessary to consider the criteria to be used to perform the abovementioned investigation.

3) Establishment of the Restoring Force Characteristics

In the case of establishing the restoring force characteristics of the building stories, the method that sums up the force-deformation curves of the frame and quake resisting wall which is individually calculated is employed. Although the propriety of this method is not yet verified, it is necessary to prove the structural behavior by large-scale experiments, vibration test, etc.

4) Treatment of Quake Resisting Wall

Using the method by which the reinforced concrete wall such as a boundary wall of the room at hotel or a wall of the surrounding core are designed, the non-resisting wall are designed by the treatment of detail and the most cases are designed for the open frame structure. It is necessary to reconsider how the method of this treatment is to aim the correct direction of the structural design.

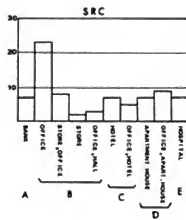


Fig. 1-a

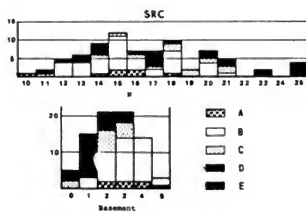


Fig. 2-a

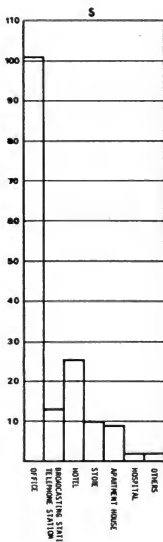


Fig. 1-b

Histogram for use of buildings

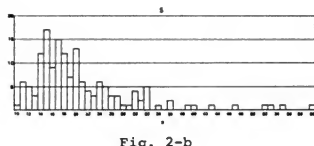


Fig. 2-b

Histogram for number of stories

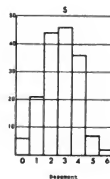


Fig. 2-b'

Relation between displacements and forces

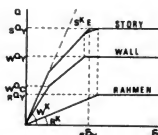


Fig. 3

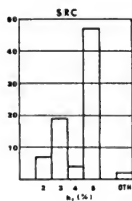


Fig. 4-a

Histogram for damping factor

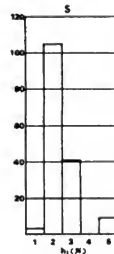


Fig. 4-b

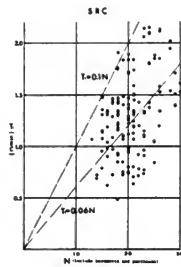


Fig. 5-a

Fundamental period vs. number of stories

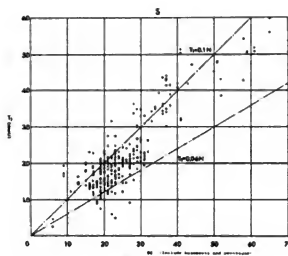


Fig. 5-b

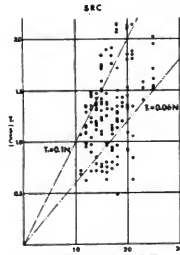


Fig. 6-a

Fundamental period vs. number of stories

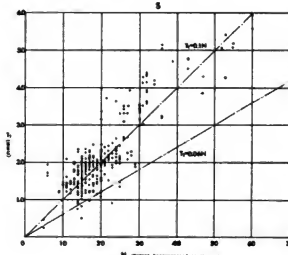


Fig. 6-b

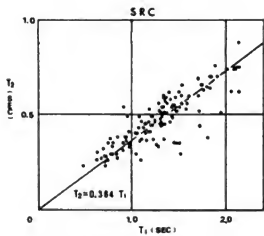


Fig. 7-a

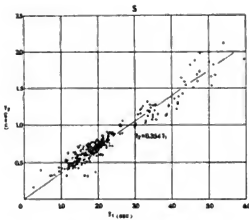


Fig. 7-b

Relation between fundamental and second order periods

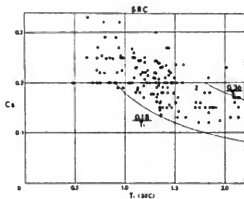


Fig. 8-a

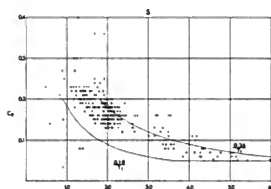


Fig. 8-b

Fundamental period vs. design base shear coefficient

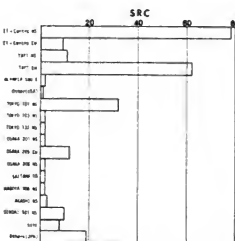


Fig. 9-a

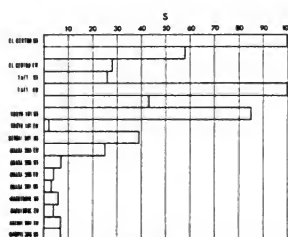


Fig. 9-b

Employed earthquake accelerograms

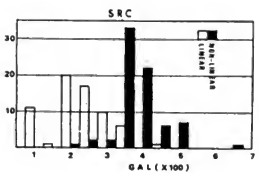


Fig. 10-a

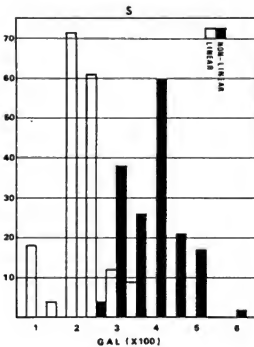


Fig. 10-b

Maximum input accelerations for elastic or inelastic response analyses

Racking Strength of Wood-frame Walls

ROGER L. TUOMI

Forest Products Laboratory, Madison, Wisconsin

ABSTRACT

Evaluation of the racking strength of wall systems has generally been limited to performance testing. Acceptance criteria for ultimate racking strength of sheathed walls are based on the strength of a wall with a let-in corner brace and horizontal board sheathing.

An analytical method for predicting racking performance has been developed that appears promising. It is independent of panel size, and small-scale tests can be used to augment the more costly standard tests. A small-scale loading apparatus was designed for rapid testing of wall sections.

Let-in corner braces using today's construction methods and materials no longer meet even the minimum level of acceptance. This is due to the elimination of horizontal board sheathing and the reduction in actual lumber sizes which took place since the racking performance standards were established.

Racking stiffness is an important performance consideration that has not been investigated. New testing apparatus has been designed that will make possible future evaluations of racking stiffness.

KEYWORDS: Racking strength; Windloads; Inplane shear forces; Corner brace; Racking stiffness

INTRODUCTION

The racking strength of a wall system is defined as its ability to resist horizontal inplane shear forces. These forces arise primarily from wind, but are also present under earthquake loadings. Current design procedures in the United States for calculating wind forces are published by the American National Standards Institute (1).^{1/}

Evaluation of wood-frame wall systems has generally been limited to performance testing. This technique has been used because no analytical method for predicting racking performance has yet been accepted.

BACKGROUND

For the first half of this century, wood-framed walls were typically built with horizontal board sheathing with let-in corner braces. With the development of plywood and fiberboards, the building industry abandoned the traditional board sheathing in favor of the more labor-efficient sheet products.

In 1949, the Federal Housing Administration (FHA) established minimum performance standards (2) as the basis for accepting new sheathing materials. The original standard was intended as an interim measure until a permanent one could be introduced. None has yet been developed, but a standard racking test procedure was approved by the American Society for Testing and Materials (ASTM) (3). With this procedure, the standard test panels are 8-by 8-foot (2.4- x 2.4-m) wall sections, fabricated with nominal 2- by 4-inch (50- x 100-mm) lumber and covered with two sheets of 4- by 8-foot (1.2- x 2.4-m) sheathing. This construction simulates conventional platform construction with studs spaced 16 inches (400 mm) apart.

Considerable wall testing, conducted prior to 1949, indicated that horizontal board sheathing with let-in corner bracing provided a minimum racking strength of 5,200 lbf (23 kN) for the 8-foot (2.4-m) square wall sections. Experience with existing houses

^{1/} Underlined numbers in parenthesis indicate references listed at end of this report.

showed this to be an adequate level of performance. All structural sheathing materials were required to meet this standard.

With the new emphasis on energy-efficient construction, many nonstructural sheet products are appearing on the market. This has forced many builders to revert to mechanical bracing systems, such as let-in lumber or metal straps.

STRUCTURAL SHEATHING

Development of Theory

After testing several standard wall panels at the Forest Products Laboratory (FPL), it became apparent that racking strength was controlled by fastener capacity rather than by the shear strength of the sheet material. FPL then developed a theory to predict racking strength of sheathing materials mechanically fastened to a stud frame. The equation was derived by an energy formulation whereby the externally applied load is resisted by the internal energy absorbed by the fasteners. The frame is assumed to distort like a parallelogram while the sheathing remains rectangular. The structural analog is shown on figure 1. The equation for the resistance provided by the perimeter nails of a single sheet of sheathing is:

$$R = \overline{sr} \sin \alpha \left[n + m - \frac{2}{3} \left(\frac{n^2 - 1}{n} \cos^2 \alpha + \frac{m^2 - 1}{m} \sin^2 \alpha \right) \right] \quad (1)$$

where

R is racking strength of one sheet of material (lbf or N),

\overline{sr} is product of slip times resistance of a single fastener (ultimate lateral load)

(lbf or N),

α is arctan (base of sheet divided by its height),

n is number of nail spaces on one horizontal edge, and

m is number of nail spaces on one vertical edge.

The total racking strength provided by the perimeter nails of a wall assembly is then the above result times the number of sheets of material plus the strength of the stud frame.

However, this relationship is complicated by the fact that most sheets also have interior or field nails. These field nails, being closer to the centroid of the sheet, offer far less resistance than the perimeter nails (5 to 10 pct), but their contribution should nonetheless be considered.

The above equation can be modified to include the contribution of the interior fasteners, and racking coefficients calculated for standard sheet sizes. A Forest Products Laboratory report, "Lightframe Walls--A Theoretical Solution for Predicting Racking," will be available later this year. It will cover the development of this theory in detail and will include racking coefficients in table form.

Small-Scale Tests

The theoretical equation considers the geometry of the sheathing, the number of horizontal and vertical nails, and the lateral resistance of the fasteners, but is independent of panel size. Figure 2 shows the correlation between theoretical and actual racking strength of both 2- by 2-foot (0.6- x 0.6-m) and 8- by 8-foot (2.4- x 2.4-m) test panels.

Since the full-scale 8- by 8-foot (2.4- x 2.4-m) tests are cumbersome and expensive to run, FPL designed a small-scale loading apparatus. It consists of a pantograph frame which is pinned at four corners. The lower member can swing freely but will always remain horizontal. The two structural members and the pinned-connector straps form a parallelogram at all times, eliminating the need for hold-down devices at the corners. The principal advantage in this arrangement is that the applied load direction can be reversed to study the effect of cyclic loading.

Deflection readings are obtained by measuring the change in diagonal length between opposite corners of the test specimen. The current ASTM Standard (3) requires three simultaneous measurements: gross horizontal corner deflection, slip, and rotation. The net racking deflection must then be calculated for each load level. With the diagonal displacement method, loads and net deflections are obtained directly.

Lateral Nail Tests

Since the lateral nail strength of fasteners is a parameter needed for predicting racking strength, it is important that the lateral nail tests represent the actual wall construction.

Two standard nail tests are used in the United States--ASTM D 1037 (4) and ASTM D 1761 (5). ASTM D 1037 was designed for evaluating the properties of wood-base fiber and particle panel materials. With this method, the nail shank is supported by a steel stirrup and is pulled through the edge of the sheet material. This method is adequate for lower strength materials, but may not indicate the mode of failure in actual racking joints.

With stronger materials, such as plywood, the joint failure may occur in the lumber rather than the sheathing. To better simulate the actual joint for higher strength sheathing, a modified version of the ASTM D 1761 test procedure is recommended. This test was designed for conducting lateral nail tests in wood. The modification recommended is that the cleat is a piece of sheathing material and the block is an actual piece of framing lumber taken from the test panel. Thus, the actual materials from the racking tests are mated in the lateral nail tests.

The distance between the nail and the edge of the sheathing is also very important. The effect of edge distance on lateral nail strength is shown in figure 3. A 3/4-inch (19-mm) end distance was selected for the value used in equation (1) because it best represents the displacement of the tension corner nails, which are the critical ones. Nails along a vertical joint, where two sheets butt together, are closer to the edge, but their displacement direction is essentially parallel to the edge rather than toward it. Half the nails have displacement components toward the center and are not affected by edge distance.

LET-IN CORNER BRACES

Many changes in construction practice have occurred since FHA established the minimum performance standard. Horizontal board sheathing is no longer used, and the actual size of dimension lumber has been reduced. Some building codes currently accept the let-in corner

brace when nonstructural sheathing is used. However, few tests have been made on walls with let-in corner bracing since the performance standard was developed.

FPL conducted a few tests to determine the capacity of let-in corner braces with today's materials. The first tests did use horizontal board sheathing to reaffirm the FHA requirements, and 5,200 lbf (23 kN) was attainable. The horizontal board sheathing supports the brace against outward buckling and also reinforces the stud frame. This was not the case, however, when the horizontal boards were eliminated.

Let-in corner braces are generally 1- by 4-inch (25- x 100-mm) boards cut into the frame and secured with two nails per stud crossing. They can act either in tension or compression depending upon the load direction. Figure 4 shows a typical brace under compression loading. Braces loaded in this manner failed violently in buckling like a slender column, or else the stud frame slowly came apart. The strength of compression braces was calculated by the following equation for an ideal column:

$$P = \frac{a\pi^2 EI}{L^2} \sin\alpha \quad (2)$$

in which

P is applied racking force (lbf or N),

α is angle between brace and vertical member,

a is end condition coefficient (use a = 1 for pinned),

E is modulus of elasticity of the brace (psi or kPa),

I is moment of inertia of the brace (in.⁴ or mm⁴), and

L is unsupported clear distance between studs along the brace (in. or mm).

This approach worked fairly well for braces with a modulus of elasticity up to about 1.6 million psi (11,000 MPa), but beyond that stiffness the stud frame simply came apart. The ultimate load when good quality braces are used is controlled by the stud wall and is around 3,600 lbf (16 kN).

When loaded in tension, racking strength is provided primarily by the lateral nail strength of the nails which secure the brace to the studs. The maximum racking load is

lower for braces loaded in tension. Further discussion on braces is presented in an upcoming FPL Report, "Racking Strength of Let-in Corner Bracing, Sheet Materials, and the Effect of Rate of Loading." This report should be available in a few months.

FUTURE RESEARCH

One important consideration that has not been resolved for racking performance is that of racking stiffness. Traditionally, racking tests have been run essentially to failure without much attention to the shape of the load-deflection curves. The initial loading produces a parabolic curve with no well-defined stiffness value or limit of proportionality.

However, in the few cases where cyclic loading was performed, the load-deflection curve became fairly linear and reproducible. This was true for lateral nail tests, wall racking tests, and full-scale house tests. Figure 5 is an example of a wall racking test cycled five times prior to loading to failure. The first loading does produce a degree of set or seating of the fasteners, but it appears to be a constant value for a given load level.

In equation (1), the lateral fastener strength was given as sr , the product of slip times resistance or stiffness. If this stiffness property can be better defined, then it would be possible to predict racking resistance for any level of deformation.

FPL recently built a new racking frame that is capable of cyclic load reversals. It can be programmed to cycle between desired limits of displacement or load level. Also, the frequency can be adjusted to simulate earthquake excitation or dynamic wind response. Load-deflection data can be monitored after 1, 10, 100, 1,000, or any desired number of cycles. A study is scheduled for later this year to use this new apparatus in an attempt to develop racking stiffness information.

SUMMARY

A relationship between theoretical and actual racking strength has been developed that appears quite promising. Small-scale tests can be used to augment the more cumbersome and

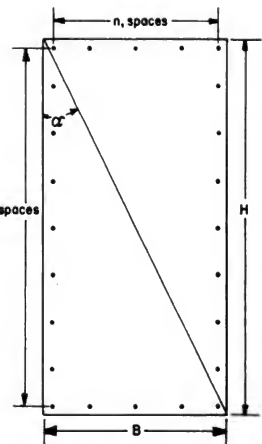
expensive standard tests. The small-scale tests should provide a quick and easy way to estimate the racking properties of new sheet materials.

The actual performance of let-in corner braces, without the horizontal board sheathing, is well below the 5,200 lbf (23 kN) level required by FHA. Although the strength and stiffness of the brace are important, a level is reached where the stud frame controls ultimate strength.

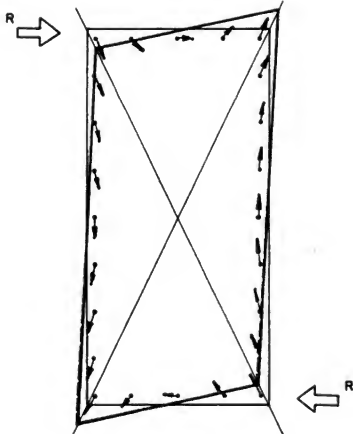
Racking stiffness is an important performance consideration that has not been investigated. A new test apparatus has recently been designed that should enable researchers to study the stiffness properties of wall systems under cyclic loading. These tests, together with a theoretical design approach, should provide a means for predicting racking resistance at various levels of load or deflection below ultimate strength.

REFERENCES CITED

1. American National Standards Institute (1972). American national standard building code requirements for minimum design loads in buildings and other structures. ANSI A58. 1-1972.
2. Federal Housing Administration (1949). A standard for testing sheathing materials for resistance to racking. FHA Tech. Cir. No. 12. Washington, D.C.
3. American Society for Testing and Materials (1968). Standard methods of conducting strength tests of panels for building construction. ASTM E 72-68. Philadelphia, Pa.
4. American Society for Testing and Materials (1964). Standard methods of evaluating the properties of wood-base fiber and particle panel materials. ASTM D 1037-64. Philadelphia, Pa.
5. American Society for Testing and Materials (1968). Standard methods of testing metal fasteners in wood. ASTM D 1961-68. Philadelphia, Pa.



ORIGINAL PANEL



DISTORTION UNDER LOAD

Figure 1. Original panel shows parameters necessary to calculate racking strength.

Under load, the frame distorts like a parallelogram while the sheathing remains rectangular. The direction and relative magnitude of the nail displacements are shown under load.

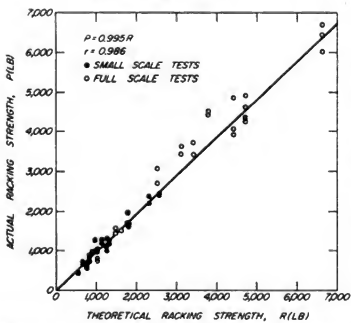


Figure 2. The relationship between theoretical and actual racking strength for both full-scale and small-scale test specimens.

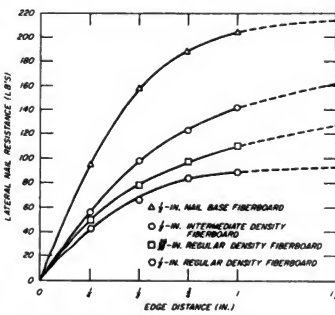


Figure 3. Lateral nail strength at various edge distances for four types of fiberboard sheathing.

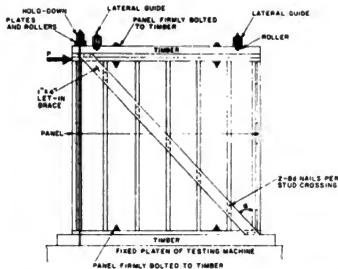


Figure 4. Schematic diagram of a let-in corner brace being loaded in compression.

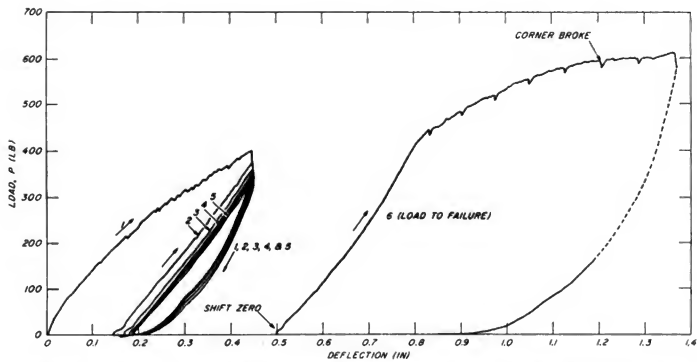


Figure 5. Typical load-deflection pattern for cyclic loading of wall panel. Curve becomes fairly linear after the first cycle seats the fasteners.

EXAMINATION FOR AN EVALUATION METHOD OF
DAMAGE TO EXISTING WOODEN HOUSES CAUSED BY EARTHQUAKES
Kaoru Ichihara, Director
Eiich Kuribayashi, Chief, Earthquake Engineering Section
Tadayuki Tazaki, Research Member
and
Takayuki Hadate, Research Member
All of Public Works Research Institute

ABSTRACT

In an effort to help draft an earthquake disaster mitigation program, an evaluation method for damages of structures by earthquakes is proposed. Concepts of the ratios of razed houses and probability theories with number of razed houses have been employed in the method.

KEYWORDS: Damages of structure by earthquake; disaster mitigation; probability theory; ratio of razed houses; wooden houses

1. INTRODUCTION

A consideration in the evaluation of damages of structures by future earthquakes is proposed herein. This would help in drafting an earthquake disaster mitigation program. Prior to evaluating the losses of lives and damages to the structures, the damages of houses were assigned an index in terms of the whole losses and damages.

For instance, H. Mizuno and S. Horiuchi presented relationships between the ratios of outbreak of fires and those of totally destroyed dwelling houses caused by past earthquakes since the Great Kanto Earthquake in 1923 as shown in Fig. 1 (1). And relationships between the losses of human lives and those of razed houses in the Fukui Earthquake in 1948 are presented as shown in Fig. 2 (2).

The equivalent ratio of razed house (defined in Chapter 2), which could be considered as an index of principal damage, is assumed as follows.

- (1) The equivalent ratio of razed houses normally expresses a seismic intensity even in the vicinity subjected to severe earthquakes, where data on ground motions are rarely obtained.
- (2) Wooden houses are common dwellings in this country, and much data on damages of wooden houses by earthquakes have been reported.

In this report, the equivalent ratio of razed houses at a respective site by a strong earthquake was estimated by applying statistical relationships among the equivalent ratios, epicentral distances and magnitude (Richter Scale) of the earthquakes reported at the last Joint Meeting (3,4). Furthermore the results of the evaluation were compared with actual damages at the site caused by the earthquakes.

2. DEFINITIONS OF DISTRIBUTION OF DAMAGE RATIOS OF EXISTING WOODEN HOUSES CAUSED BY PAST EARTHQUAKES (3)

Using the statistics of disaster documents on short distant earthquakes, Fukui Earthquake ($M = 7.3$, 1948), Izu-hanto Oki Earthquake ($M = 6.8$, 1974), and Ebino Earthquake ($M = 6.1$, 1968), relationships among ratios of razed houses, epicentral distances and magnitudes of earthquakes were reported (3). The equivalent ratio of razed houses is defined as:

$$D_1, \% = \frac{\text{Number of Razed Houses} + 0.5 \times \text{Numbers of Half Razed Houses}}{\text{Total Number of Existing Houses}} \times 100$$

Conclusively, the ratio D_1 in the area of diluvium or tertiary is given as D_{II} and D_1 in the area of alluvium is given as D_{III} ,

$$D_{II} = 1/164 \times 10^{0.625M + 0.025\Delta M - 0.272\Delta} \quad (1)$$

$$D_{III} = 1/73 \times 10^{0.576M + 0.026\Delta M - 0.248\Delta} \quad (2)$$

where Δ = epicentral distances

M = magnitudes of earthquakes (Richter Scale)

3. AN EVALUATION METHOD OF DAMAGE TO WOODEN HOUSES

In the previous chapter, the quantitative relationships among the equivalent ratio of razed houses, epicentral distance, and magnitude are given in Eq. (1) and (2). In order to estimate the distribution as for the equivalent ratios in Tokyo, Kawasaki and Yokohama districts, the earthquake is assumed as follows:

magnitude = medium class as 6 to 7,
focal depth = less than 50 km,
epicenter = assumed as the same point located at the epicenter of Ansei-Yedo Earthquake (1855), i.e., E139.8°, N35.8°.

In general, wooden houses behave elastically with relatively small amplitudes of deformation induced by ground motions, and elasto-plastically with relatively large amplitudes. H. Umemura proposed critical seismic lateral force coefficients at a point from elastic to elasto-plastic states as 0.4 for one story houses and as 0.6 for two story houses. M. Mononobe proposed the relationship between the ratio of razed houses and seismic coefficient K as Eq. (3) assuming a Gaussian Distribution,

$$D_2 = \frac{100}{\sqrt{2\pi}\sigma} \int_{-\infty}^K e^{-(K-K_0)^2/2\sigma^2} dK \quad (3)$$

where K_0 = average resistivity

σ = the parameter expressing uniformity of resistivity

Fig. 3 shows the estimated results by applying Eq. (3) to Noubi Earthquake ($K_0 = 0.40$, $\sigma = 0.053$), Fukui Earthquake ($K_0 = 0.40$, $\sigma = 0.071$), Kanto Earthquake ($K_0 = 0.45$, $\sigma = 0.071$), and Sempoku Earthquake ($K_0 = 0.47$, $\sigma = 0.105$). According to this figure, the original ratios of razed houses D_2^* corresponding to the critical seismic coefficient of 0.4 and 0.6 are 20 to 50% and 90 to 100%, respectively. So the multiplier δ for the original ratio of razed houses of two stories normalized by those of one story becomes 1.8 to 5.0. In this report, δ is assumed to be 1.8.

In Eq. (2), the average depth of alluvial deposits is assumed to be 10 to 30 m. The equivalent ratio of razed houses at the area of thicker alluvium will be greater. Fig. 4 shows the relationship between the equivalent ratio of razed houses and the depths of alluvial deposits in Tokyo and Yokohama districts during the Kanto Earthquake. The data from the investigations by H. Kawasumi, Y. Ohsaki, S. Omote and S. Miyamura are used in this estimation. According to this figure, the multipliers γ for the equivalent ratio in the area with various depth of alluvial deposits are evaluated as shown in Table 1. These multipliers are normalized by the ratio at alluvial deposits 10 to 30 m deep.

* $D_2 = \frac{\text{number of razed houses}}{\text{total number of existing houses}}$

Fig. 5 shows the deviations of the equivalent ratio of razed houses in subground type II for the Fukui Earthquake. The numbers on the abscissa in this figure correspond to those equivalent ratios of razed houses in Table 2. The deviations shown in Fig. 5 are relatively large. Comparing the deviations in Fig. 5 with the numbers of existing wooden houses N in Table 2, it can be assumed that 'N' also affects the equivalent ratio. In this report, the deviation is assumed to be a binomial distribution. Risk Indexes, RI, which means upper control limits for three standard deviations of the equivalent ratios are introduced as follows:

$$\left. \begin{aligned} RI &= D_1^U / D_1^L && \text{in \%} \\ \left. \begin{aligned} D_1^U \\ D_1^L \end{aligned} \right\} &= \bar{D}_1 \pm \sqrt{\bar{D}_1(100-\bar{D}_1)/N} && \text{in \%} \end{aligned} \right\} \dots\dots (4)$$

in which

D_1^U = upper limit of the deviation of the equivalent ratio of razed houses.

D_1^L = lower limit of the deviation of the equivalent ratio of razed houses.

\bar{D}_1 = the average equivalent ratio of razed houses in the area of a certain range of epicentral distance.

A binomial distribution can be approximated to a normal distribution when N is sufficiently large and \bar{D}_1 is sufficiently small. The difference between these distribution functions is given by Eq. (6),

$$\begin{aligned} P_{b-n} &= P \text{ binomial} - P \text{ normal} \\ &= \sum_{R=0}^c \frac{N!}{R!(N-R)!} (\bar{D}_1)^R (1-\bar{D}_1)^{N-R} \\ &\quad - \int_{-\infty}^{(c+1/2-N\bar{D}_1)/\sqrt{N\bar{D}_1(1-\bar{D}_1)}} \frac{1}{\sqrt{2\pi}} e^{-\frac{u^2}{2}} du \dots (6) \end{aligned}$$

The relationship of P_{b-n} and R^* is shown in Fig. 6. According to this figure, a binomial distribution approximates to a normal distribution having an error of 2% when N exceeds 100. If RI is greater than 10, which means that the actual equivalent ratio D_1 exceeds D_1^U , RI can be considered being affected by other factors than earthquake intensity, i.e., sub-ground condition.

*R = number of razed houses + 0.5 x number of half razed houses.

= number of equivalent razed houses.

The estimated equivalent ratios of razed houses \hat{D}_{1I} and \hat{D}_{1II} , considering the difference of resistivity between the houses of two stories and those of one story, the depth of alluvial deposit and the sample size of the existing houses in the areas are given as follows:

$$\hat{D}_{1I} = \delta \cdot RI \cdot D_{1I}^U \quad \text{in \%} \quad (7)$$

$$\hat{D}_{1II} = \epsilon \cdot RI \cdot D_{1II}^U \quad \text{in \%} \quad (8)$$

in which

$$\epsilon = \delta + \gamma$$

$$D_{1I}^U = D_{1I} + 3 \sqrt{D_{1I} (100 - D_{1I}) / N}$$

$$D_{1II}^U = D_{1II} + 3 \sqrt{D_{1II} (100 - D_{1II}) / N}$$

$$\delta = \begin{cases} 1.00 & \text{in the area where most houses are one floor} \\ 1.80 & \text{in the area where most houses are two floor} \end{cases}$$

γ ; given in Table 1

D_{1I} , D_{1II} ; given by Eq.(1), (2)

RI ; given by Eq.(5)

The procedure stated above was applied to Tokyo, Kawasaki and Yokohama districts and Fig. 7 shows the results. In this estimation, the values of RI were obtained from the Fukui Earthquake data. The value of δ was assumed to be 1.80, because most of the existing wooden houses are two stories. The average depth of alluvial deposit in ward k was estimated as follows:

$$h_{km} = \frac{\sum_{i=1}^n (\frac{h_i + h_{i+1}}{2}) A_i}{\sum_{i=1}^n A_i} \quad (9)$$

in which

h_i = the depth of alluvial deposit

A_i = the area in which depth is between h_i and h_{i+1}

In Fig. 7, upper, middle and lower numerals in each ward correspond to the estimated equivalent ratios of razed houses destroyed by the assumed earthquake of magnitude 6.0, 6.5 and 7.0, respectively.

4. CONSIDERATION

Based on the examination described herein for the evaluation method of damage to existing wooden houses by earthquakes, the estimated ratio of razed houses and the actual

ratio reported in the document of razed houses in the Ansei-Yedo Earthquake (1855) comprehensively agree with each other except minor errors.

Here, one of the evidences of the evaluation method for the damage ratios as well as their distributions could be given. Using these, it would be possible to totally evaluate the losses and damages by the earthquakes.

5. ACKNOWLEDGEMENTS

The author appreciates their cooperation listed below:

- 1) Prime Minister's Office, Statistics Bureau, National Census Department
- 2) Tokyo Metropolis, General Affair Bureau, Disaster Countermeasures Division
- 3) Fukui Pref., Fire and Disaster Prevention Department
- 4) Fukui Prefectural Library
- 5) Ishikawa Pref., Statistics Department
- 6) Kagoshima Pref., Fire and Disaster Prevention Department
- 7) Yebino City Office, Iino Branch and Shinko Branch

6. REFERENCES

- 1) H. Mizuno, S. Horiuchi, Study on the Estimation of Fires in Earthquakes, Proceedings of the Japan Society of Architects, 250, 1976.
- 2) H. Mizuno, S. Horiuchi, Study on the Relationship Between the Ratio of the Outbreak of Fires and That of the Totally Destroyed Dwelling Houses Caused by the Earthquakes, Proceedings of the Japan Society of Architects, 247, 1976.
- 3) E. Kuribayashi, T. Tasaki and T. Hadate, Relationships Between Earthquake Damage of Existing Wooden Houses and Seismic Intensities, U. S. Japan Panel on Wind and Seismic Effects, Eighth Joint Meeting, UJNR, May 18-26, 1976.
- 4) E. Kuribayashi, T. Hadate, Y. Hoshiba, Characteristics of Distribution of Damages Caused by Earthquakes, Journal of the P.W.R.I., Ministry of Construction, 18-9, 1976.
- 5) H. Unemura, Research on the Estimation of Architectural Damages by Earthquakes, Tokyo Metropolis Disaster Prevention Committee, 1970.
- 6) T. Mochizuki, Research and Earthquake Response Analysis to Estimate the Damage of Wooden Houses in Tokyo, Proc. of the Japan Society of Architects, 230, 1970.
- 7) N. Mononobe, Earthquake Engineering in Civil Engineering Structures.
- 8) Investigations on the Damages of Hokuriku Earthquake, Report of Public Works Research Institute, Ministry of Construction, No. 78, 1949.
- 9) H. Kawazumi, Damage Distribution and Earthquake in Tokyo, Architecture Magazine, 773, 1951.
- 10) Y. Ohsaki, Earthquake Damage of Wooden Buildings and Depth of Alluvial Deposit, Proc. of Japan Society of Architects, 72, 1962.
- 11) S. Omote, S. Miyamura, Relationships Between Damage Distribution in Earthquake in Yokohama and Nagoya City, and Subground Conditions, Architecture Magazine, 773, 1951.
- 12) Memorandum of the Statistics on Houses, Prime Minister's Office, Statistics Bureau, National Census Department.

- 13) Subgrounds around Tokyo Bay, 17, Planning Bureau, Ministry of Construction, edited by Tokyo Bay Development Committee.
- 14) Tokyo Metropolis, Documents of Ansei-Yedo Earthquake, 1973.
- 15) N. Koiwai, K. Miyawaki, Determination of Earthquake Hazards in Densely Populated Areas and Preventive Measures to be Considered in Urban Planning, Proc. of 5th Joint Meeting, U.S. and Japan Panel on Wind and Seismic Effects, UJNR, Tokyo, May 14-16, 1973.
- 16) K. Kanai, Damages of Wooden Houses Caused by Earthquakes, Bulletin of Earthquake Institute, 29, 1951.
- 17) Tokyo Metropolis Disaster Prevention Committee, Research for Short Distant Earthquakes, Vol. 1, 2, 3, 1974 to 1975.
- 18) Classified Maps of Subground, Land Planning Agency.
- 19) J. Fukuda, Introduction to the Applied Statistics, Nikkankogyo Shimbunsha.

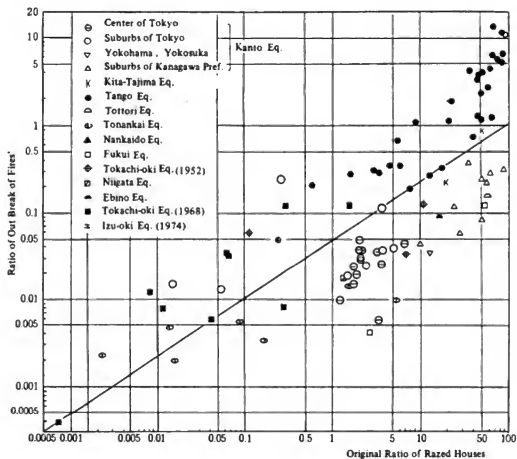


Fig. 1 Relationships between Fires and Razed Houses¹⁾⁽²⁾

Table 1 Multiplier for Depths of Alluvial Deposits.

Depth of Alluvial Deposit	District γ	Tokyo	Yokohama
		3.60	1.17
$40 \text{ m} > H \geq 30 \text{ m}$		3.60	1.17
$H \geq 40 \text{ m}$		8.80	1.23

Table 2 Equivalent Ratio of Razored Houses in Fukui Earthquake

Index	Town or Village	Epicentral Distance (Km)	Number of Existing Houses	Equivalent Ratio of Razored Houses (%)
1	Iz	4.1	497	98
2	Maruoka	4.7	1,680	30
3	Narita	2.7	2,418	95
4	Hyogo	2.0	320	100
5	Higashijugo	1.4	904	99
6	Ohashi	4.5	568	100
7	Ohraki	3.4	415	99
8	None	5.0	780	88
9	Natsume	9.2	535	24
10	Nakafujishima	6.5	806	100
11	Kibe	5.5	770	85
12	Hanashige	8.5	508	80
13	Honayo	5.6	760	92
14	Morita	5.2	1,773	97
15	Kanareza	6.2	1,230	72
16	Awara	7.8	1,254	86
17	Kawasaki	5.6	692	99
18	Higashifujishima	9.0	747	100
19	Izobe	6.8	880	99
20	Goryogashima	8.1	300	90
21	Takahoko	5.6	1,366	96
22	Nishifujishima	9.2	674	75
23	Shinbo	9.2	310	36
24	Umo	7.5	756	50
25	Tashiro	15.7	31	58
26	Fukui	10.5	17,805	69
27	Maruoka	10.2	1,501	56
28	Yoshizaki	15.0	159	90
29	Kitsugata	11.7	844	88
30	Tsubos	10.1	703	73
31	Rokujo	14.7	563	94
32	Okabo	11.6	644	91
33	Yoshino	13.7	262	75
34	Daishoji	18.5	3,353	39
35	Shioya	15.4	741	88
36	Miki	16.1	431	40
37	Sagoe	15.6	115	35
38	Kasimonju	19.0	545	30
39	Shimononju	17.0	565	94
40	Sakau	15.9	708	62
41	Tatematsu	17.7	856	2
42	Nishihago	17.5	448	10
43	Amatau	16.3	647	1
44	Mango	18.8	565	30
45	Sandani	15.2	284	3
46	Togo	17.3	813	49
47	Yoshikawa	21.9	591	1
48	Katayamazu	24.4	1,416	14
49	Rita Nakayama	25.0	828	31
50	Nakagawa	23.3	760	23
51	Katagami	22.3	397	11
52	Yutaka	24.7	486	1
53	Shizu	21.8	570	5
54	Iburibashi	24.0	491	3
55	Kuritabe	27.0	865	6
56	Rita Shinjo	25.5	519	2
57	Kunitaka	26.5	947	2
58	Ishii Nakayama	24.0	585	4
59	Yasano	27.0	604	1
60	Meageri	40.0	1,598	1
61	Minato	42.2	279	2
62	Hieshuna	42.0	375	1
63	Yoshida	41.5	336	1

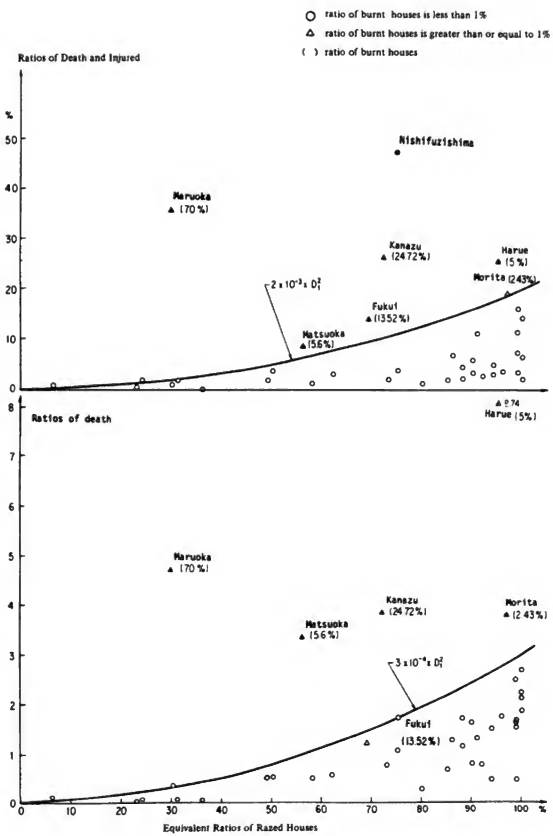


Fig. 2 Relationships between Equivalent Ratio of Razored Houses and Losses of Lives in Fukui Earthquake³⁾

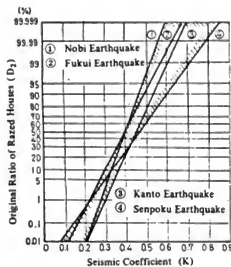


Fig. 3 Relationships between Original Ratio of Razed Houses and Seismic Coefficient by N.Monomobe⁷⁾

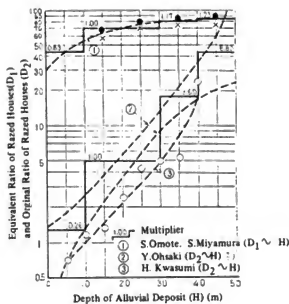


Fig. 4 Relationships between Equivalent or Original Ratio of Razed Houses and Depths of Alluvial Deposits

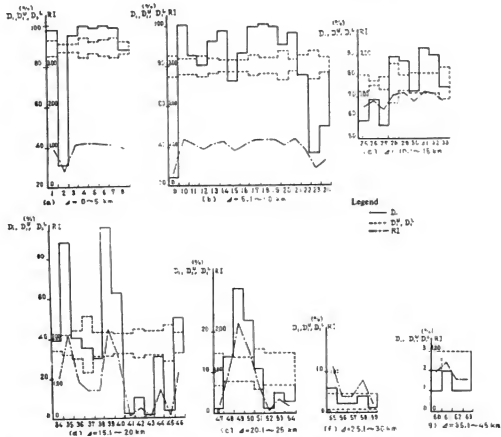


Fig. 5 Equivalent Ratio of Razed Houses and Its Deviation in Fukui Earthquake.

Table 3 Equivalent Ratio of Razed Houses in Ansei-Yedo Earthquake

Group	Equivalent Ratio of Razed Houses	Equivalent Ratio of Razed Houses Obtained from Documents ¹⁴⁾	Estimated Equivalent Ratio of Razed Houses
1 (Chiyoda Ward)	46%		35%
2 (Chuo Ward)		8	26
3 (Minato Ward)		80	34
4 (Bunkyo Ward)		68	46
5 (Taito Ward)		51	54
6 (Sumida Ward)		80	100
7 (Koto Ward)		76	84

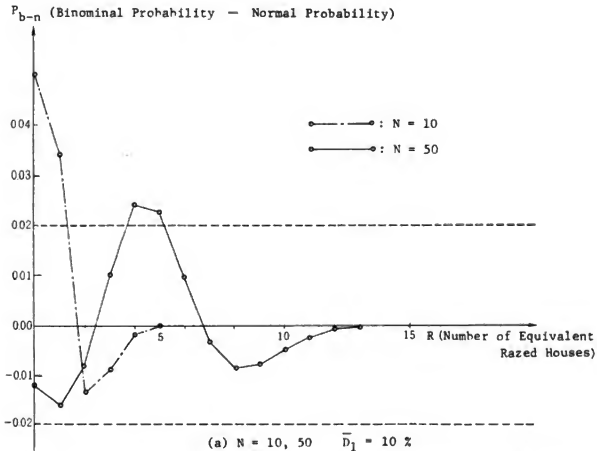


Fig. 6 Influence of Number of Existing Houses on Binomial and Normal Distributions

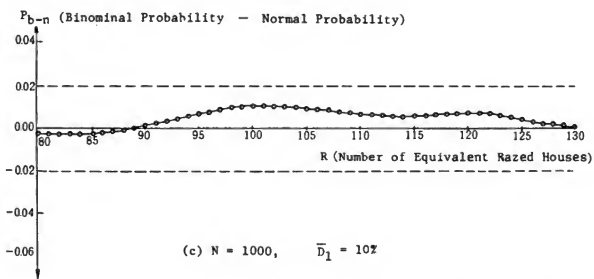
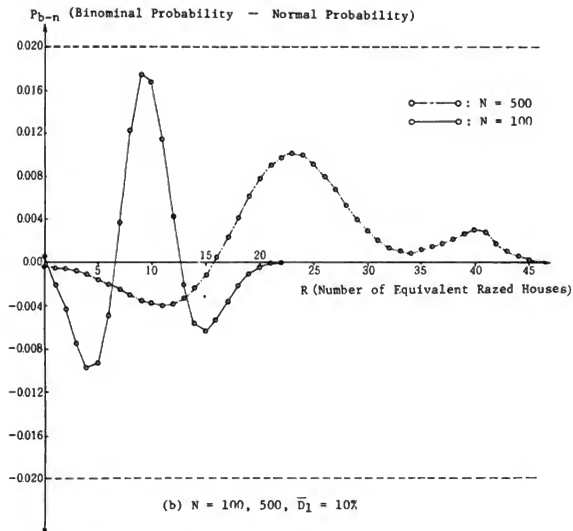


Fig. 6 Influence of Number of Existing Houses on Binomial and Normal Distributions

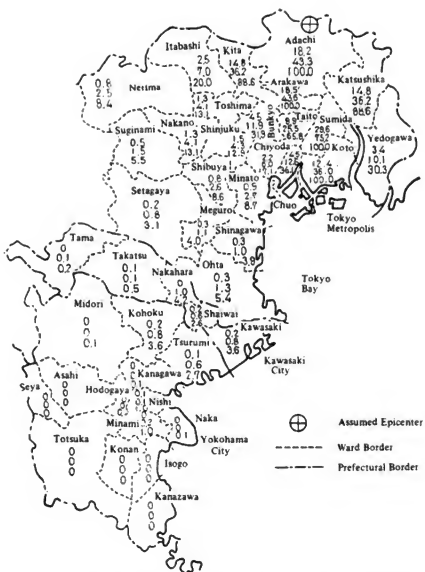


Fig. 7 Estimated Equivalent Ratio of Razed Houses at Each Ward in Tokyo, Kawasaki and Yokohama districts

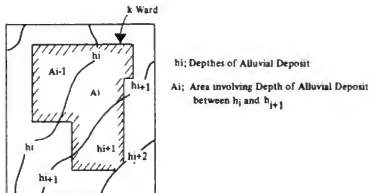


Fig. 8 Determination of Average Depths of Alluvial Deposits in k Ward.



Fig. 9 Distribution of Equivalent Ratio of Razed Houses Obtained from Documents of Ansei-Yedo Earthquake 14)

Table 4 Documents on Damages in Suburbs of Tokyo Caused by Ansei-Yedo Earthquake.

Title of Document	CONTENTS								Today's Place Name	
	Number of Houses 396, Mostly Damaged 150 ~ 140, Totally Damaged 17									
Tokyo Metro History of Mikawashima Town History of Shinagawa Ward	Location	Number of Houses	Totally Damaged	Partly Damaged	Totally Damaged Warehouses	Partly Damaged Warehouses	Dead	Wounded	Near Asakusa, Nippon in Akasaka Ward	
	Riganjihomori	460	41		25		1	1		
	Nishidohomi	305	32		12					
	Kitaohomi	267	35		6					
	Iriyamero	191	20		2					
	Shimofukuro	48	6							
	Mine		11							
	Arai tube		5							
	Ichinokura		1	3	1					
						1 (Gate of Tannery House, Half Damaged)				
	Kugahara		3		5					
	Kitakamata		12		8					
	Ohnmaru	1	2		3					
	Magono		1	86	3					
	Kirigoro	17	1							
	Ikegami		2							
	Shimochegani		1	4	3		1	1		
	Mitsutaka				1					
	Yukigaya				5					
	Nakanoh	63	1	2	5					
	Nianoya		1							
	Ohyama	65	20		1					
	Kanimeguro				7					
	Ohi	462								
	Shimoyagakubo	51			1					
	Eminoyagakubo	36								
	Togoshi	141								
	Tosivana			1 (Half Damaged)						
	Kanjoheki	26								
	Shimonoheki	49								
	Irukishi	39								
	Yotsukaitakuichi	64								
	Shimotekanava	88	10	23	3					
	Shinagawa-oku	1631	14 (Half Damaged)	382 (Mostly Damaged)	217 (Partly Damaged)					
			14 (Partly Damaged)							
Record of Personal Experience of Big Earthquake and Big Wind	In Kamomei Village, most houses were destroyed, turned up and down.								Kamei in Katsushika Ward	
History of Yodogawa Ward Nakaguchi Book	Saigasaki Village, Number of Houses; 48, Population; 245, Totally Damaged; 8, Half Damaged; 13 Totally Damaged; 11, Half Damaged; 45									
(Kanagawa Pref.) History of Kawasaki City History of Yokohama City	Number of Houses; 1726, Totally Damaged; 21, Half Damaged; 21 Ichiba Village, Number of Houses; 130, Totally Damaged; 1, Half Damaged; 2 Uchiboda Village, Number of Houses; 244, Totally Damaged; 6, Half Damaged; 1								Near Ichibana-cho, Ichiba-cho, Uchiboda-cho in Yokohama Ward. Near Uchiboda in Yokohama Ward.	

by T. Onogi

RELATIONSHIP BETWEEN MODIFIED MERCALLI INTENSITY
AND WOOD FRAME DWELLING EARTHQUAKE INSURANCE

Karl V. Steinbrugge

Insurance Services Office, San Francisco, California, U.S.A.

and

S. T. Algermissen

U.S. Geological Survey, Denver, Colorado, U.S.A.

ABSTRACT

Traditionally, earthquake insurance rates have been based on business judgment tempered by engineering input obtained from analyses of observed earthquake damage. The development of loss simulation techniques has provided important new input for improvement of the basis for earthquake insurance rates. Some important loss simulation results are reviewed. Modified Mercalli intensity can be directly related to dwelling loss and is an important parameter in dwelling loss simulation studies. Careful additional study of existing dwelling loss data (such as is available for the 1971 San Fernando, California, earthquake) together with well planned damage studies after future earthquakes will lead to greatly improved loss estimates. Probabilistic loss models should also be developed for dwelling loss studies and the effects of parameter uncertainties taken into account.

KEYWORDS: Earthquake losses; Earthquake insurance; Loss simulation; Intensity-loss relationships

INTRODUCTION

The traditional property insurance method is to establish rate levels based on insurance loss experience gained over the years. Unfortunately, earthquake insurance loss data do not exist in any meaningful way. In the United States, earthquake insurance was not written on dwellings at the time of the 1906 San Francisco shock. Practically no earthquake insurance was carried by homeowners prior to the 1925 Santa Barbara earthquake, the 1933 Long Beach earthquake, and the 1952 Kern County earthquake. Little was carried in the most heavily shaken areas of the 1971 San Fernando shock. Dwelling loss data from elsewhere in the world do not exist in an insurance loss sense and are usually complicated by non-relevant construction.

Over the years, earthquake insurance rates have been generally based on business judgment which was tempered by engineering judgment in turn based on observations of damage in earthquakes. There were no alternate methods. In recent years, simulation studies on dwelling earthquake losses tend to confirm the appropriateness of long established dwelling rates -- this newer methodology will be discussed in more detail in the next section of this paper.

The judgment procedures which were used for over half a century are adequate for small volumes of business. In recent years, however, there have been an increasing number of inquiries and statements from Federal and California state authorities regarding the possibility of mandation of earthquake insurance for dwellings. In California alone, dwelling values at risk in a single major event are in terms of many billions of dollars. This, in turn, has made research economically feasible for dwelling insurance rates as well as a need to examine possible industry capacity problems. It follows that it has become appropriate to develop alternate loss determination methodologies. Methods for estimation of losses to wood frame dwellings are discussed in this paper; however, the techniques discussed here are generally applicable to other classes of construction, if the building units are widely distributed in the affected area.

ECONOMIC CONSTRAINTS

Any kind of basic earthquake insurance study, whether for the private or public sector, requires an understanding of monetary loss associated with specific earthquakes. Monetary loss, usually expressed as a percentage of value, must be relatable to (a) earthquake magnitude, (b) nature and duration of ground motion, and (c) a practical classification of buildings according to damage patterns. Historic records of Modified Mercalli intensities have important functions in these earthquake insurance loss studies since these intensities may, in many cases, be equated to monetary loss.

The detail and refinement of any earthquake loss estimates intended for practical insurance application will be limited principally by costs. In actuality, the engineering costs involved in field examining dwellings, identifying them by class or damage type, and recognizing local geologic hazards must be borne by the insurance purchaser. To these costs must be added overhead and taxes. In the private sector's competitive marketplace,

a complex dwelling classification system will substantially increase total costs and, while better results are obtained in an engineering-science sense, normally will make the entire process economically unfeasible. For example, the current class rated earthquake insurance premium (i.e., rate manual basis) for a \$50,000 wood frame dwelling in San Francisco or Los Angeles would not exceed \$100 annually for the usual case. If individual engineering inspections and analysis were made and periodically updated (say not exceeding 10-year intervals) these engineering costs plus overheads of accounting, filing, etc., would probably substantially exceed \$10 per year. Assuming a minimum of \$10 per year, this would amount to a 10 percent increase in premium over class rating (i.e., no inspections) -- probably enough to lose a competitive edge in the private sector. Unfortunately, it has yet to be shown that the cost-benefit would be sufficiently favorable to all concerned to warrant inspections. Indeed, based on fire insurance experience, specific rating of single family dwellings is quite unwarranted. Alternative to all of the foregoing, cost differentials probably would remain the same even if insurance were issued by the public sector, unless subsidized (eventually being paid by the public through taxes).

In past practice, the approach has been to group all single family wood frame dwellings into one class and disregard construction variants, thereby eliminating high cost engineering field inspections and reducing paperwork to that which can be readily processed by the homeowner, his agent, and office clerks. It has been practical to map principal structurally poor ground areas and apply a rate penalty in major communities where insurance may be commonly carried.

Practical dwelling sub-classes could include age approximations and story height. Date of construction determined or estimated to the nearest decade is useful since age reflects, in a general way, earthquake resistive construction practices and the possible amount of deterioration over time. Microzonation has not yet been developed to a state where it can be applied on a uniform and consistent basis from city to city and is relatable to usable loss figures, and therefore is not part of present insurance rating programs. In summary, economics dictates that wood frame dwellings be simply classed, with possible rating variants being based on easily determined factors such as age, story height, geographic location by political boundaries, and location in major structurally poor ground areas.

SIMULATED LOSS TECHNIQUES

A fundamental advance in improving the basis for earthquake insurance rates has been the development of earthquake loss simulation techniques. Several important dwelling loss

simulation studies have been published in recent years^{1,2,3,4}, in addition to general discussions of the simulation technique⁵.

Direct economic losses resulting from earthquakes depend upon: (1) the distribution and kinds of property at risk, (2) the ground shaking and ground failures of various types associated with earthquakes, and (3) the relationships between (1) and (2) that result in economic loss. In loss simulation studies, the distribution of property at risk is estimated in some manner. The seismicity of the area considered is modeled either deterministically or probabilistically and losses are computed using damage-ground motion and damage-ground failure relationships. As an example, consider the San Francisco area. In the San Francisco area, earthquakes have damage patterns that are related to and can be quantified with respect to earthquake magnitude, length of fault displacement, geographic damage distribution throughout the affected area by class of construction, and other similar measurable characteristics. Using the earthquake history of the area, it is possible to simulate the damage and losses for any postulated or known distribution of buildings by construction class for any given earthquake or set of earthquakes. The total losses for each class of construction for the entire historic record can be developed by summation. In other words, the total dollar loss for any class of construction and for any geographic distribution can be computed for any given earthquake in the San Francisco area. It then follows that the total loss for all earthquakes listed in the historic record can be determined and the simulated average annual loss established. Alternately, a probabilistic simulation model may be constructed, incorporating uncertainties in inventory, seismicity, ground motion, and resulting losses to buildings. Isoseismal maps and the related intensity data play a key role in simulation studies. Of paramount importance is the need to relate intensity to monetary loss. While the concepts are simple, the computational details can be complex; the cited references^{1,2,3,4}, describe the methodology preferred by the authors. Some important results from simulation studies in California are given in Table 1. The losses in Table 1 are losses associated with ground shaking and do not include losses associated with ground failure. Losses to dwellings from ground

¹Anonymous, "Summary and Recommendations," in Studies in Seismicity and Earthquake Damage Statistics, 1969, U.S. Coast and Geodetic Survey, 23 (1969).

²K. V. Steinbrugge, F. E. McClure and A. J. Snow, "Appendix A," in Studies in Seismicity and Earthquake Damage Statistics, 1969, U.S. Coast and Geodetic Survey, 142 (1969).

³S. T. Algermissen, J. C. Stepp, W. A. Rinehart, and E. P. Arnold, "Appendix B," in Studies in Seismicity and Earthquake Damage Statistics, 1969, U.S. Coast and Geodetic Survey, 68 (1969).

⁴W. A. Rinehart, S. T. Algermissen, and Mary Gibbons, "Estimation of Earthquake Losses to Single Family Dwellings," U.S. Geol. Survey Open-File Rept. 76-156, 57 plus appendices (1976).

⁵D. C. Friedman, "Computer Simulation of the Earthquake Hazard," Proc. Conf. on Geologic Hazards and Public Problems, May 27-29, 1969, U.S. Govt. Printing Office, 153-181 (1970).

shaking have been shown to be far more important than losses from ground failure in the San Francisco Bay area⁶, and this is believed to be true throughout California. Other interesting results have also been obtained for dwellings in California. Figure 1 is a map of California with the state somewhat arbitrarily divided into a northern, middle, and southern portion. Using the known historical seismicity of the state from 1801 to 1967, average dollar losses to dwellings in northern, middle, and southern California were found to be in the ratio of 1.00:0.19:1.25. The distribution of dwellings units taken from the 1960 United States Census (updated to 1967) was used as inventory. Figure 1 also shows seismic risk zones in California as defined by Algermissen⁷. Assuming the same seismicity and inventory as above, average dollar losses per dwelling in seismic risk zone 3 (Figure 1) were found to be approximately 100 times the losses per dwelling in zone 2.

Using the historical earthquake record 1801-1967 in California and the 1967 distribution of dwellings in California, dwelling losses as a function of earthquake magnitude may also be obtained. Figure 2 shows the distribution of dwelling loss with magnitude in California⁶. Note that because of the exponential distribution of earthquakes with magnitude and the nature of the damage to dwellings, the larger earthquakes in California do not account for the greatest losses.

One inherent weakness of all known simulation studies involves the need to accurately know the actual monetary losses to dwellings as a function of each intensity. This loss information should be known by construction component*, by age, by height, and by local surficial geologic characteristics if the results are to be transferable to other regions. It is also necessary to carefully define loss (personal vs. impersonal, building vs. content, etc.) and value (cash vs. replacement for older buildings, etc.). It would be wrong to apply loss figures derived from older rotten foundation houses to new earthquake resistive ones, for example. A specific instance of the detail required, the average loss to painted gypsumboard partitions for MM=VIII should be known as a percentage to dwelling market value (or other value) by building age, height, etc. Techniques exist to answer these kinds of questions, but all techniques involve varying degrees of judgment based on appropriate experience by engineers, architects, contractors, etc. Obviously, tabulated actual loss experience data would be better than value judgments.

Good progress in simulation studies, then, will come from appropriately gathered actual loss experience in order to supplement or revise current judgmentally determined

⁶S. T. Algermissen, W. A. Rinehart, and J. C. Stepp, "Techniques for Seismic Zoning: Economic Considerations," Proc. Int'l. Conf. on Microzonation for Safer Construction, Seattle, Washington, Vol. II, 943-956 (1972).

⁷S. T. Algermissen, "Seismic Risk Studies in the United States," Proc. 43, World Conf. on Earthquake Eng., Vol. 1, 14-27 (1969).

*Construction component is defined as an assembly of materials within a dwelling which is readily identifiable and has a recognizable damage pattern. Painted gypsum on interior wood stud partitions is one such example.

monetary values. A review of past and current literature has shown practically nothing of substantial value beyond that cited in the references of this paper.

POST-EVENT ANALYSIS: SAN FERNANDO 1971 CASE STUDY

The first major post-earthquake study which related monetary losses to intensity was conducted after the 1971 San Fernando, California earthquake. The Pacific Fire Rating Bureau surveyed the damage to approximately 12,000 single family wood frame dwellings located in the most heavily shaken areas. Their survey form identified the following items, among others:

Location by city block.

Age group: (a) pre-1940, (b) 1940-49, and (c) post-1949.

Number of stories.

Floor construction.

Degree of damage to: (a) foundations, (b) wood frame, (c) interior finish by type of finish, (d) exterior finish by type of finish (including veneer), and (e) chimney.

Ground disturbance, if any, including faulting.

Improved loss data for input to simulation studies is best obtained from information carefully gathered shortly after an earthquake. When these loss data are related to intensity, then the loss relationships may be applied to isoseismal maps of other earthquakes or directly to simulated loss studies. Some work in progress is worth reviewing.

Intensity-Loss Correlations:

Figure 3 is an isoseismal map of the most heavily shaken dwelling areas. This map was based on a literal reading of the definitions of the Modified Mercalli scale with respect to dwellings. The base map for Figure 2 (i.e., map without isoseismal lines) is Figure 16 from reference 8; each tract includes a number of city blocks and has boundaries selected to enhance sample consistency (i.e., similar values, similar age of construction, etc.). Three different vibrational intensities are shown: VII, VIII, and IX. Additionally, some faulting and related ground breakage areas are, by definition, Intensity X. However, adjacent to and comingled with Intensity X areas are vibrational intensities of VII, VIII, and IX.

In Figure 3, the "average dwelling loss" for each tract may be interpreted as an equivalent of an average intensity for that tract. This suggests correlating Modified Mercalli intensity in terms of percent loss. A crude but reasonable correlation based on Figure 3 plus extensive personal knowledge of the area is as follows:

MM VII: 2 percent to and including 5 percent dwelling loss

MM VIII: 6 percent to and including 10 percent dwelling loss

MM IX: 11 percent and greater dwelling loss

⁸K. V. Steinbrugge, E. E. Schader, H. C. Bigglestone, and C. A. Weers, "San Fernando Earthquake, February 9, 1971," Pacific Fire Rating Bureau, 93 plus map (1971).

For the purposes of this paper, this correlation will be used as a tentative relationship between intensity and dwelling loss. This correlation is restricted to vibrational damage, and therefore excludes the geologic effects in MM VII-X areas. It should be recognized that the foregoing relationship between dwelling loss and intensity is partially judgmental since there is no other way to relate the subjective wording in the Modified Mercalli definition to numerical loss values. In any event, it is a rational correlation.

A possible improvement in the San Fernando intensity-loss correlations is to re-examine the basic data for the 12,000 dwellings by sub-dividing the tracts into smaller units. The isoseismal lines may vary somewhat but the correlations are expected to stand.

The loss-intensity correlations as given above are not transferable to most other communities. They are only transferable to communities having comparable amounts of dwelling construction as to story height, age of construction finishes, etc. For example, the dwelling age distribution in the San Fernando study area was:

Pre-1940	5.3 percent
1940-49	38.2 percent
Post-1949	56.5 percent

with 94.2 percent of the study area being one story. The identical ground motion striking a community of predominately older two story dwellings would cause much larger losses than those in San Fernando; thus the intensity-loss correlations for San Fernando would not be transferable to the other community discussed below.

If, however, the damage surveys for 12,000 dwellings were sorted (sub-classed) by age, height, and other factors, then the resulting intensity-loss correlations for each item could be transferable to many other communities. For an over-simplified example, a California community consisting of 50 percent 1940-49 one-story dwellings plus 50 percent one-story post-1949 dwellings (all other construction features identical) would have computable losses for MM VII, VIII, and IX. In summary, it is possible to synthesize the potential dwelling loss for MM VII, VIII, and IX for any community if the number and distribution of appropriate dwelling sub-classes are known and if loss-intensity correlations for these sub-classes are known.

Damage Factors:

An important item in detailed simulation involving insurance deductibles is a knowledge of damage distribution among "identical" dwellings or among "identical construction components" of dwellings. For example, in a tract of 100 identical homes having 4 percent average dwelling loss, the actual loss distribution might be:

Under 1 percent loss	40 homes	6 percent - 10 percent loss	5 homes
1 percent - 3 percent loss	30 homes	11 percent - 20 percent loss	3 homes
4 percent - 5 percent loss	20 homes	Over 20 percent loss	2 homes

Assume a 5-percent insurance deductible, the actual loss over the deductible is not zero, i.e., the average loss (4 percent) minus the deductible (5 percent). Thus, average values cannot be used. This introduces the need for a loss distribution function which in previous studies has been termed "damage factor."

Damage factor is defined as the ratio of the number of structures having a specified degree of loss for a given construction component to the number of structures in the tract under study. For the 1971 San Fernando earthquake, the damage factors were computed and grouped according to intensities with results as shown in Table 2. This information is transferable to other communities having similar construction component characteristics.

PROSPECT

While detailed sophisticated studies on earthquake insurance rate levels and affects of insurance deductibles on aggregate losses may give a feeling of confidence, in many ways these studies are no better than their data base. Any studies involving the losses over time must be based on, or be consistent with, losses over the historic record. The use of Modified Mercalli intensities and their resulting isoseismal maps becomes inescapable in retrospective insurance simulation loss studies since, for better or worse, these are the best available data.

Substantially improved loss information from the 1971 San Fernando earthquake plus that expected to be obtained after future shocks, is expected to greatly improve the quality of the numerical output. Concurrently, simulation studies should continue to be conducted, particularly with the view towards simplification. Probabilistic loss models should also be developed and compared with loss estimates obtained using historical seismicity as input.

TABLE 1
CALIFORNIA EARTHQUAKE LOSS SUMMARY
Loss in Dollars (1968 base)
(From Table 3 of Reference 3)

	Total	\$250 Deductible	Per Damaged Dwelling ¹	Per Dwelling Unit ²
San Francisco, 1906				
Total affected area	\$1,156,370,424	\$ 863,129,283	\$916	\$ 302
Nine Bay Area Counties ³	1,013,524,447	772,763,546	992	870
Long Beach, 1933				
Total affected area	\$97,520,100	412,586,399	750	197
100 Year Period				
Entire state	6,539,698,400	2,766,142,200	385	1,216
Nine Bay Area Counties ³	2,328,105,900	1,137,936,900	436	1,997
Los Angeles and Orange Counties	2,752,299,700	1,090,291,000	377	1,285

¹Dwellings sustaining some damage were used. For the 100 year period, dwellings may be repeatedly damaged.

²All dwellings (damaged and undamaged) within the geographical area considered for the IV isoseismal of the earthquake.

³Marin, Sonoma, Napa, Solano, San Francisco, Santa Clara, Contra Costa, Alameda and San Mateo Counties.

TABLE 2
DAMAGE FACTORS FOR 1971 SAN FERNANDO EARTHQUAKE
 From Steinbrugge, et al (1971) data (reference 8)

Construction Component	Degree of Damage*	Damage Factor (%) for MM Intensity				
		(% of Dwellings Having Given Degree of Damage)	VII	VIII	IX	VII-X
Structural -- foundation	None	98.7%	88.4%	61.4%	82.8%	
	Slight	0.8%	9.4%	29.3%	9.0%	
	Moderate	0.4%	1.8%	6.0%	4.7%	
	Severe	0.1%	0.4%	3.3%	3.5%	
		100.0%	100.0%	100.0%	100.0%	
Structural -- frame	None	94.0%	67.6%	39.9%	72.8%	
	Slight	5.1%	25.6%	45.3%	35.5%	
	Moderate	0.5%	4.9%	8.7%	7.1%	
	Severe	0.4%	1.9%	6.1%	4.6%	
		100.0%	100.0%	100.0%	100.0%	
Exterior -- stucco	None	26.3%	6.7%	2.9%	31.9%	
	Slight	72.6%	87.3%	81.4%	55.7%	
	Moderate	1.0%	5.1%	10.3%	9.0%	
	Severe	0.1%	0.9%	5.4%	3.4%	
		100.0%	100.0%	100.0%	100.0%	
Exterior -- wood	None	87.1%	55.6%	35.7%	63.7%	
	Slight	8.7%	36.2%	37.0%	23.3%	
	Moderate	3.7%	4.2%	15.6%	7.8%	
	Severe	0.5%	4.0%	11.7%	5.2%	
		100.0%	100.0%	100.0%	100.0%	
Exterior -- other	None	90.7%	71.5%	37.7%	83.4%	
	Slight	7.2%	11.2%	27.5%	10.0%	
	Moderate	2.1%	7.8%	11.6%	3.3%	
	Severe	---	9.5%	23.2%	3.3%	
		100.0%	100.0%	100.0%	100.0%	
Chimney (1 chimney)	None	84.9%	58.5%	29.9%	66.7%	
	Slight	5.1%	22.4%	39.1%	13.5%	
	Moderate	6.8%	6.6%	8.3%	9.6%	
	Severe	2.5%	8.9%	19.6%	5.8%	
	Total	0.7%	3.6%	3.1%	4.4%	
		100.0%	100.0%	100.0%	100.0%	

*See Steinbrugge, et al (1971), page 20, for summary definitions (reference 6). Field inspectors used this terminology which, in turn, was related to percent loss.



Figure 1.--Seismic risk zones in California (after Reference 1). The hatched area represents zone 2 and the remainder of the state, zone 3. The heavy black lines divide the state into northern, middle, and southern California as used in this report.

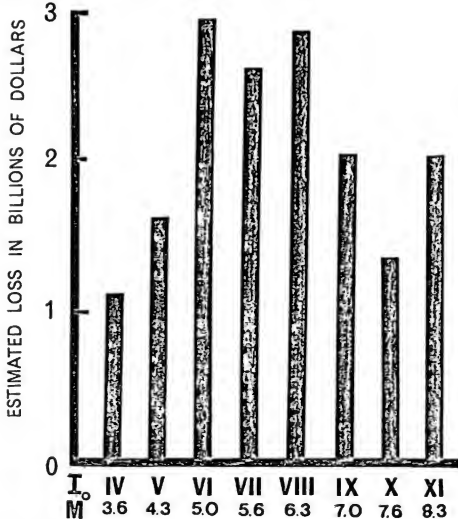


Figure 2.—Estimated dollar losses to wood frame dwellings in California as a function of maximum Modified Mercalli intensity (I_0) and equivalent mean magnitude (M). Historical earthquakes in California for the period 1801-1967 were used as the seismicity input. The spatial distribution of dwellings and their characteristics were assumed constant at the 1967 level for the loss simulation study. (Adapted from Reference 6).

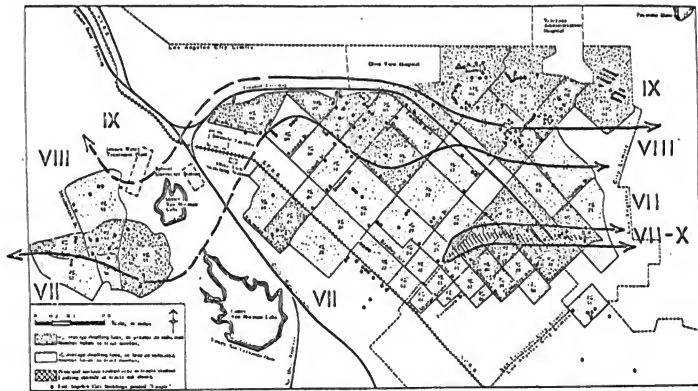


Figure 3.—Modified Mercalli intensities based on observed dwelling damage, San Fernando, California, earthquake of 1971.

Warrants for Retrofitting Highway Bridges

Anatole Longinow
and
Ernest Bergmann
IIT Research Institute, Chicago, Illinois

and

James D. Cooper
Federal Highway Administration, Washington, D.C.

ABSTRACT

A methodology for determining whether or not to seismically retrofit an existing bridge is presented. The method is based on the concept of identifying and comparing the importance of the bridge to its structural integrity. Criticality factors which are expressed in terms of bridge classification and its importance to the social, medical, economic, and security needs of a geographical area following a natural disaster are developed. Structural factors, which estimate a bridge's ability to withstand an earthquake, are determined analytically or by inspection. The criticality and structural factors are compared to determine if a bridge warrants retrofitting. The method is demonstrated by example.

KEYWORDS: Earthquake; Bridges; Retrofit decision

INTRODUCTION

A bridge is a vital link in any road network. If a disaster occurs, a bridge may be destroyed or damaged to the extent that it cannot sustain traffic or it blocks an intersecting road. A method is presented to identify and quantify the criticality, or worth, of a bridge in relation to the road, the road network, the community, and the national defense/security system. The criticality is then compared to the capability of the structure to withstand the disaster and a method is established to determine whether or not retrofit is warranted.

Specifically, the worth of a bridge can be evaluated in terms of:

- Administration/Transportation System Effects. The City, County, State, and Federal highway organizations classify roads and streets. These classifications are based on plans which relate the importance of the roads and streets to the normal emergency transportation needs of the community and the nation.
- Social/Survival Effects. Social/survival effects involve the ability of the community to meet its short term emergency needs following a disaster. Normally the social/survival effects are considered in the administration/transportation system plans for the roads and streets. There are instances, however, in which those plans have been dated by changes within or near the community (e.g., a subdivision was added, a hospital was built, etc.), or the effect on the community was not considered in the original plan.
- Security/Defense Effects. Security/defense effects concern the importance of the bridge in regard to its ability to move troops and equipment to, and within, an area to maintain law and order or to meet a threat to the security of the area, region, or Nation.
- Economic/Personal Effects. Following a disaster, the recovery process begins. The economic/personal effect relates the community need for the bridge to return to its predisaster social and business status.

Each measure of worth (e.g., Social/Survival Effects) has measures of effectiveness (e.g., Medical Support) which relate to the need for the bridge. The measures of effectiveness can be grouped, quantified, or qualified to allow an engineer to make a relative assessment of the worth of the bridge.

The measures of worth for each effect can be interrelated to allow overall assessment of the need for the bridge. After all bridges within an area of interest are analyzed, they can be separated into two categories: 1) retrofit is required to enable the bridge to withstand the earthquake, or 2) retrofit is not required because either the bridge can withstand the earthquake or the loss of the bridge does not justify the retrofit expense. Since highway budgets are finite, it is probable that some additional priority system will be needed to rank the bridges in the first category. The ranking can be achieved by applying a cost-benefit analysis and the retrofit budget can then be allocated according to this ranking. A discussion of the cost-benefit analysis is not included in this report. The state-of-the-art of evaluating the worth of the bridge, in terms of the effects identified, does not allow the worth to be graded rigorously enough to permit a meaningful cost-benefit analysis.

It is noted that a significant amount of research is required to identify and quantify each of the effects which are briefly described above. Therefore, only a brief discussion of the basic methodology, the elements of the methodology, preliminary weighting of criticality factors, and sample calculations to illustrate the methodology are presented.

METHODOLOGY

The procedure for assessing the worth of a bridge is described in this section. It represents a sequential evaluation of worth by considering the resulting effects caused by the loss of the bridge.

Procedural Flow Diagram

A decision diagram for evaluating whether or not a bridge warrants retrofit is illustrated in Figure 1. Each block or diamond in the procedural flow diagram is an element; the work elements are rectangular and the decision elements are diamonds. The measures of worth are evaluated in sequence (Elements 1, 3, 5, and 7). The output of each work element is a criticality factor (CF), rated from 0 through 3, which relates the worth of the bridge to the particular measure of worth. The higher the criticality factor the more the bridge is worth to that particular element. As an illustration, the bridge may be evaluated in terms of its worth to the social/survival effects (Element 3). A criticality factor of 3 indicates that the bridge is critical (e.g., it is the only ambulance route); a factor of 2 indicates that the bridge is desired; a factor of 1 indicates that it is convenient; and a factor of 0 indicates that it is expendable.

Decision points (Elements 2, 4, 6, and 10) are inserted between work elements. These decision points act as filters to reduce the effort needed to make a retrofit decision. At each of the first three decision points (Elements 2, 4, and 6), a criticality factor of 3 (CF=3) indicates that the bridge is of sufficient worth to merit an evaluation. If a criticality factor of less than 3 is selected, the evaluation process is continued until work Element 8 is reached.

In work Element 8, the highest criticality factor of the four measures of worth (Elements 1, 3, 5, and 7) is selected. Similarly, a structural factor (SF) is selected (Element 9) which relates the capability of the bridge to survive damage from the disaster.

The structural factors are graded over the same range as the criticality factor. A structural factor of 3 indicates that the bridge is sound; SF=2 indicates the bridge is probably sound; SF=1 indicates the bridge is probably unsound; and SF=0 indicates that the bridge is unsound.

Next, the criticality and structural factors are compared (CF - SF). If the difference is less than or equal to zero, retrofit of the bridge is not warranted.

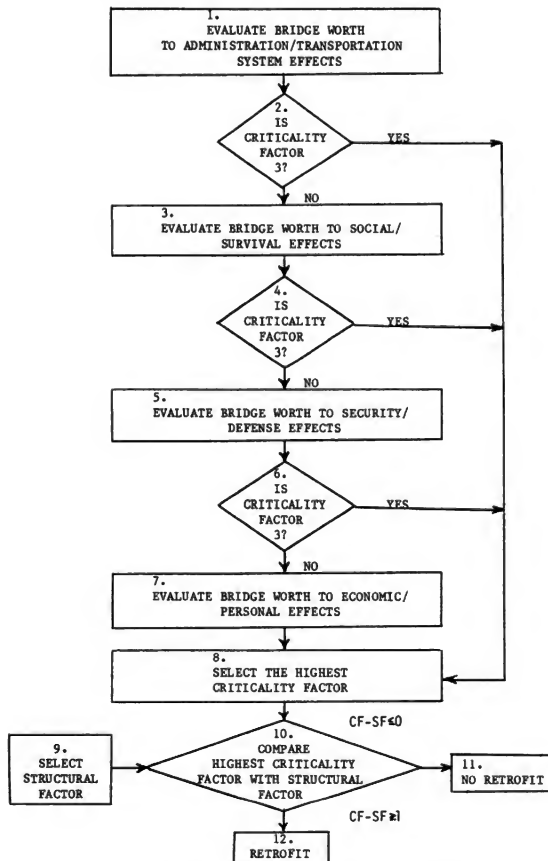


Figure 1 Bridge Retrofit Warrant Procedural Flow Diagram

If the difference is greater than or equal to 1, then retrofit is warranted. Table I lists the retrofit decision elements. This table, or the criteria illustrated in Figure 1, can be used as the basis for determining whether or not a bridge warrants retrofit.

Table I
RETROFIT/NO RETROFIT DECISION TABLE

Criticality Factor (CF)	Structural Factor (SF)	CF - SF	Subjective Evaluation	Retrofit Decision
3	3	0	Critical/Sound	No
3	2	1	Critical/Probably Sound	Yes
3	1	2	Critical/Probably Unsound	Yes
3	0	3	Critical/Unsound	Yes
2	3	-1	Desired/Sound	No
2	2	0	Desired/Probably Sound	No
2	1	1	Desired/Probably Unsound	Yes
2	0	2	Desired/Unsound	Yes
1	3	-2	Convenient/Sound	No
1	2	-1	Convenient/Probably Sound	No
1	1	0	Convenient/Probably Unsound	No
1	0	1	Convenient/Unsound	Yes
0	3	-3	Expendable/Sound	No
0	2	-2	Expendable/Probably Sound	No
0	1	-1	Expendable/Probably Unsound	No
0	0	0	Expendable/Unsound	No

Structural Factor (SF)

3 = Sound

2 = Probably Sound

1 = Probably Unsound

0 = Unsound

Criticality Factor (CF)

3 = Critical

2 = Desired

1 = Convenient

0 = Expendable

ADMINISTRATION/TRANSPORTATION SYSTEM (ATS) EFFECTS

Highway systems are grouped into a number of different classifications for administrative, planning, and design purposes. At least three different types of systems exist which affect the administration and operation of highways. These are State-county-local administrative systems, commercial-industrial-residential-recreational systems, and the Federal-Aid System. However, they all serve to develop a complete integrated highway system.

The most basic classification system for administration purposes groups highways and streets into two broad classes: systems serving rural areas or connecting urban areas, and streets or highways serving urban areas.

The rural area classification system contains following levels of road classes:

- Interstate,
- Primary (excluding interstate),
- Secondary roads with volume greater than 1,000 vehicles per day
- Secondary roads with traffic less than 1,000 vehicles per day (may be subdivided into 500-1,000, 100-400, under 100),
- Feeder roads (same as secondary roads under 1,000), and
- Tertiary roads.

A quantitatively similar system for urban areas includes:

- Expressways,
- Arterials,
- Collectors, and
- Local roads and streets.

The classification criteria for rural roads are possibly more self-explanatory than the criteria for urban streets. Table II lists the major function of each type of urban road.

Table II
URBAN ROADWAY FUNCTIONS

System	Function
Expressway System (Including freeways and parkways)	Provides for expeditious movement of large volumes of through traffic between areas and across the city, and not intended to provide land-access service.
Major Arterial System	Provides for through traffic movement between areas and across the city and direct access to adjoining property; subject to necessary control of entrances, exits, and curb use.
Collector Street System	Provides for traffic movement between major arterial and local streets, and direct access to adjoining property.
Local Street Systems	Provides for direct access to adjoining land and for local traffic movement.

The classifications carry with them a set of suggested minimum design standards which are in keeping with the importance of the system and are related to the specific transportation services the system is to perform. The functions of the rural road system hierarchy are essentially similar to the urban road system.

It is likely that exceptions to the classifications described above occasionally will occur and adjustments in assigned values could be made. Such differences are most likely to be the result of radically altered transportation patterns which have rendered portions of the system obsolete or of recent demands which outstrip the ability of the administrative system to provide an adequate roadway.

More specific information on classification criteria may be found in reference 1.

Criticality Factors

A procedure for determining the criticality factor for ATS effects is outlined below.

1. Get Federal-Aid Highway Map of region of interest from Federal Highway Administration (FHWA) or from State Department of Transportation.
2. Identify the bridge on the map.
3. Identify the road or street leading to and from the bridge.
4. Identify the road or street (if any) passing under the bridge.
5. Identify the classification of the two roads or streets from the legend on the map.
6. Select a criticality factor from Table III based on the highest of the two road or street classifications.

Table III
CRITICALITY FACTORS FOR ATS EFFECTS

Criticality Factor (CF)	Road or Street Classification	
	Rural	Urban
3	Interstate	Expressway
2	Primary	Major Arterial
1	Secondary	Collector
0	Tertiary	Local

SOCIAL/SURVIVAL (S/S) EFFECTS

Evaluation of the social/survival effect is based on the need for roadways immediately following a disaster. It is possible to use roadways with degraded levels of performance as long as continuous routes can be established. When evaluating the S/S effects on a system, the primary requisite should be identifying a system which can facilitate the emergency services listed in Table IV as rapidly as possible.

It is obvious that the evaluation of the worth of a bridge in the social/survival related context is compounded by the uncertainty of where the disaster might strike and the complexity of the transport network. However, a subjective approach is presented for consideration.

Obtain a detailed map of an area and determine the extent to which the locality has developed disaster plans. Bridges of interest can be readily identified, the population density estimated, the road network illustrated, and important service facilities (e.g., hospitals, fire stations, etc.) identified on the map. After the local departments involved in disaster related operations are interviewed, a disaster scenario can be developed. The significance of the transport network, particularly bridges, can be subjectively established and appropriate criticality factors selected.

Criticality Factors

A procedure for determining the criticality factor for S/S effects is outlined below.

1. Get detailed map of area.
2. Identify bridges of interest on the map.
3. Identify segment of community or area which would be affected by the disaster.
4. Identify hospitals, fire stations, police stations, reservoirs, and power stations.
5. Identify preferred fire and police route by telephone calls or visits to the respective departments.
6. Identify alternate routes in the event that the bridge of interest is destroyed.
7. Identify utilities carried by bridge.
8. Select criticality service from Table IV.
9. Record the associated criticality factor.

Table IV
CRITICALITY FACTORS FOR S/S EFFECTS

Criticality Factor (CF)	Criticality Service (Subjective Evaluation)	Services Considered
3	Survival Related	. Communications
2	Health Related	. Energy
1	Comfort Related	. Evacuation
0	Insignificant	. Medical Support . Food . Water . Law Enforcement . Fire and Disaster

SECURITY/DEFENSE (S/D) EFFECTS

The 1973 Federal-Aid Highway Act requires that a revised plan for defense highways be developed by each individual State. The plan will include, as a minimum, the Interstate and the Federal-Aid primary routes, although some routes may be deleted if this is considered appropriate by the State. The defense highway network will provide connecting routes to important military installations, industries, and resources not served by the primary routes and will include locations of the following:

- Military bases, national guard installations, supply depots, etc.
- Hospitals, medical supply centers, emergency depots, etc.
- Major airports
- Defense industries including those that could easily or logically be converted to such
- Refineries, fuel storage and distribution centers
- Major railroad terminals, railheads, docks, truck terminals
- Major power plants including hydroelectric centers at major dams

- Major communications centers
- Other facilities that the State considers important relating to national defense or natural disaster emergencies.

Bridges are considered a part of the Security/Defense Road Network data bank and can be classed in terms of critical, noncritical, nonbypassable, and bypassable. Information on the administration and operation of this data bank can be found in reference 2.

Criticality Factors

A procedure for determining the criticality factor for S/D effects is outlined below.

1. Determine bridge location.
2. Obtain:
 - Road Section No.
 - Miles from beginning of section
 - Bypass Code
 - Average Daily Traffic
 - Criticality (this information is sometimes available)
3. With criticality and bypass data enter Table V.
4. Record criticality factor.

Table V
CRITICALITY FACTORS FOR S/D EFFECTS

Criticality Factor (CF)	Bridge Criticality/ Alternate Route
3	Critical Structure/Nonbypassable
2	Critical Structure/Bypassable
1	Noncritical Structure/Nonbypassable
0	Noncritical Structure/Bypassable

ECONOMIC/PERSONAL (E/P) EFFECTS

The measure of worth of a bridge, during the recovery period, relates to: (1) the amount of traffic which normally passes over the bridge; and (2) the somewhat rare instances in which a severed bridge isolates a community from its primary source of business.

The average annual daily traffic, AADT, listed in Table VI, as it relates to the criticality factors, is in general agreement with the road or street classifications listed in Table III. Some adjustment can be made by the investigator to characterize the importance of a particular bridge within the environment of a particular community. For instance, the AADT over a bridge in a rural environment may be significantly below the top category ($\text{AADT} \geq 80,000$), but the bridge, as the only link between two communities, may have a higher level of importance than would be indicated by the AADT alone. A weighting factor, then, could be applied to the AADT which provides the adjustment. It is important, however, to maintain consistency when applying the weighting factors to each bridge in the geographical area of interest so that the relative importance of each bridge is characterized.

Criticality Factors

A procedure for determining the criticality factor is outlined below.

1. Identify the road and the road section (intersection, town, milepost, etc.) on which the bridge is located.
2. Determine the estimated average annual daily traffic over the bridge.
3. Enter Table VI at the appropriate level of traffic.
4. Select and record the criticality factor.

Table VI
CRITICALITY FACTORS FOR E/P EFFECTS

Criticality Factor (CF)	Average Annual Daily Traffic* (AADT) Over Bridge
3	80,000 - Up
2	25,000 - 79,999
1	5,000 - 24,999
0	0 - 4,999

*AADT is the total yearly volume (number of cars passing a particular point) divided by the number of days in the year.

EARTHQUAKE EFFECTS ON BRIDGES

To better understand seismic effects on structures, seismic damage to bridge abutments, piers, girders and supports has been documented. Damage typically occurs to bridges having the following inherent weak details: 1) bearings, 2) substructures, and 3) foundations. Types of failure most often observed are: tilting, settling, sliding, cracking, and overturning of substructures; displacement, cracking, and dislodging of girders at supports; shearing or pulling out of anchor bolts and crushing of concrete at supports; crushing of concrete columns; pulling out of reinforcing bars at column caps or footings; and settlement of approach roads and slippage of wingwalls from abutments.

A study entitled "Seismic Retrofitting of Existing Highway Bridges," reported in the Proceedings of the Sixth Joint UJNR Panel Conference, was conducted to identify and define through structural analyses practical techniques and criteria for retrofitting existing bridges to increase resistance to seismic forces. Simplified mathematical models of seven existing highway bridges representing predominant types of construction were used for developing general retrofit concepts. Each bridge was analyzed for dynamic structural

response when subjected to an analysis earthquake. Failure mechanisms which correspond closely to observed failure mechanisms described above were identified for each of the bridges, and five preliminary general retrofit concepts were identified, including the following:

1. Superstructure horizontal motion restrainers for hinges, expansion joints, bearings, etc.
2. Bearing restrainers - vertical.
3. Bearing area widening techniques.
4. Column or pier strengthening.
5. Foundation strengthening.

Several alternatives were developed for each concept.

No simple, straightforward, totally reliable method exists to determine the susceptibility of a bridge to damage. Time, location, and magnitude of an earthquake cannot be predicted. Therefore, mathematical analysis of a large number of bridges in a geographical region becomes impractical because of prohibitive cost and excessive time.

The procedure outlined below represents an initial attempt to quantify a structural factor (SF) to be used in making the decision on whether or not to retrofit. It relies heavily on engineering judgment and is based solely on observed damage caused by past earthquakes. Additional thoughts should be given to quantification of the structural factor.

Structural Factors

The procedure for determining the structural factor is:

1. Determine the structural type.
2. Examine the structure for known vulnerable details.
3. Enter Table VII.
4. Select and record the structural factor.

Table VII
STRUCTURAL FACTORS FOR EXISTING BRIDGES

Structural Factor (SF)	Bridge Type - Details
0	<p>Simply supported single and multiple span bridges or</p> <p>Reinforced concrete slab bridges with two hinges or hangars in any one span or in adjacent spans.</p>
1	<p>Continuous span bridges with at least one hinge or</p> <p>Concrete bridges with expansion joints on one or both sides of inverted T caps.</p>
2	<p>Simply supported spans with continuous, composite slabs or</p> <p>Long, continuous, composite reinforced concrete slab bridges without expansion joints in adjacent spans having a hinge or</p> <p>One, two, or three span bridges with high backfilled or bin type abutments.</p>
3	<p>Single span, rigid frame bridges or</p> <p>Continuous, multiple span bridges without expansion joints.</p>

The State of California relies solely on recognition of bridge type, identified in Table VII, to determine whether or not retrofit is warranted. Structures having a structural factor equal to 0 or 1 are considered for retrofit while those having a structural factor equal to 2 or 3 are not considered for retrofit.

SAMPLE PROBLEM

Evaluate the two-span, simply supported bridge on U.S. 45 over Des Plaines River, near Chicago, Illinois.

Criticality Factor Based on ATS Effects (Element 1, Figure 1)

1. A map of the area containing the bridge indicates:
 - . U.S. 45 leads to and from the bridge
 - . There is no road or street passing under the bridge
 - . The road crossing the bridge is classed as "major arterial" - the road is a four-lane highway in an urban area
2. From Table III the criticality factor is 2, (CF) = 2.
3. From Figure 1, Element 2, the next point of evaluation is Element 3.

Criticality Factor Based on S/S Effects (Element 3, Figure 1)

1. If the bridge is down, the communities of Hickory Hills and Justice would be isolated from Hodgkins.
2. Alternate routes between those communities would be the toll road bridge, Wentworth Avenue Bridge, Route 171 Bridge, and the Harlem Avenue Bridge.
3. The route (U.S. 45) is a preferred police and fire department route; however, the bridge is not critical to emergency services.
4. Hospitals, police, and fire services exist on both sides of the bridge.
5. The bridge is considered insignificant and from Table IV a criticality factor of 0 (CF = 0) is selected.
6. From Figure 1, Element 4, the next point of evaluation is Element 5.

Criticality Factor Based on S/D Effects (Element 5, Figure 1)

1. From the Planning Department of the Illinois Department of Transportation, Springfield, Illinois, the following data on the bridge was obtained.

. Road Section No. [Kind 2, designation 1, No. 12] ¹	
Item 679 ²	
. Miles from beginning of section	<u>0.5</u>
. Bypass Code	<u>6</u> ³
. Average annual daily traffic	<u>44,300</u>
. Criticality	<u>NC</u>

2. From Table V, the criticality factor is 1 (noncritical structure/nonbypassable), CF = 1.

3. From Figure 1, Element 6, the next point of evaluation is Element 7.

Criticality Factor Based on E/P Effects (Element 7, Figure 1)

1. Average annual daily traffic over bridge is 44,300 (from Regional State Department of Transportation, Planning Department).
2. From Table VI, the criticality factor is 2, (CF = 2).
3. From Figure 1, Element 7, the next point of evaluation is Element 8.

1. Indicates type of road (conformity to Federal code not yet completed).
2. Indicates the location of bridge (State code).
3. Indicates number of miles of bypass required if bridge is out.

Selection of Highest Criticality Factor (Element 8, Figure 1)

<u>Effect</u>	<u>Criticality Factor</u>
ATS	2
S/S	0
S/D	1
E/P	2

1. The highest criticality factor is 2 (CF = 2).
2. Select structural factor (Element 9), Figure 1.

Structural Factor (SF) Element 9, Figure 1

- . From Table VII, the structural factor for the bridge is 0 (SF = 0). The bridge is unsound in the event of an earthquake. (A separate analytical study, not reported herein, conducted for the bridge verified that the bridge is unsound in the event of a strong earthquake.)
- . From Figure 1, the next point of evaluation is Element 10.

Comparison of Highest Criticality Factor with Structural Factor (Element 10, Figure 1)

- . CF - SF = 2 - 0 = 2.
- . From Figure 1, the final point in the process is Element 12.

Based on the foregoing methodology, a bridge retrofit is warranted.

CLOSING STATEMENT

A new procedure has been presented which may help administrations decide which, if any, highway bridges situated in seismically active areas should be structurally upgraded to resist future earthquake induced damage. This represents the first attempt to identify,

prior to the occurrence of an earthquake, what the worth or loss of a bridge means to a community. It is recognized, however, that the method has shortcomings, particularly when used to evaluate a group of bridges in a given geographic area. Undoubtedly, funds will not be available to upgrade those structures which warrant retrofitting. This will require further analysis, probably a yet-to-be-developed cost-benefit analysis. Also, a structural factor (SF) which is based on current bridge inspection reports should be developed and included in the methodology. And finally, the weighting of criticality factors (CF) should be examined--perhaps more effects than the four discussed should be considered.

Although the methodology was developed specifically for the purpose of identifying those existing bridges which warrant seismic retrofitting, it can be modified and used as a tool to identify those existing structures vulnerable to damage caused by other types of natural disasters.

REFERENCES

1. Standards for Street Facilities and Services, Procedural Manual 7A, National Committee on Urban Transportation, Public Administration Service, Chicago, 1958.
2. U.S. Department of Transportation, Federal Highway Administration--Federal-Aid Program Manual, Volume 4, Chapter 7, Section 2, Washington, D.C.
3. Cooper, J. D., Robinson, R. R., and Longinow, A., "Seismic Retrofitting of Existing Highway Bridges," Proceedings of the Sixth Joint UJNR Panel Conference, NBS Special Publication 444, U.S. Department of Commerce, Washington, D.C., April 1976.
4. "Seismic Retrofitting Measures for Highway Bridges," Contract DOT-FH-11-8847 with IIT Research Institute, Office of Development, Federal Highway Administration, Washington, D.C., 1977.

CRITERION ON THE EVALUATION OF SEISMIC SAFETY
OF EXISTING REINFORCED CONCRETE BUILDINGS
Kiyoshi Nakano, Masaya Hirosewa and Shin Okamoto
Building Research Institute, Ministry of Construction

ABSTRACT

The outline of "Criterion on the Evaluation of Seismic Safety of Existing Reinforced Concrete Buildings" by the Ministry of Construction is discussed in detail. The evaluation method consists of three steps with use of various seismic indices.

KEYWORDS: Evaluation method of seismic safety; non-structural elements; reinforced concrete buildings; structural elements; seismic safety index.

1. INTRODUCTION

This report describes the outline of "Criterion on the Evaluation of Seismic Safety of Existing Reinforced Concrete Buildings" which was compiled by the joint committee chaired by Dr. H. Umemura, Professor of Tokyo University, with the commission by the Ministry of Construction, Japanese Government.

The buildings which this criterion covers are low-and medium-rise reinforced concrete buildings constructed by ordinary construction methods, and items for evaluation are not only super-structure itself but also non-structural elements such as exterior finish elements. Further, these evaluation methodologies consist of three steps, from simple first screening to complicated third screening.

The result of evaluation is expressed by the continuous numerical values but the result shall be judged by the engineer who uses this criterion considering individual and social impacts caused by presumed damages.

Moreover, the results by this criterion on damaged and un-damaged buildings in the Tokachi-oki earthquake (1968) are shown as a reference for the judgment.

2. THE CONSTITUTION OF THE SYNTHESIS INDEX REPRESENTING SEISMIC SAFETY

2.1 Definition of Seismic Index

The seismic safety of a building is represented in the following two numerical indexes and the larger value means the higher seismic safety.

Seismic Index of Structure: I_s

Seismic Index of Non-Structural Elements: I_N

2.2 Constitution of I_s -Index

I_s -index shall be calculated by Eq. 1 for both the longitudinal and ridge directions at each floor of the building under consideration.

However, the following G-Index, T-Index and S_D -Index in the first screening are the constants to a particular building independent of the floor location and direction.

$$I_s = E_0 \times G \times S_D \times T \quad (1)$$

where,

E_0 = Seismic Sub Index of Basic Structural Performance

G = Seismic Sub Index of Ground Motion

S_D = Seismic Sub Index of Structural Design

T = Seismic Sub Index of Time-Depended Deterioration

2.3 Calculation of Seismic Index of Structure I_s

1) General

In order to calculate the value of I_s -Index, any one of the first, the second and the third evaluation method may be used. However, the value of G-Index may be taken as 1.0 for all cases.

2) The First Evaluation Method

E_0 -Index is calculated from the horizontal strength of a building, based on the sum of the horizontal area of columns and walls and on their assumed unit strength.

S_D -Index is evaluated based on the results of the eight check points concerning planning and section of the building.

T-Index is evaluated, based on the age of the building and the observed results of the distortion and cracks in columns and walls.

3) The Second Evaluation Method

E_0 -Index is calculated from the ultimate horizontal strength, failure modes and ductility of columns and walls with the assumption of infinitely strong floor system.

S_D -Index is evaluated based on the results of calculated horizontal rigidity distribution and vertical mass and rigidity distribution in addition to the results of the check points in the first evaluation method.

T-Index is evaluated from the investigated quantitative results on structural crackings, distortion, changes in quality and deterioration of the building.

4) The Third Evaluation Method

E_0 -Index is calculated from the ultimate horizontal strength, failure modes and flexibility of columns and walls, based on failure mechanism of frames with consideration of strength of beams and overturning of walls.

S_D -Index and T-Index may be taken as the same values used in the second evaluation.

3. DETERMINATION AND CONSTITUTION OF SEISMIC SUB INDEX OF BASIC STRUCTURAL PERFORMANCE, E_0

3.1 General

E_0 -Index in each evaluation method is expressed as function of sub-index of strength C (bearing capacity of the building) and of sub-index of ductility F (deformation ability of the building) and so on.

3.2 The First Evaluation Method

1) General

After dividing the vertical members of the frame into the following three categories, E_0 -Index is calculated based on the simply calculated values of C-index and F-index as follows:

- a. column: column with clear height (h_o) equal to or shorter than the depth of column (D).
- b. extremely short column: column with h_o equal to or shorter than twice D.
- c. wall: reinforced concrete wall with or without surrounding framing members.

2) E_0 -index of buildings without the extremely short columns

E_0 -index of buildings without the extremely short columns may be calculated from Eq. 2,

$$E_0 = \frac{n+1}{n+i} (C_w + a_1 \cdot C_c) \times F_w \quad (2)$$

where,

n = total number of stories of the building

j = number of stories of the floor under inspection counted from the first story

C_w = C-index of wall, calculated by Eq. 6

C_c = C-index of column, calculated by Eq. 7

α_1 = (Sum of the lateral shear forces beared by columns in the displacement at the ultimate strength of walls)/ (Sum of the ultimate strength of the columns); may be taken as equal to 0.7, except in case of $C_w = 0$ where α_1 may be taken as equal to 1.0.

F_w = F-index of walls; may be taken as equal to 1.0.

3) E_0 -index of buildings with extremely short columns

E_0 -index of buildings with extremely short columns shall be equal to the larger of two following values of E_0 : E_0 calculated from Eq. 2 neglecting the extremely short columns and E_0 calculated by Eq. 3.

However, in case that the extremely short columns are the secondary seismic elements defined below, E_0 -index shall be computed by Eq. 3. The structural elements whose vertical loads can not be sustained by surrounding structural elements such as beams, walls, and columns, after having reached to their maximum capacity under lateral seismic loads, are defined as the secondary seismic elements.

$$E_0 = \frac{n+1}{n+i} (C_{sc} + \alpha_2 \cdot C_w + \alpha_3 \cdot C_c) \times F_{sc} \quad (3)$$

where,

C_{sc} = C-index of extremely short columns, calculated by Eq. 8.

C_w = C-index of walls, calculated by Eq. 6

C_c = C-index of columns not including extremely short columns, calculated by Eq. 7.

α_2 = (Sum of the lateral shear forces beared by walls in the displacement at the ultimate strength of extremely short columns)/(Sum of the ultimate strength of the walls); may be taken as 0.7.

α_3 = (Sum of the lateral shear forces beared by the ordinary columns in the displacement at the ultimate strength of the extremely short columns)/(Sum of the ultimate strength of the ordinary columns); may be taken as 0.5.

F_{sc} = F-index of extremely short columns; may be taken as 0.8.

3.3 The Second Evaluation Method

1) General

Vertical structural members, that is, columns and walls, are classified into the five following categories: a) flexural columns, b) flexural walls, c) shear columns, d) shear walls, and e) extremely brittle columns.

These classifications are made by comparing the load carrying capacity of each member for flexure with that for shear. Shear columns may be classified as extremely brittle columns, provided that its clear height is less than twice its depth.

The ultimate strength of each member subjected to flexure and shear may be determined in accordance with Eqs.(9) to (14) in Section 4.2.

The F-index of flexural columns and flexural walls may be determined by Eqs. (20) to (23). The F-index of the other members is fixed to the following values:

F = 1.0 for shear columns and shear walls

F = 0.8 for extremely brittle columns

Having determined the F-values of all columns and walls, they are grouped into three or less, and then C-index of i group may be obtained as follows: $C_i = (\text{Sum of the ultimate strength of the members belonging to } i\text{-group})/\Sigma W$ (= total weight of the portion above the floor under inspection). E_0 -index will thus be obtained in accordance with the following articles 2) and 3).

2) E_0 -index of buildings without extremely brittle columns

E_0 -index of buildings without extremely brittle columns may be determined as the larger of two values computed by Eq. 4 and by Eq. 5. However, in the case that the shear columns are classified as the secondary seismic elements, E_0 -value should be determined by Eq. 5.

$$E_0 = \frac{n+1}{n+i} \sqrt{(C_1 \times F_1)^2 + (C_2 \times F_2)^2 + (C_3 \times F_3)^2} \quad (4)$$

where,

C_1 = C-index of the members classified into the 1st group, which have relatively low value of F-index

C_2 = C-index of the members classified into the 2nd group, which have medium value of F-index

C_3 = C-index of the members classified into the 3rd group, which have relatively high value of F-index.

F_1 = F-index of 1st group, taken as the least value of F-indexes of the members classified into the 1st group

F_2 = F-index of the 2nd group, taken as the least value of the F-indexes of the members classified into the 2nd group

F_3 = F-index of the 3rd group, taken as the least value of the F-indexes of the members classified into the 3rd group.

$$E_0 = \frac{n+1}{n+i} (C_1 + \alpha_2 C_2 + \alpha_3 C_3) \times F_1 \quad (5)$$

where,

α_2 = (The sum of the lateral shear forces beared by the 2nd group members, corresponding to the displacement at the ultimate strength of the 1st group members)/(The sum of the ultimate strength of the 2nd group members); may be taken as the values shown in Table 1.

α_3 = (The sum of the lateral shear forces beared by the 3rd group members, corresponding to the displacement at the ultimate strength of the 1st group members)/(The sum of the ultimate strength of the 3rd group members); may be taken as the values shown in Table 1.

3) E_0 -index of the buildings with extremely brittle columns

E_0 -index of the buildings with extremely brittle columns should be the highest of the following three values:

- The value computed by Eq. 4, neglecting the extremely brittle columns,
- The value computed by Eq. 5, neglecting the extremely short columns, and

c) The value computed by Eq. 5 considering the extremely short column as the first group.

However, when the extremely short columns are the secondary seismic elements, E_0 -values should be computed based on the condition c).

3.4 The Third Evaluation Method

1) General

The lateral load carrying capacity and failure mode of vertical structural members may be determined from consideration of the flexure or shear failure of beams and overturning capacity of walls. The vertical structural members are then classified into the following eight categories: a) flexural columns, b) flexural walls, c) shear columns, d) shear walls, e) extremely brittle columns, f) beam yield type columns (columns whose lateral load carrying capacity depends on the flexural yield of beams), g) beam shear failure type columns (columns of which lateral load carrying capacity depends on the shear failure of beams), and h) overturning type walls (walls of which lateral load carrying capacity depends on their overturning capacity).

F-index for the members classified into a) and b) may be determined by the equations shown in Section 5 and for others the F-index may be fixed to the following values.

$F = 1.0$ for shear columns and walls

$F = 0.8$ for extremely short columns

$F = 3.0$ for beam yield type columns

$F = 1.5$ for beam shear failure type columns

$F = 2.0$ for overturning type walls

2) Grouping of vertical structural members and determination of E_0 -index

The grouping of vertical structural members in accordance with their F-index and the determination of E_0 -index may be performed as in the 2nd evaluation method.

4. CALCULATION OF STRENGTH INDEX, C, AND DETERMINATION OF FAILURE MODE

4.1 First Evaluation Method

The C-index for the 1st evaluation method at a floor may be determined by the following equations using the cross sectional areas of columns and walls at the floor and the assumed ultimate strength in terms of mean shear stress,

$$C_w = \frac{1}{w \cdot \sum A_f} (\tau_{w1} \cdot A_{w1} + \tau_{w2} \cdot A_{w2} + \tau_{w3} \cdot A_{w3}) \quad (6)$$

$$C_c = \frac{\tau_c}{w} \times \frac{A_{sc}}{\sum A_f} \quad (7)$$

$$C_{sc} = \frac{\tau_{sc}}{w} \times \frac{A_{sc}}{\sum A_f} \quad (8)$$

where,

C_w = C-index of walls
 C_c = C-index of columns
 C_{sc} = C-index of extremely short columns
 τ_{w1} = Mean shear stress of walls at their strength, with surrounding columns at both ends. It may be assumed as equal to 30 kg/cm^2
 τ_{w2} = Mean shear stress of walls at their strength, with columns at one end. It may be assumed as equal to 20 kg/cm^2
 τ_{w3} = Mean shear stress of walls at their strength, without columns. It may be assumed as equal to 10 kg/cm^2
 τ_c = Mean shear stress of columns at their strength. It may be assumed as equal to 10 kg/cm^2 , except in the case of 7 kg/cm^2 for columns whose h_o/D are equal to or exceed 6.0.
 τ_{sc} = Mean shear stress of extremely short columns at their strength. It may be assumed as equal to 15 kg/cm^2
 A_{w1} = Sum of the horizontal sectional area of walls, with surrounding columns at both ends, which are effective in the direction under inspection at the floor (cm^2)
 A_{w2} = Sum of the horizontal sectional area of walls with surrounding column at one end, which are effective in the direction under inspection at the floor (cm^2)
 A_{w3} = Sum of the horizontal sectional area of walls without surrounding columns, which are effective in the direction under inspection at the floor (cm^2)
 A_c = Sum of the horizontal sectional area of columns at the floor in which the sectional area of columns included in A_{w1} and A_{w2} shall not be considered (cm^2)
 A_{sc} = The sum of horizontal sectional area of extremely short columns at the floor (cm^2)
 A_f = Total floor area above the floor under inspection (cm^2)
 w = [Total weight (including dead and live load) above the floor under inspection]/
 ΣA_f

4.2 Second Evaluation Method

- 1) The strength index, C for the second evaluation method is obtained from the ultimate strength of the vertical structural members based on the assumption of the infinitively stiff horizontal diaphragm.
- 2) The flexural strength of section of the members, may be calculated from the following equations.
 - a) The flexural strength of section of rectangular columns, may be obtained from Eq. 9

For $N_{max} \geq N > 0.4 bDF_c$

$$M_u = \{0.8 a_t \cdot \sigma_y \cdot D + 0.12b \cdot D^2 \cdot F_c\} \left(\frac{N_{max} - N}{N_{max} - 0.4bDF_c} \right)$$

For $0.4 bDF_c \geq N > 0$

$$M_u = \{0.8 a_t \cdot \sigma_y \cdot D + 0.5N \cdot D \left(1 - \frac{N}{bDF_c} \right) \}$$

For $0 > N \geq N_{min}$

$$M_u = 0.8 a_t \cdot \sigma_y \cdot D + 0.4N \cdot D$$

(9)

where,

N_{max} . = Ultimate strength of columns under axial compression = $b \cdot D \cdot F_c + a_g \cdot \sigma_y$ (kg)

N_{min} . = Ultimate strength of columns under axial tension = $-a_g \cdot \sigma_y$ (kg)

N = Axial load of column (kg)

a_t = Area of tension reinforcement of column (cm^2)

a_g = Gross area of longitudinal reinforcement of column (cm^2)

b = Width of column (cm)

D = Depth of column (cm)

σ_y = Yield strength of reinforcement (kg/cm^2)

F_c = Compressive strength of concrete (kg/cm^2)

b) The ultimate flexural strength of section of a column with wing walls at both sides may be obtained from Eq. 10

For $N \leq \{0.5 a_e (0.9 + \beta) - 13p_t\} b \cdot D \cdot F_c$

$$M_u = \{0.9 + \beta\} \cdot a_t \cdot \sigma_y \cdot D + 0.5N \cdot D \left\{ 1 + 2\beta - \frac{N}{a_e \cdot b \cdot D \cdot F_c} \left(1 - \frac{a_t \cdot \sigma_y}{N} \right)^2 \right\} \quad (10)$$

For $N > \{0.5 a_e (0.9 + \beta) - 13p_t\} b \cdot D \cdot F_c$, M_u may be calculated also by Eq. 10 supposing

that $N = \{0.5 a_e (0.9 + \beta) - 13p_t\} b \cdot D \cdot F_c$

where,

$a_e = A/l_w \cdot b$

A = total sectional area

l_w = total horizontal length measured out-to-out of wing wall

$\beta = (\text{Length of compression zone})/D$

The other notations are the same as in Eq. 9.

c) Ultimate flexural strength of walls with surrounding columns at both ends may be calculated by Eq. 11

$$M_u = a_t \cdot \sigma_y \cdot l_w + 0.5 (a_w \cdot \sigma_{wy}) \cdot l_w + 0.5N \cdot l_w \quad (11)$$

where,

a_t = Area of longitudinal reinforcement of tension side column

σ_y = Yield strength of longitudinal reinforcement of tension side of column (cm^2)

a_w = Area of vertical reinforcement of wall (cm^2)

σ_{wy} = Yield strength of vertical reinforcement of wall (kg/cm^2)

b = Width of compression side column (cm)

l_w = Length of wall, measured center to center of column.

3) The ultimate shear strength of section of members may be determined by the following equations

a) Ultimate shear strength of section of rectangular columns may be obtained by Eq. 12.

$$Q_{su} = \left\{ \frac{0.053 p_t^{0.23} (180 + F_c)}{M/Q \cdot d + 0.12} + 2.7 \sqrt{p_w \cdot \sigma_{wy}} + 0.1 \sigma_o \right\} b \cdot x_j \quad (12)$$

$$1 \leq M/Q \cdot d \leq 3$$

where,

p_t = Tensile reinforcement ratio (%)

p_w = Shear reinforcement ratio. When p_w exceeds 0.012, p_w should be taken as equal to 0.012.

σ_{wy} = Yield strength of shear reinforcement (kg/cm^2)

σ_o = Axial stress of column (kg/cm^2). When σ_o exceed $80 \text{ kg}/\text{cm}^2$, σ_o should be taken as equal to $80 \text{ kg}/\text{cm}^2$

d = Effective depth of column, = $(D - 5)$ cm

M/Q = May be taken as equal to $h_o/2$, where, h_o is clear height of column.

b) The ultimate shear strength of section of a column with wing walls may be calculated by Eq. 13.

$$Q_{su} = 0.8 \sqrt{F_c} \left(\frac{l_w}{h_o} \right) EA + 0.5 \left\{ p_w \cdot \sigma_{wy} + p_s \cdot \sigma_{sy} \frac{t(l_w - D)}{b \cdot D + 0.1N} \right\} b \cdot D + 0.1N \quad (13)$$

where,

p_w = Shear reinforcement ratio of column

σ_{wy} = Yield strength of shear reinforcement of column (kg/cm^2)

p_s = Lateral reinforcement ratio of wing wall, = $a_w/t \cdot s$

Where a_w = Sectional area of a pair of lateral reinforcement of wing wall (cm^2)

S = Spacing of lateral reinforcements (cm)

t = Depth of wing wall

σ_{sy} = Yield strength of lateral reinforcement of wing wall (kg/cm^2)

N = Axial force of column (kg)

h_o = Clear depth of column (cm)

c) The ultimate shear strength of section walls with surrounding columns at both ends may be obtained by Eq. 14.

$$Q_{su} = \left\{ \frac{0.053 p_t^{0.23} (180 + F_c)}{M/(Q \cdot l) + 0.12} + 2.7 \sqrt{p_{we} \cdot \sigma_{wy} + 0.1 \sigma_o} \right\} \times b \cdot e \cdot j \quad (14)$$

where,

b_e = Equivalent depth of wall, = A/l (cm)

A = Sum of sectional area of wall and column (cm^2)

l = End-to-end distance between columns

p_{te} = $100 \times a_t / (b_e \cdot l)$ (%)

a_t = Total sectional areas of axial reinforcement of tension side column (cm^2)

p_{we} = Equivalent lateral reinforcement ratio of wall, = $a_w / (b_e \cdot S)$

Where, a_w = Sectional areas of lateral reinforcement of wall (cm^2)

S = Spacing of lateral reinforcements (cm)

σ_{wy} = Yield strength of above reinforcement (kg/cm^2)

σ_o = $\Sigma N / (b_e \cdot l)$ (kg/cm^2)

Where ΣN represents the total axial force sustained by wall and columns

j = May be taken as l_w or $0.8 \times l$

In the case of walls with opening, the ultimate strength of section may be obtained by multiplying the following reduction factors, to the strength obtained by Eq. 14.

$$\tau = 1 - (\text{Equivalent opening peripheral ratio}) \quad (15)$$

where,

$$(\text{Equivalent opening peripheral ratio}) = \sqrt{\frac{\text{Area of opening}}{h \times l_w}}$$

h = Story height

4) Determination of the failure mechanism and lateral strength of each member.

a) In the case of columns, lateral strength can be taken as the smaller one out of the shear force, c_{Mu}^0 at the flexural strength of section obtained by Eq. 16 and the ultimate shear force c_{su}^0 obtained by Eqs. 12 and 13.

Determination of the failure mechanism and the lateral strength of a column at the mechanism can be performed as follows.

When $c^Q_{Mu} < c^Q_{su}$, the member is defined as flexural column, and the lateral strength of the column, c^Q_u may be taken as c^Q_{Mu} .

When $c^Q_{Mu} \geq c^Q_{su}$, the member is defined as shear column, and the lateral strength of the column, c^Q_u may be taken as c^Q_{su} .

$$\text{Where } c^Q_{Mu} = \frac{M_{uu} + M_{ub}}{h_o} \quad (16)$$

M_{uu} = Ultimate flexural strength of section at the top of the column

M_{ub} = Ultimate flexural strength of section at the bottom of the column

h_o = Clear height of column

b) In case of walls, the shear force at the ultimate flexural strength of section of a member, w^Q_{Mu} may be obtained by Eq. 17. Then the failure mechanism and the lateral load carrying capacity at the mechanism may be determined as follows:

When $w^Q_{Mu} < w^Q_{su}$ = the member is defied as flexural wall, and the lateral strength at the mechanism, w^Q_u may be taken as w^Q_{Mu} .

When $w^Q_{Mu} \geq w^Q_{su}$ = the member is defined as shear wall, and the lateral strength at the mechanism, w^Q_u may be taken as w^Q_{su} .

$$\text{Where } w^Q_{Mu} = \theta \cdot \frac{M_u}{h_w} \quad (17)$$

w^Q_u = Ultimate flexural strength of wall at the floor under consideration

h_w = Total height of the wall measured from the floor under consideration

θ = 2 (When the top portion of vertically continuous wall is under consideration, θ may be taken as equal to 1.0.)

4.3 Third Evaluation Method

1) General

The lateral load carrying capacity of each vertical structural elements may be obtained, based on the following three failure mechanisms in addition to the mechanisms considered in the 2nd evaluation method; a) beam yield type columns, b) beam shear type columns and c) overturning type walls.

2) Flexural and shear strength of beam sections

The flexural and shear strength of beam sections may be computed by Eq. 10 and Eq. 11, respectively, substituting $N = 0$ or $\sigma_0 = 0$ into these equations. Here, the effect of the

reinforcements in slabs, may be considered for the computation of the flexural strength of beams. For the computation of the flexural strength of beam sections the following simple equation is also applicable,

$$M_u = 0.9 \cdot a_t \cdot \sigma_y \cdot d \quad (18)$$

where,

a_t = Area of tensile reinforcement

σ_y = Yield strength of tensile reinforcement

d = Effective depth of a beam cross-section

3) Determination of the lateral load carrying capacity of vertical members and the failure mode of the members.

a) Columns

Columns are classified into the following four types; flexural failure column, shear failure column, beam yield type column and beam shear type column. Based on the ultimate strength of columns and beams, the maximum end moments of all members at all nodal points are determined. Comparing the sum of the end moments of beams with that of columns at each nodal point, the ultimate moment distribution of columns is determined by the nodal limit analysis. Considering the above moment distribution, the ultimate strength of the column, cQ_u , may be computed by Eq. 19.

$$cQ_u = (\text{Sum of ultimate moment capacity at top and bottom ends of column}) / (\text{Clear height of column}) \quad (19)$$

b) Walls

Walls are idealized by cutting off from the other framing members at the mid-span of connecting beams. The lateral load carrying capacity of the idealized walls may be taken as the least of the three following lateral loads determined under inverse triangular distribution of lateral loads; resultant lateral loads acting above the floor under inspection (at which the walls reach their flexural yield strength), shear strength or overturning capacity. The failure mode of walls corresponds to the mechanism on which the determination of their lateral load carrying capacity is based.

5. DETERMINATION OF SUB-INDEX OF DUCTILITY F

5.1 General

The sub-index of ductility of members except flexural columns and flexural walls is fixed to the constant values shown in Article 1) of 3.4. F-index of flexural columns and flexural walls may be determined as follows.

5.2 Determination of F-index of Flexural Columns and Flexural Walls.

a) F-index of flexural columns may be obtained by equation 20, based on the ductility factor of the columns determined by Eq. 22 in 5.3.

$$F = \frac{\sqrt{2(\mu - 1)}}{0.75(1 + 0.5\mu)} \quad (20)$$

b) F-index of flexural walls is obtained by Eq. 21 using their shear strength, w_{su}^0 and flexural strength, w_u^0 .

$$\text{when } w_{su}^0/w_u^0 \leq 1.3 \quad = F = 1.0 \quad (21)$$

$$\text{when } w_{su}^0/w_u^0 \geq 1.4 \quad = F = 2.0$$

$$\text{when } 1.3 < w_{su}^0/w_u^0 < 1.4 = F = -12.0 + 10 \times \frac{w_{su}^0}{w_u^0}$$

5.3 Determination of Ductility Factor μ of Flexural Columns.

Ductility factor μ of flexural columns may be computed by Eq. 22. However, F should be 1.0 provided that any one of the conditions described in Eq. 23 are corresponded.

$$\mu = \mu_o - k_1 - k_2 \quad (22)$$

$$\text{here } 1 \leq \mu \leq 5$$

$$\text{where, } \mu_o = 10 \left(\frac{c_{su}^0}{c_u^0} - 1 \right)$$

$k_1 = 2.0$ (k_1 may be zero provided that shear reinforcement spacing is less than eight times the diameter of longitudinal reinforcement.)

$$k_2 = 30 \left(\frac{c_u^T}{F_c} - 0.1 \right) \geq 0$$

c_{su}^0 = Shear strength of column

c_u^0 = Lateral strength of column

c_u^T = $c_u^0/b \cdot j$

b = Width of column

j = Distance between compressive resultant forces and tensile resultant forces.

F_c = Compressive strength of concrete

Conditions in which F should be 1.0;

$$N_s/bDF_c > 0.4, (N_s \text{ corresponds to axial forces of columns at their failure mechanism})$$

$$c_u^T/F_c > 0.2$$

$$p_t > 1\%, \text{ where } p_t \text{ is tensile reinforcement ratio.}$$

$$h_o/D \leq 2.0, \text{ where } h_o \text{ is clear height of columns.}$$

(23)

6. SEISMIC SUB-INDEX OF STRUCTURAL PROFILE, S_D

6.1 General

This index becomes effective only in combination usage with E_o -index for evaluating the effect of the structural profile and the distribution of mass or stiffness for the seismic safety of buildings. Though only one value of S_D -index may be determined for a building in the 1st screening, S_D -index should be determined for each floor and each direction in 2nd screening.

6.2 Judgment Items

- a) For the 1st screening the following items may be examined.

Items concerning plan profile; i) irregularity of plan, ii) length-width ratio in plan, iii) clearance of expansion joints, iv) presence of open hall and v) other special profiles in plan.

Items concerning elevation profile; vi) presence of underground stories, vii) uniformity of story height, viii) presence of piles, and ix) other special profiles in section.

- b) In the second screening the following items may be examined in addition to the items considered in the 1st screening.

- i) Eccentricity of the center of gravity and the center of rigidity in plan.
- ii) Weight-stiffness ratio at a story to that at the story directly above.

6.3 Determination of S_D -index

The influence factor, C_i which represents the degree of influence of each judgment item may be computed using the grading factor, G_i , which varies 1.0 to 0.8 in accordance with the situations of each item and the adjusting factor for the range of the influence of each item, R_i . Then, the S_D -index is obtained by the mutual multiplication of C_i as shown in Eq. 24.

$$S_D = C_1 \times C_2 \times \dots \times C_n$$

(24)

$$C_i = 1 - (1 - G_i) \times R_i$$

7. SEISMIC SUB-INDEX OF TIME DEPENDED DETERIORATION

7.1 General

This index aims to evaluate the effect of the structural defects, such as cracks, excessive deflections, superannuations, and so on for the seismic safety of the buildings. Only single value for a building is determined in both the 1st and 2nd evaluation methods, respectively.

7.2 First Evaluation Method

T-index for the 1st evaluation method may be taken as the minimum value of reduction factors determined by checking the prepared questionnaire in accordance with the degree of the structural defects as cracks, deflections, superannuations, and so on observed in structural members.

7.3 Second Evaluation Method

T-index for the 2nd evaluation method may be calculated by Eq. 25, where p_{si} and p_{ti} in Eq. 25 are the sum of the demerit points concerning about structural cracks and deflection, and deterioration and superannuations, respectively. These demerit points are obtained by checking the prepared questionnaire at each story and T-factor is taken as the average of T_i determined at i-story.

$$T = (T_1 + T_2 + \dots + T_n)/N \quad (25)$$

$$T_i = (1 - p_{si})(1 - p_{ti})$$

where,

T_i = T-index of i-story

N = Number of stories examined

p_{si} = The sum of the demerit points at i-story concerning about structural cracks and deflections.

p_{ti} = The sum of the demerit points at i-story concerning about deterioration and superannuation.

In the third evaluation method, the same value of T-index as the value determined in the second evaluation method may be used.

8. SEISMIC INDEX OF NON-STRUCTURAL ELEMENTS, I_N

8.1 General

This index aims to evaluate the dangerousness in earthquakes caused by the collapse or the fall of non-structural elements such as the finish of exterior walls. For this index, screening methods from 1st to 3rd are also applied. I_N -index is determined for every wall surface in every story.

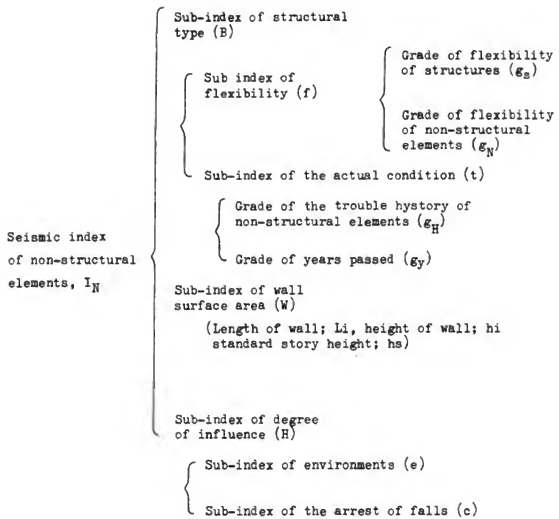
8.2 Outline of Determination of I_N -index

The constitution of the sub-indexes used for determination of I_N -index is shown on the following page.

The values of sub-indexes, g_s , g_N , g_H , g_y , e and c are given in tables. Sub-index f and t are given as matrix of g_s and g_N and of g_H and g_y , respectively. The other sub-indexes are calculated by given equations.

Thus the I_N -index may be computed by Eq. 26.

$$I_N = -\frac{\frac{EB \cdot W \cdot H \cdot L_j}{L_j}}{1 - \frac{\overbrace{(f + (1-f) \cdot t)}^B \cdot \overbrace{\left\{0.5 + \frac{0.5h_j}{h_s}\right\}}^W \cdot \overbrace{\left(\sum e \cdot c\right) L_j}^H}{\sum L_j}} \quad (26)$$



9. SEVERAL FEATURES OF CRITERION

9.1 Adoption of Seismic Index of Non-structural Elements

The seismic safety of buildings should be examined not only from a viewpoint of the safety of structural elements from collapse, but also from the viewpoint of the safety of non-structural elements such as finishing materials of exterior walls directly facing to streets from their fall. Because the reinforced concrete buildings in Japan have relatively large lateral strengths, the structures themselves seldom fall instantaneously even under the strong earthquake motions. Actually, the experience of past earthquake damages indicates that most buildings survived from catastrophic destructions. Even in the cases of buildings which were unfortunately destroyed and fell, the residents of the buildings had enough time to escape from the buildings.

Therefore, it becomes important to protect people from injury due to the fall of the non-structural elements such as finishing materials of exterior walls.

Though there is not sufficient experimental and empirical information concerning the performance of non-structural elements under earthquake loads, the safety evaluation of non-structural elements by I_N -index is attempted in this criterion taking into account the relative flexibility of structure itself and non-structural elements.

9.2 Adoption of Screening Method

The structural safety evaluation considered in this criterion consists of a sequence of steps from 1st to 3rd evaluation. This procedure is repeated in successive cycles, the assumptions and details of the calculations being refined in each successive cycle when necessary for a reliable estimate of structural performance. The repetitive procedure is called "Screening," and is believed to be the fastest and the most practical method for reasonably evaluating the structural adequacy of a large number of buildings subjected to strong earthquake motions.

9.3 Evaluation and Judgment of Seismic Safety

The evaluation of the seismic safety in a broad sense is taken more precisely in the following senses:

- 1) Evaluation of seismic safety; to express the seismic safety of structures with continuous quantity such as seismic index proposed in this criterion.
- 2) Judgment of seismic safety; to judge the adequacy of buildings for seismic safety taking into account various conditions such as their use, their importance and their age, based on the seismic index obtained by the evaluation seismic safety.

This criterion aims to evaluate the seismic safety as defined above and the judgment is left to the engineers who use this criterion.

The results by this criterion applied on damaged and un-damaged buildings in the Tokachioki earthquake of 1968 are summarized in the appendix of this criterion. These results will be helpful in performing the judgment of the seismic safety.

9.4 Adoption of Seismic Sub-indexes, S_D , T and G to Seismic Index, I_S

Seismic sub-indexes, S_D and T which represent the quality of structural design and time depended deterioration, respectively, are taken into account in this criterion as the sub-indexes of synthesis index representing seismic safety, I_S , in addition to the seismic sub-index of basic structural performance E_o which is related to the lateral load carrying capacity and the deformation capacity of structures. In this criterion, the quantitative evaluation of such sub-indexes are attempted using a check list system. Moreover, the seismic sub-index representing the intensity of input ground motions to the base of a building, which depends on the seismicity of its location and on the relationship between its dynamic characteristics and the type of soil, is defined as G in this criterion. The standard value of this sub-index is taken as equal to 1.0 and decreasing value with increase of the earthquake danger in the location is assumed. However, G-index is fixed to 1.0 in this criterion because of the difficulty of the evaluation of the earthquake danger at present.

9.5 Consideration of Seismic Sub-index of Ductility, F to Seismic Sub-index of Basic Structural Performance, E_o .

In the basic sub-index representing the earthquake resistant ability of structures, E_o , not only strength but also deformation capacity are considered as follows.

- 1) Critical conditions defined by the failure of brittle members.

The lateral load carrying capacity of a building depends on the failure of brittle structural members, provided that the building consists of structural members with various deformation capacity, and, therefore, is not always the sum of the ultimate lateral strength of every structural member. In general, critical displacements at the ultimate strength

of brittle structural members are small because of their high stiffness, and then the ductile members which have relatively low stiffness might not reach their ultimate strength at the critical displacements.

Moreover, the brittle members show significant reduction of load carrying capacity after they reach their ultimate strength.

Therefore, the failure of brittle structural members becomes one of critical conditions for evaluating the seismic performance of buildings. In this criterion, such critical conditions are expressed in Eqs. 2, 3 and 5. In these equations, α means one of the reduction factors of the strength for ductile members considering the compatibility of the displacement at the failure of brittle members. The value of α which is taken as 0.5 to 0.7 in these equations is determined empirically, based on many test results on the yield displacements.

On the other hand, the failure of brittle members causes often the local collapse of buildings because they become ineffective in sustaining vertical loads. Therefore, in this criterion, the failure of brittle members is considered to be one of the critical conditions on the safety of buildings even if the lateral load carrying capacity of the buildings as a whole is not affected by it. Such a critical condition is considered in Eq. 3 or 5.

2) Critical condition of buildings consisted of the structural members which have various deformation capacity.

It is not always easy to evaluate the seismic safety of the buildings consisted of the structural members which have various deformation capacities. In the case of a building consisted of structural members which have nearly the same deformation capacities, it is possible to evaluate its earthquake resistance, based on the assumption of the equal energy concept proposed by Blume, et al., which implies that the potential energy stored by the elastic system at maximum deflection is the same as that stored by the elasto-plastic system at maximum deflection. In the case of a building consisted of, for example, some brittle shear walls and ductile columns, its seismic resistance ability changes with change of the ratio of the load carrying capacity of walls to that of columns or change of deformation capacity of framing members. For evaluating the seismic safety of such type of structures, Eq. 4 is proposed, based on many non-linear dynamic analyses of combined structures of brittle shear walls and ductile frames responding to ground motions recorded during severe earthquakes.

3) Relation between required ductility factor of non-linear system and seismic sub-index, F .

Non-linear dynamic analyses of structures responding to earthquake motions have shown that the required ductility factor of the elasto-plastic systems whose yield shear factor is C_y , may be estimated from the elastic spectral response acceleration, C_E . Blume, et al., for example, have shown that the required ductility factor of reinforced concrete structures is given by the following equation

$$C_E/C_y = \sqrt{2\mu - 1}$$

where,

C_y = Yield shear factor of elasto-plastic system.

C_E = Spectral response acceleration of elastic system.

μ = Required ductility factor of elasto-plastic system.

This equation is based on the equal energy concept as mentioned in Article 2). Comparing the above equation with the results obtained from dynamic analyses on single degree of freedom systems with elasto-plastic and degrading stiffness load-deflection relationship, it is evident that the above equation may be an upper bound.

For determining the seismic sub-index, F , given in Eq. 20, the same approach as mentioned above has been applied, based on the non-linear dynamic analyses responding to the ground motions recorded during severe earthquakes carried out on the single degree of freedom oscillator having degrading tri-linear load-deflection relationship which seemed to be a typical load-deflection relationship of reinforced concrete structures.

The reciprocal of the seismic sub-index, $1/F$, in this criterion is one of the upper bound for the ratio of the yield shear factor of degrading tri-linear system to the elastic spectral response acceleration.

4) Determining the required ductility factor of structural members of multistory frames from the response ductility factor obtained from non-linear dynamic analyses of one mass system.

The ductility demand obtained from the non-linear dynamic response analyses on one mass system cannot be claimed to give an accurate assessment of the ductility demand of each structural member of the multistory frame responding to non-linearly strong earthquakes. In this criterion, however, it is supposed that the ductility demand of each structural member is assumed to be the same as the response ductility factor obtained by the non-linear dynamic analyses of one mass system.

Many experimental studies have been carried out recently on the ductility behavior of the flexural yield type structural members. However, there are still a lack of information concerning about the quantitative estimation of allowable ductility in accordance with structural details of the members. The equation 22 is proposed provisionally for estimation of the allowable ductility of flexural columns with some restricting conditions in which ductile behavior can not be expected.

In the cases of walls, even the experimental studies on the ductility behavior have not been performed sufficiently. Therefore, the F -index is directly given by Eq. 24 for walls for safe-side estimation instead of the estimation of F -index from the allowable ductility factor as in the case of columns.

9.6 Recommendations for repairs to improve the earthquake resistant characteristics of buildings

When insufficient seismic safety of buildings comes into question as a result of the application of this criterion, appropriate repairs may be required for improving the

earthquake resistant characteristics of the buildings. The recommendations for repairs are also provided for this purpose. These recommendations deal with the procedures of repairs in accordance with strength requirements or ductility requirements of the structural members. The method of evaluating the seismic safety for the repaired buildings, some attention for the practice of repairs, and some design details for repairs are also provided in these recommendations.

Table 1. Value of α_2 and α_3 in Eq. 5

The 2nd or 3rd group	The 1st group	Extremely short column	Shear column or shear wall
Flexural column		0.5	0.7
Flexural wall		0.7	1.0
Shear column or shear wall		0.7	—

TRANSFERRING THE TECHNOLOGY FOR WIND-RESISTANT

BUILDINGS TO DEVELOPING COUNTRIES

Noel J. Raufaste, Jr.

National Bureau of Standards, Gaithersburg, Maryland

ABSTRACT

The National Bureau of Standards project to develop improved design criteria for low-rise buildings to better resist high winds was recently completed. It contained two essential parts. The first included developing technology to reduce wind damage to buildings through improved building practices. The second part centered around making sure these improved building practices actually reached the individuals who construct and live in buildings. The latter has traditionally received minimum attention. This paper presents a method for getting the results of the NBS wind research to the building community which includes building owners and users who need it most. A 3-level approach to this method is described. The method used can be a model for other research projects aimed at technical, semi-technical, or even semi-literate audiences.

KEYWORDS: Buildings, design criteria, developing countries, technology transfer, wind-loads

INTRODUCTION

This paper discusses efforts in transferring the technical results on the effect of wind on low-rise buildings in developing countries to the local building community and to homeowners and low-technology craftsman who often build their dwellings from local materials. The homeowner and craftsmen group generally do not understand the highly technical results produced by this project; but they want a method to keep their home from collapsing in a storm. One component of this project attempted to do just that -- to transfer project information to the general public. Actual use of this technology by the general public will demonstrate the real payoff of the research.

The Center for Building Technology, of the U.S. National Bureau of Standards (NBS), recently completed this three and a half year study of the effect of wind on low-rise buildings. The project sponsored by the Agency for International Development was aimed at improving building practices -- in high wind-prone developing nations worldwide. Two previous papers discuss the technical aspects of this study -- "High Wind Study in the Philippines," and "Wind Loads on Low-Rise Buildings," published in the NBS Special Publications 470 and 477, both titled Wind and Seismic Effects. The papers were presented at the 7th and 8th joint meetings of the US/Japan Panel on Natural Resources, respectively.

Most of the data collection activities (full-scale and wind-tunnel experiments) were centered in the Philippines. This was the host country; its environment provided a natural wind laboratory. There was a significant technical contribution by the local Philippine building community, represented by the projects local coordinating group known as the Philippine Advisory Committee; (high level officials from the private and government building organizations) in all phases of the study. Also, the other participating countries (Jamaica, Bangladesh) constantly asked about the relevance of our research to local codes and standards, building materials, and socio-economic aspects of their countries. The project team recognized that the research results be consistent with, sensitive to, and relevant to improving local building practices.

The project developed improved design criteria for wind loads on buildings; provided technical material to serve as the basis for better building practices; produced a method to estimate extreme wind speeds; and documented essential information in the areas of design wind speeds and pressure coefficients, economic forecasting, socio-economic and architectural concerns, and construction detailing practices. These results are described in the next section.

PROJECT RESULTS

Three levels of information were developed to reach three major audience classes. At the first level, highly technical information is aimed at technical groups responsible for producing similar complementary research and for implementing disaster mitigation programs.

For this group a 5-volume report, Building to Resist the Effect of Wind¹, was produced which detailed the research progress and technical outputs.

The second level of information is aimed at local builders and home owners who hand-craft houses on a limited scale. For them, guidelines were produced, 43 Rules - How Houses Can Better Resist High Wind². These 43 rules were designed to make the technical results more understandable and useable for those concerned with implementing only general building practices.

The third level of information is aimed at the general public. The medium is a 2-color poster that illustrates through simple and bold graphics, wind hazards, and presents four methods to reduce damage and injury -- and most important -- tells where to go for more information. As with the 43 Rules it was designed to be reprinted in local languages.

Level-One Information: Highly Technical Audience

Technical results were published in five companion volumes. Contents of each volume are summarized. "Estimation of Extreme Wind Speeds and Guide to the Determination of Wind Forces," reviews probabilistic techniques for the analysis of existing data and the selection of design wind speeds. Simplified procedures for the calculation of wind pressure acting on building surfaces were developed. These procedures and associated design criteria provide building professionals with more reliable design loads. The data can form the basis for wind load design codes and standards in developing countries.

"A Guide for Improved Masonry and Timber Connections in Buildings," presents recommendations for good construction practices and details, especially for countries experiencing extreme wind. The report serves as a reference for improving building practices.

"Forecasting the Economics of Housing Needs: A Methodological Guide," presents a method for a nation's planners, economists, public officials, and other decision makers to assess housing needs for up to 20 years into the future.

Information on the cultural and socio-economic factors that affect building practices was developed as, "Housing in Extreme Winds: Socio-Economic and Architectural Considerations." The report discusses how strong, inexpensive, locally available building materials can be integrated with good building design. The report addresses the Philippines, Jamaica and Bangladesh.

An "Overview" volume containing an executive summary serves as an introduction and background to the technical material. It was developed for the decision maker who may not have the time to read the substantive technical material of the other four volumes yet is sufficiently familiar with the project to direct his staff to particular volumes of interest.

¹The Building Science Series 100, Building To Resist The Effect of Wind, Volumes 1-5 may be purchased from the Superintendent of Documents, U.S. Government Printing Office, Washington, DC 20402.

²This report may be ordered as NBSIR 77-1197 under its title from the National Technical Information Service, 5285 Port Royal Road, Springfield, VA 22161.

As the technical results were being developed emphasis was placed on: 1) producing data that could be developed into performance criteria (focuses on user requirements and the attributes necessary to satisfy them) and 2) producing reproducible models.

Level-Two Information: Semi-Technical Audience

A second or intermediate level of material was developed for local housing agencies, builders, and building owners. This material, 43 Rules - How Houses Can Better Resist High Wind, is a guide presenting ways to better design new and existing buildings. The information is presented in a manner for translation into a local country's language.

The audience can be considered the middle level of the housing trade, such as the local builder, contractor, designer, housing authority. For them, especially in developing nations, code enforcement is not the problem, just simple, safe practices are. This report provides suggestions to improve building practices. For example, local housing authorities and lending institutions will learn from 43 Rules that houses with lengthy roof overhangs will need special precautions such as tie-downs and learn that buildings with long roof overhangs should be designed in a manner that permits wind to pass through. Also, they will find that roofs should be designed with slopes approaching 30 degrees since this angle minimizes wind damages.

Another intended target of this publication is the leader (often unofficial) of local political units, called in the Philippines, "barrios" -- although such units occur on a worldwide basis. If this individual reads the 43 Rules he is in a good position to encourage his jurisdiction to adopt appropriate recommendations to improve building practices for new buildings and the use of certain retrofit practices for use on existing buildings. To reach this rather special audience, 43 Rules could be printed in local languages. Likewise, 43 Rules can be used by squatter and nonsquatter settlements and also can be used to improve public buildings (such as schools and community centers) and multi-family dwellings.

A 1976 award-winning 16 mm, 18 minute color movie³, also was produced by NBS to educate the audience that information is available to reduce wind damages to buildings and inform the audience about how the information was developed.

Level-Three Information: Lay Audience

⁴ A poster was produced that graphically depicts damages due to wind. It is based on information learned during this three and a half year research project. The idea to develop this poster was based on information learned from frequent discussions with members of the various participating countries and on feedback from two regional conferences where draft project results were communicated and discussed (Manila, Philippines and Kingston, Jamaica).

³ Available on free loan from Association Sterling Films, 600 Grand Avenue, Ridgefield, NJ 07657 or may be purchased from the National Audio-Visual Center, General Services Administration, Washington, DC 20409.

⁴ Copies of the poster are available from the author at the National Bureau of Standards, Center for Building Technology, Washington, DC 20234.

The conference audiences were composed of representatives of the building community (architects; engineers; regulatory, codes and standards officials; academia; manufacturers; builders and contractors; government agencies; and building users). They believed if research (any research) is to have a significant impact on the entire country, each citizen must be able to benefit directly from it and be able to implement the research results.

The poster was designed as an educational tool to illustrate critical principles of improved building practices and most importantly to identify a local contact for additional information. It is printed in two sizes; the smaller size for internal office use and the larger one for hanging on fences or telephone poles.

CONCLUSION

In the United States, Japan and other developed countries, the building codes and standards systems are aimed at protecting the public health, safety, and general welfare as they relate to the construction and occupancy of buildings. Results from this project will have an impact on those codes and standards dealing with wind loads. When building research takes place in developed countries, its results normally find their way into practices by way of the law. In developing countries, this usually is not the case.

The research covered by this project (applicable to both developed and developing countries) dealt in part with aspects that in developing countries has little code enforcement. Thus, for these users to implement the research, they must be made aware of the information, learn how to obtain the data, and be informed how to initiate improving their building practices.

This phase of the project addressed the traditional role of "technology transfer." However, it was aided by classifying the audience into three levels and then carefully tailoring the results to meet each audience's needs.

U.S. DEPT. OF COMM. BIBLIOGRAPHIC DATA SHEET		1. PUBLICATION OR REPORT NO. NBS SP-523	2. Gov't Accession No.	3. Recipient's Accession No.
4. TITLE AND SUBTITLE WIND AND SEISMIC EFFECTS Proceedings of the Ninth Joint Panel Conference of the U.S.-Japan Cooperative Program in Natural Resources May 24-27, 1977, Tokyo, Japan		5. Publication Date September 1978 6. Performing Organization Code		
7. AUTHOR(S) H. S. Lew, Editor		8. Performing Organ. Report No.		
9. PERFORMING ORGANIZATION NAME AND ADDRESS NATIONAL BUREAU OF STANDARDS DEPARTMENT OF COMMERCE WASHINGTON, D.C. 20234		10. Project/Task/Work Unit No. 11. Contract/Grant No.		
12. Sponsoring Organization Name and Complete Address (Street, City, State, ZIP) National Bureau of Standards Department of Commerce Washington, D.C. 20234		13. Type of Report & Period Covered Final 14. Sponsoring Agency Code		
15. SUPPLEMENTARY NOTES Library of Congress Catalog Card Number: 78-600082				
16. ABSTRACT (A 200-word or less factual summary of most significant information. If document includes a significant bibliography or literature survey, mention it here.) The Ninth Joint Meeting of the U.S.-Japan Panel on Wind and Seismic Effects was held in Tokyo, Japan on May 24-27, 1977. The proceedings of the Joint Meeting include the program, the formal resolutions, and the technical papers. The subjects covered in the paper include (1) characteristics of strong winds; (2) wind loads on structures and design criteria; (3) earthquake prediction; (4) earthquake ground motions and soil failures; (5) seismic loads on structures and design criteria; (6) design of special structures; (7) earthquake hazard reduction program; and (8) quantitative evaluation of damages caused by winds and earthquakes.				
17. KEY WORDS (six to twelve entries; alphabetical order; capitalize only the first letter of the first key word unless a proper name; separated by semicolons) Accelerograph; codes; design criteria; disaster; earthquakes; earthquake hazards; ground failures; seismicity; solids; standards; structural engineering; structural responses; wind loads; and winds.				
18. AVAILABILITY <input checked="" type="checkbox"/> Unlimited <input type="checkbox"/> For Official Distribution. Do Not Release to NTIS <input checked="" type="checkbox"/> Order From Sup. of Doc., U.S. Government Printing Office Washington, D.C. 20402, SD Stock No. SN003-093 <input type="checkbox"/> Order From National Technical Information Service (NTIS) Springfield, Virginia 22151		19. SECURITY CLASS (THIS REPORT) UNCLASSIFIED	21. NO. OF PAGES 518	
		20. SECURITY CLASS (THIS PAGE) UNCLASSIFIED	22. Price 6.75	

*There's
a new
look
to...*

DIMENSIONS

... the monthly magazine of the National Bureau of Standards. Still featured are special articles of general interest on current topics such as consumer product safety and building technology. In addition, new sections are designed to . . . PROVIDE SCIENTISTS with illustrated discussions of recent technical developments and work in progress . . . INFORM INDUSTRIAL MANAGERS of technology transfer activities in Federal and private labs. . . DESCRIBE TO MANUFACTURERS advances in the field of voluntary and mandatory standards. The new DIMENSIONS/NBS also carries complete listings of upcoming conferences to be held at NBS and reports on all the latest NBS publications, with information on how to order. Finally, each issue carries a page of News Briefs, aimed at keeping scientist and consumer alike up to date on major developments at the Nation's physical sciences and measurement laboratory.

(please detach here)

SCRIPTION ORDER FORM

er my Subscription To DIMENSIONS/NBS at \$12.50. Add \$3.15 for foreign mailing. No additional tage is required for mailing within the United States or its possessions. Domestic remittances uld be made either by postal money order, express money order, or check. Foreign remittances uld be made either by international money order, draft on an American bank, or by UNESCO ions.

d Subscription to:

NAME-FIRST, LAST

COMPANY NAME OR ADDITIONAL ADDRESS LINE

STREET ADDRESS

CITY

STATE

ZIP CODE

EASE PRINT

Remittance Enclosed
(Make checks payable
to Superintendent of
Documents)

Charge to my Deposit
Account No. _____

MAIL ORDER FORM TO:
Superintendent of Documents
Government Printing Office
Washington, D.C. 20402

NBS TECHNICAL PUBLICATIONS

PERIODICALS

JOURNAL OF RESEARCH—The Journal of Research of the National Bureau of Standards reports NBS research and development in those disciplines of the physical and engineering sciences in which the Bureau is active. These include physics, chemistry, engineering, mathematics, and computer sciences. Papers cover a broad range of subjects, with major emphasis on measurement methodology, and the basic technology underlying standardization. Also included from time to time are survey articles on topics closely related to the Bureau's technical and scientific programs. As a special service to subscribers each issue contains complete citations to all recent NBS publications in NBS and non-NBS media. Issued six times a year. Annual subscription: domestic \$17.00; foreign \$21.25. Single copy, \$3.00 domestic; \$3.75 foreign.

Note: The Journal was formerly published in two sections: Section A "Physics and Chemistry" and Section B "Mathematical Sciences."

DIMENSIONS/NBS

This monthly magazine is published to inform scientists, engineers, businessmen, industry, teachers, students, and consumers of the latest advances in science and technology, with primary emphasis on the work at NBS. The magazine highlights and reviews such issues as energy research, fire protection, building technology, metric conversion, pollution abatement, health and safety, and consumer product performance. In addition, it reports the results of Bureau programs in measurement standards and techniques, properties of matter and materials, engineering standards and services, instrumentation, and automatic data processing.

Annual subscription: Domestic, \$11.00; Foreign \$13.75

NONPERIODICALS

Monographs—Major contributions to the technical literature on various subjects related to the Bureau's scientific and technical activities.

Handbooks—Recommended codes of engineering and industrial practice (including safety codes) developed in cooperation with interested industries, professional organizations, and regulatory bodies.

Special Publications—Include proceedings of conferences sponsored by NBS, NBS annual reports, and other special publications appropriate to this grouping such as wall charts, pocket cards, and bibliographies.

Applied Mathematics Series—Mathematical tables, manuals, and studies of special interest to physicists, engineers, chemists, biologists, mathematicians, computer programmers, and others engaged in scientific and technical work.

National Standard Reference Data Series—Provides quantitative data on the physical and chemical properties of materials, compiled from the world's literature and critically evaluated. Developed under a world-wide program coordinated by NBS. Program under authority of National Standard Data Act (Public Law 90-396).

NOTE: At present the principal publication outlet for these data is the *Journal of Physical and Chemical Reference Data* (JPCRD) published quarterly for NBS by the American Chemical Society (ACS) and the American Institute of Physics (AIP). Subscriptions, reprints, and supplements available from ACS, 1155 Sixteenth St. N.W., Wash., D.C. 20056.

Building Science Series—Disseminates technical information developed at the Bureau on building materials, components, systems, and whole structures. The series presents research results, test methods, and performance criteria related to the structural and environmental functions and the durability and safety characteristics of building elements and systems.

Technical Notes—Studies or reports which are complete in themselves but restrictive in their treatment of a subject. Analogous to monographs but not so comprehensive in scope or definitive in treatment of the subject area. Often serve as a vehicle for final reports of work performed at NBS under the sponsorship of other government agencies.

Voluntary Product Standards—Developed under procedures published by the Department of Commerce in Part 10, Title 15, of the Code of Federal Regulations. The purpose of the standards is to establish nationally recognized requirements for products, and to provide all concerned interests with a basis for common understanding of the characteristics of the products. NBS administers this program as a supplement to the activities of the private sector standardizing organizations.

Consumer Information Series—Practical information, based on NBS research and experience, covering areas of interest to the consumer. Easily understandable language and illustrations provide useful background knowledge for shopping in today's technological marketplace.

Order above NBS publications from: Superintendent of Documents, Government Printing Office, Washington, D.C. 20402.

Order following NBS publications—NBSIR's and FIPS from the National Technical Information Services, Springfield, Va. 22161.

Federal Information Processing Standards Publications (FIPS PUB)—Publications in this series collectively constitute the Federal Information Processing Standards Register. Register serves as the official source of information in the Federal Government regarding standards issued by NBS pursuant to the Federal Property and Administrative Services Act of 1949 as amended, Public Law 89-306 (79 Stat. 1127), and as implemented by Executive Order 11717 (38 FR 12315, dated May 11, 1973) and Part 6 of Title 15 CFR (Code of Federal Regulations).

NBS Interagency Reports (NBSIR)—A special series of interim or final reports on work performed by NBS for outside sponsors (both government and non-government). In general, initial distribution is handled by the sponsor; public distribution is by the National Technical Information Services (Springfield, Va. 22161) in paper copy or microfiche form.

BIBLIOGRAPHIC SUBSCRIPTION SERVICES

The following current-awareness and literature-survey bibliographies are issued periodically by the Bureau:

Cryogenic Data Center Current Awareness Service. A literature survey issued biweekly. Annual subscription: Domestic, \$25.00; Foreign, \$30.00.

Liquified Natural Gas. A literature survey issued quarterly. Annual subscription: \$20.00.

Superconducting Devices and Materials. A literature survey issued quarterly. Annual subscription: \$30.00. Send subscription orders and remittances for the preceding bibliographic services to National Bureau of Standards, Cryogenic Data Center (275.02) Boulder, Colorado 80302.

U.S. DEPARTMENT OF COMMERCE
National Bureau of Standards
Washington, D.C. 20234

OFFICIAL BUSINESS

Penalty for Private Use \$300

POSTAGE AND FEES PAID
U.S. DEPARTMENT OF COMMERCE
COM-215



SPECIAL FOURTH-CLASS RATE
BOOK